THE UNIVERSITY OF QUEENSLAND

AUSTRALIA

Cane toad toxins: Mystery revealed

Venkatanambi Kamalakkannan

Master of Biotechnology

A thesis submitted for the degree of Doctor of Philosophy at

The University of Queensland in 2014

Institute for Molecular Bioscience

Abstract

Cane toads (*Bufo marinus*) were introduced to Australia as a biocontrol agent for the beetle pests of sugarcane. An ill-advised attempt at biocontrol, the cane toad experiment proved remarkably unsuccessful. Not only did cane toads fail to control the beetles, they became an invasive poisonous pest and threat to many native predator species and ecosystems across northern Australia. All subsequent attempts to control the cane toad invasion have proved unsuccessful. In an attempt to address this challenge we recently set out to investigate cane toad chemical ecology – arguing that better knowledge of cane toad toxins and pheromones would reveal weaknesses that might be exploited for control.

In preliminary investigations into cane toad toxins Capon group reported that the chemical composition of cane toad toxin secretions was more complex than previously reported and that bacteria isolated from the cane toad parotoid gland were capable of *in vitro* biotransformation of cane toad toxins. In our current investigations we have (i) characterized an array of bufadienolides and arginyl amides, and developed analytical methods for quantification in cane toad toxins (ii) Analysis of cane toad toxins determined the variation of chemical diversity based on various handling methods (iii) cane toad toxins are hydrolysed by BtH during secretion from conjugates (bufotoxins) to non-conjugates (bufagenins), (iv) there are two types of microbes present in parotoid gland, a former that can degrade bufagenins and a latter that can biotransform bufagenins to other analogues (vii) cane toad eggs contains bufagenins and bufolipins (conjugates with fatty acids) and (viii) evaluation of pharmacological toxicity of cane toad toxins (an SAR study) using *in vitro* cytotoxicity against mammalian cells and bacteria and activation of mNOS pathway by arginyl amides.

Cane toad toxin as always been identified as a single entity and the mystery (such as protoxin to toxin conversion of cane toad toxins, role of BtH and relationship between biotransformation and degradation bacteria) has been elaborated in the current thesis. Knowledge of the full story behind cane toad toxins, inclusive of bufagenins and bufotoxins, and the role of biotransforming enzymes and bacteria, is the first step in "knowing the enemy". We are hopeful that this knowledge will inform future control solutions.

Declaration by author

This thesis is composed of my original work, and contains no material previously published or written by another person except where due reference has been made in the text. I have clearly stated the contribution by others to jointly-authored works that I have included in my thesis.

I have clearly stated the contribution of others to my thesis as a whole, including statistical assistance, survey design, data analysis, significant technical procedures, professional editorial advice, and any other original research work used or reported in my thesis. The content of my thesis is the result of work I have carried out since the commencement of my research higher degree candidature and does not include a substantial part of work that has been submitted to qualify for the award of any other degree or diploma in any university or other tertiary institution. I have clearly stated which parts of my thesis, if any, have been submitted to qualify for another award.

I acknowledge that an electronic copy of my thesis must be lodged with the University Library and, subject to the General Award Rules of The University of Queensland, immediately made available for research and study in accordance with the *Copyright Act 1968*.

I acknowledge that copyright of all material contained in my thesis resides with the copyright holder(s) of that material. Where appropriate I have obtained copyright permission from the copyright holder to reproduce material in this thesis.

Publications during candidature

No publications

Publications included in this thesis

No publications included

Contributions by others to the thesis

I acknowledge that MALDI imaging discussed in Chapter 4 was performed in collaboration with Dr. Brett Hamilton (Prof Deon Ventor group, Mater Hospital, Brisbane) while I provided the necessary tissue samples dissected from cane toads. Electron microscopy discussed in Chapter 4 was performed in collaboration with Dr. Kathryn Green (IMB). Ion Torrent Sequencing of toad RNA was performed in collaboration with Dr. Darren Korbie (IMB) and shotgun sequencing with Dr. Eivind Undheim. In-house mNOS activation assay was performed in collaboration with Dr. Zeinab Khalil and cytotoxicity assay with Dr Xiaocong Huang. All the above experiments were planned (with all the necessary samples including tissues or cells, natural or synthetic compounds), conceptualized and outcomes processed by me for better understanding of cane toad toxins.

Statement of parts of the thesis submitted to qualify for the award of another degree

None

Acknowledgements

"Though fate is against fulfilment one's effort has ready payment"
- Thirukkural

Australian and New Zealand Standard Research Classifications (ANZSRC)

030101 Analytical Spectrometry, 45%

060107, Enzymes, 35%

030502, Natural Products chemistry, 20%

Fields of Research (FoR) Classification

0601, Biochemistry and Cell Biology, 50%

0301, Analytical Chemistry, 40%

0605 Microbiology, 10%

Table of contents

Chapter 1
Cane toad introduction in Australia and its aftermath

Chapter 2
Full characterization, identification and quantification of the cane toad parotoid toxins

Chapter 3
Chemo-anatomy: Bufadienolide composition in cane toad parotoid toxin and parotoid secretion

Chapter 6

Characterization of the cane toad egg extracts, with the emphasis on bufadienolides (bufolipins)

Chapter 7

Comparative analysis of the pharmacological properties of individual cane toad toxins

List of Figures

List of tables

List of Schemes

Abbreviations

BtH – Bufotoxin hydrolase

DAPI – 4',6'-diamidino-2-phenylindole

FdA – fluorescein diacetate

H&E – Haematoxylin Eosin

MALDI – Matrix assisted laser desorption/ionization

Na^+/K^+ ATPase – Sodium potassium ATPase

PAS – Periodic acid-Schiff

PBS – Phosphate buffer saline

SDS PAGE – Sodium dodecyl sulfate polyacrylamide gel electrophoresis

Chapter 1: Cane toad introduction in Australia and its aftermath

1.1 *B. marinus* in Australia

The cane toad belongs to the family Bufonidae, which consists of 33 genera and more than 470 species, with 258 species belong to the genus *Bufo*.[1] The cane toad and its relatives, among the most primitive groups of broad skulled toads,[2] are generally found in the Americas, Africa and Eurasia.

Figure 1.1 Adult male cane toad (*Bufo marinus*) Photograph by Alexis Barrett

The snout to vent length (SVL) of the cane toads is 10 – 15 cm in the wild and in some cases larger, especially when in captivity. Female cane toads have been reported with a SVL of more than 20 cm and a weight of 1.5 kg.[3] Cane toads possess a broad head with a truncated snout. Immediately behind the head of the cane toad are the parotoid glands, which secrete a milky-white toxin. Cane toads have a characteristic dry warty skin and are usually brown to olive brown in colour with a pale whiter to yellowish belly (Figure 1.1).[2] The life cycle of the cane toad comprises egg – tadpole – juvenile – adult – egg stages like other amphibians, with a clutch size varying depending on the size and age of the female cane toad, ranging from 4000 – 36000 eggs per adult.[1] The egg/tadpole survival rate is generally low as cane toad tadpoles themselves are major predators of cane toad eggs, consuming more than 99% of laid eggs.[4] The average life expectancy of a cane toad in the wild is 10 – 15 years.[5]

Parotoid glands are macroglands containing numerous vesicles or microglands (Figure 1.2A).[6] They play a major role in chemical defence against predatory attacks and microorganisms.[7] The parotoid secretions are stored in the microglands and are discharged upon manual compression of parotoid gland.[8] The cane toads can inflate their lungs during a predatory attack to position the parotoid gland towards the source of danger and then secrete the toxin when exposed to physical pressure.[6] Dissected parotoid glands display large numbers of alveoli containing large bottle shaped glands with a narrow slit like opening lined by a thick epithelium through which the toxin passes when physical pressure is applied (Figure 1.2B).[9]

Figure 1.2 *B. marinus* in wild. Toxin is stored in parotoid glands as indicated by an arrow (left). Parotoid microgland (PM) filled with toxin, toxin exit duct as indicated by black arrow (right).

The cane toad (*Bufo marinus*) was introduced into various countries, including Australia, Fiji and Hawaii, as a biocontrol agent for the beetle pests of sugarcane. However, the introductions turned out to be largely unsuccessful as the cane toads failed to feed specifically on the beetle pests. For example, the cane toad was introduced in June 1935 from Hawaii to Cairns, Queensland, for the control of greyback cane beetle (*Dermolepida albohirtum*) and Frenchi beetle (*Lepidiota frenchi*).[10] Since then, the cane toad has been reported to have some significant effects on the native predator populations.[3]   The major concern is the threat to the Australian native predator populations from ingestion of the toxic cane toads.[11] A large number of deaths have been reported among the native predators including lizards,[12] snakes,[13] quolls,[14] crocodiles[11] and domestic animals.[15] Cane toads are the only species in Australia to deploy bufadienolides for defense and the local predators are more susceptible since they are not evolved to overcome bufadienolide poisoning. Moreover, the cane toad population has increased significantly, extending from Queensland to New South Wales colonising more than 1 million km^2 and more importantly across the Northern Territory to the Western Australia.[3] Therefore, the need for the control of cane toad populations is urgent and significant. Figure 1.3 illustrates the distribution of cane toads in Australia as of 2007.

Figure 1.3 Distribution of cane toads in Australia as of 2007. (Reproduced from Shanmuganathan et al 2007).[10]

1.2 Chemistry of *Bufo* sp parotoid glands

The cane toad parotoid gland secretion contains a mixture of various classes of compounds.[16] The major class of chemicals reported from the cane toad toxin are the bufadienolides[17, 18] and biogenic amines (catecholamines, indolylalkylamines).[19]

1.2.1 Catecholamines

B. marinus parotoid secretions have been reported to contain catecholamines such as adrenaline (**1.1**), noradrenaline (**1.2**) and dopamine (**1.3**) (Figure 1.4).[19] The catecholamines in the parotoid secretion are potent neurotransmitters and vasoconstrictors.[6, 20]

adrenaline (**1.1**)   noradrenaline (**1.2**)   dopamine (**1.3**)
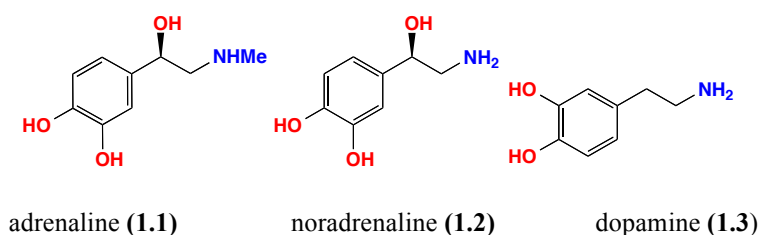
Figure 1.4 Structure of major catecholamines reported from parotoid secretions of the cane toad

1.2.2 Indolealkylamines

More than twenty indolealkylamine derivatives have been attributed to *Bufo* species. Indolealkylamines such as bufotenine (**1.4**), bufotenidine (**1.5**), dehydrobufotenine (**1.6**), bufothionine (**1.7**) and serotonin (**1.8**) have been isolated from skin and parotoid gland secretions of

4

B. marinus (Figure 1.5).[21] Bufotenine is known for its hallucinogenic properties, an activity that has seen it became a drug of abuse, and a scheduled and restricted substance.[22]

bufotenine **(1.4)**   bufotenidine **(1.5)**   dehydrobufotenin **(1.6)** bufothionine **(1.7)**   serotonin **(1.8)**
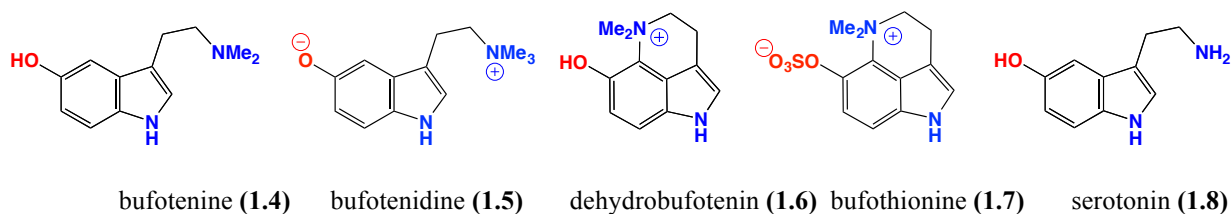
Figure 1.5 Structure of major indole alkylamines reported from parotoid secretions of the cane toad

1.2.3 Bufadienolides

Since the biogenic amines from the cane toad, *B. marinus* have been well studied, the focus of my research was on the bufadienolides. Although several competing trivial nomenclatures for bufadienolides can be found in the literature, for the purpose of this thesis we adopt the sub-class nomenclature of bufagenins, bufotoxins, bufolipins, bufagenin sulfates and bufagenin glycosides. Following the convention, bufadienolides with an unsubstituted C-3 hydroxyl are termed as bufagenins and those bearing a C-3 ester linkage to a diacid aminoacid amide are termed bufotoxins. Bufagenins bearing a C-3 ester linkage to a fatty acid are termed bufolipins. Bufagenins bearing a C-3 sulfate are referred to as bufagenin sulfates, while bufagenins bearing a C-3 glycosides are referred to as bufagenin glycosides.

About 100 bufadienolides have been reported from *Bufo* species, of which only 30 have been attributed to *B. marinus*.[18] Bufadienolides are known for their cardiotonic properties which have seen them used traditionally as a local anaesthetic.[19] Bufadienolides like marinobufagenin are structurally similar to cardenolide cardioactive glycosides such as ouabain (found in milk weed, **1.10**) and digoxin (foxglove, **1.11**). Biosynthesis of bufadienolides is still not well understood, but cholesterol is a well established precursor.[23] Bufadienolides are reported to be inhibitors of the Na^+/K^+ ATPase pump found in heart muscle, an activity they have in common with cardioactive glycosides such as digitalis.[24, 25]

cholesterol **(1.9)**   ouabain **(1.10)**

5

digoxin (**1.11**)
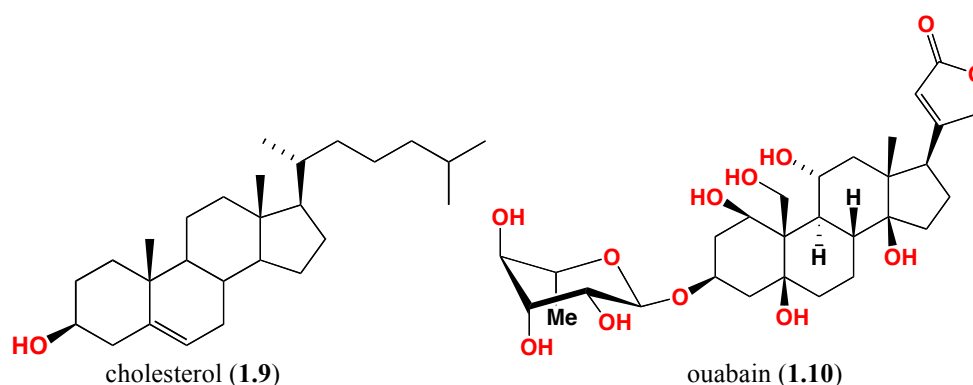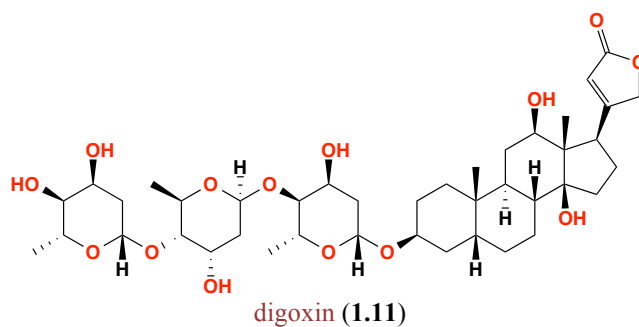
Bufadienolides have been isolated from various sources including plants and animals. The first report of a bufadienolide was scillarenin A (**1.12**) from the Egyptian Squill.[26] Since then bufagenins have been reported from various plants sources such as *Kalanchoe*,[27] *Scilla*,[28] *Melianthus*,[29] *Helleborous[30]* and animal sources including toads (*Bufonidae*),[31] snakes (*Rhabdopis* spp)[32] and fireflies (*Photinus* spp).[33] Mammalian bufadienolides have been known for two decades and include marinobufagenin (**1a**), first reported in 1993 from human cataract and kidneys.[34, 35] Mammalian bufadienolides also reported from *Bufo* species, include marinobufagenin (**1a**), marinobufotoxin (**1c**) and telocinobufagenin (**2a**).[36, 37] This chapter will discuss more about bufadienolides reported from the Bufonidae, especially from *B. marinus* (also known as *Rhinella marina*).[9] The species name for cane toads has been debated in the last 10 years but in this thesis we emphasized "*Bufo marinus*" as majority of the literature sources have adopted this species name.

scillarenin A (**1.12**)
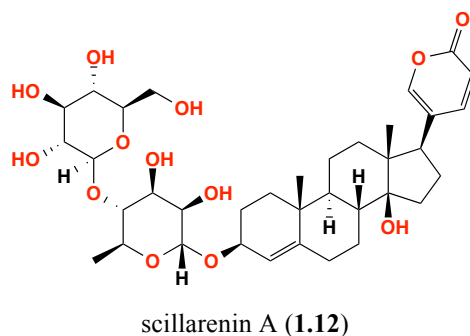
1.2.3.1 Bufagenins

Bufagenins possess steroidal A/B *cis* and C/D *cis* ring junctions with an α-pyrone ring at C-17, and a hydroxyl at C-3 (Figure 1.6). The first repeated bufagenin was acetylcinobufagenin (**1.13**), described in 1930 by Jensen et al., from *B. marinus*.[38] Since then bufagenins have been reported from various plants and animal sources[18] as well as cane toad parotoid secretions and include compounds such as bryophillin B (**1.14**), 12β-hydroxyscillirosidin (**1.15**) and gamabufotalin (**1.16**).[18, 39] Bufagenins have been reported to be potent inhibitors of Na^+/K^+ ATPase.[25]

6

Other known biological activities attributed to bufagenins include antimicrobial,[40] antitumour,[41] antileishmanial and antitrypanosomal,[7] anti-apoptotic,[42] anti-angiogenic,[43] and activation of the ClC-3 chloride channel (anti-metastasis).[44]

acetylcinobufagenin **(1.13)**
from *B. marinus*

bryophillin B **(1.14)**
from *K. gracilis*

12β-hydroxyscillirosidin **(1.15)**
from *Drimia robusta*

gamabufotalin **(1.16)**
from *R. tigrinus*
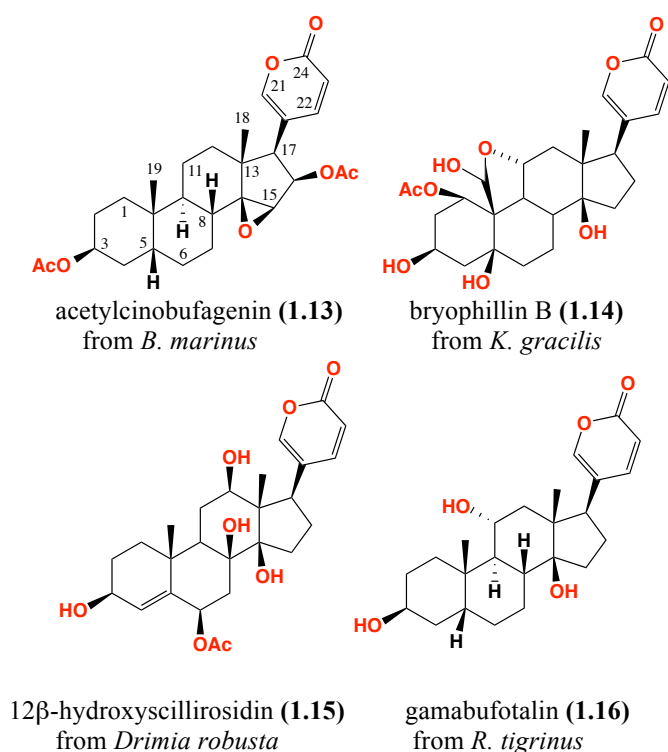
Figure 1.6 Examples of bufagenins found in plants and animals

1.2.3.2 Bufotoxins

The first reported bufotoxin was marinobufotoxin (**1c**), described from the American toad *B. marinus* by Chen et al in 1930 (Figure 1.7).[38] Since the initial report approximately 35 bufotoxins have been reported from other *Bufo* spp.[18] Bufotoxins from *B. marinus* are predominantly diacid arginyl esters however, bufotoxins containing other aminoacid variations, such as histidine and glutamine have also been reported from *Bufo melanostictus* and *Bufo japonicas*.[45, 46] Parotoid secretions from *Bufo* spp have also been reported to contain trace amounts of bufotoxins with differing diacids, such as pimeloyl,[17] succinoyl[39] glutaroyl[18] and adipoyl[39] esters of arginine. Bufotoxins are also inhibitors of Na^+/K^+ ATPase with potencies ranging from sub micromolar to micromolar levels.[25, 47] Marinobufotoxin (**1c**) has been reported to be biosynthesized in human Y1 adrenal cells and it is the first bufadienolide to be identified from *in vitro* mammalian cell cultures.[37] The role of bufotoxins in mammals is not well understood, however some reports suggest their role in sodium retention in kidneys.[48]

marinobufotoxin (**1c**) from *B. marinus*   hellebritoxin (**5c**) from *R. tigrinus*
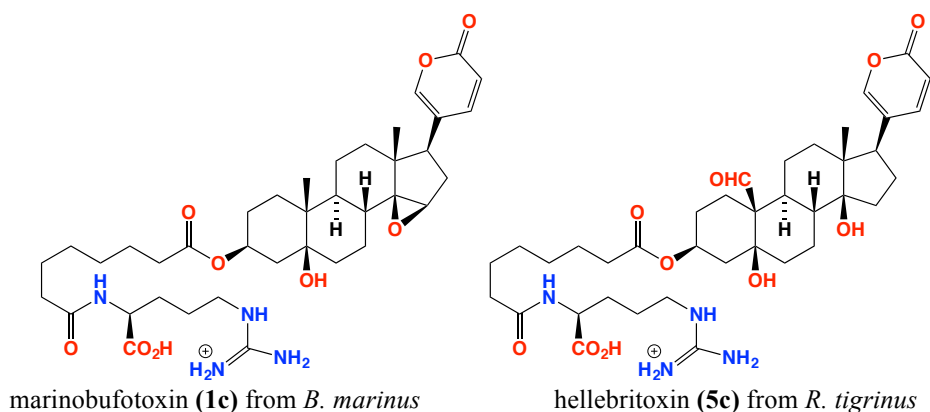
Figure 1.7 Examples of bufotoxins found in toads and snakes

1.2.3.3 Bufolipins

The first bufolipins to be reported were bufolipin A, bufolipin B and bufolipin C isolated and characterized (Note: Subsequent to this 1998 report, our laboratory coined the bufolipin terminology to provide a logical framework for describing this unique class of bufadienolides) from the ovaries of the cane toad *B. marinus*, by Matsukawa et al in 1998 (Figure 1.8).[31] Unlike bufotoxins, bufolipins are composed of a mono-carboxylic acid ester side chain with a hydroxyl group attached to the terminal of the fatty acid. To date, there have been only two literature reports of bufolipins,[31, 49] where bufolipin A was isolated from the eggs of *B. marinus* while the rest were isolated from ovaries.[31,49] Bufolipins, like other bufadienolides, are inhibitors of Na^+/K^+ ATPase and are more potent than their counterparts, bufotoxins.[31] More recently, in studies carried out in our laboratory, bufolipin A was reported to have an attractant pheromone effect on *B. marinus* tadpoles.[49]
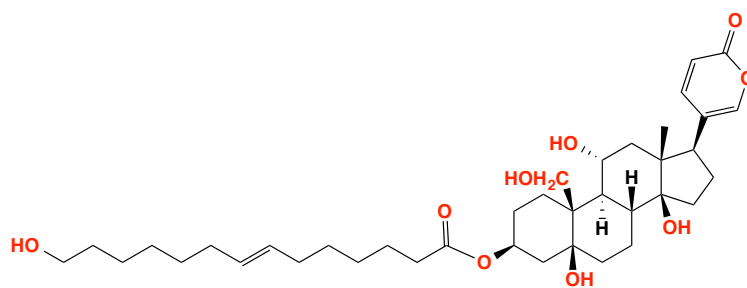
bufolipin A (**1h**)
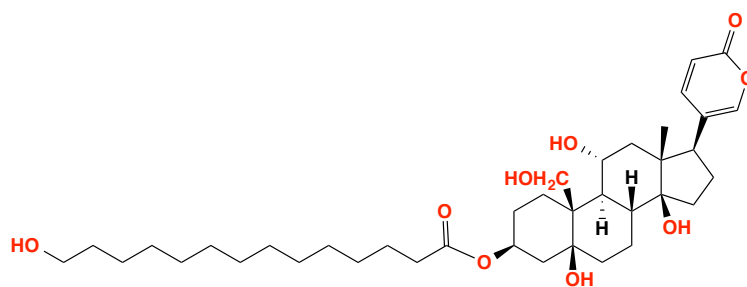
bufolipin B (**2h**)
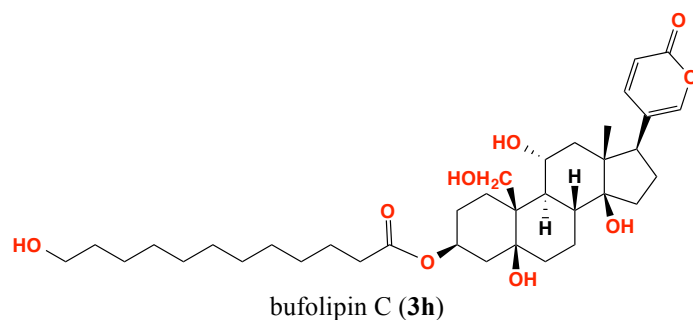
bufolipin C (**3h**)

Figure 1.8 Bufolipins found in eggs/ovaries of the cane toad

1.2.3.4 Bufagenin sulfates

The first reported bufagenin sulfate was bufalin-3-sulfate (**3f**) from *B. vulgaris* (Japanese toad), described in 1974 by Shimada et al (Figure 1.9).[50] Sulfated bufadienolides have since been detected in *Bufo* spp plasma, bile and skin,[51-53] and are weak inhibitors of Na⁺/K⁺ ATPase compared to bufagenins and bufotoxins.[51] It has been postulated that sulphation of bufagenins in toads is a detoxification strategy,[54] as the sulfates are more water soluble and more easily excreted.[55]

bufalin 3- sulfate (**3f**) - from *B. vulgaris*

hellebrigenol 3- O-sulfate from *B. melanostictus* (**5f**)
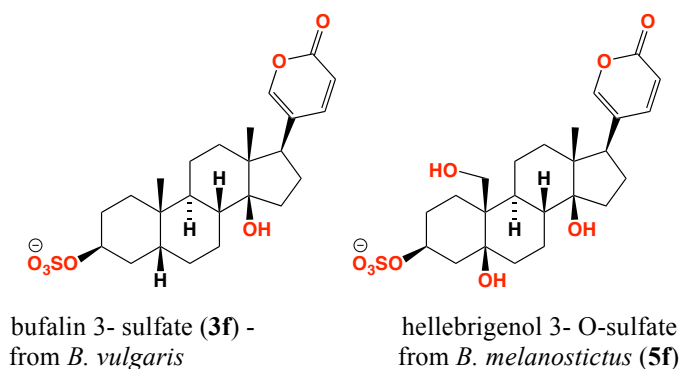
Figure 1.9 Examples of bufagenin sulfates found in toads

1.2.3.5 Bufagenin glycosides

Scillaren A (**1.12**) was the first bufagenin glycoside reported by Stoll et al in 1933.[26] In plants, bufadienolides predominately occur as glycosides with sugar units at 3-OH of bufagenins (Figure 1.10). *Urginea maritima* and *Urginea altissima* have been a great source of bufagenin glycosides.[56] Bufagenin glycosides were responsible for 33% of cattle deaths (12,000) annually, indicating the levels of toxicity and causing a great influence on agriculture industry in those regions native to bufagenin glycosides harbouring plants. More than 50 bufagenin glycosides have been reported from Crassulaceae (*Kalanchoe tomentose*, *Tylecodon wallichii*, etc) and Hyacinthaceae (*Urginea* spp.).[18, 56] Shimada et al reported that doubly linked glycosides exhibited higher cardiotonic activity than their respective bufagenins.[25] L-rhamnose promotes cardiotonic activity (eg scilliglaucosidin-α-L-rhamnoside) while D-rhamnose subititution showed less/no activity (eg scilliglaucosidin-β-D-rhamnoside).[57]

kalanchoside A (**1.17**)
from *Kalanchoe gracilis*)

scilliroside (**1.18**)
from *Urginea maritima*
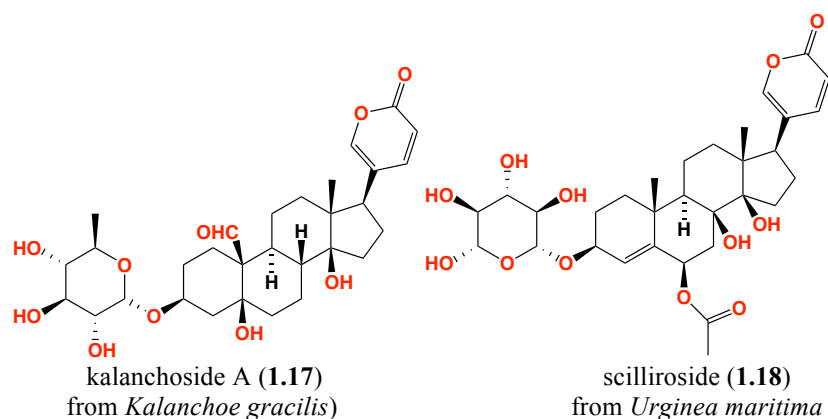
Figure 1.10 Examples of bufagenin glycosides from plants

1.2.4 Bufadienolides from *B. marinus*

The Bufonidae are a rich source of bufadienolides including bufagenins, bufotoxins, bufolipins and bufagenin sulfates, with bufagenins being the dominant structure class[58, 59] Bufadienolides have been reported from various tissues of *B. marinus* such as skin, parotoid secretions, oviducts/eggs, plasma and tadpoles (Figures 1.11 – 1.13).[31, 51, 52, 60] A list of *B. marinus* bufadienolides from various tissue sources and regions is summarized in Table 1.1.

1.2.4.1 Parotoid secretions

Parotoid secretions are a rich source of bufadienolides, consisting of bufagenins and minor amounts of bufotoxins.[17,37,51] Seven bufagenins, marinobufagenin (**1a**), telocinobufagenin (**2a**), bufalin (**3a**), resibufogenin (**4a**), hellebrigenin (**5a**), arenobufagenin (**6a**) and marinoic acid (**8a**) and five bufotoxins, marinobufotoxin (**1c**), telocinobufotoxin (**2c**), bufalitoxin (**3c**), marinobufagenin

pimeloylarginine (**8c**) and bufalin pimeloylarginine (**9c**) have been reported from parotoid secretions of *B. marinus*.[17, 61, 62] In some cases HPLC-DAD analysis of parotoid secretions detected bufagenins as the dominant chemistry, with trace levels of bufotoxins.[58] Whether bufotoxins are present in parotoid secretions remains unclear, and more work is required.[19,35] Shimada et al, hypothesized that bufotoxins were the precursors of bufagenins.[63] Curiously the relative and absolute bufagenins composition of parotoid secretion can vary, with *B. marinus* sampled in Australia exhibiting >30 bufadienolides with significant amounts of marinobufagenin (**1a**), telocinobufagenin (**2a**), bufalin (**3a**) and resibufagenin (**4a**), and traces of arenobufagenin (**6a**) and hellebrigenin (**5a**) and bufotoxins.[17]

1.2.4.2 Skin

B. marinus skin is a rich source of bufotoxins and bufagenin sulfates compared to parotoid secretions which are dominated by bufagenins.[52] The reason for such a variation has never been investigated and is addressed in this thesis (Chapter 3). Bufotoxins found in *B. marinus* skin include marinobufotoxin (**1c**), telocinobufotoxin (**2c**) and marinobufagenin-3-pimeloylarginine (**8c**), while bufagenin sulfates include marinobufagenin-3-sulfate (**1f**) and resibufogenin-3-sulfate (**4f**).[52] The only report of a bufagenin detected from the skin of *B. marinus* was that of marinosin (**9a**) by Matsukawa et al, in 1998.[64]

1.2.4.3 Plasma and bile

Distribution of bufadienolides in plasma is similar to that of the skin, as it predominantly contains bufotoxins and bufagenin sulfates. Two bufotoxins, telocinobufotoxin (**2c**) and arenobufotoxin (**6c**), and three bufagenin sulfates, telocinobufagenin-3-sulfate (**2f**), bufalin-3-sulfate (**3f**) and arenobufagenin-3-sulfate (**6f**) have been reported from the plasma of *B. marinus*.[51,65] Interestingly, a bufagenin glucuronide was claimed, but as the identification of a glucuronyl bufadienolide structure was based solely on the HPLC-DAD retention time, this claim lacks credibility.[51] Lichtstein et al, identified the bufagenin, resibufogenin (**4a**) in the plasma of *B. marinus*.[65] To date the bufagenin sulfates, marinobufagenin-3-sulfate (**1f**) and 12β-hydroxytetrahydroresibufogenin (**7f**) have been identified in the bile of *B. marinus*. Sulfation and glucuronidation of xenobiotics are known to be mediated by cytochrome P450 enzymes during the phase two of xenobiotic metabolism, a process designed to facilitate excretion.[66,67] Since sulfation improves plasma solubility, it is perhaps not surprising that bufagenin sulfates are detected in plasma and bile.[55]

1.2.4.4 Eggs/oviducts

Eggs (pre-laying) were reported to contain bufagenins, however, compared to bufagenins found in adult *B. marinus* parotoid secretions, the bufagenins on the eggs are poly-hydroxylated.[68] Poly-hydroxylation of bufadienolides could provide better solubility characteristics for toxin on the surface of eggs. Surprisingly, oviducts contain polyhydroxylated bufagenins (such as eggs) and bufolipins.[31]

Five bufagenins, 11α-hydroxymarinobufagenin (**10a**), 11α,19-dihydroxymarinobufagenin (**11a**), 11α-hydroxytelocinobufagenin (**12a**), 19-hydroxytelocinobufagenin (**13a**) and 11α,19-dihydroxytelocinobufagenin (**14a**) have been reported from pre-laid eggs of *B. marinus*, of which **10a** and **13a** are also found in oviducts.[31] Four other bufagenins, telocinobufagenin (**2a**), hellebrigenin (**5a**), arenobufagenin (**6a**) and 5β-hydroxyarenobufagenin (**15a**) and three bufolipins, bufolipin A (**1h**), bufolipin B (**2h**) and bufolipin C (**3h**) were isolated from oviducts of *B. marinus*.[31] In a recent report, bufolipin A was isolated from laid eggs while several other bufolipins and bufagenins were also identified.[49] It was also postulated that the defence mechanism in *B. marinus* eggs could be attributed to the bufadienolides passed on from the ovaries (since the composition of bufadienolides was similar in eggs and ovaries). It is also important to note the *de novo* biosynthesis of bufadienolides does not commence until the juvenile stages of the cane toad life cycle.[60]

1.2.4.5 Tadpoles

Tadpoles were reported to contain only bufagenins, but in lower amounts compared to egg or adult stages.[60] Bufagenins that were identified in parotoid secretions, marinobufagenin (**1a**), telocinobufagenin (**2a**), resibufagenin (**4a**), hellebrigenin (**5a**) and arenobufagenin (**6a**) were also identified in tadpoles.[60] Interestingly, bufagenin levels in tadpoles vary in concentration based on different developmental stages. For instance, stage 21 (early) showed moderate levels of **1a**, **2a**, **5a** and **6a**; while stage 25 (middle) showed low levels of **4a** and **6a**; but stage 44/45 (late) showed substantial levels of **2a**, **4a** and **6a** and moderate levels of **1a** and **5a**.[60] This pattern not only indicated the distribution of bufadienolides within the various developmental stages, but also lead to insights into the onset of bufadienolide biosynthesis as the metamorphic and juvenile stages showed restoration of bufadienolide composition found in parotoid secretions.

Table 1.1 List of bufadienolides from various tissues of *B. marinus* reported from various countries

Tissue	Country of origin	bufagenins	bufotoxins	bufolipins	bufagenin sulfates	bufagenin glycosides
parotoid	Australia, Japan	1a, 2a, 3a, 4a, 5a, 6a, 8a	1c, 2c, 3c, 8c, 9c			
skin	Japan	9a	1c, 8c, 2c		1f, 4f	
bile	Japan, US				1f, 7f	
plasma	Japan, US	4a	2c, 6c		2f, 3f, 6f	1g
eggs/oviducts	Japan, Australia	2a, 5a, 6a, 10a, 11a, 12a, 13a, 14a, 15a		1h, 2h, 3h		
tadpoles	Australia	1a, 2a, 4a, 5a, 6a				
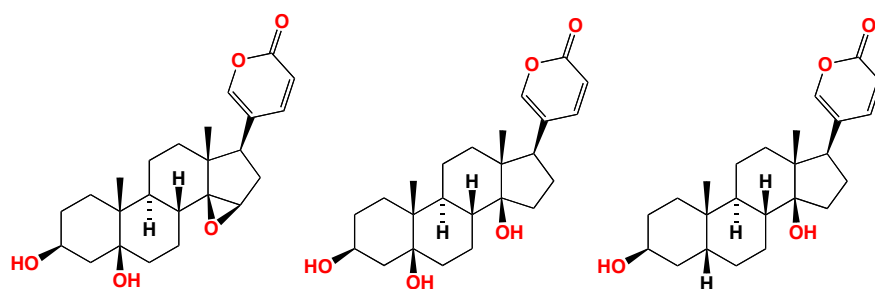
marinobufagenin **(1a)**   telocinobufagenin **(2a)**   bufalin **(3a)**
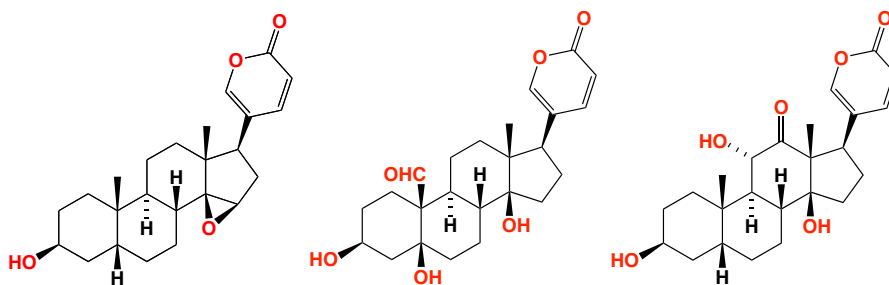
resibufagenin **(4a)**   hellebrigenin **(5a)**   arenobufagenin **(6a)**
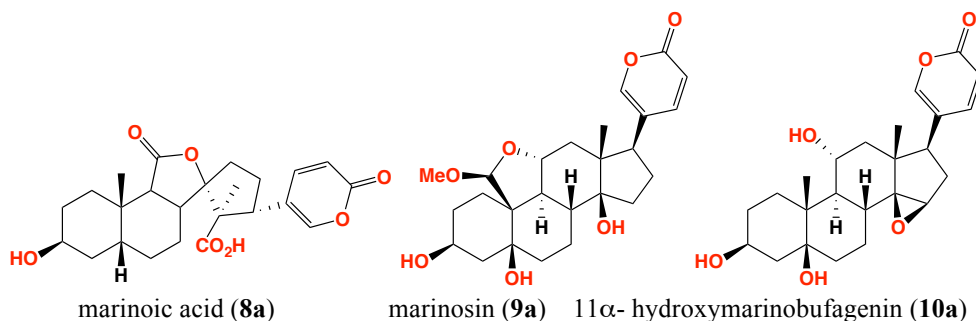
marinoic acid **(8a)**   marinosin **(9a)**   11α- hydroxymarinobufagenin **(10a)**

11α-hydroxy
telocinobufagenin (**11a**)

11α,19-dihydroxy
marinobufagenin (**12a**)

11α,19-dihydroxy
telocinobufagenin (**13a**)

19-hydroxy
telocinobufagenin (**14a**)

5β-hydroxyarenobufagenin (**15a**)
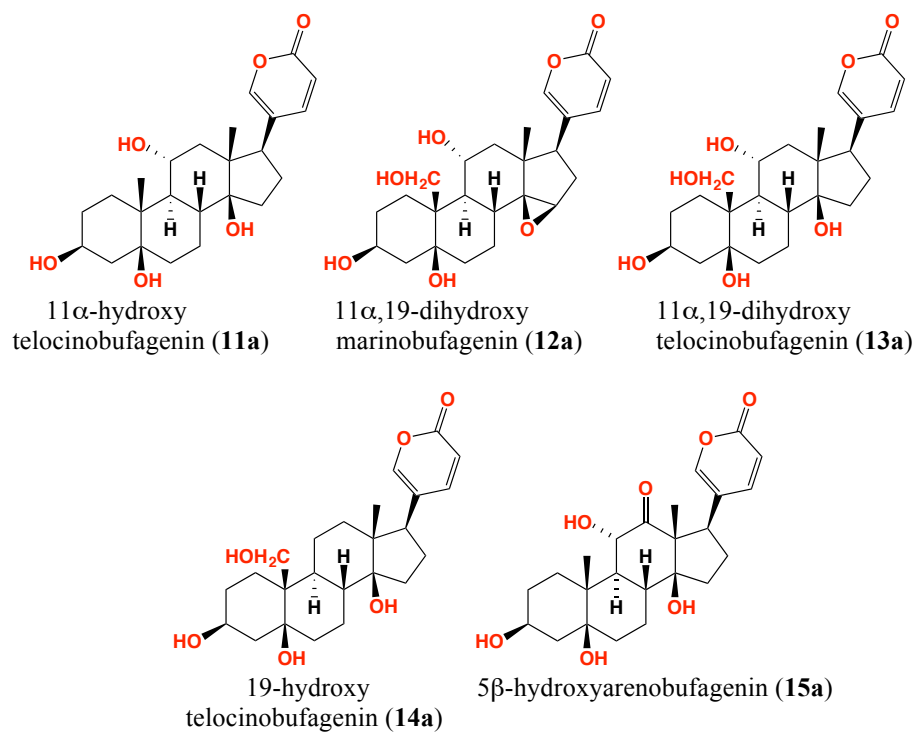
Figure 1.11 Bufagenins from *B. marinus*

marinobufotoxin **(1c)**

telocinobufotoxin **(2c)**

bufalitoxin **(3c)**

resibufotoxin **(4c)**

14

arenobufotoxin (**6c**) marinobufagenin-3-pimeloylarginine (**8c**)

bufalin-3-pimeloylarginine (**9c**)
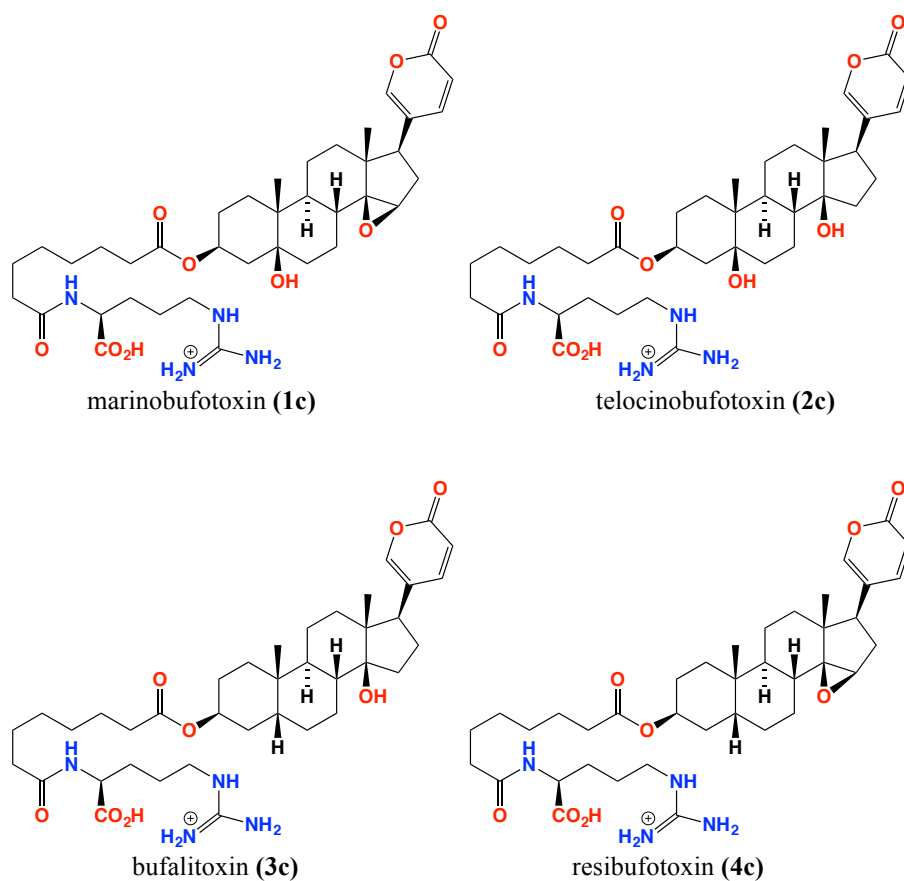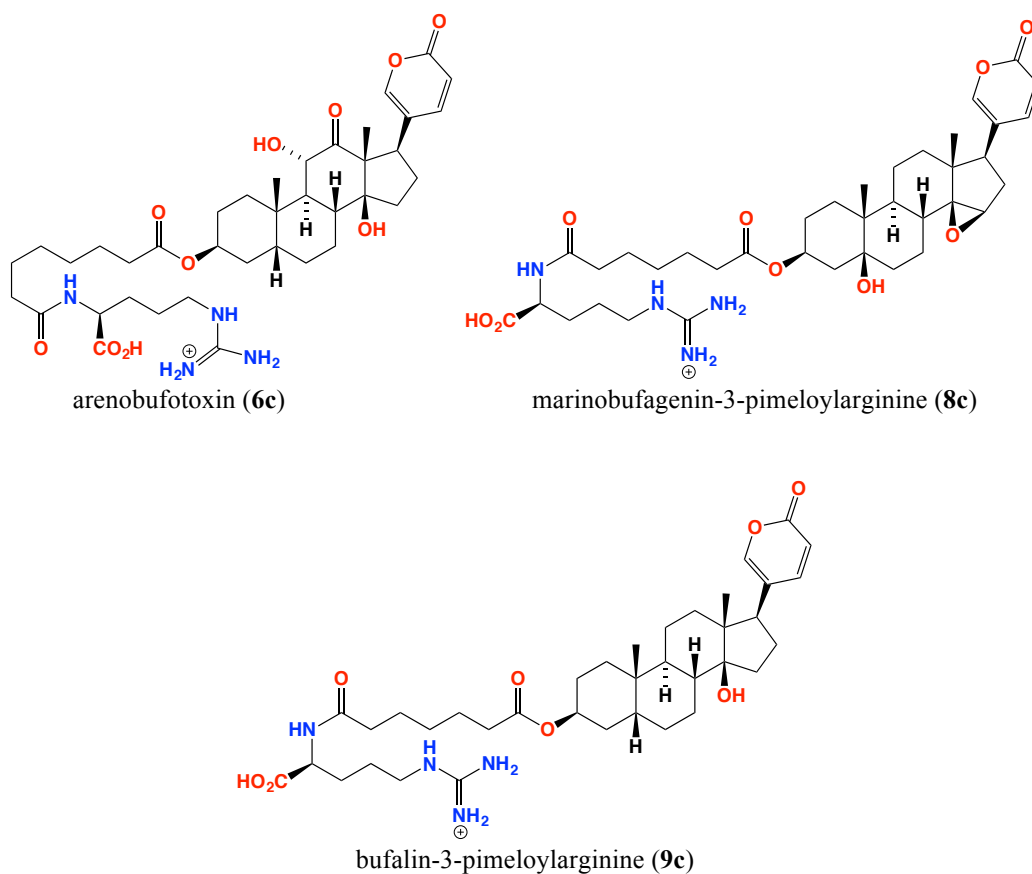
Figure 1.12 Bufotoxins from *B. marinus*

marinobufagenin-3-sulfate (**1f**) telocinobufagenin-3-sulfate (**2f**) bufalin-3-sulfate (**3f**)

resibufagenin-3-sulfate (**4f**) arenobufagenin-3-sulfate (**6f**) 12β-hydroxytetrahydro
resibufagenin 3-sulfate (**7f**)
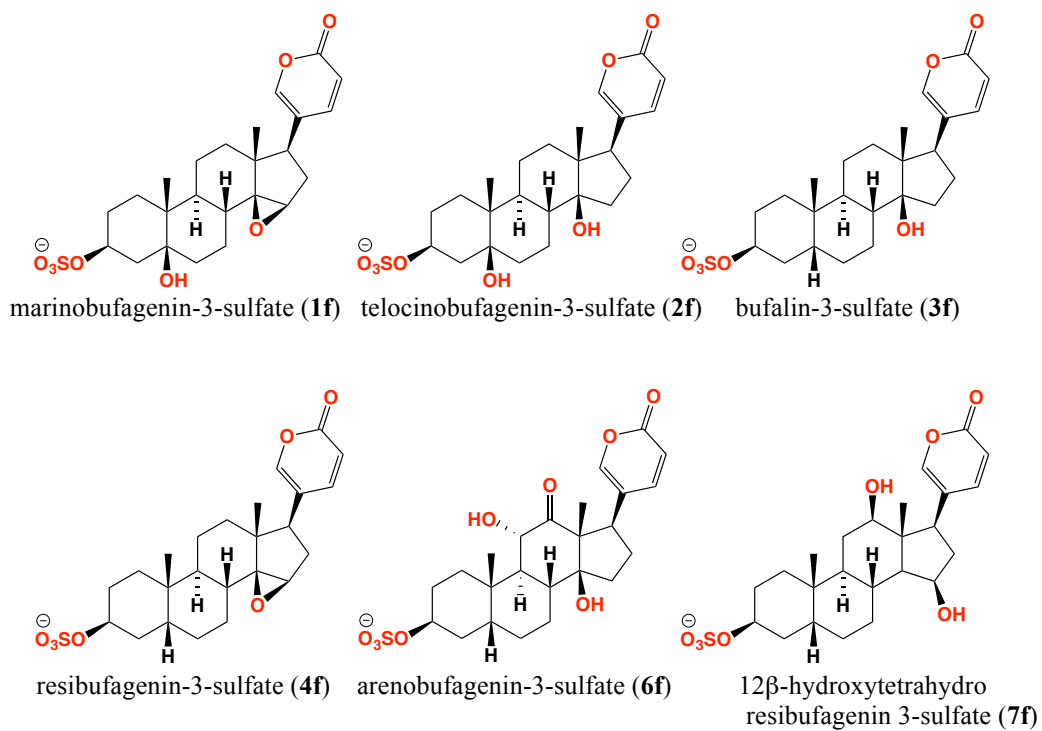
Figure 1.13 Bufagenin sulfates from *B. marinus*

1.2.5 Pharmacology of cane toad bufadienolides

Bufadienolides from *B. marinus* have been attributed various pharmacological properties. They are predominantly described as inhibitors of cardiac/kidney Na^+/K^+ ATPase, as well as antimicrobial,[40] antitumour,[41] antileishmanial and antitrypanosomal,[7] anti-apoptotic,[42] anti-angiogenetic,[43] chloride channel activators[44] and anti-viral[69]. However, bufotoxins, bufolipins and bufagenin sulfates/glycosides have only been subjected to Na^+/K^+ ATPase inhibition in different cell types and no other pharmacological interactions have been described. One of the major challenges encountered in comparing the biological/ecological properties of different bufadienolides is the lack of consistent, quantifiable and relevant bioassay data. A list of pharmacological properties of cane toad bufadienolides is summarized in Table 1.2.

1.2.5.1 Inhibition of Na^+/K^+ ATPase

The sodium-potassium activated adenosine triphosphatase (Na^+/K^+ ATPase) is a plasma membrane spanning protein complex that utilizes the energy released during the hydrolysis of ATP for the transport of sodium and potassium ions across the cell membrane. The pump plays an essential role in maintaining the concentration of sodium and potassium ions across the cell membrane. The main function of this electrochemical gradient is to provide energy for the transport of metabolites and nutrients like glucose, amino acids and ions like H^+, Ca^+ and Cl^- across the membrane and also for the regulation of cell volume and action potential of muscle.[70]

The Na^+/K^+ ATPase contains two subunits (α and β) associated in a 1:1 ratio (Figure 1.14). Basically, four α subunit isoforms occur in association with three β subunit isoforms to generate various Na^+/K^+ ATPase isozymes with specific transport and pharmacological properties.[71] The α subunit (110 kDa) provides the binding sites for the ligands to induce or inhibit the enzyme complex whereas the β (300 amino acids)[72] subunit plays a vital role in orientation and stabilization of the α subunit.[70] The γ subunit (10 kDa) of Na^+/K^+ ATPase was reported much later[73] and its role is still uncertain, but there has been a recent report which describes the γ subunit as an activator of Na^+/K^+ ATPase in pig kidney outer medulla.[74]
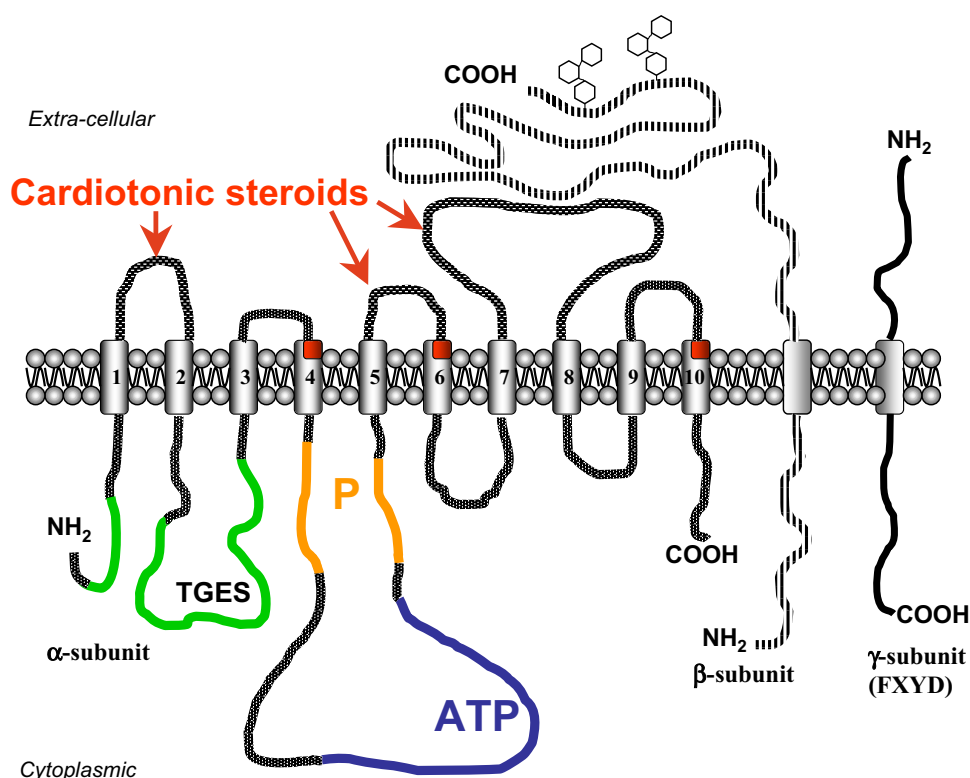
Figure 1.14 Diagrammatic representation of the membrane bound Na^+/K^+ ATPase pump showing the binding of cardiotonic steroids to the transmembrane domains of α subunit. Green – dephosphorylation mediated by TGES motif, Orange – phosphorylation region, purple – ATP binding pocket (Taken from Bagrov *et al*. Pharm. Rev. 2009).[75]

The inhibitory activity of the bufadienolides against Na^+/K^+ ATPase is reportedly similar to that of the plant derived ouabain (**1.10**) and digoxin (**1.11**).[31] Ouabain (**1.10**) was reported to inhibit Na^+/K^+ ATPase by binding to the α subunit.[76] Na^+/K^+ ATPase in humans contains three isoforms of α subunits, $α_1$, $α_2$ and $α_3$ expressed at various levels in various individuals, but the affinity of ouabain to all the isoforms is uniform.[77]

Marinobufagenin and ouabain exhibited highest affinity to different isoforms ($α_1$ and $α_3$) of Na^+/K^+ ATPase in rat aorta,[78] although both resulted in comparable Na^+/K^+ ATPase inhibition in C7-MDCK cells grown in the presence of marinobufagenin and ouabain.[47] When the Na^+/K^+ ATPase pump is inhibited, the intracellular concentration of Na^+ is slightly increased, which in turn affects the Na^+/Ca^{2+} exchange pump leading to increased levels of intracellular Ca^{2+} in the sarcoplasm of myocytes, causing a positive inotropic effect (increased muscular contractions).[79] Besides positive inotropy an increase in the extracellular concentrations of K^+ (hyperkalemia) has also been reported.[80] The genetic variations in the Na^+/K^+ isoforms are substantial as some species are immune to the cane toad toxin while others are highly susceptible. The bufadienolide diversity in the cane toad may play a significant role in antagonising a wide array of Na^+/K^+ isoforms thereby targeting a range of predators.

Although several pharmacological properties are described for cane toad bufadienolides, inhibition of Na^+/K^+ ATPase pump is of great significance as it appears to correlate to the ecological properties exhibited against predators. Several studies have been performed to understand the interaction of bufadienolides, especially bufagenins, against cardiac/kidney Na^+/K^+ ATPase.[81,82] However these studies were conducted on different cell types, in different assay systems using different readout technologies by different researchers at different time periods. In short, comparative structure activity relationship (SAR) data is simply not reliable.

In 1985 Shimada et al reported the inhibition of Na^+/K^+ ATPase isolated from guinea pig heart using an HPLC-based quantification system.[25,83] Forty-six bufadienolides, with variations in the steroid backbone and side chain conjugation were assessed as Na^+/K^+ ATPase inhibitors.[7] Briefly, the guinea pig Na^+/K^+ ATPase was incubated with bufadienolides and ATP was added to the reaction mixture. After stopping the enzymatic reaction, the conversion of ATP to ADP was measured by HPLC analysis. Although, the assay was purported to quantify the enzyme activity, and suffered from a number of limitations, Shimada et al nevertheless concluded that bufotoxins were more toxic as Na^+/K^+ ATPase inhibitor than bufagenins, bufagenin sulfates or glycosides.[25]

In another report, Akimova et al, employed a ouabain radioligand displacement assay using MDCK cells to measure the displacement properties of a range of bufadienolides.[47] Contradicting Shimada et al, Akimova et al concluded the bufagenins exhibited more toxicity or higher Na^+/K^+ ATPase inhibition compared to bufotoxins, with bufalin (**3a**) showing the highest inhibition. Overall, marinobufagenin (**1a**), telocinobufagenin (**2a**) and bufalin (**3a**) showed high potencies against Na^+/K^+ ATPase isolated from various tissues (brain, kidney or heart).

Na^+/K^+ ATPase inhibition of bufolipins has also been reported in dog kidney Na^+/K^+ ATPase using a calorimetric based assay system. Interestingly, bufolipins showed high potency by inhibiting Na^+/K^+ ATPase in sub micromolar concentrations (0.1 μM), which is comparable to bufalin (**3a**) reported from other research groups.[31] Since different research group used different assay systems to report the Na^+/K^+ ATPase inhibition exhibited by various structure class of bufadienolides, it is difficult to suggest the hierarchy of potencies. However, based on the values of IC_{50}, it could be suggested that bufagenins>bufolipins>bufotoxins>bufagenin sulfates/glycosides. However, the conclusion could also be disputed as bufotoxins in some assays showed more potency than bufagenins. A complete list of cane toad bufadienolides and their Na^+/K^+ ATPase inhibition profile has been summarized using a pie chart based on their potency and the available data in the literature (Figure 1.15). A majority of cane toad bufadienolides have not yet been investigated for Na^+/K^+

ATPase inhibition assay. However, at least one member from each of the bufadienolide structure class has been investigated for the inhibition of Na^+/K^+ ATPase. A standard quantification experiment for Na^+/K^+ ATPase inhibition including all the cane toad bufadienolide structure class would be significant to investigate the relative toxicity exhibited by cane toad toxins.

Na^+/K^+ ATPase activity
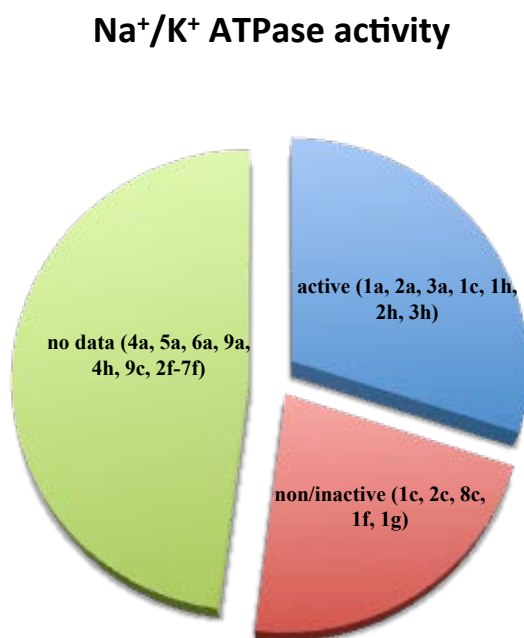
Figure 1.15 List of cane toad bufadienolides structure class based on inhibition of Na^+/K^+ ATPase sorted from the published literature

1.2.5.2 Cytotoxicity studies of *B. marinus* bufadienolides

Bufadienolides have been reported to exhibit anti-cancer activity based on the cytotoxicity studies using human cancer cell lines.[18] Cytotoxicity activities of *B. marinus* bufadienolides were conducted by researchers using various cell lines. Kamano et al, conducted a structure-activity relationship study of bufadienolides (bufagenins and bufagenin hemiesters), including *B. marinus* bufagenins using primary liver carcinoma cell line, PLC/PRF/5.[84] Bufagenins were found to be more cytotoxic than bufagenin hemiesters, but no bufotoxins were included in this study. In another study, Cunha-Filho et al, performed cytotoxicity assays on marinobufagenin (**1a**), telocinobufagenin (**2a**), bufalin (**3a**) and hellebrigenin (**5a**) using MDA-MB435 (melanoma), HL-60 (leukaemia), HCT-8 (colon), SF295 (glioblastoma) and PBLs (peripheral blood lymphocytes).[41] Interestingly in both studies bufalin (**3a**) exhibited the highest cytotoxicity (IC_{50} at sub nanomolar levels) while other bufagenins exhibited sub micromolar to 1 μM IC_{50} levels. Telocinobufagenin-3-sulfate was subjected to cytotoxicity studies using A549 (non-small-cell lung cancer), U373 (glioblastoma), HS683 (oligodendroglioma) and MCF-7 (breast cancer) cell lines and was reported to be non-cytotoxic.[54] In summary bufagenin sulfates appear to be the least cytotoxic bufadienolides followed

by bufagenin hemiesters. Bufagenins exhibit the highest levels of cytotoxicity, while bufotoxins are less cytotoxic.

1.2.5.3 Other biological activities of *B. marinus* bufadienolides

Marinobufagenin (**1a**) and telocinobufagenin (**2a**) were reported to exhibit modest antibiotic activity against *Escherichia coli* (MIC 16 and 64 μg/mL) and weak to negligible antibiotic activity against *Staphylococcous aureus* (MIC 128 μg/mL).[40] Anti-apoptotic activity of bufalin (**3a**) has been investigated in LNCaP (human Prostate Carcinoma) and MCF10A (human breast epithelial) cell lines. Following treatment with bufalin (**3a**), both cancer lines exhibited increased caspase mediated apoptotic modulation in androgen mediated and non-mediated cell types.[42] Anti-protozoan activity of telocinobufagenin (**2a**) and hellebrigenin (**5a**) were investigated against *Leishmania* (L.) *chagasi* promastigotes and *Trypanozoma cruzi* trypomastigotes. Both the bufadienolides were active against *Leishmania* (L.) *chagasi* while only hellebrigenin (**5a**) was active against *Trypanozoma cruzi*.[7]

Table 1.2 List of pharmacological properties reported on various bufadienolide structure classes isolated from *B. marinus* reported from various countries

Pharmacological properties (cell/tissue types)	bufagenins	bufotoxins	bufolipins	bufagenin sulfates	bufagenin glycosides
Na$^+$/K$^+$ ATPase inhibition					
human kidney[82]	**1a, 2a**				
C7-MDCK cells[47]	**1a, 3a**	**1c, 2c**			
dog kidney/pig brain[85]	**3a**				
guinea pig heart[81]	**1a, 2a**	**1c, 2c, 8c**			
guinea pig heart[25]	**1a**	**1c**		**1f**	**1g**
dog kidney[31]			**1h, 2h, 3h**		
Cytotoxicity					
PLC/PRF/5 cells[84]	**1a, 2a, 3a, 4a, 5a**				
HL-60, HCT-8, SF295, MDA-MB435, PBLS[41]	**1a, 2a, 3a, 5a**				
A549, U373, HS683, MCF-7[54]				**2f**	
Antibiotic – *E. coli* and *S. aureus*[40]	**1a, 2a**				
Apoptotic activity LNCaP, MCF10A[42]	**3a**				
Anti-leishmania[7]	**2a, 5a**				
Anti-trypanosome[86]	**5a**				

1.2.6 Control strategies for cane toad

The control strategies for cane toad can be divided into three major categories, physical, chemical and biological.

1.2.6.1 Physical

The physical control method is a comparatively low technology solution for the control of cane toads. It involves the use of traps[87] or containers for capturing toads and fencing barriers to avoid the migration of the cane toad.[88] Although the method offers temporary local control of cane toad populations, it cannot be regarded as a permanent solution. Moreover, the method is labour intensive and time consuming. Non-profit organisations, such as The Kimberley Toadbusters, support the physical control of the cane toads through various campaign programmes and creating awareness among the local people.[89]

1.2.6.2 Biological

The biological control approach favours the use of recombinant viruses, bacteria or parasites that are lethal and self-replicating, to colonize the toad population.

Viral delivery method

It was postulated that recombinant strains of *Bohle iridovirus* containing foreign DNA encoding globin could be used to challenge tadpole with adult cane toad globin, leading to increased mortality rates (80%-100%) in the test population of cane toad metamorphs.[90] This strategy proved to be scientifically and technically non-feasible, and arguably politically naïve, as it required the non-reliable, uncontrolled release of a genetically modified virus – with unknown ecological consequences. The approach was not surprisingly abandoned but not until it had diverted valuable resources away from the more ecologically responsible and scientifically feasible solutions.

Daughterless toad strategy

Daughterless toad technology involves a sex skewing strategy where the number of female toads is decreased drastically leading to accumulation of a male dominated population. Introducing the male sex-determining genes to the cane toad population would generate a genetically modified cane toad, which would be introduced into the environment.[10] By incorporating these genes, the development of ovaries in the female cane toads would be blocked, leading to development of testes thereby generating male progeny.[10] The resulting male tadpoles remain as males while the females will reverse sex and develop as males. The offspring of the daughterless toads would spread the incorporated gene to the following generation. In this way the female population is vastly reduced and on the other hand the male population is greatly increased and surpasses the former. As a result, the male toads will run out of their breeding partners and the cane toad population can be greatly controlled. Although the sex determining genes in cane toads have been reported[91] this method was shown not to be applicable based on model studies which required a large number of genetically modified toads to be released into the environment.[10]

Sterile male strategy

The strategy involves the production of fertile males whose off springs are sterile males. Most of the animals are diploid (2n) in nature possessing two of each chromosome per nuclei. In this strategy, genetically modified male cane toads would be generated which are polyploid (4n), by duplication of their entire genome.[92] These male cane toads survives as the level of duplication is even (balanced meiosis) and when interacts with diploid female cane toads, generates triploid progeny (3n) which are sterile in nature due to uneven number of chromosomes (disrupted meiosis). Thus, the F1 progeny are sterile male cane toad tadpoles. Moreover, the reproductive output of the

female cane toads is also greatly reduced.[10,92] Again, as imaginative as the strategy appeared, it lacked feasibility and was abandoned.

Discussion

The biological approach has largely been abandoned. Two major problems involved are the scientific and technical ability to deliver, as well as safety of any implement. On the matter of safety, the use of recombinant viruses in the environment is risky as the viruses may revert pathogenicity and more importantly the specificity of the recombinant viruses must be fully investigated to prevent the infection of other organisms. Likewise, introduction of genetically modified toads may result in the transmission of foreign DNA among the toad population leading to mutations, which might affect the ecological balance. Quite apart from the failure of science to deliver, even with a biological solution in hand it would be questionable if deployment would be authorized.

1.2.6.3 Chemical

Given the risks and limitations of the biological control method, a number of chemical approaches were considered. To develop a chemical approach requires careful analysis of the cane toad toxins in an ecological context, to identify possible solutions for the cane toad control. The chemical approach is exemplified by recent developments from our laboratory in the area of alarm[49] and attractant[93] pheromones and the microbial biotransformation of bufadienolides.[17]

Pheromones (Alarm)

Pheromones are chemical substances that are secreted by an individual and are recognized by another individual of the same species, triggering a behavioural response.[93] For example, cane toad tadpoles flee (Figure 1.16) when exposed to the water extract of crushed tadpole con-specifics suggesting the presence of alarm pheromones.[94] An ability to identify such alarm would be significant for an individual to confront pressure induced by its environment or predators.[94]

Figure 1.16 Cane toad tadpoles flee in response to crushed conspecifics (Taken from: Capon et al., 2009).[95]

Although cane toad tadpoles exhibit a stray flight response,[96-98] the chemical composition of the alarm pheromone remained unknown. In a recent study, our lab in collaboration with the Shine lab (U Syd) explored the observation that chronic exposure of cane toad tadpoles to the alarm pheromones (water extract of crushed conspecific) leads to premature metamorphs with low survival rates. More importantly, the pheromone had no effect on the native frog species.[98] This collaboration also explained and identified a tadpole attractant pheromone present in *B. marinus* eggs and used this to develop a bait/trap system.[49] Insights into cane toad chemical ecology are pivotal to exploring and applying effective chemical control solutions. For instance, distributing the synthetic alarm pheromone through waterways like lakes, dams, etc during the breeding season may interrupt the development of cane toad tadpoles and thereby lead to reduction in their population. More information about *B. marinus* pheromones is discussed in further chapters (Chapter 5). Currently the bait system has been translated to field trials (in ponds) with various bufolipin ananlogues and their ability to attract tadpoles is being performed (unpublished).

Biotransformation of bufadienolides

The biotransformation of certain bufadienolides by bacteria[99-101] and plant cells[102] has already been reported. For instance, resibufagenin (**4a**) when exposed to the cultures of *Mucor subtilissimus* was converted into 11 products,[99] while exposure to *Pseudomonas aeruginosa* produced a single product, 3-oxoresibufogenin (**16a**).[100] The biotransformation of bufadienolides suggests the possibility of broadening of chemical diversity of the bufadienolides existing in the parotoid gland. In a recent report, the microbial biotransformation of marinobufagenin (a bufadienolide isolated from the cane toad parotoid secretion) was reported.[17] Bacterial strains from the parotoid gland, ovary, tongue and stomach of a mature female cane toad were recovered and grown in liquid cultures in the presence of marinobufagenin (**1a**).

3-oxoresibufogenin (**16a**)
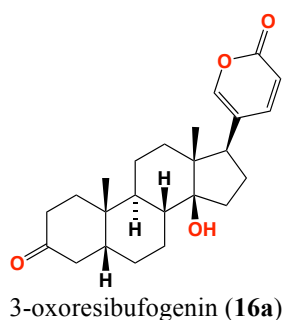
Comomonas testosteroni is a gram-negative bacterium that utilizes C_{19} - C_{27} steroids as its carbon source for growth.[103-105] Exposure of marinobufagenin (**1a**) to liquid cultures of *C. testosteroni* for 96 h was performed and the products were isolated by solvent extraction from the broth and were subjected to HPLC-DAD-MS analysis. This observation supports the hypothesis that bacteria present in the parotoid gland may manipulate bufadienolide diversity, either to make the toxin more

effective against range of predators by diversifying the chemistry or by detoxifying *B. marinus* parotoid secretions by biotransforming the cardiac steroids into less toxic analogues. Further information on biotransformation of cane toad toxins is discussed in detail in successive chapter (Chapter 4).

1.3 PhD research project

1.3.1 Aims

To better understand cane toad bufadienolides, including chemical diversity, stability and biology, as well as biosynthesis, distribution and ecology.

1.3.2 Objectives

To achieve the proposed aims several objectives were undertaken:

- ➢ Develop analytical methodology capable of detecting all class of bufadienolides in quantifiable amounts (Chapter 2)
- ➢ Carry out bufadienolide quantification in various cane toad tissues such as adult parotoid glands and eggs (Chapter 3&5)
- ➢ Analysis of storage of toxins within the parotoid gland *in situ* (Chapter 3)
- ➢ Stability of parotoid secretions against microbial biotransformation (Chapter 4)
- ➢ Pharmacological properties of cane toad bufadienolides (Chapter 6)

1.4 References

1. Hamilton, N. H. R.; Halliday, D. C. T.; Tarmo, S.; Bary, J.; Venables, D.; Robinson, A., Captive care and breeding of marine toads, *Bufo marinus*. *Journal of Herpetological Medicine and Surgery* **2005,** *15*, 21-27.
2. Glasby, C.; Ross, G.; Beesley, P.; Study, A. B. R., *Fauna of Australia: Amphibia & Reptilia*. Australian Government Publishing Service 1993.
3. Lever, C., *The cane toad: the history and ecology of a successful colonist*. Westbury Academic and Scientific Publishing2001.
4. Hearnden, M. N. Reproductive and larval ecology of *Bufo marinus* (Anura: bufonidae). James Cook University of North Queensland **1991**.
5. Tyler, M., *Australian frogs*. Viking O'Neil **1989**.
6. Toledo, R. C.; Jared, C., Cutaneous granular glands and amphibian venoms. *Comparative Biochemistry and Physiology a-Physiology* **1995,** *111*, 1-29.
7. Tempone, A. G.; Pimenta, D. C.; Lebrun, I.; Sartorelli, P.; Taniwaki, N. N.; de Andrade, H. F.; Antoniazzi, M. M.; Jared, C., Antileishmanial and antitrypanosomal activity of bufadienolides isolated from the toad *Rhinella jimi* parotoid macrogland secretion. *Toxicon* **2008,** *52*, 13-21.
8. Hostetle.Jr; Cannon, M. S., Anatomy of parotoid gland in bufonidae with some histochemical findings .1. *Bufo marinus*. *J. Morphol.* **1974,** *142*, 225-239.
9. Jared, C.; Antoniazzi, M. M.; Jordao, A. E. C.; Silva, J.; Greven, H.; Rodrigues, M. T., Parotoid macroglands in toad (*Rhinella jimi*): Their structure and functioning in passive defence. *Toxicon* **2009,** *54*, 197-207.
10. Shanmuganathan, T.; Pallister, J.; Doody, S.; McCallum, H.; Robinson, T.; Sheppard, A.; Hardy, C.; Halliday, D.; Venables, D.; Voysey, R.; Strive, T.; Hinds, L.; Hyatt, A., Biological control of the cane toad in Australia: a review. *Anim. Conserv.* **2010,** *13*, 16-23.
11. Letnic, M.; Webb, J. K.; Shine, R., Invasive cane toads (*Bufo marinus*) cause mass mortality of freshwater crocodiles (*Crocodylus johnstoni*) in tropical Australia. *Biol. Conserv.* **2008,** *141*, 1773-1782.
12. Griffiths, A. D.; McKay, J. L., Cane toads reduce the abundance and site occupancy of Merten's water monitor (*Varanus mertensi*). *Wildl. Res.* **2007,** *34*, 609-615.
13. Phillips, B. L.; Shine, R., An invasive species induces rapid adaptive change in a native predator: cane toads and black snakes in Australia. *Proc. R. Soc. B-Biol. Sci.* **2006,** *273*, 1545-1550.
14. Cardoso, M. J.; Eldridge, M. D. B.; Oakwood, M.; Rankmore, B.; Sherwin, W. B.; Firestone, K. B., Effects of founder events on the genetic variation of translocated island populations: implications for conservation management of the northern quoll. *Conserv. Genet.* **2009,** *10*, 1719-1733.
15. Reeves, M. P., A retrospective report of 90 dogs with suspected cane toad (*Bufo marinus*) toxicity. *Aust. Vet. J.* **2004,** *82*, 608-611.
16. Lyttle, T., Misuse and legend in the toad licking phenomenon. *International Journal of the Addictions* **1993,** *28*, 521-538.
17. Hayes, R. A.; Piggott, A. M.; Dalle, K.; Capon, R. J., Microbial biotransformation as a source of chemical diversity in cane toad steroid toxins. *Bioorg. Med. Chem. Lett.* **2009,** *19*, 1790-1792.
18. Steyn, P. S.; van Heerden, F. R., Bufadienolides of plant and animal origin. *Nat. Prod. Rep.* **1998,** *15*, 397-413.
19. Clarke, B. T., The natural history of amphibian skin secretions, their normal functioning and potential medical applications. *Biol. Rev. Camb. Philos. Soc.* **1997,** *72*, 365-379.
20. Erspamer, V., *Bioactive secretions of the amphibian integument. In: H. Heatwole and G.T. Barthalmus (Eds.)*. Surrey Beatty & Sons: Sydney, 1994.
21. Hurst, J., *Chemical signals in vertebrates 11*. Springer 2008.

22. Shen, H. W.; Wu, C.; Jiang, X. L.; Yu, A. M., Effects of monoamine oxidase inhibitor and cytochrome P450 2D6 status on 5-methoxy-N,N-dimethyltryptamine metabolism and pharmacokinetics. *Biochem. Pharmacol.* **2010,** *80*, 122-128.

23. Dewick, P., *Medicinal natural products: a biosynthetic approach.* Wiley **1997**.

24. Flier, J.; Edwards, M. W.; Daly, J. W.; Myers, C. W., Widespread occurrence in frogs and toads of skin compounds interacting with the ouabain site of Na^+,K^+-ATPase. *Science* **1980,** *208*, 503-505.

25. Shimada, K.; Ohishi, K.; Fukunaga, H.; Ro, J. S.; Nambara, T., Studies on steroids .213. structure activity relationship of bufotoxins and related-compounds for the inhibition of Na^+, K^+-adenosine triphosphatase. *J. Pharmacobio-Dyn.* **1985,** *8*, 1054-1059.

26. Stoll, A.; Suter, E.; Kreis, W.; Bussemaker, B. B.; Hofmann, A., The cardioactive substances of psyllium. Scillaron A - Communication on cardiac glycosides. *Helv. Chim. Acta* **1933,** *16*, 703-733.

27. Kupchan, S. M.; Ognyanov, I., Isolation and structural elucidation of a novel naturally-occurring bufadienolide orthoacetate. *Tetrahedron Lett.* **1969**, 1709-&.

28. Dias, C.; Graca, J. A. B.; Goncalves, M. L., *Scilla maderensis*, TLC screening and positive inotropic effect of bulb extracts. *J. Ethnopharmacol.* **2000,** *71*, 487-492.

29. Kupchan, S. M.; Hemingwa.Rj; Hemingwa.Jc, Tumor inhibitors .44. isolation and characterization of hellebrigenin 3-acetate and hellebrigenin 3,5-diacetate, bufadienolide tumor inhibitors from *Bersama abyssinica*. *J. Org. Chem.* **1969,** *34*, 3894-.

30. Puglisi, S.; Speciale, A.; Acquaviva, R.; Ferlito, G.; Ragusa, S.; De Pasquale, R.; Iauk, L., Antibacterial activity of *Helleborus bocconei* Ten. subsp siculus root extracts. *J. Ethnopharmacol.* **2009,** *125*, 175-177.

31. Matsukawa, M.; Mukai, T.; Akizawa, T.; Miyatake, S.; Yoshioka, M.; Morris, J. F.; Butler, V. P., Isolation and characterization of novel endogenous digitalis-like factors in the ovary of the giant toad, *Bufo marinus*. *J. Nat. Prod.* **1998,** *61*, 1476-1481.

32. Hutchinson, D. A.; Mori, A.; Savitzky, A. H.; Burghardt, G. M.; Wu, X. G.; Meinwald, J.; Schroeder, F. C., Dietary sequestration of defensive steroids in nuchal glands of the Asian snake *Rhabdophis tigrinus*. *Proc. Natl. Acad. Sci. U. S. A.* **2007,** *104*, 2265-2270.

33. Meinwald, J.; Wiemer, D. F.; Eisner, T., Defense-mechanisms of arthropods .61. lucibufagins .2. esters of 12-oxo-2-beta,5-beta,11-alpha-trihydroxybufalin, the major defensive steroids of the firefly *Photinus pyralis* (Coleoptera, Lampyridae). *J. Am. Chem. Soc.* **1979,** *101*, 3055-3060.

34. Lichtstein, D.; Gati, I.; Samuelov, S.; Berson, D.; Rozenman, Y.; Landau, L.; Deutsch, J., Identification of digitalis-like compounds in human cataractous lenses. *Eur. J. Biochem.* **1993,** *216*, 261-268.

35. Bagrov, A. Y.; Shapiro, J. I.; Fedorova, O. V., Endogenous Cardiotonic Steroids: Physiology, Pharmacology, and Novel Therapeutic Targets. *Pharmacol. Rev.* **2009,** *61*, 9-38.

36. Dmitrieva, R. I.; Bagrov, A. Y.; Lalli, E.; Sassone-Corsi, P.; Stocco, D. M.; Doris, P. A., Mammalian bufadienolide is synthesized from cholesterol in the adrenal cortex by a pathway that is independent of cholesterol side-chain cleavage. *Hypertension* **2000,** *36*, 442-448.

37. Yoshika, M.; Komiyama, Y.; Konishi, M.; Akizawa, T.; Kobayashi, T.; Date, M.; Kobatake, S.; Masuda, M.; Masaki, H.; Takahashi, H., Novel digitalis-like factor, marinobufotoxin, isolated from cultured Y-1 cells, and its hypertensive effect in rats. *Hypertension* **2007,** *49*, 209-214.

38. Jensen, H.; Chen, K. K., Chemical studies on toad poisons. III. The secretion of the tropical toad, *Bufo marinus*. *J. Biol. Chem.* **1930,** *87*, 755-759.

39. Shimada, K.; Fujii, Y.; Yamashita, E.; Niizaki, Y.; Sato, Y.; Nambara, T., Studies on steroids .119. studies on cardiotonic steroids from skin of japanese toad. *Chem. Pharm. Bull.* **1977,** *25*, 714-730.

40. Filho, G. A. C.; Schwartz, C. A.; Resck, I. S.; Murta, M. M.; Lemos, S. S.; Castro, M. S.; Kyaw, C.; Pires, O. R.; Leite, J. R. S.; Bloch, C.; Schwartz, E. F., Antimicrobial activity of the bufadienolides marinobufagin and telocinobufagin isolated as major components from skin secretion of the toad *Bufo rubescens*. *Toxicon* **2005,** *45*, 777-782.

41. Cunha, G. A.; Resck, I. S.; Cavalcanti, B. C.; Pessoa, C. O.; Moraes, M. O.; Ferreira, J. R. O.; Rodrigues, F. A. R.; dos Santos, M. L., Cytotoxic profile of natural and some modified bufadienolides from toad *Rhinella schneideri* parotoid gland secretion. *Toxicon* **2010,** *56*, 339-348.

42. Yu, C. H.; Kan, S. F.; Pu, H. F.; Jea Chien, E.; Wang, P. S., Apoptotic signaling in bufalin- and cinobufagin-treated androgen-dependent and -independent human prostate cancer cells. *Cancer Sci.* **2008,** *99*, 2467-2476.

43. Li, M. M.; Wu, S.; Liu, Z.; Zhang, W.; Xu, J.; Wang, Y.; Liu, J. S.; Zhang, D. M.; Tian, H. Y.; Li, Y. L.; Ye, W. C., Arenobufagin, a bufadienolide compound from toad venom, inhibits VEGF-mediated angiogenesis through suppression of VEGFR-2 signaling pathway. *Biochem. Pharmacol.* **2012,** *83*, 1251-1260.

44. Liu, J. S.; Zhang, D. M.; Li, Y.; Chen, W. M.; Ruan, Z. X.; Deng, L. J.; Wang, L. W.; Tian, H. Y.; Yiu, A.; Fan, C. L.; Luo, H.; Liu, S. W.; Wang, Y.; Xiao, G. K.; Chen, L. X.; Ye, W. C., Discovery of Bufadienolides as a Novel Class of ClC-3 Chloride Channel Activators with Antitumor Activities. *J. Med. Chem.* **2013,** *56*, 5734-5743.

45. Shimada, K.; Ohishi, K.; Nambara, T., Isolation of bufotalin 3-suberoyl-histidine and 3-suberoyl-3-methylhistidine esters from the skin of *Bufo melanostictus* schneider. *Tetrahedron Lett.* **1984,** *25*, 551-552.

46. Shimada, K.; Nambara, T., Isolation of Marinobufagin 3-Suberoyl-L-Glutamine Ester from the Skin of Bufo-Americanus. *Tetrahedron Lett.* **1979**, 163-164.

47. Akimova, O. A.; Bagrov, A. Y.; Lopina, O. D.; Kamernitsky, A. V.; Tremblay, J.; Hamet, P.; Orlov, S. N., Cardiotonic steroids differentially affect intracellular Na^+ and $Na^+_{(i)}$/ $K^+_{(i)}$-independent signaling in C7-MDCK cells. *J. Biol. Chem.* **2005,** *280*, 832-839.

48. Puschett, J. B.; Agunanne, E.; Uddin, M. N., Emerging Role of the Bufadienolides in Cardiovascular and Kidney Diseases. *American Journal of Kidney Diseases* **2010,** *56*, 359-370.

49. Crossland, M. R.; Haramura, T.; Salim, A. A.; Capon, R. J.; Shine, R., Exploiting intraspecific competitive mechanisms to control invasive cane toads (*Rhinella marina*). *Proc. R. Soc. B-Biol. Sci.* **2012,** *279*, 3436-3442.

50. Shimada, K.; Fujii, Y.; Nambara, T., Isolation of bufalin-3-sulfate from skin of *Bufo vulgaris formosus* boulenger. *Tetrahedron Lett.* **1974**, 2767-2768.

51. Butler, V. P.; Morris, J. F.; Akizawa, T.; Matsukawa, M.; Keating, P.; Hardart, A.; Furman, I., Heterogeneity and lability of endogenous digitalis-like substances in the plasma of the toad, *Bufo marinus*. *Am. J. Physiol. Regul. Integr. comp. Physiol.* **1996,** *271*, R325-R332.

52. Shimada, K.; Nambara, T., Studies on steroids .148. Isolation and characterization of cardiotonic steroid conjugates from the skin of *Bufo marinus* (L) schneider. *Chem. Pharm. Bull.* **1979,** *27*, 1881-1886.

53. Lee, S. S.; Derguini, F.; Bruening, R. C.; Nakanishi, K.; Wallick, E. T.; Akizawa, T.; Rosenbaum, C. S.; Butler, V. P., Digitalis-Like Compounds of Toad Bile - Sulfation and Reduction of Bufadienolides Decrease Potency of Na^+,K^+-Atpase Inhibition. *Heterocycles* **1994,** *39*, 669-686.

54. Gao, H.; Zehl, M.; Kaehlig, H.; Schneider, P.; Stuppner, H.; Moreno Y. Banuls, L.; Kiss, R.; Kopp, B., Rapid Structural Identification of Cytotoxic Bufadienolide Sulfates in Toad Venom from *Bufo melanosticus* by LC-DAD-MS and LC-SPE-NMR. *J. Nat. Prod.* **2010,** *73*, 603-608.

55. Yi, L.; Dratter, J.; Wang, C.; Tunge, J. A.; Desaire, H., Identification of sulfation sites of metabolites and prediction of the compounds' biological effects. *Anal. Bioanal. Chem.* **2006,** *386*, 666-674.

56. Krenn, L.; Kopp, B., Bufadienolides from animal and plant sources. *Phytochemistry* **1998,** *48*, 1-29.

57. Shimada, K.; Ishii, N.; Ohishi, K.; Ro, J. S.; Nambara, T., Studies on steroids .223. structure-activity relationship of cardiac steroids having a doubly linked sugar and related-compounds for the inhibition of Na^+,K^+-adenosine triphosphatase. *J. Pharmacobio-Dyn.* **1986,** *9*, 755-759.

58. Gao, H.; Zehl, M.; Leitner, A.; Wu, X.; Wang, Z.; Kopp, B., Comparison of toad venoms from different Bufo species by HPLC and LC-DAD-MS/MS. *J. Ethnopharmacol.* **2010,** *131*, 368-76.

59. Jing, J.; Ren, W. C.; Li, C.; Bose, U.; Parekh, H. S.; Wei, M. Q., Rapid identification of primary constituents in parotoid gland secretions of the Australian cane toad using HPLC/MS-Q-TOF. *Biomed. Chromatogr.* **2013,** *27*, 685-687.

60. Hayes, R. A.; Crossland, M. R.; Hagman, M.; Capon, R. J.; Shine, R., Ontogenetic Variation in the Chemical Defenses of Cane Toads (*Bufo marinus*): Toxin Profiles and Effects on Predators. *J. Chem. Ecol.* **2009,** *35*, 391-399.

61. Chen, C.; Osuch, M. V., Biosynthesis of bufadienolides-3beta-hydroxycholanates as precursors in *Bufo marinus* bufadienolides synthesis. *Biochem. Pharmacol.* **1969,** *18*, 1797-.

62. Matsukawa, M.; Akizawa, T.; Morris, J. F.; Butler, V. P.; Yoshioka, M., Marinoic acid, a novel bufadienolide-related substance in the skin of the giant toad, *Bufo marinus*. *Chem. Pharm. Bull.* **1996,** *44*, 255-257.

63. Shimada, K.; Miyashiro, Y.; Nishio, T., Characterization of in vitro metabolites of toad venom using high-performance liquid chromatography and liquid chromatography-mass spectrometry. *Biomed. Chromatogr.* **2006,** *20*, 1321-1327.

64. Matsukawa, M.; Akizawa, T.; Ohigashi, M.; Morris, J. F.; Butler, V. P.; Yoshioka, M., A novel bufadienolide, marinosin, in the skin of the giant toad, *Bufo marinus*. *Chem. Pharm. Bull.* **1997,** *45*, 249-254.

65. Lichtstein, D.; Kachalsky, S.; Deutsch, J., Identification of a ouabain-like compound in toad skin and plasma as a bufodienolide derivative. *Life Sci.* **1986,** *38*, 1261-1270.

66. Schanzer, W., Metabolism of anabolic androgenic steroids. *Clin. Chem.* **1996,** *42*, 1001-1020.

67. Kirkpatrick, R. B.; Green, M. D.; Hagey, L. R.; Hofmann, A. F.; Tephly, T. R., Effect of side-chain length on bile-acid conjugation - glucuronidation, sulfation and coenzyme-a formation of nor-bile acids and their natural c-24 homologs by human and rat-liver fractions. *Hepatology* **1988,** *8*, 353-357.

68. Akizawa, T.; Mukai, T.; Matsukawa, M.; Yoshioka, M.; Morris, J. F.; Butler, V. P., Structures of novel bufadienolides in the eggs of a toad, *Bufo marinus*. *Chem. Pharm. Bull.* **1994,** *42*, 754-756.

69. Cui, X. Y.; Inagaki, Y.; Xu, H. L.; Wang, D. L.; Qi, F. H.; Kokudo, N.; Fang, D. Z.; Tang, W., Anti-hepatitis B Virus Activities of Cinobufacini and Its Active Components Bufalin and Cinobufagin in HepG2.2.15 Cells. *Biol. Pharm. Bull.* **2010,** *33*, 1728-1732.

70. Rose, A. M.; Valdes, R., Understanding the sodium-pump and its relevance to disease. *Clin. Chem.* **1994,** *40*, 1674-1685.

71. Crambert, G.; Hasler, U.; Beggah, A. T.; Yu, C. L.; Modyanov, N. N.; Horisberger, J. D.; Lelievre, L.; Geering, K., Transport and pharmacological properties of nine different human Na,K-ATPase isozymes. *J. Biol. Chem.* **2000,** *275*, 1976-1986.

72. Shull, G. E.; Lane, L. K.; Lingrel, J. B., Amino-acid-sequence of the beta-subunit of the (Na^+/ K^+) ATPase deduced from a cDNA. *Nature* **1986,** *321*, 429-431.

73. Collins, J. H.; Forbush, B.; Lane, L. K.; Ling, E.; Schwartz, A.; Zot, A., Purification and characterization of an (Na^+/ K^+)-ATPase proteolipid labeled with a photoaffinity derivative of ouabain. *Biochim. Biophys. Acta* **1982,** *686*, 7-12.

74. Cortes, V. F.; Veiga-Lopes, F. E.; Barrabin, H.; Alves-Ferreira, M.; Fontes, C. F. L., The gamma subunit of Na^+, K^+-ATPase: Role on ATPase activity and regulatory phosphorylation by PKA. *Int. J. Biochem. Cell Biol.* **2006,** *38*, 1901-1913.

75. Morth, J. P.; Pedersen, B. P.; Toustrup-Jensen, M. S.; Sorensen, T. L. M.; Petersen, J.; Andersen, J. P.; Vilsen, B.; Nissen, P., Crystal structure of the sodium-potassium pump. *Nature* **2007,** *450*, 1043-U6.

76. Flier, J. S.; Maratosflier, E.; Pallotta, J. A.; McIsaac, D., Endogenous digitalis-like activity in the plasma of the toad *Bufo marinus*. *Nature* **1979,** *279*, 341-343.

77. Wang, J. N.; Velotta, J. B.; McDonough, A. A.; Farley, R. A., All human Na$^+$-K$^+$-ATPase alpha-subunit isoforms have a similar affinity for cardiac glycosides. *Am. J. Physiol. Cell. Physiol.* **2001,** *281*, C1336-C1343.

78. Fedorova, O. V.; Bagrov, A. Y., Inhibition of Na/K ATPase from rat aorta by two Na/K pump inhibitors, ouabain and marinobufagenin - Evidence of interaction with different alpha-subunit isoforms. *Am. J. Hypertens.* **1997,** *10*, 929-935.

79. Kometiani, P.; Li, J.; Gnudi, L.; Kahn, B. B.; Askari, A.; Xie, Z. J., Multiple signal transduction pathways link Na$^+$/K$^+$-ATPase to growth-related genes in cardiac myocytes - The roles of Ras and mitogen-activated protein kinases. *J. Biol. Chem.* **1998,** *273*, 15249-15256.

80. Weiner, I. D.; Wingo, C. S., Hyperkalemia: A potential silent killer. *J. Am. Soc. Nephrol.* **1998,** *9*, 1535-1543.

81. Shimada, K.; Sato, Y.; Nambara, T., Studies on steroids .230. Occurrence of marinobufotoxin and telocinobufotoxin homologs in the skin of *Bufo bankorensis* borbour. *Chem. Pharm. Bull.* **1987,** *35*, 2300-2304.

82. Touza, N. A.; Pocas, E. S. C.; Quintas, L. E. M.; Cunha, G.; Santos, M. L.; Noel, F., Inhibitory effect of combinations of digoxin and endogenous cardiotonic steroids on Na$^+$/K$^+$-ATPase activity in human kidney membrane preparation. *Life Sci.* **2011,** *88*, 39-42.

83. Shimada, K.; Ohishi, K.; Nambara, T., A high-performance liquid-chromatographic method for the assay of Na$^+$, K$^+$-adenosine triphosphatase inhibition. *J. Pharmacobio-Dyn.* **1985,** *8*, 64-68.

84. Kamano, Y.; Kotake, A.; Hashima, H.; Inoue, M.; Morita, H.; Takeya, K.; Itokawa, H.; Nandachi, N.; Segawa, T.; Yukita, A.; Saitou, K.; Katsuyama, M.; Pettit, G. R., Structure-cytotoxic activity relationship for the toad poison bufadienolides. *Bioorg. Med. Chem.* **1998,** *6*, 1103-1115.

85. Hilton, P. J.; McKinnon, W.; Gravett, E. C.; Peron, J. M. R.; Frampton, C. M.; Nicholls, M. G.; Lord, G., Selective inhibition of the cellular sodium pump by emicymarin and 14 beta anhydroxy bufadienolides. *Steroids* **2010,** *75*, 1137-1145.

86. Pettit, G. R.; Kamano, Y., Bufadienolides .28. Marinobufotoxin. *J. Org. Chem.* **1974,** *39*, 3003-3006.

87. Greenlees, M. J.; Brown, G. P.; Webb, J. K.; Phillips, B. L.; Shine, R., Effects of an invasive anuran the cane toad (*Bufo marinus*) on the invertebrate fauna of a tropical Australian floodplain. *Anim. Conserv.* **2006,** *9*, 431-438.

88. Brown, G. P.; Phillips, B. L.; Webb, J. K.; Shine, R., Toad on the road: Use of roads as dispersal corridors by cane toads (*Bufo marinus*) at an invasion front in tropical Australia. *Biol. Conserv.* **2006,** *133*, 88-94.

89. Somaweera, R.; Somaweera, N.; Shine, R., Frogs under friendly fire: How accurately can the general public recognize invasive species? *Biol. Conserv.* **2010,** *143*, 1477-1484.

90. Pallister, J.; Voysey, R.; Olsen, V.; Hyatt, A., In *Science of cane toad invasion and control. Proceedings of the invasive animals CRC/CSIRO/QLD NRM & W cane toad workshop, Brisbane*; Molloy, K. L.; W.R., H., Eds.: Canberra: Invasive Animals Cooperative Reserach Centre, 2006; pp 89-93.

91. Abramyan, J.; Ezaz, T.; Graves, J. A. M.; Koopman, P., Z and W sex chromosomes in the cane toad (*Bufo marinus*). *Chromosome Res.* **2009,** *17*, 1015-1024.

92. Mahony, M.; Clulow, J.; Molloy, K.; Henderson, W. In *Control of cane toads by sterile male release and inherited sterility*, Science of cane toad invasion and control. Proceedings of the invasive animals CRC/CSIRO/QLD NRM&W cane toad workshop, Brisbane **2006**; pp 134-150.

93. Karlson, P.; Luscher, M., Proposed biological term pheromone - reply. *Nature* **1959,** *183*, 1835-1835.

94. Hagman, M.; Shine, R., Understanding the toad code: Behavioural responses of cane toad (*Chaunus marinus*) larvae and metamorphs to chemical cues. *Austral. Ecol.* **2008,** *33*, 37-44.

95. Capon, R. J., Myth busting - cane toads in Australia. *Chemistry in Australia* **2009**, pp 3 - 6.

96. Chivers, D. P.; Smith, R. J. F., Chemical alarm signalling in aquatic predator-prey systems: A review and prospectus. *Ecoscience* **1998,** *5*, 338-352.
97. Summey, M. R.; Mathis, A., Alarm responses to chemical stimuli from damaged conspecifics by larval anurans: Tests of three neotropical species. *Herpetologica* **1998,** *54*, 402-408.
98. Hagman, M.; Hayes, R. A.; Capon, R. J.; Shine, R., Alarm cues experienced by cane toad tadpoles affect post-metamorphic morphology and chemical defences. *Funct. Ecol.* **2009,** *23*, 126-132.
99. Zhan, J. X.; Guo, H. Z.; Ning, L. L.; Zhang, Y. X.; Guo, D., Efficient preparation of derivatives of resibufogenin using microbial catalytic technique. *Planta Med.* **2006,** *72*, 346-350.
100. Zhan, J. X.; Liu, W. H.; Guo, H. Z.; Zhang, Y. X.; Guo, D., Selective dehydrogenation of resibufogenin and cinobufagin at 3-OH by *Pseudomonas aeruginosa. Enzyme Microb. Technol.* **2003,** *33*, 29-32.
101. Zhan, J. X.; Zhang, Y. X.; Liu, W. H.; Guo, H. Z.; Guo, D., Directional modifications of resibufogenin by *Mucor subtilissimus* and *Pseudomonas aeruginosa. Biocatal. Biotransform.* **2003,** *21*, 141-143.
102. Ye, M.; Ning, L. L.; Zhan, J. X.; Guo, H. Z.; Guo, D., Biotransformation of cinobufagin by cell suspension cultures of *Catharanthus roseus* and *Platycodon grandiflorum. J. Mol. Catal. B-Enzym.* **2003,** *22*, 89-95.
103. Skowasch, D.; Mobus, E.; Maser, E., Identification of a novel *Comamonas testosteroni* gene encoding a steroid-inducible extradiol dioxygenase. *Biochem. Biophys. Res. Commun.* **2002,** *294*, 560-566.
104. Marcus, P. I.; Talalay, P., Induction and purification of alpha-hydroxysteroid and beta-hydroxysteroid dehydrogenases. *J. Biol. Chem.* **1956,** *218*, 661-674.
105. Talalay, P.; Dobson, M. M.; Tapley, D. F., Oxidative degradation of testosterone by adaptive enzymes. *Nature* **1952,** *170*, 620-621.

Chapter 2: Full characterization, identification and quantification of cane toad bufadienolides

2.1 Introduction

A principle objective of this aspect of my research project is to develop analytical methodology capable of identifying and quantifying bufadienolides from various tissues of cane toads. Although bufagenins have been reported as the dominant bufadienolides in cane toad parotoid secretions,[1,2] with bufotoxins sometimes acknowledged as minor constituents, these studies do not employ optimized analytical methodology.[3] This chapter describes the development of analytical methodology to identify and quantify bufagenins and bufotoxins. Discussion on the analysis of bufolipins will be presented in chapter 6, and since bufagenin sulfates and glycosides are rare in cane toads,[4] their analysis is not a priority for this project.

Bufadienolides can be analysed by HPLC-DAD, although traditional methods such as prep-TLC[5] had been described in the literature. While normal phase silica HPLC has been investigated,[6] reverse phase HPLC has proved to be more effective.[1,7] Detection of bufadienolides using a diode array detector (DAD) is greatly facilitated by a characteristic UV absorbance (300 nm) of the C-17 α-pyrone ring. Different bufadienolides exhibit different retention times on reverse phase HPLC columns, with bufagenins appearing as sharp peaks[8] while bufotoxins appearing as broad peaks due to the presence of the charged arginyl moiety.[4] To unambiguously differentiate and quantify various bufadienolide classes from a given tissue sample (such as skin or parotoid secretion), requires analytical methodology optimized to detect specific bufadienolide structure classes.

Specific objectives

- ➢ To generate a bufadienolide standards library inclusive of bufagenins and bufotoxins
- ➢ To develop highly sensitive analytical methods optimized to detect and quantify bufagenins and bufotoxins
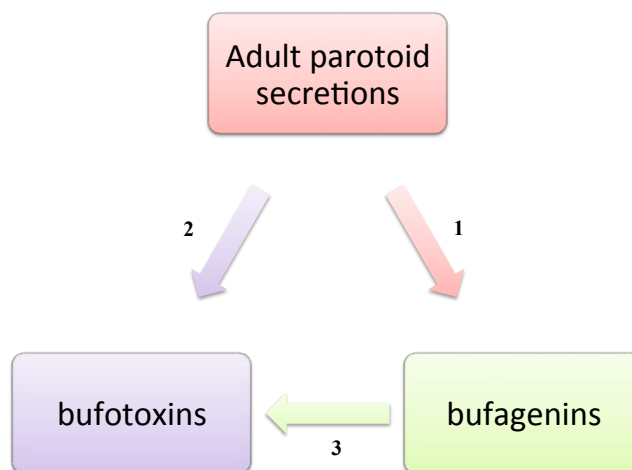
Figure 2.1 Scheme describing strategy for assembling a bufagenin/bufotoxin standard library. Dissection of parotoid glands from cane toads followed by solvent partitioning to obtain a mixture of either (1) bufagenins or (2) bufotoxins. (3) – conversion of bufagenins to bufotoxins

The approaches for the development of cane toad toxin library are based on factors such as the availability of resources, and the feasibility of the process (Figure 2.1). A reserve of > 500 frozen cane toads preserved at −20 °C provided a source of parotoid glands. Solvent partitioning and extraction followed by normal and reverse phase HPLC proved very successful at yielding bufagenins. Bufagenins obtained from adult parotoid secretions were then subjected to esterification with suberic and pimelic acid to obtain pure bufagenin esters, which were then coupled with L-arginine to yield bufotoxins. A highly sensitive analytical method was developed to analyse these bufagenin and bufotoxin standards and to analyse the bufadienolide composition of various cane toad tissues (Chapter 3).

2.2 Results and discussion

2.2.1 To generate a library of bufagenin standards

The first objective was to develop a library of standards for the detection and quantification of bufadienolides (and diacid arginyl amides) in cane toad tissues. The development of such a library includes the isolation, characterization and identification of a panel of bufagenins and bufotoxins. The parotoid glands from 120 frozen cane toads were dissected and extracted with ethyl acetate (EtOAc). After *in vacuo* concentration, the EtOAC solubles (a yellow oil) were triturated with *n*-hexane followed by *n*-BuOH (Figure 2.2). The residual parotoid gland tissues were triturated with water to solubilize all polar compounds. The organic layer contained all the bufadienolides while the water layer contained amines and amides. The EtOAc solubles were subjected to normal phase HPLC (See Experimental Section 1.2) to yield marinobufagenin (**1a**) (3 g), telocinobufagenin (**2a**)

(402 mg), bufalin (**3a**) (620 mg). The remaining crude extract retained by the column was eluted with 30% methanol/hexane, dried *in vacuo*, re-dissolved in methanol and was subjected to reverse phase HPLC purification to yield resibufagenin (**4a**) (7 mg), hellebrigenin (**5a**) (3.4 mg) and bufalin-3-acetate (**7a**) (2.8 mg). Marinobufagenin (**1a**) constituted 70% of the ethyl acetate fraction of the EtOAc solubles. Gao et al, previously reported the identification of bufagenins from the parotoid secretions of *B. marinus* and the present analysis is in agreement with that finding. The bufagenins isolated from the cane toad parotoid secretions were characterized using HPLC-DAD-MS, NMR and HRMS and identified to be **1a**, **2a**, **3a**, **4a**, **5a** and **7a**, respectively (refer to Appendix), consistent with prior studies.[1, 9, 10]
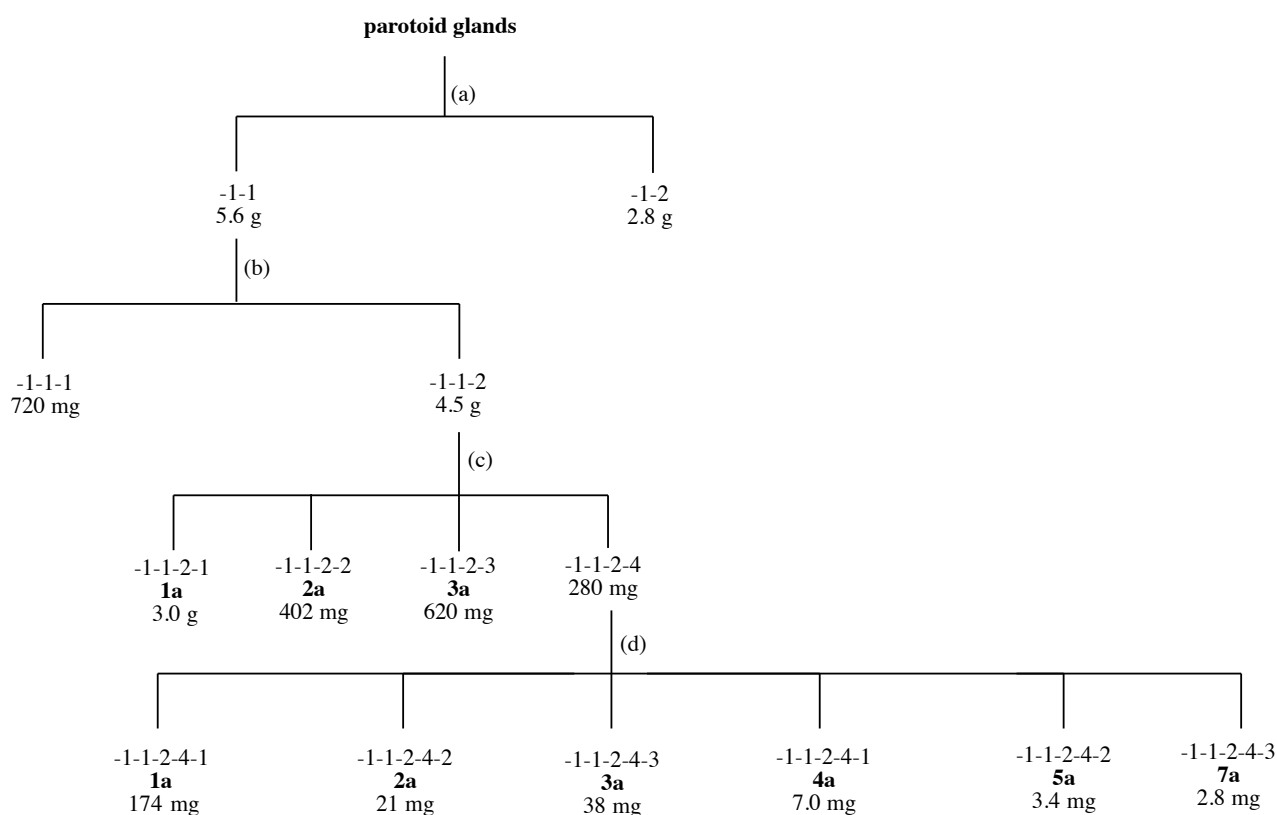
(a) Sequential solvent extraction [EtOAc (-1-1), H_2O (-1-2)]
(b) Sequential trituration [*n*-hexane (-1-1-1), *n*-butanol (-1-1-2)]
(c) Preparative NP-HPLC: 50 g SNAP cartridge (Flash chromatography silica column), eluting with 10.0 mL/min 60-100% EtOAc/*n*-hexane
(d) Semi-preparative RP-HPLC: Zorbax C_{18} column, 250 x 9.4 mm, 5 μm, 3.5 mL/min, eluting with 10-100% MeCN/H_2O over 15 min

Figure 2.2 Isolation scheme for bufagenins from cane toad parotoid gland secretions
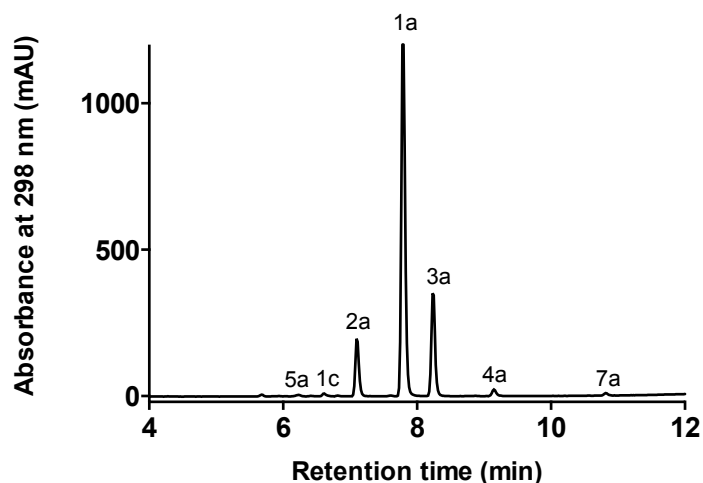
Figure 2.3 HPLC chromatogram (298 nm) of EtOAc solubles from cane toad parotoid secretion. Marinobufagenin (**1a**), telocinobufagenin (**2a**), bufalin (**3a**), resibufagenin (**4a**), hellebrigenin (**5a**) bufalin-3-acetate (**7a**) and marinobufotoxin (**1c**) analysed using Method 1

marinobufagenin (**1a**)   telocinobufagenin (**2a**)   bufalin (**3a**)

resibufagenin (**4a**)   hellebrigenin (**5a**)   bufalin acetate (**7a**)
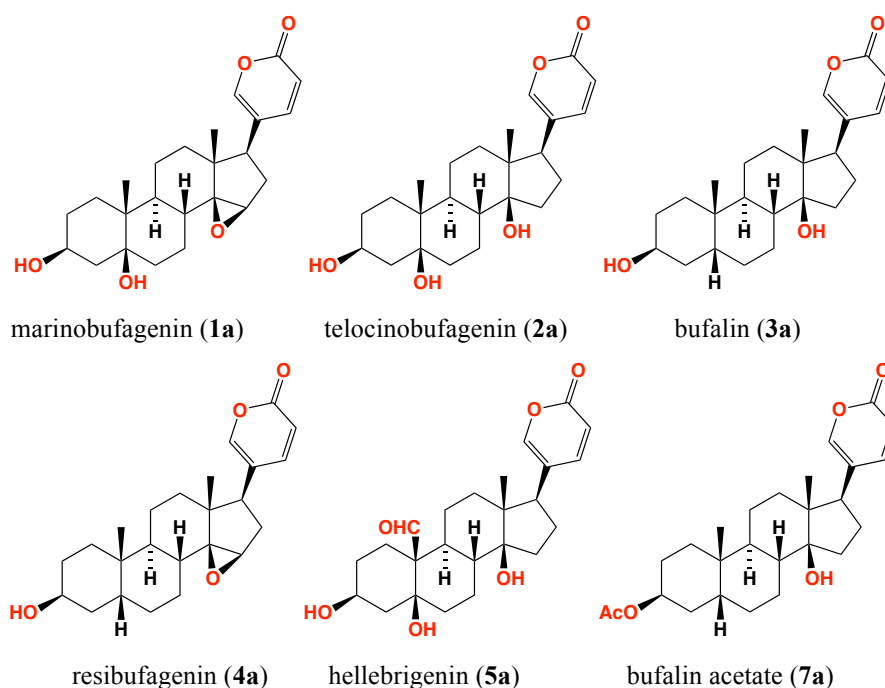
Figure 2.4 Bufagenins isolated from cane toad parotoid secretions

Characterization of **1a** from Australian cane toad parotoid secretions has been previously reported.[1] In our study **1a** was obtained as a pale white solid with HR(+)ESIMS analysis revealing a quasi-molecular ion (m/z 401.2323 [M+H]$^+$) consistent with the molecular formula $C_{24}H_{32}O_5$ (Δmmu 0.4).[1] The ^{1}H NMR and ^{13}C NMR (CD$_3$OD) data for **1a** was identical to the literature data (Appendix Figure S1, Table S1).[11] The UV-vis spectrum of **1a** exhibited the characteristic α-pyrone ring absorbance. All of the above confirmed that **1a** was marinobufagenin.

Characterization of **2a** from Australian cane toad parotoid secretions has been previously reported.[1] In our study **2a** was obtained as a pale white solid with HR(+)ESIMS analysis revealing a quasi-molecular ion (m/z 403.2479 [M+H]$^+$) consistent with the molecular formula $C_{24}H_{34}O_5$ (Δmmu 0.4).[1] The ^{1}H NMR and ^{13}C NMR (CD$_3$OD) data for **2a** was identical to the literature data (Appendix Figure S2, Table S1).[7] The UV-vis spectrum of **2a** exhibited the characteristic α-pyrone ring absorbance. All of the above confirmed that **2a** was telocinobufagenin.

Characterization of **3a** from Australian cane toad parotoid secretions has been previously reported.[1] In our study **3a** was obtained as a pale white solid with HR(+)ESIMS analysis revealing a quasi-molecular ion (m/z 387.2530 [M+H]$^+$) consistent with the molecular formula $C_{24}H_{34}O_4$ (Δmmu 0.1).[1] The ^{1}H NMR and ^{13}C NMR (CD$_3$OD) data for **3a** was identical to the literature data (Appendix Figure S3, Table S1).[12] The UV-vis spectrum of **3a** exhibited the characteristic α-pyrone ring absorbance. All of the above confirmed that **3a** was bufalin.

Characterization of **4a** from Australian cane toad parotoid secretions has been previously reported.[1] In our study **4a** was obtained as a pale white solid with HR(+)ESIMS analysis revealing a quasi-molecular ion (m/z 407.2190 [M+H]$^+$) consistent with the molecular formula $C_{24}H_{32}O_4$ (Δmmu -0.05).[1] The ^{1}H NMR and ^{13}C NMR (CD$_3$OD) data for **4a** was identical to the literature data (Appendix Figure S17, Table S1).[12] The UV-vis spectrum of **4a** exhibited the characteristic α-pyrone ring absorbance. All of the above confirmed that **4a** was resibufagenin.

Characterization of **5a** from Australian cane toad parotoid secretions has been previously reported.[1] In our study **5a** was obtained as a pale white solid with HR(+)ESIMS analysis revealing a quasi-molecular ion (m/z 417.2272 [M+H]$^+$) consistent with the molecular formula $C_{24}H_{32}O_6$ (Δmmu 0.2).[1] The ^{1}H NMR and ^{13}C NMR (CD$_3$OD) data for **5a** was identical to the literature data (Appendix figure S4, Table S5).[7] The UV-vis spectrum of **5a** exhibited the characteristic α-pyrone ring absorbance. All of the above confirmed that **5a** was hellebrigenin.

Characterization of **7a** from cane toad parotoid secretions has not been previously reported. In our study **7a** was obtained as a pale white solid with HR(+)ESIMS analysis revealing a quasi-molecular ion (m/z 428.2272 [M+H]$^+$) consistent with the molecular formula $C_{26}H_{36}O_5$ (Δmmu −0.7). The ^{1}H NMR and ^{13}C NMR spectrum (CD$_3$OD) of natural **7a** was identical to the synthetic compound (Appendix Figure S5, Table S6). The UV-vis spectrum of **7a** exhibited the characteristic α-pyrone ring absorbance. All of the above confirmed that **7a** was bufalin-3-acetate. Bufalin-3-acetate was

synthesized from bufalin using a partial synthesis strategy (Sec 2.2.2). Synthetic bufalin-3-acetate was co-injected along with crude parotoid secretions to confirm **7a** to be bufalin-3-acetate.

2.2.1.1 HSQC signatures analysis for bufagenins

Bufagenins, comprising of a typical steroidal A/B and C/D cis ring junctions exhibit a complicated and overlapping signals of methylenes which are difficult to identify using a standard ^{1}H or ^{1}H-^{1}H COSY spectra. In our analyses on bufadienolides, we investigated the common signatures exhibited by the structural functionality of the bufagenins (such as carboxylations) using HSQC. These signatures would then represent a fingerprint for the specific functionality of the bufagenins. This analyses would also be applied to bufotoxins (Page 44) and possibly extended to other bufagenin structure classes such as bufolipins. The HSQC fingerprinting analysis would be significant in identifying bufadienolides that are present in lower quantities (in <500 µg).

Bufagenins (such as **1a** – **7a** as shown above) exhibit varying levels of oxidation in a manner that is not immediately recognizable in standard ^{1}H and ^{13}C NMR spectra, this is particularly evident where functionalization occurs at quaternary carbons – for example hydroxylations at C-5 and C-14. In an effect to provide better empirical spectroscopic tools to assist in the identification of common bufagenin scaffolds, we examined the HSQC spectra of **1a** – **4a** across δ_H 0.6 – 3.7 and δ_C 14.0 – 67.0 to compare the upfield methylene envelop region to determine if the data could be used to fingerprint key structural features.

As anticipated, HSQC fingerprinting analysis of bufagenins exhibited four distinct clustering of contours based on the substitutions at C-5 and C-14. The HSQC spectrum of bufagenins (**1a** – **4a**) clearly indicated the presence of a α-pyrone ring (δ_H 6.26 – 8.0; δ_C 149.6 – 164.6) and two tertiary methyls (δ_H 0.78 – 0.98; δ_C 17.2 – 24.5). All four bufagenins, **1a** – **4a**, differ in levels of oxidation, for example, marinobufagenin (**1a**) and telocinobufagenin (**2a**) possess a 5-OH substitution whereas bufalin (**3a**) and resibufagenin (**4a**) do not, leading to diagnostic HSQC signatures. These signatures are highlighted in Figures 2.5 – 2.8 with different colours; brown for 5-OH and magenta for 5-H (Figures 2.5 – 2.8).

Another HSQC signature was attributed to the presence of C-14 epoxide vs hydroxylation. For example, whereas marinobufagenin (**1a**) and resibufagenin (**4a**) possessed a $\Delta^{14,15}$ epoxide, telocinobufagenin (**2a**) and bufalin (**3a**) possessed a C-14 hydroxyl, leading to diagnostic HSQC signatures. These signatures are highlighted in Figures 2.5 – 2.8.
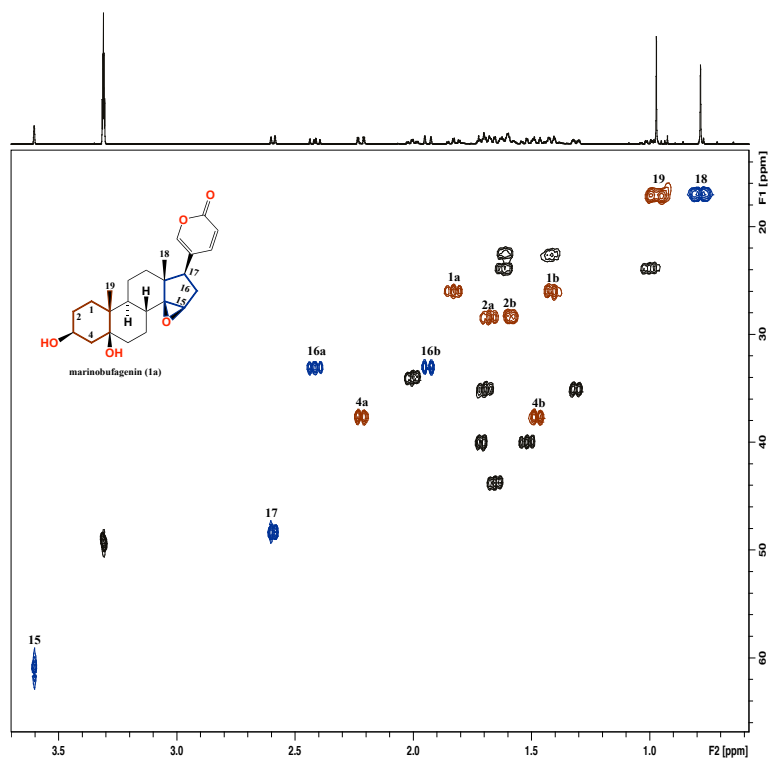
Figure 2.5 Expansion of HSQC (CD$_3$OD, 600 MHz) spectrum of marinobufagenin (**1a**) showing 5-OH (brown) and $\Delta^{14,15}$ epoxide (purple) signatures
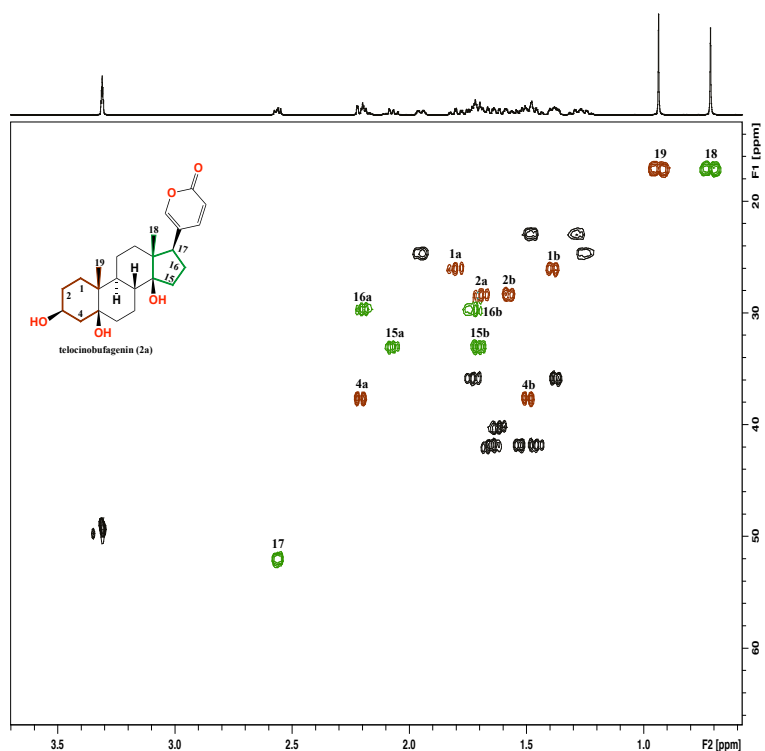
Figure 2.6 Expansion of HSQC (CD$_3$OD, 600 MHz) spectrum of telocinobufagenin (**2a**) showing 5-OH (brown) and 14-OH (green) signatures
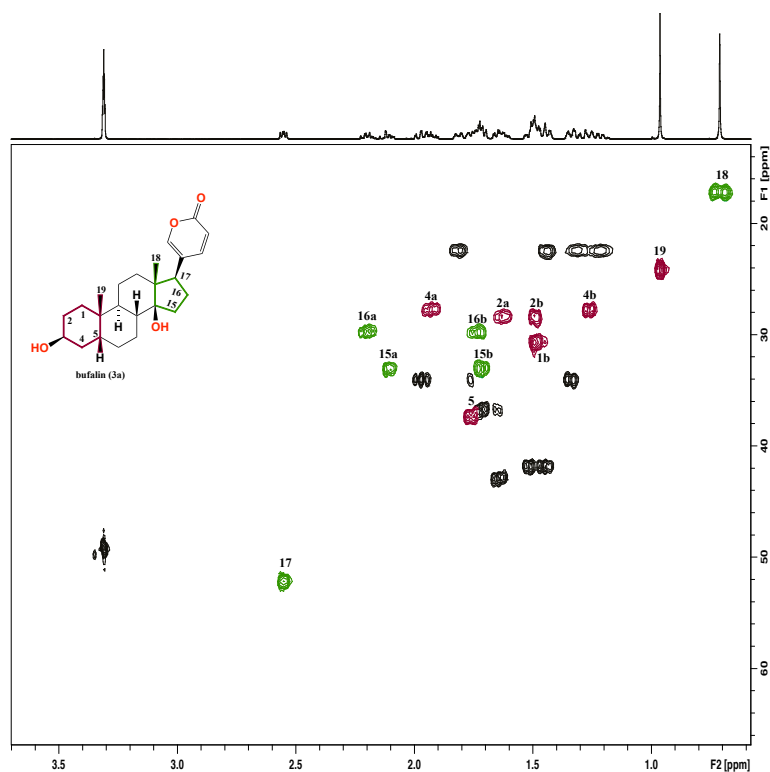
Figure 2.7 Expansion of HSQC (CD₃OD, 600 MHz) spectrum of bufalin (**3a**) showing 5-H (magenta) and 14-OH (green) signatures
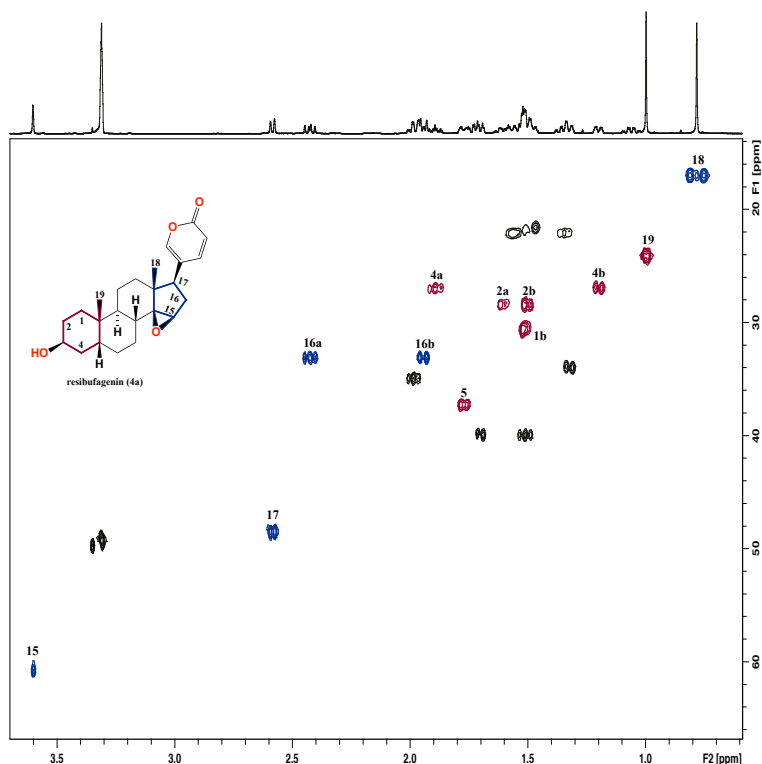
Figure 2.8 Expansion of HSQC (CD₃OD, 600 MHz) spectrum of resibufagenin (**4a)** showing 5-H (magenta) and $\Delta^{14,15}$ epoxide (purple) correlations

HSQC fingerprinting does appear to provide a valuable means to recognize quarternary oxidation levels about C-5 and C-14, and could be useful in identifying both known and new bufagenins. This

approach can also be extended to bufotoxins and bufolipins as discussed later in this thesis. Since hellebrigenin (**5a**) and bufalin-3-acetate (**7a**) exhibited differences about C-3 (acetate) and C-10 (keto) they were not included in this current HSQC fingerprinting analysis. However, with a larger set of analogues to compare it is likely that additional HSQC signatures could be identified.

2.2.2 To generate a library of bufotoxin standards

Bufotoxins have previously been reported from the extraction of thousands of cane toad skins[6,13] and as minor components from the parotoid secretions.[1] The (apparent) lack of a reliable natural source necessitated a semi-synthesis approach, where we converted bufagenins to pure bufotoxins. Bufotoxins were prepared from previously isolated bufagenins by a two-step synthetic strategy where a bufagenin ester of suberic acid (DMAP; 3 h at 60 °C in DCM) was coupled to L-arginine (iBuClCOO-, MeOH/TFA, $(C_2H_5)_3N$ for 4 h at – 10 °C) to form the bufotoxin[14] (Figure 2.7).
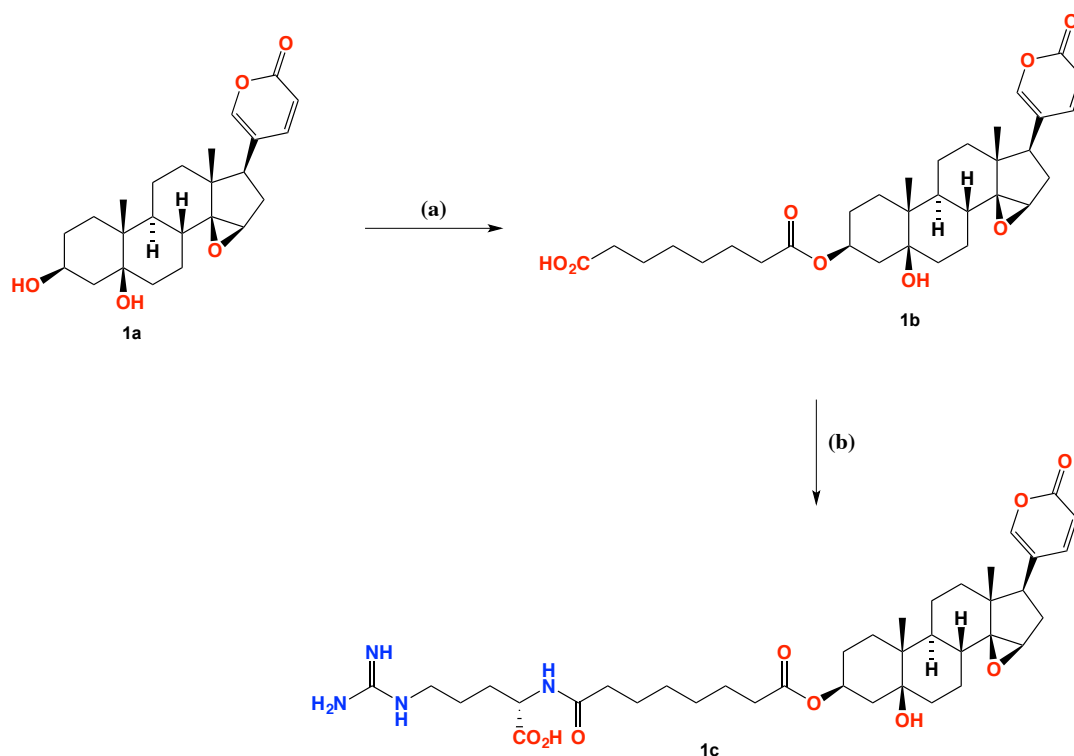
Figure 2.9 (a) marinobufagenin (**1a**) was treated with suberic anhydride and DMAP for 3 h at 60 °C in DCM (78%). (b) – The bufagenin suberate ester (**1b**) was treated with L-arginine monohydrochloride, triethylamine, isobutyl chloroformate and methanol in THF for 4 h at – 10 °C (77%).

The bufagenin esters, **1b**, **2b, 3b, 5b** and **6b**, were subjected to purification using a C_{18} SPE cartridge (20-100% MeCN) followed by semi-preparative HPLC (Zorbax SB C18 column, 250 × 9.4 mm, 5 µm, 3.5 mL/min, gradient from 90% H_2O/MeCN to 100% MeCN over 25 min, hold at 100% MeCN for 5 min, with isocratic 0.01% modifier (TFA)), after which they were subjected to full spectroscopic characterization.

In our study, **1b** was obtained as a pale white solid, with HR(+)ESIMS analysis revealing a quasi-molecular ion (m/z 557.3138 [M+H]$^+$) consistent with the molecular formula $C_{32}H_{44}O_8$ (Δmmu −2.8). The ^{1}H NMR spectra (CD$_3$OD) of **1b** showed the purity of the compound (Appendix Figure S6, Section 2.4.3.3). The UV-vis spectrum of **1b** exhibited the characteristic α-pyrone ring absorbance. All of the above confirmed that **1a** was marinobufagenin-3suberate.

In our study **2b** was obtained as a pale white solid with HR(+)ESIMS analysis revealing a quasi-molecular ion (m/z 581.3110 [M+H]$^+$) consistent with the molecular formula $C_{34}H_{44}O_8$ (Δmmu −0.1). The ^{1}H NMR spectra (CDCl$_3$) of **2b** showed the purity of the compound (Appendix Figure S7, Section 2.4.3.2). The UV-vis spectrum of **2b** exhibited the characteristic α-pyrone ring absorbance. All of the above confirmed that **2b** was telocinobufagenin-3-suberate.

In our study **3b** was obtained as a pale white solid with HR(+)ESIMS analysis revealing a quasi-molecular ion (m/z 543.3313 [M+H]$^+$) consistent with the molecular formula $C_{32}H_{46}O_7$ (Δmmu 0.6). The ^{1}H NMR spectra (CD$_3$OD) of **3b** showed the purity of the compound (Appendix Figure S8, Section 2.4.3.1). The UV-vis spectrum of **3b** exhibited the characteristic α-pyrone ring absorbance. All of the above confirmed that **3b** was bufalin-3-suberate.

In our study **5b** was obtained as a pale white solid with HR(+)ESIMS analysis revealing a quasi-molecular ion (m/z 543.3109 [M+H]$^+$) consistent with the molecular formula $C_{31}H_{42}O_8$ (Δmmu −0.8). The ^{1}H NMR spectra (CD$_3$OD) of **5b** showed the purity of the compound (Appendix figure S21, Section 2.4.3.3). The UV-vis spectrum of **5b** exhibited the characteristic α-pyrone ring absorbance. All of the above confirmed that **5b** was marinobufagenin-3-pimelate.

In our study **6b** was obtained as a pale white solid with HR(+)ESIMS analysis revealing a quasi-molecular ion (m/z 551.2992 [M+Na]$^+$) consistent with the molecular formula $C_{32}H_{44}O_8$ (Δmmu -1.3). The ^{1}H NMR spectra (CD$_3$OD) of **6b** showed the purity of the compound (Appendix Figure S25, Section 2.4.3.1). The UV-vis spectrum of **6b** exhibited the characteristic α-pyrone ring absorbance. All of the above confirmed that **6b** was bufalin-3-pimelate.

The bufagenin esters were then coupled to L-arginine to form bufotoxins. Synthetic bufotoxins, **1c**, **2c**, **3c**, **8c** and **9c**, were purified using semi-preparative HPLC (Zorbax SB C$_{18}$ column, 250 × 9.4 mm, 5 μm, 3.5 mL/min, gradient from 90% H$_2$O/MeCN to 100% MeCN over 25 min, hold at 100% MeCN for 5 min, with constant 0.01% modifier (TFA)) and dried *in vacuo* to yield an oily residue.

HPLC-DAD-MS analysis confirmed that marinobufotoxin (**1c**) was converted into its TFA adduct during handling, a transformation that could be avoided by eliminating TFA from the HPLC method. Purified bufotoxins were characterized using NMR spectroscopy (^{1}H, ^{13}C and HSQC) and HRMS (Appendix Figure S9, Table S7).

Characterization of **1c** from Australian cane toad parotoid secretions has been previously reported.[1] In our study, **1c** was obtained as a pale white solid with HR(+)ESIMS analysis revealing a quasi-molecular ion (m/z 713.4120 [M+H]$^+$) consistent with the molecular formula $C_{38}H_{56}N_4O_9$ (Δmmu −0.3).[1] The ^{1}H NMR and ^{13}C NMR spectrum (CD$_3$OD) for **1c** was identical to the literature data (Appendix Figure S9, Table S7).[11] The UV-vis spectrum of **1c** exhibited the characteristic α-pyrone ring absorbance. All of the above confirmed that **1c** was marinobufotoxin. Moreover, as **1c** was synthesized from marinobufagenin-3-suberate (**1b**), which was in turn prepared from authentic natural marinobufagenin (**1a**), we can be confident that the structure is as proposed.

Characterization of **2c** from Australian cane toad parotoid secretions has been previously reported (Figure 2.14).[1] In our study **2c** was obtained as a pale white solid with HR(+)ESIMS analysis revealing a quasi-molecular ion (m/z 715.4277 [M+H]$^+$) consistent with the molecular formula $C_{38}H_{58}N_4O_9$ (Δmmu 0.3).[1] The ^{1}H NMR and ^{13}C NMR spectrum (CD$_3$OD) of **2c** was identical to the literature data (Appendix Figure S10, Table S8).[6] The UV-vis spectrum of **2c** exhibited the characteristic α-pyrone ring absorbance. All of the above confirmed that **2c** was telocinobufotoxin. Moreover, as **2c** was synthesized from telocinobufagenin-3-suberate (**2b**), which was in turn prepared from authentic natural telocinobufagenin (**2a**), we can be confident that the structure is as proposed.

Characterization of **3c** from Australian cane toad parotoid secretions has been previously reported (Figure 2.14).[1] In our study **3c** was obtained as a pale white solid with HR(+)ESIMS analysis revealing a quasi-molecular ion (m/z 699.4327 [M+H]$^+$) consistent with the molecular formula $C_{37}H_{58}N_4O_8$ (Δmmu −0.3).[1] The ^{1}H NMR and ^{13}C NMR spectrum (CD$_3$OD) of **3c** was identical to the literature data (Appendix figure S11, Table S9).[15] The UV-vis spectrum of **3c** exhibited the characteristic α-pyrone ring absorbance. All of the above confirmed that **3c** was bufalitoxin. Moreover, as **3c** was synthesized from bufalin-3-suberate (**3b**), which was in turn prepared from authentic natural bufalin (**3a**), we can be confident that the structure is as proposed.

Characterization of **8c** from Australian cane toad parotoid secretions has been previously reported (Figure 2.14).[1] In our study **8c** was obtained as a pale white solid with HR(+)ESIMS analysis

revealing a quasi-molecular ion (m/z 699.3971 $[M+H]^+$) consistent with the molecular formula $C_{37}H_{54}N_4O_9$ (Δmmu −0.05).[1] The ^{1}H NMR and ^{13}C NMR spectrum (CD_3OD) of **8c** was identical to the literature data (Appendix figure S24, Table S11).[6] The UV-vis spectrum of **8c** exhibited the characteristic α-pyrone ring absorbance. All of the above confirmed that **8c** was marinobufagenin pimeoyl-L-arginine. Moreover, as **8c** was synthesized from marinobufagenin-3-pimelate (**5b**), which was in turn prepared from authentic natural marinobufagenin (**1a**), we can be confident that the structure is as proposed.

Characterization of **9c** from Australian cane toad parotoid secretions has been previously reported (Figure 2.14).[1] In our study **9c** was obtained as a pale white solid with HR(+)ESIMS analysis revealing a quasi-molecular ion (m/z 685.4172 $[M+H]^+$) consistent with the molecular formula $C_{36}H_{54}N_4O_8$ (Δmmu −0.08).[1] The ^{1}H NMR and ^{13}C NMR spectrum (CD_3OD) of **9c** was identical to the literature data (Appendix figure S23, Table S10).[16] The UV-vis spectrum of **9c** exhibited the characteristic α-pyrone ring absorbance. All of the above confirmed that **9c** was bufalin pimeoyl-L-arginine. Moreover, as **9c** was synthesized from bufalin-3-pimelate (**6b**), which was in turn prepared from authentic natural bufalin (**3a**), we can be confident that the structure is as proposed.

^{1}H NMR spectrum of bufotoxins revealed more complicated signals compared to respective bufagenins due to the signals overlapping from C3-suberoyl-L-arginine conjugate. A search for complete NMR structure description for bufotoxins other than marinobufotoxin (**1c**) in literature revealed only non-detailed structure elucidation (with few distinct signals) from the 1970's.[6] However, the ^{1}H NMR spectrum for bufotoxins (**1c**, **2c**, **3c**, **8c** and **9c**) matched the data reported by Hayes et al in 2008.[1]

2.2.2.1 An empirical HSQC signature analysis for bufotoxins

Investigation of bufotoxin HSQC spectra was performed as described earlier for bufagenins, revealing comparable diagnostic signatures for marinobufotoxin (**1c**) telocinobufotoxin (**2c**) and bufalitoxin (**3c**).
The 5-OH/5-H and $\Delta^{14,15}$ epoxide/14-OH motifs revealed diagnostic HSQC signatures across the methylene envelop region of the steroid framework.
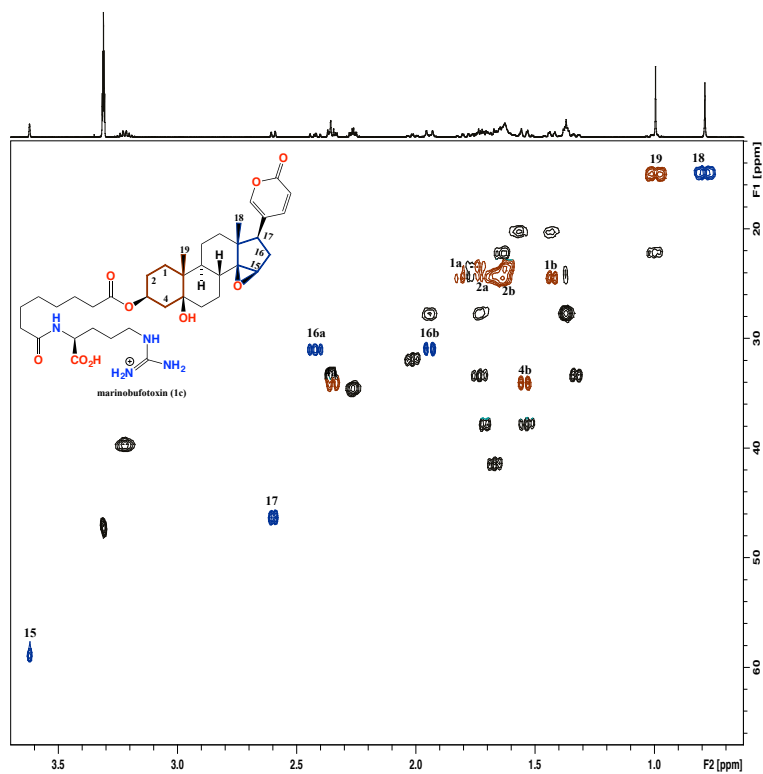
Figure 2.10 Expansion of HSQC (CD$_3$OD, 600 MHz) spectrum of marinobufotoxin (**1c**) showing 5-OH (brown) and $\Delta^{14,15}$ epoxy (purple) signatures
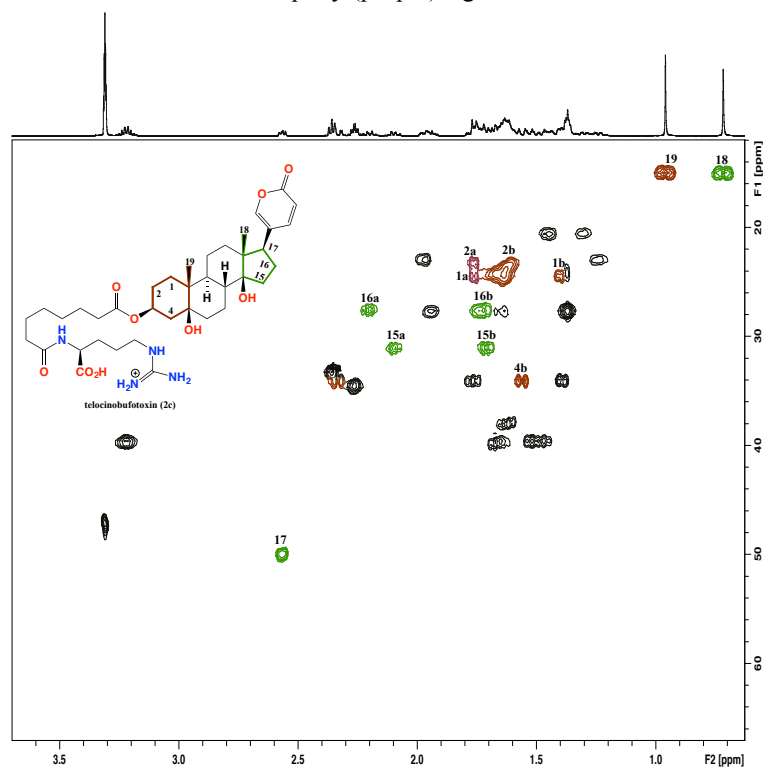
Figure 2.11 Expansion of HSQC (CD$_3$OD, 600 MHz) spectrum of telocinobufotoxin (**2c**) showing 5-OH (brown) and 14-OH (green) signatures
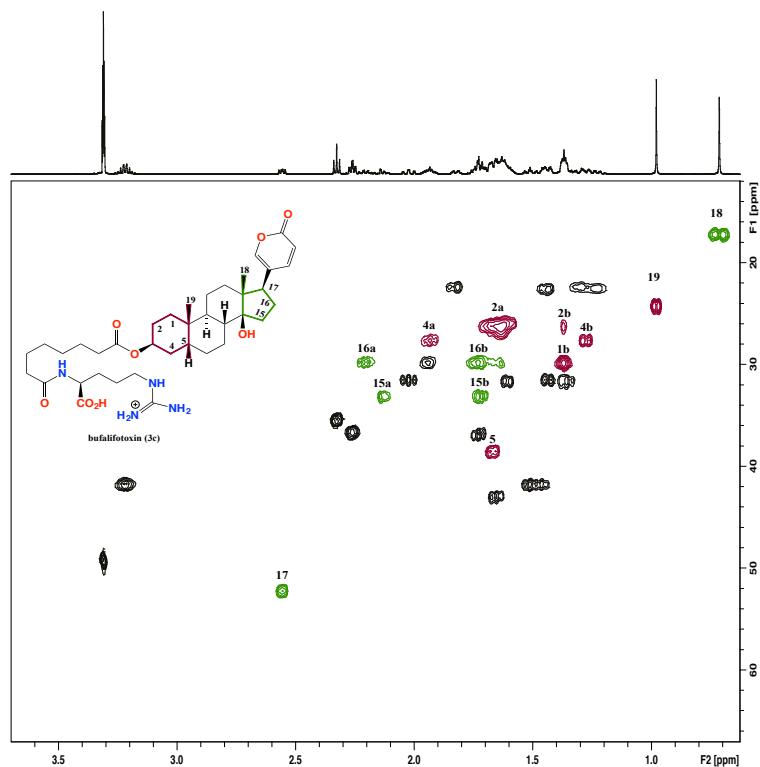
Figure 2.12 Expansion of HSQC (CD₃OD, 600 MHz) spectrum of bufalitoxin (**3c**) showing 5-H (magenta) and 14-OH (green) signatures

2.2.2.2 HSQC fingerprints for 5-OH vs 5-H bufagenins
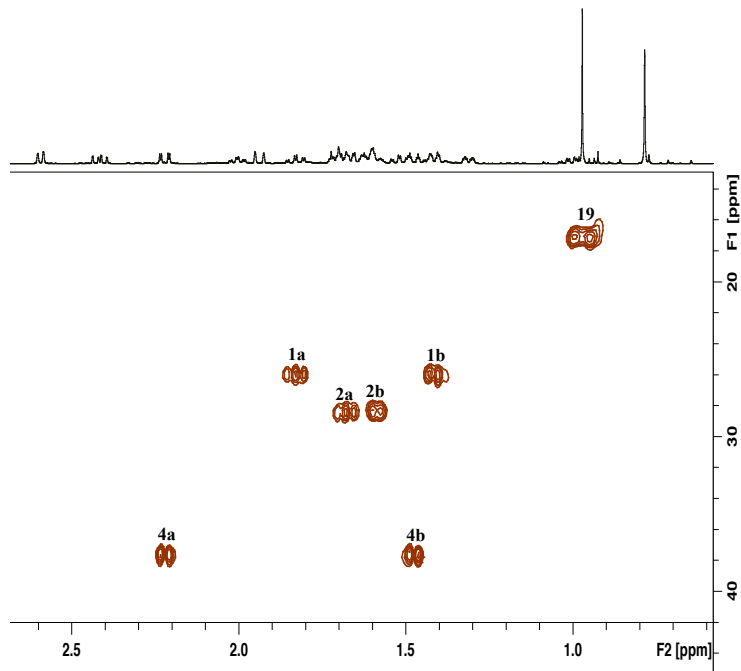
Figure 2.13 Expansion of HSQC (CD₃OD, 600 MHz) fingerprint of 5-OH bufagenins (brown)
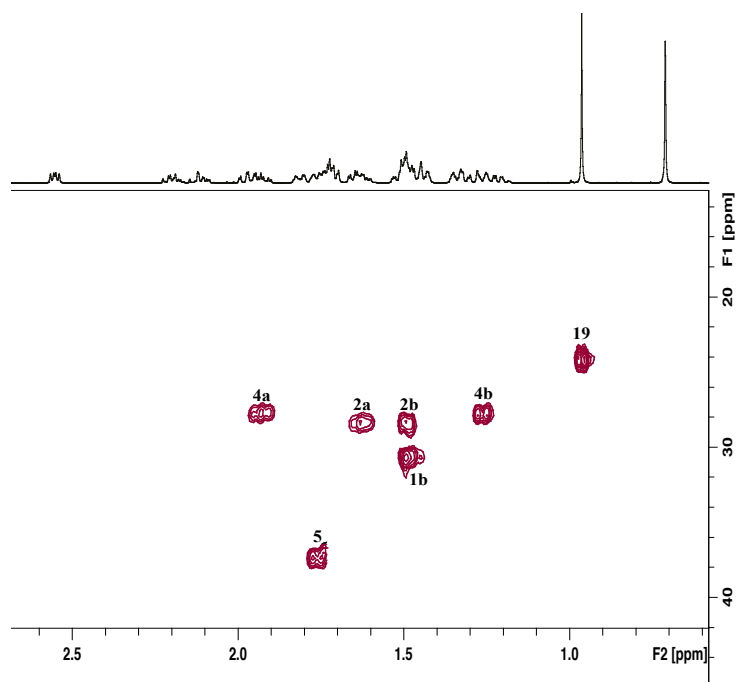
Figure 2.14 Expansion of HSQC (CD$_3$OD, 600 MHz) fingerprint of 5-H bufagenins (magenta)

2.2.2.3 Empirical HSQC rules for 14-epoxy vs 14-OH
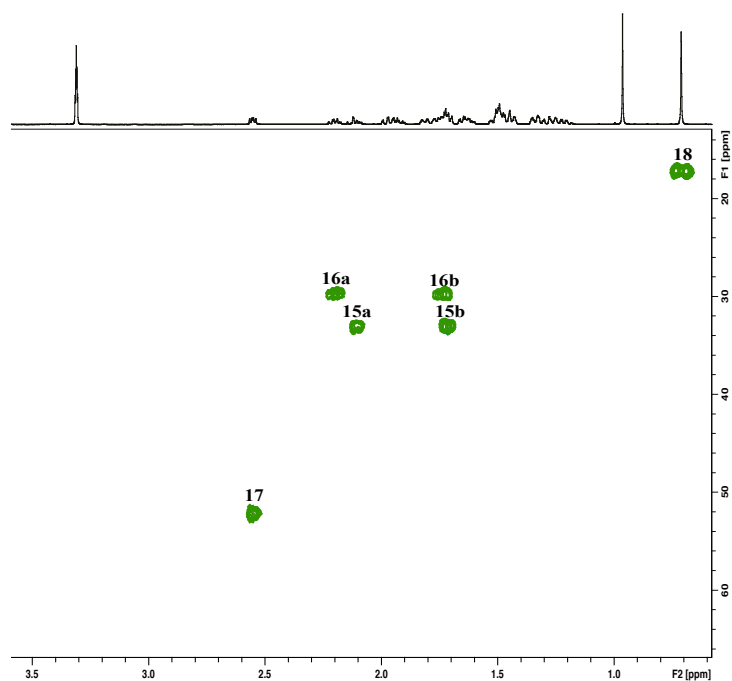
Figure 2.15 Expansion of HSQC (CD$_3$OD, 600 MHz) fingerprint of 14-OH bufagenins (green)
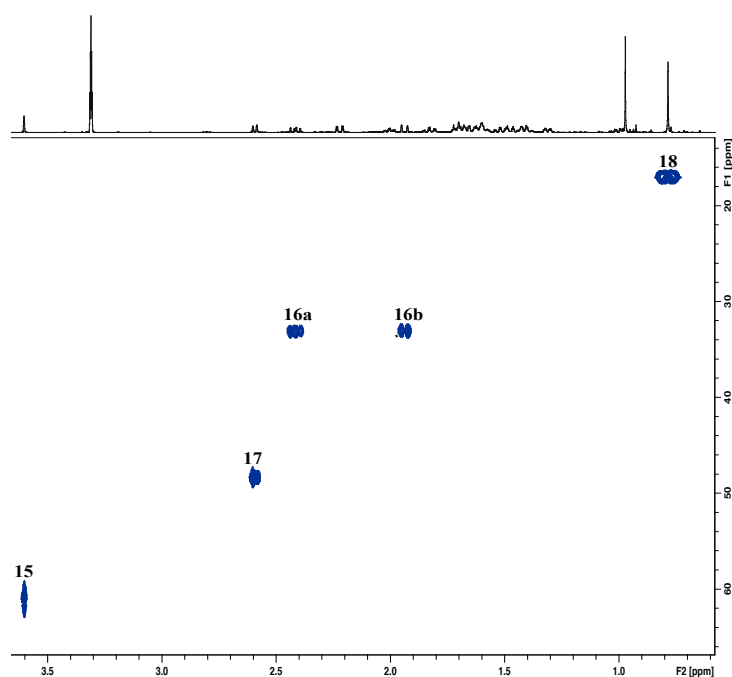
Figure 2.16 Expansion of HSQC (CD$_3$OD, 600 MHz) fingerprint of 14-epoxy bufagenins (purple)

These data suggests that HSQC fingerprinting analysis is not only applicable to identify bufagenins but also bufotoxins, and can potentially be extended to identify bufadienolides both known and new (Chapter 3).
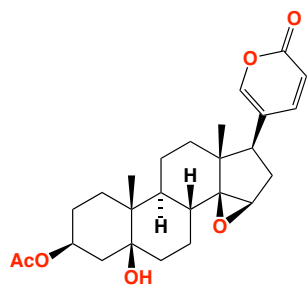
marinobufagenin-3-acetate (**8b**) marinobufagenin-3-succinate (**9b**)   marinobufagenin-3-pimelate (**5b**)
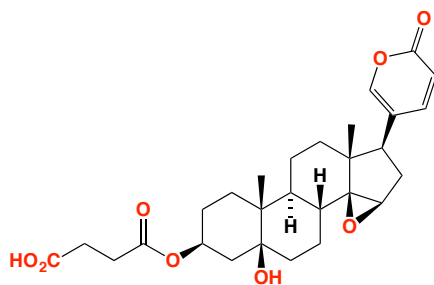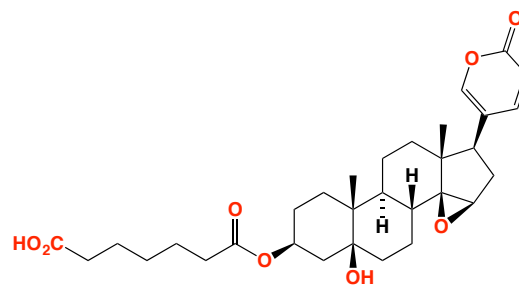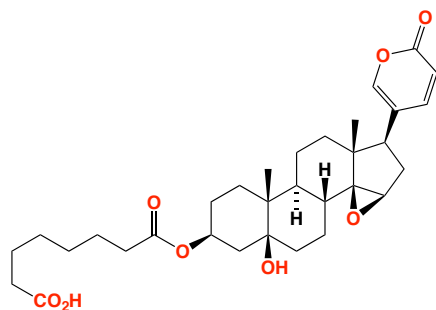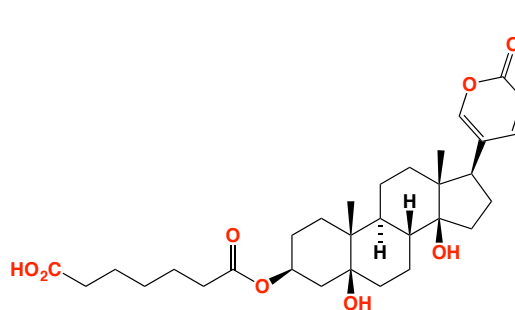
marinobufagenin-3-suberate (**1b**)   telocinobufagenin-3-pimelate (**6b**)   bufalin-3-acetate (**7a**)
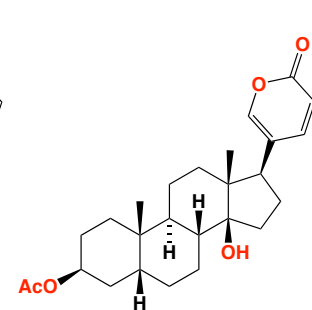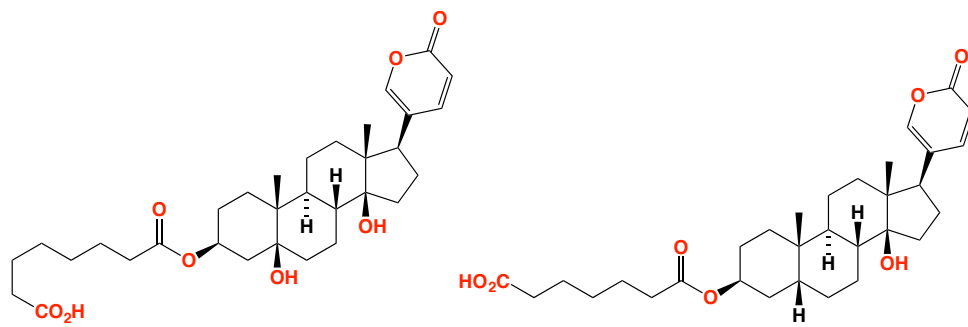
telocinobufagenin-3-suberate (**2b**)

bufalin-3-pimelate (**7b**)
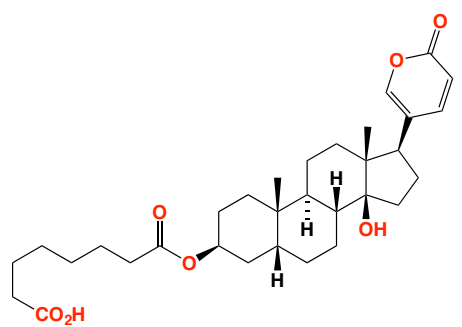
bufalin-3-suberate (**3b**)

Figure 2.17 Bufagenin esters synthesized from bufagenins
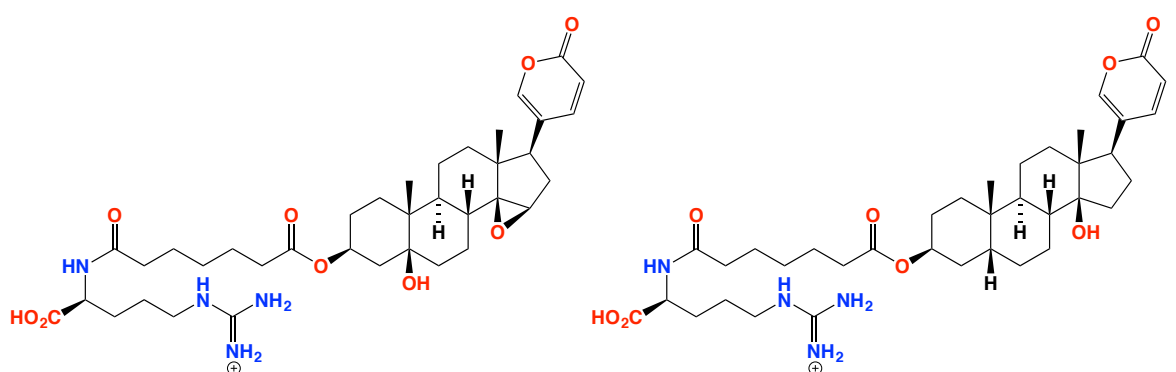
marinobufagenin pimeloyl-L-arginine (**8c**)

bufalin pimeloyl-L-arginine (**9c**)
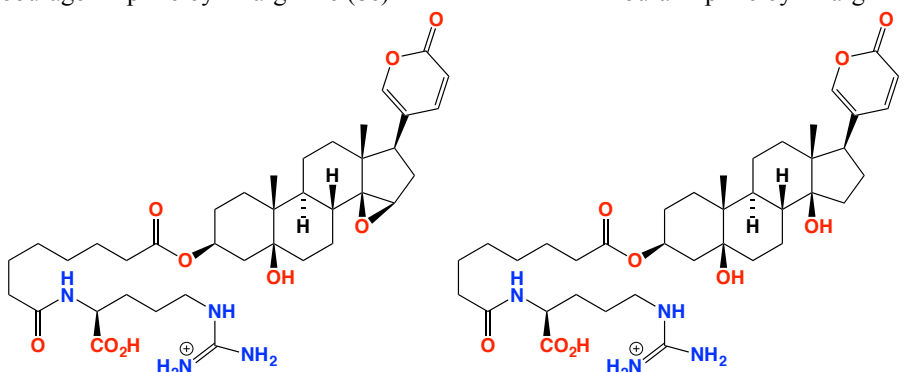
marinobufotoxin (**1c**)

telocinobufotoxin (**2c**)

bufalitoxin (**3c**)
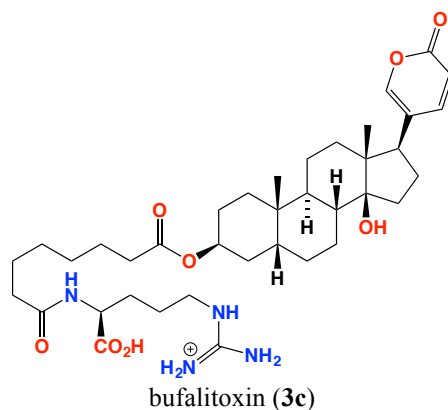
Figure 2.18 Bufotoxins synthesized from bufagenin esters

2.2.3 HPLC-DAD methodology to analyse bufagenins

An HPLC-DAD based analytical methodology was developed specifically for bufagenins by evaluating several reverse phase columns including C_3, C_8, C_{18}, CN (cyano) and phenyl columns with C_{18} (Zorbax, SB, 4.6 × 150 mm, 5 μm) providing the best resolution. Solvent conditions including MeOH/H_2O and MeCN/H_2O, across varying gradients (linear/isocratic) with and without TFA (0.01%) were also evaluated (Figure 2.19). A linear gradient of MeCN/H_2O with TFA (0.01%) showed high resolution of bufagenins (Method 1, refer section 2.) based on the peak area, peak height and the retention time of the respective bufagenin.
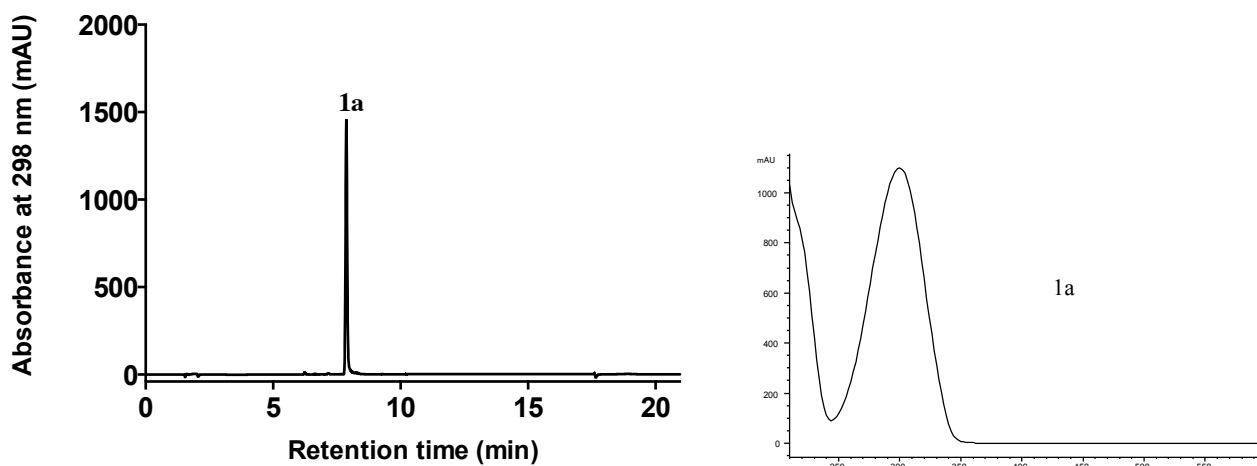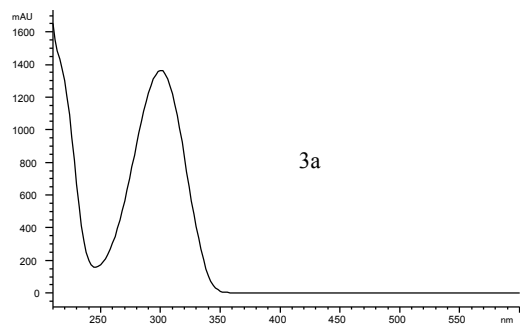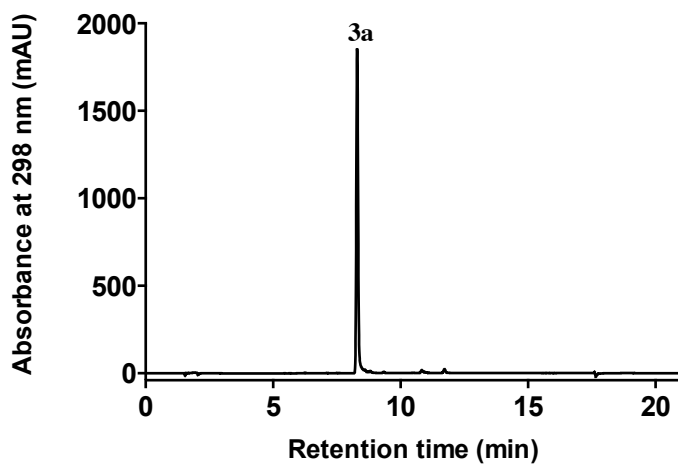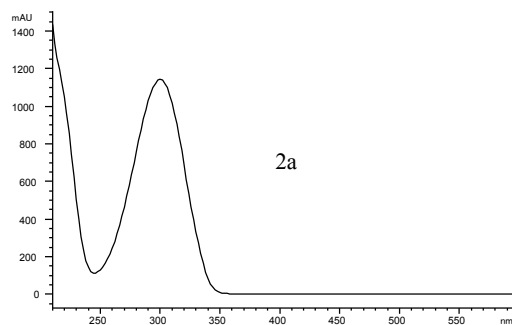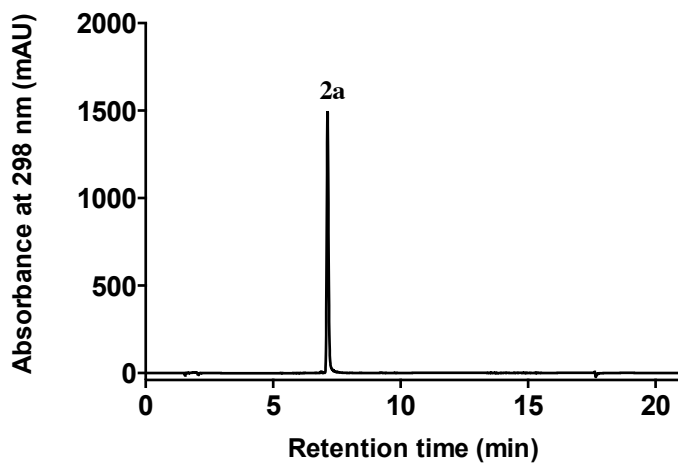
Figure 2.19 HPLC chromatograms (298 nm) and UV-Vis spectrum of marinobufagenin (**1a**), telocinobufagenin (**2a**) and bufalin (**3a**) respectively analysed using Method 1 (refer page 77)

2.2.3.1 Quantification of bufagenins

Having assembled authentic standards of a range of bufagenins, and having developed an optimized HPLC-DAD analytical methodology, it was important to evaluate this method for its applicability for quantitation analyses. As the DAD response for the α-pyrone moiety was constant across all bufagenins, it was deemed sufficient to calibrate against marinobufagenin (**1a**) as a representative of all bufagenins. A series of pure standards concentrated solutions of **1a** were prepared (3.9, 7.8, 15.6, 31.2, 62.5, 125, 250, 500, 1000 and 2000 μM). Injection of 10 μL from each standard solution delivered fixed amounts of **1a** (0.02, 0.04, 0.07, 0.13, 0.25, 0.5, 1, 2, 4 and 8 μg) (in triplicates). A plot of the DAD (298 nm) response (Figure 2.20) indicated a linear response across the range 0.02 to 8 μg (r^2=0.9978). This study provided a calibration curve that could be used to measure the concentration of **1a** (or any bufagenin) in a sample of unknown concentration, provided the mass of bufagenin injected per analyses fell within the linear range of 0.02 – 8 μg/injection.
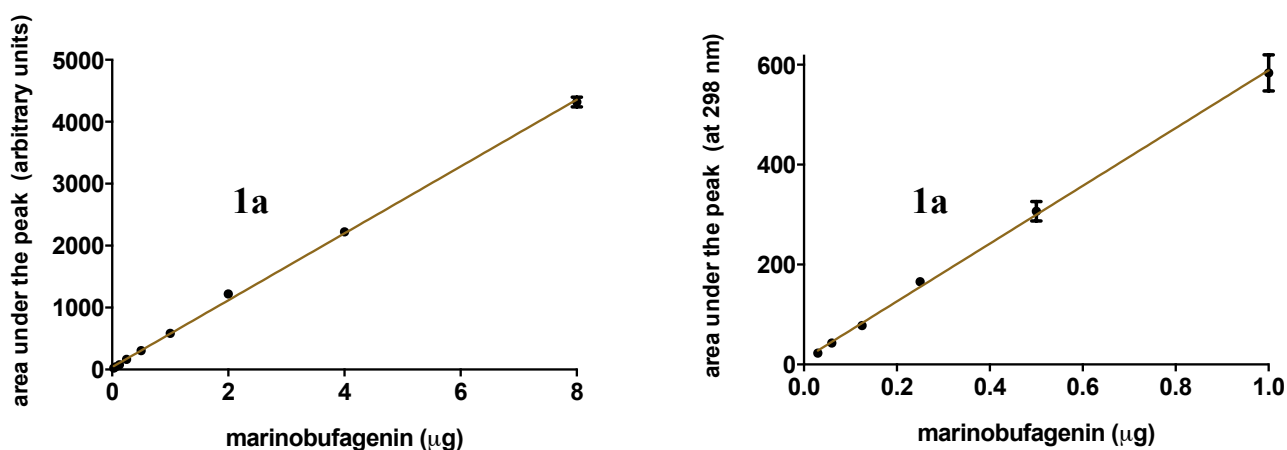
Figure 2.20 Concentration curve and UV-vis spectrum of marinobufagenin (**1a**)

2.2.4 HPLC-DAD methodology for bufotoxins

Bufotoxins are more polar compared to bufagenins due to the presence of arginyl amide conjugate, which also results in broad peaks when analysed using HPLC-DAD.[4, 10] Like the HPLC-DAD analytical methodology development with bufagenins, several reverse phase columns, such as C_3, C_8, C_{18}, CN (cyano) and phenyl columns (Zorbax, SB, 4.6 × 150 mm, 5 μm) were evaluated as well as MeOH/H_2O and MeCN/H_2O, with or without TFA (0.01%) (Figure 2.21). A C_{18} column with a linear gradient of MeCN/H_2O with TFA (0.01%) exhibited the best resolution (Method 2) based on the peak area, peak height and the retention time of the respective bufotoxin.
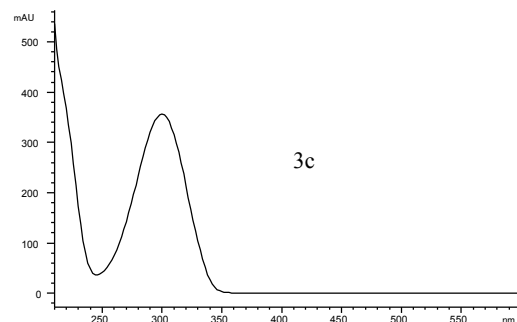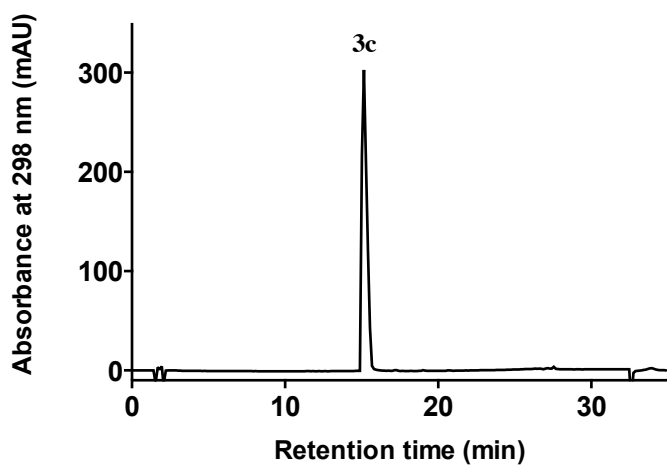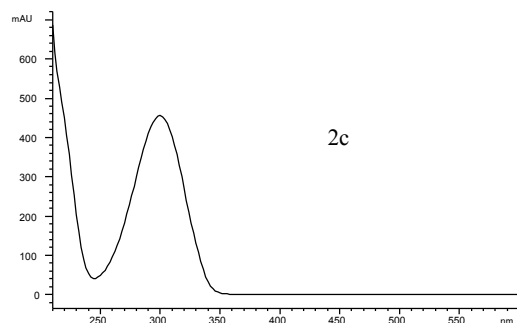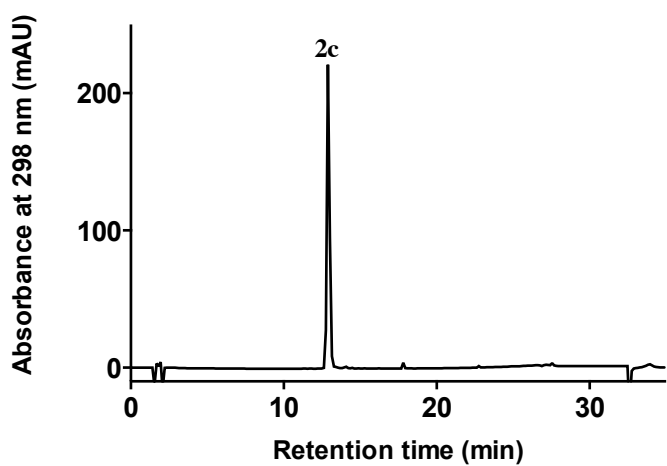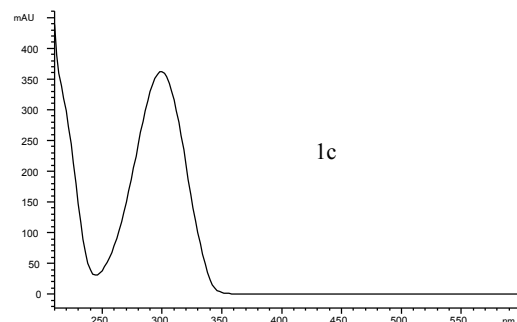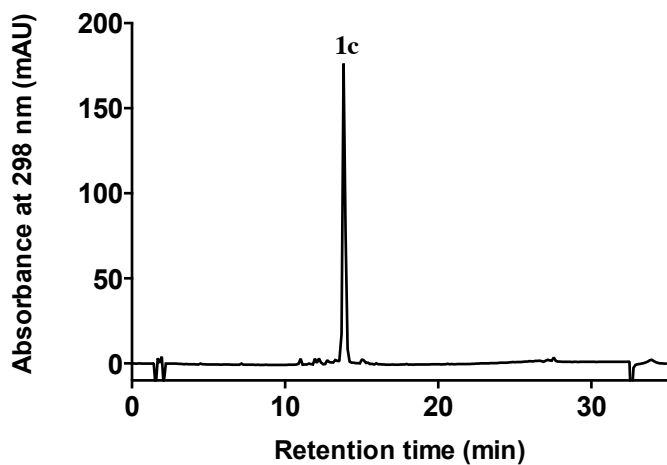
Figure 2.21 HPLC chromatograms (298 nm) and UV-vis spectrum of marinobufotoxin (**1c**), telocinobufotoxin (**2c**) and bufalitoxin (**3c**) using Method 2 (refer page 77)

2.2.4.1 Quantification of bufotoxins

Having assembled authentic standards of a range of bufotoxins, and having developed an optimized HPLC-DAD analytical methodology, it was important to evaluate this method so as to permit quantitation analyses. As the DAD response for the α-pyrone moiety was constant across all bufotoxins, it was deemed sufficient to calibrate against marinobufotoxin (**1c**) as a representative of all bufotoxins. A series of pure standards concentrated solutions of 1a were prepared (3.9, 7.8, 15.6, 31.2, 62.5, 125, 250, 500, 1000 and 2000 μM). Injection of 10 μL from each standard solution delivered fixed amounts of 1a (0.02, 0.04, 0.07, 0.13, 0.25, 0.5, 1, 2, 4 and 8 μg) (in triplicates). A plot of the DAD (298 nm) response (Figure 2.22) indicated a linear response across the range 0.02 to 8 μg (r^2=0.9994). This study provided a calibration curve that could be used to measure the concentration of **1c** (or any bufotoxin) in a sample of unknown concentration, provided the mass of bufotoxin injected per analyses fell within the calculated range of 0.02 – 8 μg/injection.
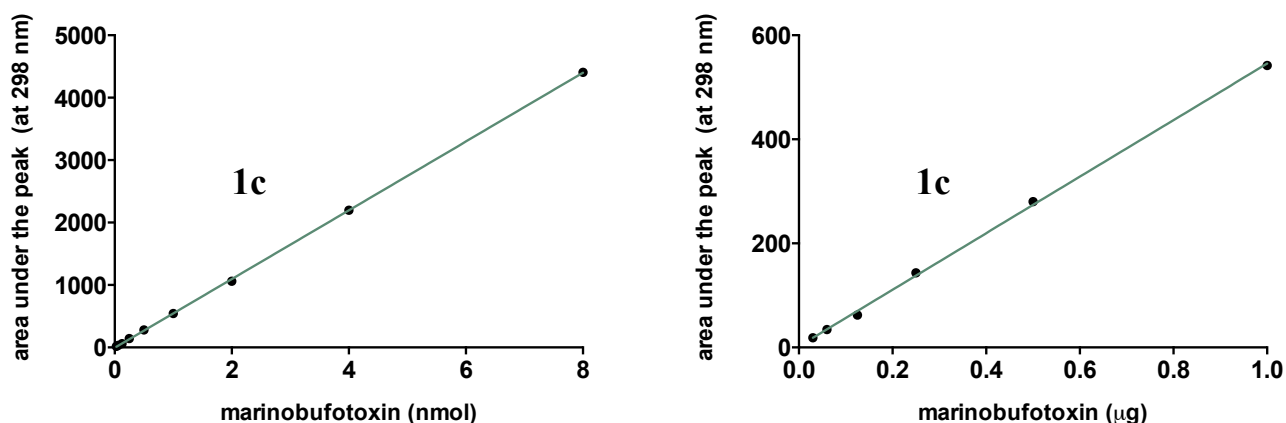
Figure 2.22 Concentration curve and UV-vis spectrum of marinobufotoxin(**1c**)

2.2.5 Analysis of bufadienolides from live cane toad parotoid secretions

Our pure bufagenin standards were isolated from frozen adult cane toad parotoid secretions, however, Hayes et al previously identified bufotoxins as minor components in parotoid secretions sourced from living cane toads. To explore this apparent contradiction we examined, parotoid secretions from live cane toads using our optimized analytical methodology specific for bufagenins and bufotoxins. Handling of parotoid secretions was of concern as the texture of toxin varies from sticky or pasty secretion to waxy solid if left to dry (data not shown). Two different approaches were investigated to handle the parotoid secretions.

2.2.5.1 Approach 1

Parotoid secretions from the left parotoid gland of three adult cane toads were squeezed onto a petridish and left for an hour to turn into a waxy solid. A pipette tip was used to scrap off parotoid secretion from the petridish and was directly dropped into methanol, mixed until homogenous solution and evaporated to dryness under N_2 at 40 °C.

HPLC-DAD analysis of the parotoid secretions recovered from live cane toads was dominated by bufagenins **1a**, **3a** and **4a** (66%), accompanied by significant amounts of bufotoxins **1c** and **2c** (34%). This analysis also detected dehydrobufotenin (**1.6**) (*) (Figure 2.23).
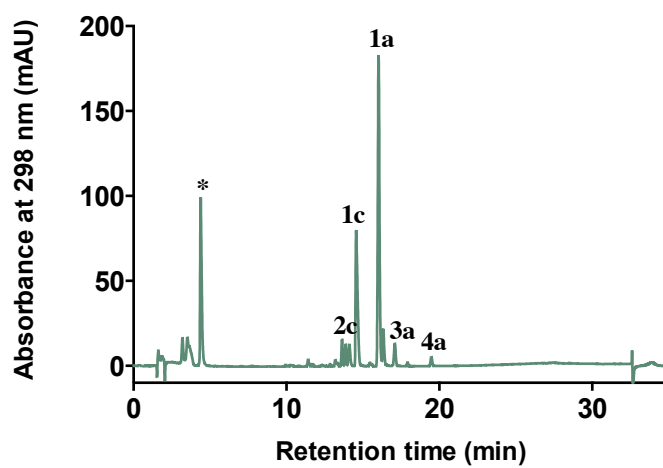
Figure 2.23 HPLC profile (298 nm) of live cane toad parotoid secretion squeezed on a petridish. Dehydrobufotenin (**1.6**), marinobufagenin (**1a**), bufalin (**3a**), resibufagenin (**4a**), marinobufotoxin (**1c**) and telocinobufotoxin (**2c**)

2.2.5.2 Approach 2

Parotoid secretions from the right parotoid gland were squeezed directly onto water and let for one hour retaining the sticky nature of the toxin. Subsequently, an aliquot of parotoid secretion in water was dispensed and dried under N_2 at 40 °C.

HPLC-DAD analysis of the parotoid secretions recovered from live cane toads revealed a higher ratio of bufagenins (89%) to bufotoxins (11%) (Figure 2.24) than measured in approach 1 (above). This observation suggests that post secretion and under certain conditions bufotoxins transformed into bufagenins. This was the first indication of such a transformation and has significant ecological implication given the very different levels of biological activity attributed to bufagenins vs bufotoxins.
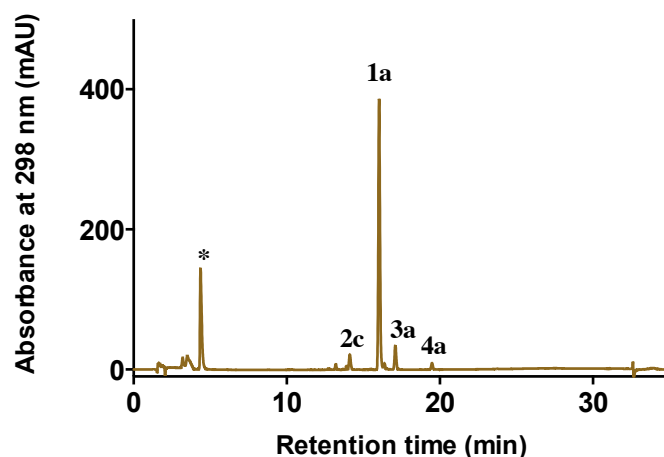
Figure 2.24 HPLC profile (298 nm) of adult parotoid secretion squeezed into water. Dehydrobufotenin (**1.6**), marinobufagenin (**1a**), bufalin (**3a**), resibufagenin, (**4a**) and telocinobufotoxin (**2c**)

The breakdown of bufotoxins to bufagenins could proceed by two plausible mechanisms

1. Proteolysis of the arginyl amide followed by hydrolysis of the suberoyl ester, to deliver the corresponding bufagenin together with arginine and suberic acid (Mechansim 1)

2. Hydrolysis of the suberoyl ester to deliver the corresponding bufagenin accompanied by intact suberoyl-L-arginine (Mechanism 2)
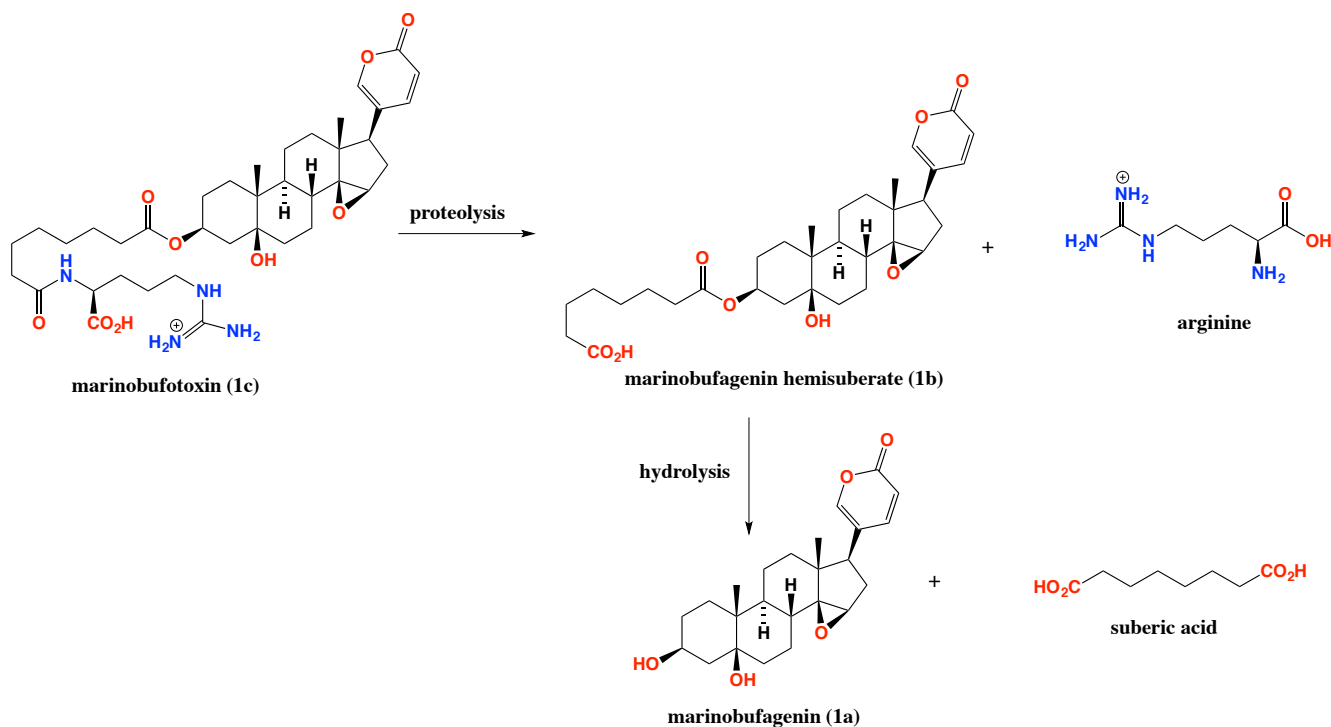
Figure 2.25 Mechanism 1 – Transformation of marinobufotoxin (**1c**) to marinobufagenin-3-suberate (**1b**) and arginine followed by marinobufagenin (**1a**) and suberic acid

56
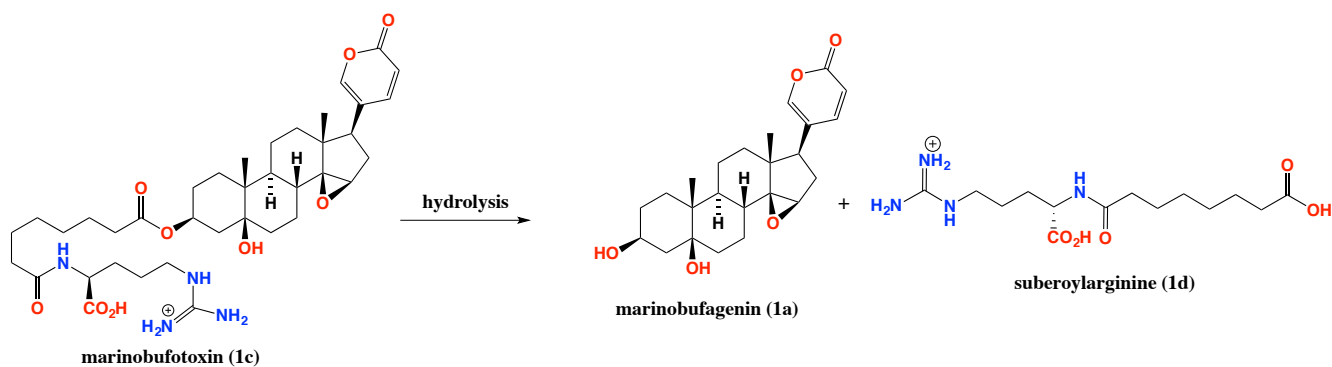
Figure 2.26 Mechanism 2 – Transformation of marinobufotoxin (**1c**) to marinobufagenin (**1a**) and suberoyl-L-arginine (**1d**)

To differentiate between these two hypotheses we developed and applied analytical methods to detect arginine, bufagenin suberate and suberoyl-L-arginine.

2.2.6 Analytical methodology to identify arginine

Although there is extensive literature about the isolation and characterization of bufadienolides (including bufotoxins), the configuration in the arginine of C-3 suberoylarginine conjugates of bufotoxins has never been reported. However, bufotoxins have always been represented to contain L-arginine in all of the published reports.[15, 17-19] Also, an analytical methodology to identify arginine in the parotoid secretions would be significant to determine the breakdown of bufotoxins through previously proposed mechanisms (Figure 2.25) during handling of the parotoid secretions. To detect arginine in the parotoid secretions and to determine the configuration of arginine, C_3-Marfey's analysis was performed on crude cane toad parotoid secretions. Since parotoid secretions directly squeezed into water showed high levels of bufagenins, it was chosen as a medium to identify arginine, as the lower the butotoxins, the higher the arginine level (Figure 2.23). Parotoid secretion was squeezed into water (5 mL), mixed using a vortex followed by partitioning with *n*-BuOH (5 mL) to solubilize all the bufadienolides. The water-soluble fraction was then dried *in vacuo* and was subjected to acid hydrolysis using 6M HCl to hydrolyse all the conjugated amino acids followed by derivatization with C_3-Marfey's reagent in the presence of 1M $NaHCO_3$. The reaction was stopped by the addition of 1M HCl, dried *in vacuo*, re-dissolved in MeCN (1 mg/mL) and was analysed using HPLC-DAD-MS co-injected with derivatized amino acid standards (Figure 2.27).
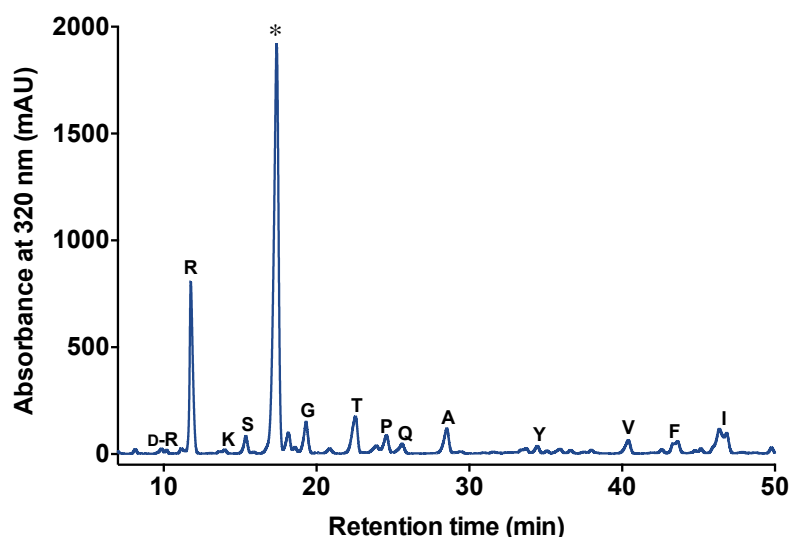
Figure 2.27 HPLC chromatogram (320 nm) of C$_3$ Marfey's analysis on water soluble fraction of parotoid secretions. * - Marfey's reagent (for peak annotation refer to Table 2.1)

Table 2.1 List of amino acids identified in water solubles of parotoid secretion using C$_3$-Marfey's analysis

Amino acid	Retention time (min)
L-histidine (H)	8.1
L-lysine (K)	9.8, 13.6
D-arginine (D-R)	10.2
L-arginine (R)	11.7
L-serine (S)	15.4
L-glycine (G)	19.3
L-aspartate (D)	20.8
L-threonine (T)	22.4
L-proline (P)	24.6
L-glutamine (Q)	25.6
L-alanine (A)	28.5
L-tyrosine (Y)	34.5
L-valine (V)	40.3
L-phenylalanine (F)	43.6
L-isoleucine (I)	46.4

C$_3$ Marfey's analysis clearly indicated the presence of high amounts of L-arginine in the parotoid secretion based on HPLC-DAD analysis (Figure 2.27). The analysis also indicated that transformation of bufotoxins to bufagenins and arginyl amides could occur through mechanism 2 (Figure 2.25) since no free L-arginine (or any amino acid) was detected in the water solubles of the

cane toad parotoid secretions, which is further, described in section 2.2.9. Analytical methodology to detect suberic acid would determine the hypothesis. A direct way of detecting suberic acid in the parotoid secretions would be to detect bufagenin suberates as cleavage of arginine from bufotoxin would significantly release bufagenin suberates. Interestingly, 14 other amino acids could also be identified indicating the presence of some source of peptides or proteins co-secreted with the parotoid secretions (Table 2.1). Bufotoxins with amino acid variations except arginine was not detected during previous analyses on *B. marinus* parotoid secretions. Hence, the source of amino acids could be from a peptide/protein. Moreover, D-arginine was also identified in low amounts based on UV detection while its function in parotoid secretions is unknown.

2.2.7 Analytical methodology to detect bufagenin suberate

Bufagenin suberates standards were synthesized previously during the synthesis of bufotoxin standards from pure bufagenins isolated from adult cane toad parotoid secretions. The standards were co-injected with the *n*-BuOH solubles of parotoid secretions squeezed into water (Section 2.2.5) and analysed using analytical methodology for bufagenins (Figure 2.28). No bufagenin suberate could be detected in the parotoid secretions indicating that transformation of bufotoxin through mechanism 1 may not fit the hypothesis (Figure 2.25). In addition to HPLC-DAD based detection, a single ion extraction of masses specific for the bufagenin suberates and other diacid conjugates also confirmed their absence.
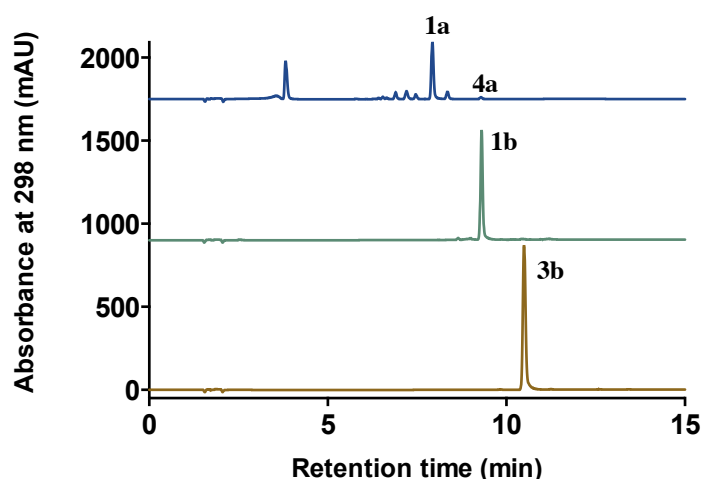
Figure 2.28 HPLC-DAD traces of co-injection of organic fraction of parotoid secretion with bufagenin suberates. Marinobufagenin (**1a**), resibufagenin (**4a**), marinobufagenin-3-suberate (**1b**), bufalin-3-suberate (**3b**)

The presence of substantial amounts of L-arginine in the parotoid secretion (C₃ Marfey's analysis) could be attributed to the presence of arginyl amides in substantial quantities in the water soluble

part of parotoid secretions. Arginyl amides, like the amino acid arginine must be water-soluble, hence, the detected L-arginine could be a hydrolysed product of suberoyl-L-arginine formed from mechanism 2. Hence, bufotoxins are proposed to undergo transformation by direct breakdown of suberoyl-L-arginine (**1d**) to form bufagenins (Figure 2.26). The observation also indicated the presence of free arginyl amides present in the parotoid secretions that had never been identified before using HPLC-DAD. Hence, it is hypothesized *that there is a fourth structure class present in the B. marinus parotoid secretions other than bufadienolides, catecholamines and indole alkaloids, namely arginyl amides*. It can also be concluded that arginine present in bufotoxins is L-arginine and the previous reports of the structure could be considered as correctly representing the configuration. A literature search on the arginyl amides returned only one hit where **1d** was identified during the chemical analysis of the Chinese traditional medicine, Chansu, prepared from the skin of the parotoid glands of *Bufo* species.[18] Mass corresponding to suberoyl-L-arginine (**1d**) was identified during an ESI-MS analysis of parotoid secretions from *B. marinus*.[2] Bufagenin conjugates with suberoyl-L-arginine and pimeloyl-L-arginine have been described previously from parotoid secretions of *Bufo* species and from Chansu.[9, 18]

2.2.8 To generate a library of diacid arginyl amides

A major drawback in the detection of arginyl amides is the lack of a characteristic UV chromophore making it difficult to isolate and characterize using HPLC-DAD. Hence, the detection and quantification of arginyl amides in the parotoid secretions requires a chemical derivatization method that could introduce a UV chromophore for detection using DAD. A synthetic strategy was undertaken to synthesize arginyl amides standards and subsequent identification using a specific analytical methodology (Figure 2.29). Since arginyl amides have not been studied before, its biological activity is as yet unknown (will be discussed in later chapters).
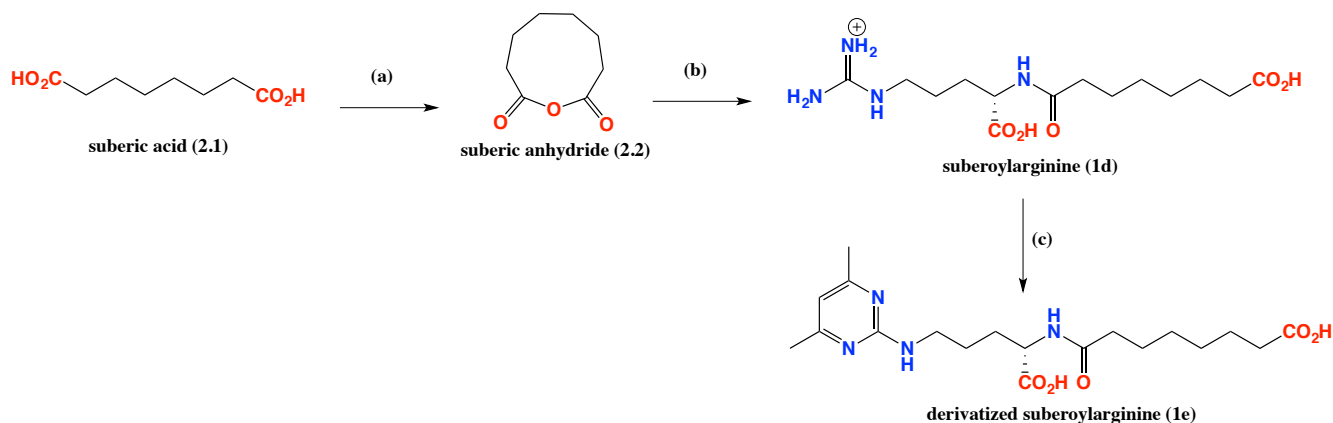
Figure 2.29 Scheme of synthesis for arginyl amides standards with suberoyl-L-arginine (**1d**) as an example. (a) – reflux for 2 h with acetic anhydride, (b) –coupling with L-arginine monohydrochloride at pH 8.2 at room temperature for 24 h, (e) – reflux for 7 h with 2,4-pentanedione and pyridine.

From C$_3$-Marfey's analysis, it was determined that arginine of the daicid arginyl amide is L-arginine and hence arginyl amides were synthesized with diacids containing various chain lengths and L-arginine. The amides were synthesized by coupling L-arginine with adipic, pimelic, suberic and azeloic anhydrides, respectively.[20] The anhydrides were obtained by heating the dicarboxylic acids with acetic anhydride at reflux. Immediately after the synthesis, the anhydrides were dried *in vacuo* and were subjected to coupling with L-arginine monohydrochloride (Figure 2.29).

The pKa values for the alpha amino group and the guanidino group of arginine are 9.04 and 12.48 respectively. The reaction was maintained between pH 8 and 9 to permit the free amine (alpha amino group) to undergo nucleophilic addition to the anhydride to form an amide bond (Appendix Figure S14, Table S12). Arginyl amides with varying chain lengths (4, 5, 6 and 7 methylenes) were synthesized (Table 2.2) and the purification was performed using ion-exchange chromatography (Dowex 50WX2, strong cation exchange resin, 200-400 dry mesh, 1 mL/min) with a linear gradient of 0 – 2 M HCl. Characterization was performed with NMR spectroscopy (^{1}H, ^{13}C, HSQC, HMBC and COSY) and HRMS.

Table 2.2 List of synthesized diacid arginyl amides

Chain length (n)	amide	yield
4	adipoyl-L-arginine (**2d**)	61%
5	pimeloyl-L-arginine (**3d**)	57%
6	suberoyl-L-arginine (**1d**)	58%
7	azeloyl-L-arginine (**4d**)	55%

A derivatization method was adopted to specifically modify the individual amides to be UV detectable (Figure 2.29).[21] The amides were converted to their respective pyrimidine analogues by the cyclization of the guanidino group of the arginine in the presence of 2,4-pentanedione (Table 2.3).

The synthesized amides (Figure 2.30) were subjected to the 2,4-pentanedione derivatization reaction and pure pyrimidine analogues of amides were isolated and characterized by semi-preparative HPLC, NMR spectroscopy (^{1}H, ^{13}C, HSQC, HMBC and COSY) and mass spectrometry.

Table 2.3 List of all 2,4-pentanedione derivatized arginyl amides

Chain length (n)	derivatized amide	yield
4	derivatized adipoyl-L-arginine (**2e**)	83%
5	derivatized pimeloyl-L-arginine (**3e**)	72%
6	derivatized suberoyl-L-arginine (**1e**)	90%
7	derivatized azeloyl-L-arginine (**4e**)	88%

All the derivatized diacid arginyl amides (Figure 2.31) would be used as standards to identify and quantify the presence of arginyl amides in any given tissue sample (such as parotoid secretion). An analytical methodology to specifically identify derivatized amides was developed which will be discussed in the next section. Quantification of arginyl amides standards would be performed using the analytical methodology and generate a standard concentration curve which would be used as a tool to calculate absolute amounts of arginyl amides in a given tissue sample.

adipoyl-L-arginine (**2d**)

pimeloyl-L-arginine (**3d**)

suberoyl-L-arginine (**1d**)

azeloyl-L-arginine (**4d**)
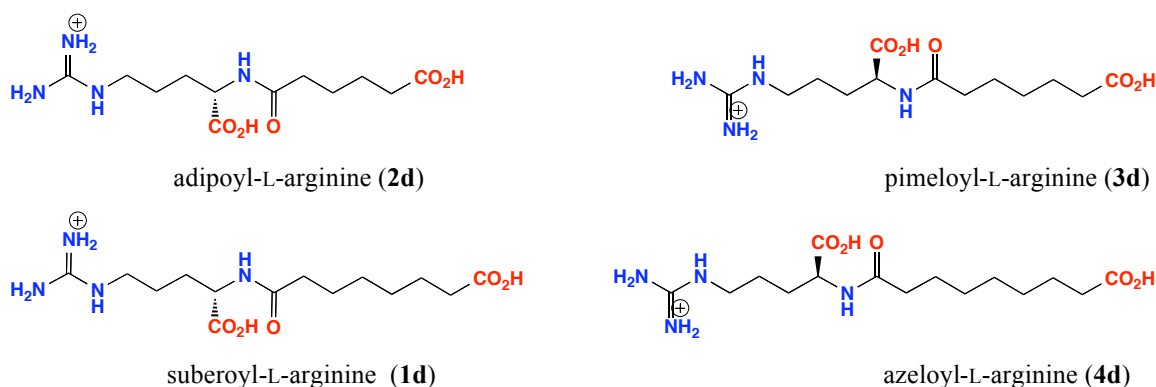
Figure 2.30 List of synthesized arginyl amides

derivatized adipoyl-L-arginine (**2e**)

derivatized pimeloyl-L-arginine (**3e**)

derivatized suberoyl-L-arginine (**1e**)

derivatized azeloyl-L-arginine (**4e**)
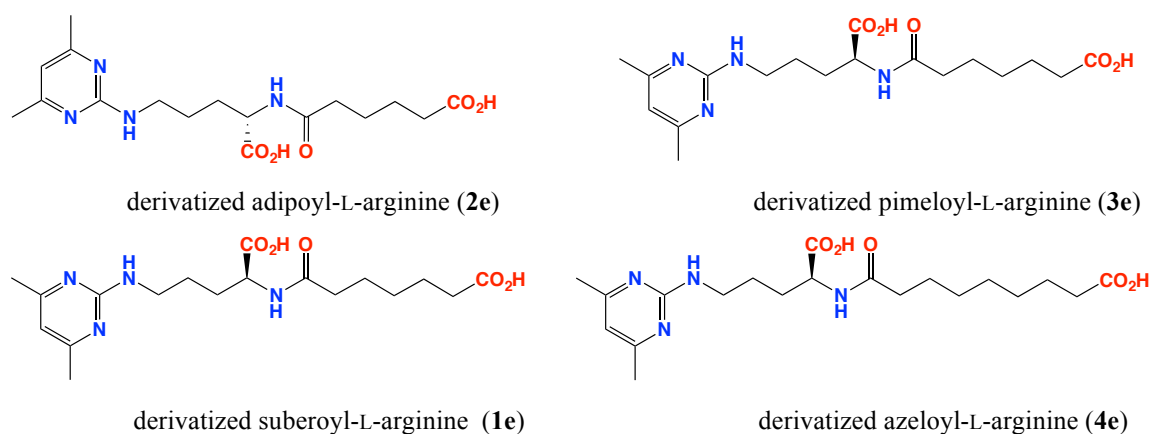
Figure 2.31 List of derivatized synthetic arginyl amides

2.2.9 Analytical methodology for arginyl amides

2.2.9.1 Analytical methodology 1 for arginyl amides – HPLC-DAD-MS

A primary analytical methodology (Method 3a, refer 2.4.7) for the detection of arginyl amides involves an HPLC-DAD-MS based approach based on the ionization of the derivatized amides. Following the derivatizaion of arginyl amide standards with 2,4-pentanedione, a single ion extraction analysis was performed based on the mass (m/z) of the derivatized amides and the search returned a distinct ionization pattern for all four different amides (Figure 2.32). This approach would be suitable for arginyl amides that are present in less amounts or difficult to identify using absorption measured by HPLC-DAD.
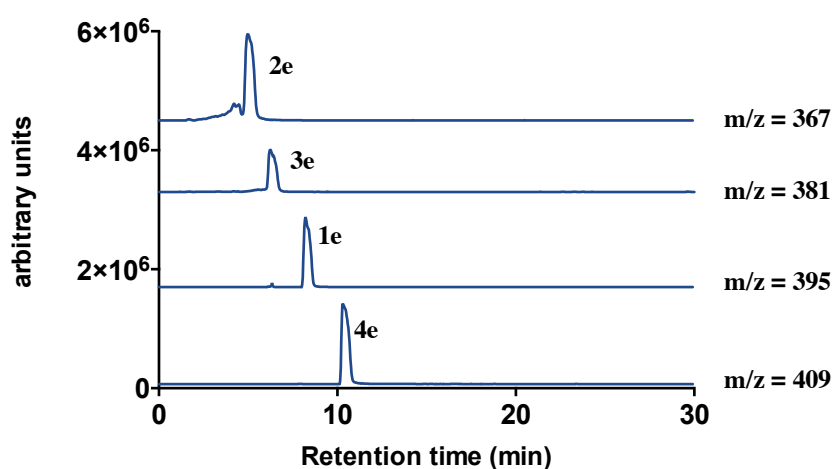
Figure 2.32 Single ion extraction of derivatized arginyl amides standards in ESI positive ion reflectron mode analysed using Method 3a (refer page 77). **2e** – derivatized adipoyl-L-arginine, **3e** – derivatized pimeloyl-L-arginine, **1e** – derivatized suberoylargiinne, **4e** – derivatized azeloyl-L-arginine

Surprisingly, the analytical methodology also revealed that derivatized arginyl amide standards showed a better resolution under HPLC-DAD-MS profile (Figure 2.33). A search for the suberoyl-L-arginine (**1d**), the major arginyl amide, in crude water solubles of the parotoid secretion co-eluted with dehydrobufotenine (**1.6**, major indole alkaloid) as a broad peak. However, since the derivatized amide (**1e**) has a different retention time and a better resolution (narrow peak) under HPLC-DAD-MS, the problem of co-eluting or complexing of arginyl amides with other derivatives would be avoided while detecting individual arginyl amides. The two arginyl amides that were identified using Method 3a on crude water solubles of parotoid secretion include pimeloyl-L-arginine (**3d**) and suberoyl-L-arginine (**1d**) while no free L-arginine was detected.
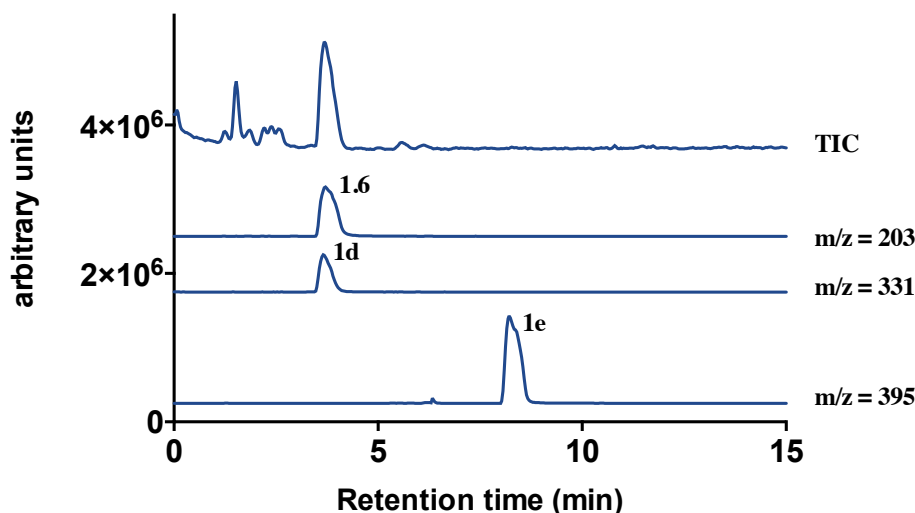
Figure 2.33 Single ion extraction chromatograms from crude water solubles of parotoid secretion in ESI positive ion mode analysed using Method 3a (refer page 77). **TIC** – total ion current, dehydrobufotenine (**1.6**), suberoyl-L-arginine (**1d**), derivatized suberoyl-L-arginine (**1e**)

2.2.9.2 Analytical method for detection of arginyl amides

Arginyl amides standards when analysed using HPLC-DAD did not elicit a good response, however, a small peak was observed at 210 nm but at higher concentrations (>2 mg/mL). Derivatized amides were subjected to HPLC-DAD analysis using several reverse phase columns including C_3, C_8, C_{18}, CN (cyano) and phenyl with C_{18} (Zorbax, SB, 4.6 × 150 mm, 5 μm) showing the best resolution based on the peak area, peak height and the retention time of the respective arginyl amide. MeCN/H_2O solvent gave better resolution compared to MeOH/H_2O with TFA (0.01%). The absorbance (DAD) elicited by the derivatized amides is attributed to the pyrimidine ring (320 nm) formed from the cyclization of guanidine group of the arginine. Since the derivatized amides have a distinctive and characteristic UV absorbance at 320 nm it is significant to identify arginyl amides among other structure classes such as bufadienolides (298 nm) and alkaloids (210 nm) in a given tissue sample (Method 3b, refer 2.4.7). The derivatized amides are less polar and methanol soluble compared to arginyl amides that are water-soluble. Crude extract from a tissue sample would be partitioned with EtOAC/H_2O or *n*-BuOH/H_2O to separate bufadienolides and arginyl amides. The water solubles containing arginyl amides would be further subjected to derivatization with 2,4-pentanedione followed by analysis using HPLC-DAD (Figure 2.34).
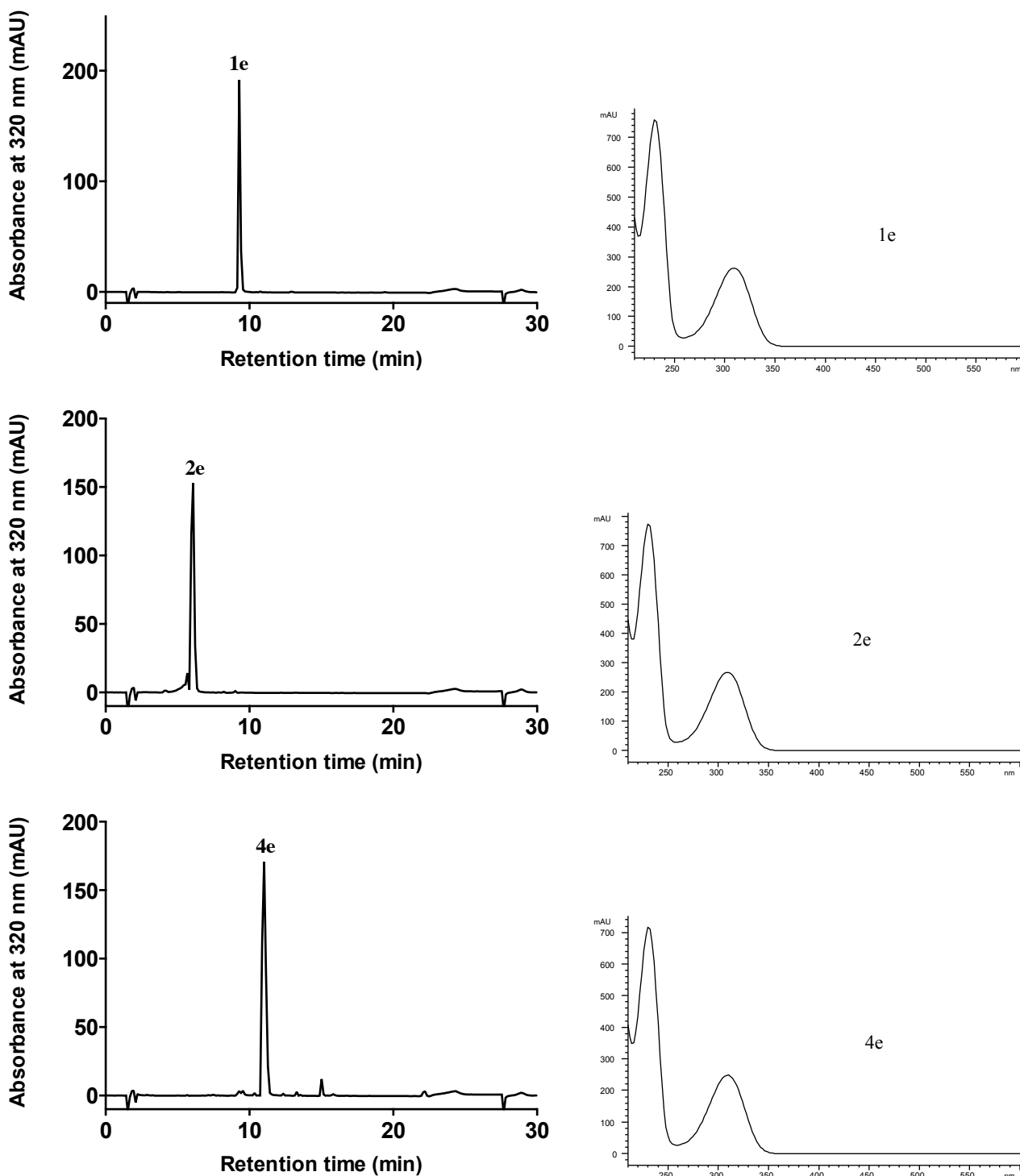
Figure 2.34 HPLC chromatogram (320 nm) and UV-vis spectrum of 2,4-pentanedione derivatized arginyl amides (1 mM; 10 µL) analysed using Method 3b (refer page 77). **1e** – derivatized suberoyl-L-arginine, **2e** – derivatized adipoyl-L-arginine and **4e** – derivatized azeloyl-L-arginine

2.2.9.3 Quantification of arginyl amides

Free arginyl amides were identified in the *B. marinus* parotoid secretions leading to indication of presence of significant quantities based on ionization as identified using HPLC-DAD-MS (Figure 2.33). Gao et al, reported the presence of suberoyl-L-arginine (**1d**) in the parotoid secretions of *B. marinus* based on the mass spectrometry analysis.[3] Since arginyl amides are not detetcted using

DAD, derivatized amides were subjected to quantitation studies using the analytical method for arginyl amdies previously described. This means the crude extract from the tissue under study must be derivatized with 2,4-pentanedione followed by analysis using HPLC-DAD using analytical Method 3.

Having assembled authentic standards of a range of pyrimidine derivatives, and having developed an optimized HPLC-DAD analytical methodology, it was important to evaluate this method so as to permit quantitation analyses. As the DAD response for the pyrimidine moiety was constant across all derivatized amides, it was deemed sufficient to calibrate against derivatized suberoyl-L-arginine (**1e**) as a representative of all bufagenins. A series of pure standards concentrated solutions of **1e** were prepared (3.9, 7.8, 15.6, 31.2, 62.5, 125, 250, 500, 1000 and 2000 μM). Injection of 10 μL from each standard solution delivered fixed amounts of **1a** (0.02, 0.04, 0.07, 0.13, 0.25, 0.5, 1, 2, 4 and 8 μg) (in triplicates). A plot of the DAD (320 nm) response (Figure 2.35) indicated a linear response across the range 0.02 to 8 μg (r^2=0.9960). This study provided a calibration curve that could be used to measure the concentration of **1e** (or any pyrimidine derivative) in a sample of unknown concentration, provided the mass of pyrimidine derivatives injected per analyses fell within the linear range of 0.02 – 8 μg/injection. Another interesting observation about the derivatized arginyl amides is that, unlike other bufadienolides, they can be detected by DAD at 320 nm, which means that a specific detection method is now available to exclusively detect arginyl amides. (Figure 2.35).

Concentration curves for other derivatized amides are described elsewhere (Appendix Figure S29). The current investigation of arginyl amides in the parotoid secretions has revealed interesting findings since identification of arginyl amides has not been reported previously. The quantification of arginyl amides in the parotoid secretions may be significant for the toxicity of the cane toad parotoid secretions. 2,4-pentanedione derivatized crude extracts from a given sample could therefore be analysed using method 3b. Quantification of concentration for specific arginyl amides identified by comparison with standards can be done using the standard concentration curve. Following the calculation of absolute amounts in the crude extract, the amount present in the given tissue sample could be accurately determined.
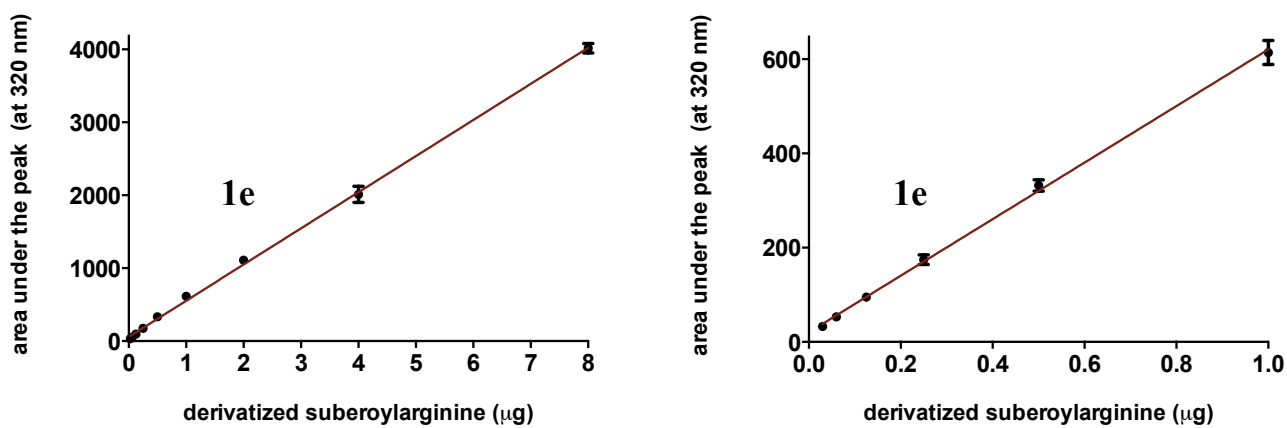
Figure 2.35 Concentration curve and UV-vis spectrum of derivatized suberoyl-L-arginine (**1e**)

2.3 Conclusion

The chemical diversity in parotoid secretions obtained from frozen *B. marinus* corresponded to the previously published literature, however, only bufagenins and no bufotoxins were identified as mentioned in some previous reports. A cane toad toxin library consisting of bufagenins, bufotoxins and arginyl amides was developed by various approaches as mentioned earlier to obtain significant quantities of compounds for quantification of toxin in various tissues.

Bufagenin standards were directly isolated from parotoid secretions while bufotoxin standards were partially synthesized from bufagenins. All the standards were characterized for their purity and structure using analytical HPLC-DAD, HPLC-DAD-MS, NMR and HRMS. Having developed standards, a specific analytical methodology for identification of bufagenins and bufotoxins was developed. Quantification of the standards was performed by employing the analytical methodologies specific for each structure class with known amounts. Concentration curves were generated using UV absorbance (area under the curve) and absolute amount of each standard. Having developed an analytical separation and quantification methodology, absolute amounts of bufadienolides in any given tissue sample (parotoid secretions, eggs) could be determined. A HSQC finger printing analysis of bufadienolides was developed to identify the key substitution patterns in the steroidal A and D rings of new/unknown bufagenins as well as bufotoxins.

During the analysis of parotoid secretions from live cane toads, handling of the toxin was determined to have an effect on the chemical profiling of the bufadienolides in the parotoid secretions. Bufotoxins were identified in significant amounts from dried parotoid secretions while the amounts dropped in parotoid secretions stored in water, although bufagenins were identified to be the dominant class of bufadienolides in either ways of handling. The investigation clearly suggested that there is a transformation of bufotoxins to bufagenins and arginyl amides. The observations also led to the presence of a new structure class, diacid arginyl amides in the parotoid secretions. To identify and quantify diacid arginyl amides in the parotoid secretions, standards were synthesized and derivatized with 2,4-pentanedione facilitating a UV response when detected using HPLC-DAD.

C_3-Marfeys analysis on parotoid secretions indicated the presence of L-arginine, which not only confirmed the stereochemistry of arginine in bufotoxins but also indicated the presence of significant amounts of arginyl amide in the parotoid secretions. Investigations on the role of free arginyl amides in the parotoid secretions are explained in following chapter.

2.4 Experimental

2.4.1 Equipment

High Performance Liquid Chromatography (HPLC) was performed using an Agilent 1100 Series Separations Module equipped with Agilent 1100 series diode array and/or multiple wavelength detectors and Agilent 1100 series fraction collector, controlled using ChemStation Rev.9.03A. Electrospray Ionisation Mass Spectra (ESI-MS) were acquired using an Agilent 1100 Series separations module equipped with an Agilent 1100 Series LC/MSD mass detector in both positive and negative ion modes. NMR spectra was obtained on a Bruker Avance DRX600 spectrometer, in the solvents indicated and referenced to residual proton signals in deuterated solvents.

2.4.2 Isolation of bufagenins from parotoid secretions

Parotoid glands from 120 frozen toads were dissected and were manually disrupted in a beaker containing ethyl acetate to release all the secretions. The organic layer was collected and was dried *in vacuo* at 40 °C and subjected to purification by flash chromatography (Biotage) with a linear gradient of 60-100% EtOAc/*n*-hexane using 50 g normal phase silica column (SNAP cartridge). Each peak was collected in clean glass test tubes. Peaks corresponding to bufalin (**3a**) and telocinobufagenin (**2a**) were again subjected to purification by HPLC to isolate the minor peaks that was not detected by flash chromatography to yield hellebrigenin (**5a**) and bufalin-3-acetate (**7a**).

marinobufagenin (1a): yellow solid; $[\alpha]^{21}_D$ +12.5 (*c* 0.2, CHCl$_3$) (Reported: +12.2 (*c* 1.1, CHCl$_3$); ^{1}H and ^{13}C NMR (CD$_3$OD, 600 MHz) see Table S1; HRESI(+)MS m/z 401.2323 (M+H)$^+$ (calcd for C$_{24}$H$_{32}$O$_5$, 401.2322). Zorbax C$_{18}$ column, 250 × 9.4 mm, 5 μm, 3.5 mL/min, gradient from 10-100% MeCN/H$_2$O over 25 min, t_R = 13.5 (Appendix Figure S1). Yield: 66.7%

telocinobufagenin (2a): white solid; $[\alpha]^{21}_D$ −5.7 (*c* 0.16, MeOH) (Reported: −12.5 (*c* 0.9, MeOH); ^{1}H and ^{13}C NMR (CD$_3$OD, 600 MHz) see Table S2; HRESI(+)MS m/z 403.2479 (M+H)$^+$ (calcd for C$_{24}$H$_{34}$O$_5$, 403.2474). Zorbax C$_{18}$ column, 250 × 9.4 mm, 5 μm, 3.5 mL/min gradient from 10-100% MeCN/ H$_2$O over 25 min, t_R = 11.2 min (Appendix Figure S2). Yield: 8.9%

bufalin (3a): white solid; $[\alpha]^{21}_D$ −7.7 (*c* 0.2, CHCl$_3$) (Reported: −8.9 (*c* 1.2, CHCl$_3$); ^{1}H and ^{13}C NMR (CD$_3$OD, 600 MHz) see Table S3; HRESI(+)MS m/z 387.2530 (M+H)$^+$ (calcd for C$_{24}$H$_{34}$O$_4$, 387.2527). Zorbax C$_{18}$ column, 250 × 9.4 mm, 5 μm, 3.5 mL/min, gradient from 10-100% MeCN/ H$_2$O over 25 min, t_R = 14.4 min (Appendix Figure S3). Yield: 13.7%

resibufagenin (4a): white solid; $[\alpha]^{21}_D$ +37.3 (*c* 0.15, CHCl$_3$); ^{1}H and ^{13}C NMR (CD$_3$OD, 600 MHz) see Table S4; HRESI(+)MS m/z 407.2190 (M+Na)$^+$ (calcd for C$_{24}$H$_{32}$O$_4$, 407.2193). Zorbax C$_{18}$ column, 250 × 9.4 mm, 5 μm, 3.5 mL/min, gradient from 10-100% MeCN/ H$_2$O over 25 min, t_R = 15.2 min (Appendix Figure S17). Yield: 1.5%

hellebrigenin (5a): white solid; $[\alpha]^{21}_D$ +13.2 (c 0.05, CHCl$_3$) (Reported: +19.8 (c 1.074, CHCl$_3$); ^{1}H and ^{13}C NMR (CD$_3$OD, 600 MHz) see Table S5; HRESI(+)MS m/z 417.2272 (M+H)$^+$ (calcd for C$_{24}$H$_{32}$O$_6$, 417.2269). Zorbax C$_{18}$ column, 250 × 9.4 mm, 5 µm, 3.5 mL/min, gradient from 10-100% MeCN/ H$_2$O over 25 min, t$_R$ = 9.7 min (Appendix Figure S4). Yield: 0.7%

bufalin-3-acetate (7a): white solid; $[\alpha]^{21}_D$ +11.9 (c 0.095, CHCl$_3$) (Reported: −7.5 (c 1.1, CHCl$_3$); ^{1}H and ^{13}C NMR (CD$_3$OD, 600 MHz) see Table S6; HRESI(+)MS m/z 429.2272 (M+H)$^+$ (calcd for C$_{26}$H$_{34}$O$_6$, 429.2268). Zorbax C$_{18}$ column, 250 × 9.4 mm, 5 µm, 3.5 mL/min, gradient from 10-100% MeCN/ H$_2$O over 25 min, t$_R$ = 14.3 min (Appendix Figure S5). Yield: 0.6%

2.4.3 Synthesis of bufagenin esters

2.4.3.1 Synthesis of bufalin-3-suberate

A solution of bufalin (100 mg, 0.259 mmol), suberic anhydride (121 mg, 0.777 mmol) and 4-(dimethylamino)pyridine (32.2 mg, 0.259 mmol) in CH$_2$Cl$_2$ (3 mL) stirred for 3 h at 60 °C. The reaction mixture was later dried under a stream of N$_2$ at 40 °C and re-dissolved in MeOH for purification using a SPE C$_{18}$ cartridge. The purification was performed using a stepwise gradient of 20-100% MeOH/H$_2$O. Bufalin-3-suberate (**3b**) was collected in the 60% MeOH/H$_2$O fraction, dried under a stream of N$_2$ at 40 °C and purified by semi-preparative HPLC-DAD (Zorbax SB C$_{18}$ column, 250 × 9.4 mm, 5 µm, 3.5 mL/min, gradient from 90% H$_2$O/MeCN to 100% MeCN over 25 min, hold at 100% MeCN for 5 min, with isocratic 0.01% modifier (TFA)). Yield 67 mg.

^{1}H NMR (CD$_3$OD, 600 MHz) δ_H 0.72 (s, H-18), 0.98 (s, H-19), 1.65 (m, H-9), 1.73 (m, H-8), 2.28 (t, J = 14.9, 7.5 Hz, H-7′), 2.33 (t, J = 7.3 Hz, H-2′), 6.28 (dd, J = 9.7, 0.8 Hz, H-23), 7.43 (dd, J = 2.5, 0.9 Hz, H-21), 7.99 (dd, J = 9.7, 2.6 Hz, H-22) ppm.

bufalin-3-suberate (3b): white solid; $[\alpha]^{21}_D$ −9.3 (c 0.2, CHCl$_3$); ^{1}H NMR (CD$_3$OD, 600 MHz); HRESI(+)MS m/z 543.3313 (M+H)$^+$ (calcd for C$_{32}$H$_{46}$O$_7$, 543.3311) (Appendix Figure S8).

2.4.3.2 Synthesis of bufalin-3-pimelate

Bufalin-3-pimelate (was also synthesized and purified based on the above mentioned method except for the reactants, bufalin (10 mg, 0.026 mmol), pimelic anhydride (11 mg, 0.078 mmol) and 4-(dimethylamino)pyridine (3.2 mg, 0.026 mmol) to yield 5.8 mg.

^{1}H NMR (CD$_3$OD, 600 MHz) δ_H 0.72 (s, H-18), 0.98 (s, H-19), 1.64 (m, H-9), 1.73 (m, H-8), 2.27 (t, J = 7.5 Hz, H-7′), 2.33 (t, J = 7.4 Hz, H-2′), 6.28 (d, J = 9.7 Hz, H-23), 7.43 (d, J = 2.2 Hz, H-21), 7.99 (dd, J = 9.7, 2.5 Hz, H-22) ppm.

bufalin-3-pimelate (7b): white solid; $[\alpha]^{21}_D$ −7.1 (c 0.06, CHCl$_3$); ^{1}H NMR (CD$_3$OD, 600 MHz); HRESI(+)MS m/z 551.2992 (M+Na)$^+$ (calcd for C$_{31}$H$_{44}$O$_7$, 551.2979) (Appendix Figure S26).

2.4.3.3 Synthesis of bufalin-3-acetate

Bufalin-3-acetate was also synthesized and purified based on the above mentioned method except for the reactants, bufalin (10 mg, 0.026 mmol), acetic anhydride (8 mg, 0.078 mmol) and 4-(dimethylamino)pyridine (3.2 mg, 0.026 mmol) to yield 8.2 mg. (Appendix Figure S6, Table S5)

2.4.3.4 Synthesis of telocinobufagenin-3-suberate

A solution of telocinobufagenin (100 mg, 0.25 mmol), suberic anhydride (116 mg, 0.74 mmol) and 4-(dimethylamino)pyridine (30.6 mg, 0.25 mmol) in CH_2Cl_2 stirred for 3 h at 60 °C with constant stirring. The reaction mixture was later dried under a stream of N_2 at 40 °C and was re-dissolved in methanol for purification using a SPE C_{18} cartridge. The purification was performed using a stepwise gradient of 20-100% methanol/water. Telocinobufagenin-3-suberate was collected at 80% methanol fraction, dried under a stream of N_2 at 40 °C and was purified using semi-preparative HPLC-DAD (Zorbax SB C_{18} column, 250 × 9.4 mm, 5 μm, 3.5 mL/min, gradient from 90% H_2O/MeCN to 100% MeCN over 25 min, hold at 100% MeCN for 5 min, with isocratic 0.01% modifier (TFA)). Yield 86 mg.

^1H NMR (CDCl$_3$, 600 MHz) δ_H 0.69 (s, H-18), 0.99 (s, H-19), 1.66 (m, H-9), 1.98 (d, $J = 2.9$ Hz, H-15a), 2.18 (ddd, $J = 12.4, 8.7, 3.7$ Hz, H-7′), 2.32 (dd, $J = 15.4, 7.9$ Hz, H-2′), 6.25 (d, $J = 9.8$ Hz, H-23), 7.21 (dd, $J = 2.3, 0.9$ Hz, H-21), 7.90 (dd, $J = 9.7, 2.6$ Hz, H-22) ppm.

Telocinobufagenin-3-suberate (2b): white solid; $[\alpha]^{21}_D$ +17.3 (c 0.07, CHCl$_3$); ^1H NMR (CDCl$_3$, 600 MHz); HRESI(+)MS m/z 581.3109 (M+H)$^+$ (calcd for $C_{34}H_{44}O_8$, 581.3108) (Appendix Figure S7).

2.4.3.5 Synthesis of marinobufagenin-3-suberate

A solution of marinobufagenin (200 mg, 0.500 mmol), suberic anhydride (156 mg, 1.00 mmol) and 4-(dimethylamino)pyridine (61 mg, 0.50 mmol) in CH_2Cl_2 (5 mL) stirred for 3 h at 60 °C. The reaction mixture was later dried under a stream of N_2 at 40 °C and was re-dissolved in acetonitrile for purification using a SPE C_{18} cartridge. The purification was performed using a stepwise gradient of 20-100% acteonitrile/water. Marinobufagenin-3-suberate (**1b**) was collected at 60% acetonitrile fraction, dried under a stream of N_2 at 40 °C and was purified using semi-preparative HPLC-DAD (Zorbax SB C_{18} column, 250 × 9.4 mm, 5 μm, 3.5 mL/min, gradient from 90% H_2O/MeCN to 100% MeCN over 25 min, holding 100% MeCN for 5 min, isocratic 0.01% TFA). Yield 156 mg.

^1H NMR (CD$_3$OD, 600 MHz) δ_H 0.79 (s, H-18), 0.99 (s, H-19), 1.65 (m, H-9), 2.01 (td, $J = 12.1, 3.9$ Hz, H-8), 2.29 (t, $J = 7.4$ Hz, H-7′), 2.36 (ddd, $J = 10.3, 7.6, 2.7$ Hz, H-2′), 6.27 (dd, $J = 9.8, 0.8$ Hz, H-23), 7.45 (d, $J = 2.2$ Hz, H-21), 7.90 (dd, $J = 9.7, 2.5$ Hz, H-22) ppm.

marinobufagenin-3-suberate (1b): white solid; $[\alpha]^{21}_D$ +27.3 (*c* 0.1, CHCl$_3$); ^{1}H NMR (CD$_3$OD, 600 MHz); HRESI(+)MS m/z 557.3109 (M+H)$^+$ (calcd for C$_{32}$H$_{44}$O$_8$, 557.3104) (Appendix Figure S6).

2.4.3.6 Synthesis of marinobufagenin-3-pimelate

Marinobufagenin-3-pimelate (**5b**) was synthesized and purified based on the above mentioned method except for the reactants, marinobufagenin (20 mg, 0.05 mmol), pimelic anhydride (14 mg, 0.10 mmol) and 4-(dimethylamino)pyridine (6.1 mg, 0.05 mmol) to yield 14.6 mg.

^{1}H NMR (CD$_3$OD, 600 MHz) δ_H 0.79 (s, H-18), 0.99 (s, H-19), 1.64 (m, H-9), 2.01 (td, *J* = 12.2, 4.2 Hz, H-8), 2.32 (t, *J* = 7.5 Hz, H-2′), 2.35 (ddd, *J* = 10.1, 7.5, 2.8 Hz, H-7′), 6.26 (d, *J* = 9.8 Hz, H-23), 7.45 (d, *J* = 2.3 Hz, H-21), 7.90 (dd, *J* = 9.7, 2.3 Hz, H-22) ppm.

marinobufagenin-3-pimelate (5b): white solid; $[\alpha]^{21}_D$ +27.8 (*c* 0.1, CHCl$_3$); ^{1}H NMR (CD$_3$OD, 600 MHz); HRESI(+)MS m/z 543.2778 (M+H)$^+$ (calcd for C$_{31}$H$_{42}$O$_8$, 543.2776) (Appendix Figure S21).

2.4.3.7 Synthesis of marinobufagenin-3-succinate

Marinobufagenin-3-succinate (**9b**) was synthesized and purified based on the above mentioned method except for the reactants, marinobufagenin (20 mg, 0.05 mmol), succinic anhydride (10 mg, 0.10 mmol) and 4-(dimethylamino)pyridine (6.1 mg, 0.05 mmol) to yield 18.6 mg.

^{1}H NMR (CD$_3$OD, 600 MHz) δ_H 0.79 (s, H-18), 0.99 (s, H-19), 1.66 (m, H-9), 2.01 (td, *J* = 12.2, 4.0 Hz, H-8), 2.33 (dd, *J* = 15.8, 3.8 Hz, H-7′), 2.56 (m, H-2′), 6.27 (d, *J* = 9.8 Hz, H-23), 7.45 (d, *J* = 2.1 Hz, H-21), 7.90 (dd, *J* = 9.9, 2.4 Hz, H-22) ppm.

marinobufagenin -3-succinate (9b): white solid; $[\alpha]^{21}_D$ −85.9 (*c* 0.05, CHCl$_3$); ^{1}H NMR (CD$_3$OD, 600 MHz); HRESI(+)MS m/z 523.2313 (M+Na)$^+$ (calcd for C$_{28}$H$_{36}$O$_8$, 523.2302) (Appendix Figure S20).

2.4.3.8 Synthesis of marinobufagenin-3-acetate

Marinobufagenin-3-acetate (**8b**) was synthesized based on the above mentioned method except for the reactants, marinobufagenin (20 mg, 0.05 mmol), acetic anhydride (10.2 mg, 0.10 mmol) and 4-(dimethylamino)pyridine (6.1 mg, 0.05 mmol) to yield 17.7 mg.

^{1}H NMR (CD$_3$OD, 600 MHz) δ_H 0.79 (s, H-18), 0.99 (s, H-19), 2.05 (s, H-26), 2.59 (d, *J* =10.4 Hz, H-17), 3.62 (br s, H-15), 6.27 (dd, *J* =9.8, 0.7 Hz, H-23), 7.45 (d, *J* = 1.9 Hz, H-21), 7.90 (d, *J* = 1.9 Hz, H-22) ppm.

marinobufagenin-3-acetate (8b): white solid; $[\alpha]^{21}_D$ +79.9 (*c* 0.06, CHCl$_3$) (Reported: +24.1 (*c* 1.059, CHCl$_3$); ^{1}H NMR (CD$_3$OD, 600 MHz); HRESI(+)MS m/z 465.2255 (M+Na)$^+$ (calcd for C$_{26}$H$_{34}$O$_6$, 465.2248) (Appendix Figure S22).

2.4.4 Synthesis of bufotoxins

2.4.4.1 Synthesis of bufalitoxin

A solution of bufalin-3-suberate (100 mg, 0.184 mmol) in THF (8 mL) containing triethylamine (0.14 mL) was stirred for 15 min at −10 °C followed by the addition of isobutylchloroformate (0.05 mL) in THF (1 mL) and stirring was continued for further 40 min. Methanol (1 mL) was added to the reaction mixture followed by dropwise addition of freshly prepared L-arginine monohydrochloride solution (77 mg, 0.37 mmol) in a mixture of water (0.4 mL) and methanol (4 mL) over 3 min. Stirring was continued for another 3 h at −5 °C to 0 °C. The reaction mixture was then concentrated under reduced pressure yielded an oily residue, which was purified using HPLC (Zorbax SB C_{18} column, 250 × 9.4 mm, 5 μm, 3.5 mL/min, gradient from 90% H_2O/MeCN to 100% MeCN over 25 min, hold at 100% MeCN for 5 min, t_R = 11.5 min). Yield 82 mg.

bufalitoxin (3c): white solid; $[\alpha]^{21}_D$ −5.8 (*c* 0.05, MeOH) (Reported: −5.2 (*c* 0.2, MeOH); ^1H and ^{13}C NMR (CD_3OD, 600 MHz) see Table S9; HRESI(+)MS m/z 699.4327 $(M+H)^+$ (calcd for $C_{37}H_{56}N_4O_8$, 699.4318) (Appendix Figure S11).

2.4.4.2 Synthesis of bufalin pimeloyl-L-arginine

A solution of bufalin-3-pimelate (10 mg, 0.02 mmol) in THF (2 mL) containing triethylamine (0.02 mL) was stirred for 15 min at −10 °C followed by the addition of isobutylchloroformate (0.01 mL) in THF (0.2 mL) and stirring was continued for further 40 min. Methanol (0.2 mL) was added to the reaction mixture followed by dropwise addition of freshly prepared L-arginine monohydrochloride solution (7.7 mg, 0.04 mmol) in a mixture of water (0.1 mL) and methanol (0.9 mL) over 3 min. Stirring was continued for another 3 h at −5 °C to 0 °C. The reaction mixture was then concentrated under reduced pressure yielded an oily residue, which was purified using HPLC (Zorbax SB C_{18} column, 250 × 9.4 mm, 5 μm, 3.5 mL/min, gradient from 90% H_2O/MeCN to 100% MeCN over 25 min, hold at 100% MeCN for 5 min, t_R = 10.9 min). Yield 7.3 mg.

bufalin pimeloyl-L-arginine (9c): white solid; $[\alpha]^{21}_D$ +7.3 (*c* 0.07, MeOH) (Reported: −5.5 (*c* 0.18, $CHCl_3$); ^1H and ^{13}C NMR (CD_3OD, 600 MHz) see Table S10; HRESI(+)MS m/z 685.4172 $(M+H)^+$ (calcd for $C_{37}H_{56}N_4O_8$, 685.4171) (Appendix Figure S23).

2.4.4.3 Synthesis of telocinobufotoxin

A solution of telocinobufagenin-3-suberate (100 mg, 0.179 mmol) in THF (8 mL) containing triethylamine (0.14 mL) was stirred for 15 min at −10 °C followed by the addition of isobutylchloroformate (0.05 mL) in THF (1 mL) and stirring was continued for further 40 min. Methanol (1 mL) was added to the reaction mixture followed by dropwise addition of freshly prepared L-arginine monohydrochloride solution (75 mg, 0.36 mmol) in a mixture of water (0.4 mL) and methanol (4 mL) over 3 min. Stirring was continued for another 3 h at −5 °C to 0 °C. The

reaction mixture was then concentrated under reduced pressure yielded an oily residue, which was purified using HPLC (Zorbax SB C_{18} column, 250 × 9.4 mm, 5 μm, 3.5 mL/min, gradient from 90% H_2O/MeCN to 100% MeCN over 25 min, hold at 100% MeCN for 5 min, t_R = 10.1 min). Yield 81 mg.

telocinobufotoxin (2c): white solid; $[\alpha]^{21}_D$ +14.0 (c 0.05, MeOH); ^{1}H and ^{13}C NMR (CD$_3$OD, 600 MHz) see Table S8; HRESI(+)MS m/z 715.4327 (M+H)$^+$ (calcd for $C_{38}H_{58}N_4O_9$, 715.4320) (Appendix Figure S10).

2.4.4.4 Synthesis of marinobufotoxin

A solution of marinobufagenin-3-suberate (100 mg, 0.182 mmol) in THF (8 mL) containing triethylamine (0.14 mL) was stirred for 15 min at −10 °C followed by the addition of isobutylchloroformate (0.05 mL) in THF (1 mL) and stirring was continued for further 40 min. Methanol (2 mL) was added to the reaction mixture followed by dropwise addition of freshly prepared L-arginine monohydrochloride solution (75 mg, 0.36 mmol) in a mixture of water (0.4 mL) and methanol (4 mL) over 3 min. Stirring was continued for another 3 h at −5 °C to 0 °C. The reaction mixture was then concentrated under reduced pressure yielded an oily residue, which was purified using HPLC (Waters C_{18} column, 150 × 19 mm, 7 μm, 10 mL/min, gradient from 90% H_2O/MeCN to 100% MeCN over 25 min, hold at 100% MeCN for 5 min, t_R = 9.7 min). Yield 77 mg.

marinobufotoxin (1c): white solid; $[\alpha]^{21}_D$ +14.6 (c 0.1, MeOH); ^{1}H and ^{13}C NMR (CD$_3$OD, 600 MHz) see Table S7; HRESI(+)MS m/z 713.4120 (M+H)$^+$ (calcd for $C_{38}H_{56}N_4O_9$, 713.4116) (Appendix Figure S9).

2.4.4.5 Synthesis of marinobufagenin pimeloyl-L-arginine

A solution of marinobufagenin-3-pimelate (10 mg, 0.02 mmol) in THF (2 mL) containing triethylamine (0.02 mL) was stirred for 15 min at −10 °C followed by the addition of isobutylchloroformate (0.01 mL) in THF (0.2 mL) and stirring was continued for further 40 min. Methanol (0.2 mL) was added to the reaction mixture followed by dropwise addition of freshly prepared L-arginine monohydrochloride solution (7.7 mg, 0.04 mmol) in a mixture of water (0.1 mL) and methanol (0.9 mL) over 3 min. Stirring was continued for another 3 h at −5 °C to 0 °C. The reaction mixture was then concentrated under reduced pressure yielded an oily residue, which was purified using HPLC (Zorbax SB C_{18} column, 250 × 9.4 mm, 5 μm, 3.5 mL/min, gradient from 90% H_2O/MeCN to 100% MeCN over 25 min, hold at 100% MeCN for 5 min, t_R = 9.1 min). Yield 6.8 mg.

marinobufagenin pimeloyl-L-arginine (8c): white solid; $[\alpha]^{21}_D$ +18.4 (c 0.05, MeOH) (Reported: +22 (c 0.23, MeOH); ^{1}H and ^{13}C NMR (CD$_3$OD, 600 MHz) see Table S11; HRESI(+)MS m/z 699.3971 (M+H)$^+$ (calcd for $C_{37}H_{54}N_4O_9$, 699.3964) (Appendix Figure S24).

2.4.5 Synthesis of amides

2.4.5.1 Synthesis of suberic anhydride

A solution of suberic acid (1.0 g, 5.7 mmol) in acetic anhydride (5 mL) was heated at reflux for 4 h with constant stirring. The reaction mixture was then reduced *in vacuo* at 40 °C which yielded a pale yellow solid. Recrystallization from hexane/ethyl acetate yielded 750 mg (75%) of suberic anhydride.

2.4.5.2 Synthesis of pimelic anhydride

A solution of pimelic acid (1.0 g, 6.2 mmol) in acetic anhydride (5 mL) was heated at reflux for 4 h with constant stirring. The reaction mixture was then reduced *in vacuo* at 40 °C which yielded a pale yellow solid. Recrystallization from hexane/ethyl acetate yielded 640 mg (64%) of pimelic anhydride.

2.4.5.3 Synthesis of suberoyl-L-arginine

A solution of suberic anhydride (52 mg, 0.33 mmol) and L-arginine monohydrochloride (69 mg, 0.33 mmol) in water was prepared and the pH of the solution was adjusted to 8 − 9 using NaOH (40% w/v) and was left stirring overnight at room temperature. The reaction mixture was dried under a stream of N_2 at 40 °C and purification was performed using ion-exchange chromatography (Dowex 50WX2, strong cation exchange resin, 200-400 dry mesh, 1 mL/min) with a linear gradient of 0 – 2 M HCl. Pure arginyl amide eluted from 0.9 – 2 M HCl to yield 70 mg.

suberoyl-L-arginine (1d): colourless oil ; $[\alpha]^{21}_D$ +2.1 (*c* 0.08, MeOH); ^{1}H and ^{13}C NMR (CD$_3$OD, 600 MHz) see Table S12; HRESI(+)MS m/z 331.1969 (M+H)$^+$ (calcd for $C_{14}H_{27}N_4O_5$, 331.1968) (Appendix Figure S14).

2.4.5.4 Synthesis of pimeloyl-L-arginine

A solution of pimelic anhydride (50 mg, 0.35 mmol) and L-arginine monohydrochloride (73 mg, 0.35 mmol) in water was prepared and the pH of the solution was adjusted to 8 – 9 using NaOH (40% wt/vol) and was left stirring overnight at room temperature. The reaction mixture was dried under a stream of N_2 at 40 °C and purification was performed using ion-exchange chromatography (Dowex 50WX2, strong cation exchange resin, 200-400 dry mesh, 1 mL/min) with a linear gradient of 0 – 2 M HCl. Pure arginyl amide eluted from 0.9 – 2 M HCl to yield 71 mg.

pimeloyl-L-arginine (3d): colourless oil ; $[\alpha]^{21}_D$ −5.9 (*c* 0.08, MeOH); ^{1}H and ^{13}C NMR (CD$_3$OD, 600 MHz) see Table S14; HRESI(+)MS m/z 339.1637 (M+Na)$^+$ (calcd for $C_{13}H_{24}N_4O_5Na$, 339.1635) (Appendix Figure S13).

2.4.5.5 Synthesis of azeloyl-L-arginine

A solution of azelaic anhydride (57 mg, 0.33 mmol) and L-arginine monohydrochloride (69 mg, 0.33 mmol) in water was prepared and the pH of the solution was adjusted to 8 – 9 using NaOH (40% wt/vol) and was left stirring overnight at room temperature. The reaction mixture was dried under a stream of N_2 at 40 °C and purification was performed using ion-exchange chromatography (Dowex 50WX2, strong cation exchange resin, 200-400 dry mesh, 1 mL/min) with a linear gradient of 0 – 2 M HCl. Pure arginyl amide eluted from 0.9 – 2 M HCl to yield 69 mg.

azeloyl-L-arginine (4d): colourless oil ; $[\alpha]^{21}_D$ −1.8 (*c* 0.05, MeOH); ^{1}H and ^{13}C NMR (CD$_3$OD, 600 MHz) see Table S13; HRESI(+)MS m/z 345.2144 (M+H)$^+$ (calcd for $C_{15}H_{29}N_4O_5$, 345.2142) (Appendix Figure S15).

2.4.5.6 Synthesis of adipoyl-L-arginine

A solution of adipic anhydride (42 mg, 0.33 mmol) and L-arginine monohydrochloride (69 mg, 0.33 mmol) in water (5 mL) adjusted to pH 8 – 9 using NaOH (40% wt/vol) was stirred overnight at room temperature. The reaction mixture was then dried under a stream of N_2 at 40 °C and purification was performed using ion-exchange chromatography (Dowex 50WX2, strong cation exchange resin, 200-400 dry mesh, 1 mL/min) with a linear gradient of 0 – 2 M HCl to yield adipoyl-L-arginine (**2d**) (67 mg).

adipoyl-L-arginine (2d): colourless oil ; $[\alpha]^{21}_D$ −6.4 (*c* 0.05, MeOH); ^{1}H and ^{13}C NMR (CD$_3$OD, 600 MHz) see Table S15; HRESI(+)MS m/z 303.1305 (M+H)$^+$ (calcd for $C_{12}H_{23}N_4O_5$, 303.1302) (Appendix Figure S12).

2.4.6 Synthesis of derivatized amide standards

A known amount of pure arginyl amide (10 mg) was subjected to derivatization with 2,4-pentanedione and pyridine (2:1) for a period of 12 h at reflux. The reaction mixture was later dried under a stream of N_2 at 40 °C and was subjected to purification by HPLC (Zorbax C_{18} Semi-prep column, 250 × 9.4 mm, 5 μm, 3.0 mL/min, gradient from 10-100% MeCN over 25 min).

Derivatized adipoyl-L-arginine (2e): ^{1}H NMR (CD$_3$OD, 600 MHz) δ_H 1.65 (m, H-3), 1.67 (m, H-10), 2.28 (t, *J* = 13.8 Hz, H-5), 2.31 (t, *J* = 13.8 Hz, H-2), 2.40 (s, H-12), 3.52 (m, H-11), 4.46 (m, H-7), 6.64 (s, H-13) ppm. Yield: 9 mg (Appendix Figure S19). Slight brownish oil; $[\alpha]^{21}_D$ +1.6 (*c* 0.05, MeOH); HRESI(+)MS m/z 367.1976 (M+H)$^+$ (calcd for $C_{17}H_{26}N_4O_5$, 367.1976).

Derivatized pimeloyl-L-arginine (3e): ^{1}H NMR (CD$_3$OD, 600 MHz) δ_H 1.63 (m, H-3), 2.26 (m, H-2, H-6), 2.30 (s, H-13, H-15), 3.44 (m, H-12), 4.44 (m, H-8), 6.45 (s, H-14) ppm. Yield: 7.2 mg (Appendix Figure S25). Slight brownish oil; $[\alpha]^{21}_D$ +2.8 (*c* 0.06, MeOH); HRESI(+)MS m/z 381.2132 (M+H)$^+$ (calcd for $C_{18}H_{28}N_4O_5$, 381.2132).

Derivatized suberoyl-L-arginine (1e): ^{1}H NMR (CD$_3$OD, 600 MHz) δ$_H$ 1.60 (m, H-3), 1.67 (m, H-12), 2.17 (m, H-7), 2.20 (m, H-2), 2.40 (s, H-14), 3.49 (m, H-13), 4.46 (m, H-9), 6.64 (s, H-15) ppm. Yield: 8.3 mg (Appendix Figure S16). Slight brownish oil; [α]$^{21}_D$ +2.3 (c 0.09, MeOH); HRESI(+)MS m/z 395.2289 (M+H)$^+$ (calcd for C$_{19}$H$_{30}$N$_4$O$_5$, 395.2289).

Derivatized azeloyl-L-arginine (4e): ^{1}H NMR (CD$_3$OD, 600 MHz) δ$_H$ 1.60 (m, H-3), 1.66 (m, H-13), 2.28 (m, H-8), 2.32 (m, H-2), 2.40 (s, H-15), 3.49 (m, H-14), 4.42 (m, H-10), 6.64 (s, H-16) ppm. Yield: 8.8 mg (Appendix Figure S18). Slight brownish oil; [α]$^{21}_D$ +4.4 (c 0.08, MeOH); HRESI(+)MS m/z 409.2460 (M+H)$^+$ (calcd for C$_{20}$H$_{32}$N$_4$O$_5$, 409.2458).

2.4.7 Analytical methodology for detection of various structure classes of cane toad toxins

Table 2.4 Analytical methods for the detection of bufadienolides and amides

	Method	Structure class	Conditions
HPLC-DAD	Method 1	bufagenins	Zorbax C$_{18}$ column, 150 × 4.6 mm, 5 μm, 1 mL/min, gradient from 90% H$_2$O/ MeCN to 100% MeCN over 15 min, hold at 100% MeCN over 5 min, with constant 0.01% modifier (TFA).
HPLC-DAD	Method 2	bufotoxins	Zorbax C$_{18}$ column, 150 × 4.6 mm, 5 μm, 1 mL/min, gradient from 90-50% H$_2$O/ MeCN over 15 min, 50-30% H$_2$O/ MeCN over 5 min, 30% H$_2$O/ MeCN to 100% MeCN over 5 min, hold at 100% MeCN for 5 min, with constant 0.01% modifier (TFA).
HPLC-DAD-MS	Method 3a	amides	Zorbax C$_{18}$ column, 150 × 4.6 mm, 5 μm, 1 mL/min, gradient from 90% H$_2$O/ MeCN to 70% H$_2$O/ MeCN over 20 min, 90% H$_2$O/ MeCN – 100% MeCN over 2 min, hold at 100% MeCN over 3 min, with constant 0.01% modifier (TFA).
HPLC-DAD	Method 3b	amides	Zorbax C$_{18}$ column, 150 × 4.6 mm, 5 μm, 1 mL/min, gradient from 90% H$_2$O/ MeCN to 70% H$_2$O/ MeCN over 20 min, 90% H$_2$O/ MeCN – 100% MeCN over 2 min, hold at 100% MeCN over 3 min, with constant 0.01% modifier (TFA).

2.4.8 Derivatization of amides from parotoid toxin/secretion as pyrimidines

Parotoid glands from 10 frozen toads were dissected and manually disrupted in a beaker containing ethyl acetate to release all the secretions. The organic layer was collected and distilled water was added to the left over parotoid gland fractions and sonicated for 5 min. The aqueous extract was collected and was reduced to dryness under a stream of N_2. The left over residue was heated at reflux with pyridine and 2,4-pentanedione for 7 h. The reaction mixture was then reduced to dryness under a stream of N_2 at 40 °C. The residues were redissolved in methanol (1 mg/mL), filtered using 0.45 μm PTFE filter and was analysed using HPLC-DAD.

2.5 Appendix

Table S1 NMR (CD$_3$OD, 600 MHz) data for marinobufagenin (**1a**)
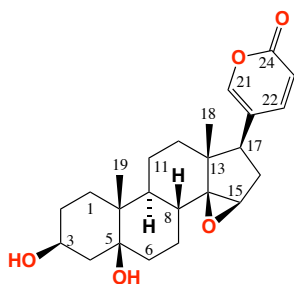
Pos.	Experimental data δ_H (m, J in Hz)	δ_C	Literature data[a] $\delta_C{}^a$	δ_H (m, J in Hz)^a
1a	1.83 (ddd, 14.5, 14.5, 4.1)	26.2	26.2	1.83 (ddd, 14.3, 14.3 3.9),
1b				1.41*
2a	1.67*	28.6	28.7	1.67*, 1.58*
2b	1.58*			
3	4.12 (m)	69.2	69.2	4.13 (m)
4a	2.22 (dd, 14.9, 3.2)	37.8	37.9	2.22 (dd, 14.8, 3.2)
4b	1.79 (m)			1.79*
5		75.9	76.2	-
6a		35.3	35.3	1.68*
6b	1.31 (ddd, 13.1, 4.1, 3.1)			1.31 (ddd, 13.2, 4.1, 3.0)
7a	1.62*	24.1	24.1	1.61*
7b	0.99 (m)			0.99 (m)
8	2.01 (td, 12.3, 3.9)	33.9	34.3	2.00 (ddd, *12.1, 12.1, 3.1*)
9	1.65*	43.9	44.0	1.65*
10		42.1	42.2	-
11a	1.60*	22.8	22.8	1.60*
11b				1.41*
12a		40.3	40.3	1.71*
12b	1.51 (m)			1.51*
13		46.3	46.3	-
14		76.2	75.9	-
15	3.60 (br s)	61.3	61.3	3.60 (br s)
16a	2.43 (ddd, 15.4, 10.1, 1.3)	33.3	33.3	2.42 (ddd, 15.4, 10.1, 1.4)
16b	1.94 (d, 15.4)			1.94 (d, 15.4)
17	2.59 (d, 10.1)	48.6	48.6	2.60 (d, *10.1*)
18	0.78 (s)	17.2	17.2	0.78 (s)
19	0.92 (s)	17.4	17.4	0.92 (s)
20		124.6	124.6	-
21	7.45 (dd, 2.5, 0.8)	151.9	151.9	7.45 (dd, 2.5, 0.8)
22	7.90 (dd, 9.7, 2.5)	149.6	149.7	7.90 (dd, 9.7, 2.5)
23	6.26 (dd, 9.7, 0.9)	115.5	115.5	6.26 (dd, 9.7, 0.8)
24		164.6	164.6	-

δ_H 1.4 – 1.9 – overlapping resonances

* – J coupling constants could not be determined due to overlap with other signals

[a] – structure comparison with the published literature, NMR (600 MHz, CD$_3$OD)[11]

Table S2 NMR (600 MHz, CD$_3$OD) data for telocinobufagenin (**2a**)
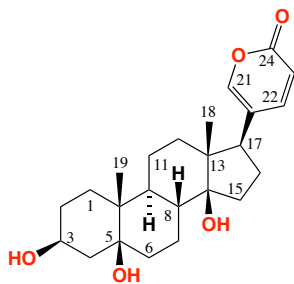
Pos.	Experimental data δ_H (m, *J* in Hz)	δ_C	Literature data[a] $\delta_C{}^a$	δ_H (m, *J* in Hz)[a]
1a	1.83 (ddd, 14.5, 14.5, 4.1)	26.3	26.0	1.80
1b				1.38
2a	1.67*	28.6	28.3	1.69
2b	1.58 (m)			1.58
3	4.13 (m)	69.2	68.8	4.13 (m)
4a		37.9	37.5	2.21
4b				1.49
5		76.3	76.0	
6a		36.1	35.8	1.73
6b				1.38
7a	1.95 (m)	24.9	24.6	1.95
7b	1.25 (m)			1.26
8	1.65*	42.1[b1]	41.8	1.65
9	1.62 (d, 3.21)	40.5	40.1	1.62
10		42.2[b1]	41.7	
11a		23.2	22.8	1.49
11b	1.28 (m)			1.28
12a	1.53 (m)	42.1[b1]	41.8	1.53
12b	1.46*			1.45
13		49.7	49.5	
14		86.2	85.9	
15a	2.07 (dd, 9.4, 2.2)	33.3	32.9	2.07
15b	1.70*			1.70
16a		29.9	29.5	2.19
16b				1.73
17	2.56 (d, 10.3)	52.3	51.9	2.56
18	0.71 (s)	17.4[b2]	17.0	0.71
19	0.93 (s)	17.4[b2]	17.1	0.93
20		125.2	124.8	
21	7.43 (d, 2.5)	151.6	150.2	7.43
22	7.99 (dd, 9.7, 2.5)	149.5	149.1	7.99
23	6.28 (dd, 9.7, 0.9)	115.5	115.2	6.28
24		164.9	164.7	

δ_H 1.2 – 1.8 – overlapping resonances
* – J coupling constants could not be determined due to overlap with other signals
[a] – structure comparison with the published literature, NMR (600 MHz, CD$_3$OD)[7]
[b1,2] – signals are interchangeable

Table S3 NMR (600 MHz, CD$_3$OD) data for bufalin (**3a**)
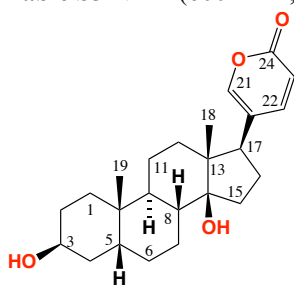
	Experimental data		Literature data[a]	
Pos.	**δ$_H$ (m, *J* in Hz)**	**δ$_C$**	**δ$_C$[a]**	**δ$_H$ (m, *J* in Hz)[a]**
1b		30.9	29.7	1.50
2a	1.62*	28.7	27.9	1.62
2b				1.52
3	4.07 (m)	67.8	66.9	4.16
4a	1.98 (dd, 14.0, 3.1)	34.3	33.4	1.93
4b				1.38
5	1.76*	37.6	36.0	1.77
6a	1.94 (m)	28.1	26.6	1.90
6b	1.27 (m)			1.27
7a	1.81 (m)	22.7[b1]	21.4	1.73
7b				1.29
8	1.64*	43.2	42.5	1.55
9	1.71*	36.6[b2]	35.8	1.62
10		37.0[b2]	35.4	
11a		22.7[b1]	21.5	1.44
11b	1.22 (ddd, 16.1, 12.4, 3.9)			1.21
12a	1.52*	42.1	40.9	1.52
12b				1.37
13		49.9	48.4	
14		86.3	85.5	
15a	2.11 (ddd, 11.6, 9.4, 2.2)	33.3	32.8	2.06
15b	1.71*			1.71
16a	2.20 (ddd, 15.5, 10.3, 1.3)	30.1	28.8	2.20
16b	1.73*			1.75
17	2.56 (d, 10.3)	52.4	51.4	2.49
18	0.73 (s)	17.5	16.6	0.72
19	0.98 (s)	24.5	23.8	0.97
20		125.2	122.7	
21	7.44 (d, 2.5)	150.6	148.6	7.25
22	8.01 (dd, 9.8, 2.6)	149.5	146.8	7.83
23	6.29 (dd, 9.8, 0.9)	115.6	115.4	6.29
24		164.9	162.5	

δ$_H$ 1.2 – 2.0 – overlapping resonances
* – J coupling constants could not be determined due to overlap with other signals
[a] – structure comparison with the published literature, NMR (500 MHz, CD$_3$OD)[12]
[b1,2] – signals are interchangeable

Table S4 NMR (600 MHz, CD$_3$OD) data for resibufagenin (**4a**)
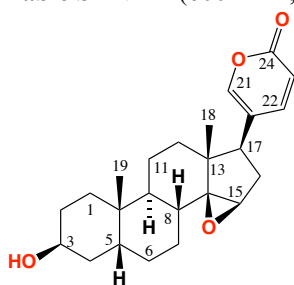
Pos.	Experimental data δ_H (m, *J* in Hz)	δ_C	Literature data[a] $\delta_C{}^a$	δ_H (m, *J* in Hz)[a]
1b		30.9	29.6	1.51
2a	1.62*	28.8	27.9	1.54
2b				
3	4.07 (m)	67.8	66.9	4.13
4a		35.3	33.3	1.88
4b				1.35
5		37.6[b1]	36.0	1.76
6a	1.89 (m)	27.3	25.8	1.85
6b	1.20 (m)			1.20
7a	1.47*	21.9[b2]	20.8	1.50
7b	1.05 (ddd, 17.4, 13.3, 4.3)			0.95
8		35.2	33.6	1.98
9		37.5[b1]	39.4	1.60
10		36.7	35.6	
11a	1.56*	22.4[b2]	21.1	1.51
11b				1.33[c]
12a		40.2	39.5	1.38
12b	1.70 (m)			1.65
13		46.5	45.3	
14		76.0	74.8	
15	3.60 (br s)	61.3	59.9	3.52
16a	2.43 (ddd, 15.4, 10.1, 1.3)	33.4	32.5	2.36
16b	1.94 (m)			1.95
17	2.59 (d, 10.1)	48.6	47.9	2.45
18	0.78 (s)	17.3	16.9	0.78
19	0.99 (s)	24.4	23.8	0.98
20		124.7	122.3	
21	7.45 (dd, 2.5, 0.8)	151.9	149.7	7.23
22	7.90 (dd, 9.7, 2.5)	149.8	147.1	7.78
23	6.26 (dd, 9.7, 0.9)	115.6	115.4	6.24
24		164.7	162.1	

δ_H 1.42 – 2.00 – overlapping resonances

* – J coupling constants could not be determined due to overlap with other signals

[a] – structure comparison with the published literature, NMR (500 MHz, CD$_3$OD)[12]

[b1,2] – signals are interchangeable

82

Table S5 NMR (600 MHz, CD₃OD) data for hellebrigenin (**5a**)
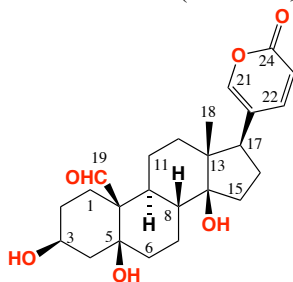
	Experimental data		Literature data[a]	
Pos.	**δ_H (m, J in Hz)**	**δ_C**	**δ_C[a]**	**δ_H (m, J in Hz)[a]**
1a		18.7	18.4	1.70
1b				2.13
2a	1.72*	27.7	27.3	1.72
2b	1.65*			1.67
3	4.14 (m)	68.1	67.7	4.14
4a		38.7	38.4	1.50
4b				2.20
5		75.9	90.1	
6a		37.6	37.2	1.67
6b	2.10 (dd, 14.9, 3.2)			2.10
7a	1.37 (m)	25.4	25.0	1.38
7b				2.15
8	1.95 (dt, 12.6, 3.6)	43.2	42.7	1.95 (dt, 12.6, 3.6)
9	1.70*	40.7	40.3	1.71[c]
10		56.4	55.9	
11a	1.55 (dd, 13.7, 3.4)	23.7	23.4	1.55 (dd, 13.7, 3.4)
11b	1.19 (m)			1.19 (m)
12a	1.42 (m)	41.7	41.3	1.42 (m)
12b				1.51[d]
13		49.6	49.1	
14		85.8	85.3	
15a	2.06 (ddd, 18.2, 14.5, 4.9)	32.5	32.1	2.06 (ddd, 18.2, 14.5, 4.9)
15b	1.67*			1.67[a]
16a		29.9	29.4	2.20[e]
16b	1.74*			1.74[c]
17	2.56 (d, 10.2)	52.1	51.7	2.56 (d, 10.2)
18	0.68 (s)	17.2	17.0	0.68 (s)
19	10.06 (s)	210.3	209.1	10.06 (s)
20		125.2	124.5	
21	7.43 (d, 2.5)	150.7	150.3	7.43 (d, 2.5)
22	7.99 (dd, 9.7, 2.5)	149.4	149.1	7.99 (dd, 9.7, 2.5)
23	6.28 (d, 9.7)	115.6	115.2	6.28 (d, 9.7)
24		164.9	164.3	

δ_H 1.2 – 1.8, 2.1 – 2.4 – overlapping resonances
* – J coupling constants could not be determined due to overlap with other signals
[a] – structure comparison with the published literature, NMR (600 MHz, CD₃OD)[7]

Table S6 NMR (600 MHz, CD$_3$OD) data for bufalin-3-acetate (**7a**)
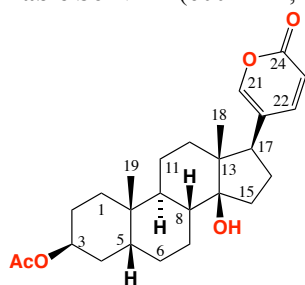
Pos.	δ_H (m, J in Hz)	δ_C
1a	2.01 (m)	31.8[b1]
1b		
2a	1.66*	26.1
2b		
3	5.07 (br t)	72.5
4a		31.7[b1]
4b	1.37 (ddd, 18.9, 15.1, 4.7)	
5	1.68*	38.6
6a	1.93 (m)	27.8
6b		
7a	1.83 (m)	22.7[b2]
7b		
8		43.1
9		36.5[b3]
10		37.1[b3]
11a	1.29*	22.6[b2]
11b	1.23 (ddd, 16.1, 12.4, 3.9)	
12a	1.51 (m)	42.0
12b	1.46*	
13		49.9
14		86.3
15a	2.13 (d, 11.8, 9.4, 2.5)	33.3
15b	1.71*	
16a	2.20 (ddd, 15.4, 10.2, 1.1)	30.0
16b		
17	2.56 (d, 10.2)	52.4
18	0.71 (s)	17.5
19	0.98 (s)	24.4
20		125.2
21	7.44 (d, 2.5)	150.6
22	8.01 (dd, 9.8, 2.6)	149.5
23	6.29 (dd, 9.8, 0.9)	115.6
24		164.9
25		172.7
26	2.03 (s)	21.4

δ_H 1.2 – 1.8 – overlapping resonances
* – J coupling constants could not be determined due to overlap with other signals
[b1-3] – signals are interchangeable
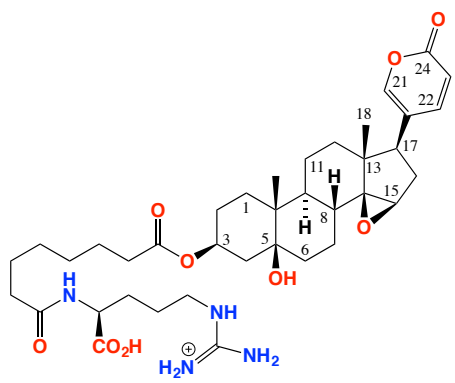
marinobufotoxin (**1c**)
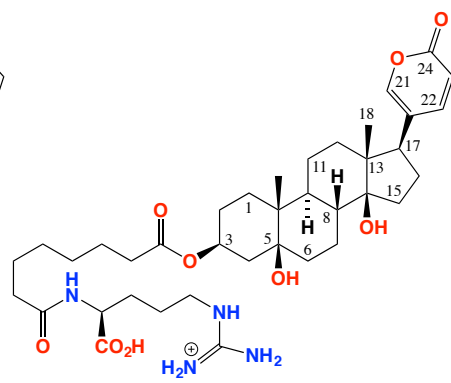
telocinobufotoxin (**2c**)
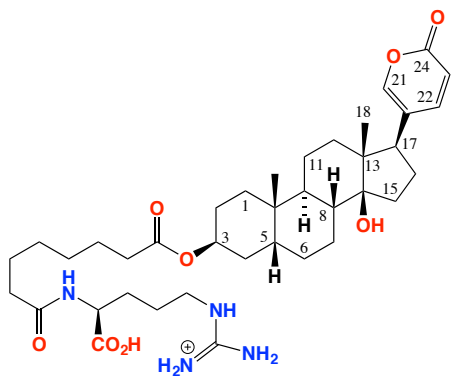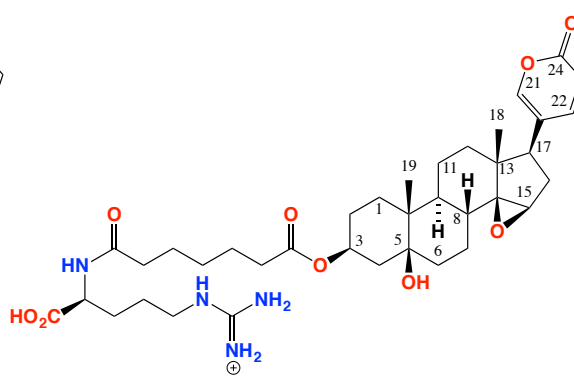
bufalitoxin (**3c**)

marinobufagenin pimeloyl-L-arginine (**8c**)
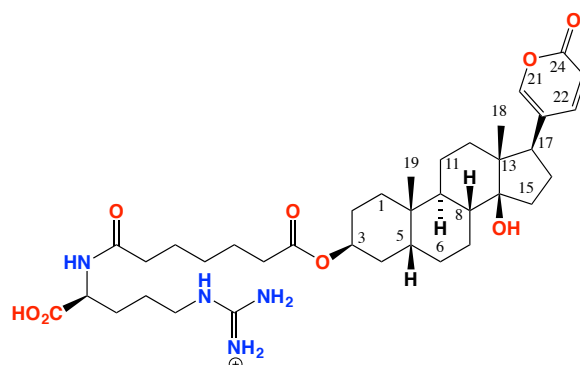
bufalin pimeloyl-L-arginine (**9c**)

Table S7 NMR (CD$_3$OD, 600 MHz) data for marinobufotoxin (**1c**)

Pos.	Experimental data δ$_H$ (m, J in Hz)	δ$_C$	Literature data[a] δ$_C$[a]	δ$_H$ (m, J in Hz)[a]
1a	1.80 (ddd, 14.3, 14.3, 3.5)	26.5[b1]	26.7	1.79 (ddd,14.2, 14.3, 3.5)
1b				1.42*
2a	1.73*	25.9[b1]	25.6	1.74*
2b	1.61*			1.61*
3	5.14 (br t, 2.6)	72.0	72.3	5.14 (m)
4a	2.34 (d, 7.6)	36.3[b2]	36.4	2.34 (dd, 15.4, 4.0)
4b				1.54*
5		74.4	74.5	
6a		35.6[b3]	35.6	1.72*
6b	1.32 (ddd, 13.5, 3.9, 3.2)			1.32(ddd, 13.5, 4.0, 3.1)
7a	1.63*	24.4	24.5	1.63*
7b	0.99 (s)			0.99* (s)
8	2.01 (td, 12.3, 3.9)	33.9	34.2	2.00 (td, 12.3, 3.9)
9	1.66*	43.7	43.7	1.66*
10		42.0[b4]	41.7	
11a	1.56*	22.5	22.5	1.56*
11b				1.42*
12a	1.70*	40.1	40.1	1.70*
12b				1.52 (ddd, 13.3, 13.3, 3.3)
13		46.2	46.2	
14		75.8	75.8	
15	3.61 (br s)	61.2	61.4	3.61 (s)
16a	2.41 (ddd, 15.5, 10.3, 1.3)	33.3	33.3	2.41 (ddd, 15.4, 10.2, 1.3)
16b				1.93*
17	2.59 (d, 10.3)	48.3	48.6	2.59 (d, 10.2)
18	0.78 (s)	17.1[b5]	17.2	0.78 (s)
19	0.98 (s)	17.2[b5]	17.3	0.98 (s)
20		124.6	124.6	
21	7.44 (dd, 2.5, 0.9)	151.4	151.9	7.44 (dd, 2.4, 0.8)
22	7.89 (dd, 9.7, 2.5)	149.6	149.7	7.89 (dd, 9.7, 2.4)
23	6.26 (dd, 9.7, 0.9)	115.4	115.5	6.26 (dd, 9.7, 0.8)
24		164.6	164.6	
1′		175.1[b7]	175.1	
2′	2.35 (t, 7.7)	35.4[b3]	35.5	2.35 (t, 7.5)
3′		26.4[b1]	26.5	1.63*
4′	1.36*	30.0[b6]	30.0	1.36*
5′		30.0[b6]	30.0	1.36*
6′		26.5[b1]	26.9	1.63*
7′	2.26 (ddd, 11.1, 7.4, 3.9)	36.8[b2]	36.8	2.26 (t, 7.4)
				2.25 (t, 7.4)
8′		174.8[b7]	174.8	
9′	4.43 (dd, 8.9, 5.1)	52.7	53.0	4.42 (dd, 9.1, 5.1)
10′		176.5	176.5	
1″a		29.8[b6]	30.0	1.93*
1″b				1.72*
2″	1.62*	26.3[b1]	26.0	1.62*
3″a	3.23 (dd, 13.7, 7.2)	42.0[b4]	42.0	3.24 (dd, 13.6, 7)
3″b	3.19 (dd, 13.7, 7.2)			3.19 (dd, 13.6, 7)
4″		158.8	158.8	

δ$_H$ 1.2 – 1.8 – overlapping resonances
* – J coupling constants could not be determined due to overlap with other signals
[a] – structure comparison with the published literature NMR (600 MHz, CD$_3$OD)[11]
[b1-7] – signals are interchangeable

Table S8 NMR (600 MHz, CD$_3$OD) data for synthetic telocinobufotoxin (**2c**)

Pos.	δ_H (m, J in Hz)	$\delta_C{}^a$
1a		26.9
1b		
2a	1.76*	25.6[b1]
2b		
3	5.17 (br t, 2.6)	72.5
4a	2.33 (d, 3.9)	36.4[b2]
4b	1.56 (m)	
5		74.6
6a		36.4[b2]
6b		
7a	1.97 (m)	25.3[b1]
7b	1.24 (m)	
8		42.0[b3]
9	1.66 (m)	40.3
10		42.1[b3]
11a		22.9
11b	1.31 (d, 4.1)	
12a	1.53 (t, 7.5)	41.7[b3]
12b		
13		49.7
14		86.2
15a	2.07 (d, 2.2)	33.4
15b	1.71*	
16a	2.20 (ddd, 15.4, 10.4, 1.3)	29.9[b4]
16b		
17	2.56 (d, 10.4)	52.3
18	0.71 (s)	17.3[b5]
19	0.93 (s)	17.4[b5]
20		125.2
21	7.45 (d, 2.5)	150.8
22	7.90 (dd, 9.7, 2.5)	149.6
23	6.26 (dd, 9.7, 0.9)	115.6
24		164.9
1′		175.2[b6]
2′	2.35 (t, 7.4)	35.5
3′	1.63*	26.5[b1]
4′	1.37*	30.0[b4]
5′		30.0[b4]
6′		26.8[b1]
7′	2.26 (ddd, 11.1, 7.4, 3.9)	36.8[b2]
8′		174.9[b6]
9′	4.43 (dd, 8.9, 5.1)	53.0
10′		176.7
1″a	1.94 (m)	29.8[b4]
1″b		
2″		26.0[b1]
3″a	3.24 (dd, 13.7, 7.2)	41.9[b3]
3″b	3.19 (dd, 13.7, 7.2)	
4‴		158.8

δ_H 1.2 – 1.8 – overlapping resonances

* – J coupling constants could not be determined due to overlap with other signals

[a] – structure comparison was performed with in house standard, NMR (600 MHz, CD$_3$OD)

[b1-6] – signals are interchangeable

Table S9 NMR assignments (600 MHz, CD$_3$OD) of synthetic bufalitoxin (**3c**)

Pos.	δ_H (m, J in Hz)	δ_C	δ_H (m, J in Hz)*
1a	1.61*	31.9[b1]	
1b			
2a		26.9[b2]	
2b			
3	5.08 (br t, 2.6)	72.3	5.05 (m)
4a	2.02 (td, 16.6, 14.5, 3.0)	31.7[b1]	
4b			
5	1.67*	38.7	
6a	1.28 (m)	27.9	
6b			
7a	1.83 (m)	22.6[b3]	
7b			
8	1.73*	36.9[b4]	
9		43.2	
10		37.1	
11a	1.31*	22.8[b3]	
11b	1.23 (ddd, 16.2, 12.3, 3.9)		
12a	1.46*	42.0[b5]	
12b	1.52 (m)		
13		49.9	
14		86.2	
15a	2.13 (ddd, 11.8, 9.4, 2.5)	33.3	
15b			
16a	2.20 (ddd, 15.5, 10.3, 1.3)	30.1[b6]	
16b			
17	2.56 (d, 10.3)	52.4[b7]	
18	0.71 (s)	17.5	0.72 (s)
19	0.98 (s)	24.5	0.98 (s)
20		125.2	
21	7.43 (d, 2.5)	150.6	7.22 (d, 2.5)
22	7.99 (dd, 9.7, 2.5)	149.5	7.83 (dd, 9.5, 2.5)
23	6.28 (dd, 9.7, 1.0)	115.6	6.22 (d, 9.5)
24		164.9	
1′		175.3[b8]	
2′	2.33 (t, 7.4)	35.6	
3′		26.2[b2]	
4′	1.37*	30.0[b6]	
5′		30.0[b6]	
6′		26.3[b2]	
7′	2.26 (ddd, 10.5, 7.4, 3.0)	36.5[b4]	
8′	-	175.1[b8]	
9′	4.43 (dd, 8.9, 5.1)	53.0[b7]	4.26 (m)
10′		176.5	
1″a		30.0[b6]	
1″b			
2″		26.5[b2]	
3″a	3.24 (dd, 13.7, 7.2)	41.9[b5]	
3″b	3.19 (dd, 13.7, 7.2)		
4″		158.8	

δ_H 1.2 – 1.8 – overlapping resonances

* – J coupling constants could not be determined due to overlap with other signals

[a] – structure comparison was performed with in house standard, NMR (600 MHz, CD$_3$OD

[b1-8] – signals are interchangeable

Table S10 NMR assignments (600 MHz, MeOD) of bufalin pimeloyl-L-arginine (**9c**)

Pos.	δ_H (m, J in Hz)	δ_C
1a	1.61*	31.9[b1]
1b		
2a	1.63*	26.9[b2]
2b		
3	5.08 (br t, 2.6)	72.3
4a	2.02 (td, 16.6, 14.5, 3.0)	31.7[b1]
4b		
5		38.7
6a	1.28 (m)	27.9
6b	1.94*	
7a	1.83 (m)	22.6[b3]
7b		
8		36.9[b4]
9	1.65*	43.2
10		37.1
11a	1.31*	22.8[b3]
11b	1.23 (ddd, 16.2, 12.3, 3.9)	
12a	1.46*	42.0[b5]
12b	1.52 (m)	
13		49.9
14		86.2
15a	2.13 (ddd, 11.8, 9.4, 2.5)	33.3
15b	1.72*	
16a	2.20 (ddd, 15.5, 10.3, 1.3)	30.1[b6]
16b		
17	2.56 (d, 10.3)	52.4[b7]
18	0.71 (s)	17.5
19	0.98 (s)	24.5
20		125.2
21	7.43 (d, 2.5)	150.6
22	7.99 (dd, 9.7, 2.5)	149.5
23	6.28 (dd, 9.7, 1.0)	115.6
24		164.9
1′		175.3[b8]
2′	2.33 (t, 7.4)	35.6
3′		26.2[b2]
4′	1.38*	30.0[b6]
5′		26.3[b2]
6′	2.26 (ddd, 10.5, 7.4, 3.0)	36.5[b4]
7′	-	175.1[b8]
8′	4.43 (dd, 8.9, 5.1)	53.0[b7]
9′		176.5
1″a		30.0[b6]
1″b		
2″		26.5[b2]
3″a	3.24 (dd, 13.7, 7.2)	41.9[b5]
3″b	3.19 (dd, 13.7, 7.2)	
4″		158.8

δ_H 1.2 – 1.8 – overlapping resonances

* – J coupling constants could not be determined due to overlap with other signals

[a] – structure comparison was performed with in house standard, NMR (600 MHz, CD$_3$OD)

[b1-8] – signals are interchangeable

Table S11 NMR assignments (600 MHz, MeOD) of marinobufagenin pimeloyl-L-arginine (**8c**)

Pos.	δ_H (m, J in Hz)	δ_C
1a	1.80 (ddd, 14.3, 14.3, 3.5)	26.5[b1]
1b		
2a		25.9[b1]
2b	1.61*	
3	5.14 (br t, 2.6)	72.0
4a	2.34 (d, 7.6)	36.3[b2]
4b		
5		74.4
6a		35.6[b3]
6b	1.32 (ddd, 13.5, 3.9, 3.2)	
7a	0.99 (s)	24.4
7b		
8	2.01 (td, 12.3, 3.9)	33.9[b4]
9	1.66*	43.7
10		42.0[b5]
11a	1.56*	22.5
11b		
12a	1.70*	40.1
12b		
13		46.2
14		75.8
15	3.61 (br s)	61.2
16a	2.41 (ddd, 15.5, 10.3, 1.3)	33.3[b4]
16b		
17	2.59 (d, 10.3)	48.3
18	0.78 (s)	17.1[b6]
19	0.98 (s)	17.2[b6]
20		124.6
21	7.44 (dd, 2.5, 0.9)	151.4
22	7.89 (dd, 9.7, 2.5)	149.6
23	6.26 (dd, 9.7, 0.9)	115.4
24		164.6
1'		175.1[b6]
2'	2.35 (t, 7.7)	35.4[b3]
3'	1.63*	26.4[b1]
4'	1.38*	30.0[b7]
5'		26.5[b1]
6'	2.26 (ddd, 11.1, 7.4, 3.9)	36.8[b2]
7'		174.8[b6]
8'	4.43 (dd, 8.9, 5.1)	52.7
9'		176.5
1''a		29.8[b7]
1''b		
2''		26.3[b1]
3''a	3.23 (dd, 13.7, 7.2)	42.0[b5]
3''b	3.19 (dd, 13.7, 7.2)	
4''		158.8

δ_H 1.3 – 1.8 – overlapping resonances
* – J coupling constants could not be determined due to overlap with other signals
[a] – structure comparison was performed with in house standard, NMR (600 MHz, CD$_3$OD)
[b1-7] – signals are interchangeable

Table S12 NMR (D₂O, 600 MHz) data for suberoyl-L-arginine (**1d**)
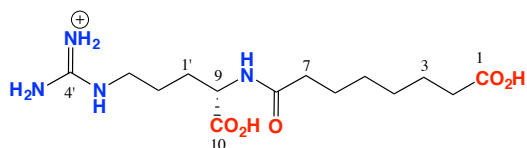
Pos.	δ_H (m, J in Hz)	δ_C
1		179.2
2	2.38 (t, 7.4)	33.7
3	1.61*	24.1[b1]
4	1.34*	27.6[b2]
5		27.7[b2]
6		24.3[b1]
7	2.32 (ddd, 9.1, 7.6, 2.2)	35.3
8		177.1
9	4.35 (dd, 9.1, 5.1)	52.8
10		176.3
1′a	1.93 (m)	27.9[b2]
1′b	1.77 (m)	
2′	1.67 (m)	25.0
3′a	3.24 (dd, 13.7, 7.2)	40.4
3′b	3.19 (dd, 13.7, 7.2)	
4′		158.2

δ_H 1.55 – 2.00 – overlapping resonances
* – J coupling constants could not be determined due to overlap with other signals
[b1,2] – signals are interchangeable

Table S13 NMR assignments (600 MHz, D₂O) of azeloyl-L-arginine (**4d**)
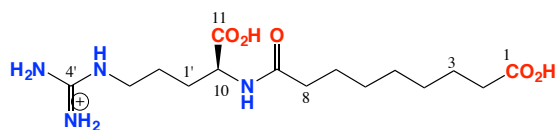
Pos.	δ_H (m, J in Hz)	δ_C
1		181.3
2	2.37 (t, 7.4)	35.6
3	1.60*	25.8[b1]
4	1.33*	29.4[b2]
5		29.4[b2]
6		26.7
7		29.6[b2]
8	2.31(ddd, 9.1, 7.6, 2.2)	37.1
9		179.2[b3]
10	4.27 (dd, 9.1, 5.1)	55.3
11		178.5[b3]
1′a	1.90 (m)	30.0[b2]
1′b	1.73 (m)	
2′	1.63*	26.1[b1]
3′	3.22 (t, 7.2)	42.1
4′		158.2

δ_H 1.55 – 2.00 – overlapping resonances
* – J coupling constants could not be determined due to overlap with other signals
[b1-3] – signals are interchangeable

Table S14 NMR assignments (600 MHz, D₂O) of pimeloyl-L-arginine (**3d**)
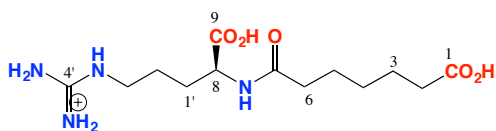
Pos.	δ_H (m, J in Hz)	δ_C
1		179.2
2	2.38 (t, 7.4)	33.5
3	1.61*	23.9[b1]
4	1.34 (m)	27.5[b2]
5		24.3[b1]
6	2.32 (ddd, 9.1, 7.6, 2.2)	35.3
7		177.1
8	4.35 (dd, 9.1, 5.1)	52.1
9		176.3
1'a	1.93 (m)	27.6 [b2]
1'b	1.78 (m)	
2'	1.66 (m)	24.9[b1]
3'a	3.24 (dd, 13.7, 7.2)	40.4
3'b	3.19 (dd, 13.7, 7.2)	
4'		158.2

δ_H 1.55 – 2.00 – overlapping resonances
* – J coupling constants could not be determined due to overlap with other signals
[b1,2] – signals are interchangeable

Table S15 NMR assignments (600 MHz, D₂O) of adipoyl-L-arginine (**2d**)
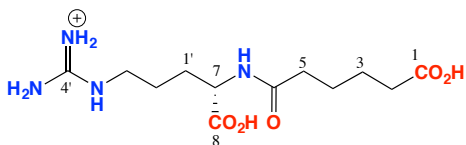
Pos.	δ_H (m, J in Hz)	δ_C
1		178.5
2	2.42 (t, 7.4)	33.4
3		23.6[b1]
4		24.3[b1]
5	2.35 (ddd, 9.1, 7.6, 2.2)	35.0
6		176.7
7	4.39 (dd, 9.1, 5.1)	52.2
8		175.5
1'a	1.95 (m)	27.6
1'b	1.79 (m)	
2'	1.67 (m)	24.6[b1]
3'a	3.23 (dd, 13.7, 7.2)	40.4
3'b	3.19 (dd, 13.7, 7.2)	
4'		156.8

δ_H 1.55 – 2.00 – overlapping resonances
* – J coupling constants could not be determined due to overlap with other signals
[b1] – signals are interchangeable

Figure S1 ¹H NMR (CD₃OD, 600 MHz) spectrum for marinobufagenin (**1a**)
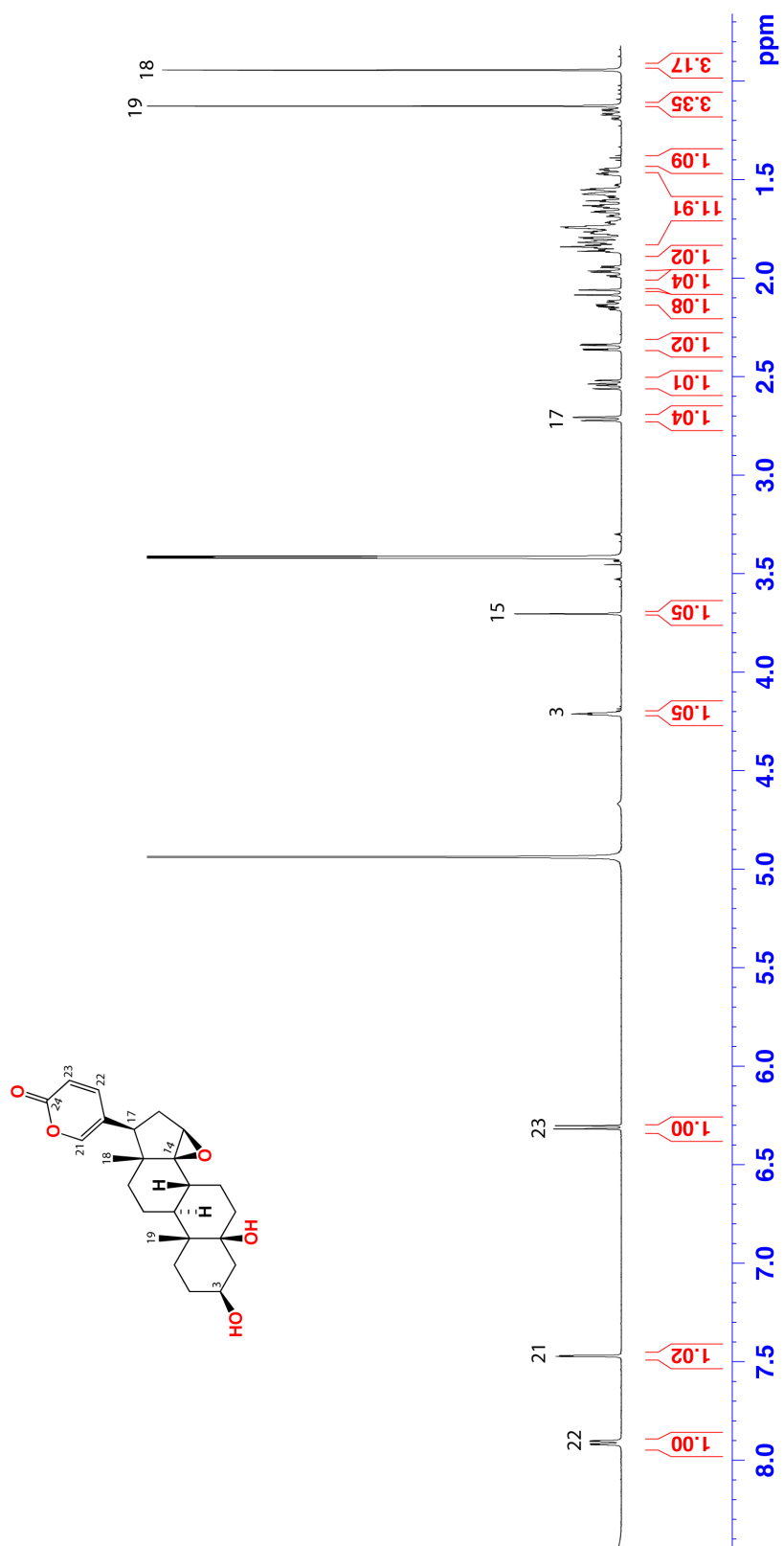
Figure S2 ^{1}H NMR (CD$_3$OD, 600 MHz) spectrum for telocinobufagenin (**2a**)
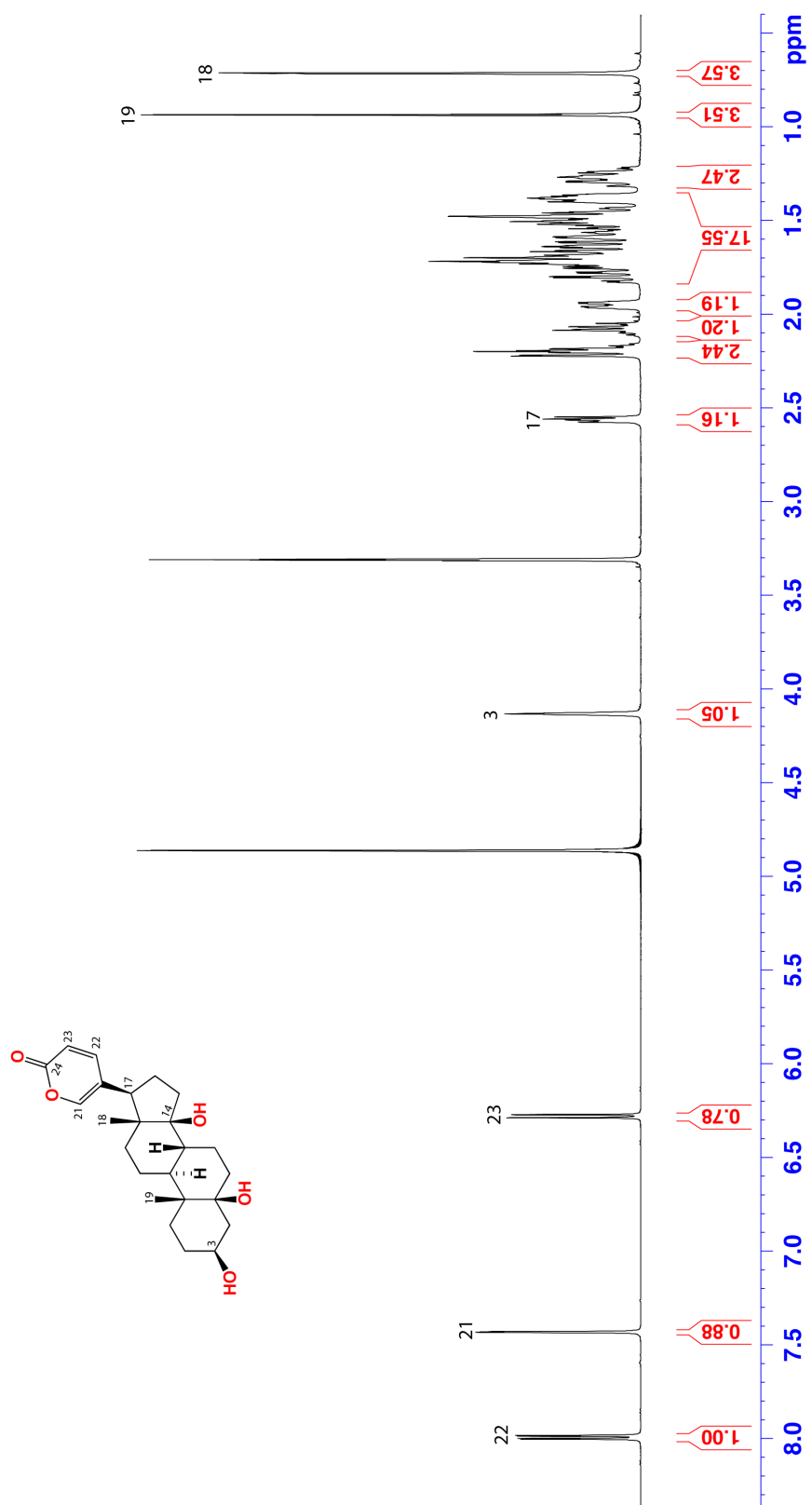
Figure S3 ¹H NMR (CD₃OD, 600 MHz) spectrum for bufalin (**3a**)
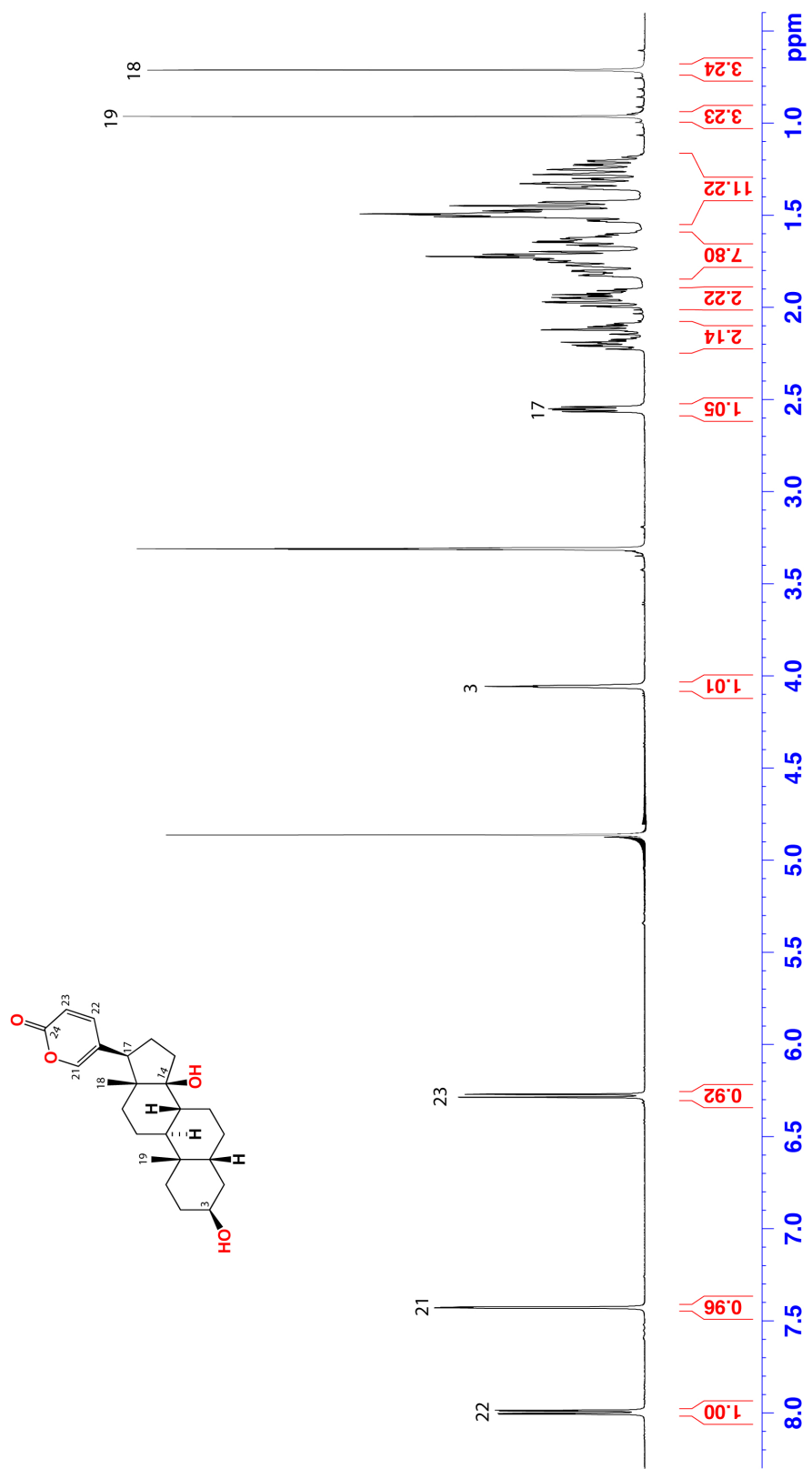
Figure S4 ¹H NMR (CD₃OD, 600 MHz) spectrum for hellebrigenin (**5a**)
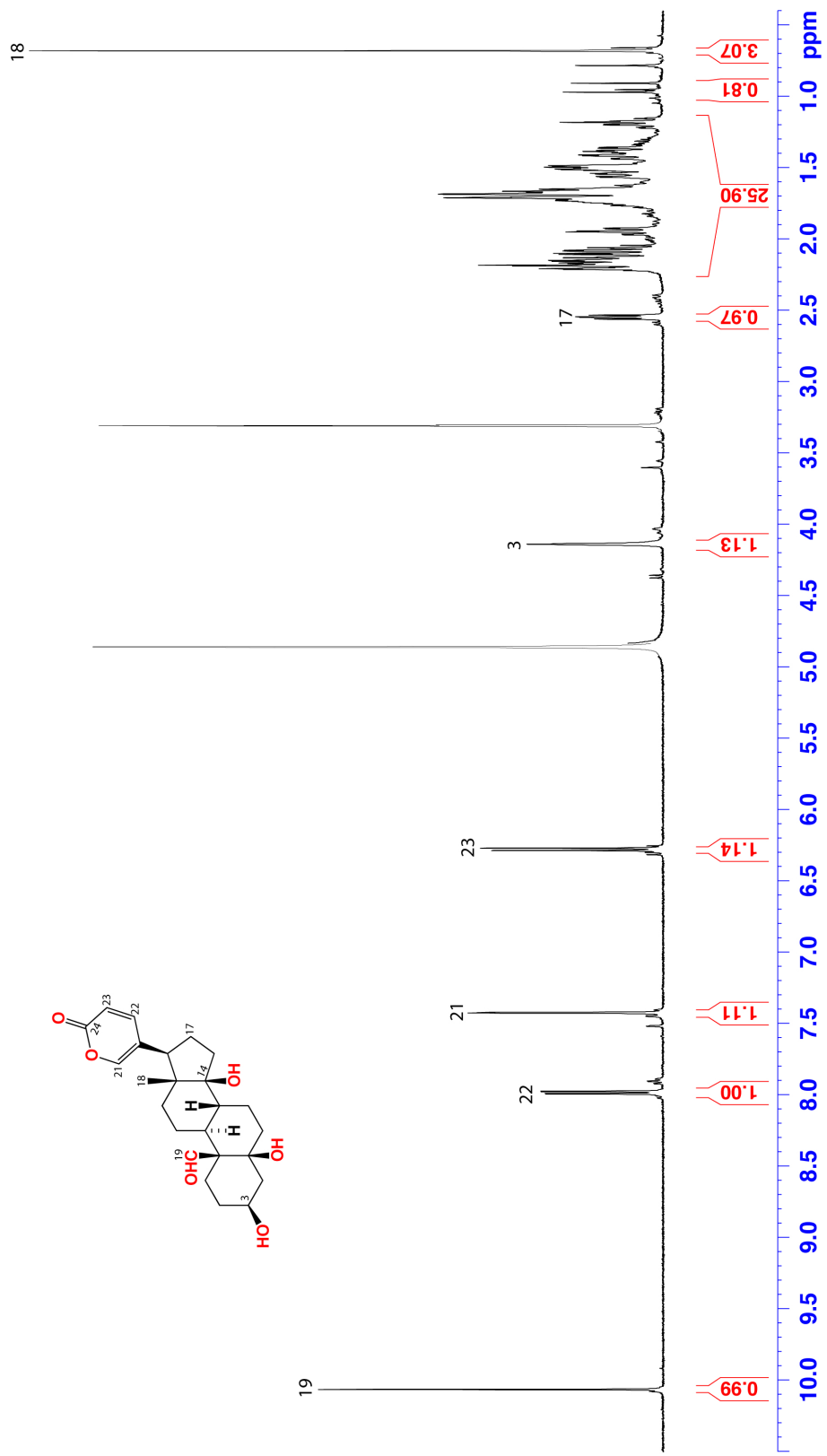
Figure S5 ¹H NMR (CD₃OD, 600 MHz) spectrum for bufalin-3-acetate (**7a**)
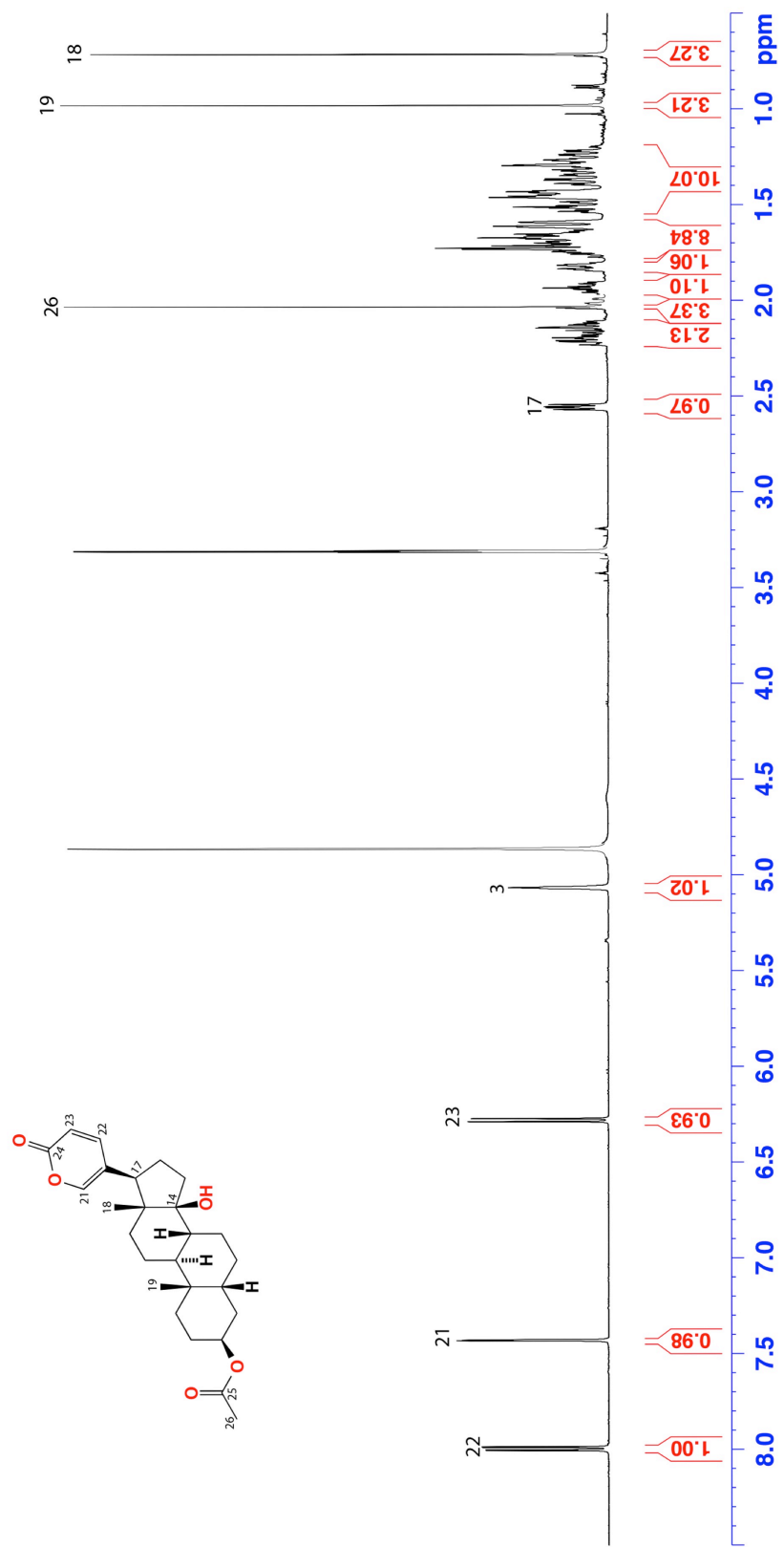
Figure S6 ^{1}H NMR (CD$_3$OD, 600 MHz) spectrum for marinobufagenin-3-suberate (**1b**)
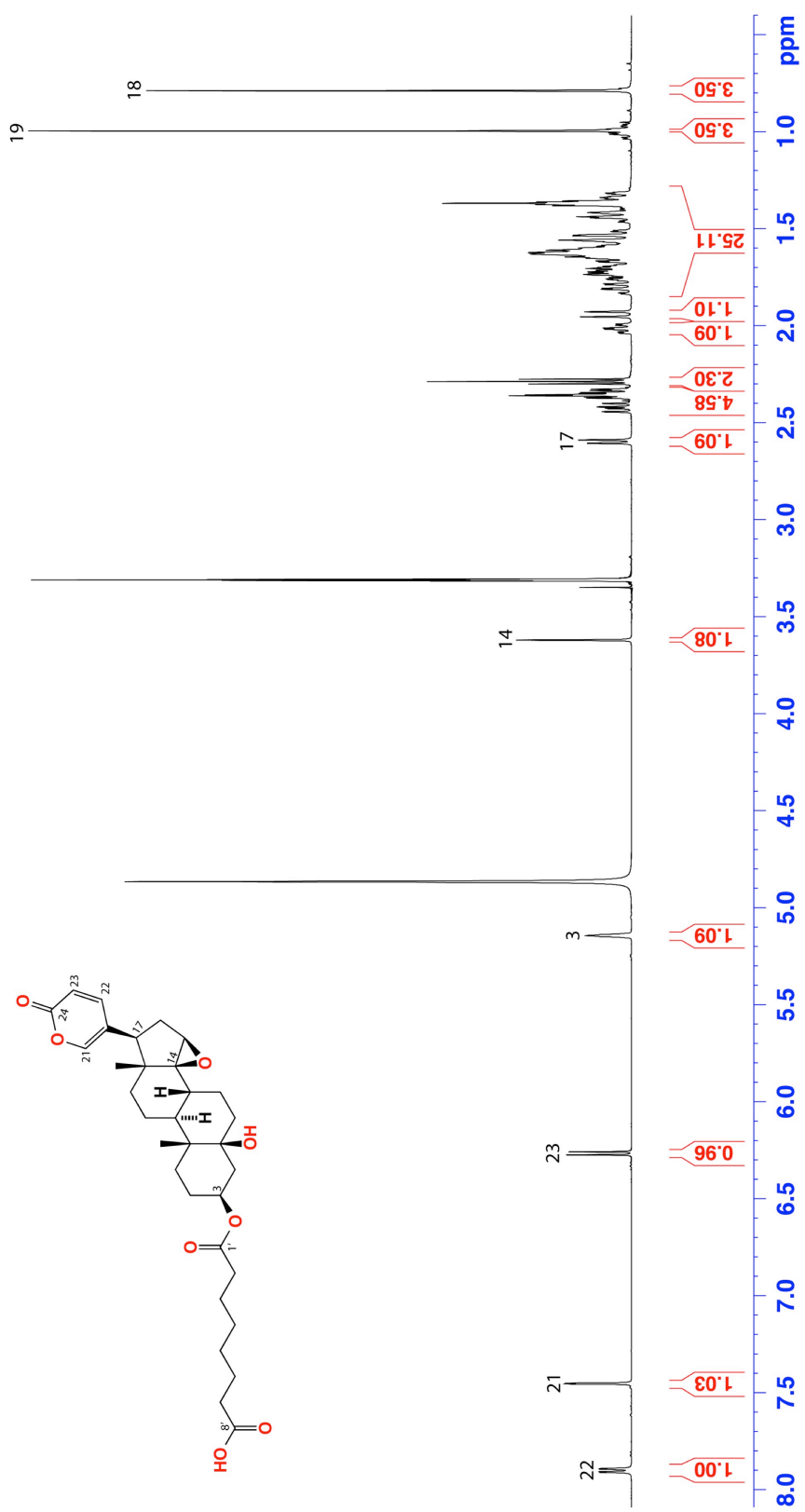
Figure S7 ¹H NMR (CD₃OD, 600 MHz) spectrum for telocinobufagenin -3-suberate (**2b**)
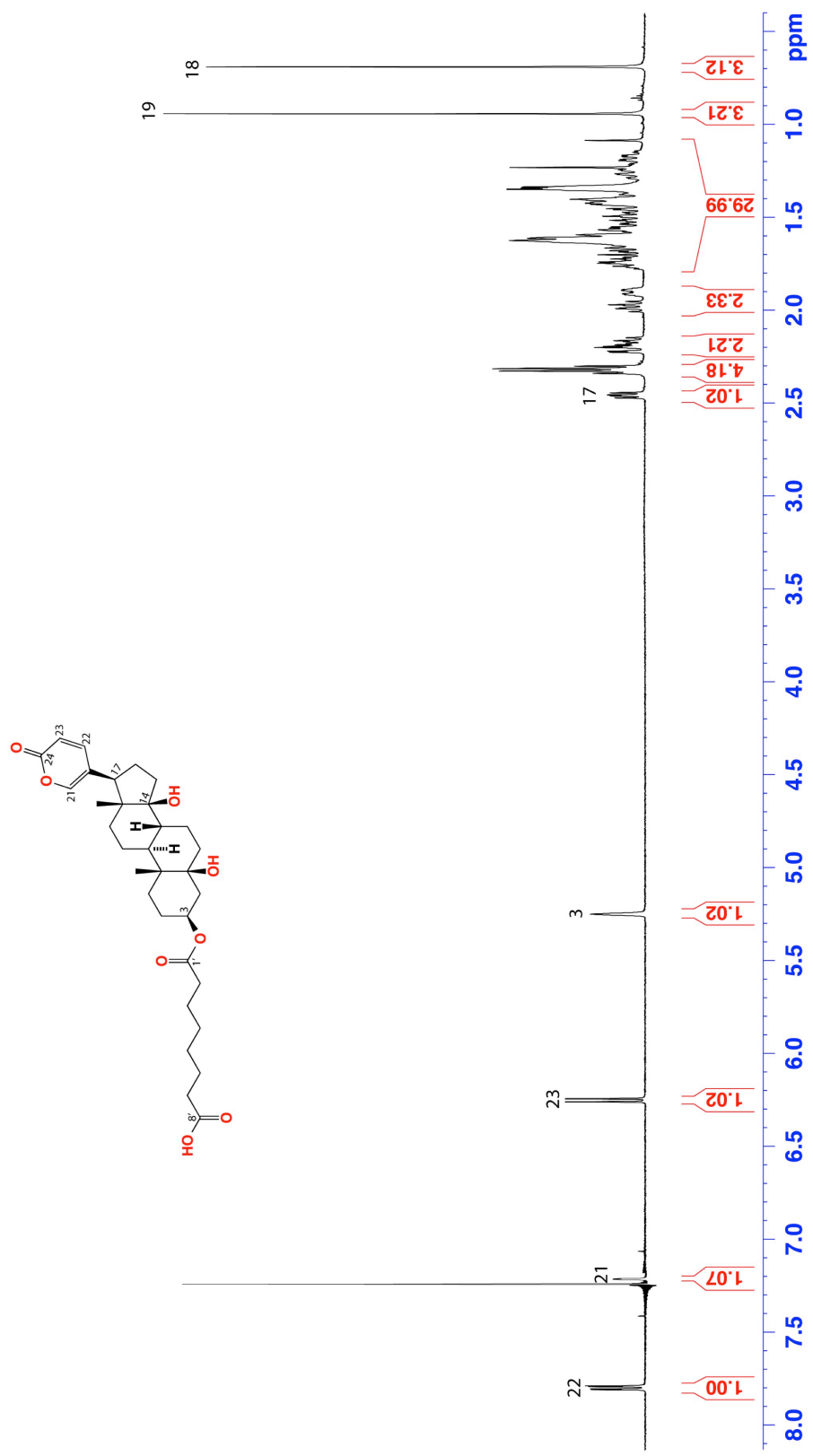
Figure S8 ¹H NMR (CD₃OD, 600 MHz) spectrum for bufalin-3-suberate (**3b**)
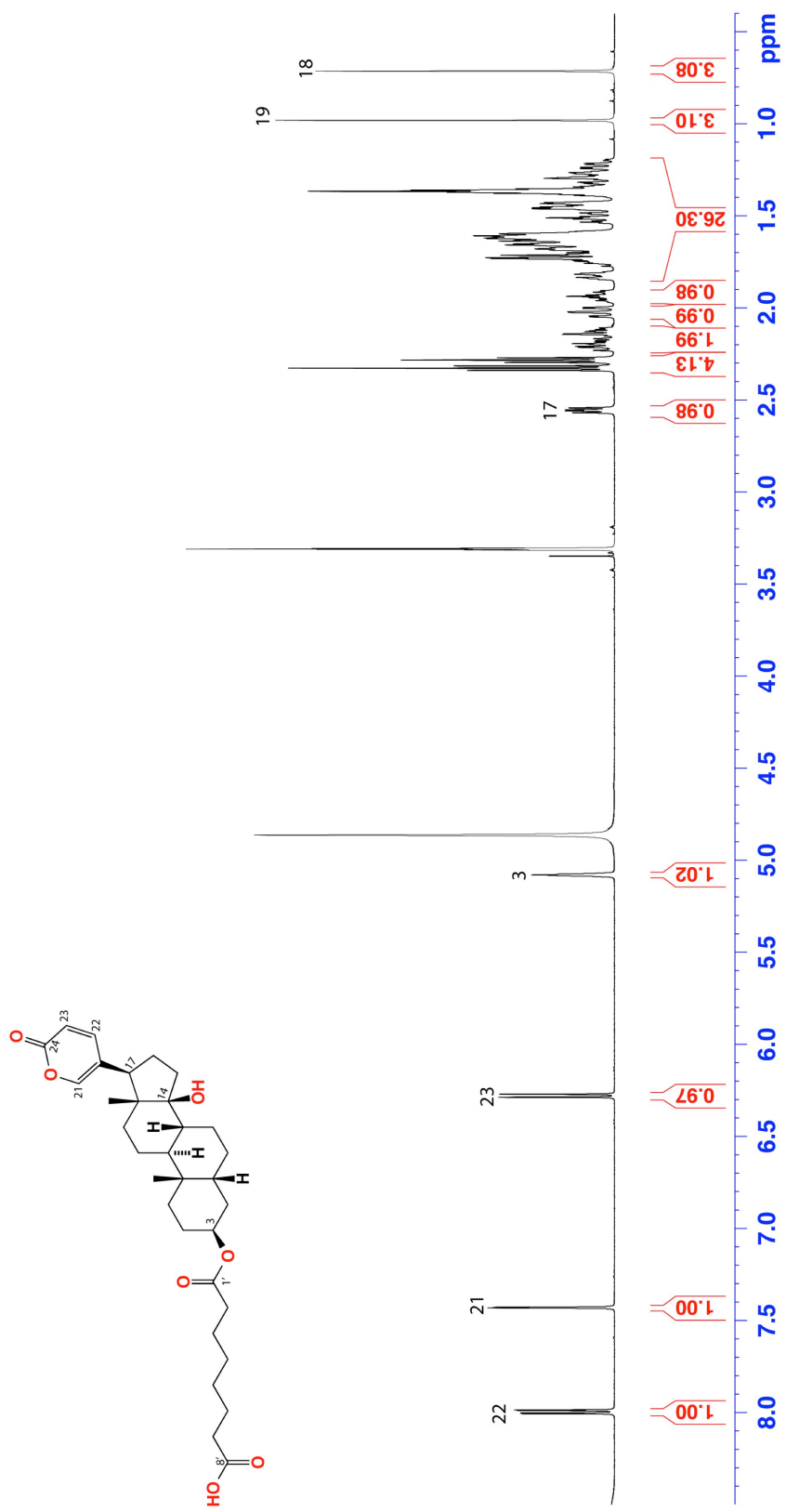
Figure S9 ¹H NMR (CD₃OD, 600 MHz) spectrum for marinobufotoxin (**1c**)
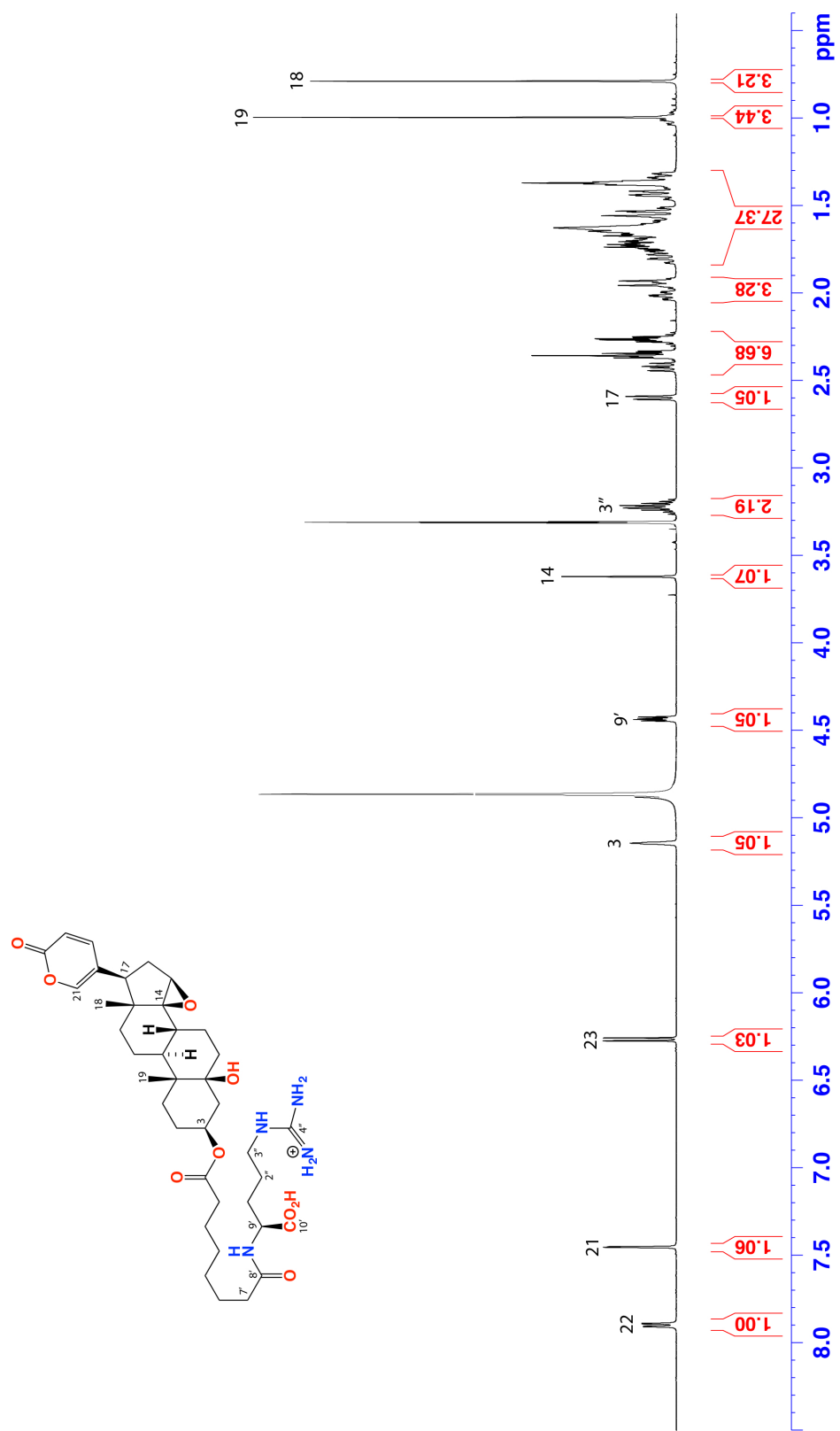
Figure S10 ^{1}H NMR (CD$_3$OD, 600 MHz) spectrum for telocinobufotoxin (**2c**)

Figure S11 ^{1}H NMR (CD$_3$OD, 600 MHz) spectrum for bufalitoxin (**3c**)

103
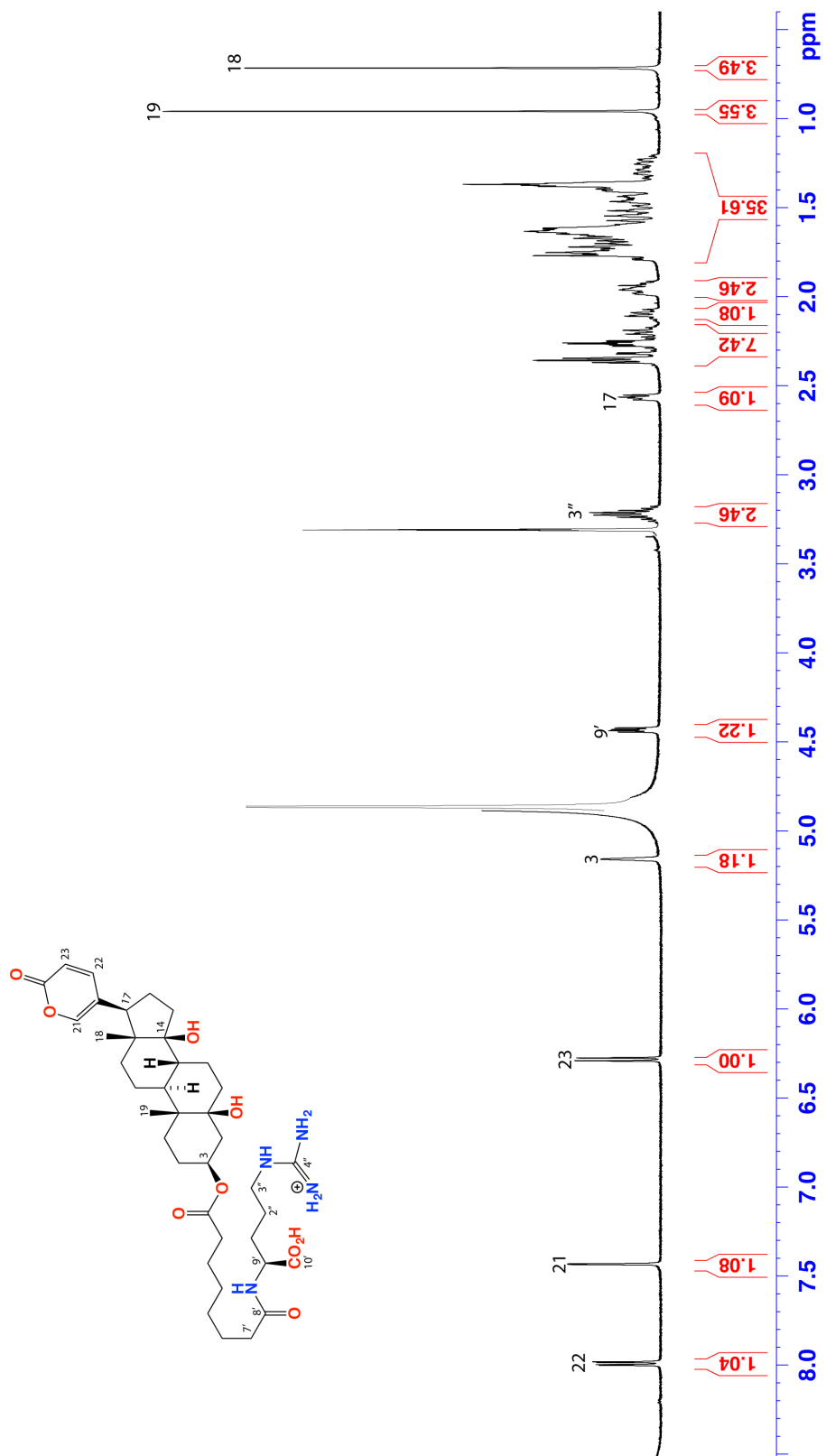
Figure S12 ^{1}H NMR (D$_2$O, 600 MHz) spectrum for adipoyl-L-arginine (**2d**)
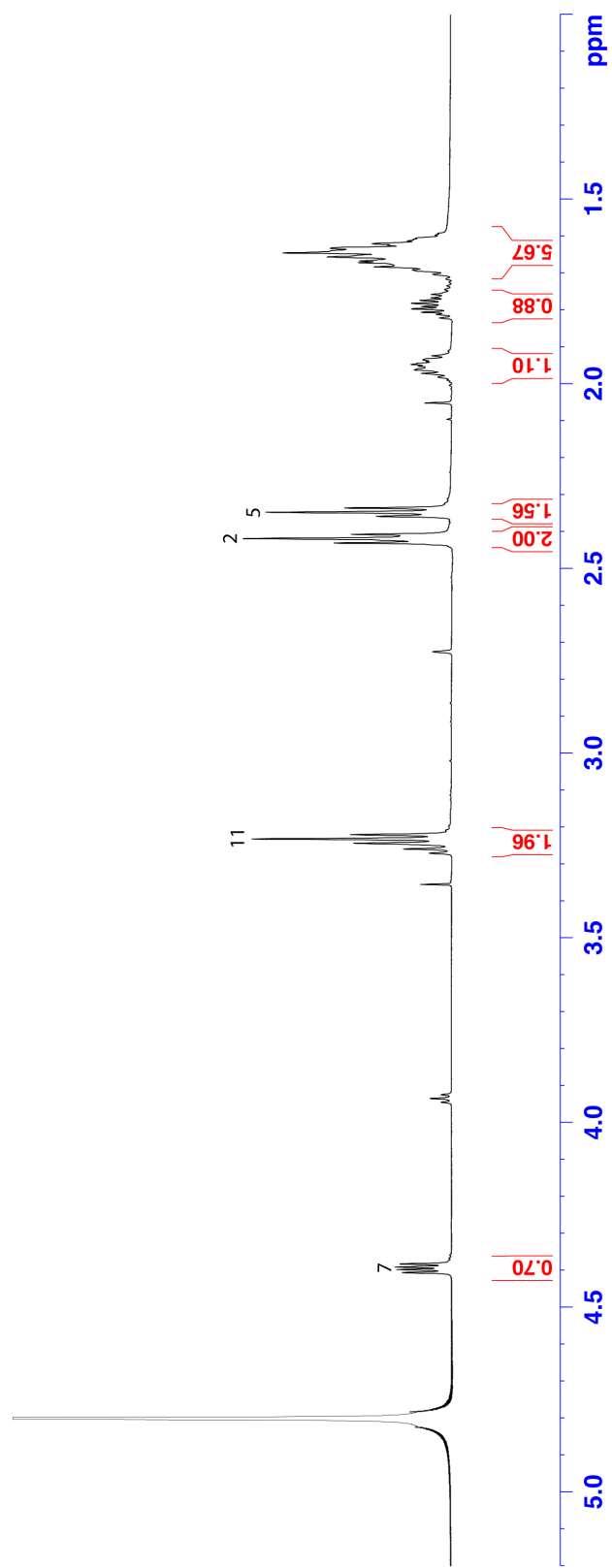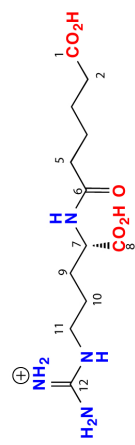
Figure S13 ^{1}H NMR (D$_2$O, 600 MHz) spectrum for pimeloyl-L-arginine (**3d**)
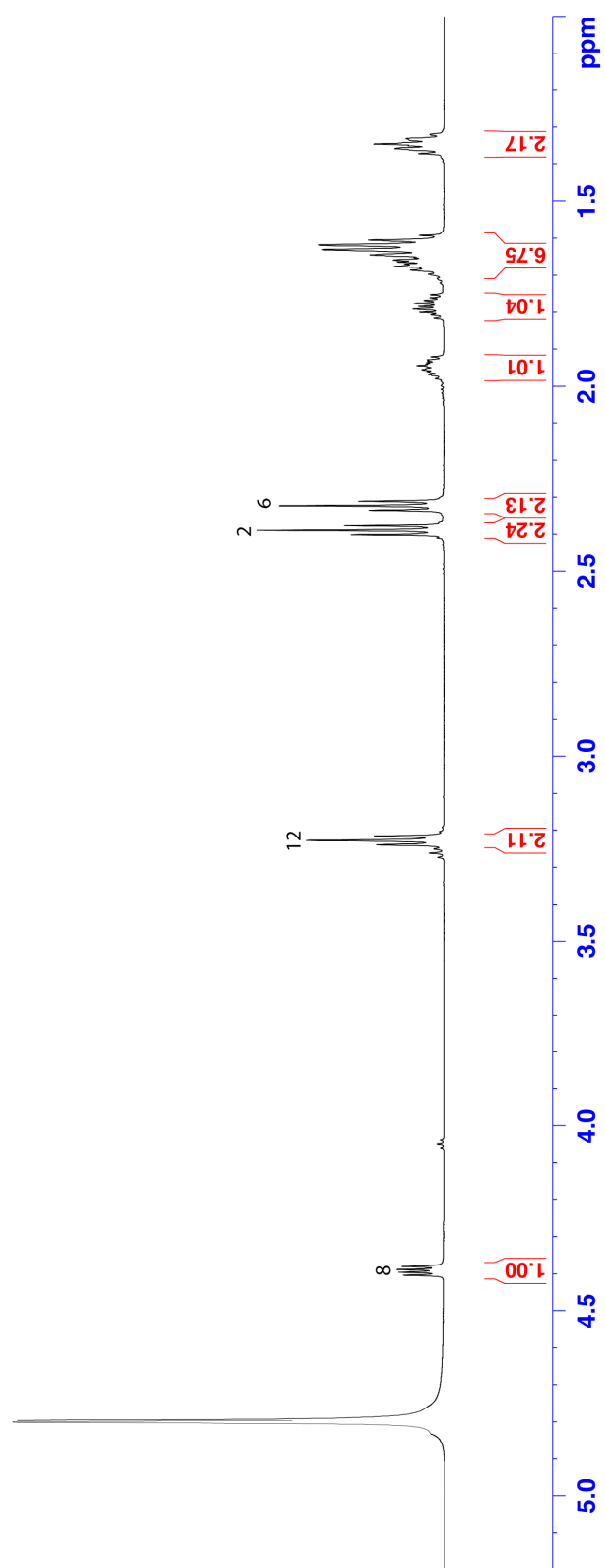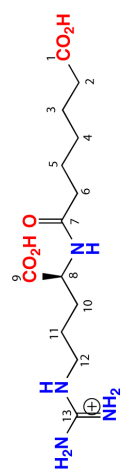
Figure S14 ^{1}H NMR (D$_2$O, 600 MHz) spectrum for suberoyl-L-arginine (**1d**)
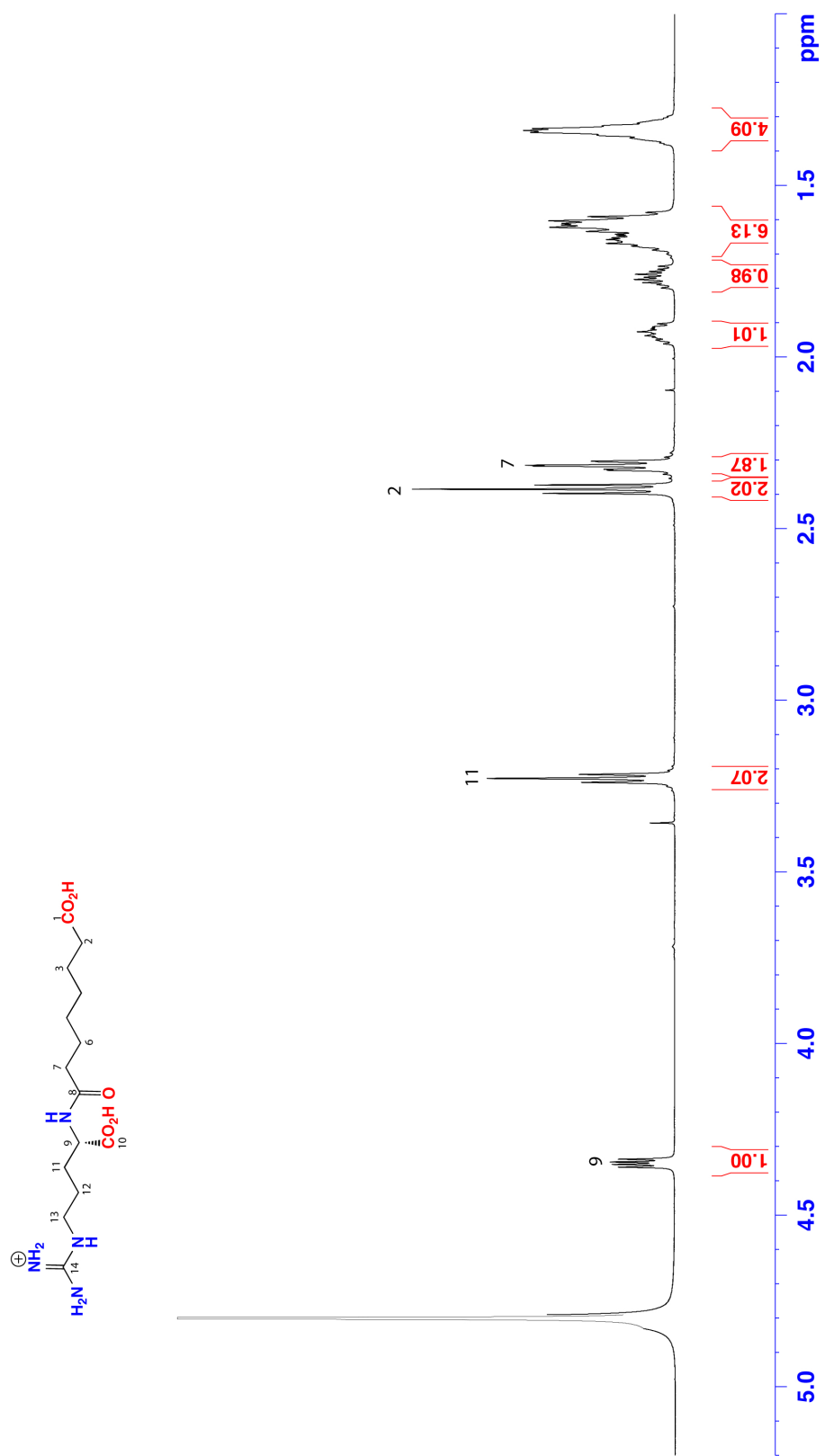
Figure S15 ^{1}H NMR (D$_2$O, 600 MHz) spectrum for azeloyl-L-arginine (**4d**)
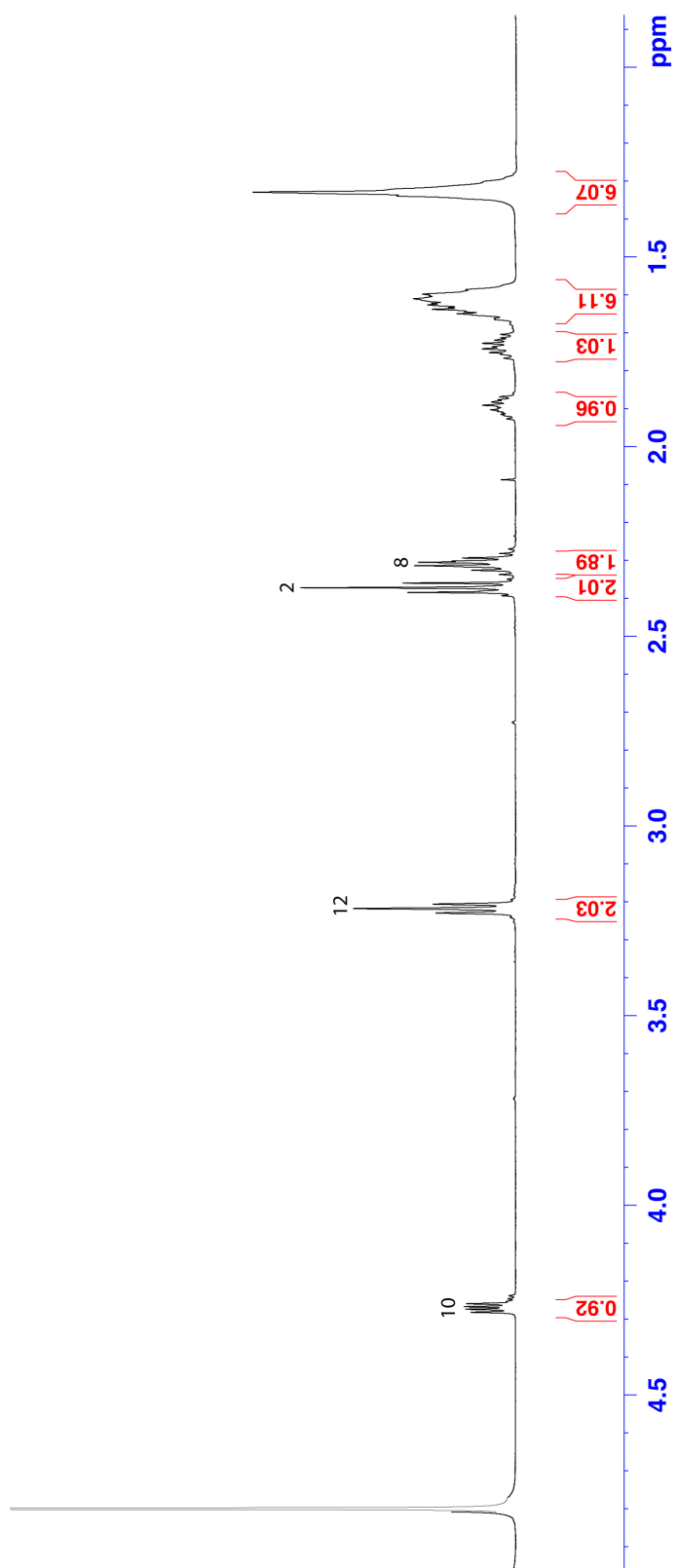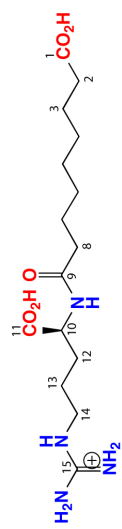
Figure S16 ^{1}H NMR (CD$_3$OD, 600 MHz) spectrum for derivatized suberoyl-L-arginine (**1e**)

108
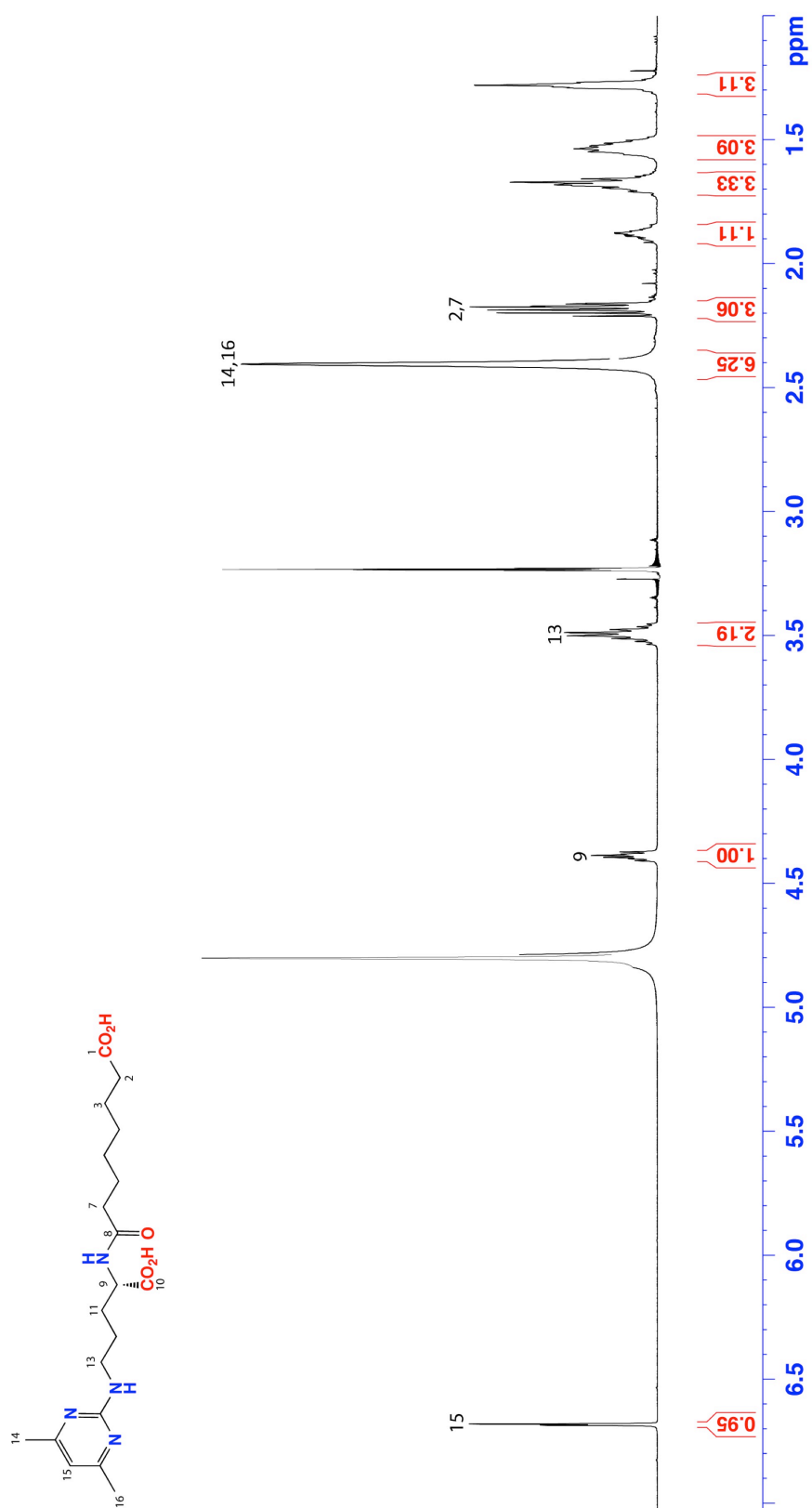
Figure S17 ^{1}H NMR (CD$_3$OD, 600 MHz) spectrum for resibufagenin (**4a**)
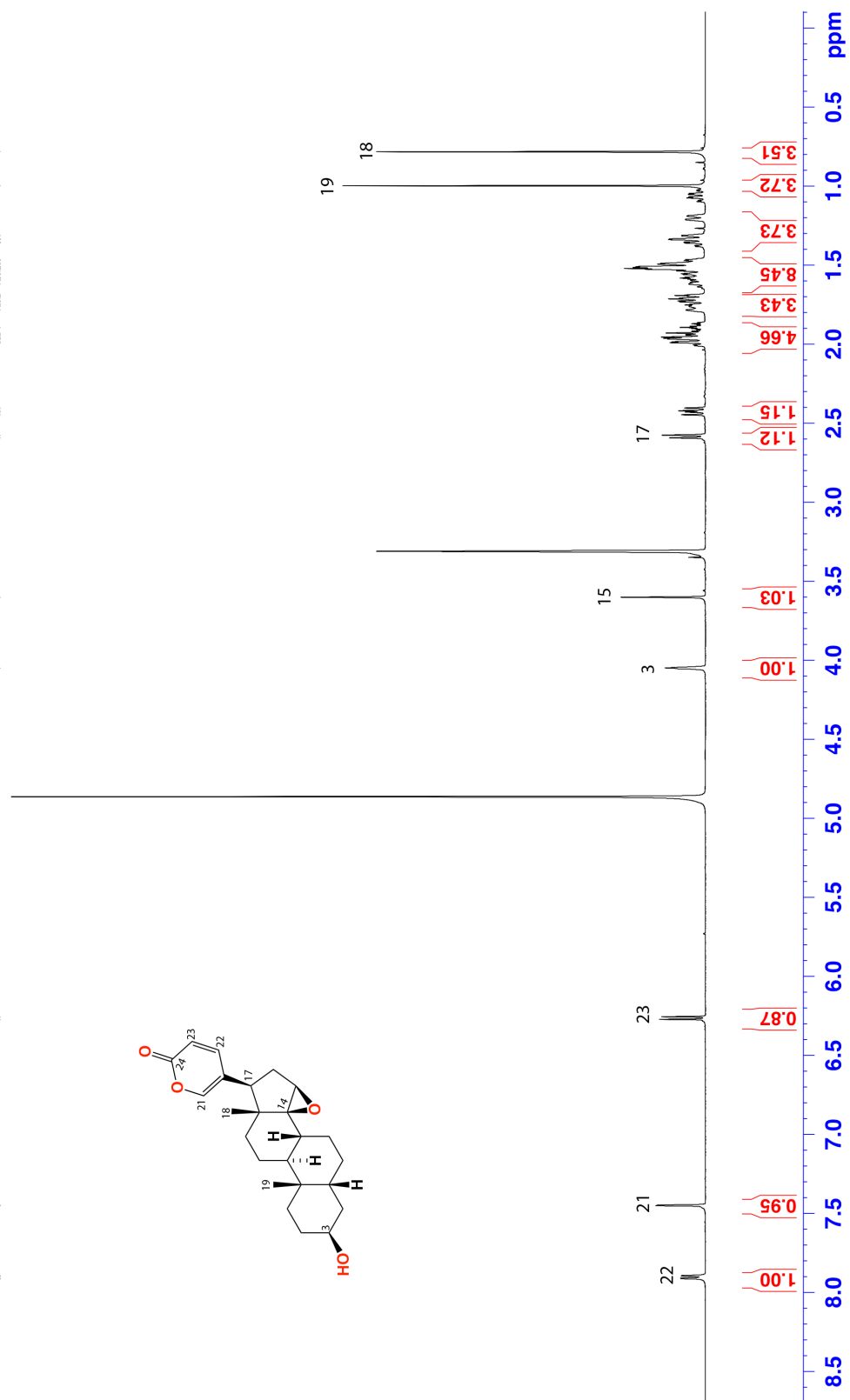
Figure S18 ¹H NMR (CD₃OD, 600 MHz) spectrum for derivatized azeloyl-L-arginine (**4e**)
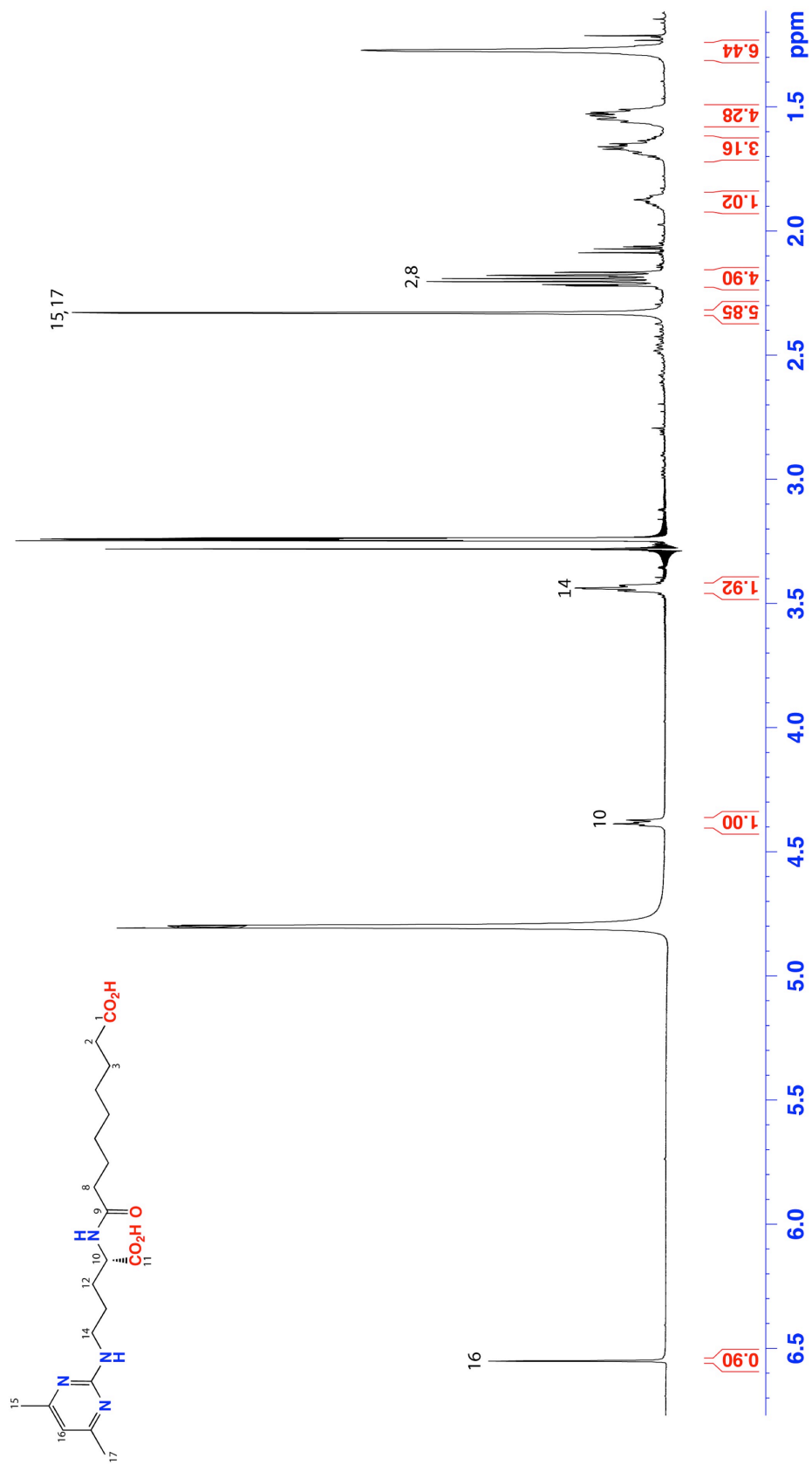
Figure S19 ^{1}H NMR (CD$_3$OD, 600 MHz) spectrum for derivatized adipoyl-L-arginine (**2e**)
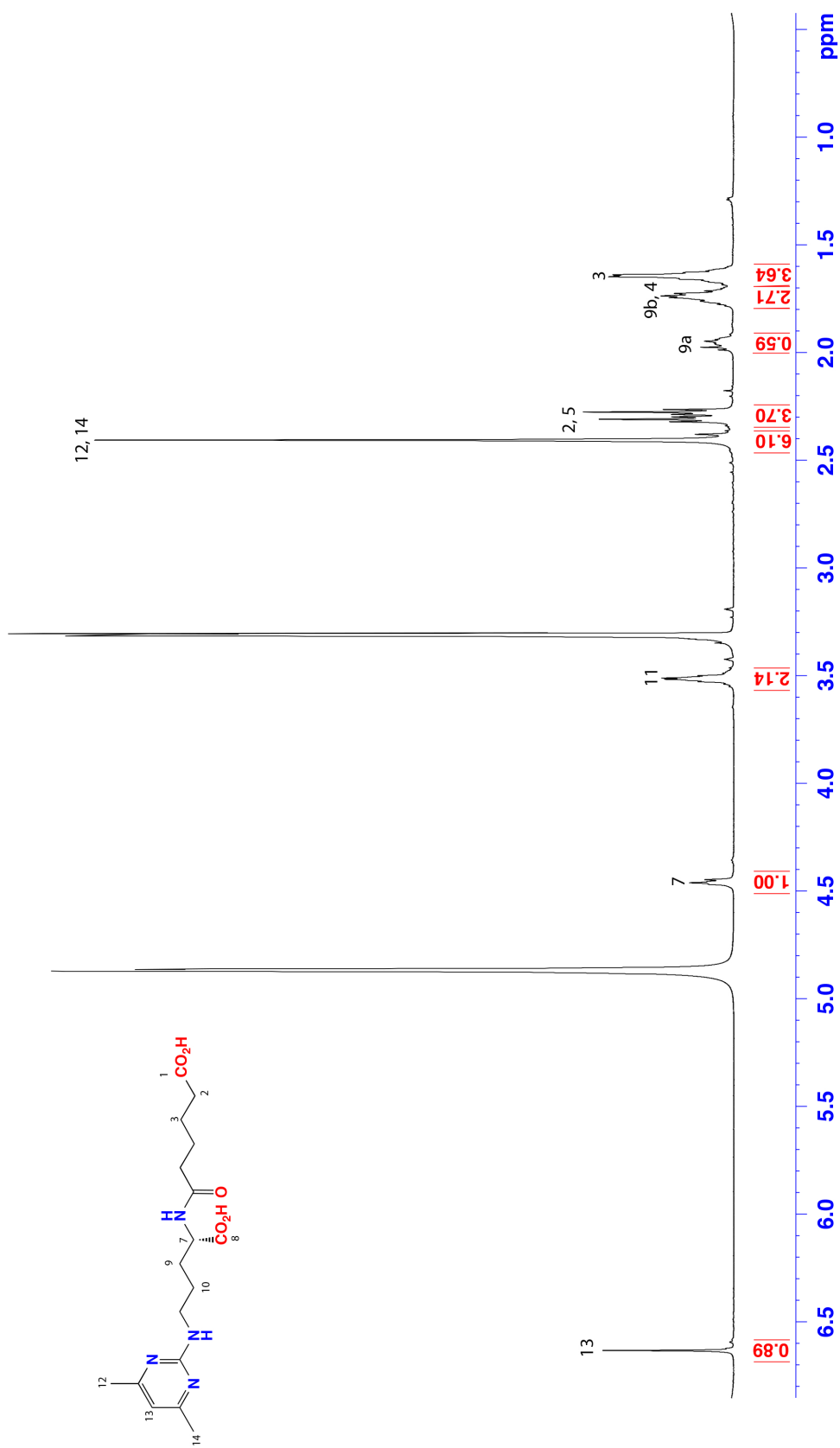
Figure S20 ¹H NMR (CD₃OD, 600 MHz) spectrum for marinobufagenin-3-succinate (**9b**)
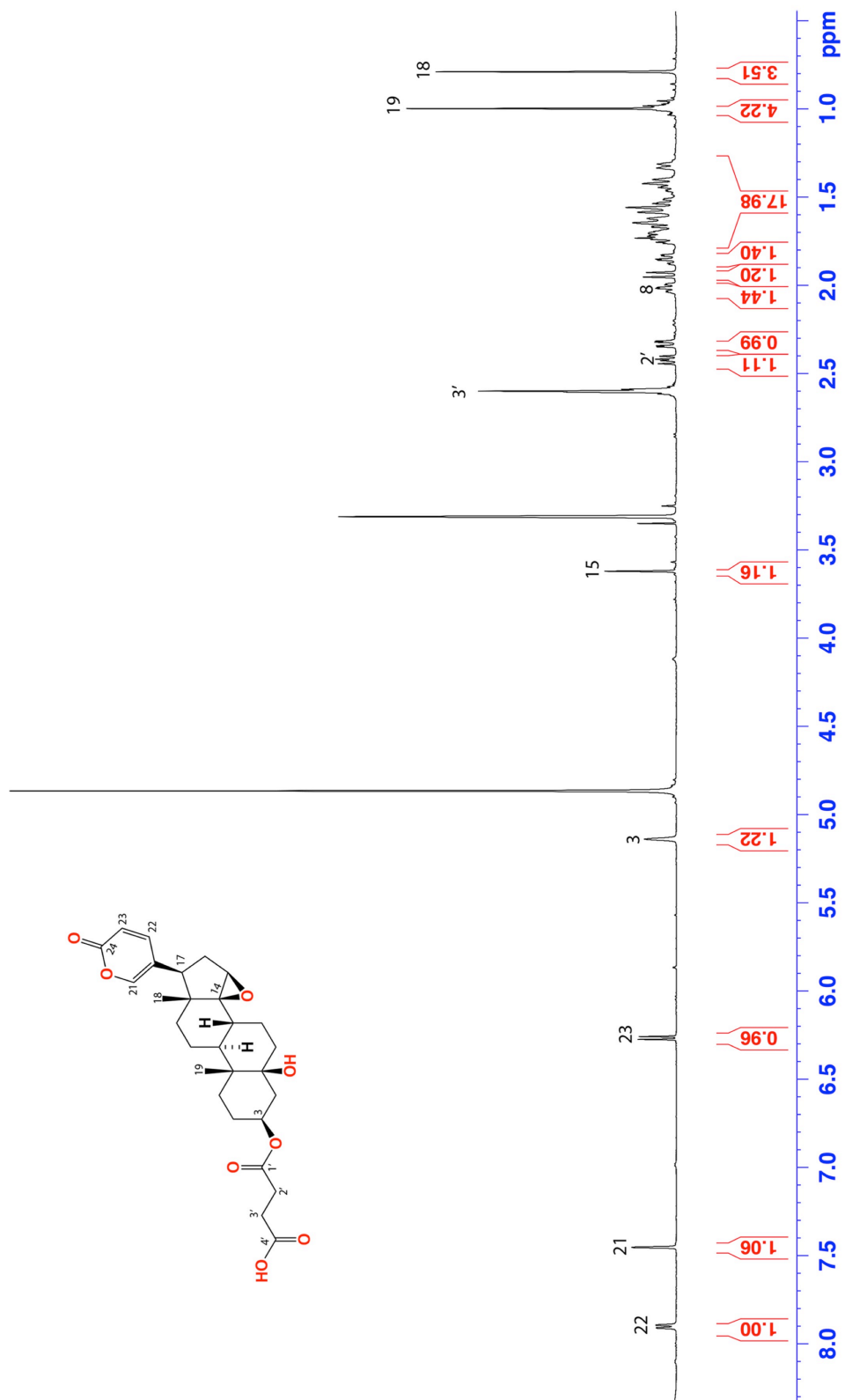
Figure S21 ^{1}H NMR (CD$_3$OD, 600 MHz) spectrum for marinobufagenin-3-pimelate (**5b**)
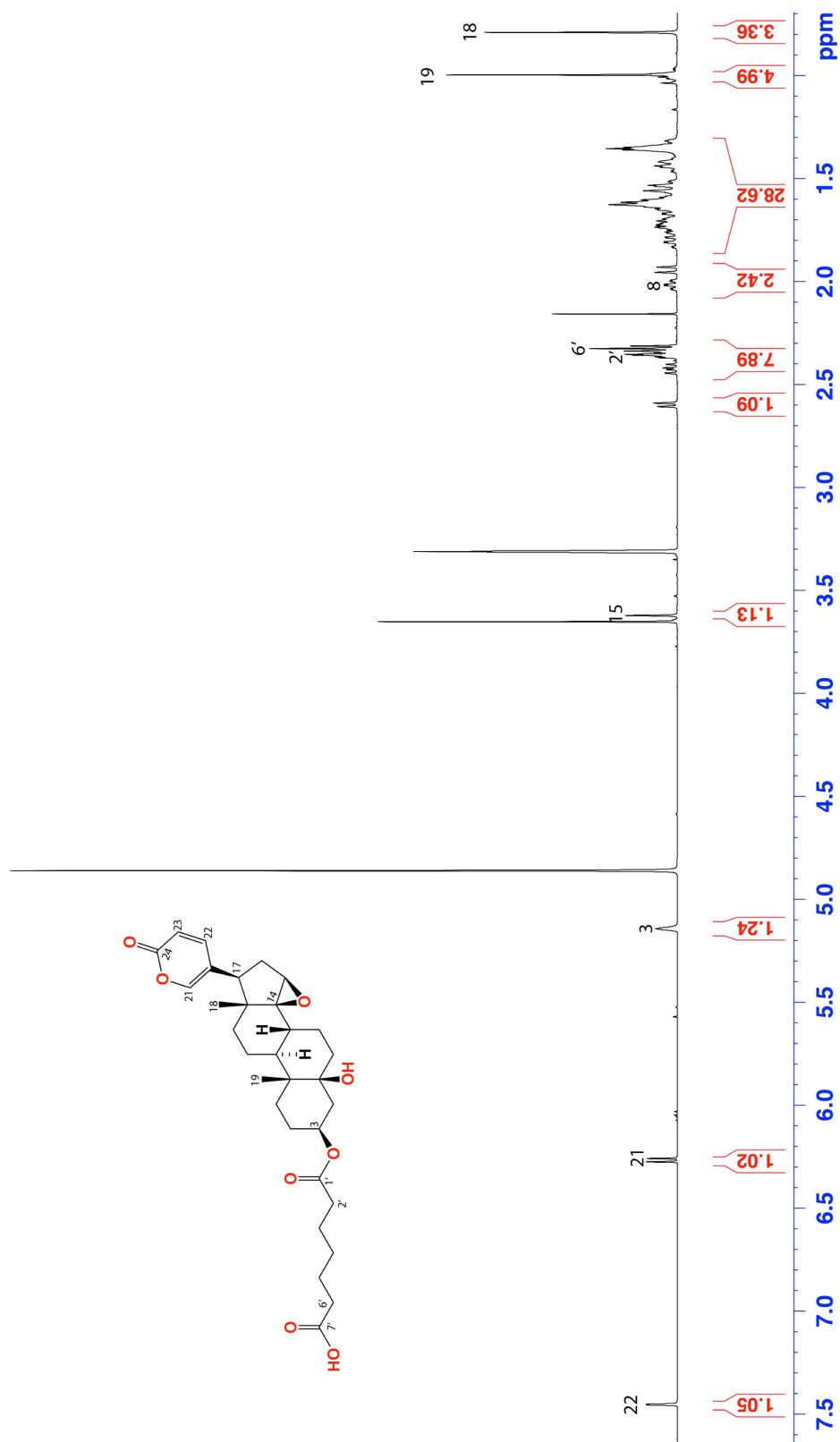
Figure S22 ¹H NMR (CD₃OD, 600 MHz) spectrum for marinobufagenin-3-acetate (**8b**)
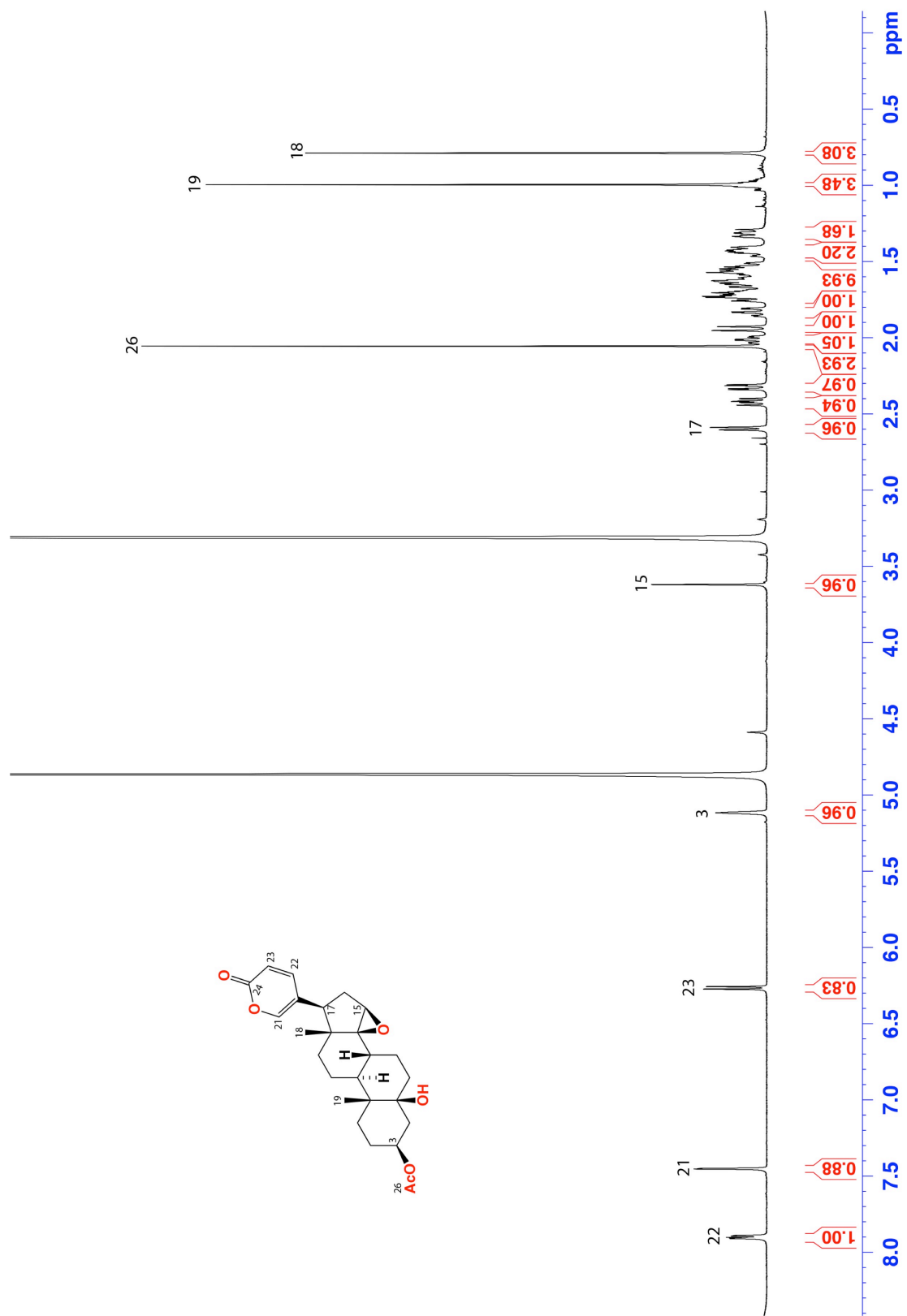
Figure S23 ^{1}H NMR (CD$_3$OD, 600 MHz) spectrum for bufalin pimeloyl-L-arginine (**9c**)
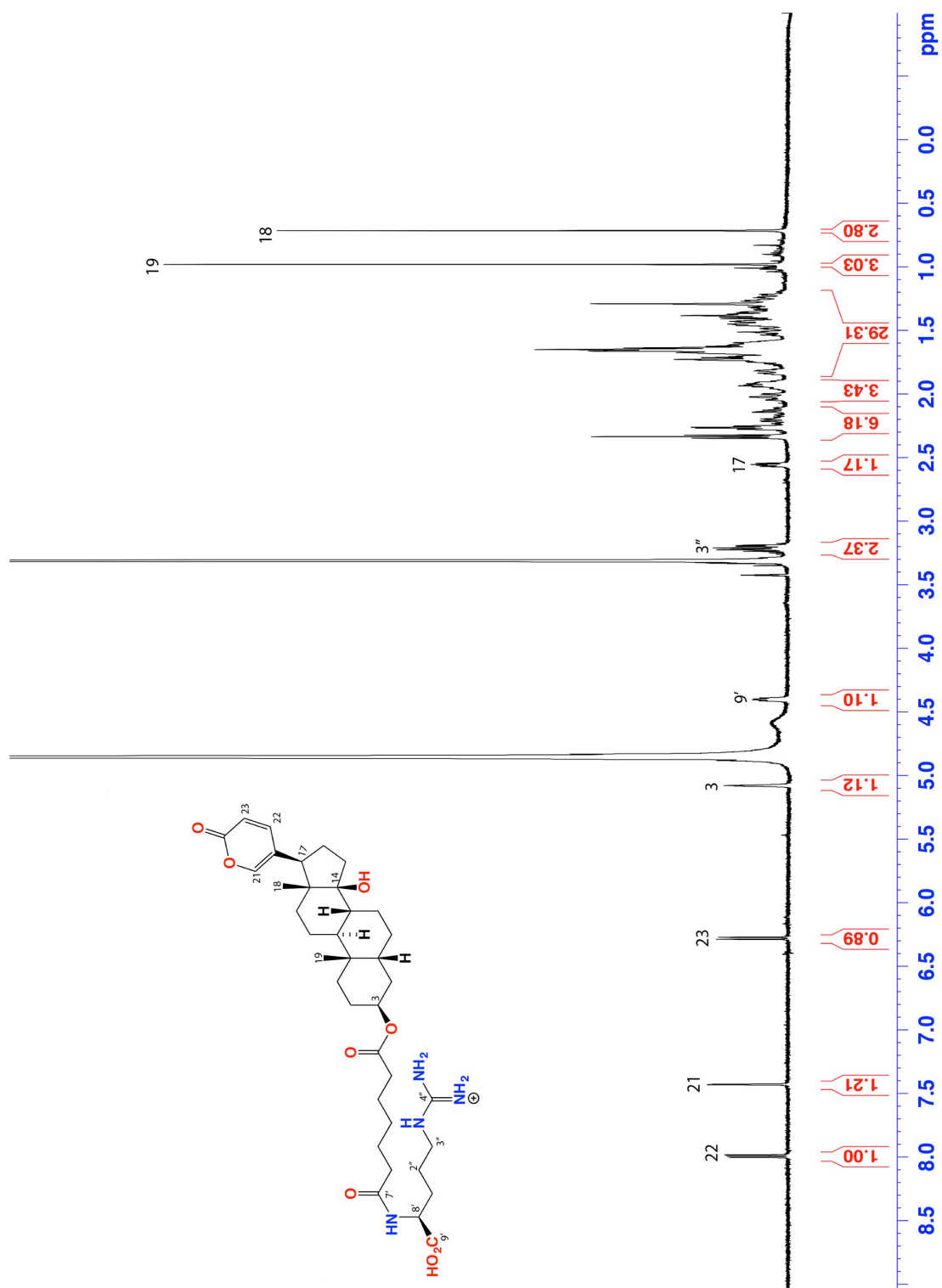
Figure S24 ¹H NMR (CD₃OD, 600 MHz) spectrum for marinobufagenin pimeloylarginine (**8c**)
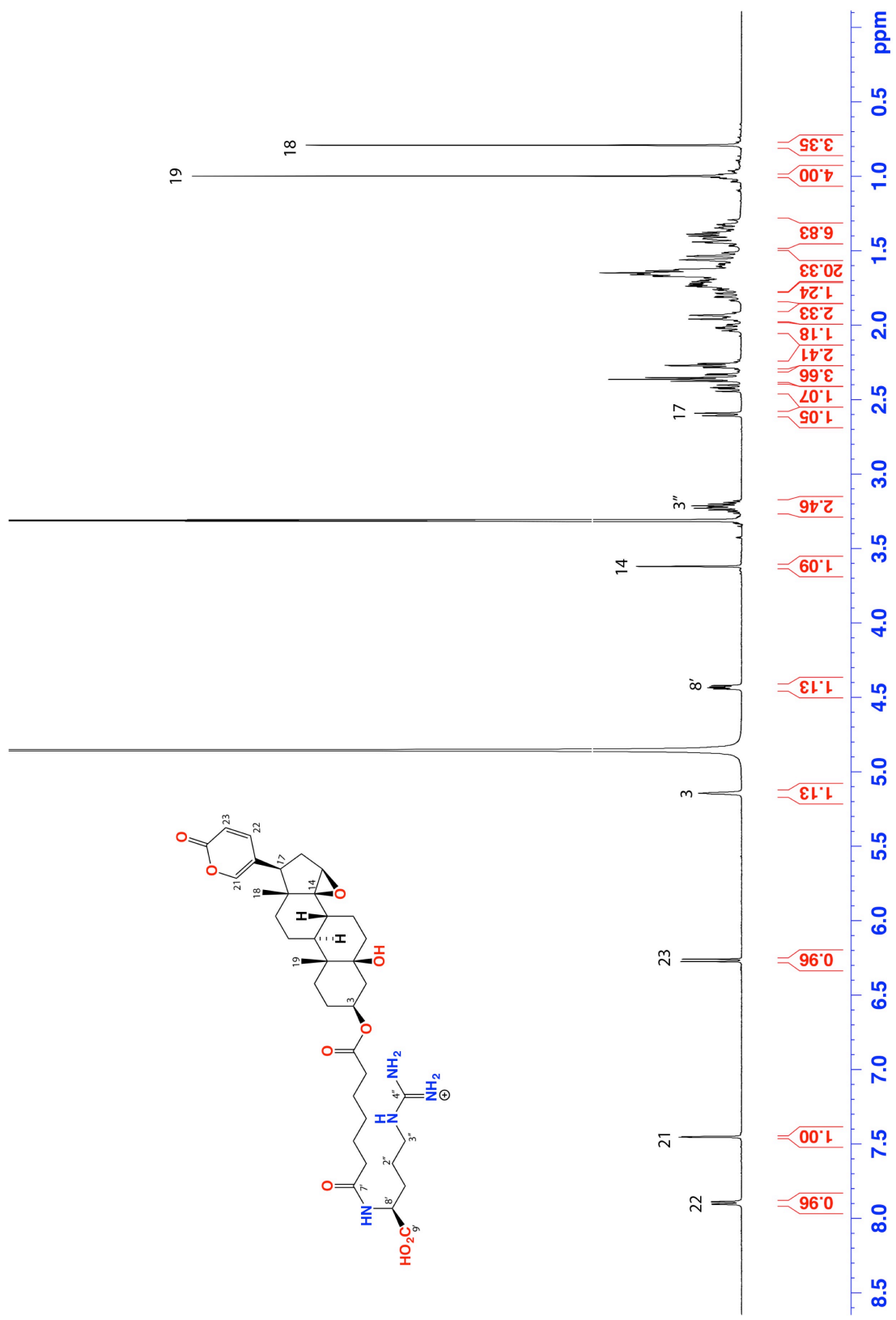
Figure S25 ¹H NMR (600 MHz, CD₃OD) spectrum for derivatized pimeoyl-L-arginine (**3e**)
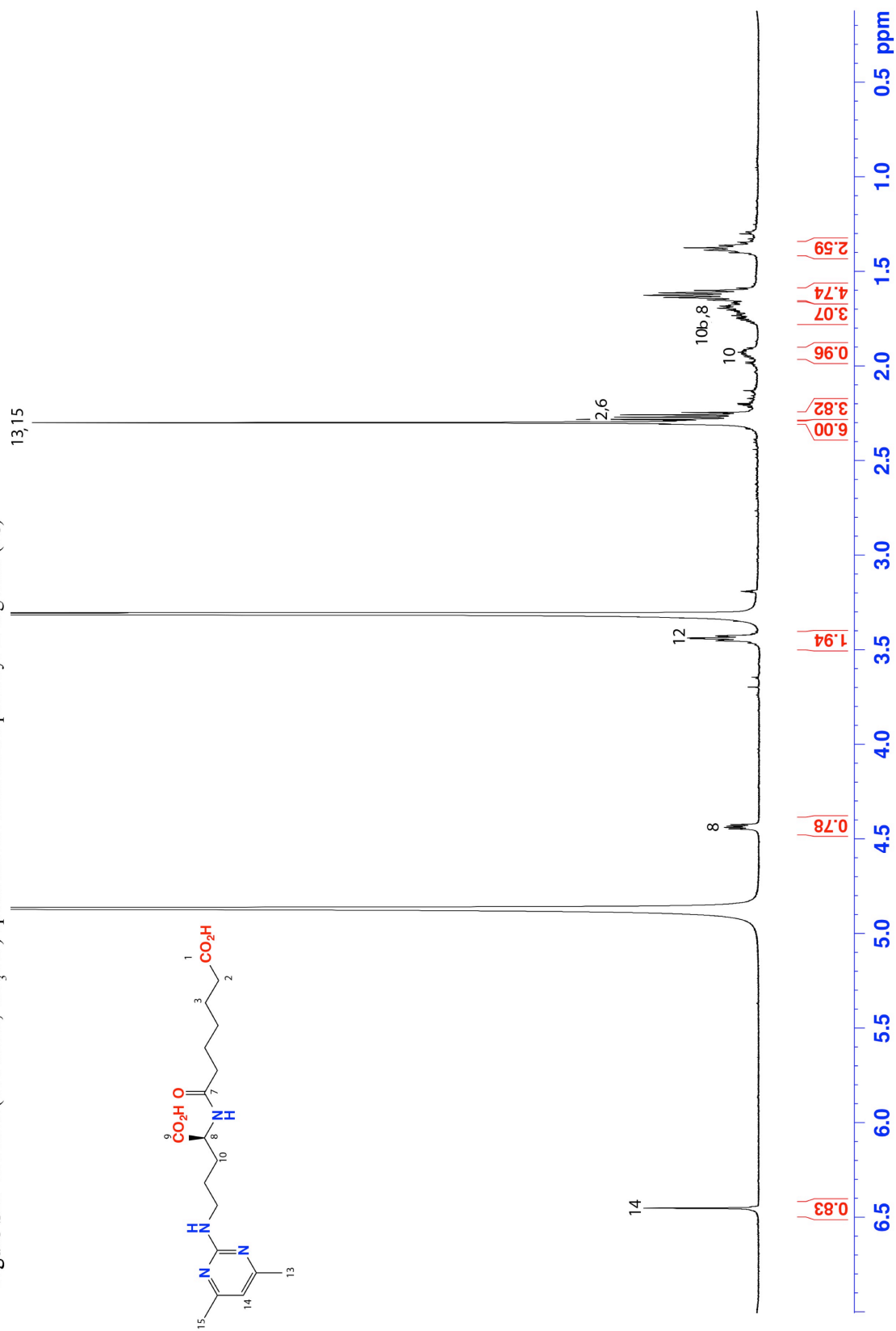
Figure S26 ^{1}H NMR (600 MHz, CD$_3$OD) spectrum for bufalin-3-pimelate (7b)

118
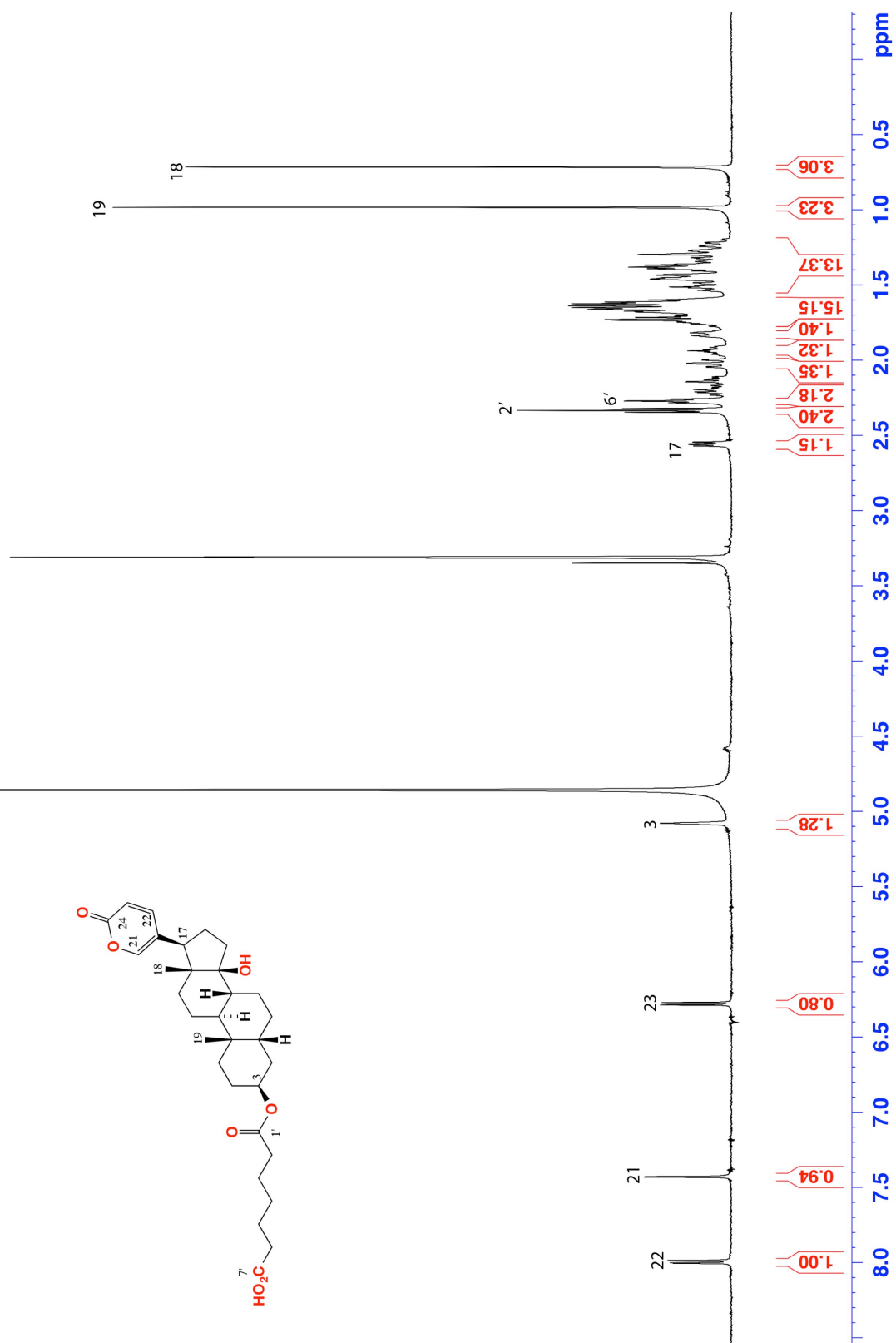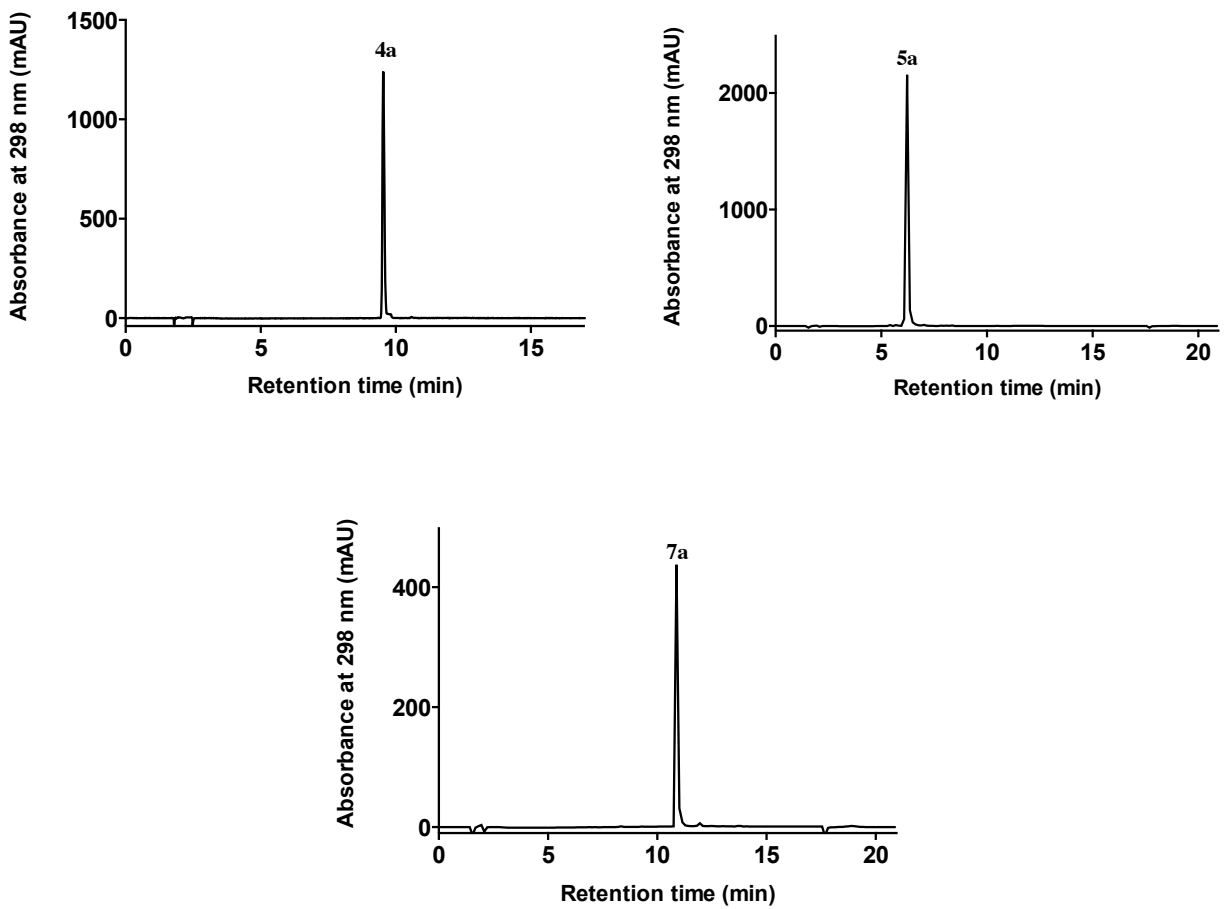
Figure S27. HPLC chromatograms (298 nm) of bufagenins from parotoid secretions analysed using Method 1
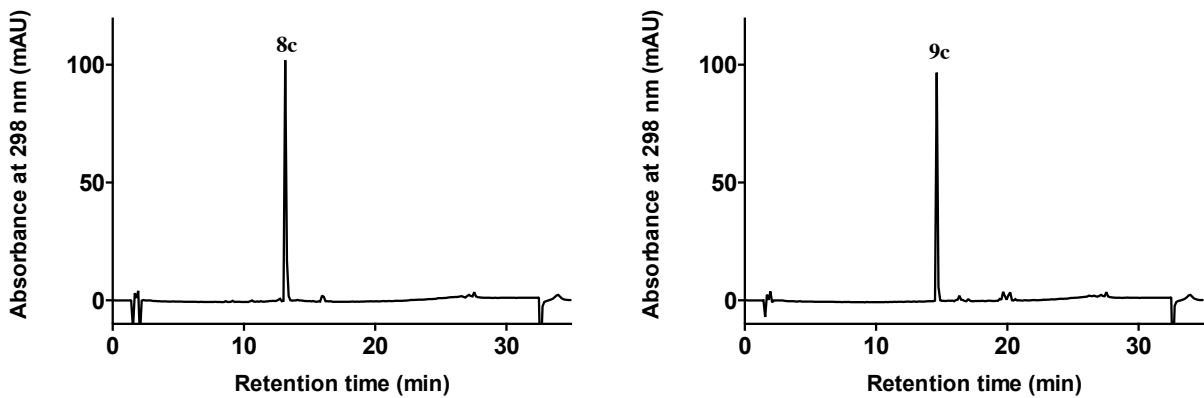
Figure S28. HPLC chromatograms (298 nm) of synthetic bufotoxins analysed using Method 2
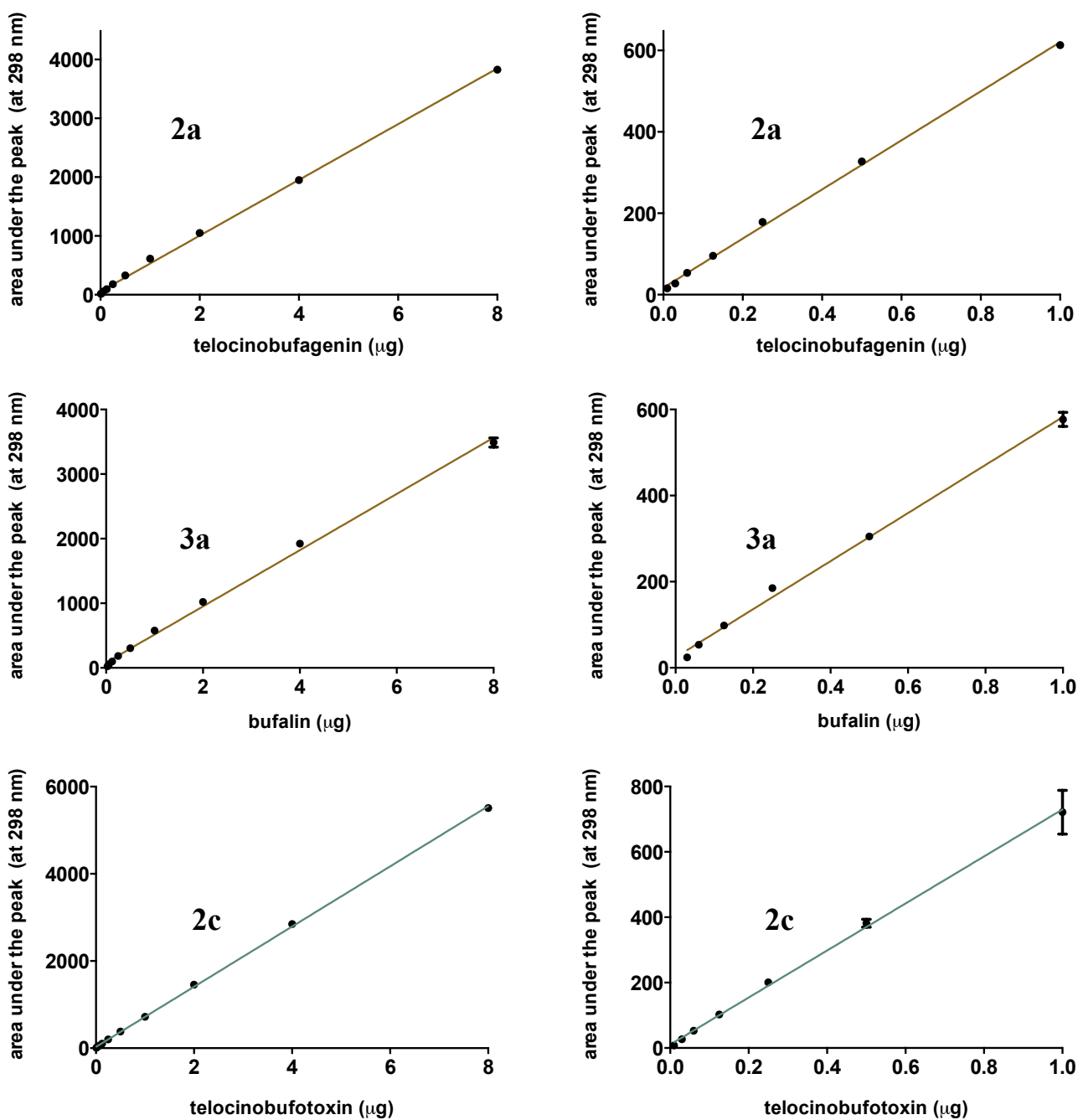
Figure S29a. Concentration curves of bufagenins and bufotoxins. Telocinobufagenin (**2a**) (r^2=0.9987), bufalin (**3a**) (r^2=0.9943) and telocinobufotoxin (**2c**) (r^2=0.9993)
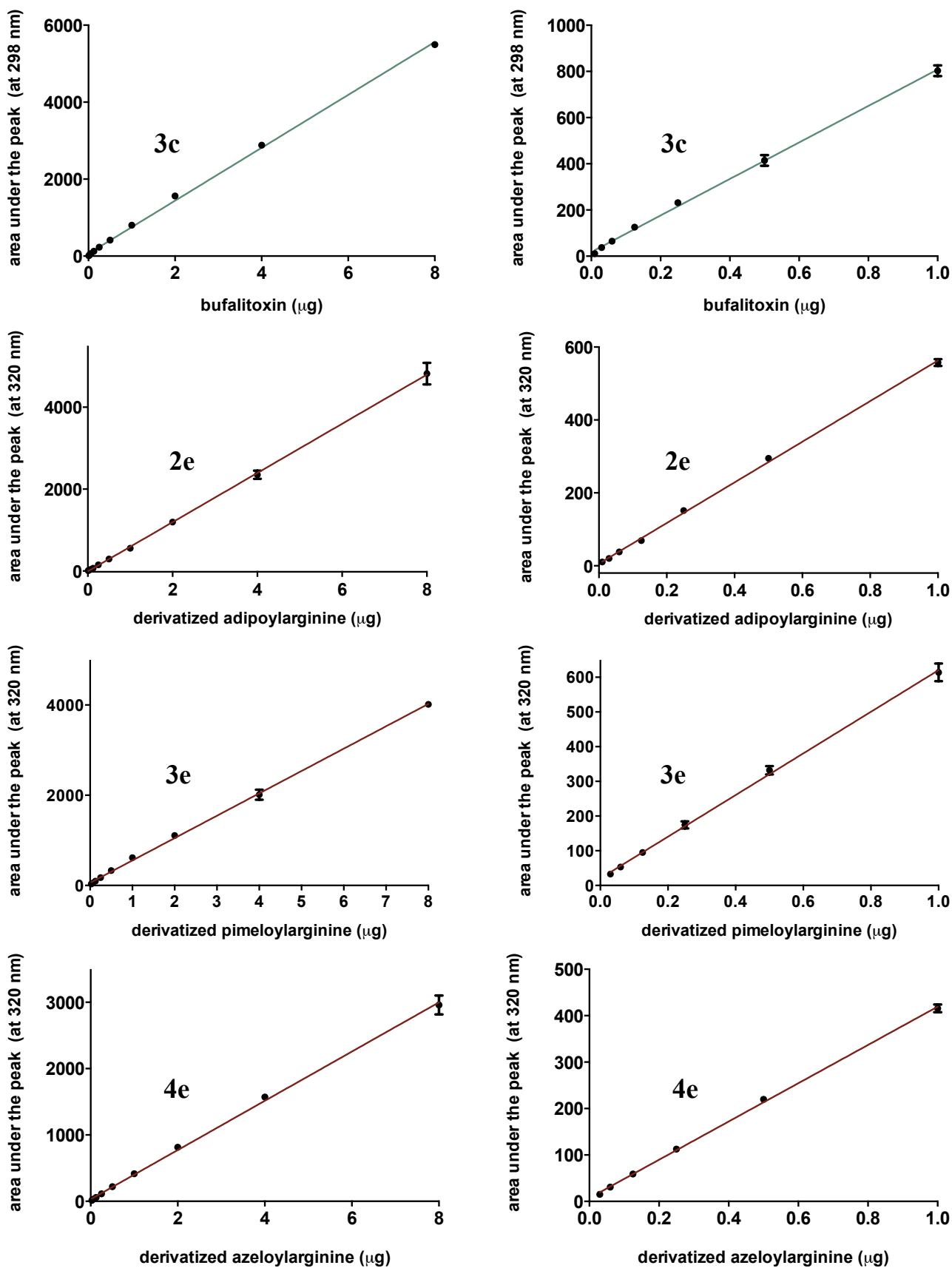
Figure S29b. Concentration curves of bufotoxins and derivatized amides. Bufalitoxin (**3c**) (r^2=0.9985), der. adipoyl-L-arginine (**2e**) (r^2=0.9925), der. pimeloyl-L-arginine (**3e**) (r^2=0.9960) and der. azeloyl-L-arginine (**4e**) (r^2=0.9938)

2.6 References

1. Hayes, R. A.; Piggott, A. M.; Dalle, K.; Capon, R. J., Microbial biotransformation as a source of chemical diversity in cane toad steroid toxins. *Bioorg. Med. Chem. Lett.* **2009,** *19*, 1790-1792.
2. Yoshika, M.; Komiyama, Y.; Konishi, M.; Akizawa, T.; Kobayashi, T.; Date, M.; Kobatake, S.; Masuda, M.; Masaki, H.; Takahashi, H., Novel digitalis-like factor, marinobufotoxin, isolated from cultured Y-1 cells, and its hypertensive effect in rats. *Hypertension* **2007,** *49*, 209-214.
3. Gao, H.; Zehl, M.; Leitner, A.; Wu, X.; Wang, Z.; Kopp, B., Comparison of toad venoms from different *Bufo* species by HPLC and LC-DAD-MS/MS. *J. Ethnopharmacol.* **2010,** *131*, 368-76.
4. Butler, V. P.; Morris, J. F.; Akizawa, T.; Matsukawa, M.; Keating, P.; Hardart, A.; Furman, I., Heterogeneity and lability of endogenous digitalis-like substances in the plasma of the toad, *Bufo marinus. Am. J. Physio. Regul. Integr. Comp. Physiol.* **1996,** *271*, R325-R332.
5. Shimada, K.; Ohishi, K.; Nambara, T., Studies on steroids .208. Bufadienolides from *Bufo asper. J. Nat. Prod.* **1985,** *48*, 159-159.
6. Shimada, K.; Nambara, T., Studies on steroids .148. Isolation and characterization of cardiotonic steroid conjugates from the skin of *Bufo marinus* (L) Schneider. *Chem. Pharm. Bull.* **1979,** *27*, 1881-1886.
7. Hutchinson, D. A.; Mori, A.; Savitzky, A. H.; Burghardt, G. M.; Wu, X. G.; Meinwald, J.; Schroeder, F. C., Dietary sequestration of defensive steroids in nuchal glands of the Asian snake *Rhabdophis tigrinus. Proc. Natl. Acad. Sci. U. S. A.* **2007,** *104*, 2265-2270.
8. Bagrov, A. Y.; Dmitrieva, R. I.; Fedorova, O. V.; Kazakov, G. P.; Roukoyatkina, N. I.; Shpen, V. M., Endogenous marinobufagenin-like immunoreactive substance - A possible endogenous Na^+K^+-ATPase inhibitor with vasoconstrictor activity. *Am. J. Hypertens.* **1996,** *9*, 982-990.
9. Jing, J.; Ren, W. C.; Li, C.; Bose, U.; Parekh, H. S.; Wei, M. Q., Rapid identification of primary constituents in parotoid gland secretions of the Australian cane toad using HPLC/MS-Q-TOF. *Biomed. Chromatogr.* **2013,** *27*, 685-687.
10. Gao, H. M.; Zehl, M.; Leitner, A.; Wu, X. Y.; Wang, Z. M.; Kopp, B., Comparison of toad venoms from different *Bufo* species by HPLC and LC-DAD-MS/MS. *J. Ethnopharmacol.* **2010,** *131*, 368-376.
11. Crossland, M. R.; Haramura, T.; Salim, A. A.; Capon, R. J.; Shine, R., Exploiting intraspecific competitive mechanisms to control invasive cane toads (*Rhinella marina*). *Proc. R. Soc. B-Biol. Sci.* **2012,** *279*, 3436-3442.
12. Reynolds, W. F.; Maxwell, A.; Telang, B.; Bedaisie, K.; Ramcharan, G., Total Assignment of the H-1 and C-13 Nmr Chemical-Shifts of 4 Bufadienolides by 2d Nmr-Spectroscopy. *Magn. Reson. Chem.* **1995,** *33*, 412-414.
13. Chen, K. K.; Kovariko.A, Pharmacology and toxicology of toad venom. *J. Pharm. Sci.* **1967,** *56*, 1535-&.
14. Pettit, G. R.; Kamano, Y., Bufadienolides .28. Marinobufotoxin. *J. Org. Chem.* **1974,** *39*, 3003-3006.
15. Pettit, G. R.; Kamano, Y.; Drasar, P.; Inoue, M.; Knight, J. C., Steroids and related natural-products .104. Synthesis of bufalitoxin and bufotoxin .36. Bufadienolides. *J. Org. Chem.* **1987,** *52*, 3573-3578.
16. Shimada, K.; Fujii, Y.; Yamashita, E.; Niizaki, Y.; Sato, Y.; Nambara, T., Studies on steroids .119. Studies on cardiotonic steroids from skin of Japanese toad. *Chem. Pharm. Bull.* **1977,** *25*, 714-730.
17. Kasai, H.; Tsubuki, M.; Shimada, K.; Nambara, T.; Honda, T., Analyses of Biologically Active Steroids: Antitumor Active OSW-1 and Cardiotonic Marinobufotoxin, by Matrix-Assisted Laser Desorption/Ionization Quadrupole Ion Trap Time-of-Flight Tandem Mass Spectrometry. *Chem. Pharm. Bull.* **2009,** *57*, 948-956.

18. Higashi, T.; Nakayama, N.; Shimada, K.; Kasai, H.; Nakazawa, H., High-performance liquid chromatography - Tandem mass spectrometry of cardiac steroids. *J. Liq. Chromatogr. Relat. Technol.* **1999,** *22*, 2283-2296.

19. Shimada, K.; Nambara, T., Studies on steroids .156. Isolation and characterization of a new type of bufotoxin from the skin of *Bufo americanus*. *Chem. Pharm. Bull.* **1980,** *28*, 1559-1562.

20. Sakai, A.; Xiang, D. F.; Xu, C. F.; Song, L.; Yew, W. S.; Raushel, F. M.; Gerlt, J. A., Evolution of enzymatic activities in the enolase superfamily: N-succinylamino acid racemase and a new pathway for the irreversible conversion of D- to L-amino acids. *Biochemistry* **2006,** *45*, 4455-4462.

21. Urban, S.; Capon, R. J.; Hooper, J. N. A., A new alkaloid from an australian marine sponge, *Spongosorites* sp. *Aust. J. Chem.* **1994,** *47*, 2279-2282.

Chapter 3: Chemo-anatomy: Bufadienolide composition in cane toad parotoid toxin and parotoid secretion

3.1 Introduction

The aim of this section of my research is to analyse bufadienolide composition and levels within adult cane toad parotoid glands. Depending on experimental method, our investigations into the chemistry of secretions obtained from live cane toads resulted in variable results – yielding different proportions of bufagenins vs bufotoxins. This finding led to new insights into the composition and storage of bufadienolides in cane toad parotoid glands. Based on the handling procedures, the composition of bufadienolides in secretion varies. To better understand this phenomenon we investigated bufadienolide composition in secretions and *in situ* (within the parotoid gland). To differentiate toxins found within versus those secreted from the parotoid gland, we adopted a clarifying terminology. A "parotoid toxin" indicates the toxin present within the parotoid gland (*in situ*) while a "parotoid secretion" indicates the toxin secreted from the parotoid gland upon manual pressure (*ex situ*).

Parotoid secretions were obtained by manual squeezing the parotoid gland onto a solid/liquid medium. As parotoid toxins are stored within the parotoid gland in numerous small microglands, parotoid toxins were obtained by micro-dissection of the parotoid gland followed by solvent extraction.

The bufadienolides content in parotoid toxins and secretions were quantified by the methods developed in chapter 2. Our study into bufadienolide composition of the parotoid toxin provides insights into the *in situ* storage of bufadienolides in adult cane toads, extending across physical (formation of secondary structures such as liposomes), chemical (stability against biological fluids such as plasma), microbiological (susceptibility to biotransformation) and biological (cytotoxicity) aspects of bufadienolides.
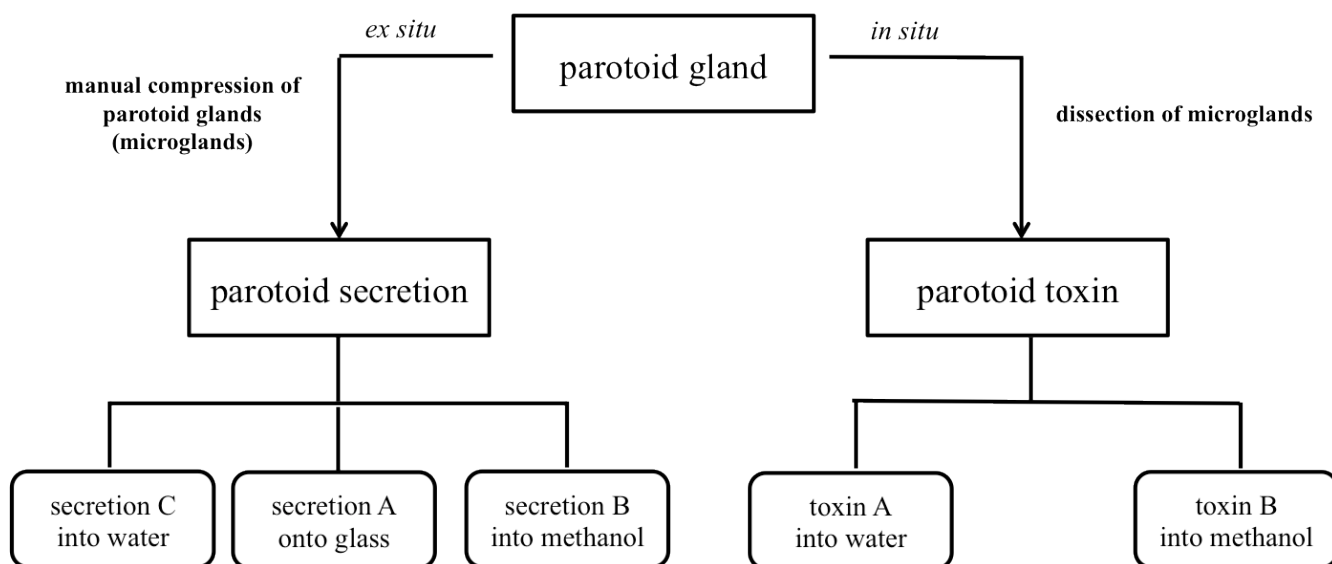
Figure 3.1 Scheme of handling of parotoid gland contents with respect to investigations on storage and delivery of cane toad toxins

Chemical analyses of *ex situ* parotoid secretions were performed by adopting various handling conditions, squeezing the parotoid secretions onto different media, glass (secretion A), MeOH (secretion B) and H_2O (secretion C). Parotoid toxins were investigated by dissecting parotoid microglands into MeOH and/or H_2O followed by analyzing for bufadienolides and arginyl amides using previously established analytical methodology. Composition of bufadienolides in parotoid secretions vs parotoid toxin would provide insights into storage and delivery of cane toad toxins.

3.2 Results and discussion

3.2.1 Micro-dissection of parotoid microglands

In situ parotoid toxin is stored in 60 – 100 small microgland like structures called parotoid microglands attached to the parotoid epithelium (Figure 3.2).[1] Each microgland is about 0.5 – 1 mm diameter and is highly vascularized. During the manual compression of the parotoid gland, the stored toxin is pushed outwards via the opening of the microgland through to the pores of the parotoid skin. It has been reported that the synthesis and storage of toxin, including bufadienolides, biogenic amines and proteins, occurs in the microglands.[2]

**parotoid gland
(dorsal)**

**parotoid gland
(ventral)**
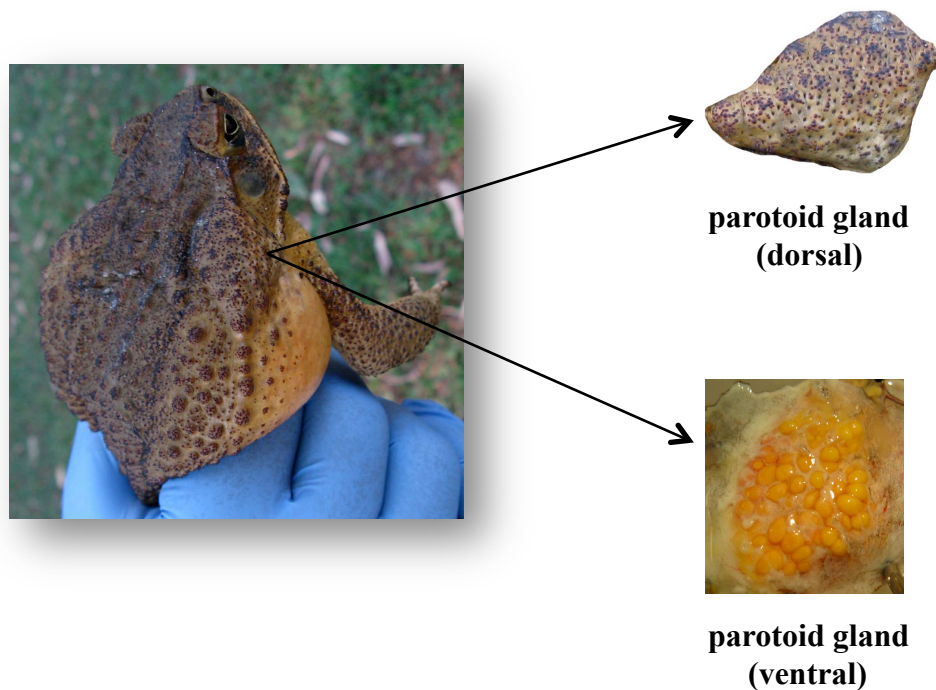
Figure 3.2 Section of parotoid gland exhibiting dorsal portion covered with thick epithelium and fine pores and the ventral portion exhibiting numerous microglands filled with parotoid toxin
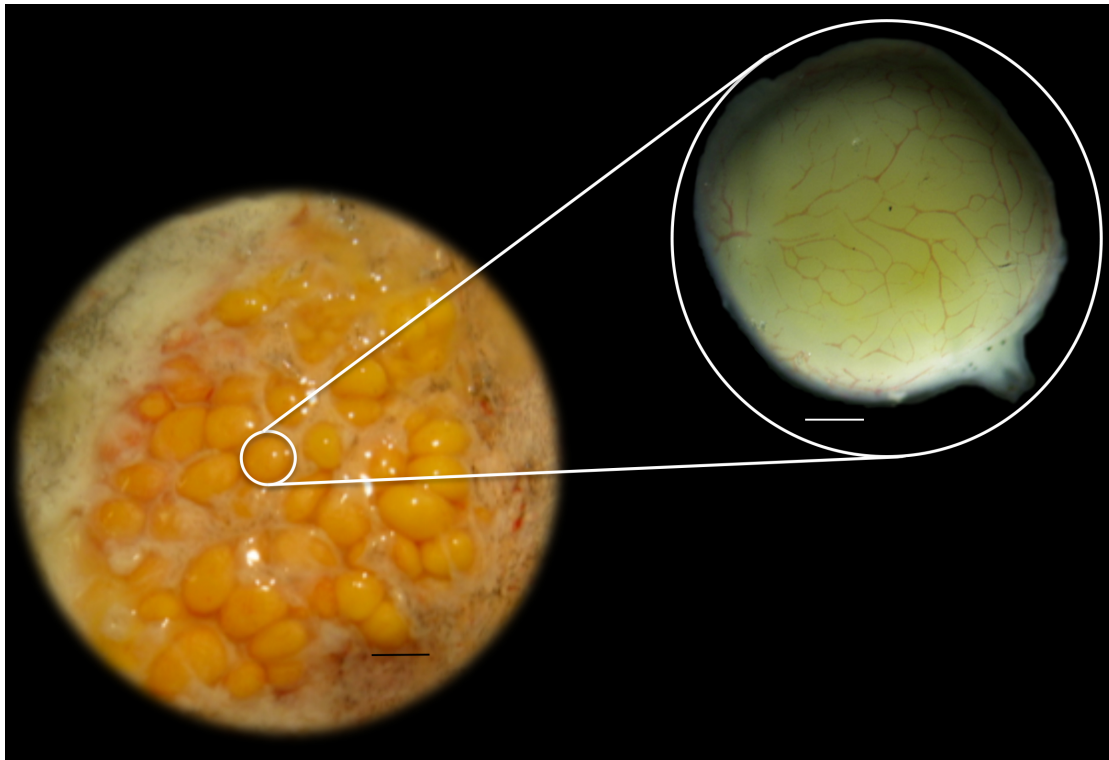
Figure 3.3 Light microscopy image of parotoid microglands (left). A parotoid microgland filled with toxin (right). Bars – black = 10 mm, white = 500 μM

Parotoid microglands are yellow to orange when filled with toxin. After manual compression of the parotoid glands to release parotoid secretion, the deflated microgland is filled with blood. Compressed parotoid microglands are smaller in size (deflated) and are bright red. Another, interesting feature of the parotoid gland is all of the toxin cannot be expelled by a single compression leaving a mix of yellow and red microglands. A previous study by Morales et al determined that a single compression of a parotoid gland leaves approximately 50% of the microglands intact.[3] The red microglands takes about 28 days to mature into a fully loaded yellow parotoid microgland (filled with toxin). This reluctance to fully deplete toxin levels during a secretion event (predatory attack) may be designed to ensure that the toad retains sufficient levels of toxin to protect against subsequent predatory attacks.[3]

Micro-dissection involves dissecting individual parotoid microglands, with the aid of a microscope (Figure 3.5). Micro-scissors and micro-tweezers were used to cut individual microglands from the surrounding epithelium, which were secured by a strong basal attachment. Isolated microglands were examined under a light microscope (Carl Zeiss, Australia) to ensure that they were not damaged during dissection.
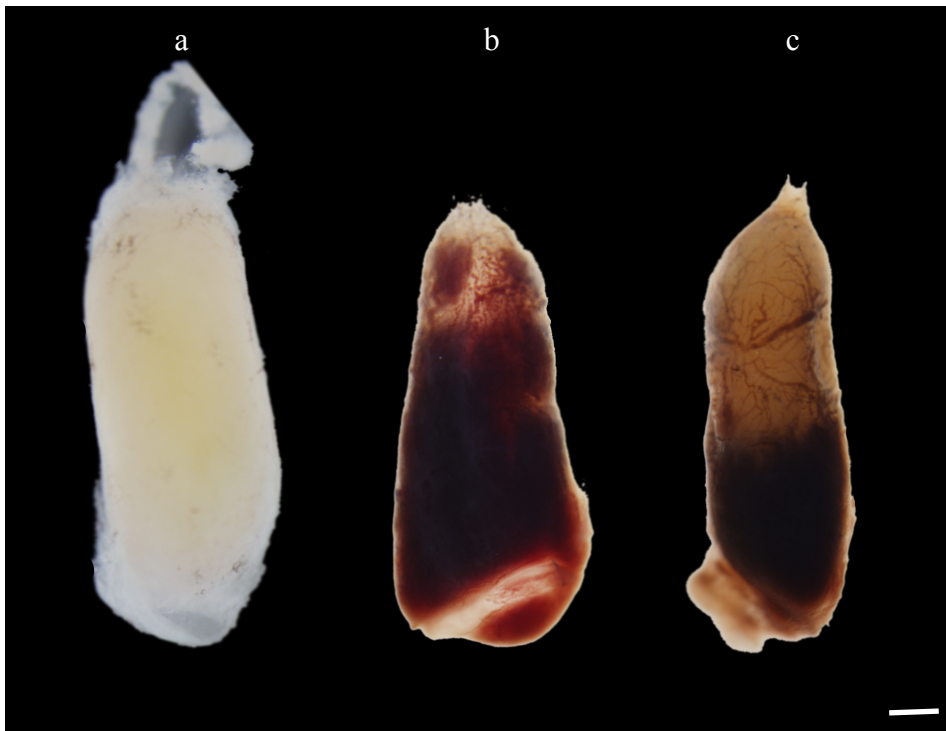
Figure 3.4 (a) Parotoid microgland filled with toxin before manual compression with evidence of toxin leakage, (b) filled with blood after manual compression of the parotoid gland and (c) partially filled with toxin and blood after manual compression of the parotoid gland, bar = 500 μm

Parotoid microglands when filled with parotoid toxin have a diameter of a 500 μm with a well-defined continuous myoepithelium (Figure 3.4). The entire parotoid microgland features a rich network of collagenous connective tissue, which was previously proposed to supply nutrients for the biosynthesis of parotoid toxin.[4] The microgland toxin exit duct also features a dense network of connective tissue and epithelium, believed to facilitate contraction and toxin release during a predatory attack. Scanning electron microscopy of intact excised microglands reveal structural elements that aids in the storage and secretion of parotoid toxin (Figures 3.5 and 3.6), whereas scanning electron microscopy of compressed (deflated) parotoid microglands reveals a ruptured or shrunk myoepithelium (Figure 3.6) and an expanded exit duct (due to the passage of parotoid toxin during the compression). The connective tissue of compressed microglands is more transparent compared to intact microglands, and shows accumulation of epithelial cells with a rich network of collagen like fibrous connective tissue.
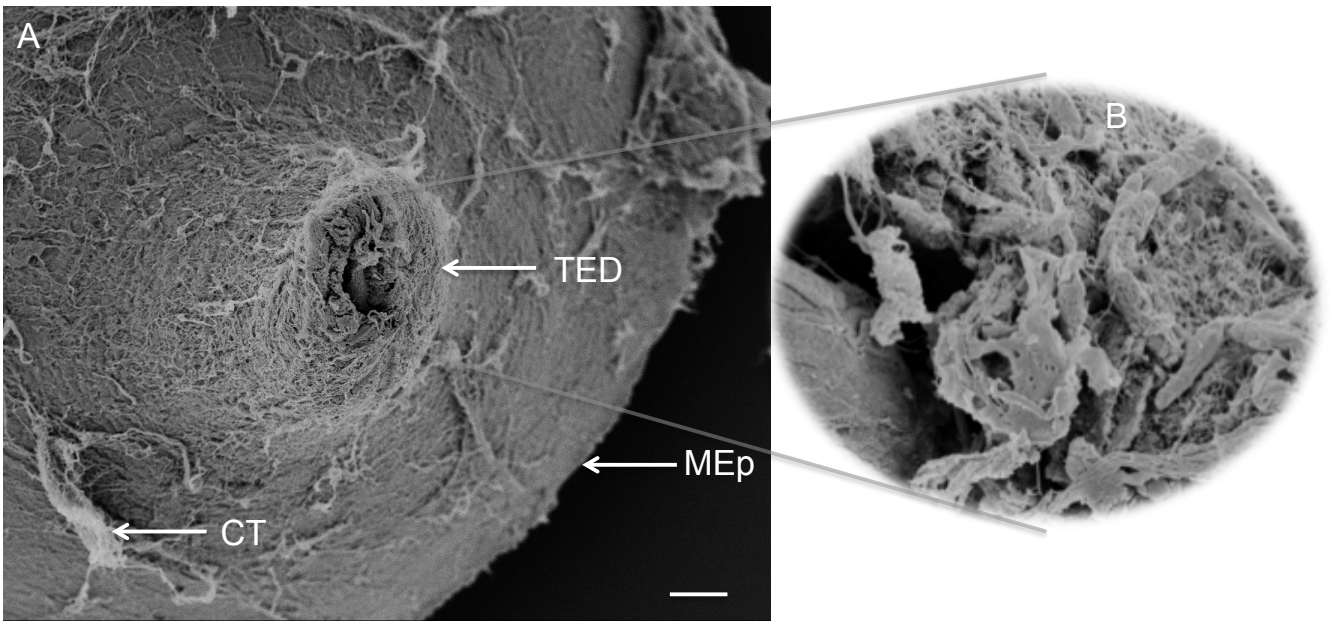
Figure 3.5 Scanning electron microscopy images of an intact parotoid microgland filled with toxin. A – structural framework of parotoid microgland, TED – toxin exiting duct, MEp – myoepithelium, CT – connective tissue, B – epithelium with a network of connective tissue.
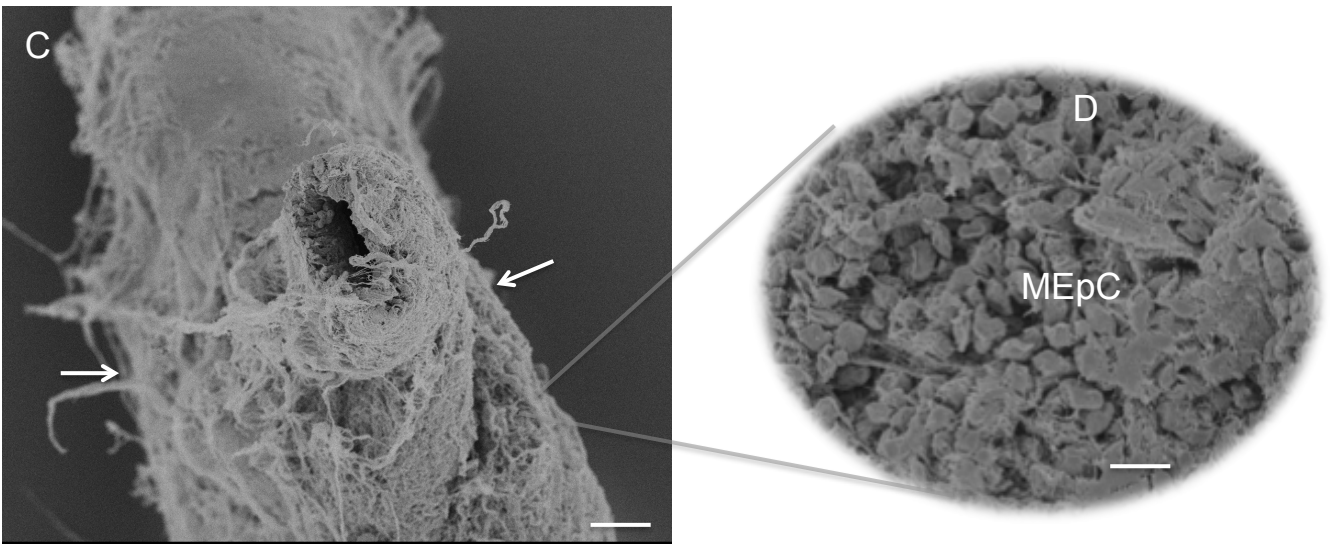
Figure 3.6 Scanning electron microscopy images of a compressed parotoid microgland filled with blood. C – structural framework of parotoid microgland, arrows pointing to ruptured/shrunk myoepithelium, D – surface of microgland with a large number of myoepihtelial cells with a network of connective tissue.

3.2.2 Chemical analysis and quantification of parotoid secretions, parotoid toxins and parotoid microglands

During preliminary analyses of parotoid secretions from live cane toads we observed that parotoid secretions squeezed into H_2O contained predominantly bufagenins with minor amounts of bufotoxins, while parotoid secretions squeezed onto a glass plate contained mostly bufagenins but with significant amounts of bufotoxins. This observation suggested that, subject to handling, bufotoxins can undergo varying degrees of conversion to bufagenins. This hypothesis was supported by the observation that expression of parotoid secretion directly into MeOH yielded only bufotoxins, while expression into H_2O followed by a short (10 – 20 min) incubation at room temperature yielded only bufagenins. All these observations were confirmed by quantitative analyses as detailed below.

3.2.2.1 Secretion A – parotoid secretion squeezed onto a glass plate

Manual compression of parotoid glands to release secretion directly on to a glass plate has been reported previously, and is often used as a standard method to obtain parotoid secretions.[5, 6] Following this strategy the parotoid gland secretions of five adult cane toads were squeezed on to a glass plate and were left for an hour during which the secretion turned into a dry waxy solid. All the toads selected for these analyses were within the mass range of 90 – 180 g, and included three female (181 g, 102 g and 149 g) and two male (103 g and 91 g) cane toads. The dry waxy parotoid secretion from each toad was dissolved from the glass surface into MeOH (5 mL) and dried under N_2 at 40 °C to yield 231 mg, 104 mg, 96 mg, 168 mg and 78 mg respectively. This result is consistent with our previous studies, where we observed that the mass of toads correlates with parotoid secretion mass yields. The dried MeOH extract was subjected to n-BuOH/ H_2O partition, and the n-BuOH solubles were dried under N_2 at 40 °C and weighed to generate 49 mg, 21 mg, 18 mg, 36 mg and 15 mg, respectively. Based on prior experience in our laboratory the n-BuOH phase contains all bufadienolides, while various indole-alkaloids and catecholamine components are concentrated in the H_2O soluble phase. The n-BuOH solubles were then re-dissolved in MeOH to a standard concentration (1 mg/mL) to generate analytes A1 – A5 which were analysed using Method 2 (Chapter 2) specific for bufagenins and bufotoxins, respectively (Figure 3.7).
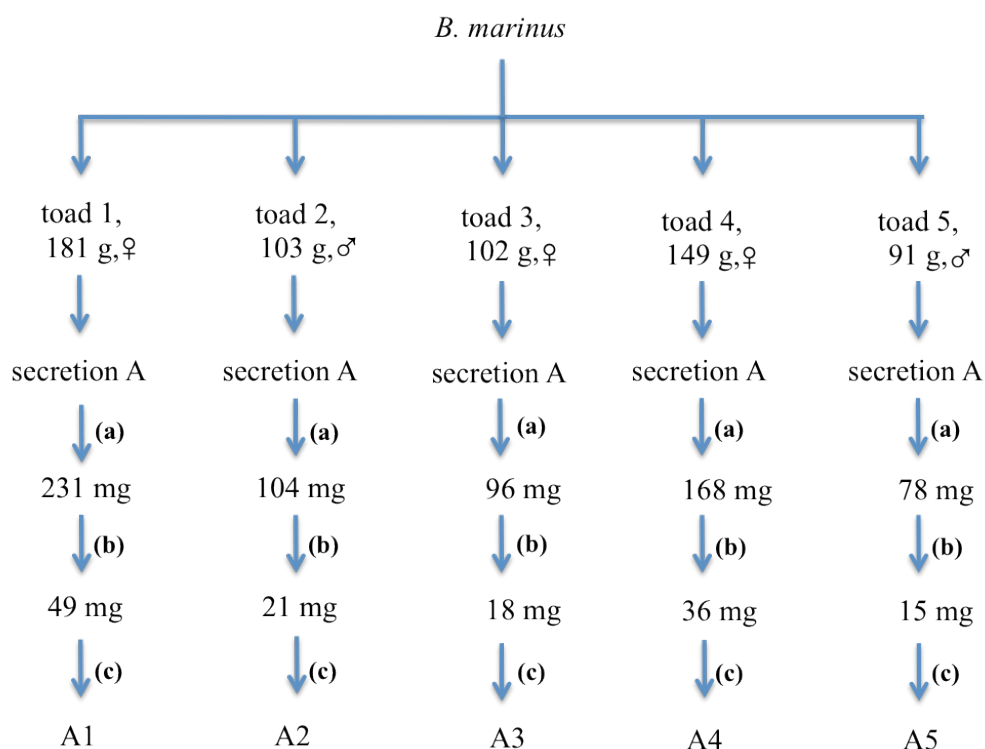
(a) – dissolved in MeOH (5 mL) dried under N_2 at 40 °C
(b) – n-BuOH/H_2O (1:1), 10 mL partition, with n-BuOH concentrated under N_2 at 40 °C
(c) – re-dissolved in MeOH (1 mg/mL), to generate analytes

Figure 3.7 Secretion A – production of analytes A1 – A5 (n-BuOH)

Aliquots (10 μL =10 μg) of A1 – A5 were analysed using HPLC Method 2 (see Chapter 2) to yield five HPLC traces (Figure 3.8). Comparison of HPLC retention times and HPLC-MS data for all peaks in the traces with authentic standards (See Chapter 2) confirmed the presence of bufagenins (**1a**, **2a**, **3a**, **4a** and **5a**) (Figure 3.9) and bufotoxins (**1c**, **2c**, **3c** and **5c**) (Figure 3.10). The area under each peak was quantified to generate relative bufadienolide percentages in A1 – A5 (Table 3.1).
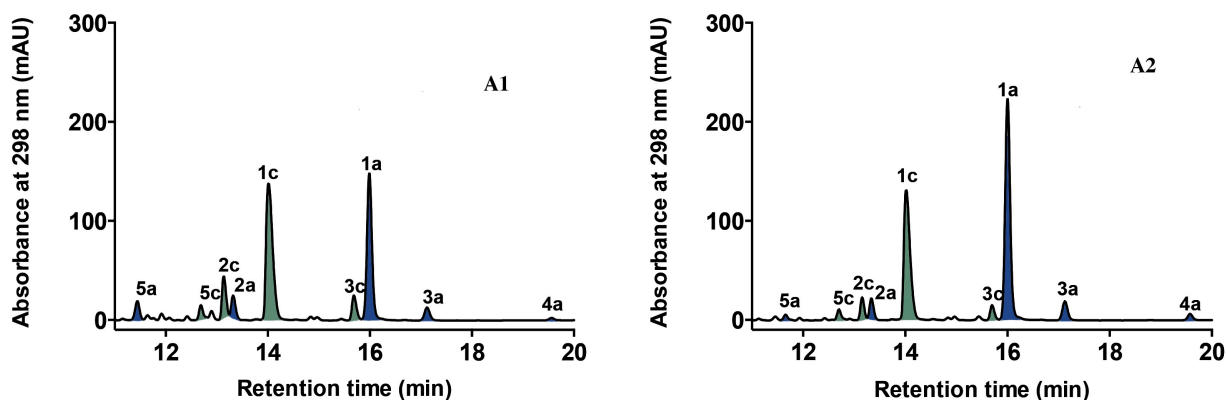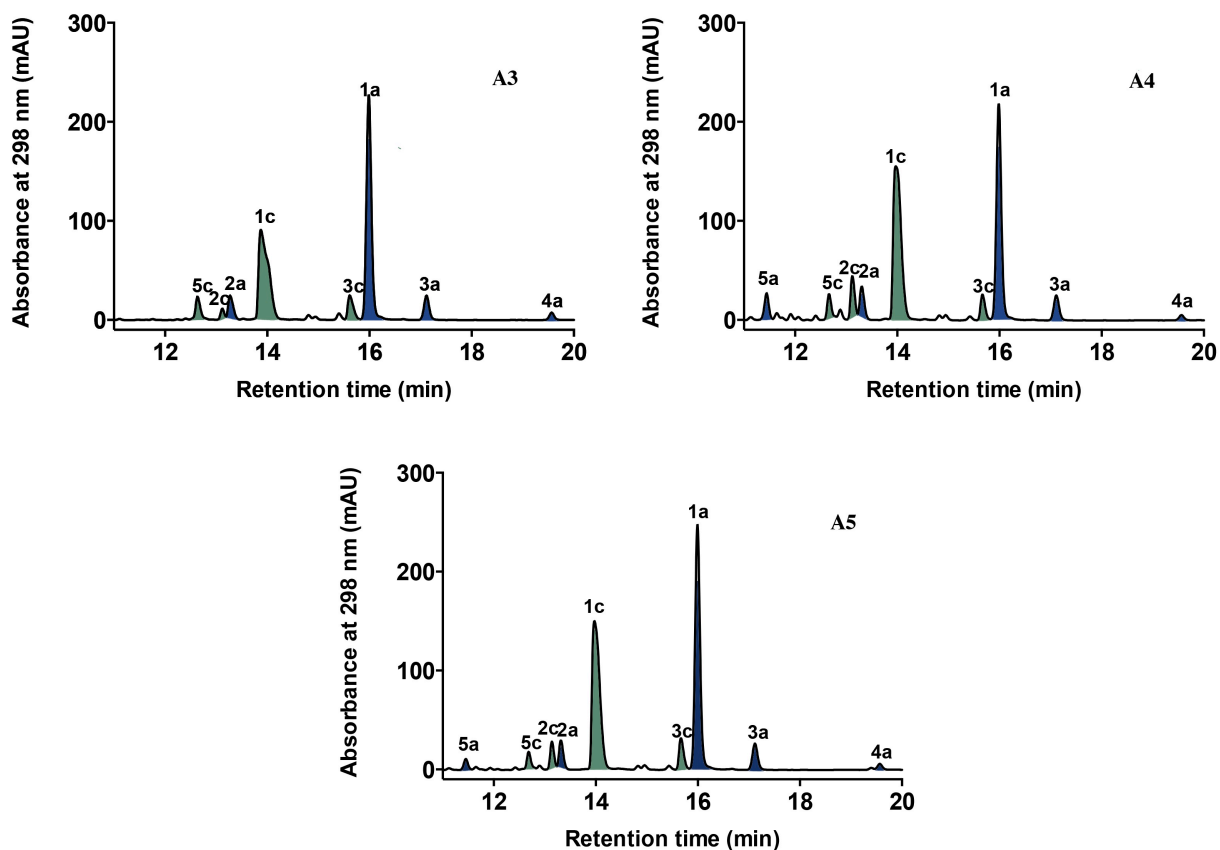
Figure 3.8 HPLC chromatogram (298 nm) of Secretion A analytes A1-A5 analysed using Method 2 (see Chapter 2). Bufotoxins (green) and bufagenins (blue). Marinobufotoxin (**1c**), telocinobufotoxin (**2c**), bufalitoxin (**3c**), hellebritoxin (**5c**), marinobufagenin (**1a**), telocinobufagenin (**2a**), bufalin (**3a**) and resibufagenin (**4a**).

marinobufotoxin (**1c**)

telocinobufotoxin (**2c**)..

bufalitoxin (**3c**)

heelbritoxin (**3c**)

marinobufagenin pimeloyl-L-arginine (**8c**)
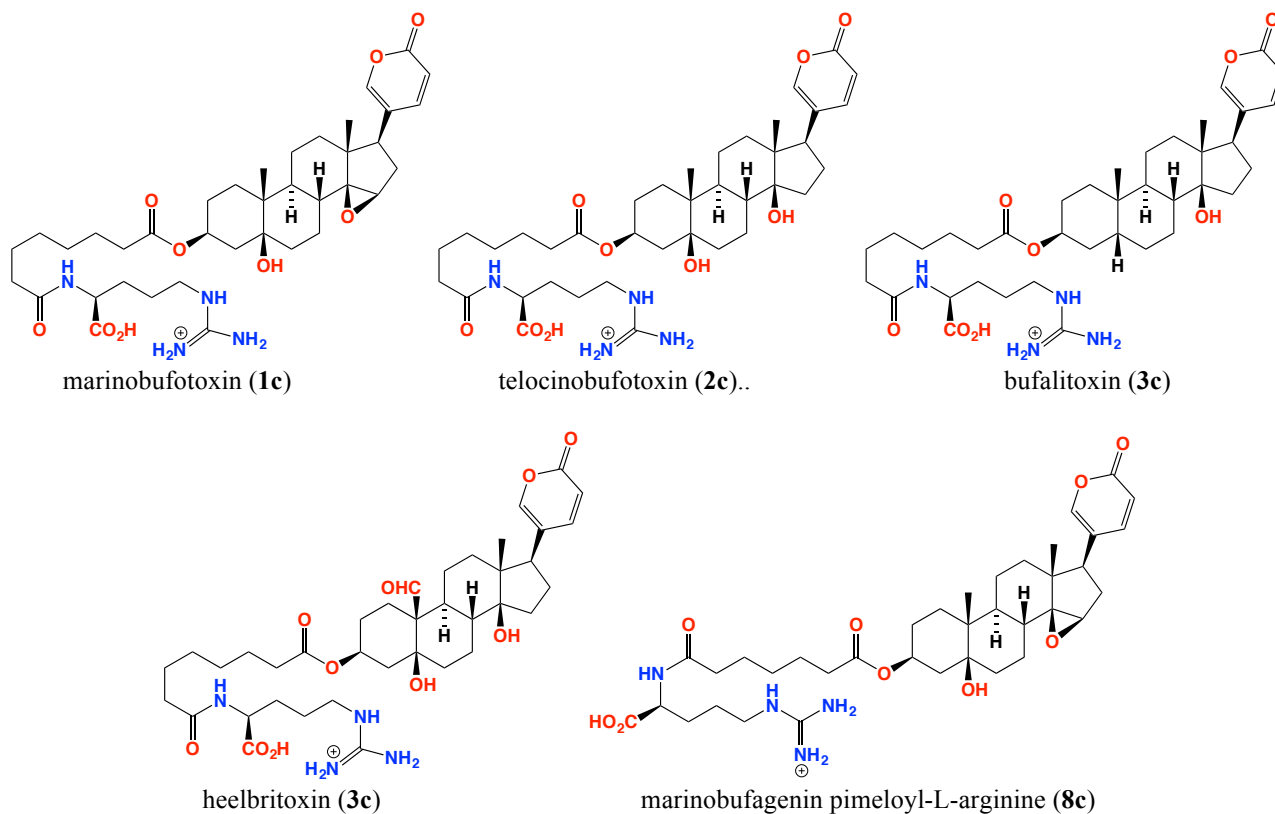
Figure 3.9 Bufotoxins identified in parotoid secretions in secretion A

133
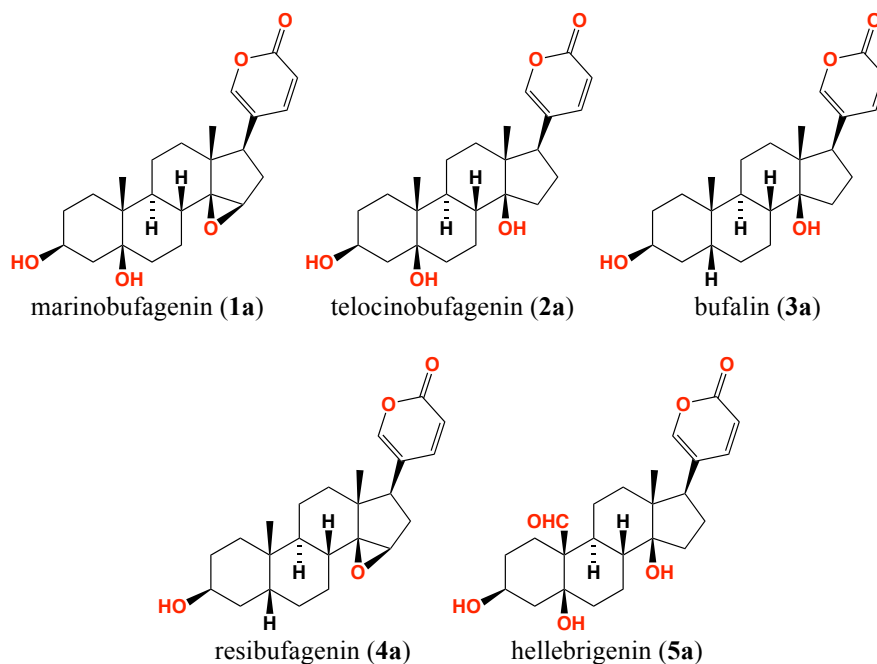
Figure 3.10 Bufagenins identified in parotoid secretions in secretion A

Table 3.1 Relative composition (%) of bufadienolides in secretion A (A1 – A5 are analytes)

Compound no.	A1 (%)	A2 (%)	A3 (%)	A4 (%)	A5 (%)
1c	41.4	34.2	33.8	38.5	37.4
2c	5.3	3.8	1.7	6.0	3.7
3c	4.4	2.7	5.3	3.7	4.7
5c	3.0	2.1	4.7	3.8	2.7
1a	33.6	46.6	43.5	34.1	40.0
2a	5.9	4.0	4.9	5.1	4.4
3a	3.0	4.2	4.8	4.1	4.5
4a	0.4	1.3	1.3	0.8	1.0
5a	3.0	1.1	<0.1	3.9	1.6

Secretion A contains an approximately 1:1 composition of bufotoxins to bufagenins with marinobufotoxin (**1c**) as the dominant bufotoxin followed by bufalitoxin (**3c**), telocinobufotoxin (**2c**) and hellebritoxin (**5c**), and marinobufagenin (**1a**) as the dominant bufagenin followed by telocinobufagenin (**2a**), bufalin (**3a**) and hellebrigenin (**5a**).

The area under each peak in the HPLC traces (Figure 3.8) was also compared against standard curves for marinobufagenin (Chapter 2, Figure 2.16) and marinobufotoxin (Chapter 2, Figure 2.18), to calculate the μg/peak per HPLC trace per compound. Table 3.2 uses these qualitative measures to calculate the weight (mg) of each bufadienolide in each secretion A sample.

Secretion A contains an approximately 1.8:1 weight composition of bufotoxins to bufagenins, with marinobufotoxin (**1c**) as the dominant bufotoxin followed by bufalitoxin (**3c**), telocinobufotoxin (**2c**) and hellebritoxin (**5c**), and marinobufagenin (**1a**) was the dominant bufagenin followed by telocinobufagenin (**2a**) and bufalin (**3a**).

Table 3.2 Absolute amounts (mg) of bufadienolides in secretion A

Compound no.	A1 (mg)	A2 (mg)	A3 (mg)	A4 (mg)	A5 (mg)
1c	25.9	7.9	6.8	18.7	5.4
2c	2.9	1.0	0.9	2.5	0.7
3c	1.9	0.8	0.5	1.0	0.6
5c	0.9	0.8	0.5	1.0	0.6
1a	12.7	6.3	5.6	9.4	4.0
2a	1.9	0.6	0.5	1.0	0.6
3a	0.5	0.6	0.5	0.7	0.6
4a	<0.1	<0.1	<0.1	<0.1	<0.1
5a	<0.1	<0.1	<0.1	0.3	<0.1

From the above analysis the total weight of bufadienolides per secretion A was calculated across toads 1 – 5 to be 46 mg, 18 mg, 15 mg, 34 mg and 12 mg respectively with the bufagenin to bufotoxin ratio in male and female toads being similar. Since cane toads deliver approximately half of their toxin content in the first compression of the parotoid gland, and possess two glands, we can estimate the total bufadienolide load per toad to be of 50 – 200 mg.

3.2.2.2 Secretion B – parotoid secretions squeezed into MeOH

Parotoid secretion was squeezed from the left parotoid gland of three adult cane toads into MeOH (5 mL) and was left for an hour at room temperature. Two female cane toads weighing, 89 g and 71 g, respectively and one male toad weighing 67 g were subjected to secretion B analyses, and the

crude yellow parotoid secretion in MeOH (5 mL) was dried under N_2 at 40 °C yielding 46 mg, 41 mg, and 38 mg respectively. The dried crude extract was subjected to n-BuOH/H_2O partition, and the n-BuOH solubles were dried under N_2 at 40 °C and weighed to generate 14 mg, 12 mg and 10 mg, respectively. The n-BuOH solubles were then re-dissolved in MeOH to a standard concentration (1 mg/mL) to generate analytes A6 – A8 and were analysed using Method 2 (Chapter 2) specific for bufagenins and bufotoxins, respectively (Figure 3.11).
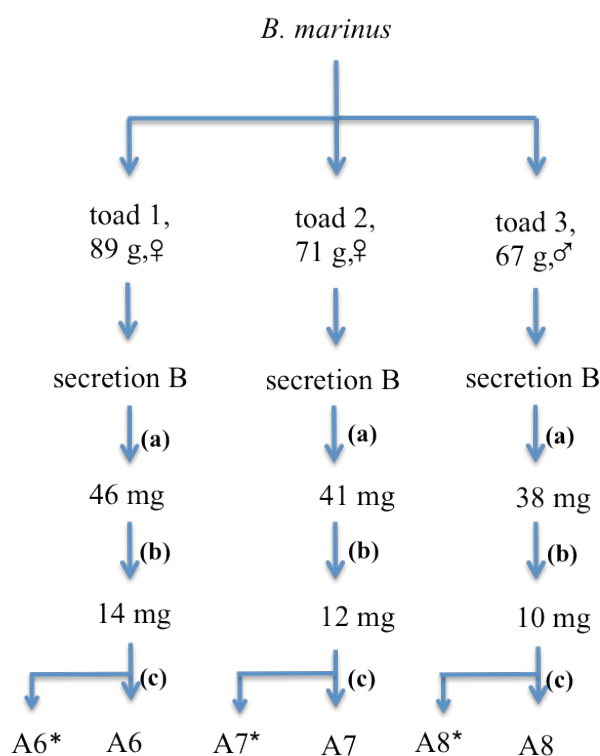
(a) – homogenized in MeOH (5 mL) dried under N_2 at 40 °C
(b) – n-BuOH/H_2O (1:1), 10 mL partition, with n-BuOH concentrated under N_2 at 40 °C
(c) – re-dissolved in MeOH (1 mg/mL), to generate analytes

Figure 3.11 Secretion B – production of analytes A6 – A8 (n-BuOH) and A6* – A8* (H_2O)

Aliquots (10 μL =10 μg) of A6 – A8 were analysed using HPLC Method 2 as described in Chapter 2 to yield three HPLC traces (Figure 3.12). Identification of bufagenins (**1a**) (Figure 3.9) and bufotoxins (**1c**, **2c**, **3c**, **5c** and **8c**) was performed as mentioned above (Figure 3.10). The area under each peak was quantified to generate relative bufadienolide percentages in A6 – A8 (Table 3.3).

Figure 3.12 HPLC chromatogram (298 nm) of Secretion B analytes A6-A8 analysed using Method 2 (see Chapter 2). Marinobufotoxin (**1c**), telocinobufotoxin (**2c**), bufalitoxin (**3c**), resibufotoxin (**4c**), hellebritoxin (**5c**), marinobufagenin pimeloyl-L-arginine (**8c**) and marinobufagenin (**1a**)

Table 3.3 Relative composition (%) of bufadienolides in secretion B

Compound no.	A6 (%)	A7 (%)	A8 (%)
1c	65.2	65.2	70.3
2c	4.1	4.2	5.5
3c	7.5	7.2	6.8
4c	0.8	0.7	3.9
5c	9.2	9.5	3.5
8c	11.8	11.9	6.8
1a	1.5	1.2	3.0

Surprisingly, HPLC-DAD analysis (298 nm) of secretion B samples showed the presence of bufotoxins predominantly (98%), with marinobufotoxin (**1c**) exhibiting the highest concentration followed by bufalitoxin (**3c**) and telocinobufotoxin (**2c**), while marinobufagenin (**1a**) was the only bufagenin identified (Figure 3.10).

The area under each peak in the HPLC traces (Figure 3.12) was also compared against standard curves for marinobufagenin (Chapter 2, Figure 2.16) and marinobufotoxin (Chapter 2, Figure 2.18), to calculate the µg/peak per HPLC trace per compound. Table 3.4 uses these qualitative measures to calculate the weight (mg) of each bufadienolide in each secretion B sample.

Secretion B contains an approximately 99:1 ratio (amount) of bufotoxins to bufagenins, with marinobufotoxin (**1c**) as the dominant bufotoxin followed by telocinobufotoxin (**2c**), bufalitoxin (**3c**) and hellebritoxin (**5c**), and marinobufagenin (**1a**) was the dominant bufagenin with no traces of other bufagenins.

In light of the significant differences observed in the bufotoxin:bufagenin ratios in secretion A and secretion B, we were keen to analyze and quantify the levels of free suberoyl-L-arginine (**1d**) (and homologs). Standards outlined in chapter 2 provided authentic standards and suitable analytical methods.

The H_2O solubles from the *n*-BuOH/ H_2O of secretion B partition were dried *in vacuo* and derivatized with 2,4-pentanedione. The resulting reaction product was dried *in vacuo*, dissolved in MeOH to a standard concentration (1 mg/mL) to generate analytes A6*-A8* which were analysed using the HPLC-DAD method (Method 3, refer section 2.4.7) described above. Comparison of HPLC retention times and HPLC-MS data for all peaks in the traces with authentic standards (See Chapter 2) confirmed the presence of derivatized suberoyl-L-arginine (**1e**) (Figure 3.13). Interestingly, only trace amounts of suberoyl-L-arginine were identified in secretion B (Figure 3.14).
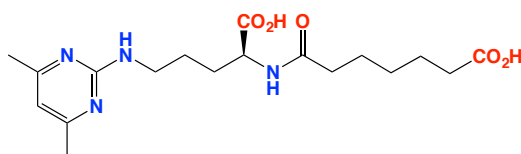
Figure 3.13 Derivatized arginyl amide identified in Secretion B preparation

The area under derivatized suberoyl-L-arginine in the HPLC traces (Figure 3.14) was compared against standard curves for suberoyl-L-arginine (Chapter 2, Figure 2.16), to calculate the µg/peak per HPLC trace per compound. Table 3.4 uses these qualitative measures to calculate the weight (mg) of suberoyl-L-arginine in each secretion B H_2O solubles. Levels of bufotoxins in secretion B correlated with the total mass of bufadienolides sampled from toads 6 – 8 with less/negligible amounts of bufagenins (<0.1 mg). Moreover, only negligible amount of suberoyl-L-arginine (<0.1 mg) was identified in secretion B. From the above analysis the total weight of bufadienolides per

secretion B was calculated across toads 6 – 8 to be 11 mg, 10 mg and 7 mg respectively, with the bufagenin to bufotoxin ratio in male and female toads being similar.
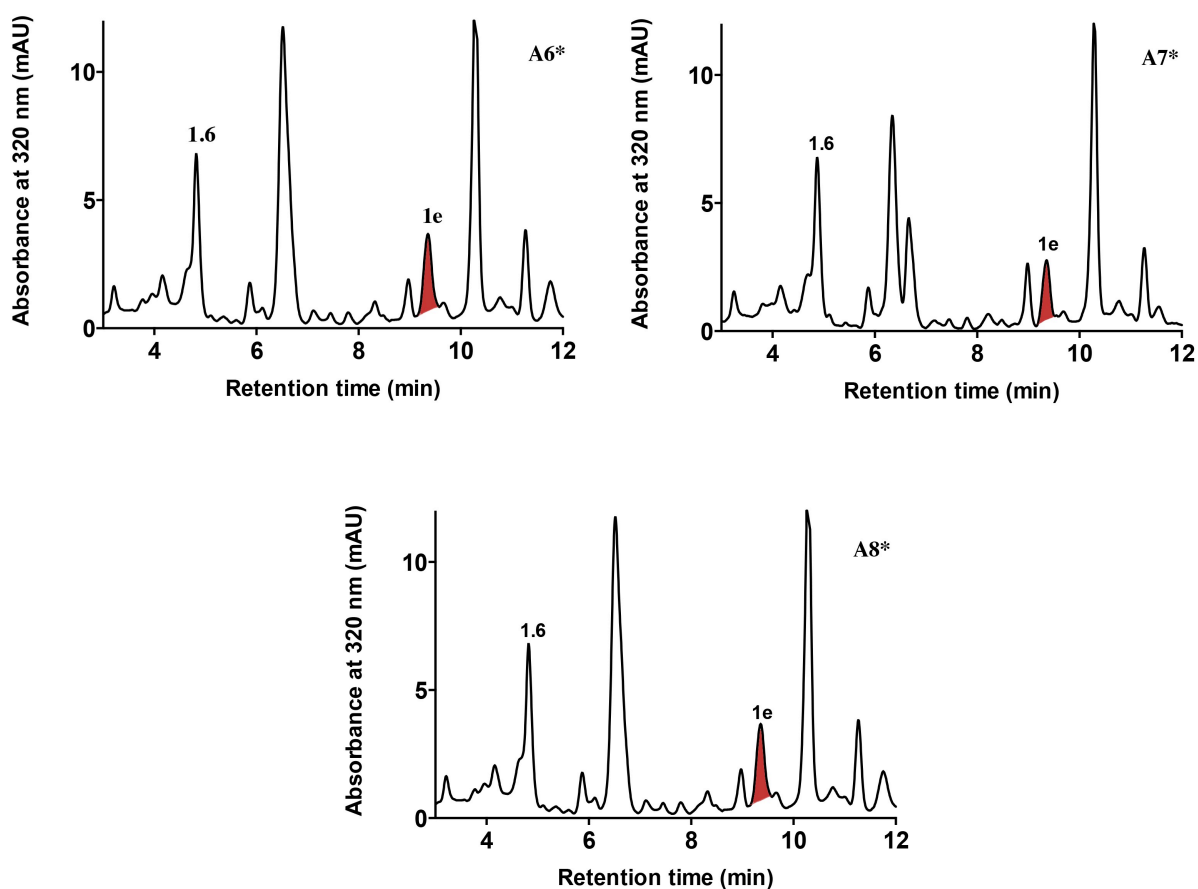
Figure 3.14 HPLC chromatogram (320 nm) of Secretion B analytes A6*-A8* analysed using Method 3 (see Chapter 2). Dehydrobufotenine (**1.6**), derivatized suberoyl-L-arginine (**1e**)

Table 3.4 Absolute amounts of bufadienolides and arginyl amides in secretion B

Compound no.	A6 (mg)	A7 (mg)	A8 (mg)
1c	7.4	6.5	4.9
2c	0.6	0.4	0.4
3c	1.0	0.7	0.5
4c	0.3	0.3	0.3
5c	1.0	0.9	0.3
8c	1.2	1.2	0.5
1a	<0.1	<0.1	<0.1
1e	<0.1	<0.1	<0.1

3.2.2.3 Secretion C – parotoid secretions squeezed into H_2O

Parotoid secretion was squeezed from the right parotoid gland of three adult cane toads into H_2O (5 mL), homogenized using a vortex and was left for an hour at room temperature to deliver a creamy yellow solution. Two female cane toads weighing, 89 g and 71 g, respectively and one male toad weighing 67 g were subjected to secretion C analyses. The crude yellow parotoid secretion in H_2O (5 mL) was dried under N_2 at 40 °C yielding 44 mg, 39 mg, and 37 mg respectively. The dried crude extract was subjected to *n*-BuOH/H_2O partition, and the *n*-BuOH solubles were dried under N_2 at 40 °C and weighed to generate 15 mg, 11 mg and 9 mg, respectively. The *n*-BuOH solubles were then re-dissolved in MeOH to a standard concentration (1 mg/mL) to generate analytes A9 – A11 and which were analysed using Method 1 (Chapter 2) specific for bufagenins, respectively (Figure 3.15).

B. marinus

toad 1,
89 g,♀

toad 2,
71 g,♀

toad 3,
67 g,♂

secretion C

secretion C

secretion C

(a)

(a)

(a)

44 mg

39 mg

37 mg

(b)

(b)

(b)

15 mg

11 mg

9 mg

(c)

(c)

(c)

A9*   A9

A10*   A10

A11*   A11
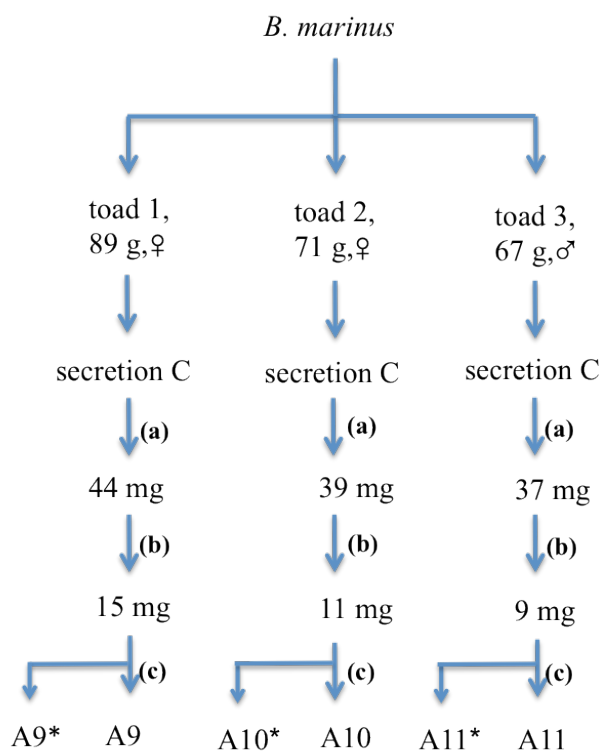
(a) – homogenized in water (5 mL) dried under N_2 at 40 °C
(b) – *n*-BuOH/H_2O (1:1), 10 mL partition, with *n*-BuOH concentrated under N_2 at 40 °C
(c) – re-dissolved in MeOH (1 mg/mL), to generate analytes

Figure 3.15 Secretion C – production of analytes A9 – A11 (*n*-BuOH) and A9* – A11* (H_2O)

Aliquots (10 µL =10 µg) of A9 – A11 were analysed using HPLC Method 2 as described in Chapter 2 to yield three HPLC traces (Figure 3.16). Identification of bufagenins (**1a**, **2a**, **3a**, **4a** and **5a**) (Figure 3.9) was performed as mentioned above. The area under each peak was quantified to generate relative bufadienolide percentages in A9 – A11 (Table 3.5).
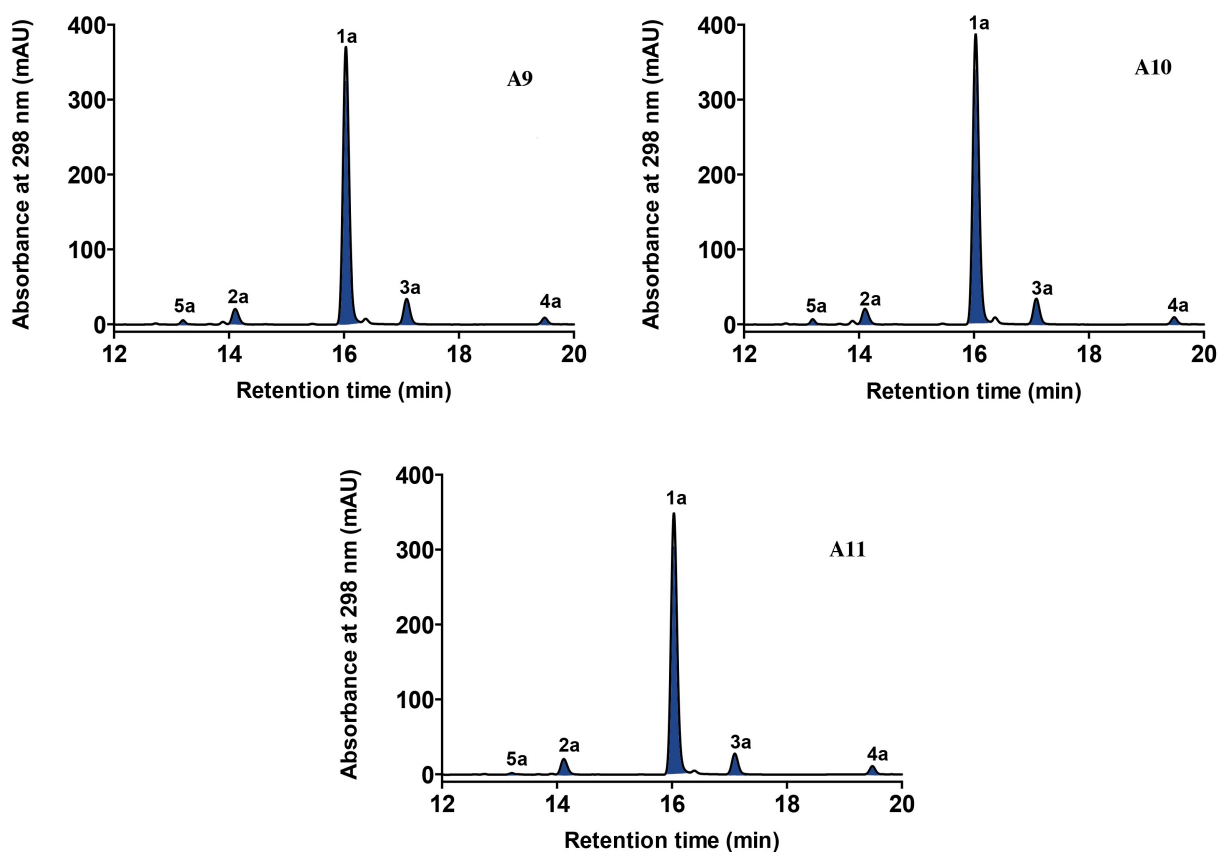
Figure 3.16 HPLC chromatogram (298 nm) of Secretion C analytes A9-A11 analysed using Method 1 (See Chapter 2). Marinobufagenin (**1a**), telocinobufagenin (**2a**), bufalin (**3a**), resibufagenin (**4a**)

Table 3.5 Relative composition (%) of bufadienolides in secretion C

Compound no.	A9 (%)	A10 (%)	A11 (%)
1a	84.3	84.5	84.9
2a	5.0	4.8	5.4
3a	7.8	7.5	6.8
4a	1.8	1.9	2.5
5a	1.0	1.2	0.5

Secretion C contains >99 % bufagenins compared to bufotoxins, with marinobufagenin (**1a**) as the dominant bufagenin followed by bufalin (**3a**), telocinobufagenin (**2a**), resibufagenin (**4a**), and hellebrigenin (**5a**). The area under each peak in the HPLC traces (Figure 3.16) was also compared against standard curves for marinobufagenin (Chapter 2, Figure 2.16), to calculate the µg/peak per HPLC trace per compound. Table 3.6 uses these qualitative measures to calculate the weight (mg) of each bufadienolide in each secretion C sample.

As detailed above, the H₂O soluble phase from the n-BuOH:H₂O partitions of secretion C were prepared and derivatized to yield analytes A9*-A11* which were analysed for suberoyl-L-arginine (**1d**) (and homologues) using the methodology outlined in chapter 2. Comparison of HPLC retention times and HPLC-MS data for all peaks, with comparison to authentic standards (See Chapter 2), confirmed the presence of derivatized arginyl amides (**1e** and **3e**) (Figure 3.17).

derivatized suberoyl-L-arginine (**1e**)   derivatized pimeloyl-L-arginine (**3e**)
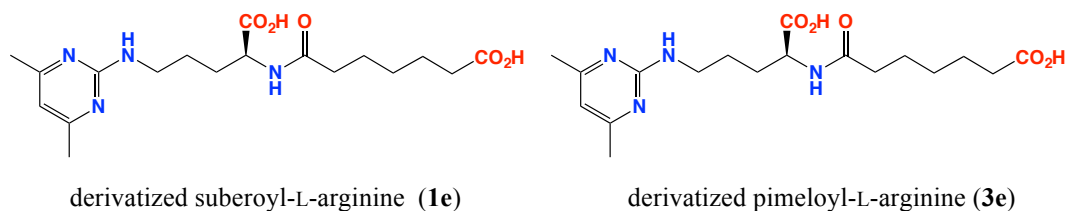
Figure 3.17 Derivatized arginyl amides detected in Secretion C preparation

The area under derivatized arginyl amides peaks in the HPLC traces (Figure 3.18) was quantified to calculate the weight (mg) of arginyl amides in each Secretion C sample, which was dominated by suberoyl-L-arginine (**1e**) with trace amounts of pimeloyl-L-arginine (**3e**). From the above analysis the total weight of bufadienolides per Secretion C was calculated across all toads 1-3 to be ~ 9 mg, 7 mg and 5 mg, respectively with the bufagenin to bufotoxin ratio in male and female toads being similar and dominated by bufotoxins (>99.9%)
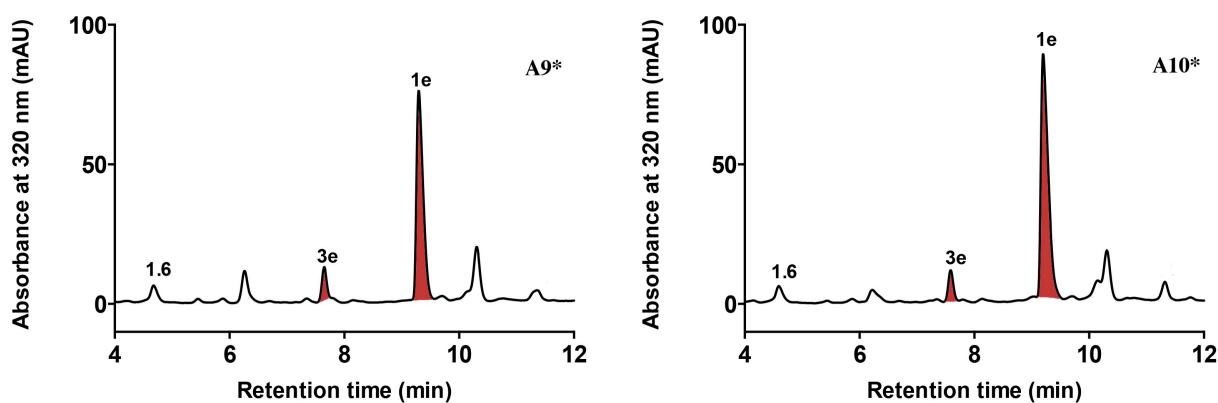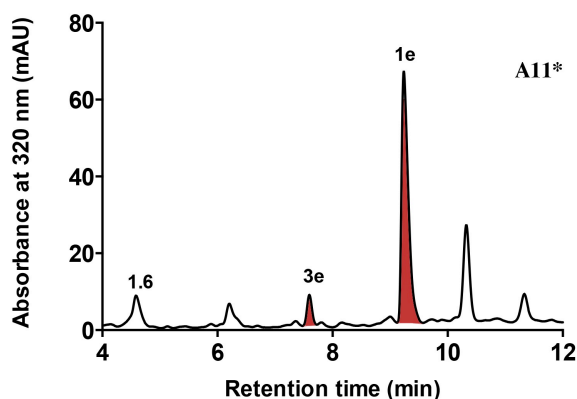
Figure 3.18 HPLC chromatogram (320 nm) of 2 Secretion C analytes A9*-A11* analysed using Method 3 (see Chapter 2). Dehydrobufotenine (**1.6**), derivatized pimeloyl-L-arginine (**3e**) and derivatized suberoyl-L-arginine (**1e**)

Table 3.6 Absolute amounts (mg) of bufadienolides and arginyl amides in secretion C

Compound no.	A9 (mg)	A10 (mg)	A11 (mg)
1a	7.6	5.7	4.6
2a	0.4	0.3	0.2
3a	0.6	0.4	0.3
4a	<0.1	<0.1	0.1
5a	<0.1	<0.1	<0.1
1e	6.8	4.9	3.8
3e	0.8	0.5	0.3

3.2.2.4 Toxin A – microgland extracted with MeOH

Two male cane toads weighing 102 g and 99 g, respectively and one female toad weighing 104 g were subjected to toxin A analyses. To investigate the composition of bufadienolides present in the parotoid toxin stored *in situ*, left parotoid glands of three adult cane toads were excised and three parotoid microglands from each parotoid gland filled with toxin were dissected, washed with PBS, weighed and immersed in MeOH (1 mL). Large well-developed parotoid microglands with an average mass of 3.4±0.4 mg (n = 9) were selected for toxin A analysis to minimize handling errors. The parotoid microglands in MeOH were homogenized using a pipette tip and left for an hour at room temperature. The crude yellow toxin A sample was dried under N_2 at 40 °C, and dried crude extract subjected to *n*-BuOH/H_2O partition. The dried *n*-BuOH solubles were dried under N_2 at 40 °C and were re-dissolved in MeOH (50 μL) and were analysed using method 2 (Chapter 2) specific for bufagenins and bufotoxins, respectively (Figure 3.19).
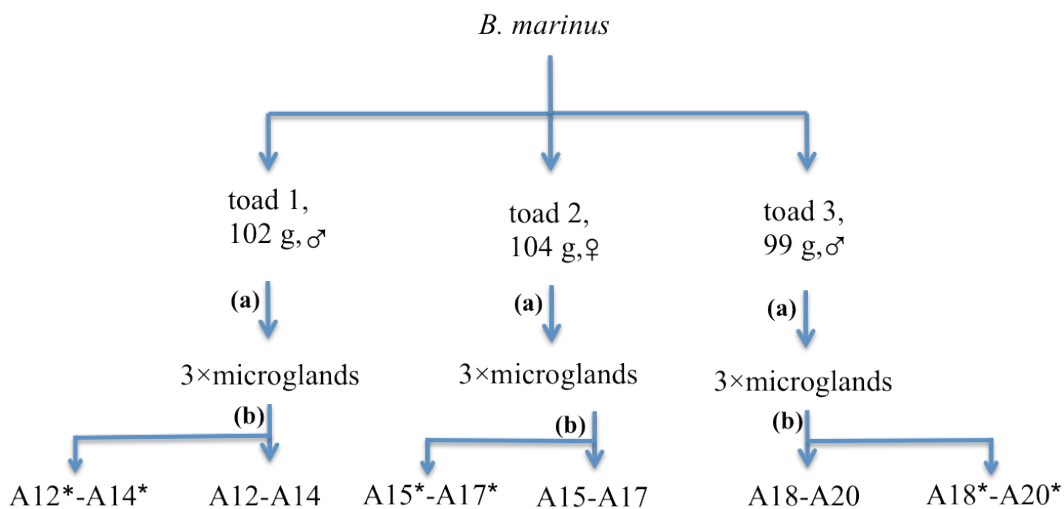
(a) – excised 3 × ~ 3.4 mg microglands per toad
(b) – extracted into MeOH, partitioned into *n*-BuOH, dried and re-dissolved in MeOH (50 μL) or H₂O (50 μL)

Figure 3.19 Toxin A – production of analytes A12 – A20 (*n*-BuOH) and A12′ – A20′ (H₂O)

Aliquots (10 μL) of A12 – A20 were analysed using HPLC Method 2 as described in Chapter 2 to yield nine HPLC traces (Figure 3.20). Identification of bufotoxins (**1c**, **2c**, **3c**, **4c**, **5c**, **8c** and **9c**) and bufagenins (**1a**) (Figure 3.9) was performed as mentioned above (Figure 3.10). The area under each peak was quantified to generate relative bufadienolide percentages in A12 – A20 (Table 3.7).
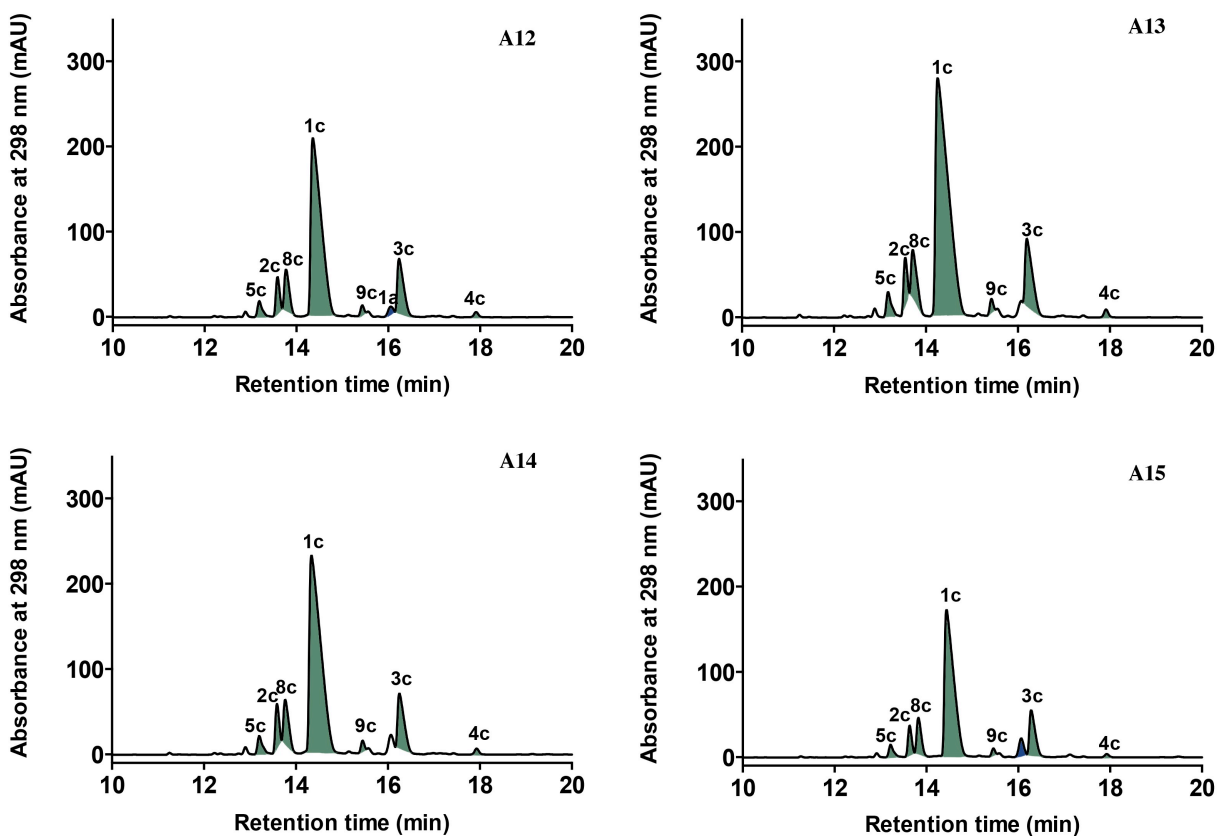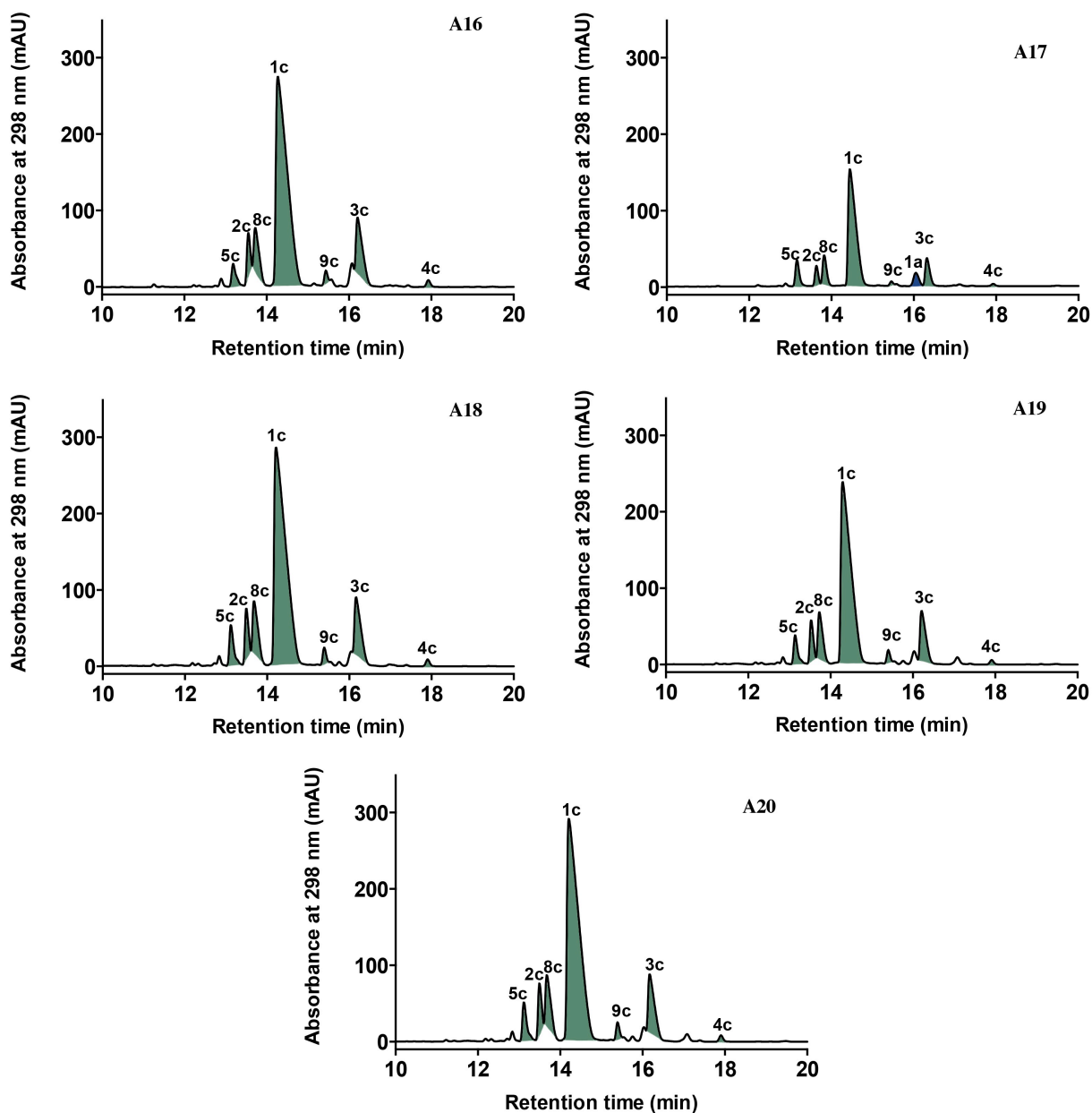
Figure 3.20 HPLC chromatogram (298 nm) of Toxin A analytes A12-A20 analysed using Method 2 (see Chapter 2). Marinobufotoxin (**1c**), telocinobufotoxin (**2c**), bufalitoxin (**3c**), hellebritoxin (**5c**), marinobufagenin pimeloyl-L-arginine (**8c**)

HPLC-DAD analysis (298 nm) of Toxin A revealed that they were dominated by >99% bufotoxins, with only trace levels of bufagenins (<1%). Bufotoxins were dominated by marinobufotoxin (**1c**) (66%) and the lone bufagenin identified was marinobufagenin (**1a**) (<1%) (Figure 3.10). This observation confirms that *in situ* cane toad toxin is composed of bufotoxins and that secretions can be prone to hydrolysis to deliver bufagenins and arginyl amides (as evidenced in secretion A and secretion C).

The area under each peak in the HPLC traces of Toxin A samples (Figure 3.20) was also compared against standard curves for marinobufagenin (Chapter 2, Figure 2.16) and marinobufotoxin (Chapter 2, Figure 2.18), to calculate the μg/peak per HPLC trace per compound. Table 3.7 uses

these qualitative measures to calculate the weight (mg) of each bufadienolide in each Toxin A sample.

Table 3.7 Relative composition (%) of bufadienolides in toxin A

Compound no.	A12 (%)	A13 (%)	A14 (%)	A15 (%)	A16 (%)	A17 (%)	A18 (%)	A19 (%)	A20 (%)
1c	64.5	64.6	64.5	65.3	64.0	65.0	64.5	64.6	64.3
2c	5.7	5.4	6.1	5.8	5.6	4.8	5.7	5.8	5.7
3c	13.3	13.1	12.0	13.0	13.5	11.5	13.3	12.1	12.0
4c	0.8	0.8	0.7	0.8	0.7	0.6	0.7	0.6	0.7
5c	2.8	2.9	2.9	2.9	3.0	5.4	3.0	4.4	4.7
8c	9.0	9.5	9.1	9.0	9.4	9.0	9.6	9.4	9.7
9c	1.7	1.8	1.7	1.7	1.8	1.2	1.7	1.9	1.8
1a	2.0	1.5	2.0	2.0	2.0	2.5	1.5	1.0	1.0

Total bufadienolides per parotoid microgland was between 50 – 250 µg depending on the size of the microgland and % bufadienolide per parotoid microgland was between 2.6 – 5.2% (Table 3.8). The bufadienolide content per microgland is broadly correlated with the weight of the microgland (Figure 3.21, r^2 = 0.9647). The nine microglands used in this study were among the larger encountered in the ~80 – 100 microglands found per parotoid gland. Based on these approximations, it is possible to estimate that the yield of bufadienolides per toad to be between 10 – 50 mg.

Table 3.8 Total amounts (µg) of bufadienolides in toxin A

	A12	A13	A14	A15	A16	A17	A18	A19	A20
A (µg)	50	250	90	82	180	74	203	143	216
B (%)	2.6	4.8	3.5	3.4	4.1	3.2	5.2	4.2	4.7

A (µg) – calculated as total mass of bufadienolides per microgland

B (%) – calculated as mass of total bufadienolides per mass of microgland
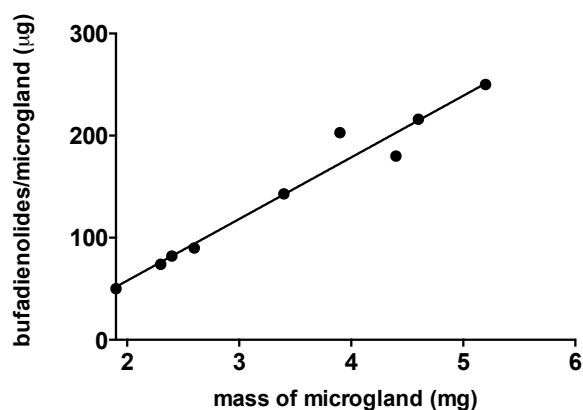
Figure 3.21 Plot between mass of microgland (mg) and total bufadienolides per microgland (μg)

Analysis of the arginyl amide content in the H_2O solubles from toxin A proceeded as described earlier. The dried H_2O soluble partitioned from each microgland was derivatized with 2,4-pentanedione, and the reaction product dried *in vacuo* and dissolved in MeOH (50 μL) to yield analytes A12*-A20*, which were analysed using the HPLC-DAD method (Method 3, refer section 2.4.7) described above. Negligible levels of arginyl amides were detected in the parotoid microgland contents confirming that arginyl amides in the parotoid secretion are a by-product of the hydrolysis of bufotoxins *in situ* and importantly, that surplus arginyl amides are not stored (accumulated) in microglands (Figure 3.22).
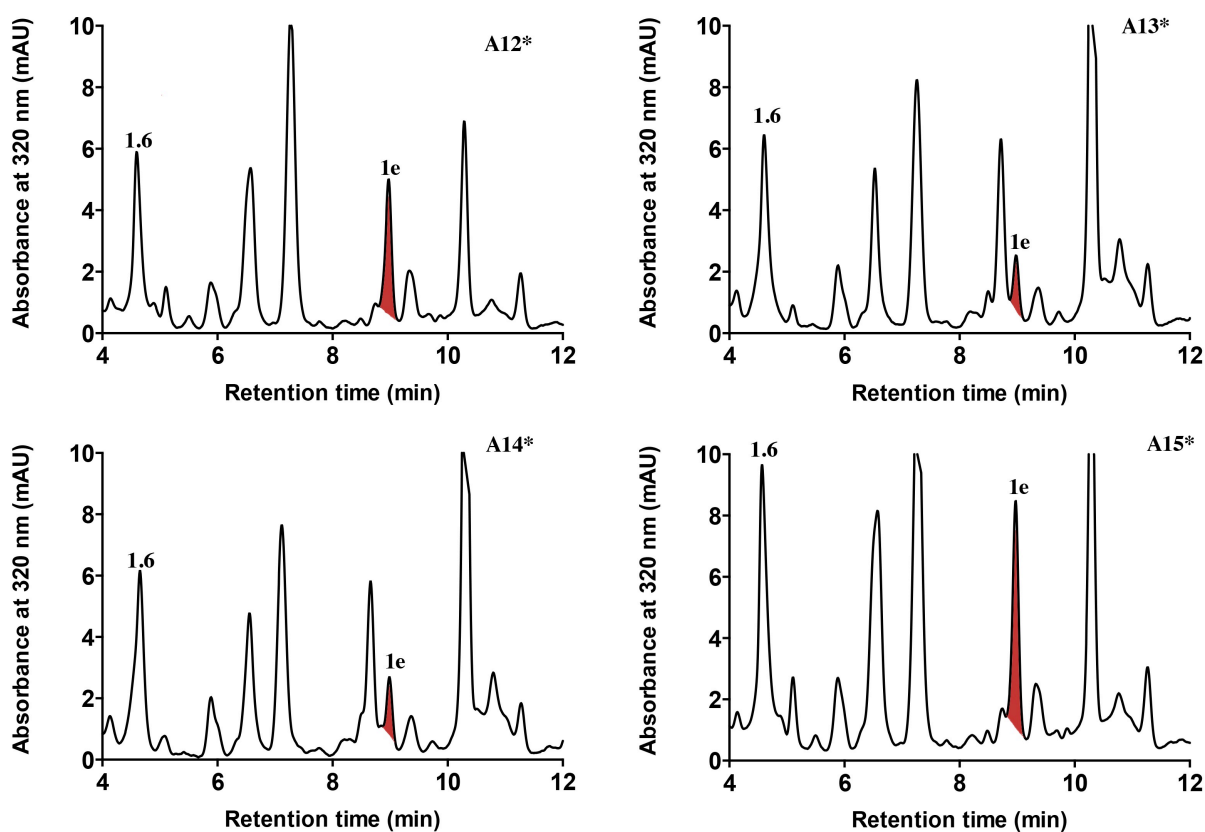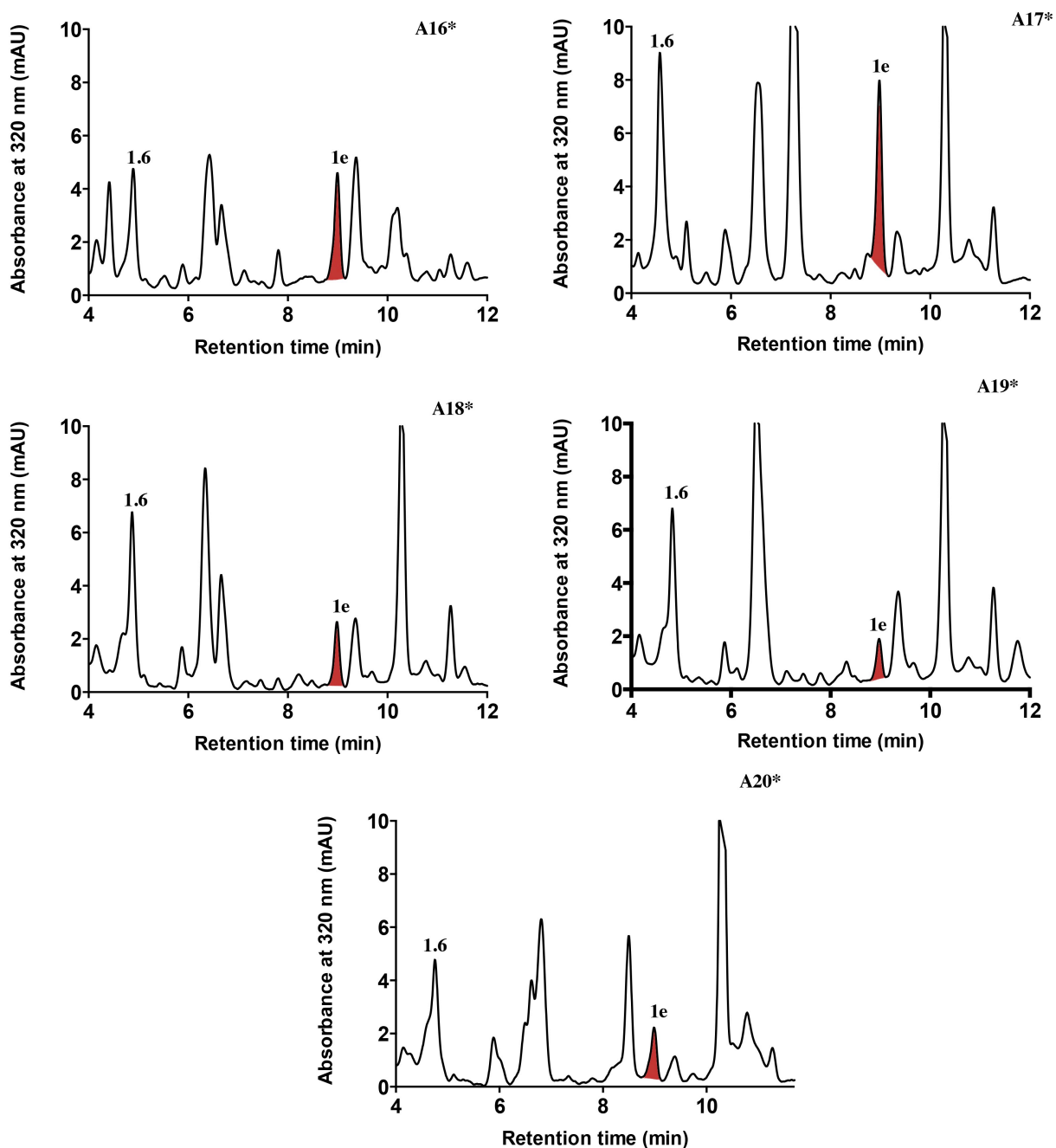
Figure 3.22 HPLC chromatogram (298 nm) of Toxin A analytes A12*-A20* analysed using Method 3 (see Chapter 2). Dehydrobufotenin (**1.6**) and suberoyl-L-arginine (**1e**)

3.2.2.5 Toxin B – microgland extracted into H_2O

Two male cane toads weighing 102 g and 99 g, respectively and one female toad weighing 104 g were subjected to toxin B analyses. Right parotoid glands of three adult cane toads were excised and three parotoid microglands from each parotoid gland filled with toxin we dissected, weighed and immersed into H_2O (1 mL). The parotoid microglands were then homogenized using a pipette tip and were left for an hour at room temperature to deliver a pale yellow solution. The crude yellow parotoid toxin B in MeOH (1 mL) was dried under N_2 at 40 °C. The dried crude extract was subjected to n-BuOH/H_2O partition and the n-BuOH solubles comprising bufadienolides were dried

under N_2 at 40 °C and re-dissolved in MeOH (50 μL) to deliver analytes A21-A29, which were analysed using Method 2 (Chapter 2) specific for bufagenins and bufotoxins, respectively (Figure 3.23).
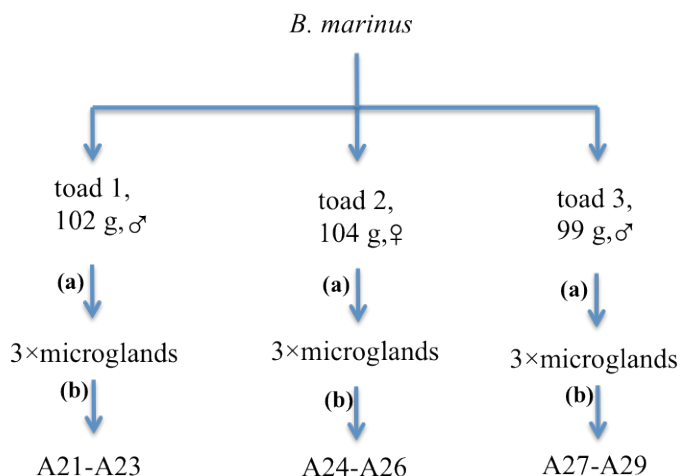
(a) – excised 3 × microglands per toad
(b) – extracted into H_2O, partitioned into *n*-BuOH, dried and re-dissolved in MeOH (50 μL)

Figure 3.23 Toxin B – production of analytes A21 – A29 (*n*-BuOH)

Aliquots (10 μL) of A21 – A29 were analysed using HPLC Method 2 (see Chapter 2) to yield nine HPLC traces (Figure 3.24). Identification of bufotoxins (**1c**, **2c**, **3c**, **4c**, **5c**, **8c** and **9c**) and bufagenins (**1a**) (Figure 3.9) was performed as mentioned above (Figure 3.10). The results obtained from the analysis were identical to toxin A (microgland treated in MeOH) where the bufadienolides composition was dominated with bufotoxins (>98%) and trace amounts of marinobufagenin was detected. The observation also indicated the absence of hydrolytic activity associated with *in situ* parotoid toxin.
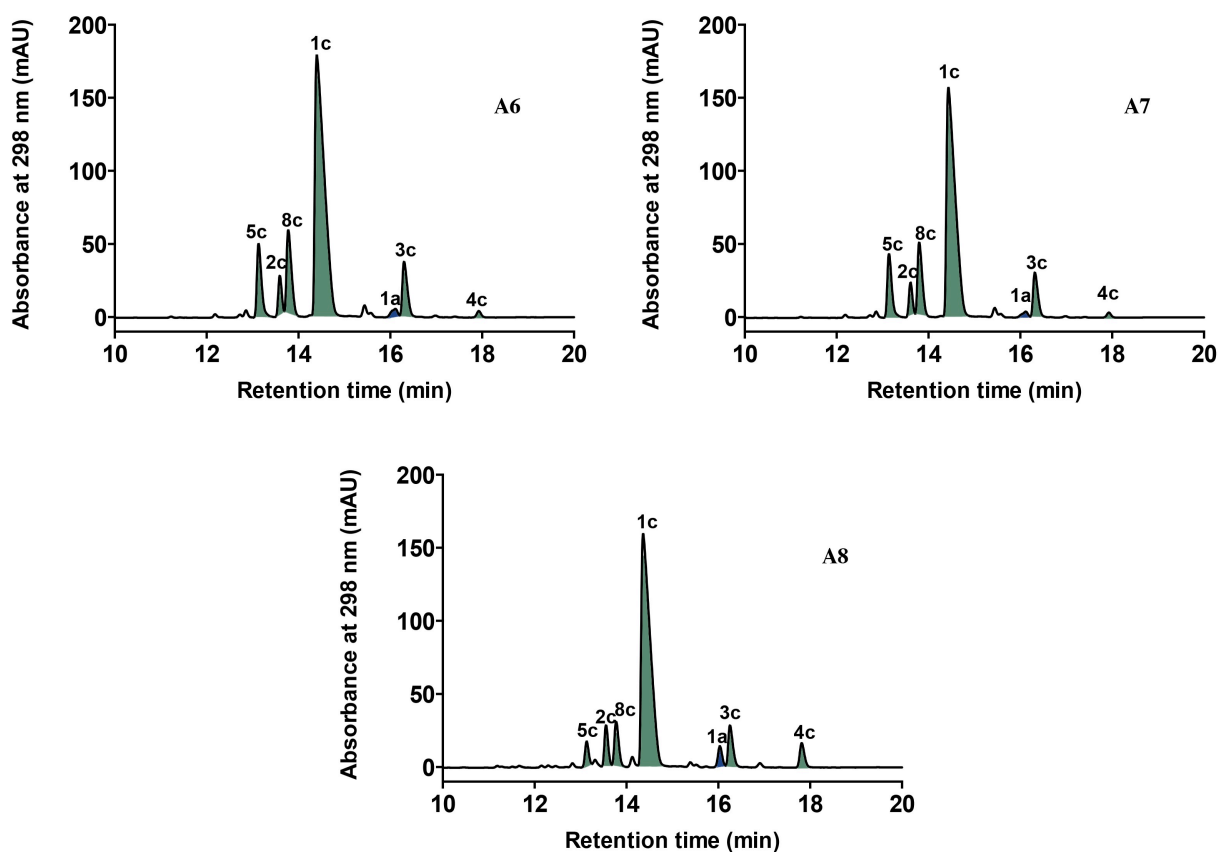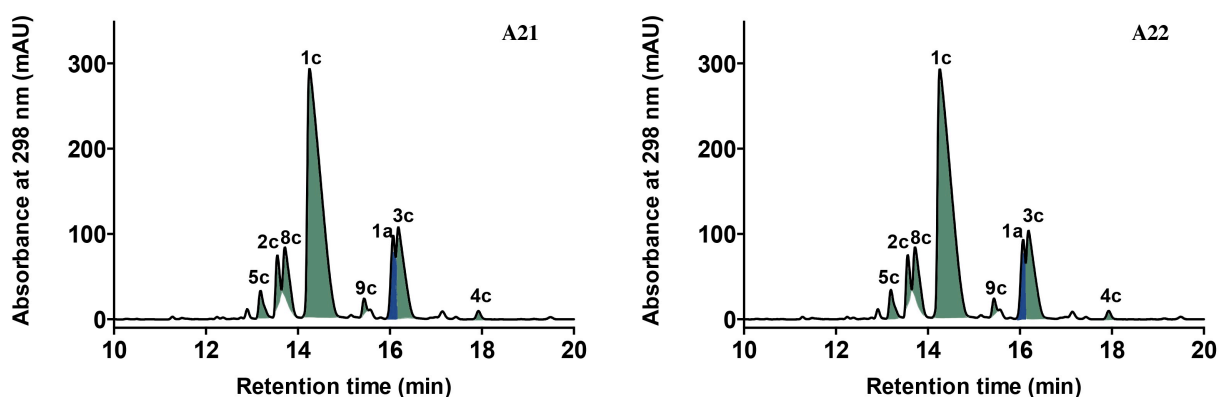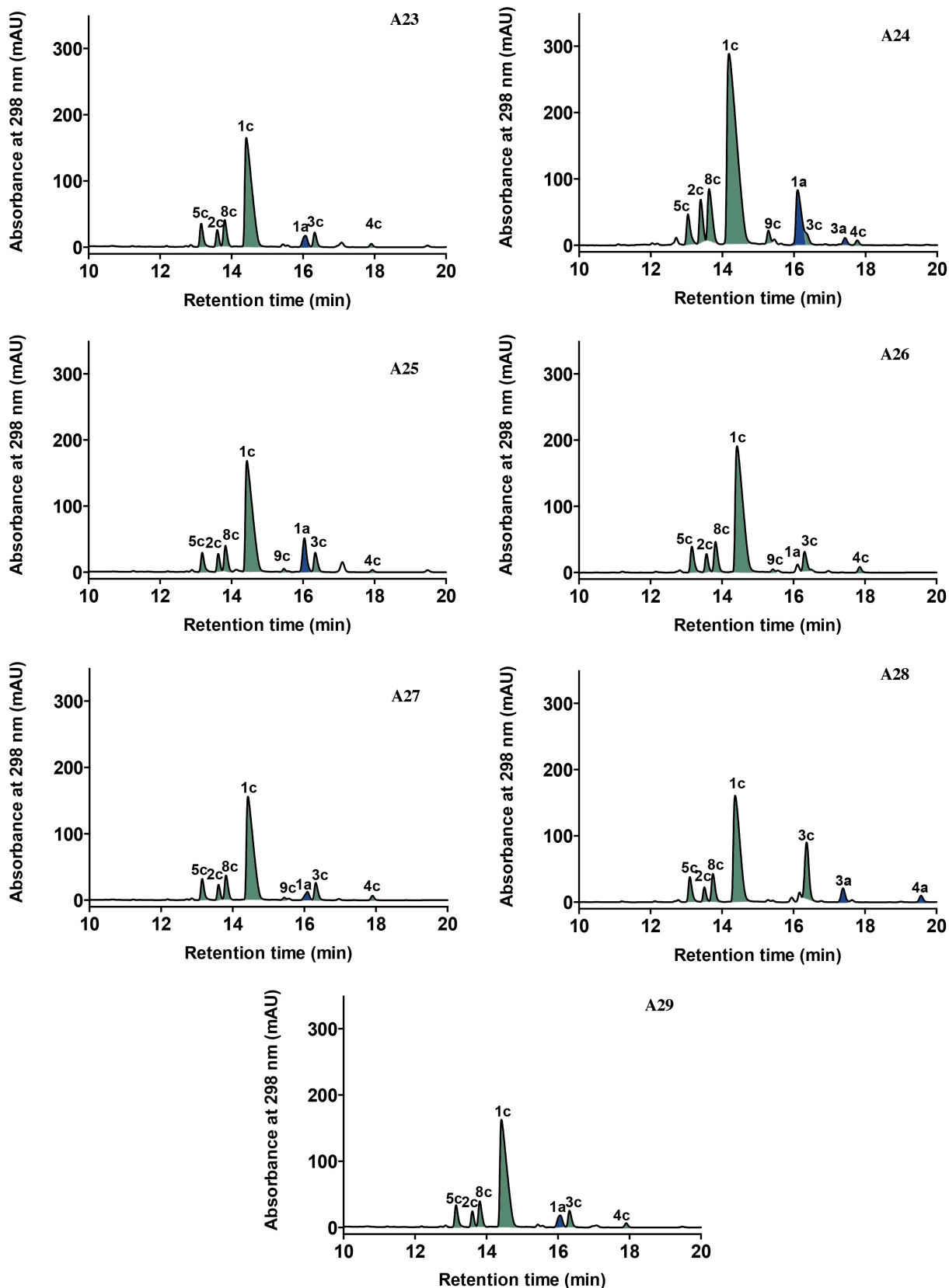
Figure 3.24 HPLC chromatogram (298 nm) of Toxin B analytes A21*-A29* analysed using Method 2 (see Chapter 2). Marinobufotoxin (**1c**), telocinobufotoxin (**2c**), bufalitoxin (**3c**), hellebritoxin (**5c**), marinobufagenin pimeloyl-L-arginine (**8c**), bufalin pimeloyl-L-arginine (**9c**), marinobufagenin (**1a**), bufalin (**3a**) and resibufagenin (**4a**)

3.2.3 Rate of hydrolysis of bufotoxins

During our analysis on handling of parotoid secretions, hydrolysis of bufotoxins to bufagenins and suberoyl-L-arginine was well established. To investigate whether the bufotoxins hydrolysis is time-dependent, the rate of hydrolysis of bufotoxins was calculated at different time intervals.

3.2.3.1 Rate of hydrolysis of bufotoxins – Secretion D

To identify the rate of conversion of bufotoxins into bufagenins, parotoid secretion from three cane toads was squeezed into H_2O (5 mL) followed by rapid mixing using a vortex to obtain a homogenous solution. Aliquots of this homogenous solution (500 μL) were quenched with MeOH (500 μL) at various time intervals ranging from 5, 10, 15, 20 and 30 min. A 0 min reading was obtained by squeezing parotoid secretions directly into MeOH (5 mL) to immediately inhibit the bufotoxin hydrolysis. All MeOH solutions were dried under N_2 at 40 °C, triturated with MeOH (1 mL), dried under N_2 at 40 °C and re-dissolved in MeOH to a standard concentration (1 mg/mL) to generate analytes A30-A50, respectively and analysed using Method 2 (Figure 3.25).
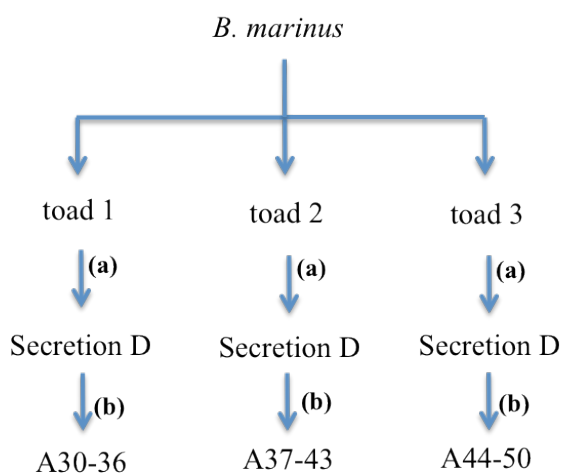
(a) – Secretion D sampling at 0, 2, 5, 10, 15, 20 and 30 min
(b) – each sample was then dried, subjected to *n*-BuOH/H_2O partition, *n*-BuOH solubles were dried, re-dissolved in MeOH (1 mg/mL)

Figure 3.25 Secretion D – production of analytes A30 – A50 (*n*-BuOH)

Aliquots (10 μL = 10 μg) of A30 – A50 were analysed using HPLC Method 2 (see Chapter 2) of which seven representative traces are shown below (Figure 3.26). Identification of bufotoxins (**1c**, **2c**, **3c**, **4c**, **5c** and **8c**) (Figure 3.9) and bufagenins (**1a**, **2a**, **3a**, **4a** and **5a**) (Figure 3.10) was performed as mentioned above.
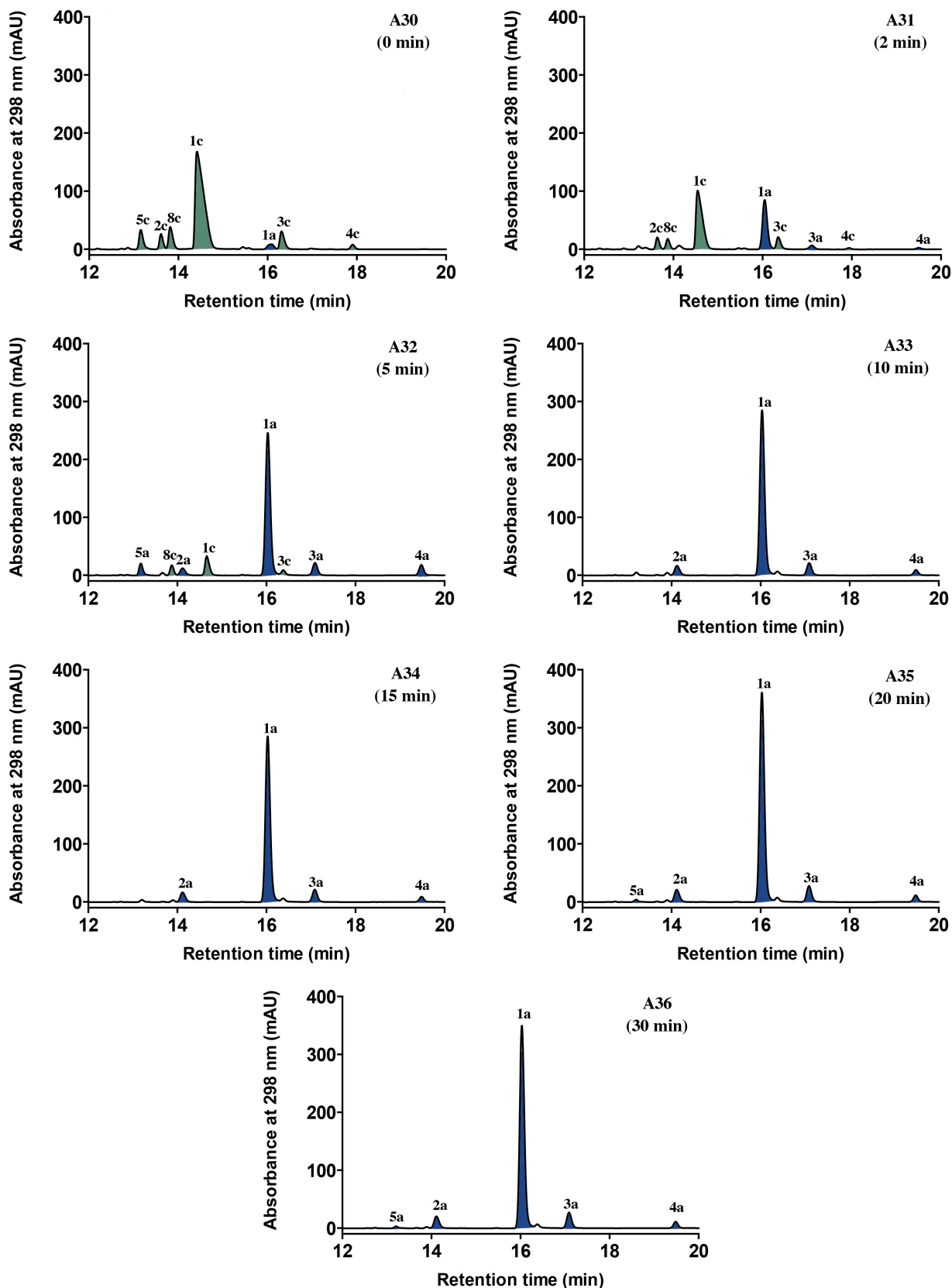
Figure 3.26 HPLC chromatograms (298 nm) representative of Secretion D analytes A30-A50 analysed using Method 2 (see Chapter 2). Marinobufotoxin (**1c**), telocinobufotoxin (**2c**), bufalitoxin (**3c**), hellebritoxin (**5c**), marinobufagenin pimeloyl-L-arginine (**8c**), marinobufagenin (**1a**), telocinobufagenin (**2a**), bufalin (**3a**), resibufagenin (**4a**) and hellebrigenin (**5a**).

The area under peaks corresponding to marinobufotoxin (representing bufotoxin) and marinobufagenin (representing bufagenin) was quantified to generate relative bufadienolide percentages in A30 – A50 and was interpreted as a graph as shown below (Figure 3.27). A curve was plotted between % of marinobufotoxin and marinobufagenin against each time interval (X axis, min) with two rows of Y-axis corresponding to hydrolysis of marinobufotoxin (green) and formation of marinobufagenin (blue).
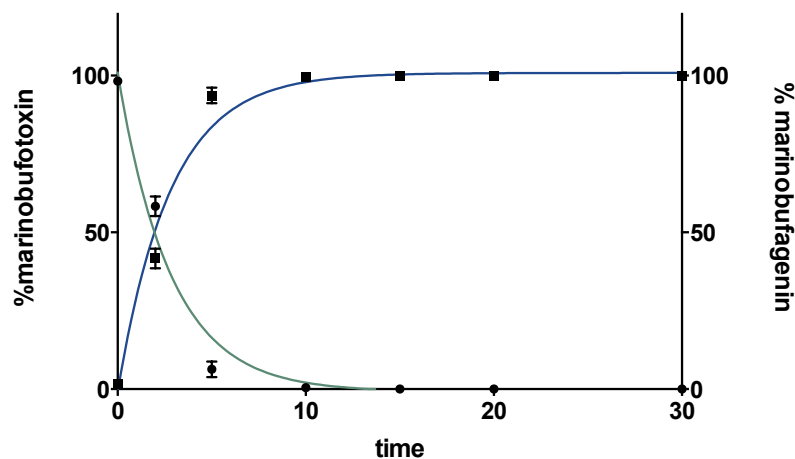
Figure 3.27 Conversion of marinobufotoxin (**1c**) to marinobufagenin (**1a**) over 30 min. Green line indicating the breakdown of bufotoxins (left Y axis), blue line indicating the formation of bufagenins (right Y axis)

From the graph (Figure 3.27, One phase decay, non-linear fit, $r^2 = 0.9806$) it is evident that the rate of hydrolytic activity in the parotoid secretion is rapid. The curve obtained from the percentage conversion of bufotoxins and bufagenins was linear until 5 min and reached the maximum (100%) through further time intervals. Rapid mixing using vortex resulted in a homogenous solution that distributed the chemistry of the parotoid secretion uniformly throughout the solution. The hydrolytic activity in the parotoid secretion resulted in the conversion of about 94% of bufotoxins into bufagenins in 5 min and then reached complete conversion (>99%) after 10 min.

From this observation, it can be determined that cane toad parotoid secretions are subject to *ex situ* hydrolysis and this reaction is rapid and converts bufotoxins into bufagenins and arginyl amides. Our previous observation of bufagenins dominating the parotoid secretion (secretion C), which was analyzed using method 1 also coincides with our current observation. The above experiment indicated that handling of cane toad parotoid toxins during the chemical analysis would play a major role in the determination of the toxin constituents. From our observations it is evident that exposure of cane toad parotoid toxin to H_2O (moisture) would increase the hydrolysis and result in rapid and quantitative conversion of bufotoxins to bufagenins. These results suggest that a hydrolase is co-secreted with the parotoid secretion.

3.2.4 Identification of bufotoxin hydrolysis in parotoid microglands – chemical approach

3.2.4.1 Toxin C – investigation of co-localization of hydrolase

An experiment was performed to identify whether the hydrolase activity detected in cane toad secretion is co-localized with bufotoxins within the microglands. In our preliminary investigations with parotoid microglands (Toxin A and Toxin B), parotoid microglands were gradually detached from their basal epithelium using micro-tweezers. However, in the current investigation, individual microglands from the parotoid glands of a male and a female toad were dissected using micro-scissors and were cut angular to the basal epithelium of the parotoid gland, as this approach would provide access to surrounding epithelium which could also contain hydrolase (Figure 3.28). During this process access to an individual microgland was gained by destroying surrounding microglands and after dissection the microgland was washed twice with PBS buffer.
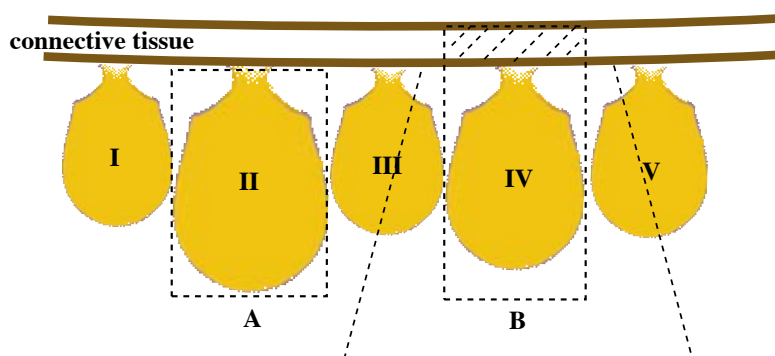
A - dissection of microgland by detaching from basal epithelium (II;Toxin A and Toxin B)

B - dissection of microgland by cutting through surrounding connective tissue by destroying adjacent microglands(III, IV and V;Toxin C)

Figure 3.28 Comparison of dissection strategies adopted in previous analyses, Toxin A, Toxin B and Toxin C

Following dissection, the microglands were homogenized using a sterile pipette tip in the presence of H_2O (500 μL) and was left at room temperature for 60 min and dried *in vacuo* and triturated with MeOH (1 mL) to solubilize all the bufadienolides. The MeOH soluble fraction was then dried *in vacuo* and was re-dissolved in MeOH to a standard concentration (1 mg/mL) to generate analytes A51-A54 which were analysed using Method 2 (Figure 3.29).
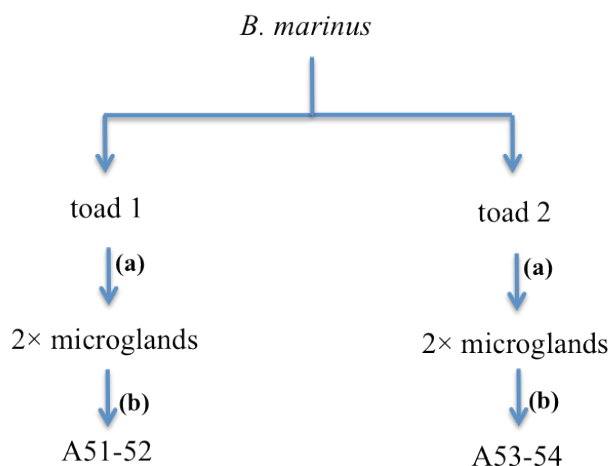
(a) – excised 2 × microglands per toad by cutting through the basal epithelium
(b) – extracted into H$_2$O, partitioned into *n*-BuOH, dried and re-dissolved in MeOH (50 μL)

Figure 3.29 Toxin C – production of analytes A51 – A54 (*n*-BuOH)

Aliquots (10 μL) of A51 – A54 were analysed using HPLC Method 2 as described in Chapter 2 to yield four HPLC traces (Figure 3.30). Identification of bufotoxins (**1c**, **2c**, **3c** and **5c**) (Figure 3.9) and bufagenins (**1a**, **2a**, **3a** and **4a**) (Figure 3.10) was performed as mentioned above.
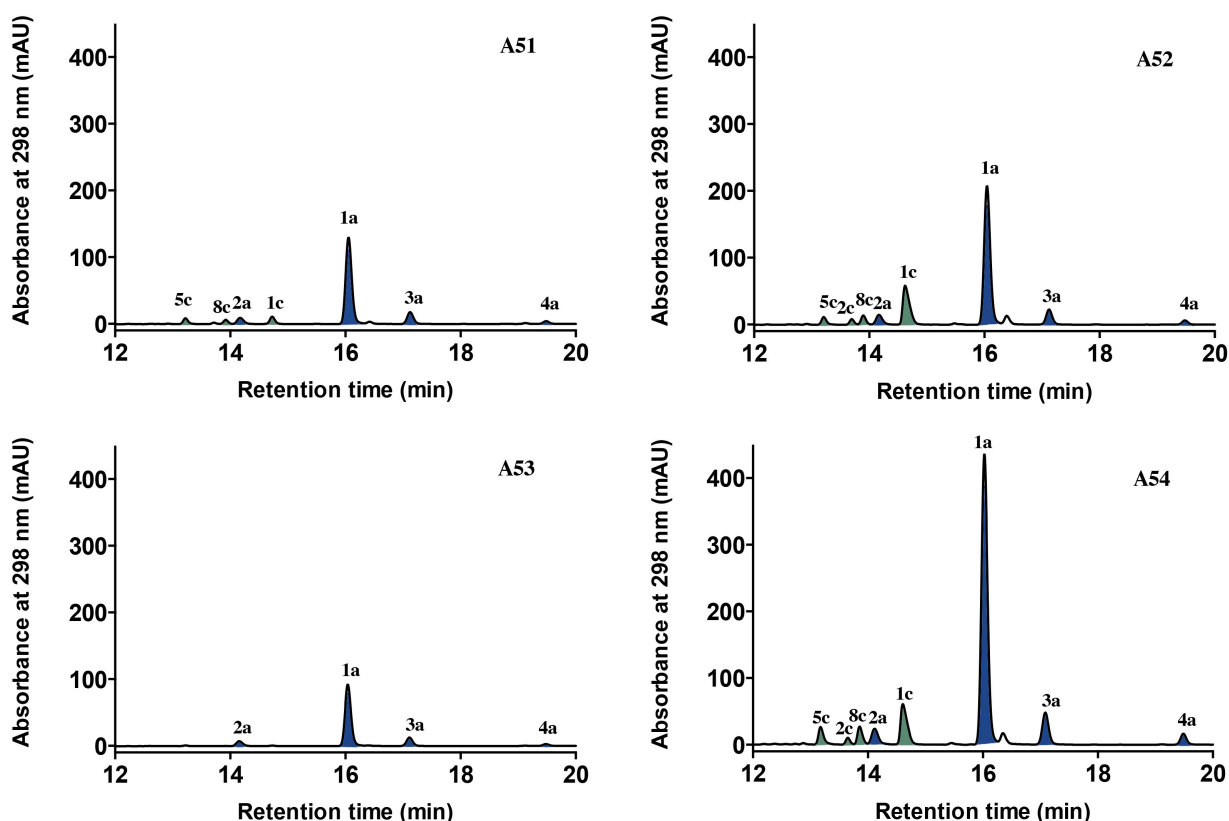
Figure 3.30 Identification of hydrolase activity in different modes of dissection. (green – microgland detached from basal epithelium, blue – microgland cut across basal epithelium), marinobufotoxin (**1c**), marinobufagenin (**1a**)

Interestingly, the analysis showed the conversion of bufotoxins into bufagenins in Toxin C prepared from microglands detached from the basal epithelium, differed from those of Toxin B which was

155

prepared from microglands cut from the basal epithelium, indicating that the mode of dissection is critical. Hydrolysis of bufotoxins to bufagenins in Toxin C was not as rapid as observed in parotoid Secretion D. For example, after 60 min >20% of bufotoxins in toxin C were unhydrolysed, however Secretion D showed >99% hydrolysis of bufotoxins after only 10 min. The analysis indicates that the amount of hydrolase present in Toxin C was far less than that in Secretion C, and more than in the Toxin A or Toxin B. These observations could be explained if the hydrolase was localized external to the parotoid microglands within the surrounding tissues, especially towards basal epithelium (just above the microglands). An imaging of parotoid microglands with different modes of dissection was applied to identify the localization of enzymes (Chapter 4).

3.2.5 Why bufotoxins? – Multi-faceted stability investigations

The preliminary analysis on cane toad parotoid toxin and secretion indicated a change in the levels of bufadienolides and arginyl amides during the secretion of parotoid gland contents. This observation also leads to insights into the significance of adapting a complex mechanism of biosynthesising a conjugated bufadienolide and hydrolysing during the secretion of the toxin. Several key features were investigated to identify the advantages of bufotoxin accumulation in parotoid glands. One of the major reasons was the stability of bufotoxins. Stability in this regard is classified into various types such as physical stability (formation of secondary structures such as micelles or liposomes for better packaging), chemical stability (resistance to proteins or other macromolecules in bodily fluids such as plasma), microbiological stability (resistance to microbial biotransformation) and toxicological stability (resistance to self-poisoning) (Figure 3.31). This chapter will focus on physical and chemical stabilities of bufotoxins while microbiological (Chapter 5) and biological stabilities (Chapter 7) will be discussed later.
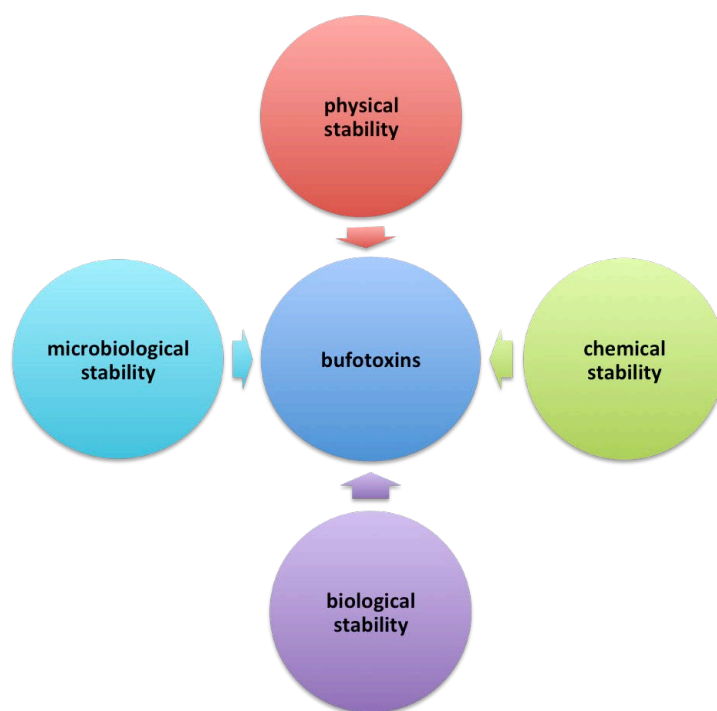
Figure 3.31 Storage of bufotoxins serves several benefits such as physical, chemical, biological and toxicological stabilities

3.2.6 Physical stability - Storage of toxins and their particle stability

Following the dissection of parotoid gland and parotoid microgland, storage of parotoid toxin within the parotoid microgland was investigated. The parotoid toxin within the microgland was reported to have shown positive reaction to Alcian blue stain by Jared et al[2] Since the toxin is rich in bufadienolides, a lipid specific stain such as Nile red would be significant in determining the storage of toxins and possibly the structure of lipid stores. To perform microscopy, a microgland was dissected from the parotoid gland of a cane toad and was stained with Nile red and mounted on a glass slide and fixed with 50% glycerol. Imaging was performed using confocal microscopy and the emission was detected using red and green filters.

The emission spectrum of Nile red stain is based on its environment, and fluorescence is observed in lipid-rich regions. Polar lipids appear bright red[7] while neutral lipid structures appears green,[8] and hence the detection filters are green and red. Since bufotoxins are polar lipids (based on the conjugation), they appeared bright red with the lipid particles resembling a ring or droplet like structures (Figure 3.32). A lipid (bufotoxin) rich environment was observed within the parotoid microgland.
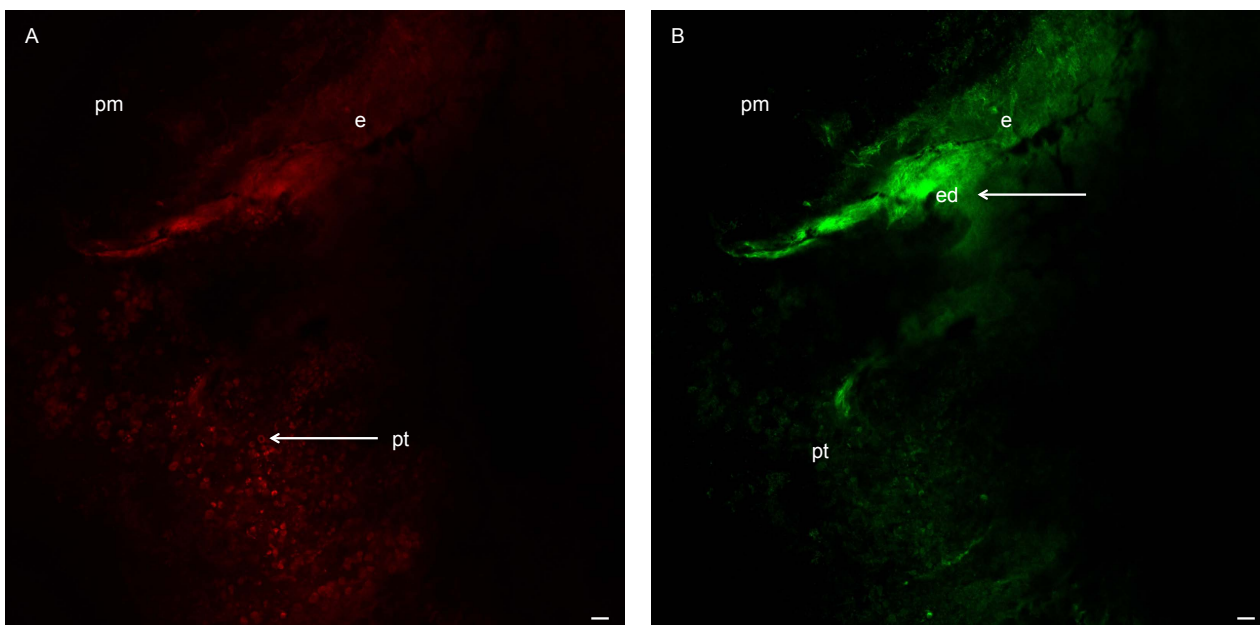
Figure 3.32 Parotoid toxin exiting from a parotoid microgland as identified by confocal microcopy stained with Nile red. A) Charged lipid bodies (bufotoxins) appear red as marked by an arrow, B) neutral lipids appear green as marked by an arrow. pm – parotoid microgland, e – epithelium, pt – parotoid toxin, ed – exit duct. Bars – 900 μm

On investigating the green emission spectra, the neutral lipid-rich region was identified to be the apical portion of the parotoid microgland, which is further connected to the toxin exit duct. The neutral lipids could be attributed to the presence of cholesterol or triglycerides, which are the major constituents of large secondary structures such as liposomes or lipid droplets.[8] Presence of secondary structures such as liposomes or lipid droplets in parotoid microglands were expected, providing the surface area required for the storage of high amounts of bufotoxins. High resolution imaging such as electron microscopy would reveal the presence of such secondary structures within the parotoid microglands. Investigation of the storage of parotoid toxin using confocal imaging indicated that the lipid rich regions within the parotoid microgland contained polar lipids (such as bufotoxins) as well as neutral lipids.

3.2.6.1 Physical properties of cane toad of parotoid toxins

Physical stability of toxin is essential as high amounts of parotoid toxin is distributed and stored within the parotoid gland (10's to 100's of mg levels of bufotoxins) and this requires the formation of stable particles. The stability of the bufotoxin particles (*in situ* toxin) must be high to package substantial amounts of steroids, and this could be achieved by forming secondary structures such as liposomes or micelles. Since bufotoxins possess a hydrophobic region attributed by steroidal rings and a hydrophilic region formed by the guanidine of the diacid arginyl amide, they could significantly form stable micelles or liposomes. While imaging the storage of toxins within the parotoid gland using Nile red stain, which is specific for lipids, particles (ring like) about 5 μm diameter were identified (Figure 3.33). These particles had a droplet like appearance with the

158

periphery stained red. Since positively charged lipids appear bright red when stained with Nile red, bufotoxins bearing the hydrophilic guanidine appeared red on the circumference of the lipid-droplet like structures while neutral lipids such as cholesterol appear green. Bufotoxins stored in the parotoid glands are possibly trapped within large lipid bodies such as lipid droplets, facilitating the storage of large toxin reserves and delivery upon a predatory attack. Lipid droplets are large globules containing rich amounts of fatty acids and sterol esters and they range from 20 nm to 100 μm.[9]
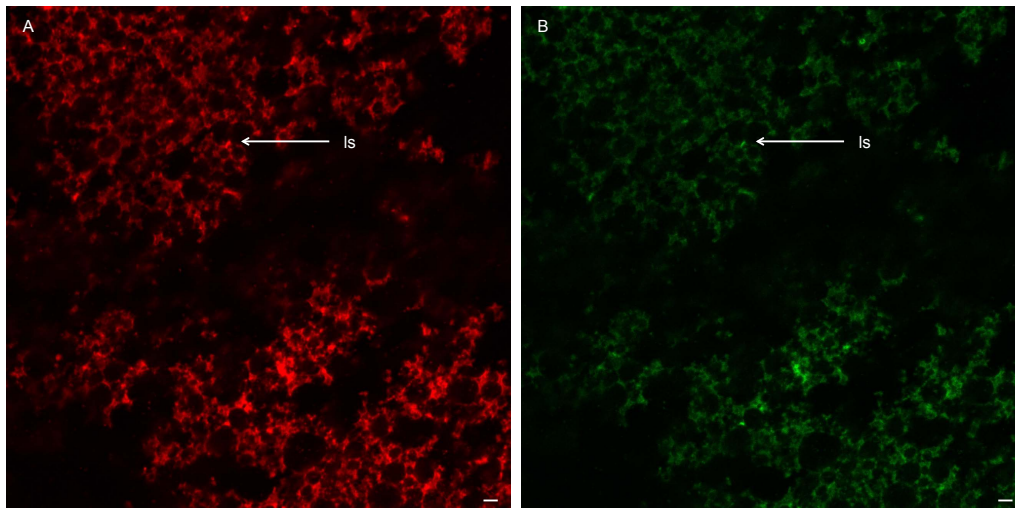
Figure 3.33 Confocal image of toxin stored within the parotoid microgland showing the structure of lipid structures. A –lipid droplet like structures with dense polar lipids (red), B – lipid structures also contains neutral lipids (green). ls – lipid structures.

Further characterization of the particle storage of parotoid toxin rich in bufotoxin was performed using electron microscopy. A transmission electron microscopy of a whole individual microgland showed insights into the packaging of bufotoxins. Lipid structures ranging from few nm to μm size were identified (Figure 3.34). Since a large amount of toxin had to be packaged and delivered through an efficient vehicle, the cane toad parotoid glands possess an effective usage of lipid droplet like structures. The small lipid structures could be disintegrated particles of large lipid structures or they could also be the precursors of large droplets. Formation of lipid droplets had been identified in human adipocytes as a storage and delivery vehicle for fatty acid esters/lipids.[10] A cane toad parotoid gland could also be compared to adipocytes due to the storage and delivery of high amounts of fatty acids including steroids (as steroidal esters). Presence of numerous fibrous particles on the lipid structures was also identified. The large lipid structures possessed significant amount of fibrilar structures compared to the small droplets exhibiting a regular pattern. From the previous observations based on Nile red staining of parotoid microgland, it is evident that bufotoxins (positively charged lipids) are attached to the lipid structures. Cane toad parotoid glands contain microglands that act as storage vesicles for toxin in the form of bufotoxins. Bufotoxins can potentially self assemble as micelle/lipid droplets to facilitate storage and delivery (secretion) as a

defense agent (Figure 3.35). Micellar structures reported in the literature have been identified to form cylindrical structures when observed under a high-resolution microscope such as TEM.[11]
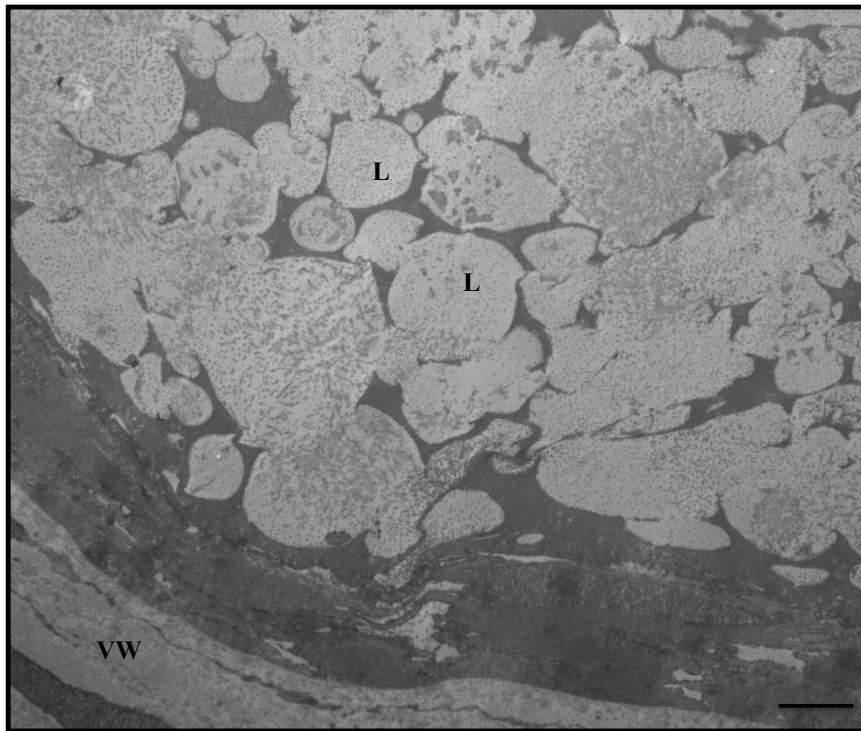
Figure 3.34 Lipid droplets observed within an individual parotoid microgland using transmission electron microscopy. L – lipid droplet, VW – microgland wall. Bar – 5 μm
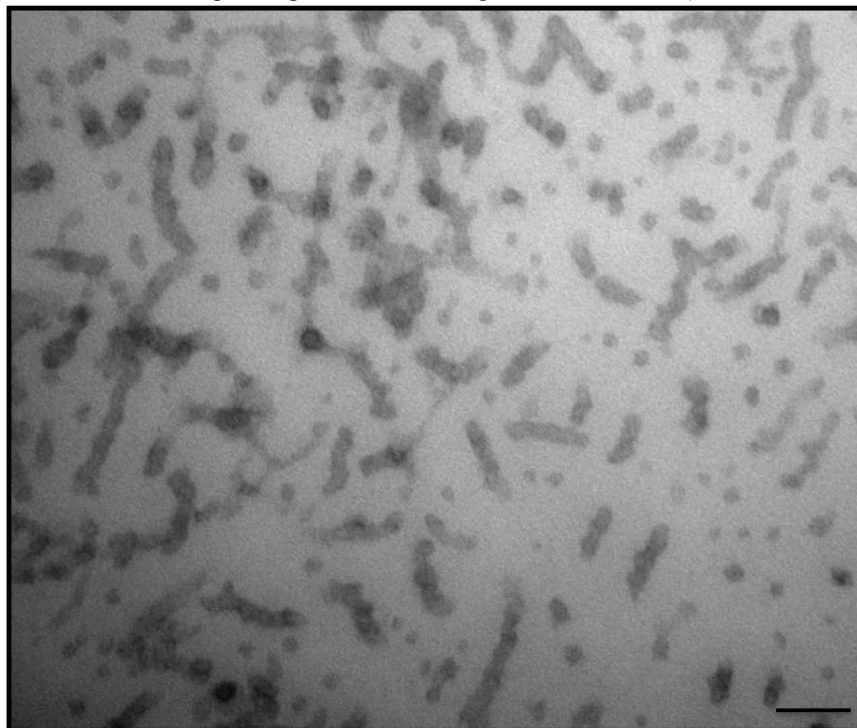
Figure 3.35 Cylindrical structures within lipid droplets, which are proposed to be micelles within an individual parotoid microgland using transmission electron microscopy. Bar – 200 nm

A combined approach of confocal imaging and electron microscopy showed some evidence of secondary structures formed within the parotoid gland for the storage of toxins. No such description of such a controlled toxin delivery system has been reported in any species other than *Bufo*. Since the toxin consists of steroidal esters (bufotoxins), a mechanism that is commonly known to deliver fatty acid esters in adipocytes could also have been adopted in Bufo toads.

Bufagenins such as bufalin (**3a**) and resibufagenin (**4a**) have been demonstrated to form highly stable structures when trapped within synthetic liposomes.[12,13] Considering the chemical stability of bufotoxins within the parotoid microglands, they could therefore likewise form highly stable bufotoxin-loaded lipid structures. Thus the in situ stored bufotoxins would be a much more practical storage mechanism than storing hydrolysed particles (*ex situ*). It is likely that the volume required to store the toxin would be much smaller for bufotoxins compared to bufagenins. In summary, storage of bufadienolides as bufotoxins enables a highly physically stable environment for *in situ* toxin storage aiding in the accumulation of concentrated amounts of bufadienolides within the parotoid gland.

3.2.7 Chemical stability of toxins to plasma and saliva

During a predatory attack on a cane toad significant amounts of bufotoxins would be released into the buccal cavity and gut of the predator where the bufotoxins would be hydrolysed into bufagenins upon exposure to body fluids such as saliva and plasma. The generated bufagenins would eventually find their way to the target cells expressing Na^+/K^+ ATPase, and in the process are exposed to body fluids such as saliva and plasma (increased plasma protein concentration). Shimada et al, reported the metabolism of marinobufotoxin (**1a**) and marinobufagenin (**1c**) after being exposed to enzymatic hydrolysis using rat or human liver cytosolic fraction.[14] About 20% of **1a** was converted into 3-dehydromarinobufagenin and 10% into 3-epimarinobufagenin after 3 h. Also, 10% of **1c** was converted into **1a** after 3 h, but the expected compound, marinobufagenin-3-suberate (**1b**) was not detected.

The bufotoxins, however, would most likely hydrolyze on contact with saliva and/or plasma before being metabolized by the liver since both saliva and plasma possess complex mixtures of proteins (enzymes including hydrolases). Hence, the chemical stability of parotoid secretion in plasma and/or saliva would indicate the hydrolysis of bufotoxins without the aid of hydrolase. The rate of formation of bufagenin would provide insights into understanding of the chemical stability of bufotoxins. If enzymes in the buccal cavity or plasma of predators could rapidly hydrolyse

marinobufotoxin (**1c**), the role of enzyme(s) co-secreted with parotoid secretions requires further analysis to determine its ecological function. Chemical stability of bufotoxins to hydrolases in plasma and/or saliva would indicate the need of an effective enzyme(s) being co-secreted to initiate rapid hydrolysis of bufotoxins for immediate activity against predators. Chemical stability of bufotoxins was investigated by determining the susceptibility of bufotoxins to body fluids such as plasma or saliva.

3.2.7.1 Stability of toxins to plasma

To determine the chemical stability of bufotoxins in plasma, a known concentration of **1c** (100 μM) was subjected to transformation in the presence of human plasma for 0 – 4 h at 37 °C. The enzymatic activity at each time interval (0, 1 and 4 h) was investigated by inhibiting the reaction, using *n*-BuOH, forming a bi-phasic mixture. The organic phase was dried, re-dissolved in MeOH (50 μL) and analysed using HPLC-DAD (Method 1).
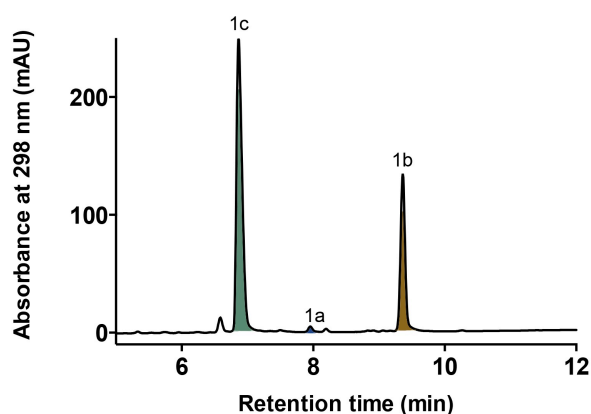
Figure 3.36 HPLC chromatogram (298 nm) of 100 μM of marinobufotoxin (**1c**) (green) in the presence of human plasma after 4 h. Marinobufagenin (**1a**) (blue) and marinobufagenin-3-hemisuberate (**1b**) (gold)

Analysis of **1c** subjected to plasma at 37 °C showed the formation of the hemi-ester, **1b** in higher amounts and minute amounts of **1a** (Figure 3.36). This is an interesting observation, as even after 4 h of exposure only 30% of bufotoxin was converted to **1b**. Only 1% of **1a** was observed, showing that the hydrolysis of bufotoxins to bufagenins in plasma is not efficient. The formation of **1a** from **1c** could be directly by the hydrolysis of C-3 suberoyl-L-arginine or **1c** could be converted into **1c** and further hydrolysed to form **1a**. The latter could be a two-step process:

1) proteolysis at C-9′ releasing marinobufagenin hemisuberate and
2) hydrolysis at C-3 releasing marinobufagenin

Breakdown of amide at C-9′ could be attributed to the proteolytic activity of peptidases/proteinases (proteases). The hemi-ester that was formed following protease attack was more stable to hydrolytic activity in the plasma, which could be the reason for the presence of less/negligible amounts of **1a**. Another reason for the production of hemi-ester instead of releasing free steroid could be that the former is less toxic than the latter. This could also be explained from the toxicity studies published in the literature that **1a** is a potent cytotoxin as well as cardiotoxic agent.[15] Hydrolysis of several esters has been reported in human plasma but esters of bufotoxins are more stable and the toads have developed a complex mechanism for their hydrolysis.[16, 17] We hypothesize that **1c** is converted into **1b** in the plasma as it is less toxic (inhibition of Na^+/K^+ ATPase) compared to **1a**, which causes severe toxicity by inhibiting Na^+/K^+ ATPase (Phase 1 metabolism).

Shimada et al, reported that when **1c** was subjected to biotransformation with mouse/human liver cytosolic fraction, resulted in the production of **1a** without forming **1b**, however, only 10% of **1a** was produced after 3 h exposure at 37 °C showing the high stability of **1c** from being metabolized by liver.[14] Half-life of marinobufotoxin in human plasma was determined by the above mentioned method with more time intervals (0, 1, 2, 4, 6, 8, 10, 12, 14, 20 and 24 h) included. The reaction was monophasic resulting in the production of **1b** while **1a** appeared in minute amounts (<5%) even after 20 h of exposure to human plasma. This clearly indicates that **1c** is highly stable against hydrolysis in the plasma (Figure 3.37). The half-life ($t_{1/2}$) of **1c** was calculated by plotting the percentage of **1c** remaining in plasma at different time intervals (h). The $t_{1/2}$ of **1c** was determined to be 7.9 h (One phase decay; r^2 = 0.9920) after exposure to human plasma for 24 h.
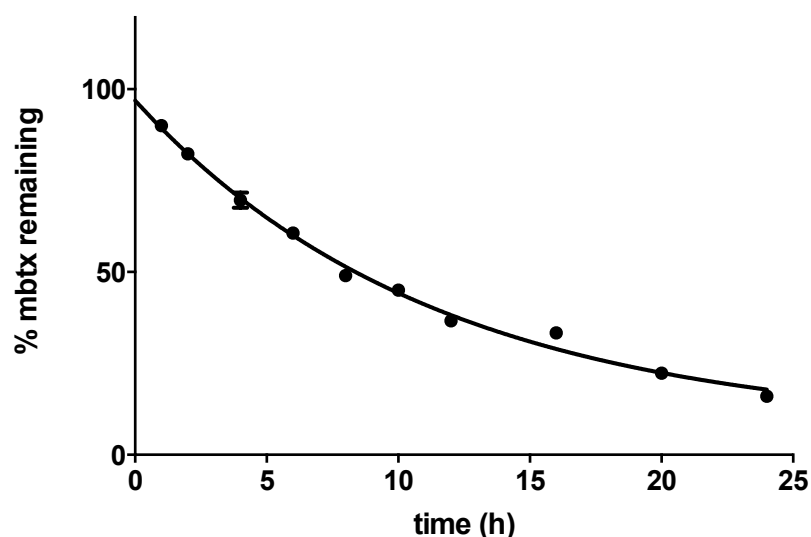
Figure 3.37 Stability of 100 μM of marinobufotoxin (**1c**) in the presence of human plasma for 24 h

The longer $t_{1/2}$ of **1c** in human plasma suggests that bufotoxins are chemically stable molecules against proteolytic activity, interestingly, they are even more stable against hydrolysis. This could

be the reason for bufotoxins hydrolysing into bufagenins during the release of the parotoid gland contents by a complex mechanism, while it should also be noted that previous studies have determined bufagenins more toxic than bufotoxins are.[18]

3.2.7.2 Stability of toxins to saliva

Stability of **1c** in saliva was also determined since during the predatory attack bufotoxins are first exposed to saliva containing mixture of proteins (such as lysozymes and other hydrolases), which could result in breakdown of bufotoxins to bufagenins and other derivatives. To determine the chemical stability of bufotoxins in saliva, a known concentration of **1c** (100 μM) was subjected to biotransformation in the presence of human saliva for 0 – 1 h at 37 °C. The enzymatic activity at each time interval (0, 15 min and 1 h) was investigated by inhibiting the reaction, using *n*-BuOH, to form a bi-phasic mixture. The organic phase was investigated using HPLC-DAD (Method 1).
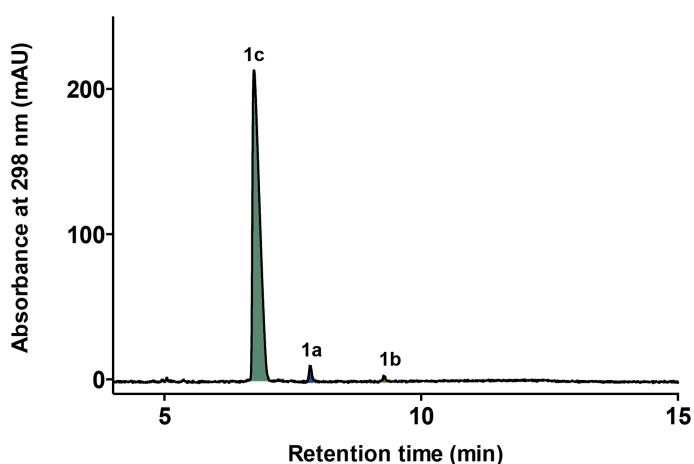
Figure 3.38 Stability of 100 μM of marinobufotoxin (**1c**) (green) in the presence of human saliva for 1 h. Marinobufagenin (**1a**) (blue) and marinobufagenin-3-hemisuberate (**1b**) (gold)

Similar to our observation in plasma experiment, the bufotoxin was highly stable to hydrolysis of the ester (<5%) (Figure 3.38). Another interesting observation was that the bufotoxins were also stable to proteolytic activity since negligible amounts of **1b** was identified using HPLC-DAD based detection. This observation suggests that **1c** is a stable molecule, which is not degraded by enzymes in saliva. Considering the rapid pace of lethal events that occurs during the predatory attack,[19] the conversion of bufotoxins into bufagenins must be at a higher rate. Hence, it is evident that the *in situ* parotoid gland hydrolase play an inevitable role in the hydrolysis of bufotoxins into bufagenins during the secretion of cane toad toxins.

3.2.8 Discussion – parotoid secretions vs parotoid toxins

The results described above reveal a level of molecular complexity associated with the chemical composition of cane toad parotoid toxin that has gone unnoticed for over 100 years. New found knowledge of cane toad parotoid toxin has implications for our understanding of cane toad chemical ecology, with possible flow on benefits in regards to control of the invasive pest. Figure 3.39 illustrates our key findings to date, which can be summarized as follows;

1. Cane toad parotoid toxin is localized *in situ* within the parotoid gland in ~ 80 – 100 microglands.
2. Cane toad parotoid toxin *in situ* is dominated by bufotoxins while the secretions contains bufagenins and arginyl amides (Figures 3.40 and 3.41).
3. The chemical composition of microgland toxin is remarkably simple, being dominated by a single bufotoxin, marinobufotoxin, with trace amounts of closely related bufotoxins (Figure 3.42).
4. During a predatory attack (or on manual compression) up to 50% of parotoid microglands will secrete their toxins via a duct, exuding a milky yellow liquid.
5. Bufotoxins are co-secreted with a hydrolase that rapidly transforms bufotoxins into bufagenins and arginyl amides.
6. Microglands do not store bufagenins and arginyl amides.
7. The bufadienolide localization and composition of male and female cane toad parotoid toxin is effectively the same.
8. The total levels of bufotoxins within the cane toad parotoid gland is ~ 50 – 200 mgs.

parotoid microgland

parotoid gland

bufotoxin

bufagenin

predatory attack or

manual expression of toxin

hydrolase
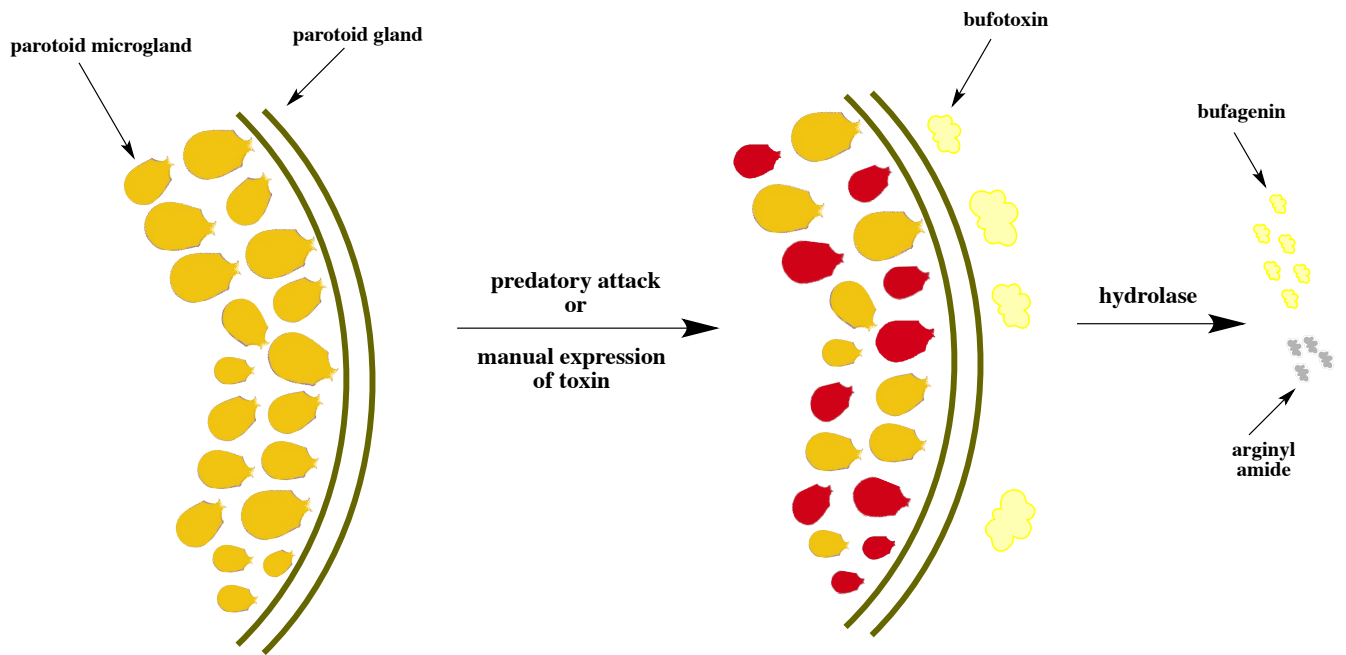
arginyl amide

1. Parotoid toxins are stored as <u>bufotoxins</u>
2. Bufotoxins are <u>not</u> co-localized with arginyl amides

1. 50% of microglands expel their bufotoxin content via a duct and reinflate with blood
2. Bufotoxins co-secrete with an enzyme (BtH) that can rapidly transform bufotoxins into bufagenins and arginyl amides

Figure 3.39 Summary on investigations of storage and delivery of cane toad parotoid toxins

parotoid gland

manual compression of parotoid glands (microglands)   *ex situ*

parotoid secretion

secretion C into water

secretion A onto glass

secretion B into methanol

Method 1 & Method 2   100%   bufagenins   bufotoxins   100%

Presence of an esterase (present in exit duct/connective tissue)

Method 3 & Method 3a   100%   suberoyl-L-arginine   0%
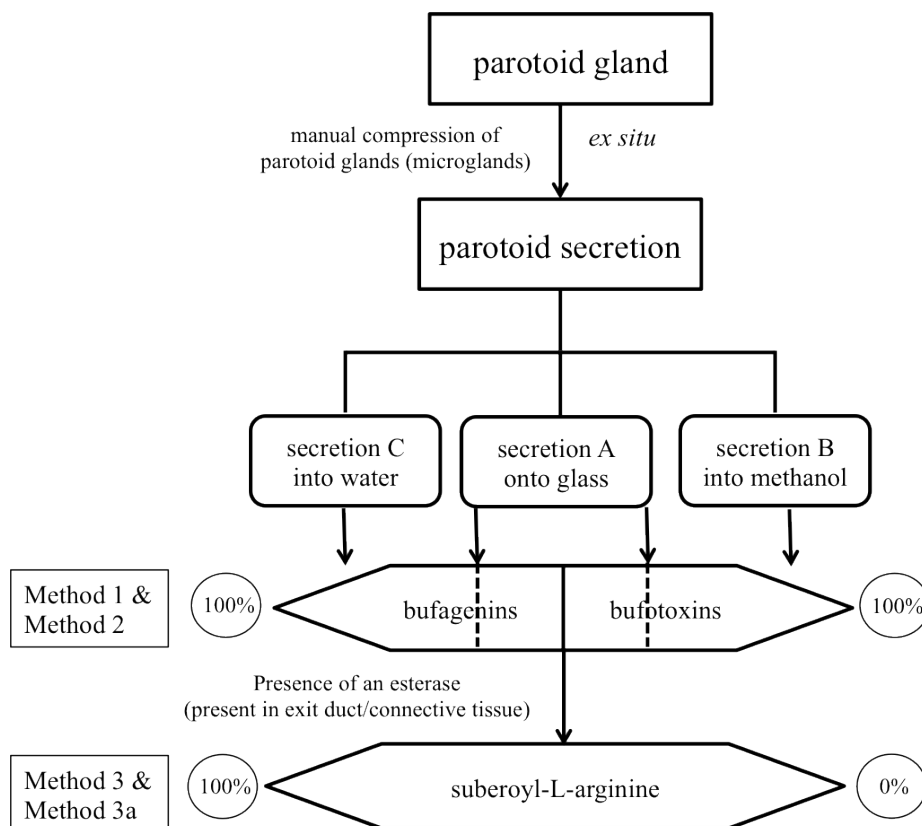
Figure 3.40 Scheme of analysis of parotoid secretions with different handling approaches yielding different composition of bufagenins vs bufotoxins

166
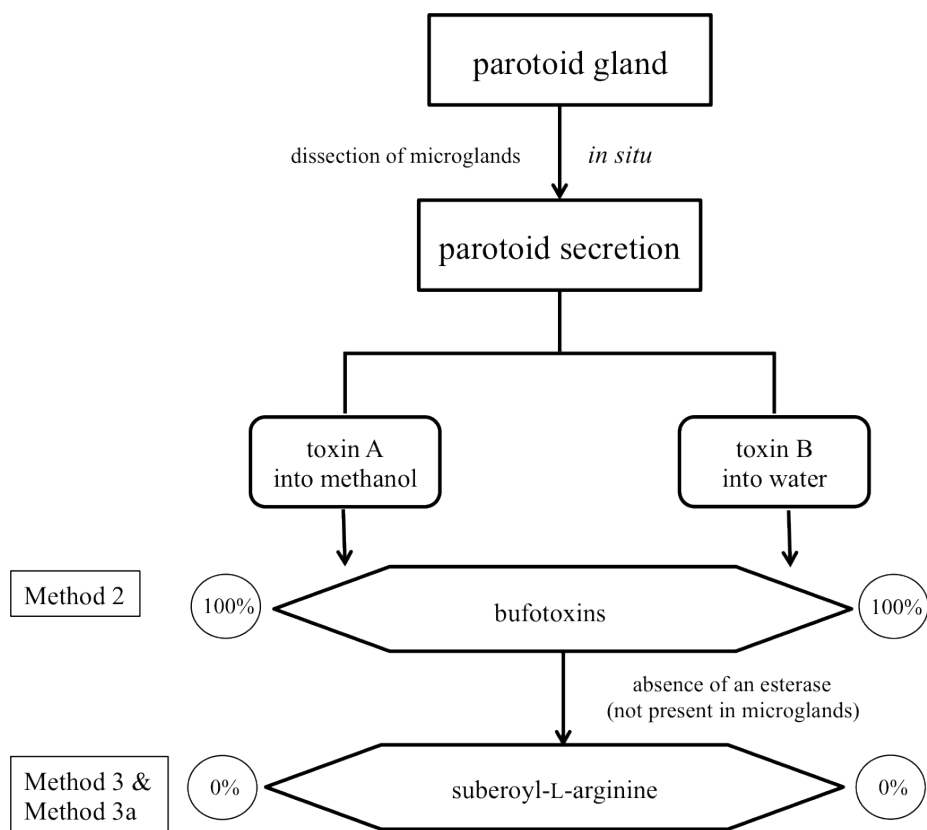
Figure 3.41 Scheme of analysis of parotoid toxin with different handling approaches yielding different composition of bufagenins vs bufotoxins
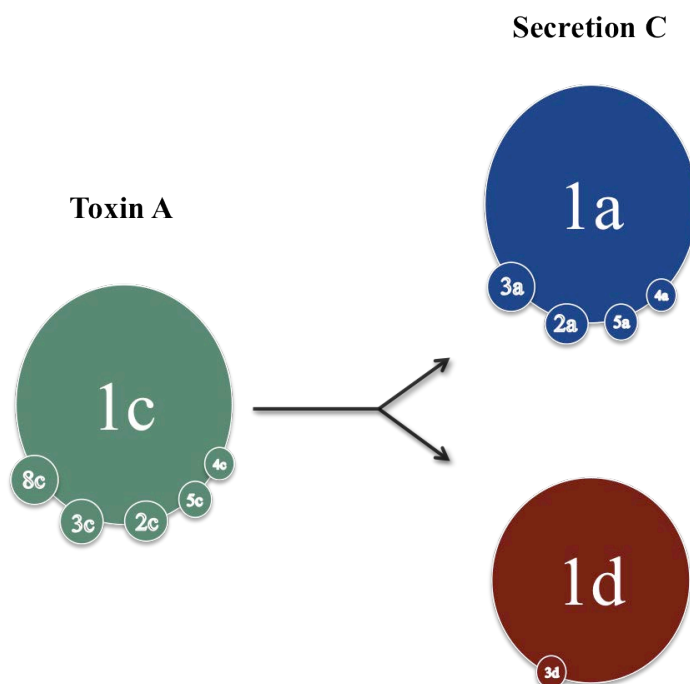
Figure 3.42 Chemical composition of parotoid toxins vs parotoid secretions. Bufotoxins (green), bufagenins (blue) and arginyl amides (red)

Although dominated by marinobufotoxin, parotoid toxin contains a range of closely related bufotoxins, all of which can be viewed as derivatives of marinobufotoxin (**1c**). These relationships are illustrated in Figure 3.43. While we can speculate conversion of bufotoxins to bufagenins is

achieved via a co-secreted hydrolase, the structure and properties of the hydrolase have to be studied, and will be explored in detail in Chapter 4. Marinobufotoxin (**1c**) could possibly be a precursor scaffold from which all the other bufotoxins are derived by *in situ* metabolic processing, including oxido-reductive enzymes. Another possibility is that marinobufotoxin could be subjected to *in situ* biotransformation by microbes. Such microbial transformations (degradation) were first reported in our laboratory in 2008.[20] The possibility that other microbes may inhabit the parotoid gland and facilitate the transformation of marinobufotoxin into one or more of other bufotoxins detected within the microglands is worthy of further investigation. Our efforts in the area will be described in Chapter 5.
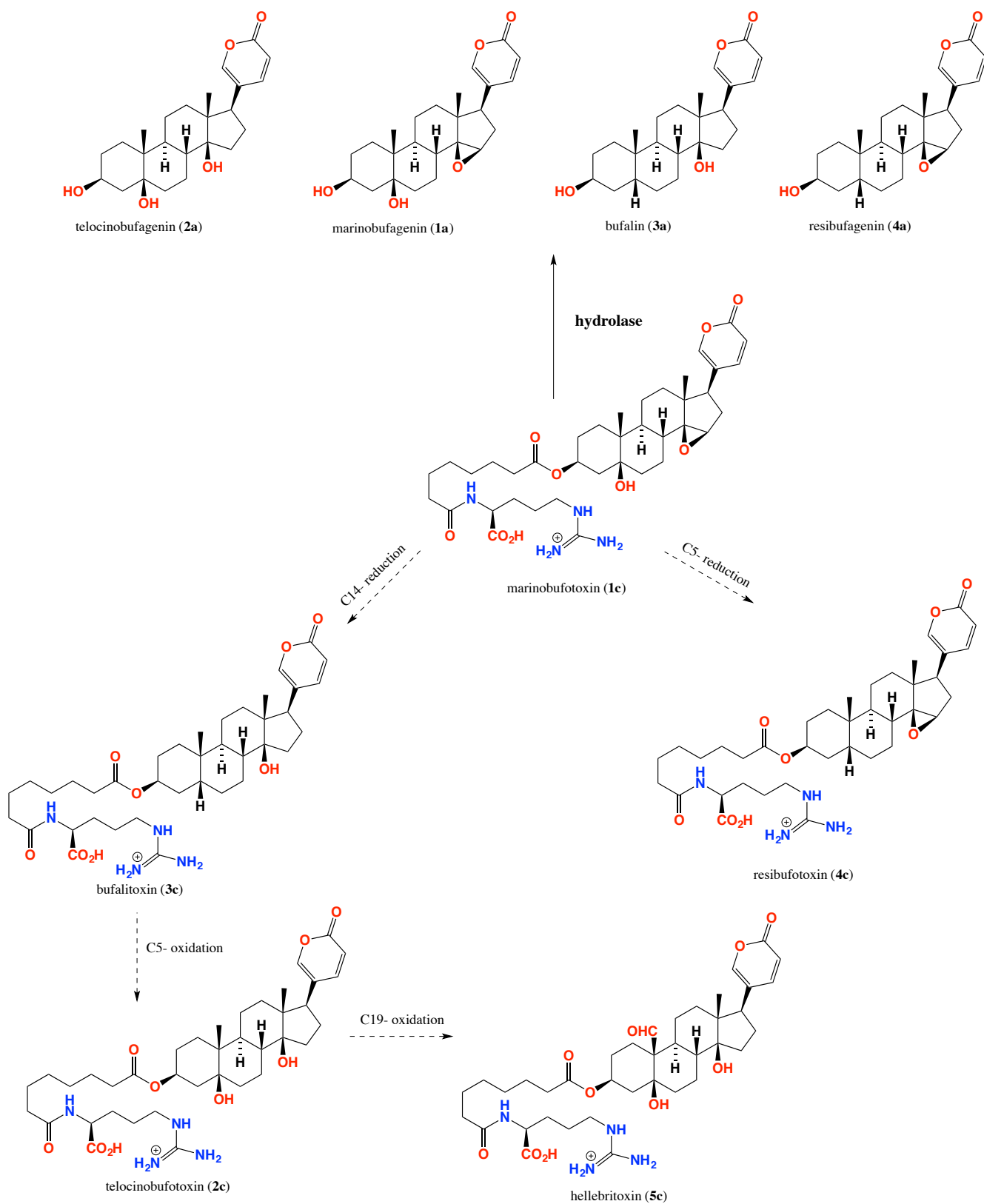
Figure 3.43 Plausible oxidation-reduction in *in situ* parotoid glands to form various bufotoxin analogues from marinobufotoxin (**1c**) and the action of hydrolase to form bufagenins from respective bufotoxins

3.3 Conclusion

Our preliminary investigation on the handling of cane toad parotoid secretions suggested the presence of bufotoxins in the parotoid secretions (chapter 2). Further investigation on the storage and delivery of cane toad parotoid toxins using the analytical methodology previously developed specifically for bufadienolide classes and arginyl amides, revealed that *in situ* parotoid toxins are stored as bufotoxins and upon release they are converted into bufagenins and arginyl amides, constituting *ex situ* parotoid secretions. Matured parotoid microglands are filled with bufotoxins and upon release, are inflated and filled with blood. This observation was also justified by the ratio of absolute amounts of bufotoxins:arginyl amides in the parotoid toxin and bufagenins:arginyl amides in the parotoid secretion analysed using our standard quantification methods. Quantification studies also showed that typical bufotoxin content in adult cane toads range between 25 – 100 mg. Also, the rapid hydrolysis of bufotoxins when the parotoid gland contents were squeezed into H_2O suggested the presence of hydrolyzing agents such as hydrolase co-secreted with the parotoid toxin. A differential dissection analysis exhibited the absence of *in situ* hydrolase within the microgland and is localized in the vicinity of the basal epithelium to which microglands are attached.

Based on our imaging studies, it was identified that bufotoxins in the parotoid gland could form highly stable particles and could be packaged around lipid structures. Chemical stability analysis using plasma/saliva indicated that bufotoxins are highly stable compounds against hydrolysis from bodily fluids. These observations suggested the possible mechanism for the hydrolysis of bufotoxins could be primarily due to the presence of some enzymes that are co-secreted, resulting in rapid hydrolysis in the presence of H_2O to release one equivalent of bufagenin and an arginyl amide each for one equivalent of bufotoxin. The proposed event that occurs during the manual compression of parotoid glands is summarized below (Figure 3.44).
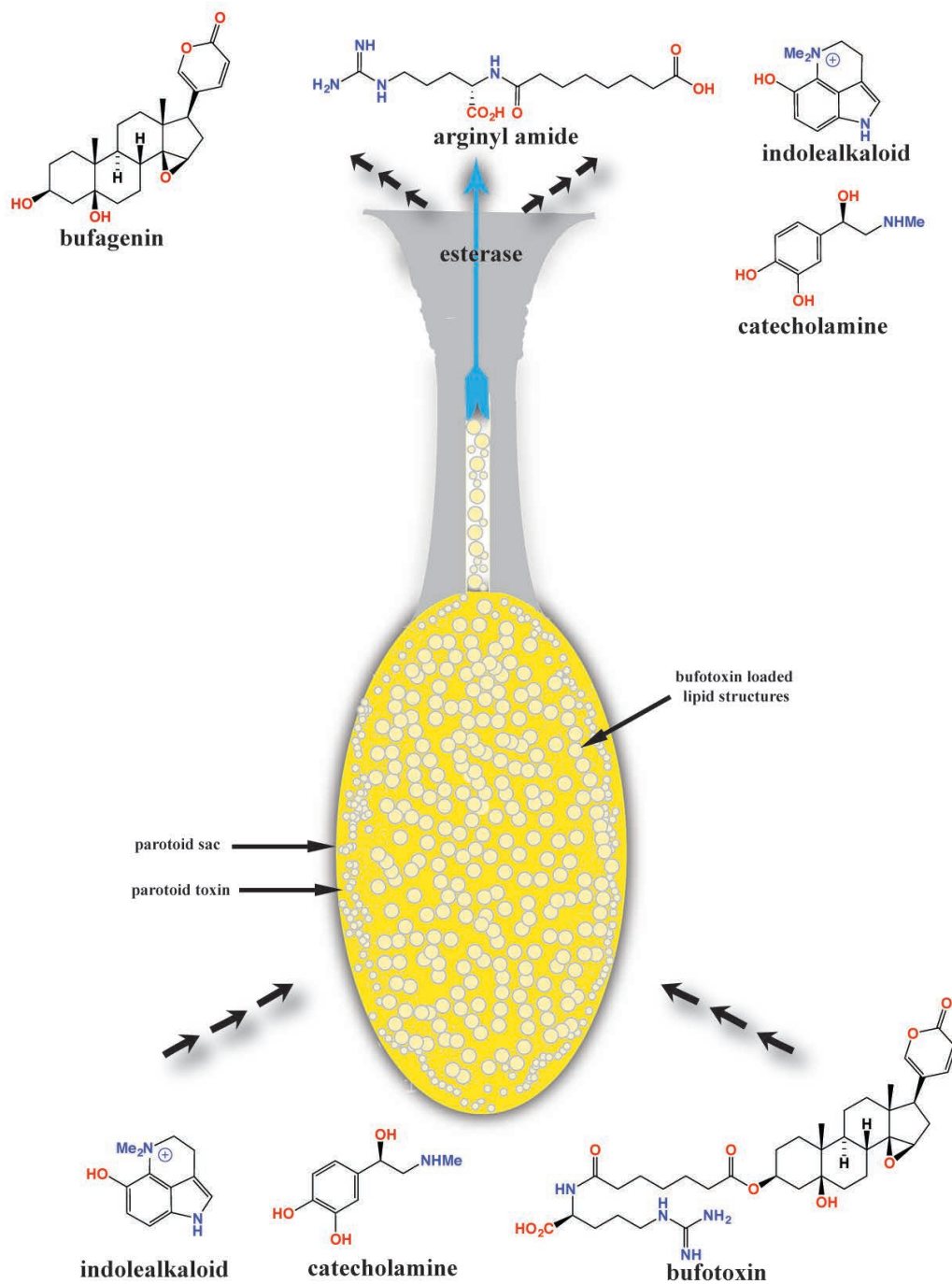
Figure 3.44 A diagrammatic representation of storage and release of parotoid toxin from a parotoid microgland based on recent findings. The secretion majorly comprised of bufagenins, however, the *in situ* toxin contains bufotoxins predominantly

3.4 Experimental

3.4.1 Micro-dissection of parotoid microglands

Parotoid glands were dissected from cane toad parotoid glands using a sterile tweezer and surgical scissors. The excised parotoid gland was washed with distilled H_2O/PBS to wash off any blood or tissues and also to maintain the moisture within the gland. Incisions were made on the ventral side of the gland to remove the thin epithelium gradually to expose the parotoid microglands that were held together by the external thin epithelium. Images of the parotoid gland and parotoid microgland were taken using Zeiss light microscope. Individual microglands were detached from the basal epithelium by the use of tweezers.

3.4.2 Secretion A – parotoid secretion squeezed onto glass plate (Figure 3.7)

Parotoid secretion from three toads (six parotoid glands) was manually squeezed onto a sterile glass plate and left for 60 min. The total secretion was collected dissolving in MeOH (10 mL) into a vial. This was followed by drying the crude parotoid secretion in MeOH under N_2 at 40 °C. The dried crude parotoid secretion was subjected to partition with n-BuOH/ H_2O, n-BuOH layers were dried under N_2 at 40 °C, re-dissolved in MeOH (1 mg/mL) to a standard concentration.

3.4.3 Secretion B – parotoid secretions squeezed into MeOH (Figure 3.11)

Parotoid glands (three) from three cane toads were squeezed to obtain the parotoid secretions directly into a vial containing MeOH (5 mL) mimicking the parotoid toxin, left for 60 min. The parotoid toxin was then dried under N_2 at 40 °C, partitioned between n-BuOH and H_2O. The dried n-BuOH layer solubles was resuspended in MeOH to a standard concentration (1 mg/mL). The dried H_2O solubles were subjected to derivatization with 2:1 ratio of 2,4-pentanedione and pyridine for 6 h at reflux, dried under N_2 at 40 °C and resuspended in MeOH to a standard concentration (1 mg/mL).

3.4.4 Secretion C – parotoid secretions squeezed into H_2O (Figure 3.15)

Parotoid glands (three) from three cane toads were squeezed to obtain the parotoid secretions directly into a vial containing H_2O (5 mL), gradually mixed until the solution is partially homogenized and left for 60 min. The parotoid secretion was then dried under N_2 at 40 °C, partitioned between n-BuOH and H_2O. The dried n-BuOH layer solubles was resuspended in MeOH to a standard concentration (1 mg/mL). The dried H_2O layer solubles was subjected to

derivatization with 2:1 ratio of 2,4-pentanedione and pyridine for 6 h at reflux, dried under N_2 at 40 °C and resuspended in MeOH to a standard concentration (1 mg/mL).

3.4.5 Toxin A – microgland extracted in MeOH (Figure 3.19)

Individual parotoid microglands were dissected from parotoid glands, washed with PBS, weighed and were directly immersed into a vial containing MeOH (500 μL). The microgland was disrupted using a pipette tip to release the parotoid toxin into MeOH and left for 60 min, dried under N_2 at 40 °C, partitioned between *n*-BuOH and H_2O. The dried *n*-BuOH layer solubles was resuspended in MeOH to (50 μL). The dried H_2O layer solubles was subjected to derivatization with 2:1 ratio of 2,4-pentanedione and pyridine for 6 h at reflux, dried under N_2 at 40 °C and resuspended in MeOH (50 μL).

3.4.6 Toxin B - microgland extracted in H_2O (Figure 3.23)

Individual parotoid microglands were dissected from parotoid glands, washed with PBS, weighed and were directly immersed into a vial containing H_2O (500 μL). The microgland was disrupted using a pipette tip to release the parotoid toxin into H_2O and left for 60 min, dried under N_2 at 40 °C, partitioned between *n*-BuOH and H_2O. The dried *n*-BuOH layer solubles was resuspended in MeOH (50 μL).

3.4.7 Secretion D – rate of hydrolysis of bufotoxin (Figure 3.25)

Left parotoid glands (three) from three cane toads were squeezed to obtain the parotoid secretions directly into a vial containing H_2O (5 mL), gradually mixed until the solution is partially homogenized. An aliquot of sample (500 μL) was obtained for each time interval ranging 5, 10, 15, 20 and 30 min and quenched with MeOH (500 μL). 0 min reading was obtained by squeezing the right parotoid gland into a vial containing MeOH (5 mL). The parotoid secretion was then dried under N_2 at 40 °C, partitioned between *n*-BuOH and H_2O. The dried *n*-BuOH layer solubles was resuspended in MeOH to a standard concentration (1 mg/mL).

3.4.8 Toxin C – co-localization of hydrolase within microgland (Figure 3.29)

Parotoid glands were excised and individual microglands were cut using micro-scissors from the basal epithelium by destroying surrounding microglands, washed with PBS and were directly immersed into a vial containing H_2O (500 μL). The microgland was disrupted using a pipette tip to

release the parotoid toxin into H_2O and left for 60 min, dried under N_2 at 40 °C, partitioned between n-BuOH and H_2O. The dried n-BuOH layer solubles was resuspended in MeOH (50 μL).

3.4.9 Imaging *in situ* parotoid toxin in parotoid microglands (Confocal imaging)

Parotoid microglands were dissected from parotoid glands as mentioned above, washed twice with sterile H_2O and were directly immersed in cold PBS solution containing 4% formaldehyde. Parotoid microglands were later immersed into a solution of Nile red stain (10 μg/mL; 300 μL) and incubated for 10 min. Nile red treated parotoid microglands were then washed twice with PBS to remove excess nile red and was fixed using a cover slip with 50% glycerol. The sample was then observed using a confocal microscope (Zeiss, Australia).

3.4.10 Imaging *in situ* parotoid toxin in parotoid microglands (Electron microscopy)

Parotoid microglands were dissected from parotoid glands as mentioned above and were washed with 4% formaldehyde solution in PBS and immersed in sodium cacodylate buffer containing 3% glutaraldehyde.

3.4.11 Stability of marinobufotoxin in plasma

Human plasma was kindly provided by Dr. Abishek Iyer (Prof Fairlie Group, IMB, UQ). Marinobufotoxin (100 μM) was made up to 1 mL with human plasma (450 μL) and incubated for various time intervals (0 – 60 min) at 37 °C. The enzymatic activity at each time interval was investigated by the addition of n-BuOH to form a bi-phasic mixture and the organic layer was extracted (2x). The organic layers were combined and dried under a stream of N_2 at 40 °C, re-dissolved in MeOH (50 μL).

3.4.12 Half-life of marinobufotoxin in plasma

Human plasma was kindly provided by Dr. Abishek Iyer (Prof Fairlie Group, IMB, UQ). Marinobufotoxin (100 μM) was made up to 1 mL with human plasma (450 μL) and incubated for various time intervals (1, 2, 4, 6, 8, 10, 12, 16, 20 and 24 h) at 37 °C. The enzymatic activity at each time interval was investigated by inhibiting the reaction, n-BuOH was added to form a bi-phasic mixture and the organic layer was extracted (2x). The organic layers were combined and dried under a stream of N_2 at 40 °C, re-dissolved in MeOH (50 μL).

Graphpad Prism was used to generate $t_{1/2}$ curves (One phase decay) for marinobufotoxin (**1c**) with area under the peak calculated at different concentrations. Relative amounts of marinobufotoxin (**1c**) were determined by calculating the area under the peak analysed using HPLC-DAD.

3.4.13 Stability of marinobufotoxin in saliva

Human saliva was collected from the research candidate (Mr. Venkatanambi Kamalakkannan). Marinobufotoxin (100 µM) was made up to 1 mL with human saliva (450 µL) and incubated for various time intervals (0 – 60 min) at 37 °C. The enzymatic activity at each time interval was investigated by inhibiting the reaction, *n*-BuOH was added to form a bi-phasic mixture and the organic layer was extracted (2x). The organic layers were combined and dried under a stream of N_2 at 40 °C, re-dissolved in MeOH (50 µL).

3.5 References

1. Hostetle.Jr; Cannon, M. S., Anatomy of parotoid gland in bufonidae with some histochemical findings .1. *Bufo marinus*. *J. Morphol.* **1974,** *142*, 225-239.
2. Jared, C.; Antoniazzi, M. M.; Jordao, A. E. C.; Silva, J.; Greven, H.; Rodrigues, M. T., Parotoid macroglands in toad (*Rhinella jimi*): Their structure and functioning in passive defence. *Toxicon* **2009,** *54*, 197-207.
3. Morales, R., Chemical synthesis and pharmacological characterization of the frog Prokineticin Bv8 and study of the mechanism of chemical defence of cane toads (*Rhinella marin*a) **2010**.
4. Hutchinson, D. A.; Savitzky, A. H., Vasculature of the parotoid glands of four species of toads (Bufonidae : *Bufo*). *J. Morphol.* **2004,** *260*, 247-254.
5. Tian, H. Y.; Luo, S. L.; Liu, J. S.; Wang, L.; Wang, Y.; Zhang, D. M.; Zhang, X. Q.; Jiang, R. W.; Ye, W. C., C-23 Steroids from the Venom of *Bufo bufo gargarizans*. *J. Nat. Prod.* **2013,** *76*, 1842-1847.
6. Crossland, M. R.; Haramura, T.; Salim, A. A.; Capon, R. J.; Shine, R., Exploiting intraspecific competitive mechanisms to control invasive cane toads (*Rhinella marina*). *Proc. R. Soc. B-Biol. Sci.* **2012,** *279*, 3436-3442.
7. Greenspan, P.; Mayer, E. P.; Fowler, S. D., Nile red - A selective fluorescent stain for intracellular lipid droplets. *J. Cell Biol.* **1985,** *100*, 965-973.
8. Martin, S.; Parton, R. G., Lipid droplets: a unified view of a dynamic organelle. *Nat. Rev. Mol. Cell Biol.* **2006,** *7*, 373-378.
9. Guo, Y.; Cordes, K. R.; Farese, R. V., Jr.; Walther, T. C., Lipid droplets at a glance. *J. Cell Sci.* **2009,** *122*, 749-752.
10. Thiam, A. R.; Farese, R. V., Jr.; Walther, T. C., The biophysics and cell biology of lipid droplets. *Nat. Rev. Mol. Cell Biol.* **2013,** *14*, 775-786.
11. Kuntsche, J.; Horst, J. C.; Bunjes, H., Cryogenic transmission electron microscopy (cryo-TEM) for studying the morphology of colloidal drug delivery systems. *Int. J. Pharm.* **2011,** *417*, 120-137.
12. Hu, K. L.; Zhu, L.; Liang, H. Y.; Hu, F. Q.; Feng, J. F., Improved Antitumor Efficacy and Reduced Toxicity of Liposomes Containing Bufadienolides. *Arch. Pharmacal Res.* **2011,** *34*, 1487-1494.
13. Li, F.; Yang, R.; Weng, Y.; Tang, X., Preparation and evaluation of lyophilized liposome-encapsulated bufadienolides. *Drug Dev. Ind. Pharm.* **2009,** *35*, 1048-1058.
14. Shimada, K.; Miyashiro, Y.; Nishio, T., Characterization of in vitro metabolites of toad venom using high-performance liquid chromatography and liquid chromatography-mass spectrometry. *Biomed. Chromatogr.* **2006,** *20*, 1321-1327.
15. Kamano, Y.; Kotake, A.; Hashima, H.; Inoue, M.; Morita, H.; Takeya, K.; Itokawa, H.; Nandachi, N.; Segawa, T.; Yukita, A.; Saitou, K.; Katsuyama, M.; Pettit, G. R., Structure-cytotoxic activity relationship for the toad poison bufadienolides. *Bioorg. Med. Chem.* **1998,** *6*, 1103-1115.
16. Stewart, D. J.; Inaba, T.; Tang, B. K.; Kalow, W., Hydrolysis of cocaine in human plasma by cholinesterase. *Life Sci.* **1977,** *20*, 1557-1563.
17. Alberti, J.; Martinet, A.; Sentellas, S.; Salva, M., Identification of the Human Enzymes Responsible for the Enzymatic Hydrolysis of Aclidinium Bromide. *Drug Metab. Dispos.* **2010,** *38*, 1202-1210.
18. Akimova, O. A.; Bagrov, A. Y.; Lopina, O. D.; Kamernitsky, A. V.; Tremblay, J.; Hamet, P.; Orlov, S. N., Cardiotonic steroids differentially affect intracellular Na^+ and $Na^+_{(i)}$/ $K^+_{(i)}$-independent signaling in C7-MDCK cells. *J. Biol. Chem.* **2005,** *280*, 832-839.
19. Crossland, M. R.; Brown, G. P.; Anstis, M.; Shilton, C. M.; Shine, R., Mass mortality of native anuran tadpoles in tropical Australia due to the invasive cane toad (*Bufo marinus*). *Biol. Conserv.* **2008,** *141*, 2387-2394.

20. Hayes, R. A.; Piggott, A. M.; Dalle, K.; Capon, R. J., Microbial biotransformation as a source of chemical diversity in cane toad steroid toxins. *Bioorg. Med. Chem. Lett.* **2009,** *19*, 1790-1792.

Chapter 4: Isolation, identification and characterization of enzyme mediating toxin hydrolysis

4.1 Introduction

The *in situ* parotoid toxin is rapidly converted into bufagenins in secretions obtained after manual compression, most likely by the action of a co-secreted bufotoxin hydrolase (BtH). Chemical analysis of the parotoid microglands (Chapter 3) clearly indicated if a BtH is present it is localized in the vicinity of the basal epithelium to which the microglands are attached, and that during manual compression of the parotoid gland or predatory attack BtH is likely to be co-secreted with toxin. Toledo et al has previously reported the anatomy of *B. marinus* parotoid gland and commented on the presence of proteins, along with bufadienolides and biogenic amines.[1] Likewise, Jared et al detected protein-like substances in specialized glands (differentiated granular glands) in the vicinity of the parotoid microglands in *Rhinella jimi* (Brazilian toad),[2] situated just above the parotoid glands near the exit pore, which would allow for co-secretion of protein (BtH) with the parotoid toxin.[2]

Although new to our understanding of toad chemical ecology, the concept of an enzyme-toxin co-secretion model has been reported as a part of the defense mechanism exhibited by bombardier beetles. In that instance, the substrate hydrogen peroxide is stored in a separate chamber which is then mixed with the catalase/peroxidase to produce free oxygen, which in turn oxidizes, hydroquinone to *p*-quinone resulting in a highly exothermic reaction reaching about 100 °C.[3, 4] While there are no reports describing the co-secretion of hydrolases and cardiotonic steroids as a defense mechanism, the identification of such a hydrolase in *B. marinus* would provide valuable insights into the ecological role and chemo-anatomy of the parotoid gland. For example, that a hydrolase (BtH) could convert a storage protoxin (bufotoxin) to a defensive toxin (bufagenins) represents an intriguing possibility.

Parotoid secretions reported in chapter 3 suggested localization of an *in situ* parotoid gland hydrolase (BtH). To detect *in situ* as well as *ex situ* BtH we explored the use of a fluorescent stain and subjecting parotoid gland preparations to fluorescent imaging. We also employed transcriptomics analyses to acquire the RNA sequence dataset from which we translated protein sequence information. Purification of BtH from parotoid secretions was achieved using gel filtration chromatography with the help of a fluorescent indicator. Structure-activity-relationship studies on BtH were performed using various bufadienolide substrates, to determine substrate specificity. Kinetics studies showed rapid hydrolysis of bufotoxin by BtH as identified previously in Chapter 3. Purified BtH was also subjected to peptide mass fingerprint analysis, which was correlated with

protein sequence information from transcriptome analyses, to characterize the complete sequence of BtH (Scheme 4.1).
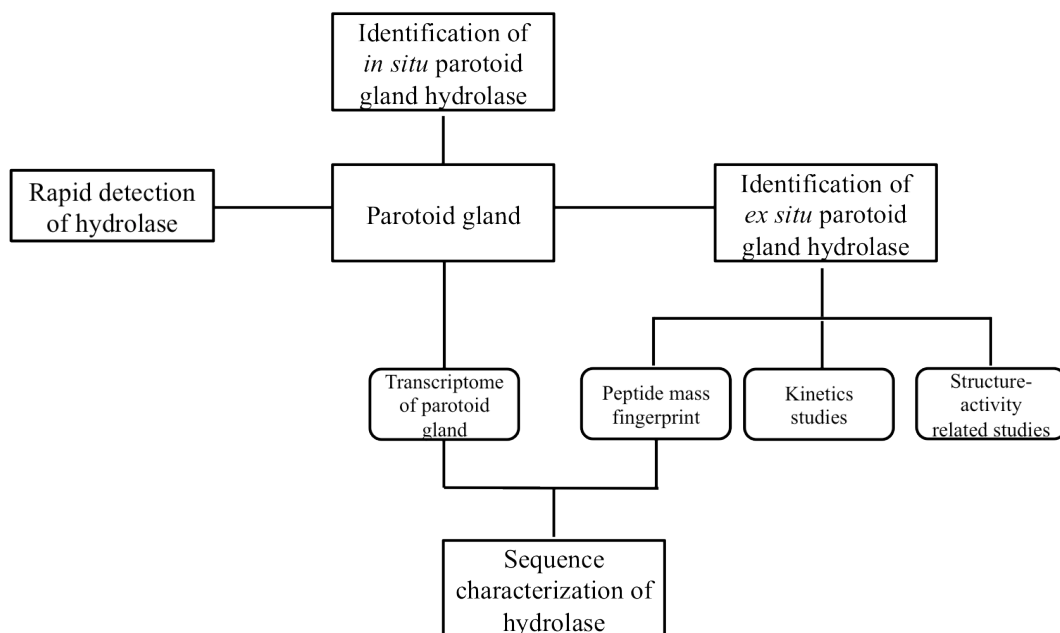
Scheme 4.1 Identification and characterization of parotoid gland hydrolase

4.2 Results and discussion

4.2.1 Fluorescein aided detection of hydrolase activity in parotoid secretions

The preliminary experiments on cane toad toxin suggested that a hydrolyzing enzyme (BtH) in the parotoid gland was co-secreted during manual compression resulting in rapid hydrolysis of bufotoxins into bufagenins and arginyl amides. For easy and rapid detection of hydrolase activity *in situ* (localization of hydrolase) and *ex situ* (isolation of hydrolase) a highly reactive fluorescent stain, fluorescein diacetate (FdA) (which is often used to detetect hydrolases) was used. We anticipated and confirmed that bufotoxin hydrolase (BtH) would accept fluorescein diacetate (FdA) as a substrate and release the fluorescent dye, fluorescein (Figure 4.1).
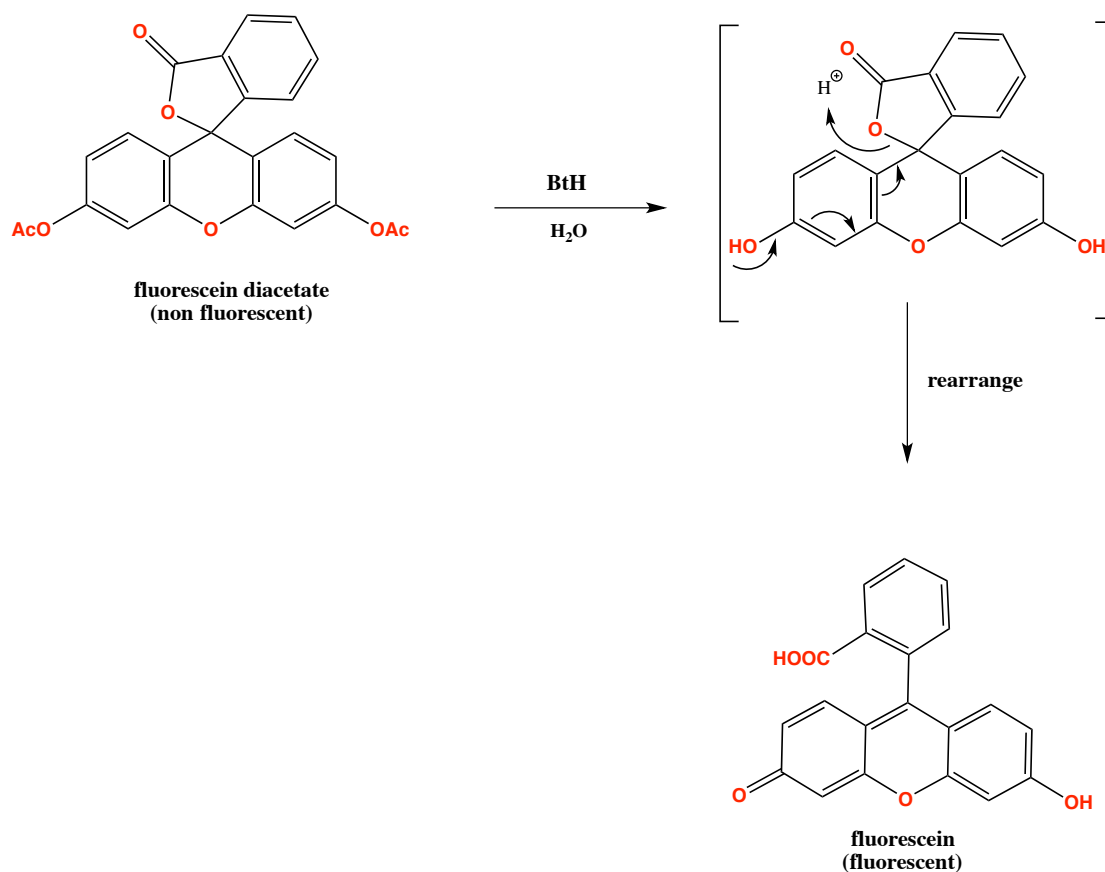
Figure 4.1 Conversion of fluorescein diacetate to fluorescein by the hydrolase in the presence of H_2O

FdA could be hydrolysed by the parotoid secretion suggesting a hydrolase enzyme with broad specificity was present in the secretion. Having fluorescent diacetate (FdA) as a BtH responsive dye, we analyzed the location, biochemistry and structure of BtH. Parotoid secretion from an adult cane toad was collected in a vial containing PBS (pH 7.4) and mixed gently using a vortex. An aliquot (1 mL) was centrifuged to remove non-polar substances (including bufadienolides) and the supernatant was collected and reacted with a solution of FdA (50 μg/mL; 100 μL) and left for 15

min. The supernatant exhibited strong fluorescence activity within 5 min of incubation indicating that BtH did accept FdA as a substrate (Figure 4.2). Due to its specificity and rapid reaction time with BtH, FdA was seen as a useful reagent that could be used to visualize the localization BtH within the parotoid gland.
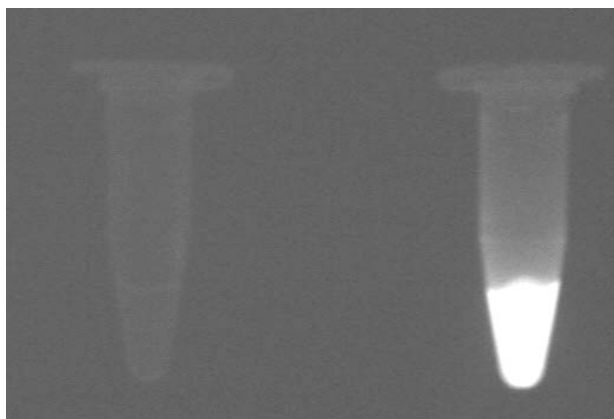
Figure 4.2 Reaction of crude parotoid secretions pellet with fluorescein diacetate exhibiting no fluorescence (left) and supernatant exhibiting strong fluorescence (right)

4.2.2 Identification of BtH

4.2.2.1 Structure of parotoid gland and microglands

Parotoid glands are large secretory glands that store parotoid toxin, and on manual compression release the stored toxin through numerous pores. Several anatomical studies have been reported on parotoid glands, describing their physical as well as biochemical features. Several lipids, proteins, carbohydrates and cell wall components have been described by Toledo et al,[1] Jared et al[2] and Hutchinson et al,[5] in an effort to better understand the storage of toxin within the parotoid gland. Notwithstanding prior studies, we elected to reexamine this matter – particularly in light of our revelations regarding bufotoxin hydrolysis. We explored the histology of the parotoid gland and its cellular/organelle components using several imaging techniques, including those listed in Table 4.1.

Table 4.1 List of stains and specificity

Stain	Specificity
Trichrome	cells, connective tissue and cytoplasm
PAS	polysaccharides (eg. glycogen) and mucinous substances (eg. Mucous and glycoproteins)
Alcian blue	acidic polysaccharides (eg. glycosaminoglycans) and mucinous substances
DAPI	DNA
Congo red	cytoplasm and erythrocytes
Mucicarmine	Microorganisms (cell wall components)

A trichrome staining of the parotoid gland revealed the structure of distinct parotoid microglands (pm), small granulated glands (gg) and a rich structural framework of collagen and cells scattered upon different regions (Figure 4.3). The contents of parotoid microglands (rich in bufotoxins) did not show any positive reaction to trichrome stain indicating the absence of cells or connective tissue within the parotoid microglands.
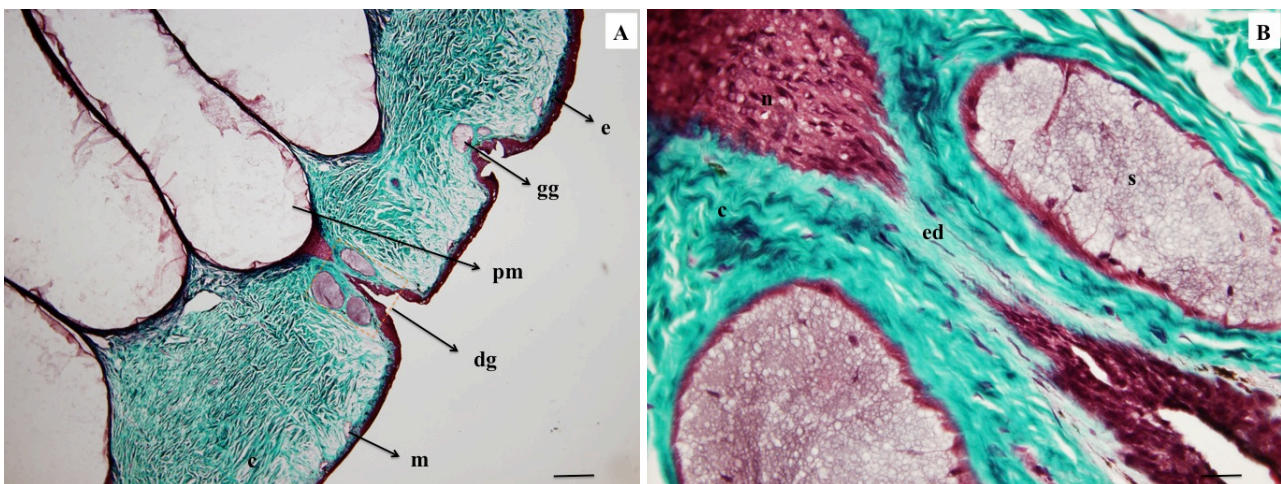
Figure 4.3 Trichrome staining of *B. marinus* parotoid gland, bright red – nuclei, pinkish red – cytoplasm, green – connective tissue. A – basic structures of parotoid gland exhibiting parotoid microgland (pm), differentiated granular glands (dg), connective tissue (CT), granular gland (g), mucinous glands (m), bar – 500 μm. B – expansion of the toxin exit duct (texd) connecting ductal epithelium (d) of parotoid microgland to the pore on parotoid skin, bar – 10 μm.

This staining showed that the basic anatomy of the *B. marinus* parotoid gland consists of a structural framework similar to the Brazilian toad, *Rhinella jimi*. The main structures of the parotoid gland include those listed in Table 4.2.

Table 4.2 List of anatomical structures in parotoid gland

Code	Structure	Description
pm	large parotoid microglands	bottle shaped glands containing parotoid toxin
d	ductal epithelium	duct at the apex of the parotoid microgland with dense cellular material
gg	granular glands	small granulated glands containing secretory material
dg	differentiated granular glands	large granulated glands at the apex of parotoid microgland adjacent to the ductal epithelium and
c	connective tissue	thick dense connective tissue consisting of collagen fibers
ed	exit duct	duct connecting the microgland to the toxin exit pore
s	secretion	secretory material within dg
m	mucous glands	scattered glands with mucinous secretions along the dermis
e	epidermis	thick calcified epidermis
n	nuclei	nucleus within cells
ge	glandular epithelial cell	epithelial cells present within differentiated granular glands
me	myo-epithelial cells	epithelial cells distributed in the surface of parotoid microglands
k	keratinocyte	keratin containing cells present in the proximity of epidermis

Histology of large parotoid microglands with Alcian blue, PAS, H&E and mucicarmine stains showed the secretion is highly positive to Alcian blue (Figure 4.4A) and mucicarmine while negative to PAS and H&E. These investigations clearly indicated the presence of polysaccharides (eg. mucopolysaccharides) within the parotoid microgland. This observation also indicated that substances such as carbohydrates are present in substantial amounts in the parotoid microglands, however, their function is currently unknown. The walls of the parotoid microgland showed the presence of high amounts of nucleated cells (thick red portion, Figure 4.3A). Hostetle et al had previously proposed that such cells were responsible for the biosynthesis of bufadienolides, although there is no direct evidence to support this hypothesis.[6] Alcian blue (Figure 4.4A) and Congo red (Figure 4.4B) revealed that parotoid microglands have foam like internal structures.
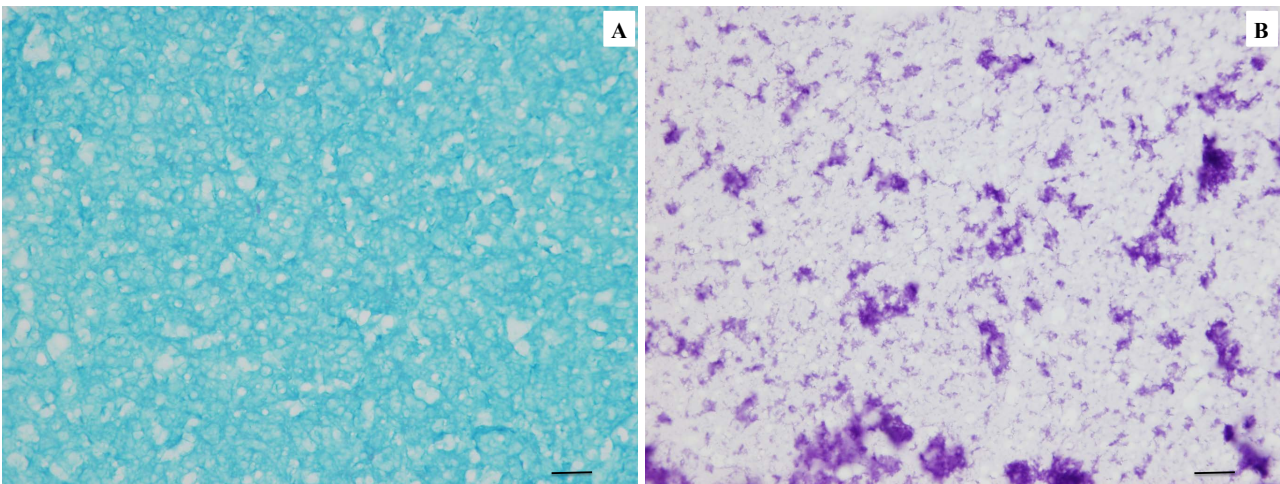
Figure 4.4 Differential staining of parotoid microglands exhibiting foam like appearances. A – Alcian blue staining, B – Congo red staining. Bars – 20 μm

The differentiated granular glands (dg) present adjacent to the ductal epithelium (Figure 4.3) were structurally different from the mucous (m) and the granular glands (gg) (Figure 4.5 E). The differentiated granular glands consist of four glands that are arranged in a circular form around the ductal epithelium. Some of these glands exhibited secretions positive to PAS staining (Figure 4.5B, Figure 4.5F), however, the nuclei of the cells (n) in the surrounding epithelium exhibited positive DAPI (Figure 4.5A), Congo red (Figure 4.5D) and Alcian blue staining. A trichrome staining of differentiated granular glands (dg) clearly indicated the presence of secretory material (s) and surrounded by secretory epithelium with two different cell types, nucleated and non-nucleated epithelial cells (Figure 4.5C). The differentiated granular glands were also previously proposed to contain proteins based on their reaction with bromophenol blue by Almeida et al and Toledo et al, however no biochemical characterization of the proposed proteins were performed.[1,7] The function of these differentiated granular glands is largely unknown. This was of major interest to our investigation to detect and identify the tissue locality of a potential BtH. Based on the location of these glands, we hypothesized that BtH is stored in and co-secreted from differentiated granular glands along with the toxins upon manual pressure on the parotoid glands.
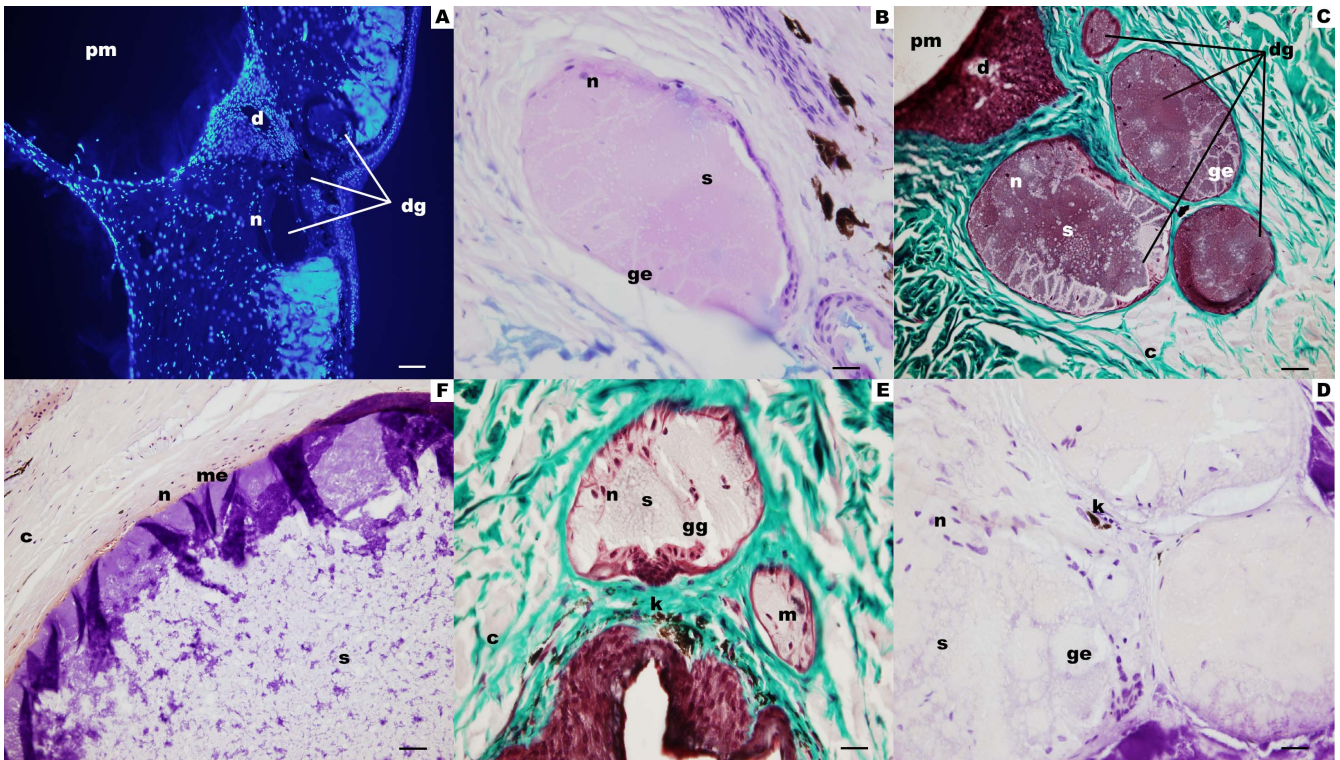
Figure 4.5 Imaging of parotoid glands using various stains. Clockwise, A – DAPI staining of parotoid gland exhibiting parotoid microgland (pm) devoid of cells, ductal epithelium (d) and differentiated accessory glands (dg) at the apex of the parotoid microgland, bar – 500 μm. B – PAS stain positive secretion (s) in the differentiated accessory gland with possibly two different cell types, the surrounding glandular epithelial cells (ge) and cells with nuclei (n), bar – 50 μm. C – parotoid gland stained with trichrome displaying islets of differentiated accessory glands (dg) filled with cytoplasmic secretion (s) and dense connective tissue (c), bar – 100 μm. D – differentiated accessory glands stained with Congo red exhibiting two cell types as with other stains, PAS and trichrome, bar – 50 μm, E – a trichrome staining indicating granular gland (gg) and small mucous gland just below the epidermis filled with secretion (s) and differentiated cells (n), bar – 50 μm, F – wall of the parotoid microgland stained with Congo red indicating the myo epithelium (me) and abundance of cell types (n) in the inter-vesicular space.

4.2.2.2 Localization of BtH

The presence of a potential BtH within the parotoid gland was investigated using fluorescent microscopy and FdA. Sections of parotoid gland was cut using a microtome and mounted on glass slides and were treated with FdA (10 μg/mL; 1% DMSO), followed by imaging using a confocal microscope with the long pass filter set for an emission wavelength of 505 and 560 nm.

A transmission (transmitted light image) exposure showed the presence of the vesicle containing toxin with four differentiated granular glands arranged in a circular form adjacent to the apex of the vesicle (narrow passage) filled with secretion as described above (Figure 4.6A). The presence of collagen around the parotoid glands and mucous glands lying under epidermis were also identified. The differentiated granular glands (dg) contain thick epithelial cells and secretion that was also highly reactive to PAS (Figure 4.6B).

Staining with FdA exhibited fluorescence of the secretion contained within the differentiated granular glands (Figure 4.6B). The surrounding layer filled with collagen around parotoid

186

microglands exhibited fluorescence, probably due to the leakage from the differentiated glands while preparing the tissue sections, or due to BtH non-specific fluorescence. Since the differentiated glands containing BtH is present in a close vicinity to the parotoid microgland and the toxin exit duct (attached to the pore), it is ideally positioned for the co-secretion with parotoid toxin. Auto-fluorescence of the tissues was also investigated, to confirm that the fluorescence exhibited by the secretion within the differentiated glands is not an artifact (due to non-specific fluorescence by FdA) or associated with some tissues (such as collagen, extracellular matrix, etc.) which can exhibit auto-fluorescence without addition of any fluorescent stain.[8] An auto-fluoresence image (without addition of FdA) clearly indicated fluorescence exhibited by the *in situ* secretion is not an artifact, even though the secretory epithelial cells (Figure 4.6C) within the differentiated glands exhibited some auto-fluorescence.
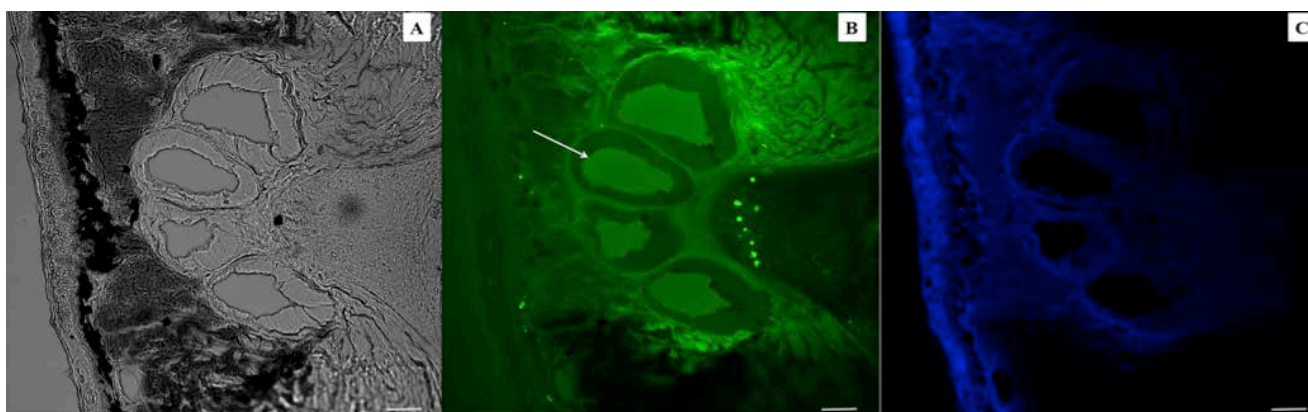
Figure 4.6 Confocal image of differentiated granular glands in the parotoid gland containing granulated cells and *in situ* secretion. A – transmission exposure, B – staining with fluorescein diacetate (arrow indicates the localized fluorescence), C – auto fluorescence. Bars – 900 μm

4.2.3 MALDI imaging on parotoid glands

Spatial localization of bufotoxins within the parotoid microglands was identified by imaging mass spectrometry, using a MALDI mass spectrometer fitted with a light microscope. Parotoid glands from two toads were excised and immediately snap frozen with liquid nitrogen followed by treatment with formalin and fixation using microwave to deactivate any enzymatic activity. Enzymatic activity was disrupted to inhibit the conversion of bufotoxins to bufagenins during the handling of the parotoid glands. Sections of parotoid gland were cut using a microtome, mounted on a MALDI-plate (CHCA matrix) and subjected to simultaneous imaging using mass spectrometry and a light microscope (imaging mass spectrometry). Overlapping the ionization pattern with the image obtained showed the spatial distribution of bufadienolides in the parotoid microglands (Figure 4.7).

The major ion detected in the total positive ion current corresponded to marinobufotoxin (**1c**) (713.2 Da, [M+H]$^+$) (Figure 4.7B), which correlated with our previous studies on the chemical profiling of the parotoid toxin. Marinobufotoxin was identified as the most abundant bufadienolide within the parotoid microgland. The second most abundant ion (699.2 Da, [M+H]$^+$) (Figure 4.7C) correlated to bufalitoxin (**3c**), and was also identified to be present around the same regions as marinobufotoxin, indicating the storage of bufotoxins is evenly distributed within the parotoid microglands. Interestingly, the observation is also in agreement with our earlier findings where marinobufotoxin (**1c**) was identified as the most abundant bufotoxin followed by bufalitoxin (**3c**) (Chapter 3).
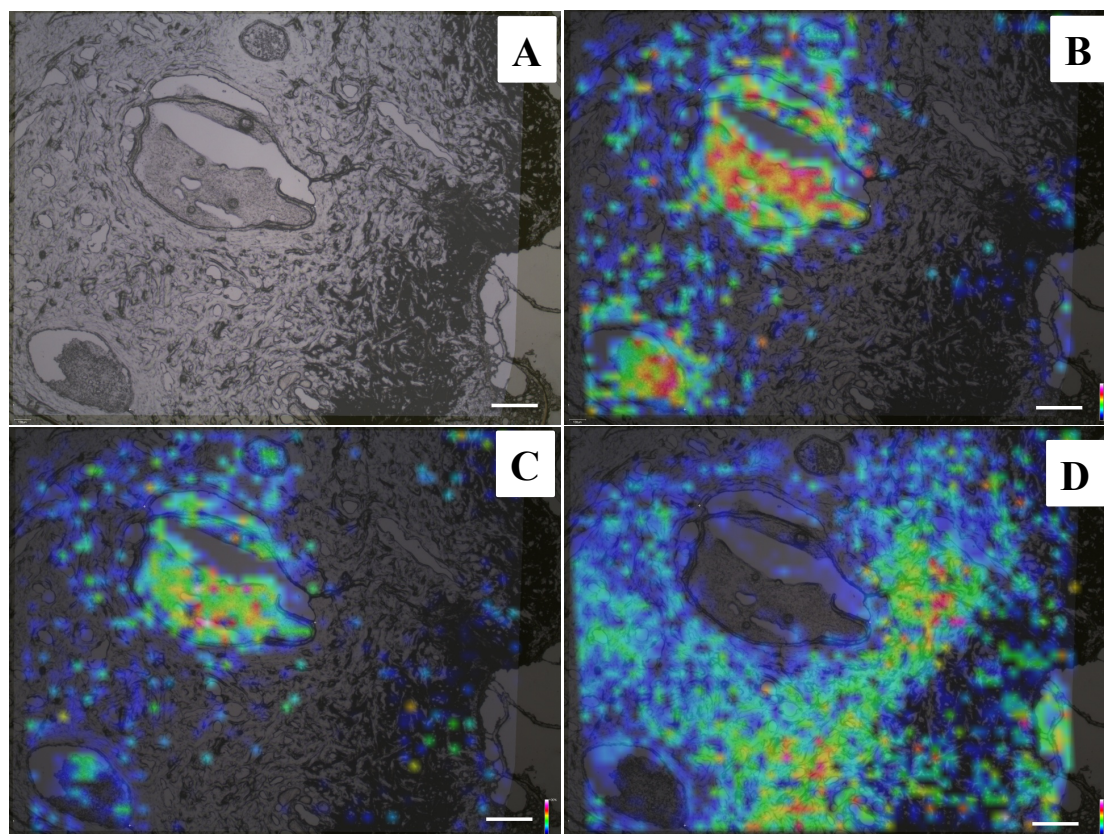
Figure 4.7 Imaging mass spectrometry of parotoid glands with *in situ* parotoid toxin rich in bufotoxins. A – light microscopy image, B – spatial distribution of marinobufotoxin (**1c**) C – spatial distribution of bufalitoxin (**3c**), D – spatial distribution of marinobufagenin (**1a**). Bars – 100 μm

By contrast, the search for the mass of marinobufagenin (**1a**) (401.2 Da, [M+H]), the dominant bufagenin in the secretion, showed a spatial distribution outside of the parotoid microgland just above the toxin exit duct (Figure 4.8). This observation was consistent with BtH mediated hydrolysis of residual bufotoxin during the handling of the parotoid gland while preparing sections using microtome.

Imaging mass spectrometry showed different spatial distribution of bufotoxins and bufagenin within the parotoid gland, supporting our earlier findings on the storage and delivery of the parotoid toxin. This observation along with confocal imaging (Figure 4.6) suggests that BtH is localized in individual glands, physically separated from the parotoid microglands.

4.2.4 Isolation of BtH from *B. marinus* parotoid secretions

B. marinus

↓ (a)

Parotoid Secretion C (see Chapter 3)

↓ (b)

A55

(c)   (d)

A56   A57

(e) ↓

A58
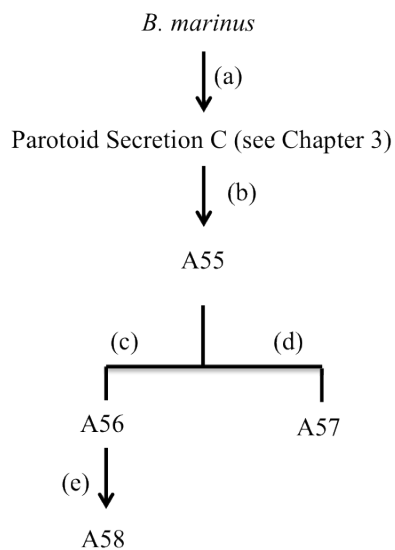
(a) – manual squeezing of parotoid secretions from adult cane toads into phosphate buffer (pH 7.4)
(b) – homogenization by syringe followed by ultrasonication for 10 min
(c) – centrifugation followed by collection of supernatant
(d) – centrifugation followed by pellet re-suspension in phosphate buffer (pH 7.4)
(e) – dialysed using Amicon filter (10 kDa)

Note : Throughout the purification process the protein mixture was maintained at 4 °C and no aggregation was encountered. The proteins were also stable in phosphate buffer at pH 7.4, hence, the same conditions were maintained for the storage

Scheme 4.2 Preparation of analytes A55 – A58

Parotoid secretions from each parotoid gland of two cane toads were squeezed into phosphate buffer saline (PBS). The parotoid secretion C (see Chapter 3) was subjected to homogenization (syringe) followed by ultrasonication to rupture any vesicles and generate analyte A55. A55 was centrifuged to remove tissue and cell debris, and the supernatants were separated as A56, while the cellular pellet was re-suspended in PBS to generate A57. A solution of FdA (50 μg/mL; 1% DMSO) in H_2O was prepared as a reagent to detect and purify BtH.

Proposed BtH mediated fluorescence was detected in the supernatants (A56), whereas pellet suspensions (A57) exhibited very little fluorescence. A56 was subjected to ultrasonication (5 min) after which it was concentrated using Amicon filters (10 kDa cut off) to remove molecules <10 kDa (eg. bufadienolides and biogenic amines) to generate analyte A58. Fluorescence generated by FdA hydrolysis was mediated by a potential hydrolase that was present in fractions A56 and A58 (Scheme 4.2). An SDS PAGE fractionation of all the analytes A55 – A58 was performed on a 12.5% SDS (sodium dodecyl sulfate) gel using Tris buffer at pH 7.4 (Figure 4.8) to separate the proteins based on charge and molecular masses. Samples were applied with a loading dye to help track the protein mixture. A molecular mass standard was also included to compare the molecular mass of proteins in the analytes. This analysis revealed bands at 10 kDa, 25 kDa, 50 kDa, 100 kDa and 150 kDa as prominent in all analytes. The concentrated fraction (A58) which exhibited

hydrolytic activity (<5 min) contained three prominent bands correlating to molecular masses of 25 kDa, 50 kDa and 100 kDa.
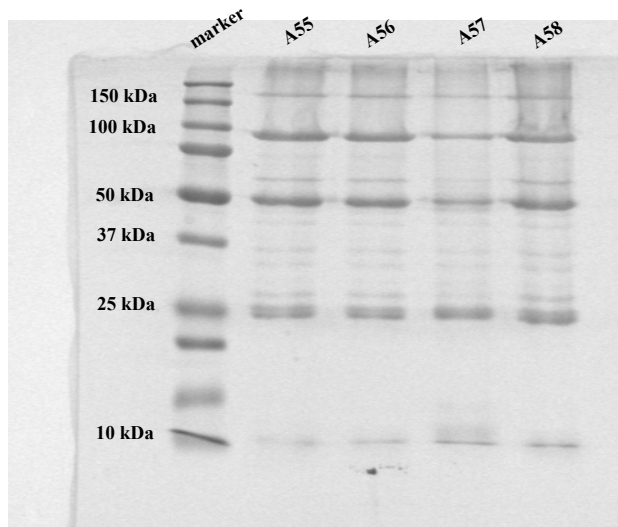
Figure 4.8 SDS PAGE analysis of analytes A55 – A58 in Tris buffer

A58 was then subjected to size exclusion chromatography to separate the proteins based on their size (or molecular mass), using a Superdex S-200 column containing 150 mM NaCl, 20 mM Na$_2$HPO$_4$ at pH 7.4. The fractions collected from gel filtration chromatography of A58 generated analytes A59 – A64 (Scheme 4.3). The analytes were subjected to SDS-PAGE as well as FdA monitoring to identify the active fraction containing BtH. The active fraction was further purified by gel filtration chromatography (Scheme 4.3).
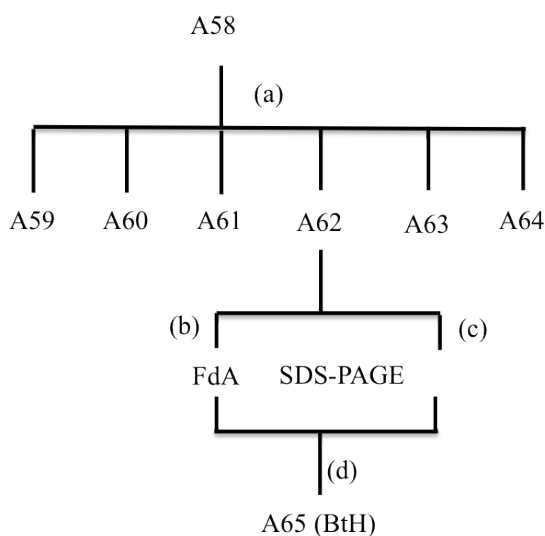
(a) – Sephadex S200 column (pH 7.4), six peaks (fractions) were observed based on the UV profile at 280 nm for 60 min and were collected individually
(b) – hydrolytic activity of each fraction was detected using FdA
(c) – fractions were then dialysed using Amicon filter (10 kDa)
(d) – gel filtration of the protein exhibiting highest hydrolytic activity using Sephadex S200 column

Scheme 4.3 Preparation of analytes A59 – A65 and their biochemical analysis
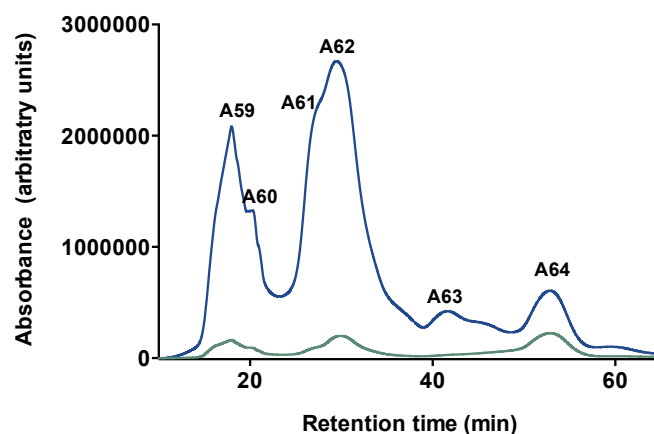
Figure 4.9 Chromatogram showing the absorbance of various proteins present in the parotoid secretions using gel filtration chromatography, S-200 column. A59 – A64 denotes the fractions that were collected. Blue – absorbance at 210 nm, green – absorbance at 280 nm

Six fractions were collected during the gel-filtration based purification (Figure 4.9) and all of them were investigated for the hydrolase activity using FdA. The fluorescence was detected using a UV transilluminator at an excitation wavelength of 254 nm. BtH mediated hydrolase activity was localized in A62 (Figure 4.10). A62 was concentrated using an Amicon filter (10 kDa cut off) to remove any residual small molecules (including bufadienolides and biogenic amines) and was subjected to SDS PAGE analysis to reveal a mixture of three proteins (Figure 4.11). Although, A61 and A62 eluted close to each other on gel filtration chromatography (Figure 4.9), A61 did not show any hydrolytic activity when treated with FdA. Furthermore, SDS-PAGE analysis revealed the presence of a 100 kDa band in A62, not seen in A61. From this data we hypothesize that the 100 kDa band observed in A62 is BtH.
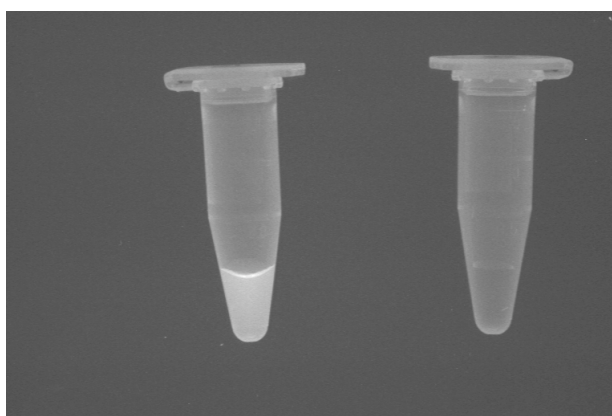
Figure 4.10 Fluorescence exhibited by A62 (left) and A61 (right) measured using FdA as the substrate after incubation for 10 min at 37 °C.
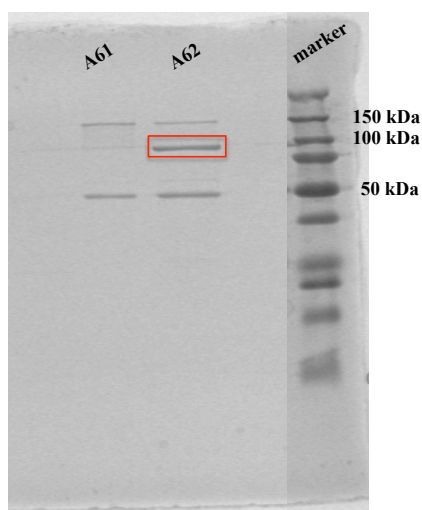
Figure 4.11 SDS PAGE analysis of A61 and A62 collected using gel filtration in Tris buffer. 100 kDa (possibly BtH) band is highlighted in red

Further purification of A62 using size exclusion chromatography (S-200 column) fitted to an FPLC-DAD gave two peaks identified as A62a and A62b. Both peaks were collected and reacted with FdA to reveal that only A62b exhibited BtH activity (Figure 4.12).
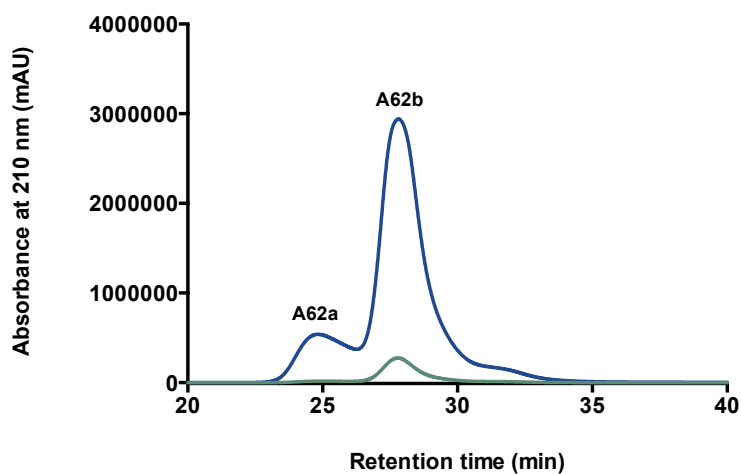
Figure 4.12 Purification of the active protein (A62b) using gel filtration chromatography, S200 column. Blue – 210 nm, green – 280 nm
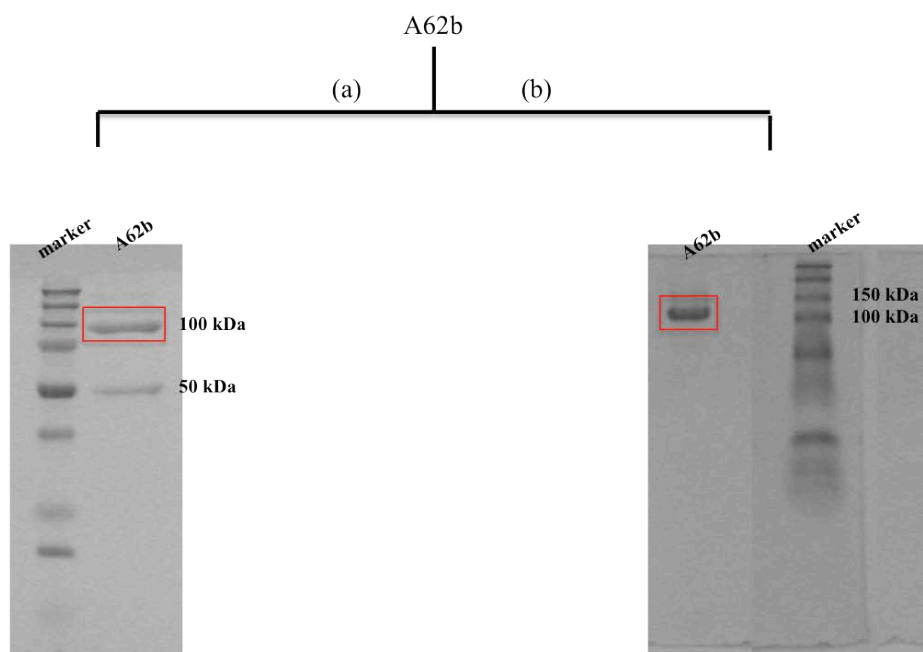
(a) – SDS PAGE analysis following reduction of active protein mixture
(b) – Native PAGE analysis without reduction of active protein mixture

Scheme 4.4 Analyses of A62b. 100 kDa band is highlighted in red

A62b was subjected to SDS-PAGE (reducing) as well as Native-PAGE (non-reducing) analyses to confirm purity (Scheme 4.4). To achieve these analyses, A62b was concentrated using Amicon filter (10 kDa cut off) and subjected to SDS – PAGE to reveal two protein bands, corresponding to molecular masses 100 kDa and 50 kDa respectively, with the former being more prominent (higher concentration) (Figure 4.14). As SDS PAGE analysis involves denaturation/reduction of protein prior to analysis this can generate protein bands corresponding to monomeric units of an oligomeric protein, leading to the possibility that the 50 kDa was a monomer of a 100 kDa dimer.

To explore this hypothesis, a Native-PAGE (non-reducing) analysis was performed on A62b without prior denaturation. Native PAGE analysis clearly showed the presence of only one protein with a molecular mass of 100 kDa (Figure 4.15), suggesting that a protein with mass 100 kDa is BtH.

4.2.5 Hypotheses

Based on the findings shown above we present two working hypotheses:
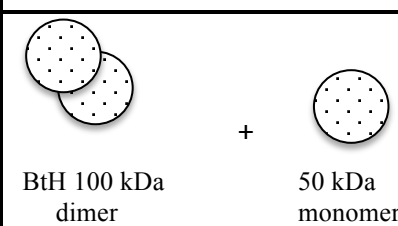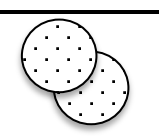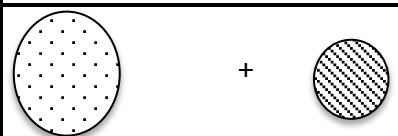
Hypothesis	SDS-PAGE	Native-PAGE
1	BtH 100 kDa dimer + 50 kDa monomer	BtH 100 kDa dimer
2	BtH 100 kDa + 50 kDa	BtH 100 kDa + 100 kDa dimer

Figure 4.13 Summary of hypotheses 1 and 2

4.2.5.1 Hypothesis 1

A62b consists of a single protein that can exist in both monomeric (50 kDa) and dimeric (100 kDa) forms. Both species are observed under SDS PAGE analysis, but only the dimeric species is evident under Native PAGE analysis. The dimeric species exhibits hydrolytic activity and can be characterized as BtH (Figure 4.13).

4.2.5.2 Hypothesis 2

A62b consists of two proteins of molecular weight 100 kDa and 50 kDa. Under SDS-PAGE analysis both species can be characterized and the hydrolytic activity associated with BtH is uniquely attributed to the 100 kDa protein. Under Native PAGE analysis the 50 kDa protein exists exclusively as a dimeric species, which co-elutes with (but is not associated with) BtH (Figure 4.13).

While we have demonstrated that BtH co-expresses with parotoid secretion and facilitates the hydrolysis of bufotoxins to bufagenins, it is interesting to speculate on the possible biosynthetic versatility of this protein. It is well established that enzymatic reactions can be reversible, suggesting that BtH may also have a role in the biosynthetic conversion of bufagenins to bufotoxins (ie. as an esterase) (Figure 4.14). Irrespective of its dual potential (hydrolase/esterase), following manual compression and secretion of toxin, there should be an upregulation of the biosynthesis of

194

both the toxic bufadienolides and BtH. To explore this possibility we turned our attention to a transcriptomic analysis.
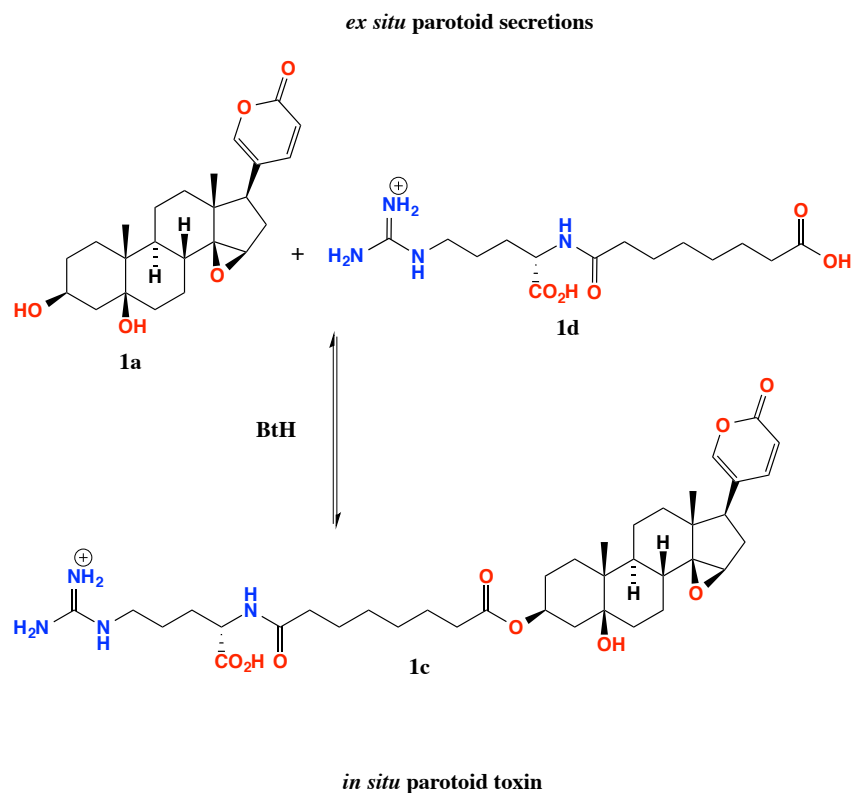
Figure 4.14 Plausible role of BtH in hydrolysis and esterification

4.2.6 Identification of BtH – a proteomic/transcriptomic approach

4.2.6.1 Transcriptomics of parotoid gland
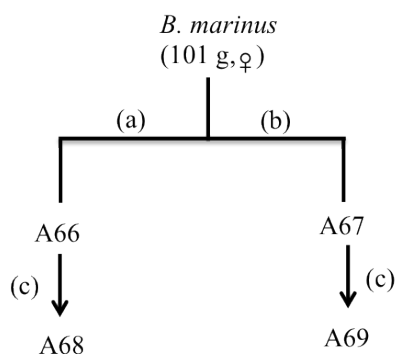
(a) – left parotoid gland was squeezed, left for 72 h and excised
(b) – right parotoid gland squeezed and immediately excised
(c) – total RNA was extracted and enriched for mRNA using Dynabeads®

Scheme 4.5 Preparation of analytes A66 – A69

The left parotoid gland of a female cane toad was subjected to manual compression leading to secretion of toxin. This toad was allowed to respond to this insult for 72 h, after which the left parotoid gland was excised and processed to generate analyte A66 (Scheme 4.5). As a negative control, the right parotoid gland from the same toad was then squeezed and excised immediately to generate analyte A67 (Scheme 4.5). RNA from both parotoid glands was isolated using a modified protocol from the supplier (Qiagen) followed by mRNA enrichment using immobilized oligo(dT) beads to generate analytes A68 and A69 from the left and right parotoid glands, respectively. The compressed parotoid gland (A68) would mimic a "stimulated" gland with the biosynthesis of bufotoxins and BtH "up-regulated", whereas the uncompressed parotoid gland (A69) would correspond to an "unstimulated" gland with biosynthesis of bufotoxins and BtH unaffected. Enriched mRNA were isolated from A68 (19.7 ng/mL) and A69 (16.7 ng/mL) and cDNA libraries constructed and subjected to Ion torrent PGM (Life Tech) sequencing. Ion torrent sequencing is one of a high throughput sequencing technology where a complementary dNTP (deoxyribonucleotide triphosphate) is added to the growing template DNA strand resulting in a release of hydrogen ions and pyrophosphate (as by products). Release of H^+ interacts with the in-built ion-sensitive sensors (eg. ISFET) resulting in an electronic signal, which is then processed by the in-built software to determine the nucleotide sequence of the entire library. The transcriptome is a dynamic phenomenon and changes over time. Ion torrent sequencing provides an RNA-seq that indicates the status of the transcriptome under study at a given instant. An illustration of the processes as applied to cane toad parotoid glands is shown in Scheme 4.6.
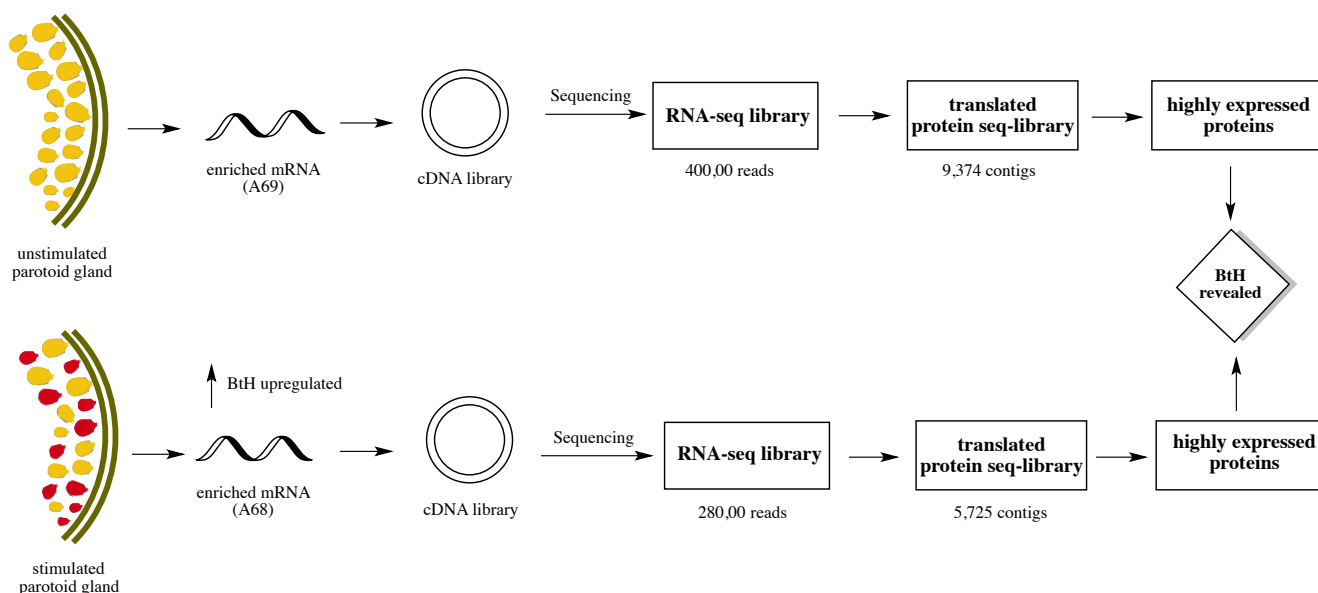
Scheme 4.6 Identification of protein sequences exhibiting high expression profiles from parotoid gland transcriptome

The transcriptome from A68 exhibited > 280,000 high quality reads, while A69 exhibited >400,000 high quality reads. The average base pair reading for each sample was ~150 bp with some reads

196

extending to 500 bp. The transcriptome assembly for A68 and A69 exhibited 2.3Mbp and 3.8Mbp consensus length, respectively. Gene ontology and annotations were performed for 5,725 contigs from A68 and 9,374 contigs from A69 which were assembled using CLC Genomics workbench using standard Ion Torrent assembly parameters. A large set of >1,000 enzymes were identified from both transcriptomes, with most involved in common processes such as cell division, transport, protein synthesis, etc. A significant differential gene expression pattern for specific enzymes involved in the biochemical pathways was observed between both A68 and A69, however, due to the vast set of data and limited amount of time, the relationship between the entire parotoid gland transcriptome and biochemical pathways is not elaborated in this thesis, which instead focuses on the sequence identification of the protein of interest, BtH.

The relative gene expression level was obtained by comparison of the number of reads and consensus lengths for each contigs from RNA-seq libraries obtained from A68 and A69. A69 exhibited high levels of expression of specific contigs (proteins) that we hypothesized may coincide with BtH. Tables 4.3 and 4.4 illustrate the contigs that exhibited high levels of expression in A68 and A69, respectively. The Contig that showed highest expression levels from A68 (contig 22) was also observed at higher expression levels in A69 (contig 37), and was attributed to a protein with a molecular mass of 100 kDa consistent with that attributed to BtH (Figure 4.15). Of note, A69 revealed another protein of high abundance (contig 61) with the molecular mass of 50 kDa (Figure 4.17). Both these high abundance gene sequences were translated to their protein sequence using ProteinPilot® and are illustrated in Figure 4.16 (100 kDa) and Figure 4.18 (50 kDa).

Table 4.3 Proteins that exhibited high expression levels in A68 (>2000 reads)

Sequence	Number of reads	Consensus length	Function
contig 84	7517	1899	type 2 cytoskeletal 75-like
contig 14	3932	2180	type 1 cytoskeletal 17
contig 22	2883	2885	Pfam 115-like
contig 15	5399	1485	heat shock cognate 71kDa
contig 111	2085	2755	nicotinamide n-methyltransferase

(protein with unknown function highlighted in red)

Table 4.4 Proteins that exhibited high expression levels in A69 (>2000 reads)

Sequence	Number of reads	Consensus length	Function
contig 79	6837	3185	nicotinamide n-methyltransferase
contig 61	5042	1768	galactoside-9
contig 157	4144	1754	Eukaryotic translation elongation factor 1 α1
contig 131	3683	1184	type 2 cytoskeletal 75-like
contig 54	3493	1553	heat shock cognate 71kDa
contig 46	3452	1809	type 1 cytoskeletal 17
contig 37*	3406	883	Pfam 115-like

(protein with unknown function highlighted in red, * represents various isoforms of the protein with different expression levels)

```
CCAACTTGGCTCCTTTTCTTTGAGGATCCTCTCCTCCTGTCCTAAGCTGTGGTACATGATCGCTAATACAATATCATAATTGCCTTACA
TTGTATTGAAGTTTTGGGACAGTTATCAAGAAATCATGTTGACTAATGAAGATTACGCCTCACTTACCAAAGGCATCCAGAATCTGAAT
TTCACAGGAGACAGTATCCCTTGTAGGCTTCTTCTTACTGGTGACACAGCATTCCCAGTACTGGAGACTCCTGCAAACAATGTTCTCAT
TGCTGCATCCAGATACGGCAAGGGACGCTTGGTTGTCATGAGCCATGAATCATATTTGAATGATCCACAATTTATGGATTTTCTGCAGA
ATGCAATATCCTGGTTGAAACCATCCTCAGAAGCAGTAATTGGCATTGAAAACAGCCTAGGTCTTTTGGCAGACACTCTGTCTAACTCT
GGACATAGAATTGACACGACCTCTGGCTTTAAGGAAGATTTGGGAGTGTTCTGCATGACACAATATAATGAAAGCCAGTTATCAGAAGT
TGTGTTATTTTTGAAGGAAGGTGGTGGTCTCCTTATTGGAGCTGAAGCCTGCCATTGGTCTGAAAGCCACCCAGAATTAAATGTTTTCT
TTGATTTTCCTGGAAACAAAATAACATCTGTAGCTGGTGTCTATTTCACTAATAAGACTGGAGAAAATGGGATTTTCCCAGCGAGTGAG
AAACCACCACCATTTCCATCTTTTAATGATGTGGACTTCTCCATGGACCTAAAACAGATCTTCAATGGGCTATCCAGTCTGGATGTTAG
TGGGGATGCTGGTGCATCTGAACTCCTACTACACGGACCTTTGACTTTTCCACTTGGACTGACTAACAGCAACCAATGTTTTTTTGGTG
CTGCATACTATGGCCGAGGACGTGTTGTAGTGGGGCCACATGAAGGCTACATTACAAGACTACAGCTGAAGTCTTTTATCCTGAATGCC
ATTTCGTGGCTGGATGCGGGAAGAAATGGGATGATTGGTGTTCAAAATGCAATGCGAGGCCTGATTCCCATACTGCAGGCTGAGGGTAT
CTCTTGTGCGACGTCCAATGTGAGTTCTGAATTCAGCATTTATTGTTGCAATTCTTATAGTGATGCTGAAGTAGACAAAATCCATCAGT
TTGTTGCAGAAGGAGGAAGTCTTCTCATTGCTGGCCATGCCTGGTACTGGTCTTACTCCCATTCAGATGTTCCTTCTCAGTATCCAGGA
AACAAAATCCTCAATAGATTTGGGATAACCATTCTGGAAAGCACCATAAACAATGGCATTTACAAAGTTCCTGAGTCAACTACTAATTC
ATATCATTTTCTCAGATCAATCTGTCAGTTTCTGAGAGACTTGAAAAATGGAGTGGAGATTAAACCCCCTCTAAGCTCCTGGTTATCAA
AGCTCAGACAAGATGTCGCGACCTATCTGAAGTTGCCTGCCACACCTCTTAGGGTGTCCCTATGGCAAGAACTTTTAAATCTGGTACAA
AATTGTAATTTACCAGAAGTGAGCAAAGAGCATCCAGTGAAAAGCCAATCCAAAGAGGCTTTTCTAATCTGTTTGGCTCAAGAAGTCGA
CTGCTTTTATGACTCATTTCAAGAGGACGCAGGAGAGCTTGATATTCAAGGAGAACCCATACATGTAGATATTGATGGCACAAATCCTG
GTGGTGATGCATGGAGAAGTACAGGGCTATACTTGCCTCCTAACAAAAAAGGAAAACTGGTATTTCCATCCTCAGCTGTGGGAAATGGT
CTCCAGGTACAAATTGGTTGTCAGTCCGATAACCTGAGCGGAGCATCAGAGTATTGTCGTGCTCCAGTGGTTGTACATAGAAAGAATGT
TGTTCGCGAGGAGGTTGTGATATCCTGTATCTGGGGAGGACTTCTTTATGTTATTGTAAAGGGGAAGAGTGAACTGGGAAATATTCCAG
TTACAATTTATGGGGCAGAACCAGCTCCAACATTTATAAATGGACAAACTAATGTTTCTTCGTGGTTGGATACATTACGCACCTCAACA
TCTCCTTGGGCTGAGCTTATTACAGAGGATATTATCCTGACTGTCCCTACTGATAAAGTCCGCTCACTAGAGGATCCTGAATCACTTAT
GTGTTTATGGGACAACATCATGTCTACAATAGCTGATCTGGCAGCTATCCCAAAGAAAATGCCTCGTCCAGAAAGAATTGTGGCCGATG
TTCAGATCTCAGCAGGTTTTATGCATGCTGGATACCCAATAATGTGCCATGTGCCAACATCAACTTCTTTAGTAACTGTTACATCATTG
AAGAGTGGCATGTGGGGGGGCTGCACATGAGCTTGGCCACAACCAGCAGAGAGGAGTTTGGGAATTCCCTCCTCACACCACAGAAGCCAC
CTGTAATCTGTGGTCAGTATATGTGCATGAAATCTTGCTGGGGATCCCAAGGGATAAAGCTCATCCTGCTCTCAAGCCGGGAGACAGAG
AACAAAGAACCAAGCAGTATGTGAAGAATGGAGCCAAACTTGATGAGTGGAACGTGTGGACAGCGCTTGAGACTTATCTTCAGCTACAA
GAGGGCTTTGGTTGGGATCCCTTCAAGCGGGTTTTCTCAGAGTATCAAACCATGTCCAACGTCAGTAATAACAAGAATGTTAAGATGAA
TCTTTGGGCAGAGAAGTTCTCTCAAGCAGTTGATAAGAACCTGGCTCCATTCTTTCAGGCCTGGGGATGGCCCATTGATGATGCTACCA
GCAACAAATTATCCACATTAAGTGAATGGGAAGAGAATCCAATGAAGAAATATGTCAGCTAAATTTCATTAAAGAAATATATAAAATGA
TCCTTCTATATTAATAAGCTTTCAGTGGCTTAAGAGG
```

Figure 4.15 Calculated nucleotide sequence of 100 kDa protein with high expression in A68 (contig 22) and A69 (contig 37)

```
MLTNEDYASLTKGIQNLNFTGDSIPCRLLLTGDTAFPVLETPANNVLIAASRYGKGRLVVMSHESYLNDPQFMDFLQNAISWLKPSSEA
VIGIENSLGLLADTLSNSGHRIDTTSGFKEDLGVFCMTQYNESQLSEVVLFLKEGGGLLIGAEACHWSESHPELNVFFDFPGNKITSVA
GVYFTNKTGENGIFPASEKPPPFPSFNDVDFSMDLKQIFNGLSSLDVSGDAGASELLLHGPLTFPLGLTNSNQCFFGAAYYGRGRVVVG
PHEGYITRLQLKSFILNAISWLDAGRNGMIGVQNAMRGLIPILQAEGISCATSNVSSEFSIYCCNSYSDAEVDKIHQFVAEGGSLLIAG
HAWYWSYSHSDVPSQYPGNKILNRFGITILESTINNGIYKVPESTTNSYHFLRSICQFLRDLKNGVEIKPPLSSWLSKLRQDVATYLKL
PATPLRVSLWQELLNLVQNCNLPEVSKEHPVKSQSKEAFLICLAQEVDCFYDSFQEDAGELDIQGEPIHVDIDGTNPGGDAWRSTGLYL
PPNKKGKLVFPSSAVGNGLQVQIGCQSDNLSGASEYCRAPVVVHRKNVVREEVVISCIWGGLLYVIVKGKSELGNIPVTIYGAEPAPTF
INGQTNVSSWLDTLRTSTSPWAELITEDIILTVPTDKVRSLEDPESLMCLWDNIMSTIADLAAIPKKMPRPERIVADVQISAGFMHAGY
PIMCHVPTSTSLVTVTSLKSGMWGAAHELGHNQQRGVWEFPPHTTEATCNLWSVYVHEILLGIPRDKAHPALKPGDREQRTKQYVKNGA
KLDEWNVWTALETYLQLQEGFGWDPFKRVFSEYQTMSNVSNNKNVKMNLWAEKFSQAVDKNLAPFFQAWGWPIDDATSNKLSTLSEWEE
NPMKKYVS
```

Figure 4.16 Translated protein sequence of 100 kDa protein with high expression in A68 (contig 22) and A69 (contig 37)

```
CTTCCTTCGGAGCCTGCAGTGAACGATCTGTAGCGCCCCTGTGGCAGTAGATGGGCTGACTTGTTGGGACTCAATGCTCCTTTATTTTA
AGAAACTCTGAAGTTATCTGTCAGCTTTACCAGTCAAAATGTGTGACGAAATCATCAAGAATCCCCCTGTTCCATACGTCACCCATTTT
CACAGTGGCATCAAGAATGGCAGCGTGTTTGTTATAAGCGGCACCGTCCTTCCCTCGGCCGAAGGGTTTATGGTCGATTTCCAGTGTGG
TACTCTTGGAAATGCTGACATTGCCTTCAATTTCAATCCACGTTTTAATGAAGGACATGTTCTTCTTAACACACGGCAGAACAATGTAT
GGAGCCCAGATGAAAATAGGTACAAGGTGCCATTTGCTAAGGAACAACCTTTTGAAATCCAGGTCCTAGTTACAGACCAAGAATATAAA
GTTTTTGTTAATAAAATATTCTTTTTGGATTATCCTCACAAAATTCCTCTGGCCAAAGTCTGTGCTTTTGGGGTAAAGGGCGATGTGAC
TCTAAGTTGTGTGGAGATCCAACCACAAATGATTGGATTCCATCATCAATATTTTCCAGAAGGACAACAGGAAAACACTCTTCCATTTG
GCACCCAGTTTCCTAGTGAAATCAAAGTTGGCACAGTGTTTATTATCAATGGCACTATCCCTCCATTACCTGACAGGTCTTACATCAAT
TTCATGTGTGGTAGTGACATAGATGATGATATTGCTTTCCATTTCAATCCTCGTTTTGATGAAGAAAAAATCATCTGCAACGCAAAGAG
AAATGGCTTTTATGACGTCAATGAAGAGAGGTCGCCACTGCGACTTAAAAAAGACCAAGCTTTTGAATTCCGGTTCCTAGTTGAAGACC
ATGCATATCAAGTTTCTTTGAATGGAGATGAACTTTTTTATTTTAGTCACAGACTTTCTCCAGACACAGTCAAGAATTTAGTAATAATG
GGCTGTGCTCTTCTGAAAAGCGTTGAGATACAAGCAGAAGCATCTGGATTCCATCATCTTTATTTTCAAGATGAACACATCTCAAAGTC
TGTTCCACTCGTGACCCCGTTTGTGGTTGGCATCAAAGAGGACACCGTGGTTAGGATTCGTGGCACTGTCCTACCAGCGACTAAAAGCT
TCTCCATAGATATCCAATGTGGTGATAAGGACACTGATGACATCGCCTTCCATCTCAATATATTTACTGGTAAAGGACATGTTTCCTGC
AATACAATGGAAAATGAAATCTGGGGGAATGAAGAACTCAAAGAAGAGATGCCATTCAAAAGGGGACAACCTTTTGAAGTCCGGATCCT
ATTCACAAGCCAAGAATACAAAGTTTCTGTGGATAGAAATCGATTTTTGGAATACGGTCACAGAATTCCTATGGAGCGGGTCAACACTT
TGGCAGTACATGGCCGTATTACTGTAAATACTGTGGAGATCAAATCACAAGGGGGTGAATTCCCTTAAAACCTCTCAAAACTGCTGACA
GCTCTGCATAGGTGACGGGAGAGCAGTGTAATCATACCTGGACTGATGGTCATCCATCTTTTATTACCCCTCCCACCGTGATTGCAAGT
GTCCTGGAGGTGGTCCCTTTCTGTTCAGTGCCCTGGCTTCTCTCTACTGAACCGTTCCTTCCTCTGCTCTGAATGGCGGCTCTAGCG
TTTTCCTAACTAGCCACTAAAGCTCCATTATGCTGTGCTGATGCAAGAAAATAAATTTAAAAAAAAAATAAAAATAA
```

Figure 4.17 Calculated nucleotide sequence of 50 kDa protein with high expression in A69 (contig 61)

```
MCDEIIKNPPVPYVTHFHSGIKNGSVFVISGTVLPSAEGFMVDFQCGTLGNADIAFNFNPRFNEGHVLLNTRQNNVWSPDENRYKVPFA
KEQPFEIQVLVTDQEYKVFVNKTFFLDYPHKIPLAKVCAFGVKGDVTLSCVEIQPQMIGFHHQYFPEGQQENTLPFGTQFPSEIKVGTV
FIINGTIPPLPDRSYINFMCGSDIDDDIAFHFNPRFDEEKIICNAKRNGFYDVNEERSPLRLKKDQAFEFRFLVEDHAYQVSLNGDELF
YFSHRLSPDTVKNLVIMGCALLKSVEIQAEASGFHHLYFQDEHISKSVPLVTPFVVGIKEDTVVRIRGTVLPATKSFSIDIQCGDKDTD
DIAFHLNIFTGKGHVSCNTMENEIWGNEELKEEMPFKRGQPFEVRILFTSQEYKVSVDRNRFLEYGHRIPMERVNTLAVHGRITVNTVE
IKSQGGEFP
```

Figure 4.18 Translated protein sequence of 50 kDa protein with high expression in A69 (contig 61)

The A68 (contig 22) and A69 (contig 37) were attributed to a protein comprising 897 amino acids and a molecular mass of 99 kDa, belonging to an uncharacterized member of the FAM-115 superfamily of proteins (Figure 4.15). An NCBI blast search of the protein yielded a highest homology (88%) hit corresponding to an uncharacterized protein reported from *Bufo Bufo gargarizans* (Asiatic toad) (Figure 4.19).[9] A comparison of this protein sequence was performed against peptides identified from the shotgun sequencing of BtH (see below), supporting its assignment as BtH.
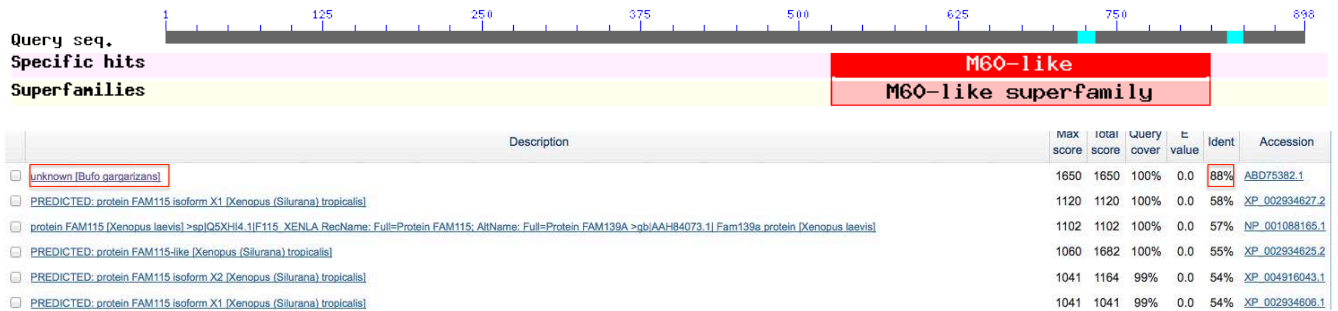
Figure 4.19 An NCBI-blast of the highest expressed protein from the stimulated parotoid gland showing similarity to *Bufo* species (as marked in red)

The A69 (contig 61) was attributed to a common protein comprising 454 amino acids and a molecular mass of 50 kDa, belonging to lectin superfamily of proteins (Figure 4.15). An NCBI blast search of the protein yielded homology hit corresponding to galectin like protein reported from *Xenopus laevis* (African clawed frogs) (Figure 4.20).[10] A comparison of this protein sequence was performed against peptides identified from the shotgun sequencing of 50 kDa protein (see below), supporting its assignment as lectin.
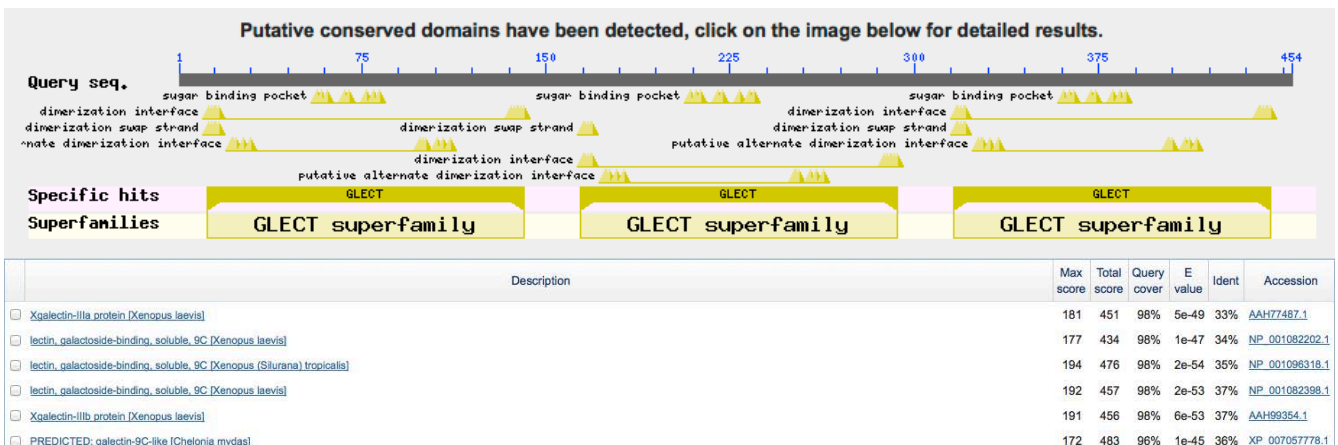
Figure 4.20 An NCBI-blast of the highest expressed protein from the stimulated parotoid gland showing similarity to galectin like protein from *Xenopus laevis*

The expression profiles of A69 with two most abundant protein, 100 kDa (BtH) and 50 kDa (lectin) correlated with the protein profile of parotoid secretions, A62b (Scheme 4.4). That said, the upregulation of BtH post manual compression of the parotoid glands also indicates the plausible role played by BtH in the biosynthesis of bufotoxins from bufagenins and arginyl amides.

4.2.6.2 Tandem mass spectrometry sequencing of BtH

BtH enriched material (A62b) was fractionated and subjected to shotgun proteomics using mass spectrometry. A62b was subjected to SDS PAGE fractionation to resolve two proteins of molecular mass 100 kDa and 50 kDa. Both bands were manually cut from the gel and individual gel spots from two bands were washed with ultrapure water and destained (40 mM NH_4CO_3/50% MeCN) and dehydrated (100% MeCN). Gel spots were rehydrated in 10 μL of 20 μg/mL proteomics grade trypsin (Sigma-Aldrich) and incubated overnight at 37°C. Digests were eluted by washing the gel spots for 20 min with each of the following solutions: 20 μL 1% formic acid, followed by 20 μL of 5% MeCN/0.5% formic acid. Both extracted proteins, 0.75 μg each was processed by LC/MS/MS analysis to generate two sets of peptides. MS2 spectra were acquired at a rate of 20 scans/s, with a cycle time of 2.3 s, and optimized for high resolution. Precursor ions with m/z between 300 – 1,800 m/z, a charge of +2 to +5, and an intensity of at least 120 counts/s were selected, with a unit mass precursor ion inclusion window of ± 0.7 Da, and excluding isotopes within 2 Da for MS2 spectra. MS2 spectra were searched against contigs translated to all six reading frames from both assembled transcriptomes (A68 and A69) using Proteinpilot v4.5 (AB Sciex) (Scheme 4.7) which uses a sequence template to match experimental MS2 spectra to the theoretical MS2 spectra it has generated from the template provided.
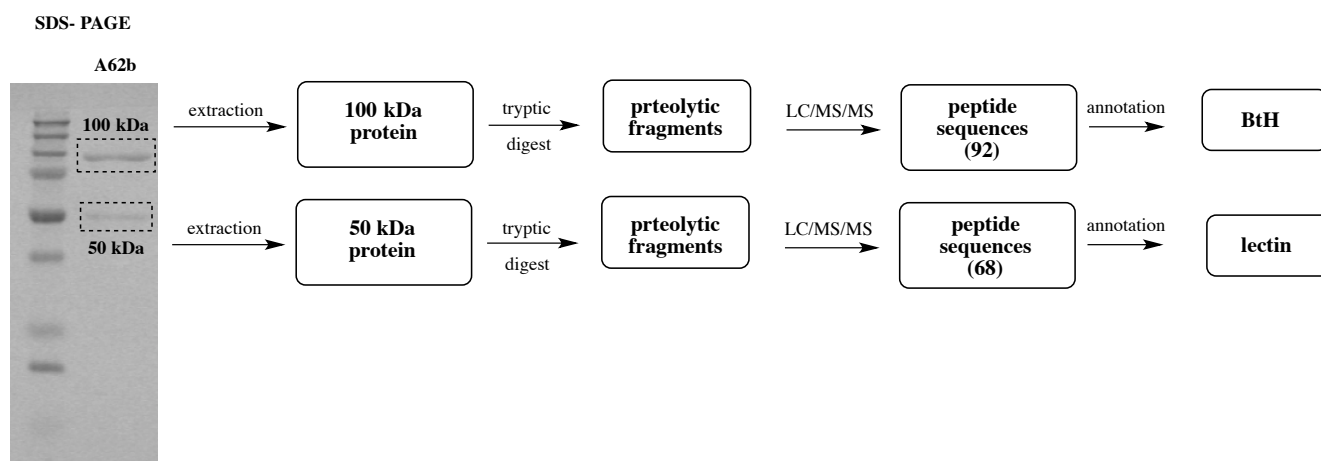
Scheme 4.7 MS/MS sequencing of 100 kDa and 50 kDa proteins obtained from A62b.

MS/MS sequencing of the tryptic digest of the 100 kDa protein extracted from the SDS PAGE gel of A62b revealed 93 individual peptides (Table 4.5) selected using high stringency parameters that required >95% sequence confidence (e.g. omitting hits with missed cleavages or ethanoloyl modifications) with a predicted mass of 100 kDa. These peptides showed high (100%) sequence homology with the putative BtH sequence established by transcriptomic analysis (contig 22, Table 4.3 and contig 37, Table 4.4), accounting for 65% coverage of the entire sequence (Figure 4.21).

Table 4.5 List of peptides generated from tryptic digest of the 100 kDa protein from SDS-PAGE fractionation of A62b and LC/MS/MS analysis

Sequence	Δppm	Sequence	Δppm	Sequence	Δppm
APVVVHR	-0.275	GWPIDDATSNK	-0.153	IQGEPIHVDIDGTN	0.285
LPATPLR	-0.187	LVVMSHESYLN	0.065	HVPTSTSLVTVTSLK	0.283
MNLWAEK	-0.022	SDVPSQYPGNK	-0.263	DKAHPALKPGDREQR	-0.474
FGAAYYGR	-0.323	STGLYLPPNKK	-0.199	LDIQGEPIHVDIDGTN	0.456
GFGWDPFK	-0.104	STIADLAAIPK	-0.165	LSTLSEWEENPMKK	0.624
IDTTSGFK	-0.166	STSLVTVTSLK	-0.05	SYSHSDVPSQYPGNK	-0.328
IGVQNAMR	-0.13	DVPSQYPGNK	-0.19	NGVEIKPPLSSWLSK	0.243
NVLIAASR	-0.151	TLSEWEENPMK	0.329	SLGLLADTLSNSGHR	0.048
QDVATYLK	-0.117	NGMIGVQNAMR	-0.233	VFSEYQTMSNVSNNK	0.321
SEVVLFLK	-0.342	DKAHPALKPGDR	-0.122	FQAWGWPIDDATSNK	0.57
DIQGEPIH	-0.235	HSDVPSQYPGNK	-0.104	FGITILESTINNGIYK	0.787
EDYASLTK	0.157	ITSVAGVYFTNK	0.403	NSLGLLADTLSNSGHR	-0.365
IILTVPTDK	0.033	MLTNEDYASLTK	0.284	SGMWGAAHELGHNQQR	0.392
NEDYASLTK	0.05	VVVGPHEGYITR	-0.081	WSYSHSDVPSQYPGNK	1.022
NNVLIAASR	-0.079	WGWPIDDATSNK	0.392	DLKNGVEIKPPLSSWLSK	0.137
SLVTVTSLK	-0.221	ETPANNVLIAASR	0.006	IQGEPIHVDIDGTNPGGDAWR	0.692
VFFDFPGNK	-0.17	AHPALKPGDREQR	-0.105	NLAPFFQAWGWPIDDATSNK	1.168
VSSWLDTLR	0.036	AWGWPIDDATSNK	0.084	DIQGEPIHVDIDGTNPGGDAWR	0.462
VVVGPHEGY	-0.37	DKAHPALKPGDRE	-0.268	TSTSPWAELITEDIILTVPTDK	1.2889
FFGAAYYGR	-0.048	SEYQTMSNVSNNK	0.514	LDIQGEPIHVDIDGTNPGGDAWR	1.025
AISWLDAGR	-0.03	SFILNAISWLDAGR	0.564	LLLTGDTAFPVLETPANNVLIAASR	0.3554
AISWLKPSSE	-0.383	SGMWGAAHELGH	0.188	GKSELGNIPVTIYGAEPAPTFINGQTN	3.689
DIILTVPTDK	-0.074	SHSDVPSQYPGNK	-0.13	DAGELDIQGEPIHVDIDGTNPGGDAWR	1.046
GMIGVQNAMR	0.109	VPESTTNSYHFLR	0.017	TGENGIFPASEKPPPFPSFNDVDFSMDLK	2.2918
GTNPGGDAWR	-0.129	ITEDIILTVPTDK	0.033		
LRQDVATYLK	0.111	GRVVVGPHEGYITR	0.071		
NVKMNLWAEK	-0.161	IDTTSGFKEDLGVF	0.376		
ESTINNGIYK	-0.778	KLSTLSEWEENPMK	0.779		
STGLYLPPNK	-0.127	LITEDIILTVPTDK	0.224		
VGPHEGYITR	-0.245	LSTLSEWEENPMK	0.008		
VHEILLGIPR	-0.026	VDIDGTNPGGDAWR	0.976		
NGVEIKPPLS	-0.241	QAWGWPIDDATSNK	0.03		
AHPALKPGDR	-0.403	VSLWQELLNLVQN	0.803		
AHPALKPGDRE	-0.157	YSHSDVPSQYPGNK	-0.071		

Δ ppm = Theoretical – calculated m/z [M+H] in ppm

MLTNEDYASLTKGIQNLNFTGDSIPCRLLLTGDTAFPVLETPANNVLIAASRYGKGRLVVMSHESYLNDP
QFMDFLQNAISWLKPSSEAVIGIENSLGLLADTLSNSGHRIDTTSGFKEDLGVFCMTQYNESQLSEVVLFL
KEGGGLLIGAEACHWSESHPELNVFFDFPGNKITSVAGVYFTNKTGENGIFPASEKPPPFPSFNDVDFSM
DLKQIFNGLSSLDVSGDAGASELLLHGPLTFPLGLTNSQCFFGAAYYGRGRVVVGPHEGYITRLQLKSF
ILNAISWLDAGRNGMIGVQNAMRGLIPILQAEGISCATSNVSSEFSIYCCNSYSDAEVDKIHQFVAEGGSL
LIAGHAWYWSYSHSDVPSQYPGNKILNRFGITILESTINNGIYKVPESTTNSYHFLRSICQFLRDLKNGVEI
KPPLSSWLSKLRQDVATYLKLPATPLRVSLWQELLNLVQNCNLPEVSKEHPVKSQSKEAFLICLAQEVD
CFYDSFQEDAGELDIQGEPIHVDIDGTNPGGDAWRSTGLYLPPNKKGKLVFPSSAVGNGLQVQIGCQSD
NLSGASEYCRAPVVVHRKNVVREEVVISCIWGGLLYVIVKGKSELGNIPVTIYGAEPAPTFINGQTNVSS
WLDTLRTSTSPWAELITEDIILTVPTDKVRSLEDPESLMCLWDNIMSTIADLAAIPKKMPRPERIVADVQI
SAGFMHAGYPIMCHVPTSTSLVTVTSLKSGMWGAAHELGHNQQRGVWEFPPHTTEATCNLWSVYVHE
ILLGIPRDKAHPALKPGDREQRTKQYVKNGAKLDEWNVWTALETYLQLQEGFGWDPFKRVFSEYQTM
SNVSNNKNVKMNLWAEKFSQAVDKNLAPFFQAWGWPIDDATSNKLSTLSEWEENPMKKYVS

Figure 4.21 Complete sequence of BtH identified from transcriptomics and compared with the data from shotgun sequencing of the 100 kDa protein isolated from SDS-PAGE fractionation of A62b. Green – peptides with 99% confidence levels, red – peptides with 60% confidence levels, yellow – peptides with <50% confidence levels, grey – peptides not identified using shotgun sequencing.

With respect to the sequence data attributed to BtH (Figure 4.18), it is interesting to note that no known protein family was observed with high sequence homology (blast InterProScan, NCBI). It is also interesting to note that the sequence for BtH does not include a "signal peptide" at the N-terminal, which is normally characterized as a short cleavable peptide sequence to direct proteins into the necessary secretory pathway.

A majority of the proteins contain a "signal peptide" at the N-terminal end for targeted delivery. Surprisingly, the translated sequence of BtH was lacking an N-terminal signal peptide indicating that it could possibly belong to the class of "leaderless secretory proteins".[11] Selected group secretory proteins including FGF-1, IL-1 and galectins belong to this class of proteins.[11-13] Eukaryotic proteins are usually secreted through classical secretory pathways involving transport and post-translational modifications in endoplasmic reticulum and Golgi.[14] Leaderless proteins are secreted via non-classical secretory pathway, which is independent of the secretory mechanism involving ER-Golgi network.[14] The fact that BtH lacks an N-terminal signal that guides its intracellular trafficking could suggest that BtH does not traffic intracellularly but is an extra cellular protein. This would be consistent with our investigation on the localization of BtH within the parotoid gland (Figure 4.6B).

MS/MS sequencing of the tryptic digest of the 50 kDa protein extracted from the SDS-PAGE gel of A62b revealed 68 individual peptides selected using high stringency parameters that required >95% sequence confidence (Table 4.6) with a predicted mass of 50 kDa. When correlated with the high frequency contigs from the transcriptomic analyses of cane toad parotoid gland both pre (A69) and post secretion (A68) using Protein Pilot, these peptides showed high sequence homology (100%) with a 50 kDa protein, detected in A69 (contig 61, Table 4.4) with 78% coverage of the entire sequence (Figure 4.22).

Table 4.6 List of peptides generated from tryptic digest of the 50 kDa protein from SDS-PAGE fractionation of A62b and LC/MS/MS analysis

Sequence	Δppm	Sequence	Δppm	Sequence	Δppm
LEYGHR	-2.3	VNTLAVHGR	-1.8	NGFYDVNEERSPLR	4.91
DQAFEFR	0.78	VTHFHSGIK	-2.41	PPVPYVTHFHSGIK	1.17
FLEYGHR	-1.75	YFQDEHISK	-1.04	NPPVPYVTHFHSGIK	1.493
HFHSGIK	-4.12	FLVEDHAYQV	2.72	EQPFEIQVLVTDQEYK	0.994
LSPDTVK	-2.17	GDELFYFSHR	0.19	MIGFHHQYFPEGQQEN	1.654
YKVPFAK	-1.81	IRGTVLPATK	-3.61	MCGSDIDDDIAFHFNPR	3.28
HRIPMER	-3.2	LKKDQAFEFR	1.96	VGTVFIINGTIPPLPDR	4.21
FLVEDHAY	-1.48	NGFYDVNEER	-1.86	TMENEIWGNEELKEEMPFK	4.69
FNEGHVLL	0.46	GTVLPATKSF	0.67	SVEIQAEASGFHHLYFQDEHISK	7.49
FYDVNEER	0.58	FLVEDHAYQVS	0.518	MIGFHHQYFPEGQQENTLPFGTQFPSEIK	2.323
GTVLPATK	-2.42	FNEGHVLLNTR	0.79		
IAFNFNPR	-0.19	HLYFQDEHISK	4.33		
NTLAVHGR	-2.08	NPPVPYVTHFH	-2.19		
RGQPFEVR	-4.33	QNNVWSPDENR	0.61		
VWSPDENR	-1.5	RNGFYDVNEER	-1.09		
KDQAFEFR	-1.61	SFSIDIQCGDK	2.04		
IFFLDYPHK	0.74	GDVTLSCVEIQPQ	0.427		
EGHVLLNTR	-2.99	GNADIAFNFNPR	2.4		
FLVEDHAYQ	2.417	IINGTIPPLPDR	2.88		
FNEGHVLLN	-1.72	IQVLVTDQEYK	-0.171		
GFYDVNEER	0.88	SVEIQAEASGFH	0.49		
GTIPPLPDR	-2.85	SVPLVTPFVVGIK	2.333		
GTQFPSEIK	-1.3	NTLPFGTQFPSEIK	2.47		
IFFLDYPHK	0.74	QNNVWSPDENRYK	1.1		
ILFTSQEYK	0.71	SLNGDELFYFSHR	5		
ITVNTVEIK	0.76	TLPFGTQFPSEIK	2.36		
NPPVPYVTH	-0.95	FLVEDHAYQVSLN	2.45		
NVWSPDENR	0.182	GFHHLYFQDEHISK	0.539		

Δ ppm = Theoretical – calculated m/z [M+H] in ppm

MCDEIIKNPPVPYVTHFHSGIKNGSVFVISGTVLPSAEGFMVDFQCGTLGNADIAFNFNPRFNEGHVLLNTR QNNVWSPDENRYKVPFAKEQPFEIQVLVTDQEYKVFVNKIFFLDYPHKIPLAKVCAFGVKGDVTLSCVEI QPQMIGFHHQYFPEGQQENTLPFGTQFPSEIKVGTVFIINGTIPPLPDRSYINFMCGSDIDDDIAFHFNPRF DEEKIICNAKRNGFYDVNEERSPLRLKKDQAFEFRFLVEDHAYQVSLNGDELFYFSHRLSPDTVKNLVIM GCALLKSVEIQAEASGFHHLYFQDEHISKSVPLVTPFVVGIKEDTVVRIRGTVLPATKSFSIDIQCGDKDTD DIAFHLNIFTGKGHVSCNTMENEIWGNEELKEEMPFKRGQPFEVRILFTSQEYKVSVDRNRFLEYGHRIP MERVNTLAVHGRITVNTVEIKSQGGEFP

Figure 4.22 Complete sequence of 50 kDa protein identified from transcriptomic analysis and compared with shotgun sequencing of the 50 kDa protein isolated from SDS-PAGE fractionation of A62b. Green – peptides with 99% confidence levels, red – peptides with 60% confidence levels and grey – peptides not identified using shotgun sequencing.

On performing an NCBI-BLAST search for the identified sequence, it returned several homologous to lectin reported from *Xenopous laevis*. An Interpro search for the identification of the function of the protein revealed the major part of the sequence showed homology to carbohydrate recognition domain of galectins and also to concanavalin A like lectins (Figure 4.23). A literature search performed on lectins showed their ability to form dimers that exhibit galactoside-binding activity.[15, 16] The presence of lectin proteins in the parotoid glands *in situ* could be attributed to the presence of rich amounts of polysaccharides[6] since lectins bind to carbohydrates. This observation clearly identified the mixture of another protein present along with BtH. The sensitiveness and reliability of

transcriptomics combined with proteomic analysis played a vital role in identifying the co-eluting protein.

Figure 4.23 Complete sequence of the 50 kDa protein identified from partial sequencing, transcriptomics and comparison with InterProScan protein database showing part of the sequence similarity to lectin like superfamily

4.2.6.3 Further purification of A62b

The protein mixture was concentrated to 1 mg/mL in Tris buffer at pH 8.0 and was injected to an anion exchange resin column (Mono S HR 5/5), with a linear gradient of 100 – 1000 mM NaCl. Identification of two distinct peaks would have indicated the presence of two different proteins as determined by our transcriptomic analysis. Surprisingly, only one narrow peak was observed. From the UV absorbance, the sample was thought to contain just one protein, 100 kDa. However, an SDS PAGE analysis of the single peak exhibited two bands, 100 kDa and 50 kDa, respectively. The observation clearly indicated the presence of two proteins co-eluting again on the anion exchange resin. A search on ExPasy database (ProtParam) for BtH and the lectin protein sequences returned the theoretical pI of the proteins to be 5.28 and 5.48, respectively. Since both the proteins had similar pI it was difficult to separate the proteins based on ion exchange chromatography (Figure 4.24).
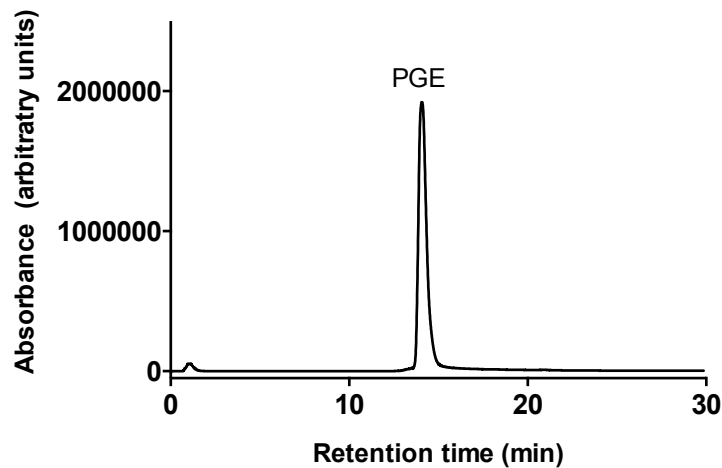
Figure 4.24 Purification of the active fraction of BtH containing 100 kDa and 50 kDa proteins using anion exchange chromatography at pH 8.0

4.2.7 Phylogenetic analysis

Homologous sequences from different species identified by BLAST were correlated with BtH sequence information to identify the phylogenetic relationship. Since there is not much information about the BtH protein family, a phylogenetic analysis would be significant in two ways: (1) identification of homologs (similar proteins) from various species – to identify species specific distribution of the homologs and (2) grouping of homologs based on age as well as function – this analysis would lead us to identify any functional relationship with other known proteins from different/same species.

There was no species-specific clustering of the sequence homolog identified from the phylogenetic analysis, with several species ranging from birds, amphibians and mammals exhibiting a match with BtH (Figure 4.22). A sequence homolog is the part of the query protein sequence that exhibits homology with BtH and it is ranked based on the degree of homology (%):

- Closely related species are shown in the first cluster consist of the Asiatic toad (*Bufo gargarizans*) and a frog (*Xenopus silurana*), (i.e. amphibians) (homology score of 100%). An unknown protein from *B. gargarizans* showed the closest match followed by a FAM115-like protein from *Xenopus silurana* (Figure 4.25).
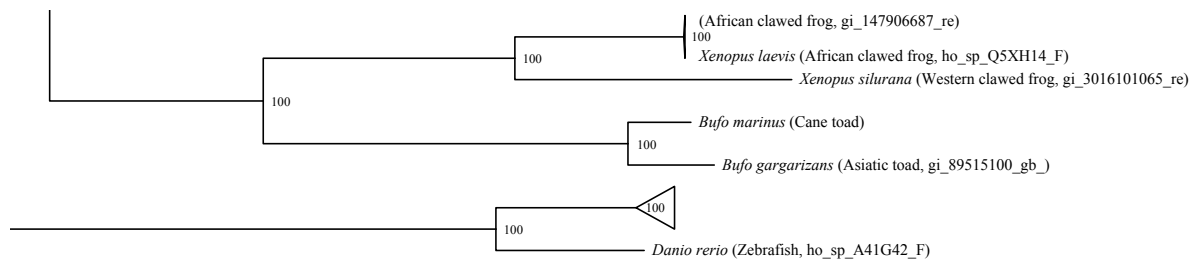
Figure 4.25 First cluster of phylogenetic tree for BtH

- Closely related species shown in the second cluster (homology score 99%) includes the orders Cetaceae, Carnivora, Artiodactyla, Perissodactyla and Rodentia (Figure 4.26).
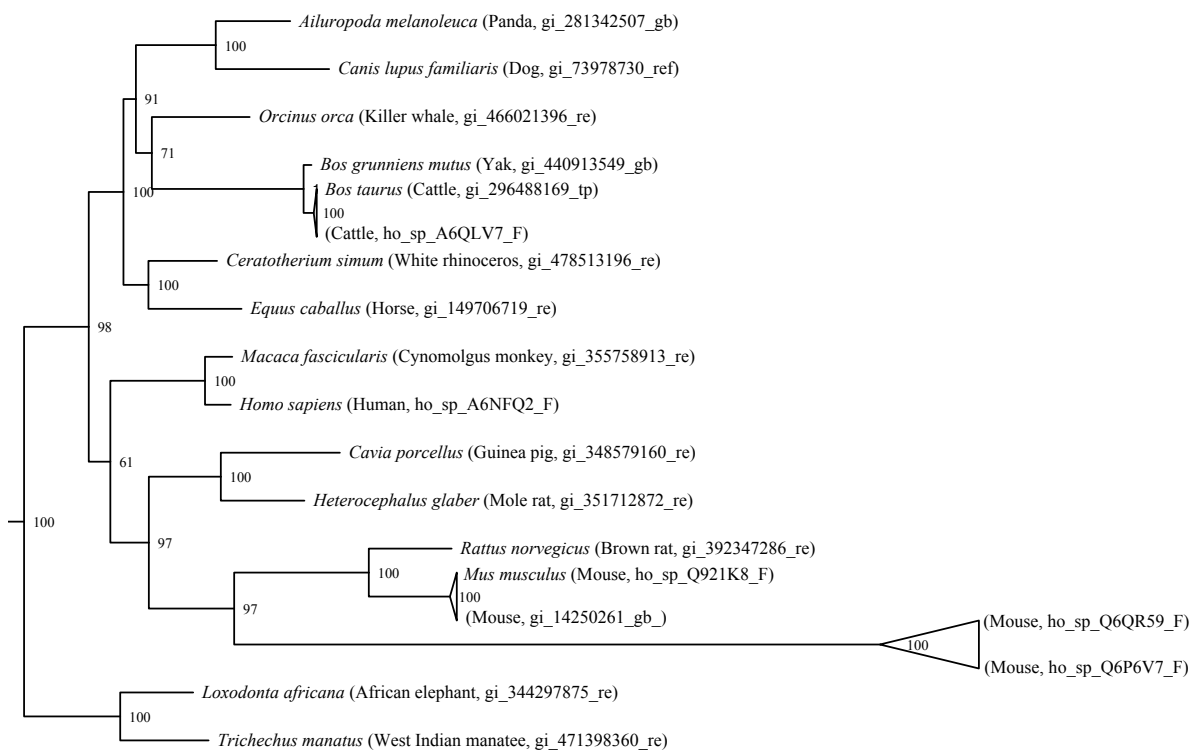
Figure 4.26 Second cluster of phylogenetic tree for BtH

- Closely related species shown in the third cluster (homology score 85 – 100%) include Primates (i.e. orangutan, chimpanzee, human, gorilla, marmoset and monkey) (Figure 4.27).
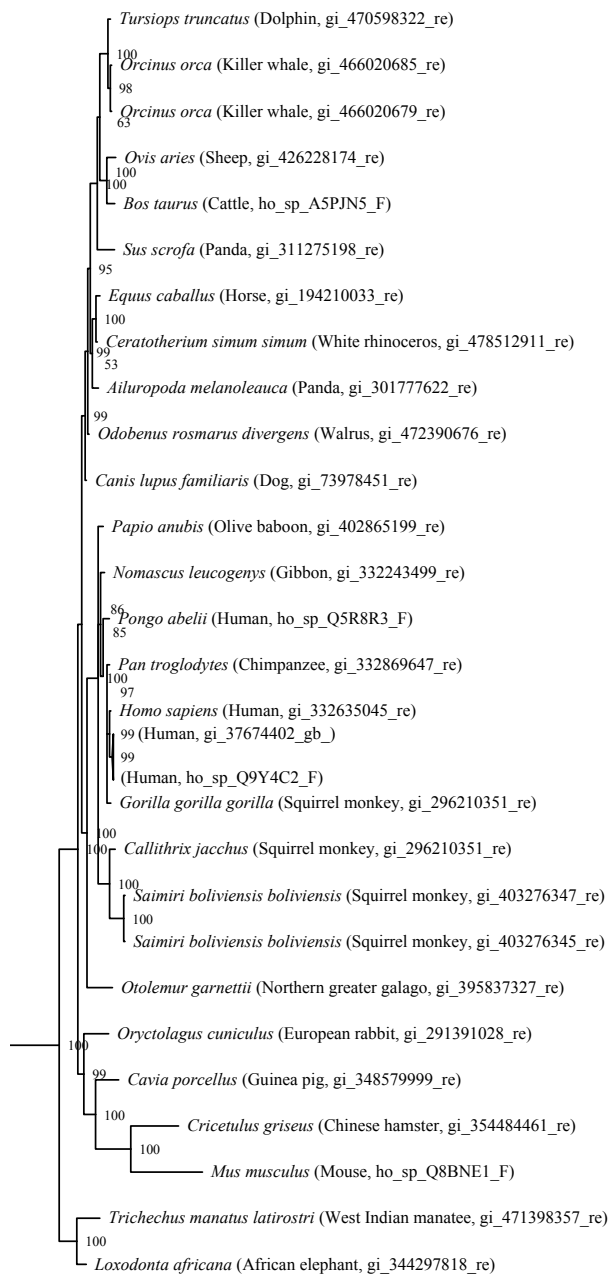
Figure 4.27 Third cluster of phylogenetic tree for BtH

Majority of the hits that showed sequence homology to BtH were exclusively identified to be member of the FAM115 protein family, which have only been predicted by genome sequencing. The full-length protein sequence homology exhibited by the matched hits was only in the range of 43 – 58%, except for an unknown protein identified by gene sequencing from *B. gargarizans* (88%). Such low homology levels also indicated that BtH could belong to new class of protein and the current investigation also indicates the high sequence conservation in BtH. The phylogenetic tree was generated with *Danio rerio* (Zebrafish) sequence (NP_001082796.1) as the root while all the other homologs were matched based on the sequence similarity with the BtH. No other known protein family showed a match with BtH.
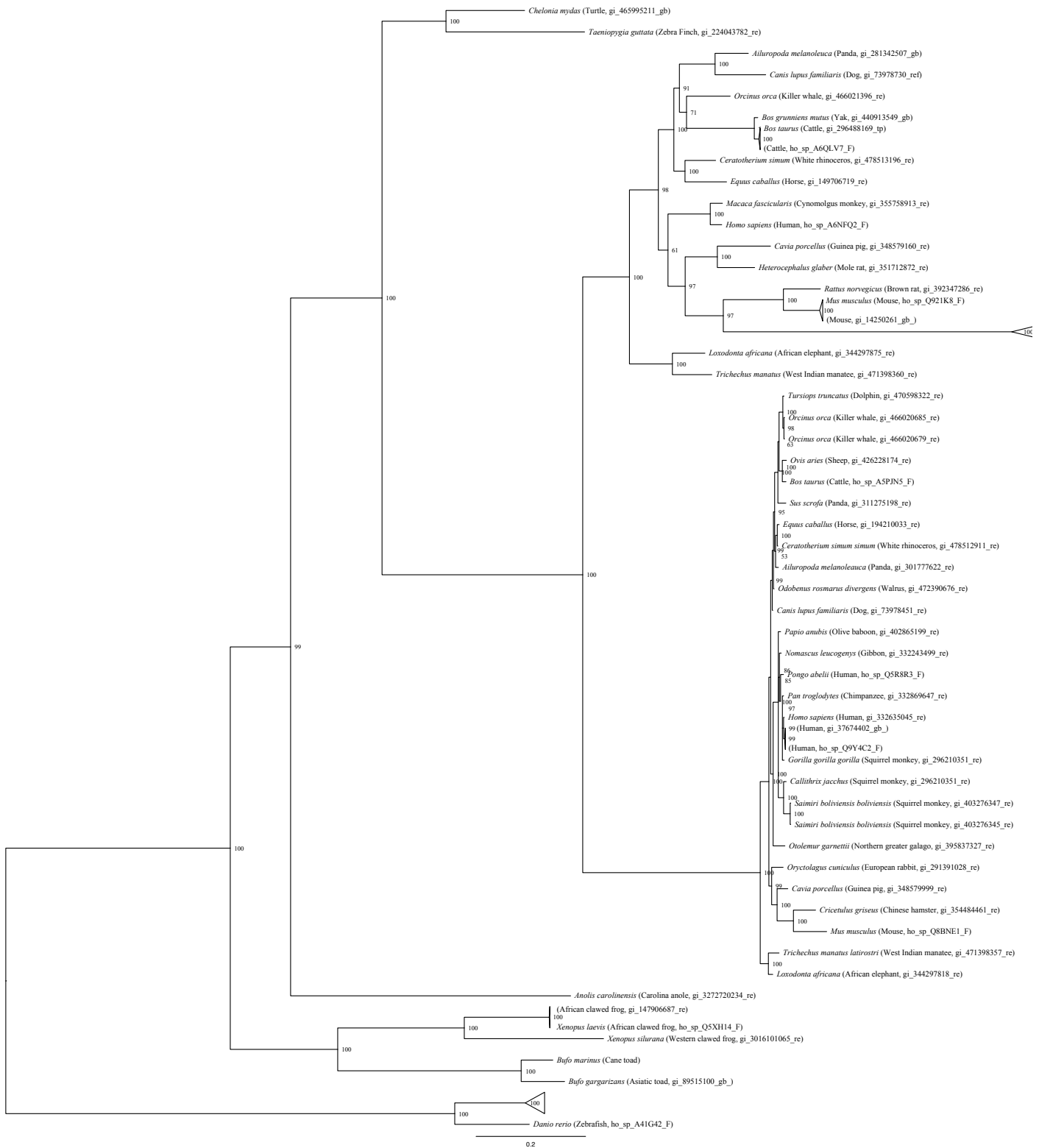
Figure 4.28 Phylogentic analysis of BtH showing matches with conserved sequences reported from different species exhibiting sequence homology and phylogenetic distance from the related homologs.

4.2.8 Kinetics of BtH – measurement of V_{max} and K_m values for the hydrolysis of bufotoxins by *in situ* hydrolase

Previous observations showed the BtH mediated hydrolysis of bufotoxins to bufagenins was rapid. To quantify this process we set out to determine the rate kinetics of V_{max} and K_m, where V_{max} denotes the maximum rate of the reaction at maximum substrate concentration, while K_m denotes the substrate concentration at which half maximal V_{max} is achieved. Subsequently the values were calculated to be $V_{max} = 22.0$ μmoles/min/mg of BtH and $K_m = 182$ nM.

As the BtH substrate (bufotoxin) is non-fluorescent and the substrate (bufotoxins) and the product (bufagenins) have virtually identical UV-Vis spectra, we elected to use HPLC-DAD methodology to determine the rate of BtH hydrolysis of bufotoxins to bufagenins. The BtH hydrolysis of the marinobufotoxin (**1c**) was measured at specific time points by quenching BtH activity by the addition of MeOH to the reaction mixture. Each time point reaction mixture was dried, re-dissolved in MeOH to a standard concentration (50 μL) and analysed using HPLC-DAD Method 1 (see Chapter 2). The conversion of marinobufotoxin (**1c**) to marinobufagenin (**1a**) was determined by calculating the area under the curve as described in Chapter 2 and Chapter 3. All BtH hydrolysis reactions were performed at 37 °C using A62b fraction (containing lectin). Hence the actual kinetics of BtH must be higher than the value measured using the cuurent assay system.

Firstly, the rate kinetics of BtH was determined by monitoring the hydrolysis of **1c** into **1a** time period by various concentrations of hydrolase. Final assay volume was 200 μL and the triplicates for each concentration of BtH was maintained with time intervals ranging from 0 – 10 min. A standard minimum concentration of marinobufotoxin (**1c**) was determined (62.5 μM) based on the UV absorbance using Method 1 as previously determined (Chapter 2). For each time interval 50 μL of the reaction was obtained and immediately quenched with MeOH (100 μL) to inhibit the hydrolysis. The resulting mixture was dried under N_2 at 40 °C and was re-dissolved in MeOH (500 μL) and filtered and again dried under N_2 at 40 °C and was re-dissolved in MeOH (50 μL) and analysed using Method 1.
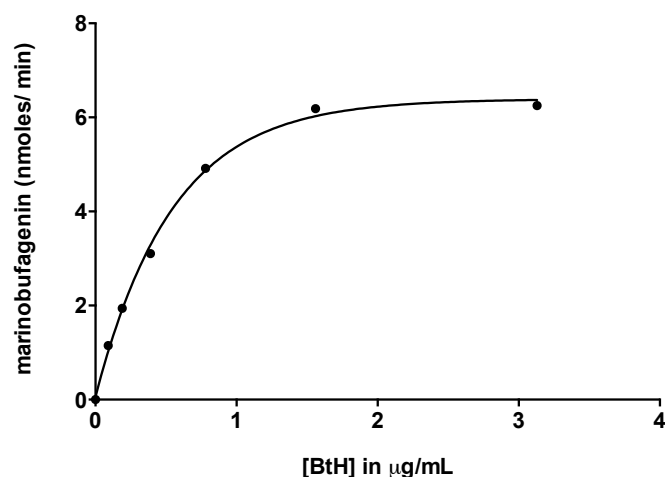
Figure 4.29 Rate kinetics of parotoid gland hydrolase (BtH) for the hydrolysis of marinobufotoxin (**1c**) at various concentrations

Number of moles of **1a** formed post the hydrolysis of **1c** was calculated for every 10 min (Figure 4.29). A graph was plotted between the number of moles of **1a** formed by various concentrations of BtH and the slope corresponded to the half maximal value, which was 0.4 μg/mL for 62.5 μM of **1c**. Concentration slightly lower than half maximal value was selected because at lower concentrations of BtH, saturation of binding sites could be achieved by increasing concentrations of substrate, **1c**. Hence, 0.2 μg/mL of BtH was the optimum concentration to determine the rate kinetics of the bufotoxin hydrolysis (in triplicates).

A constant concentration of BtH (0.2 μg/mL) was exposed to varying concentrations of **1c** and the hydrolysis was monitored for various time intervals (0 – 60 h). Rate of hydrolysis of **1c** was determined for about 10 time intervals with triplicates for each. Various concentrations of **1c** was exposed to hydrolysis, with concentrations ranging between 0 – 125 μM. Final assay volume was 1 mL and for each time point 50 μL of reaction mixture was pipetted out into 100 μL of MeOH to inhibit the hydrolysis. The resulting mixture was dried under N_2 at 40 °C and was triturated with MeOH (500 μL) and filtered and again dried under N_2 at 40 °C and was re-dissolved in MeOH (50 μL) and analysed using HPLC-DAD using Method 1.
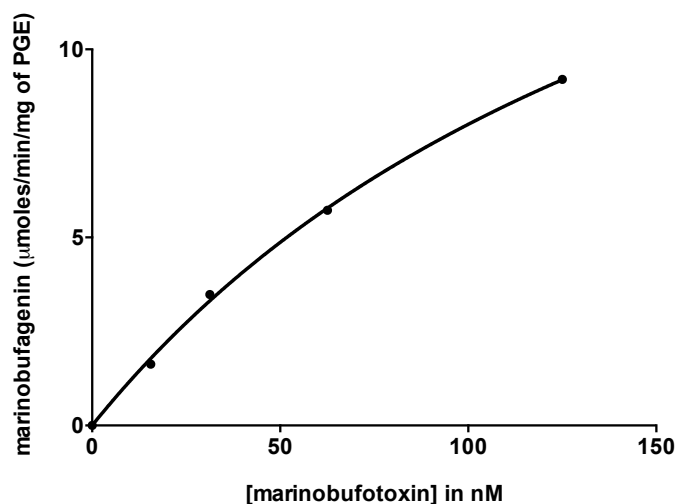
Figure 4.30 Calculation of K_m and V_{max} value for the BtH (parotoid gland hydrolase) for the hydrolysis of marinobufotoxin (**1c**) at various concentrations

The specific activity of BtH was calculated for each concentration of **1c** by determining the number of moles of marinobufagenin (**1a**) formed per min per mg of BtH (Figure 4.30). The number of moles of **1a** formed from **1c** was determined by calculating the area under the peaks from the chromatogram (298 nm) obtained from HPLC-DAD. From the graph the V_{max} was 22.0 µmoles/min/mg of BtH and K_m value was calculated to be 182 nM. A low K_m value suggests the high affinity of BtH for the substrate, while high V_{max} value determines the high rate of reaction. Preliminary analysis of hydrolysis observed in cane toad secretions also showed high rate of hydrolysis as 94% of bufotoxin in the parotoid secretions converted into bufagenins in 5 min, which is consistent with the current observation

4.2.9 Structure-activity-related studies on BtH

Parotoid gland hydrolase (BtH) was investigated for structure activity related studies with various bufadienolide moieties to understand and compare substrate specificity for bufotoxins and related structures. Reactivity of BtH with marinobufagenin esters with varying side chain lengths including marinobufagenin-3-acetate (**8b**), marinobufagenin-3-succinate (**9b**), marinobufagenin-3-suberate (**1b**), bufolipin A (**1h**) (isolation from eggs, described in chapter 6) and marinobufotoxin (**1c**) was investigated. A known amount of substrate (50 µg) was incubated with BtH (2 µg) for 60 min at room temperature and the reaction was stopped by the addition of MeOH. The reaction mixture was then dried under N_2 at 40 °C, subjected to *n*-BuOH/H_2O partition and the *n*-BuOH layer was collected and dried under N_2 at 40 °C, re-dissolved in MeOH and analysed using Method 1.

Surprisingly, following 60 min of incubation with BtH, 87% of marinobufagenin-3-hemisuberate (**1b**) (Figure 4.31A) was hydrolysed to marinobufagenin (**1a**) and 94% of marinobufotoxin (**1c**) was hydrolysed to marinobufagenin (**1a**) (Figure 4.31B). Only 2% of marinobufagenin-3-acetate (**8b**)

was hydrolysed to form marinobufagenin indicating that shorter chain length at C-3 would hinder the function of BtH (Figure 4.32). In the case of marinobufagenin-3-succinate (**9b**) (Figure 4.33A) and long chain fatty acid ester, bufolipin A (**1h**) (Figure 4.33B), no hydrolysis was observed with BtH even after incubation for 60 min indicating that both short and long chain esters are resistant to hydrolysis by BtH.
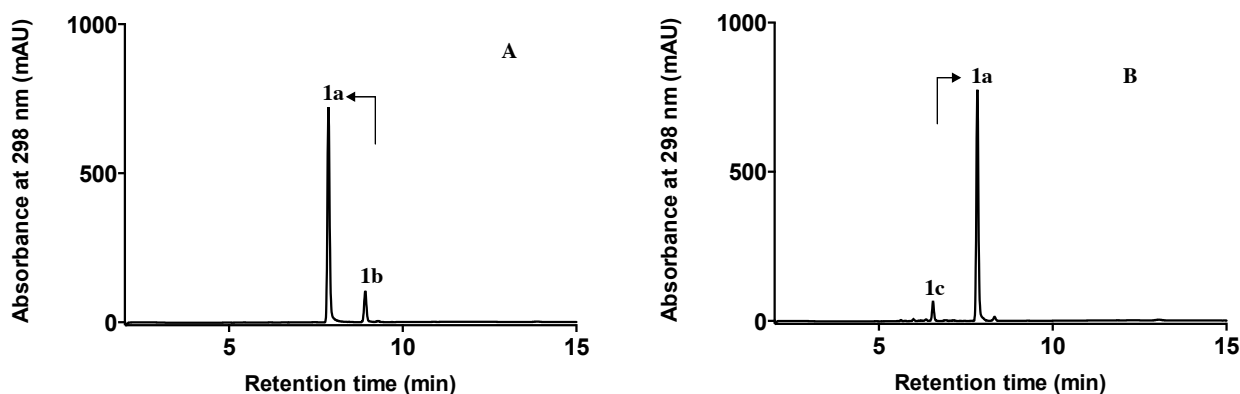
Figure 4.31 HPLC chromatograms (298 nm) indicating the structure based hydrolase activity of BtH with (A) marinobufagenin-3-suberate (**1b**) (B) marinobufotoxin (**1c**)
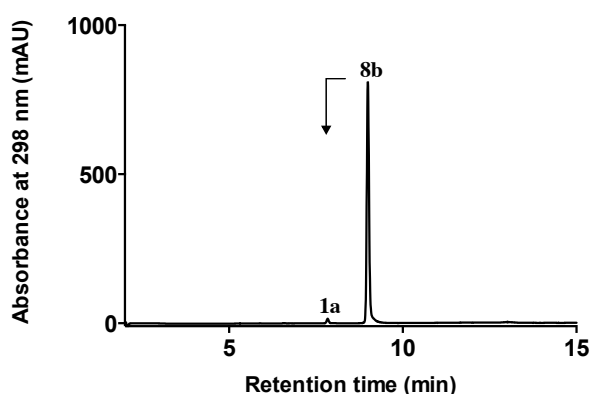
Figure 4.32 HPLC chromatogram (298 nm) indicating the structure based hydrolase activity of BtH with marinobufagenin-3-acetate (**8b**)

By comparison the analogues featuring a suberate moiety, marinobufagenin-3-suberate (**1b**) and marinobufotoxin (**1c**) alone exhibited high levels of hydrolysis (>90%) to form marinobufagenin (**1a**). These analyses clearly indicate that BtH exhibits specificity for substrates with suberate moieties (**1b** and **1c**) (n = 6) possessing 6 methylenes, but disfavours substrates with lesser/higher chain lengths such as acetate (n = 1), succinate (n = 2) and a long chain fatty acid (n = 13) (Figure 4.34).
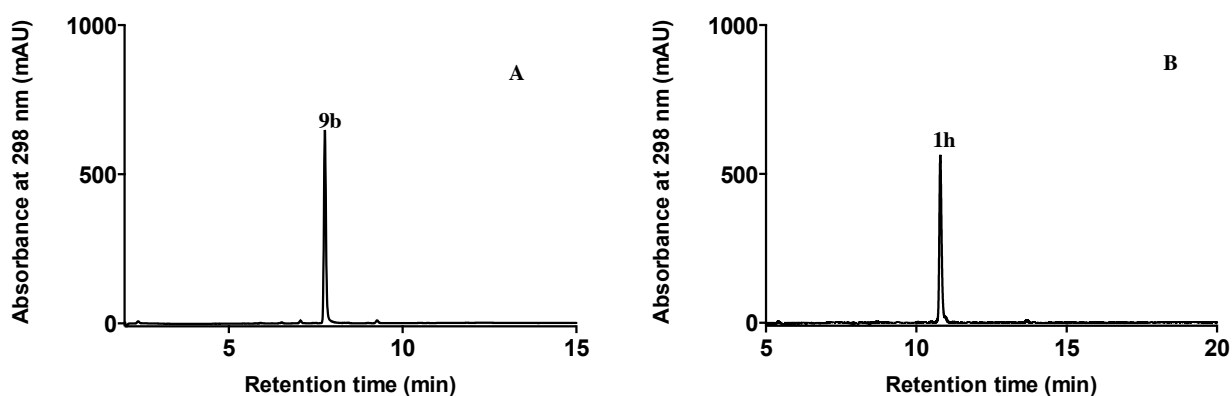
Figure 4.33 HPLC chromatograms (298 nm) indicating the structure based hydrolase activity of BtH with (A) marinobufagenin-3-succinate (**9b**) and bufolipin A (**1h**)
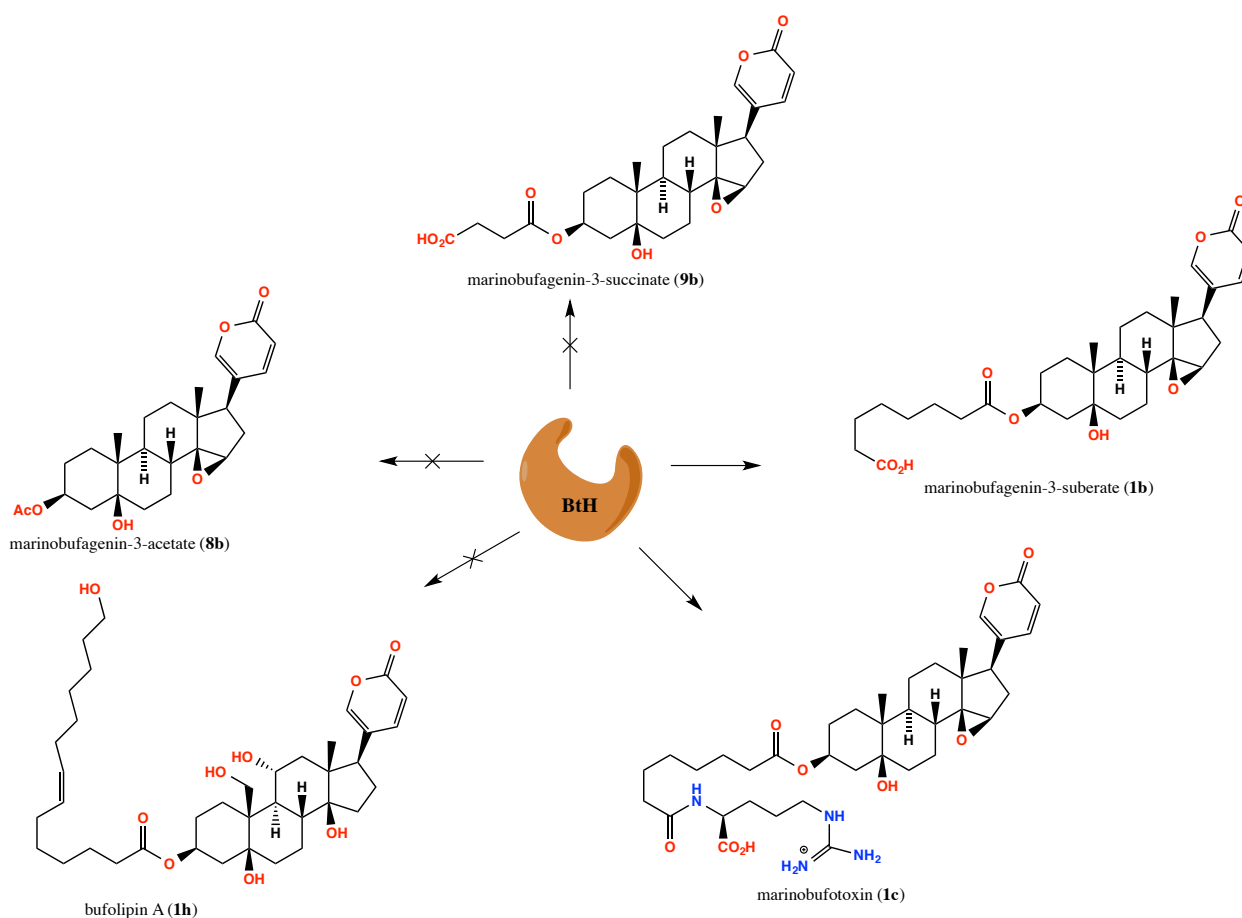
Figure 4.34 structure activity based relationship activity exhibited by BtH on various bufotoxin analogues with short and long chain variants

4.2.9.1 Inhibition of hydrolase activity by suberoyl-L-arginine

Preliminary investigations on the structure activity based function of BtH indicated that bufotoxins possessing suberoyl-L-arginine conjugate at the C-3 exhibited high specificity. This could be possibly due to the binding properties exerted by the suberoyl-L-arginine moiety on BtH, and suggests that free suberoyl-L-arginine may be a competitive inhibitor of BtH (Figure 4.35).

214
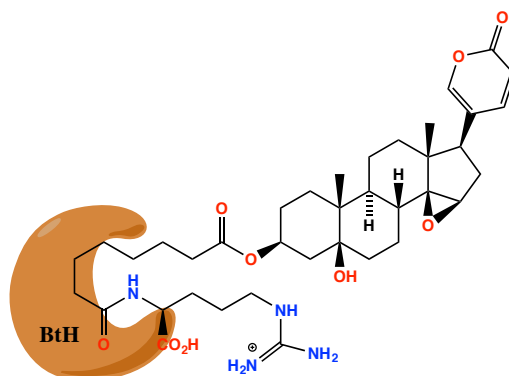
Figure 4.35 Hypothesis – suberoyl-L-arginine influences the binding characteristics of bufotoxins on BtH

To test the hypothesis, BtH was first incubated with suberoyl-L-arginine and/or arginine to compete for the binding sites in BtH, followed by the addition of marinobufotoxin (**1c**). Inhibition of the hydrolysis of **1c** would demonstrate whether suberoyl-L-arginine or L-arginine were competitive inhibitors of BtH. A UV absorption minimum was previously determined for the detection of marinobufotoxin (**1c**) (62.5 μM) using HPLC-DAD at various concentrations. The ideal concentration of hydrolase (10 μg/mL) for the hydrolysis of bufotoxins was also previously established.

Suberoyl-L-arginine (100 μL) and L-arginine (100 μL) at various concentrations, ranging from 7.8 μM (0.125× bufotoxin) to 1.25 mM (20× bufotoxin) were added to BtH (10 μg/mL) in duplicate and incubated for 15 min at 37 °C followed by the addition of 62.5 μM (100 μL) of marinobufotoxin (**1c**). The reaction was incubated for another 15 min at 37 °C. The hydrolase reaction was stopped by the addition of MeOH (300 μL) and the reaction mixture was dried *in vacuo* and triturated with MeOH (500 μL) to solubilize bufadienolides. The MeOH soluble fraction was dried *in vacuo* and re-dissolved in MeOH to a standard concentration (1 mg/mL) and analysed using Method 1 (Figure 4.36).

The HPLC-DAD based analysis of inhibition of BtH showed that suberoyl-L-arginine (**1d**) was a competitive inhibitor of BtH mediated hydrolysis of **1c** while L-arginine failed to inhibit **1c** hydrolysis (Figure 4.36). This observation suggests that during the hydrolysis of bufotoxins the released suberoyl amides could downregulate BtH hydrolysis of bufotoxins, however, in an ecological context it remains questionable whether this is likely to impede the conversion of **1c** to **1a**.
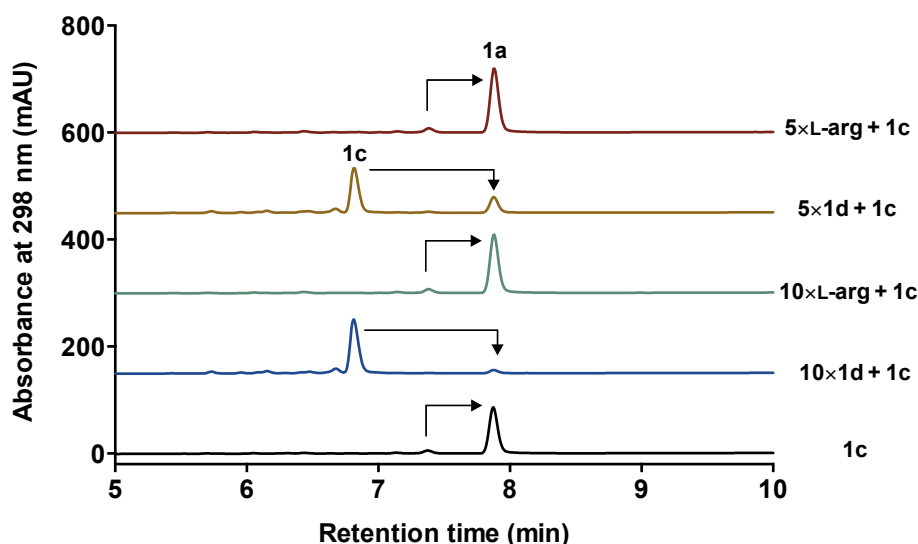
Figure 4.36 Inhibition of BtH mediated hydrolysis of marinobufotoxin (**1c**) in the presence of suberoylarginine (**1d**) and L-arginine (L-arg). Ctrl – **1c** + BtH, arrows point to the hydrolysis product, **1a**.

4.2.10 Formation of bufotoxins by BtH (a hydrolase acting as an esterase)

BtH mediated esterification of marinobufagenin (**1a**) with suberoyl-L-arginine (**1d**) to form marinobufotoxin (**1c**) would likely be impacted by several factors including substrate, temperature, pH, co-factors, hydrophobicity, etc. BtH mediated esterification trailed:

- Substrate ratio – ratios of marinobufagenin (**1a**) and suberoyl-L-arginine (**1d**) (1:1, 1:10 and 1:100).
- Temperature – 14 °C, 26 °C and 37 °C
- pH – pH 4, pH 6, pH 7 and pH 9
- co-factors – with and without co-enzyme A
- Hydrophobicity – 30%, 50%, 80% and 100% *n*-hexane/H$_2$O

None of the above experiments exhibited detectable levels of conversion of marinobufotoxin (**1c**) into marinobufagenin (**1a**). This could be due to various factors such as absence of cofactors necessary for the enzymatic activity such as ATP and NADPH or metals such as Cu, Mn, Fe, Zn while BtH could theoretically esterify bufagenins, however, our investigations, failed to demonstrate conditions under which this esterification could be detected.

4.3 Conclusion

Preliminary chemical analysis on cane toad toxins showed insights into the hydrolysis of *in situ* parotoid toxin during manual compression of the parotoid gland and that there is a hydrolase(s) co-secreted with the parotoid secretions. The key findings included evidence that BtH;

1. Is localized *in situ* at the apex of parotoid microgland
2. Co-secreted during the manual compression of the parotoid gland
3. Mediates rapid hydrolysis of marinobufotoxin
4. Exhibits high substrate specificity for bufotoxins (marinobufotoxin).
5. Is upregulated post secretion of toxin from the parotoid gland.
6. belongs to unreported class of proteins.
7. Is a 99 kDa protein with 897 amino acids with a sequence as shown in Figure 4.21.

The current studies on the cane toad parotoid gland and the toxins has widened the traditional understanding (Figure 4.37 & Figure 4.38) and showed insights into some of the complex mechanism involved during the secretion of parotoid toxin. To our knowledge the cane toad parotoid chemistry is the first of its kind to accumulate steroidal toxins as "protoxin" that are rapidly converted into free steroidal "toxin" by co-secretion of a specific hydrolase.

1. Parotoid toxins are stored in microglands as <u>bufotoxins</u>
2. Bufotoxins are <u>not</u> co-localized with arginyl amides or BtH
3. BtH is localized in specialized glands adjacent to the microgland duct

1. 50% of microglands expel their bufotoxin content via a duct and reinflate with blood
2. Bufotoxins co-secrete with BtH
3. BtH rapidly hydrolyse bufotoxins into bufagenins and arginyl amides

Figure 4.37 Summary on investigations of storage and delivery of cane toad toxins
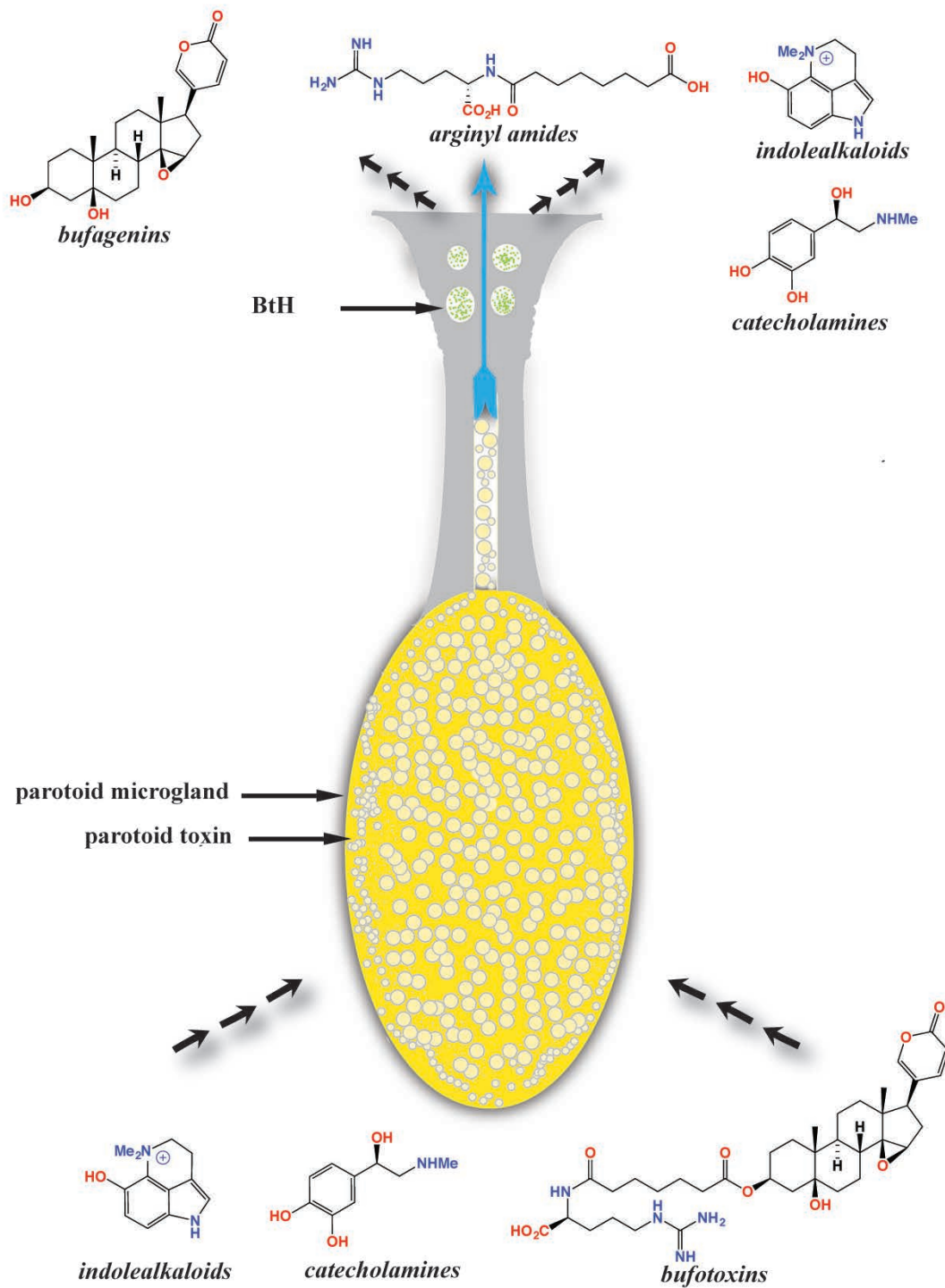
Figure 4.38 A diagrammatic representation of storage and release of parotoid toxin from a parotoid microgland based on recent findings

4.4 Experimental

4.4.1 Reaction with fluorescein diacetate

A solution of fluorescein diacetate in PBS (50 μg/mL) in 1% DMSO was prepared. Parotoid secretions were squeezed into a vial containing PBS (5 mL). An aliquot of parotoid secretion in H_2O was subjected to centrifugation (4000 rpm) and the supernatant was collected and reacted with FdA (100 μL).

4.4.2 Histology of parotoid gland

Parotoid glands from four cane toads were excised and cut into three or four pieces longitudinally and were fixed with 4% formaldehyde (pH 7.4, PBS) and embedded in paraffin sections (5 μm) stained with Mallory trichome, Haematoxylin Eosin, PAS, Alcian Blue, Congo red and DAPI stains. Images were obtained using an Olympus light microscope fitted with a 12 M-pixel digital camera.

4.4.2.1 Imaging of BtH

Parotoid glands from a cane toad were dissected and cut into thin sections after exposure to liquid nitrogen (−78 °C). The tissue sections were stained with fluorescein diacetate (10 μg/mL in 1% DMSO/H_2O) for 5 min and were washed three times with PBS to remove excess stain. The tissues were fixed with 70% EtOH/H_2O followed by washing with xylene. The dry tissues were mounted onto wax slides and then cut into 5 μm sections using a vibratome and were imaged under a confocal microscope. Confocal microscopy was performed on a Zeiss LSM510 confocal laser-scanning microscope equipped with a Zeiss 63x/1.4NA oil-immersion objective. Confocal microscopy samples were measured with emissions filtered through a 505 nm and 560 nm long-pass filters. Images were accessed using Image J software (NIH). Images were processed using Image J (USA).

4.4.3 Imaging mass spectrometry

Parotoid glands excised from three cane toads were snap frozen in liquid nitrogen (−78 °C). The frozen glands were then fixed with RCL/EtOH using a microwave based fixation for 2 min followed by stepwise treatment with 70% EtOH/H_2O, 100% EtOH and xylene before embedding in paraffin. Sections (7 μm) were cut, layered in Indium-Tin Oxide slides (Bruker Daltonics, Germany), sprayed with 7 mg/mL α-cyano-4-hydroxycinnamicacid (CHCA) in 50% MeCN and

0.2% TFA. Spectra were acquired using an Ultraflex III ToF/ToF mass spectrometer (Bruker, Germany) using linear positive mode, mass range 0.2 – 8 kDa and a resolution of 80 μm. Images were visualized using manufactureser's inbuilt software, Fleximaging 2.1 (Bruker Daltonics).

4.4.4 Isolation of BtH from parotoid secretions

Parotoid secretions from each parotoid gland of two cane toads squeezed into phosphate buffer saline (70 mL) were dispensed into two falcon tubes (35 mL each). The contents of one were homogenized using syringes (18 G, 23 G and 30 G), while the contents of the remaining tube were ultrasonicated for 2 min. Both the syringe and ultrasonicated fractions were centrifuged at 5000 rpm for 15 min and the supernatants collected in separate clean flacon tubes, while the pellets were re-suspended in PBS. Fluorescein diacetate (50 μg/mL; 1% DMSO) in H_2O was prepared to detect the hydrolytic activity during the purification of the hydrolase. Supernatant fractions were concentrated using an Amicon filter (10 kDa cut off) to workable volume (20 – 30 mL) and an aliquot (1 mL) of the concentrated supernatants purified by HPLC (Superdex S-200 column, Isocratic, Phosphate buffer comprising 150 mM NaCl, 20 mM Na_2HPO_4 at pH 7.4, 0.5 mL/min). Proteins were collected based on UV absorbance and hydrolytic activity determined by treatment with FdA detected at 500 nm.

The hydrolytically (FdA) active protein fraction (A62b) was later subjected to purification using a gel filtration column (Superdex S-200) fitted to an HPLC-DAD (Superdex S-200 column, Isocratic, Phosphate buffer comprising 150 mM NaCl, 20 mM Na_2HPO_4 at pH 7.4, 1 mL/min) was used to isolate active protein from a mixture of proteins. The isolated protein fraction was again subjected to reaction with FdA.

The hydrolytically active protein fractions (A62b) were subsequently subjected to purification using an anion exchange column fitted to an HPLC-DAD (Mono S HR 5/5 column, linear gradient, 0.1 – 1 M NaCl in 30 min, Tris buffer comprising 1M NaCl, 100 mM Tris, pH 8.0, 1 mL/min) was used to isolate active protein from a mixture of proteins. The isolated protein fraction was again subjected to reaction with FdA. Protein concentration was determined by measuring the absorbance at 280 nm using a Nanodrop and also by Bradford assay.

4.4.5 Kinetics of BtH

4.4.5.1 Optimization of BtH concentration

An aliquot of 62.5 μM of marinobufotoxin (**1c**) (50 μL) and BtH at different concentrations (0.09, 0.19, 0.38. 0.76, 1.50 and 3 μg/mL; 50 μL) was added to phosphate buffer to a final assay volume to 200 μL and the hydrolysis reaction was allowed to proceed at 37 °C with an aliquot (50 μL) collected at 10 min intervals (quenched with MeOH (100 μL) followed by drying under N_2 at 40 °C). The dried reaction mixture was triturated in MeOH (200 μL). The MeOH solubles were transferred into a new eppendorf tube and was again dried under N_2 at 40 °C, re-dissolved in MeOH (50 μL) and analysed using Method 1.

4.4.5.2 Determination of V_{max} and K_d values for BtH

An aliquot of BtH (0.2 μg/mL; 250 μL) and marinobufotoxin (**1c**) at different concentrations (15.6, 31.3, 62.5, and 125 μM; 250 μL) was added to phosphate buffer to a final assay volume to 1 mL and the hydrolysis reaction was carried out at 37 °C with an aliquot (50 μL) collected for each minute between 0 – 10 min (quenched with MeOH (100 μL) followed by drying under N_2 at 40 °C). The dried reaction mixture was triturated in MeOH (200 μL). The MeOH solubles were transferred into a new eppendorf tube and was again dried under N_2 at 40 °C, re-dissolved in MeOH (50 μL) and analysed using Method 1.

Graphpad Prism was used to generate standard curves for individual bufadienolides and amides (Section). Relative amounts of bufadienolides and amides were determined by calculating the area under the peak using Agilent Chemstation software.

4.4.6 Inhibition of BtH by amides

Suberoylarginine (100 μL) and L-arginine (100 μL) in PBS at various concentrations ranging from 9.5, 19, 39, 78.5, 156, 312.5, 625, 1250 μM were added to BtH (10 μg/mL; 50 μL) in duplicate experiments after incubating for 15 min at 37 °C. Marinobufotoxin (62.5 μM; 100 μL) was added to the reaction mixture and was incubated for another 15 min at 37 °C, after which BtH was quenched by the addition of MeOH (300 μL) and the reaction mixture was dried under N_2 at 40 °C. The triturated MeOH (500 μL) solubles at a standard concentration (1 mg/mL) were analysed by Method 1 (Figure 4.36).

4.4.7 Transcriptomics of parotoid gland

Sample was prepared for sequencing using the Ion Torrent RNA Seq kit, v1, as per the manufacturers protocol. In brief, the RNA was fragmented using RNAse III treatment, adaptor ligated, reverse transcribed and amplified, and size selected to a median size of ~200bp. Templating and sequencing used the Ion Torrent 200 sequencing kits, v2. Sample was sequenced on a 314 chip and the final FASTQ file provided.

4.4.8 Tandem mass spectrometry sequencing of BtH

BtH was subjected to SDS PAGE analysis. Gel spots were washed with ultrapure water, destained (40 mM NH_4CO_3/50% MeCN) and dehydrated (100% MeCN). Gel spots were rehydrated in 10 μL of 20 μg/ml proteomics grade trypsin (Sigma-Aldrich) and incubated overnight at 37 °C. Digests were eluted by washing the gel spots for 20 min with each of the following solutions: 20 μL 1% formic acid, followed by 20 μL of 5% MeCN/0.5% formic acid, followed by LC-MS/MS analysis (stable bond C_{18} column (2.1 mm × 100 mm, 1.8 μm particle size, 300 Å pore size) at a flow of 400 μL/min and a gradient of 1–40% solvent B (90% MeCN, 0.1% formic acid) in 0.1% formic acid over 5 min on a Shimadzu Nexera UHPLC coupled with an AB SCIEX 5600 mass spectrometer equipped with a Turbo V ion source heated to 450 °C). Peptide sequences identified by fragmentation patterns and assembled using Protein Pilot™ (AB Sciex), were compared with the transcriptome of the parotoid gland, with alignment of the protein sequences manually optimized using CLC Main Workbench software (CLC bio, Aarhus, Denmark). Sequence similarity and function information of proteins was investigated using Inter-Pro science, NCBI-BLAST and UniProt databases.

4.4.9 Phylogenetic analysis

Sequences showing similarity to BtH were previously extracted from NCBI database. The final dataset contained about 110 sequences. The sequence alignment was performed using MAFFT (algorithm). The alignment of the protein sequences were manually optimized using CLC Main Workbench software (CLC bio, Aarhus, Denmark). The phylogenetic tree was viewed and annotated using Figtree.

4.5 References

1. Toledo, R. C.; Jared, C., Cutaneous granular glands and amphibian venoms. *Comp. Biochem. Phys.A.* **1995,** *111*, 1-29.
2. Jared, C.; Antoniazzi, M. M.; Jordao, A. E. C.; Silva, J.; Greven, H.; Rodrigues, M. T., Parotoid macroglands in toad (*Rhinella jimi*): Their structure and functioning in passive defence. *Toxicon* **2009,** *54*, 197-207.
3. Dean, J.; Aneshansley, D. J.; Edgerton, H. E.; Eisner, T., Defensive spray of the bombardier beetle - a biological pulse jet. *Science* **1990,** *248*, 1219-1221.
4. Eisner, T.; Aneshansley, D. J., Spray aiming in the bombardier beetle: Photographic evidence. *Proc. Natl. Acad. Sci. U. S. A.* **1999,** *96*, 9705-9709.
5. Hutchinson, D. A.; Savitzky, A. H., Vasculature of the parotoid glands of four species of toads (Bufonidae : *Bufo*). *J. Morphol.* **2004,** *260*, 247-254.
6. Hostetle.Jr; Cannon, M. S., Anatomy of parotoid gland in bufonidae with some histochemical findings .1. *Bufo-marinus*. *J. Morphol.* **1974,** *142*, 225-239.
7. de Almeida, P. G.; Felsemburgh, F. A.; Azevedo, R. A.; de Brito-Gitirana, L., Morphological re-evaluation of the parotoid glands of *Bufo ictericus* (Amphibia, Anura, Bufonidae). *Contrib. Zool.* **2007,** *76*, 145-152.
8. Monici, M., Cell and tissue autofluorescence research and diagnostic applications. In *Biotechnology Annual Review*, El-Gewely, M. R., Ed. Elsevier **2005**; Vol. Volume 11, pp 227-256.
9. Deng, W., Identification of venom proteins from the Chinese toad, *Bufo Bufo gargarizans*, using an integrated proteomic and transcriptomic strategy. **2007**.
10. Shoji, H.; Nishi, N.; Hirashima, M.; Nakamura, T., Characterization of the Xenopus galectin family - Three structurally different types as in mammals and regulated expression during embryogenesis. *J. Biol. Chem.* **2003,** *278*, 12285-12293.
11. Bendtsen, J. D.; Jensen, L. J.; Blom, N.; von Heijne, G.; Brunak, S., Feature-based prediction of non-classical and leaderless protein secretion. *Protein Eng. Des. Sel.* **2004,** *17*, 349-356.
12. Rubartelli, A.; Cozzolino, F.; Talio, M.; Sitia, R., A novel secretory pathway for interleukin-1-beta, a protein lacking a signal sequence. *EMBO J.* **1990,** *9*, 1503-1510.
13. Tanudji, M.; Hevi, S.; Chuck, S. L., Improperly folded green fluorescent protein is secreted via a non-classical pathway. *J. Cell Sci.* **2002,** *115*, 3849-3857.
14. Nickel, W.; Seedorf, M., Unconventional Mechanisms of Protein Transport to the Cell Surface of Eukaryotic Cells. In *Annu. Rev. Cell Dev. Biol.*,2008; Vol. 24, pp 287-308.
15. Bianchet, M. A.; Ahmed, H.; Vasta, G. R.; Amzel, L. M., Soluble beta-galactosyl-binding lectin (galectin) from toad ovary: Crystallographic studies of two protein-sugar complexes. *Proteins* **2000,** *40*, 378-388.
16. Kim, B. W.; Hong, S. B.; Kim, J. H.; Kwon, D. H.; Song, H. K., Structural basis for recognition of autophagic receptor NDP52 by the sugar receptor galectin-8. *Nat. Commun.* **2013,** *4*.

Chapter 5: The ecological role of microbial biotransformation of cane toad toxins

5.1 Introduction

Bufagenins are the active ingredients of the Chinese traditional medicine Chansu, which is known for several medicinal properties including potent cardiotonic[1] and anticancer activity.[2] Since the bufagenins are potent inhibitors of cardiac Na^+/K^+ ATPase,[3] novel bufagenin analogues that are less toxic yet therapeutically significant are highly valued.

Biotransformation of bufadienolides has been widely reported by various bacteria[4-6] and plant cells[7]. For instance, cinobufagenin (**32a**) when exposed to the fungi, *Alternaria alternata* exhibited 6 biotransformation products including four oxidized compounds[8] while in the presence of *Syncephalastrum racemosum*, **32a** yielded 5 products[9] and in the presence of *Mucor spinosus* **32a** yielded two oxygenated, six hydroxylated and one acetylated product.[10]

Resibufagenin (**4a**) when exposed to the cultures of *Mucor subtilissimus* was converted into 11 products,[4] while exposure to *Pseudomonas aeruginosa* produced a single product, 3-oxoresibufogenin.[5] In another experiment, resibufagenin (**4a**) when exposed to *Mucor polymorphosporus* produced 22 biotransformation products.[11] Other bufagenins that are included in the biotransformation experiment includes marinobufagenin (**1a**), bufalin (**3a**) and cinobufagenin (**32a**).

Biotransformation of bufalin (**3a**) by *Mucor spinosus* yielded 12 analogues of bufalin.[12] Interestingly, biotransformation of bufadienolides was mostly reported in fungi and one notable actinomycetes, *Nocardia* sp. Tables 5.1 and 5.2 lists literature accounts bufagenin substrates, biotransforming organisms and biotransformation products:
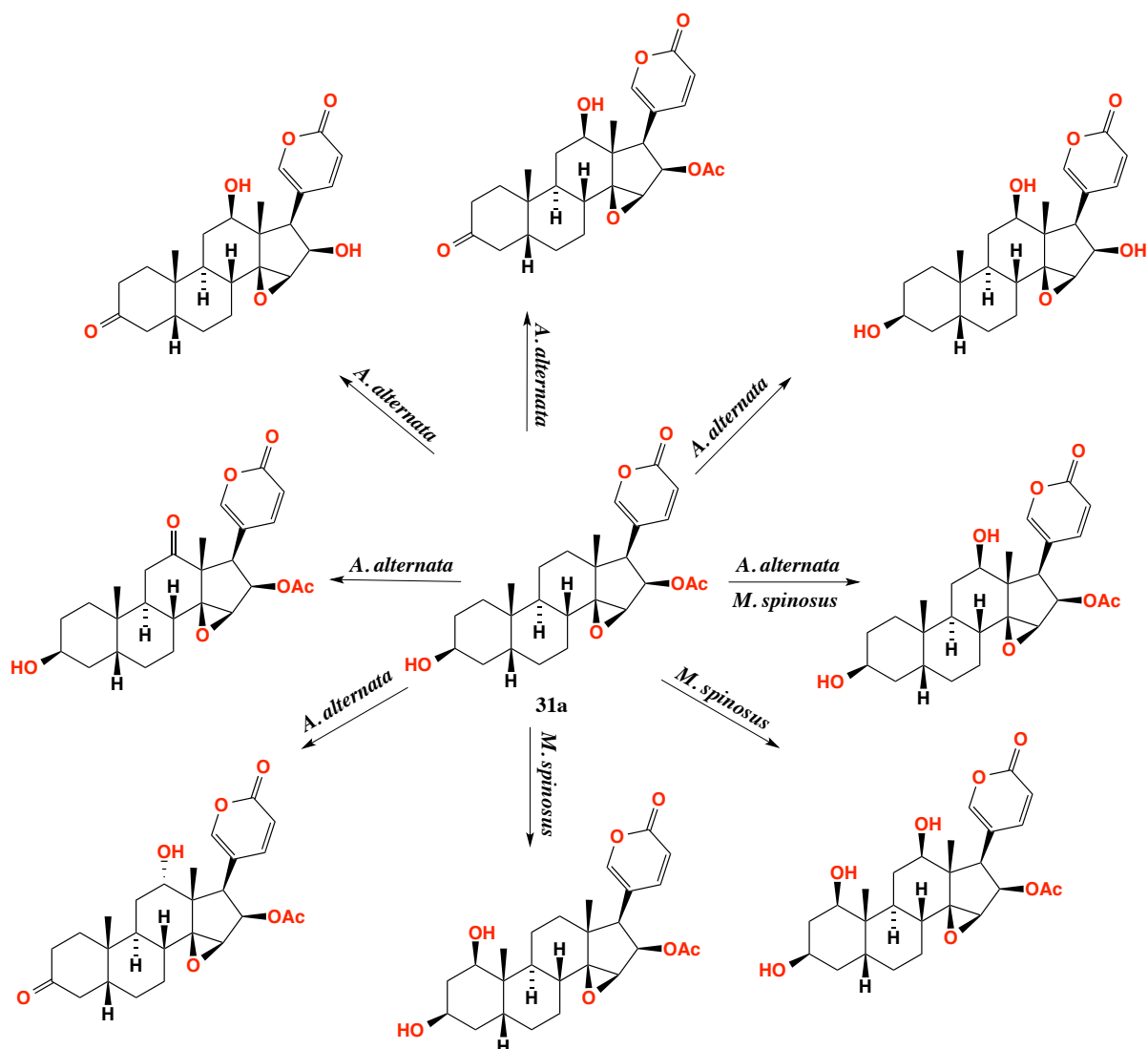
Figure 5.1 Biotransformation of cinobufagenin (**31a**) by *Alternaria alternata* and *Mucor spinosus* (Bhatti et al., 2012)

Table 5.1 List of bufagenins, biotransforming fungi and biotransformation products

Substrate	Fungi	No of Products	Reference
bufalin (**3a**)	*Mucor spinosus*	12	12
	Cunninghamella blakesleana	4	11
	Alternaria alternata	4	13
	Penicillium aurantigriseum	2	14
	Fusarium solani AS 3.1829	1	15
resibufagenin (**4a**)	*Mucor polymorphosporus*	22	11
	Mucor polymorphosporus	18	16
	Alternaria alternata	2	13
	Pseudomonas aeruginosa	1	6
	Pseudomonas aeruginosa	1	5
	Mucor subtilissimus	1	17
	Fusarium solani AS 3.1829	1	15
	Penicillium aurantigriseum	2	14
bufotalin (**30a**)	*Alternaria alternata*	3	18
cinobufagenin (**32a**)	*Alternaria alternata*	6	8
	Alternaria alternata	3	13
	Alternaria alternata	1	19
	Aspergillus niger	7	10
	Mucor spinosus	9	5
	Fusarium solani AS 3.1829	1	15
	Penicillium aurantigriseum	5	14
	Syncephalastrum racemosum	5	9

Table 5.2 List of bufagenins, biotransforming bacteria and biotransformation products

Substrate	Bacteria	No of Products	References
resibufagenin (**4a**)	*Nocardia* sp.	2	20
cinobufagenin (**32a**)	*Nocardia* sp	1	20
marinobufagenin (**1a**)	*Comamonas testorsteroni*	4	21
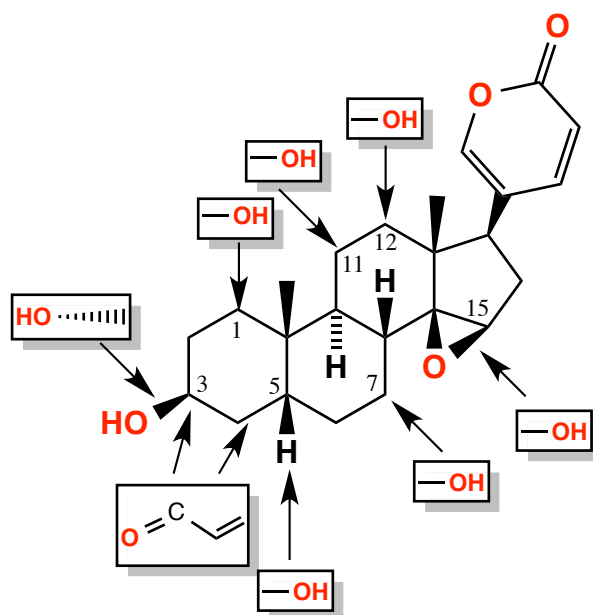
Figure 5.2 Modifications observed in biotransformation of bufagenins

Reported biotransformations of bufagenins exhibit a similarity as is evident from the biotransformation products. For instance, the most commonly observed biotransformation products are bufagenins that are 12β-hydroxylated and/or 7β-hydroxylated. Other frequent modifications include epimerization or oxidation at C-3, reduction/oxidation at C-5 and oxidation at C-15.

In an ecological context, the biotransformation of bufadienolides offers the potential to broaden the chemical diversity of the bufadienolides in the parotoid gland. However, most of the previous (published) biotransformation experiments were performed with microbes (fungi) which were not sourced from cane toads and hence, the biotransformation products previously reported are absent in parotoid secretions. In a recent report, our laboratory described the biotransformation of marinobufagenin (**1a**) by bacteria isolated from the cane toad parotoid secretion.[21] In that study, bacterial strains from the parotoid gland, ovary, tongue and stomach of a mature female cane toad were recovered and grown in liquid cultures in the presence of **1a**. The biotransforming strains were identified as *Comomonas testosteroni*, *Flavobacterium* sp. (both from parotoid gland) and *Acinetobacter johnsonii* (from the ovary).[21] *C. testosteroni* is a gram-negative bacterium that utilizes $C_{19} – C_{27}$ steroids as its carbon source for growth.[22-24] Exposure of marinobufagenin (**1a**) to liquid cultures of *Comomonas testosteroni* for 96 h, followed by solvent extraction and HPLC-DAD-ESI-MS analysis, yielded 3-epi-marinobufagenin (**17a**), 3-oxomarinobufagenin (**18a**), $\Delta^{1,4}$-3-oxoresibufogenin (**19a**) and $\Delta^{1,4}$-3-oxobufalin (**20a**) (Figure 5.3).

This observation supports the hypothesis that bacteria present in the parotoid gland may manipulate bufadienolide diversity. This process has the potential to be both advantageous, or disadvantageous to toad survival. For example, biotransformation could make the toxin more effective against range of predators and/or make it function in both aquatic and terrestrial environments. Alternatively, biotransformation could degrade bufadienolide reserves, rendering the toad less able to defend itself against predatory attacks.
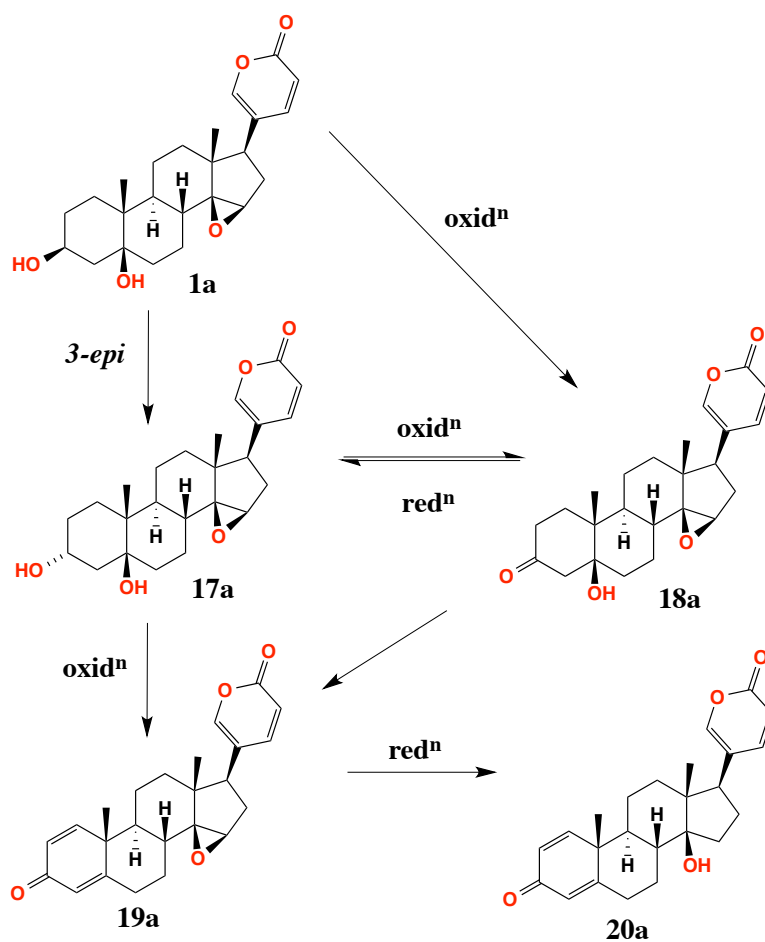
Figure 5.3 Biotransformation of marinobufagenin (**1a**) by *Comamonas testosteroni*. 3-epi-marinobufagenin (**17a**), 3-oxomarinobufagenin (**18a**), $\Delta^{1,4}$-3-oxoresibufogenin (**19a**), $\Delta^{1,4}$-3-oxobufalin (**20a**) (Hayes et al., 2009).[21]

Studies described earlier in the thesis revealed that parotoid toxins are stored as bufotoxins and are subjected to *ex situ* hydrolysis by BtH to form bufagenins and arginyl amides. *In situ* biotransformation of bufotoxins by bacteria is also worthy of investigation and are the basis of this chapter.

5.2 Results and discussion

5.2.1 Biotransformation of marinobufagenin

The capacity of *Comomonas testosteroni* (from parotoid gland) and *Acinetobacter johnsonii* (isolated from cane toad ovaries) to biotransform marinobufagenin (**1a**) was re-examined.[21] The strains were cultivated in nutrient broth (section 5.4.1.1) in the presence of **1a** and aliquots extracted with EtOAc at 24, 48 and 72 h intervals were dried under N_2 at 40 °C and re-dissolved in MeOH to a standard volume (500 μL) to generate analytes A70 – A72 (Scheme 5.1). These analytes were analysed using HPLC-DAD Method 1 (see Chapter 2) (Figure 5.4). Marinobufagenin (**1a**) extracted from nutrient broth was used as a negative control.
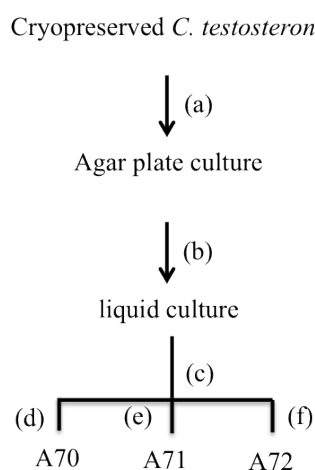
Cryopreserved *C. testosteroni*

(a)

Agar plate culture

(b)

liquid culture

(c)

(d)   (e)   (f)

A70   A71   A72

(a) – cryopreserved *C. testosteroni* recovered on nutrient agar plates
(b) – *C. testosteroni* cultivated in nutrient broth (5 mL) with marinobufagenin (**1a**)
(c) – Extraction with EtOAc, dried and re-dissolved in MeOH (100 μL)
(d) – after 24 h
(e) – after 48 h
(f) – after 72 h

Scheme 5.1 Preparation of analytes A70 – A72
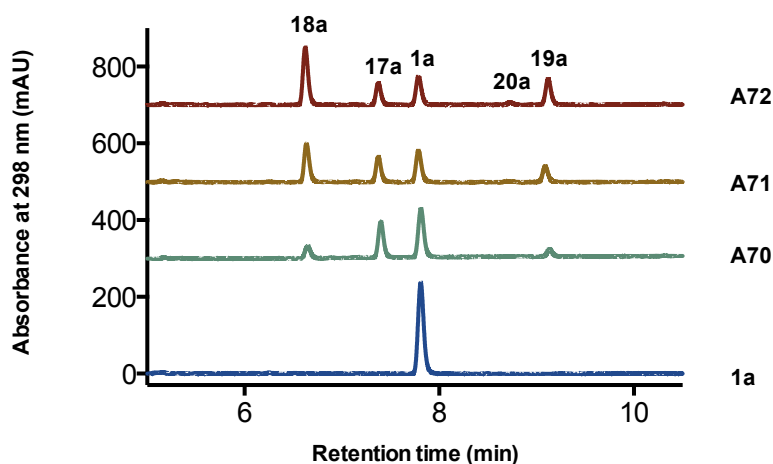
Figure 5.4 HPLC traces (298 nm) of analytes A70 - A72 analysed using Method 1. Marinobufagenin (**1a**), 3-epimarinobufagenin (**17a**), 3-oxomarinobufagenin (**18a**), $\Delta^{1,4}$-3-oxobufalin (**19a**) and $\Delta^{1,4}$-3-oxoresibufogenin (**20a**).

C. testosteroni transformed marinobufagenin (**1a**) into four products, 3-oxomarinobufagenin (**18a**), $\Delta^{1,4}$-3-oxoresibufogenin (**19a**), 3-epiresibufogenin (**17a**) and trace amounts of $\Delta^{1,4}$-3-oxobufalin (**20a**) (based on DAD response) as observed previously (Figure 5.4). The HPLC trace of analytes A70 - A72 showed marinobufagenin (**1a**) been depleted with simultaneous increase in the concentration of biotransformation products gradually over 72 h.

A. johnsonii strains were cultivated under the same condition as described above for *C. testosteroni* in the presence of marinobufagenin (**1a**) with sampling at 24, 48 and 72 h intervals generating analytes A73 – A75 (Scheme 5.2). Marinobufagenin (**1a**) extracted from uninoculated nutrient broth was used as a negative control. These analytes were analysed using the HPLC-DAD Method 1 (see Chapter 2) (Figure 5.5). *A. johnsonii* was found to transform marinobufagenin (**1a**) into three different products, 3-epimarinobufagenin (**17a**), 3-oxomarinobufagenin (**18a**) and $\Delta^{1,4}$-3-oxobufalin (**20a**) (Figure 5.5), concurred with the results obtained previously by Hayes et al.[21]

(a) – cryopreserved *A. johnsonii*, recovered on nutrient agar plates
(b) –of *A. johnsonii* cultivated in nutrient broth (5 mL) with marinobufagenin (**1a**)
(c) – Extraction of cultures with EtOAc, dried and re-dissolved in MeOH (100 μL)
(d) – after 24 h
(e) – after 48 h
(f) – after 72 h

Scheme 5.2 Preparation of analytes A73 – A75
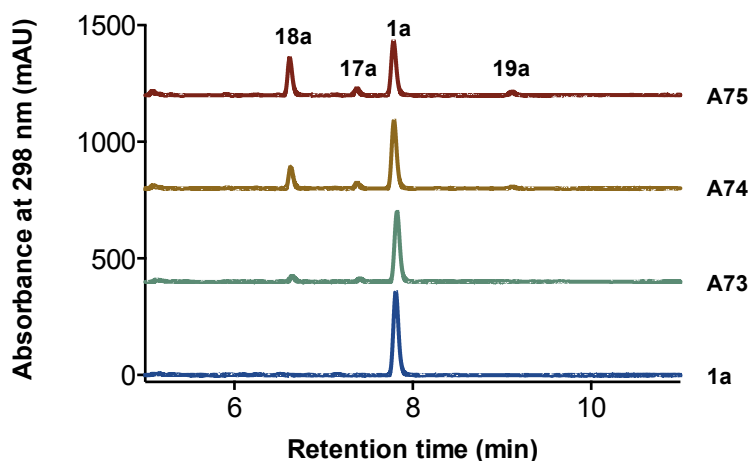
Figure 5.5 HPLC traces (298 nm) of analytes A73 - A75 analysed using Method 1. Marinobufagenin (**1a**), 3-epimarinobufagenin (**17a**), 3-oxomarinobufagenin (**18a**) and $\Delta^{1,4}$-3-oxoresibufogenin (**19a**).

marinobufotoxin (**1c**)

marinobufagenin-3-suberate (**1b**)

marinobufagenin (**1a**)
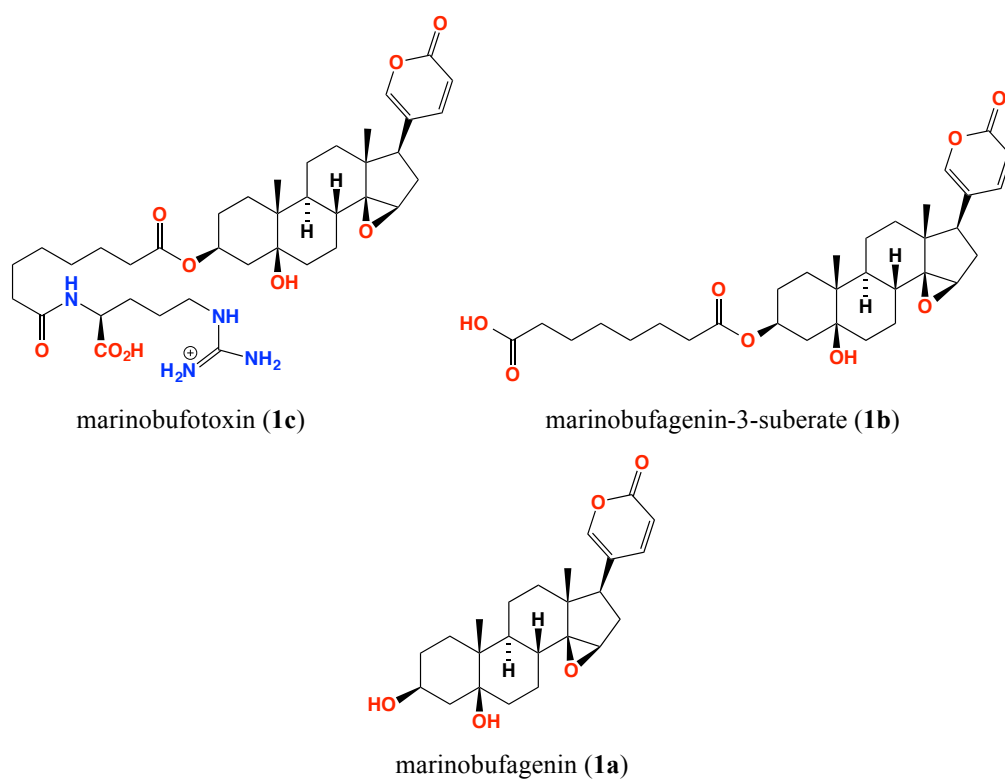
5.2.2 Biotransformation of marinobufotoxin (1c)

The objective of this study was to determine if *Comomonas testosteroni* (from parotoid gland) and *Acinetobacter johnsonii* (from ovaries) could biotransform marinobufotoxin (**1c**).[21] *C. testosteroni* strains were cultivated in nutrient broth (as described above) in the presence of marinobufotoxin (**1c**) (10 mg/mL; 50 µL) with *n*-BuOH extracts prepared at 24, 48 and 72 h intervals dried under N_2 at 40 °C and re-dissolved in MeOH to a standard volume (500 µL) to generate analytes A76 – A78 (Scheme 5.3). These analytes were analysed using the HPLC-DAD Method 1 (see Chapter 2)

(Figure 5.6). Since bufagenins were the expected biotransformation products, Method 1 was applied instead of Method 2, which is specific for bufotoxins.

(a) – cryopreserved *C. testosteroni,* recovered on nutrient agar plates
(b) – *C. testosteroni* cultivated in nutrient broth (5 mL) with marinobufotoxin (**1c**)
(c) – Extraction with *n*-BuOH, dried and re-dissolved in MeOH (100 µL)
(d) – after 24 h
(e) – after 48 h
(f) – after 72 h

Scheme 5.3 Preparation of analytes A76 – A78
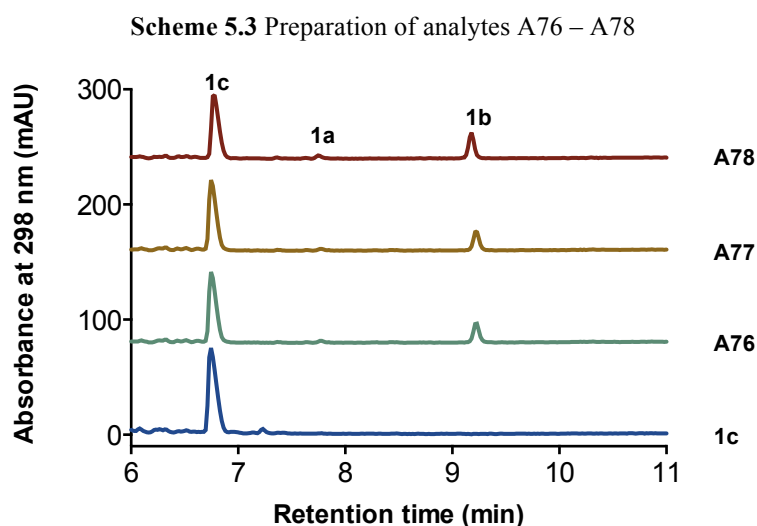
Figure 5.6 HPLC traces (298 nm) of analytes A76 – A78 analysed using Method 1. Marinobufotoxin (**1c**), marinobufagenin hemisuberate (**1b**) and marinobufagenin (**1a**).

C. testosteroni cultures exposed to marinobufotoxin (**1c**) did not show significant biotransformation to **1a**. A small percentage of **1c** was converted into marinobufagenin hemisuberate (**1b**) (11%) and marinobufagenin (**1a**) (3%) (Figure 5.6). This result suggests that C-3 suberoylarginine conjugates are resistant to bacterial biotransformation.

A. johnsonii strains were cultivated in nutrient broth (as described above) in the presence of marinobufotoxin (**1c**) (10 mg/mL; 50 µL) with *n*-BuOH extracts prepared at 24, 48 and 72 h intervals dried under N_2 at 40 °C and re-dissolved in MeOH to a standard volume (500 µL) to generate analytes A79 – A81 (Scheme 5.4). These analytes were then analysed using HPLC-DAD

Method 1 (see Chapter 2) (Figure 5.7). Marinobufotoxin (**1c**) extracted from uninoculated nutrient broth was used as negative control.
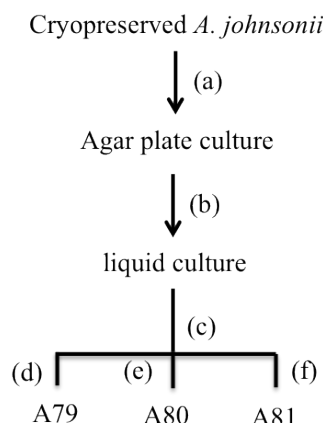
(a) – cryopreserved *A. johnsonii*, recovered on nutrient agar plates
(b) – *A. johnsonii* cultivated in nutrient broth (5 mL) with marinobufotoxin (**1c**)
(c) – Extraction of cultures with *n*-BuOH, dried and re-dissolved in MeOH (100 μL)
(d) – after 24 h
(e) – after 48 h
(f) – after 72 h

Scheme 5.4 Preparation of analytes A79 – A81
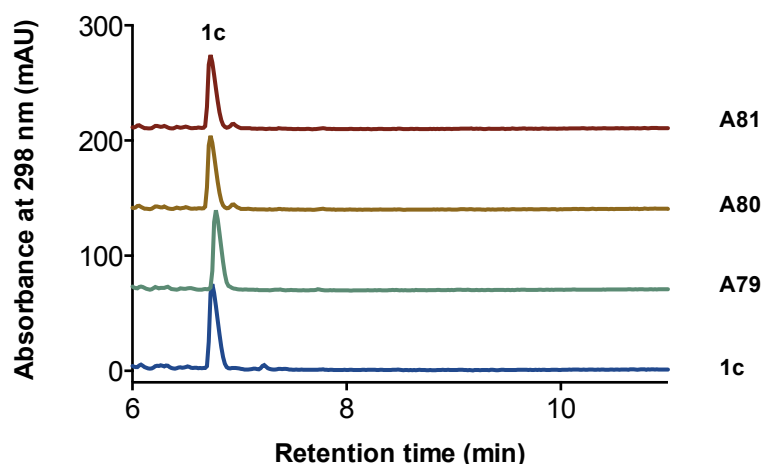
Figure 5.7 HPLC traces (298 nm) of analytes A79 – A81 analysed using Method 1. Marinobufotoxin (**1c**).

A. johnsonii cultures did not show biotransformation against **1c** (Figure 5.7). These analyses clearly indicate that bufotoxins are largely resistant to microbial biotransformation by the two bacterial isolates recovered from the parotoid gland.

The above observations suggest that biotransforming bacteria present in the parotoid glands are opportunistic as the bacteria could possibly utilize bufagenins in parotoid secretions (post predatory attack) as a source of carbon for growth. This observation does not favour the previous hypotheses by Hayes et al that *in situ* parotoid gland biotransforming bacteria could play a role in

diversification of parotoid chemistry. However, identification of microbes that could transform bufagenins into other bufagenin analogues found in parotoid secretions would be the key to suggest diversification of cane parotoid chemistry.

5.2.3 Biotransformation of marinobufagenin-3-suberate (1b)

During the biotransformation of marinobufotoxin (**1c**) by *C. testosteroni*, it was observed that a small fraction was converted into **1b** and a much smaller amount into **1a**. This raised the possibility that if *C. testosteroni* cultures was exposed to marinobufotoxin (**1c**) for an extended time period, this may convert **1b** into **1a**. To test this hypothesis, synthetic marinobufagenin hemisuberate (**1b**) (see Chapter 2), was subjected to biotransformation by *C. testosteroni* (Figure 5.8) and *A. johnsonii* (Figure 5.9). *C. testosteroni* strains cultivated in nutrient broth (as described above) in the presence of **1b** (10 mg/mL; 50 μL) were extracted with *n*-BuOH at 24, 48 and 72 h intervals, and the extracts were dried under N_2 at 40 °C and re-dissolved in MeOH to a standard volume (500 μL) to generate analytes A82 − A84 (Scheme 5.5). These analytes were analysed using HPLC-DAD Method 1. Marinobufagenin-3-suberate (**1b**) extracted from uninoculated nutrient broth was used as a negative control.

Cryopreserved *C. testosteroni*

↓ (a)

Agar plate culture

↓ (b)

liquid culture

(c)

(d)   (e)   (f)

A82   A83   A84
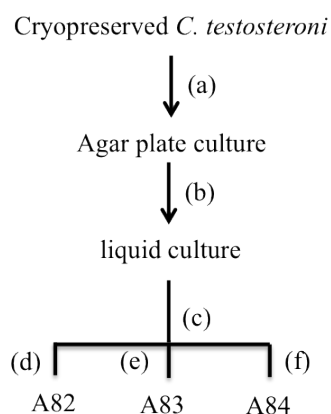
(a) – cryopreserved *C. testosteroni,* thawed and cultivated on nutrient agar plates at 26.5 °C
(b) – *C. testosteroni* cultivated in nutrient broth (5 mL) with marinobufagenin-3-suberate (**1b**)
(c) – Extraction with *n*-BuOH, dried and re-dissolved in MeOH (100 μL)
(d) – after 24 h
(e) – after 48 h
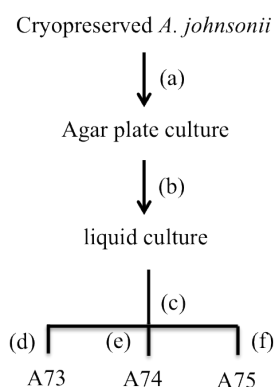**(f)** – after 72 h

Scheme 5.5 Preparation of analytes A82 − A84
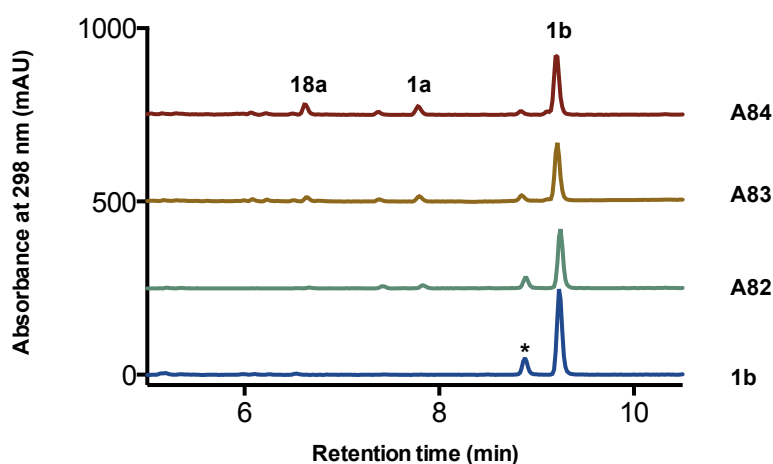
Figure 5.8 HPLC traces (298 nm) analytes A82 – A84 analysed using Method 1.marinobufagenin hemisuberate (**1b**), marinobufagenin (**1a**), 3-oxomarinobufagenin (**18a**) and * contaminant.

C. testosteroni cultures exposed to marinobufagenin-3-suberate (**1b**) did not show significant biotransformation (Figure 5.8). The HPLC trace also shows the formation of trace amounts of **1a** and **18a**, the latter as a biotransformation product of **1a** (as shown earlier).

A. johnsonii strains cultivated in nutrient broth (as described earlier) in the presence of **1b** (10 mg/mL; 50 μL) were extracted with *n*-BuOH at 24, 48 and 72 h intervals and the extracts dried under N_2 at 40 °C and re-dissolved in MeOH to a standard volume (500 μL) to generate analytes A85 – A87 (Scheme 5.6). The analytes A85 – A87 were analysed using HPLC-DAD Method 1 (Figure 5.9). Marinobufagenin-3-suberate (**1b**) extracted from uninoculated nutrient broth was used as a negative control. *A. johnsonii* cultures exposed to **1b** failed to show significant biotransformation, with 14% conversion to **1a** over 72 h compared to 15% in the case of *C. testosteroni*.
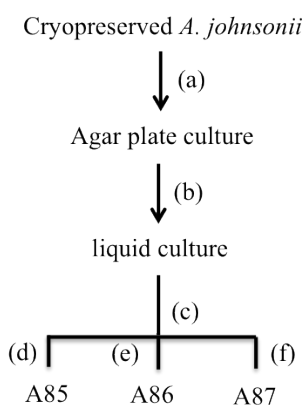
(a) – cryopreserved *A. johnsonii,* recovered on nutrient agar plates at 26.5 °C
(b) – *A. johnsonii* cultivated in nutrient broth (5 mL) with marinobufagenin-3-suberate (**1b**)
(c) – Extraction of cultures with *n*-BuOH, dried and re-dissolved in MeOH (100 μL)
(d) – after 24 h
(e) – after 48 h
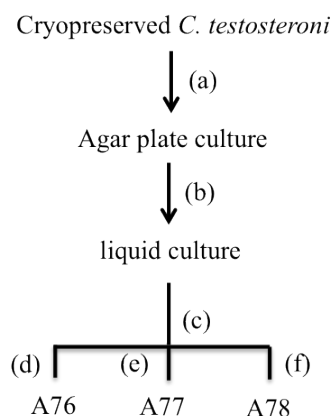**(f)** – after 72 h

Scheme 5.6 Preparation of analytes A85 – A87
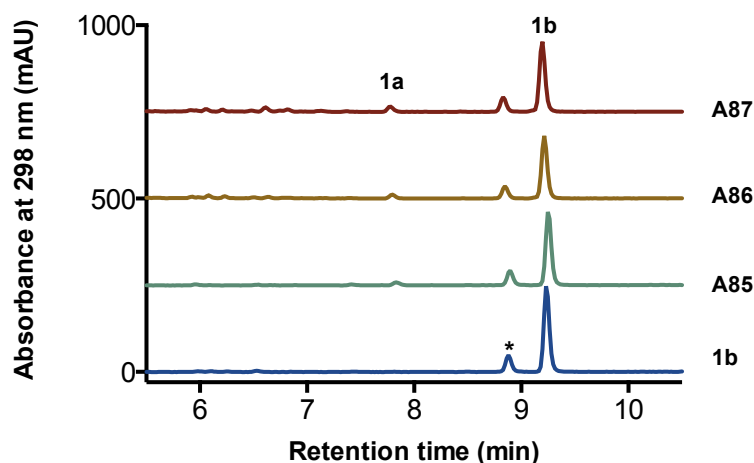
Figure 5.9 HPLC traces (298 nm) of analytes A85 – A87 analysed using Method 1. Marinobufagenin hemisuberate (**1b**), marinobufagenin (**1a**) and * contaminant.

5.2.4 Biotransformation of other bufagenins

5.2.4.1 Biotransformation of telocinobufagenin (2a)

As the microbial biotransformation of cane toad bufagenins by the bacteria isolated from parotoid glands and ovaries resulted in significant degradation of marinobufagenin we investigated the effect on other bufagenins, namely bufalin (**3a**) and telocinobufagenin (**2a**). These are the second and third most dominant bufadienolides in the cane toad parotoid secretions.

A. johnsonii strains cultivated in nutrient broth (as described earlier) in the presence of telocinobufagenin (**2a**) were extracted with EtOAc at 72 h and the extracts dried under N_2 at 40 °C and re-dissolved in MeOH to a standard volume (500 μL) to generate analyte A88 (Scheme 5.7). Analyte A88 was analysed using HPLC-DAD Method 1 (Figure 5.10). Telocinobufagenin (**2a**) extracted from uninoculated nutrient broth was used as a negative control.
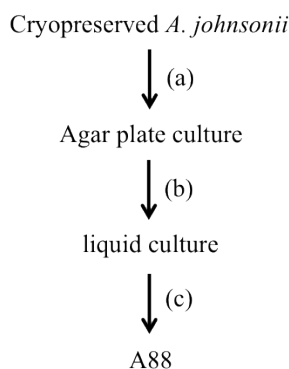
(a) – cryopreserved *A. johnsonii,* recovered on nutrient agar plates
(b) – *A. johnsonii* cultivated in nutrient broth (5 mL) with telocinobufagenin (**2a**)
(c) – Extraction of cultures with EtOAc after 72 h, dried and re-dissolved in MeOH (100 μL)

Scheme 5.7 Preparation of analyte A88

Biotransformation of **2a** (*m/z* (M+H)$^+$, 403) after 72 h showed the presence of two degradation products with *m/z* (M+H) values 401 and 383 respectively (Figure 5.11). Since **2a** is also a similar bufagenin to **1a**, we anticipated a similar microbial biodegradation. Therefore, the peak corresponding to *m/z* 401 was attributed to the C-3 oxidation product, 3-oxotelocinobufagenin (**21a**) while *m/z* 383 was attributed to $\Delta^{4,5}$-3-oxobufalin (**22a**). Hence the biotransformation steps for **2a** possibly involve the typical oxidation/dehydration products as observed previously for **1a** (Figure 5.12).
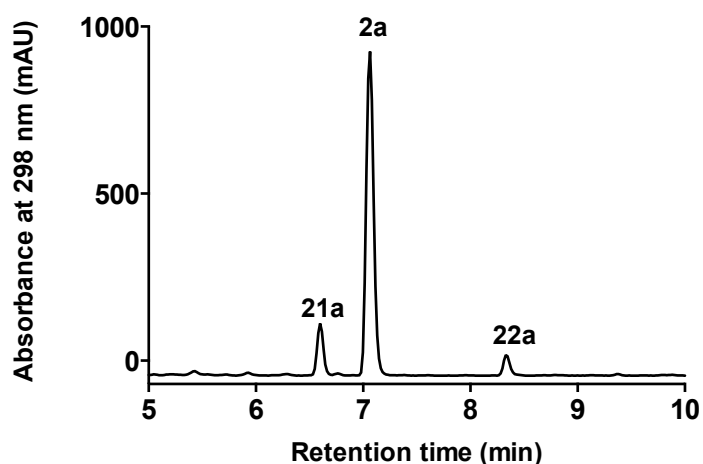
Figure 5.10 HPLC trace (298 nm) of analyte A88. Telocinobufagenin (**2a**), 3-oxotelocinobufagenin (**21a**), $\Delta^{4,5}$-3-oxobufalin (**22a**)
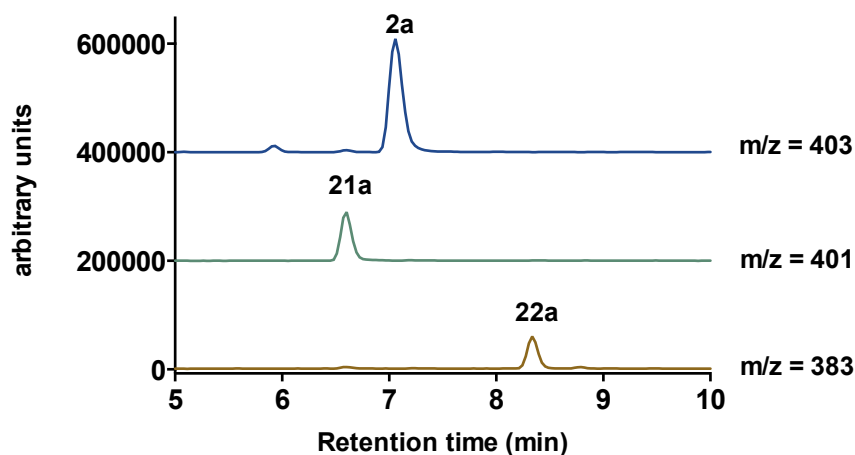
Figure 5.11 Single ion-extraction of analyte A88. Telocinobufagenin (**2a**), 3-oxotelocinobufagenin (**21a**), $\Delta^{4,5}$-3-oxobufalin (**22a**)
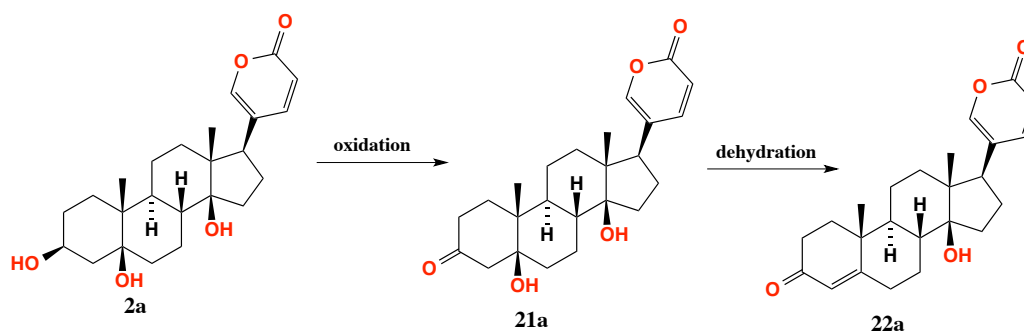
Figure 5.12 Proposed scheme and biotransformation products of telocinobufagenin (**2a**) by *A. johnsonii*. Telocinobufagenin (**2a**), 3-oxotelocinobufagenin (**21a**), $\Delta^{4,5}$-3-oxobufalin (**22a**)

5.2.4.2 Biotransformation of bufalin (3a)

Following the successful biotransformation of **2a** by *A. johnsonii*, a sample of bufalin (**3a**) was subjected to degradation by *A. johnsonii*. *A. johnsonii* strains cultivated in nutrient broth (as described earlier) in the presence of bufalin (**3a**) were extracted with EtOAc after 72 h, dried under N₂ at 40 °C and re-dissolved in MeOH to a standard volume (500 μL) to generate analyte A89 (Scheme 5.8). The analyte A89 was analysed using HPLC-DAD Method1 (Figure 5.13). Bufalin (**2a**) extracted from uninoculated nutrient broth was used as a negative control.
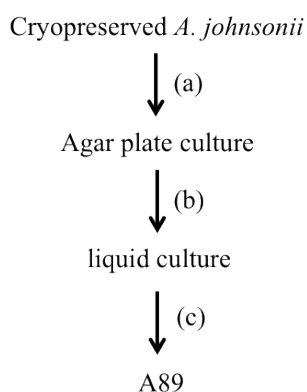
Cryopreserved *A. johnsonii*

↓ (a)

Agar plate culture

↓ (b)

liquid culture

↓ (c)

A89

(a) – cryopreserved *A. johnsonii*, recovered on nutrient agar plates
(b) –*A. johnsonii* cultivated in nutrient broth (5 mL) with bufalin (**3a**)
(c) – Extraction of cultures with EtOAc after 72 h, dried and re-dissolved in MeOH (100 μL)

Scheme 5.8 Preparation of analyte A89

Biotransformation of **3a** (*m/z* (M+H)⁺, 387) showed the presence of two degradation products with *m/z* (M+H) values of 387 and 385 respectively (Figure 5.13). A total ion current (negative mode) indicated the presence of two bufagenins eluting at the same time with the *m/z* 385 (Figure 5.14A). A single ion extraction revealed the presence of a bufagenin with m/z 387 (Figure 5.14B). Since, **3a** is structurally similar to **1a**, we anticipated a similar response to microbial biotransformation (as mentioned above), which permits assignment of *m/z* 387 as 3-epibufalin (**23a**). Of note, 3-epibufalin (**23a**) was previously reported as a degradation product in the biotransformation of **3a**

with *Penicllium aurantigriseum* and *Mucor spinosus* as well as treatment with human plasma.[12, 14, 25] The second degradation product, which corresponded to *m/z* 385 was attributed to 3-oxobufalin (**24a**), as observed previously in the biotransformation of **1a** and **2a**, and an oxidation product of either **3a** or 3-epibufalin (**23a**). The biotransformation products of **3a** by *A. johnsonii* matched with the biotransformation products of **3a** with the fungi *Penicillium aurantigriseum*.[14] Hence the biotransformation steps for **3a** possibly involve the typical oxidation products as observed with **1a** (Figure 5.15).
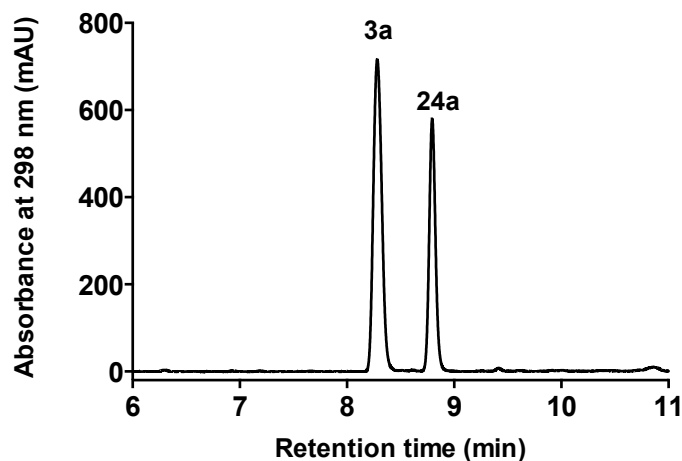
Figure 5.13 HPLC traces (298 nm) of A89 analysed using Method 1. Bufalin (**3a**), 3-oxobufalin (**24a**)
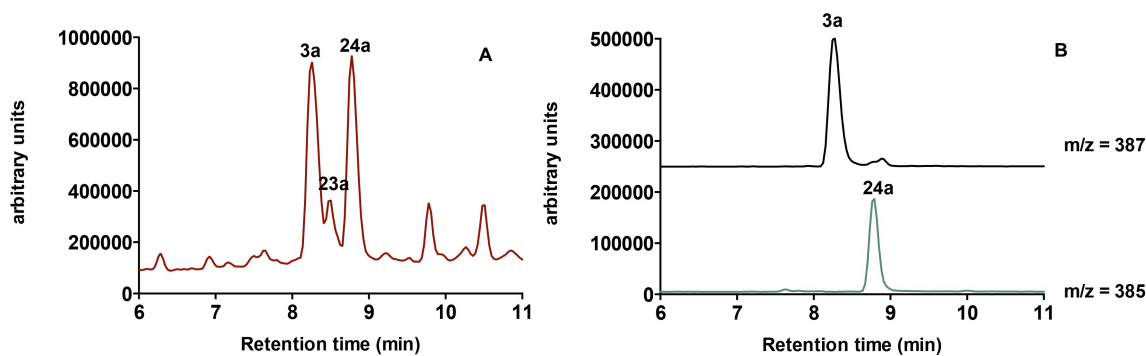
Figure 5.14 A – HPLC-DAD-MS analysis revealing total ion current (negative reflectron mode) indicating the presence of bufalin (**3a**), 3-epibufalin (**23a**) and 3-oxobufalin (**24a**). B - HPLC-DAD-MS analysis revealing single ion-extraction of analyte A89. Bufalin (**3a**) and 3-oxobufalin (**24a**)
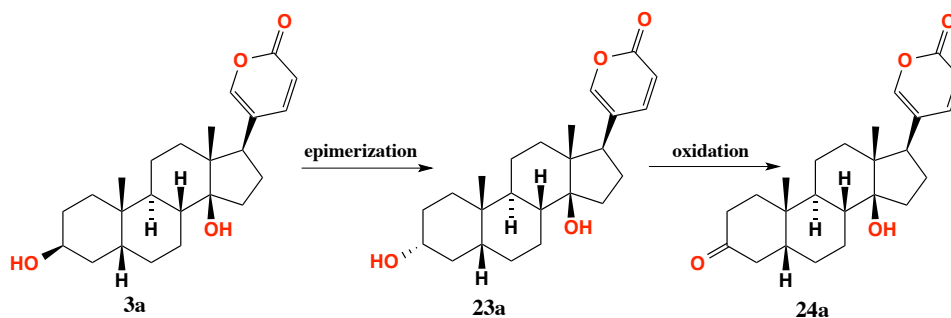
Figure 5.15 Proposed scheme and biotransformation products of bufalin (**3a**) by *A. johnsonii*. Bufalin (**3a**) and 3-oxobufalin (**24a**)

5.2.4.3 Discussion – biotransformation of bufagenins, bufotoxins and bufagenin-3-suberate

Biotransformation of **1c** and **1b** by biotransforming bacteria did not show significant modification (as in the case of **1a**) but a small fraction was transformed into marinobufagenin (**1a**). This may indicate that, only a sub-population of biotransforming bacteria is active against bufotoxins, or that the kinetics are very slow and inefficient. This observation also shows why biotransformation products of **1a** (such as **17a**, **18a**, **19a** and **20a**) are not identified in parotoid toxin. Several advantages of biosynthesizing toxins as bufotoxins have been considered (see Chapter 3) but one of the major concerns was the stability of the toxins to microbial biodegradation. Since the bufotoxins are resistant to microbial biotransformation, it is possible that *cane toads have developed a strategy to resist/overcome the microbial biodegradation of the parotoid toxins by storing bufadienolides as bufotoxins*. If toxins were stored as bufagenins, the steroid-degrading microbes would thrive in a steroid-rich environment leading to the degradation of stored toxins, and adversely impacting the chemical defence of the cane toad.

5.2.5 Identification of new bufagenin transforming microbes from parotoid gland and secretions

Given the success in documenting the biotransforming properties of the cane toad microbes (*C. testosteroni* and *A. johnsonii*), an effort was made to isolate additional biotransforming microbes. More specifically, consideration was given to isolation and characterization of microbes that could modify and diversify the structure of bufadienolides without causing degradation, as such microbes would be potent and beneficial to the cane toad.

Parotoid secretion from one of the parotoid glands from two toads was directly squeezed into sterile water and an aliquot was directly plated onto a nutrient agar plate and incubated at 26.5 °C for 7 days. The other parotoid gland from two toads were excised and an incision was made using fine scissors on the ventral side and a swab of the cut side was applied to a nutrient agar plate and incubated for 26.5 °C for 7 days. Microbial flora on the surface of the parotoid gland were isolated using the former approach while the latter method retrieved microbial flora present within parotoid gland. A 7-day incubation was deemed estimal as it would reveal both bacteria (unicellular as well as sporulating) as well as fungi. Individual colonies were selected and plated on a nutrient agar medium and incubated for 2 days for unicellular bacteria, 3 days for spore-producing bacteria and 7 days for fungi at 26.5 °C. A total of 68 strains were isolated including bacteria (63) and fungi (5) based on the morphology of the colonies.

Previously, all the biotransformation experiments with bufagenin, bufotoxins and bufagenin suberates were performed using microbial culture tubes (5 mL) on the previously isolated two active biotransforming strains, *C. testosteroni* and *A. johnsonii*. To explore the biotransforming potential of a library of 68 strains required a semi-high throughput technique. Hence, a 24-well micro bioreactor approach was used to assess such strains capable of transforming marinobufagenin (**1a**). This micro bioreactor based approach was previously optimized by Dr Zeinab Khalil from the Capon group. Micro bioreactors are valuable replacements of a traditional shaker flask for the cultivation of microbes in low volumes. Various compartments of micro bioreactor is illustrated in Figure 5.16.
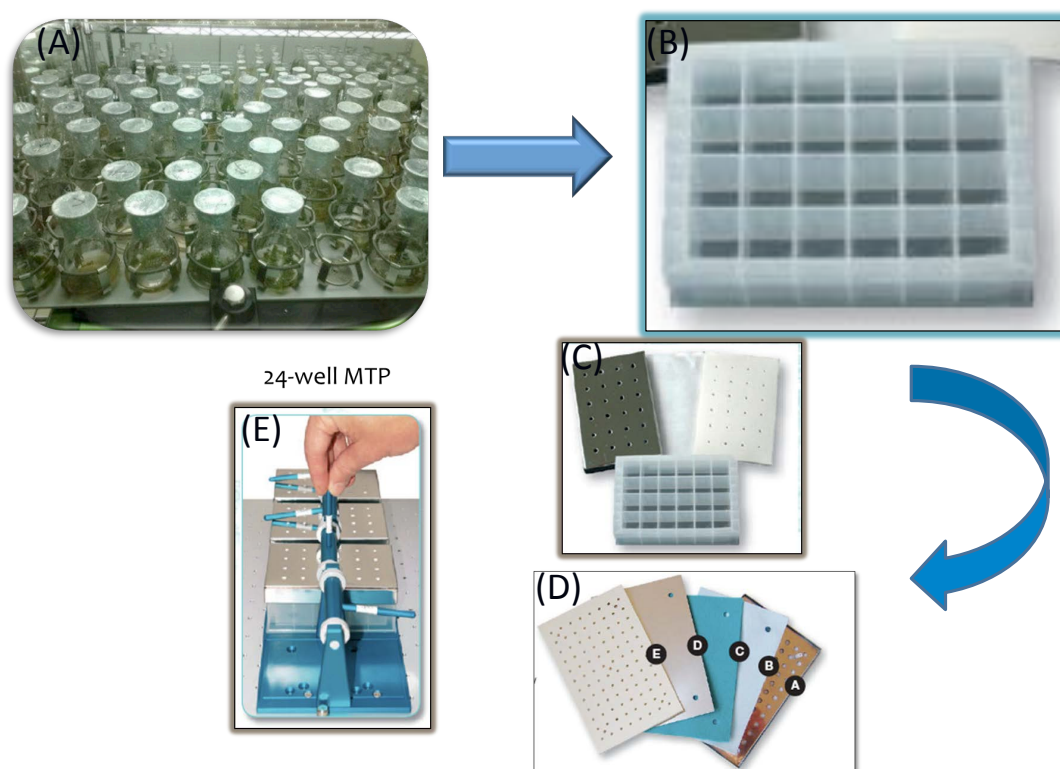
Figure 5.16 Applikon bioreactor system; (A) traditional shake flasks, (B) 24-well microbioreactor plate, (C) stainless steel cover, (D) sandwich covers, (E)- plate holder

Micro bioreactors consist of a 24 well plate for cultivation of microbes over which goes the sandwich covers providing space for aeration. The whole set up is held together by a stainless steel cover following which the micro reactors are clamped to a support, which is then subjected to constant shaking. Micro bioreactors were previously used for cultivating microorganisms in small volumes, however, the growth characteristics and secondary metabolism production is comparable with shaker flasks. [17] Hence, the micro bioreactor based cultivation of microbes was performed in the presence of a bufagenin while microbes cultured without a bufagenin served as a negative

control. A single colony from the agar plate was picked and cultured onto a nutrient broth in a micro bioreactor, sealed with a lid. Marinobufagenin (**1a**) (15 mg/mL; 3 μL) was added to the cultures after 12 h of incubation and further incubated for 36 h for bacteria and 84 h for fungi followed by extraction with EtOAc. The EtOAc extracts were dried *in vacuo* and re-dissolved in MeOH (50 μL) to generate analytes A90 − A157, which were analysed using Method 1 (Scheme 5.9).

B. marinus

Toad 1
(94 g, ♀)

Toad 2
(98 g, ♂)

(a) (b)

(a) (b)

CMB-TD03 − 25   CMB-TD26 − 38

CMB-TD39 − 56   CMB-TD57 − 70

(c)   (c)   (c)   (c)

liquid cultures   liquid cultures   liquid cultures   liquid cultures

(d)   (d)   (d)   (d)

A90 − A112   A113 − A125   A126 − A143   A144 − A157
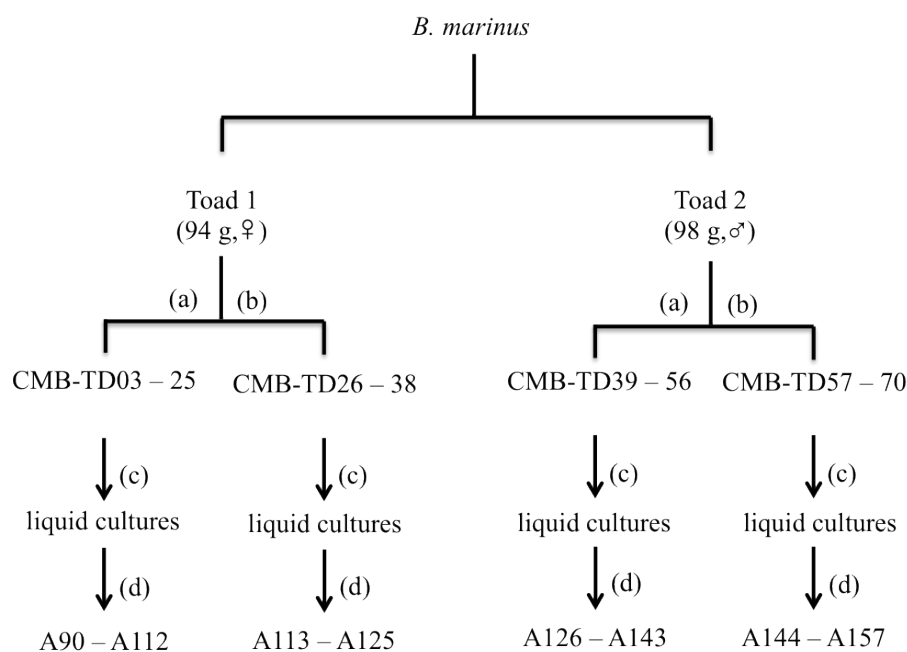
(a) – Left parotoid gland washed with H₂O, squeezed into sterile H₂O and an aliquot (50 μL) swabbed on to a nutrient agar plate, incubated for 7 days at 26.5 °C, subsequent culturing of each microbe on to a nutrient agar plate and further incubation for 7 days at 26.5 °C.
(b) – Right parotoid gland washed with H₂O, incised on dorsal epithelium and swabbed directly on to a nutrient agar plate, incubated for 7 days at 26.5 °C, subsequent culturing of each microbe on to a nutrient agar plate and further incubation for 3 days at 26.5 °C.
(c) – Pure colonies of microbes cultivated in nutrient broth (2 mL) in 24-well plates with marinobufagenin (1a) (15 mg/mL; 3 μL) for 48 h (bacteria) and 96 h (fungi)
(d) – extraction with EtOAc, dried and re-dissolved in MeOH (50 μL)

Scheme 5.9 Preparation of analytes A90 − A157

Only 4 out of 68 strains exhibited an ability to biotransform **1a** with two strains (CMB-TD-29 and CMB-TD-59) showing significant levels of biotransformation, and the remaining two only moderate levels. Interestingly, the two strains that showed highest biotransformation activity were isolated from the ventral part of the parotoid gland (*in situ*) and exhibited similar biotransformation products. The morphology of two strains resembled bacteria, one with rough colonies (white) while the other with rough to smooth colonies (off-white). Taxonomic classification remains a work-in-progress. In the former two closely eluting peaks with the same *m/z* (M+H) value of 417 were detected, along with *m/z* 363 (**25a**) and *m/z* 345 (**27a**) (Figure 5.17). The peak *m/z* 417 was identical to arenobufagenin (**6a**, *m/z* 417) previously identified by Hayes et al and confirmed with co-injection with an authentic standard (in-house library).[21] The UV profile of all biotransformed

products exhibited a characteristic bufadienolide spectrum. Another peak eluting closer to **6a** was tentatively identified as the C-3 epimer **23a**, a biotransformation seen in earlier studies. The two bacterial strains also significantly transformed **1a** to **6a** (44%) and also exhibited moderate conversion of **1a** to **26a** (12%).
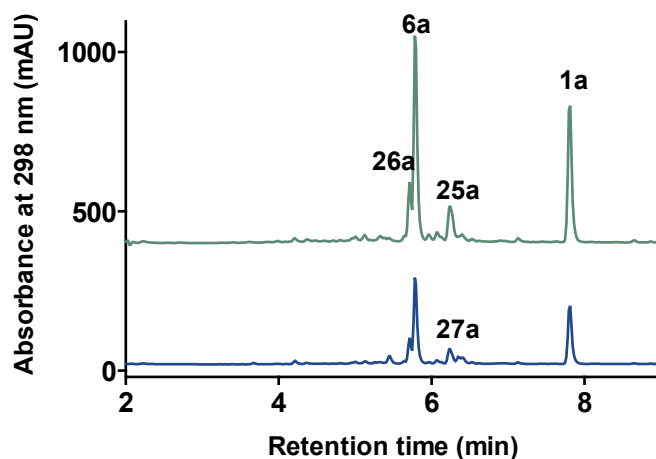
Figure 5.17 HPLC traces (298 nm) of analytes A119 (green) and A148 (blue) analysed using Method 1. Arenobufagenin (**6a**), *m/z* 363 Da (**25a**), *m/z* 417 (**26a**)

arenobufagenin (**6a**)   3-epiarenobufagenin
                                  (possible **26a**)
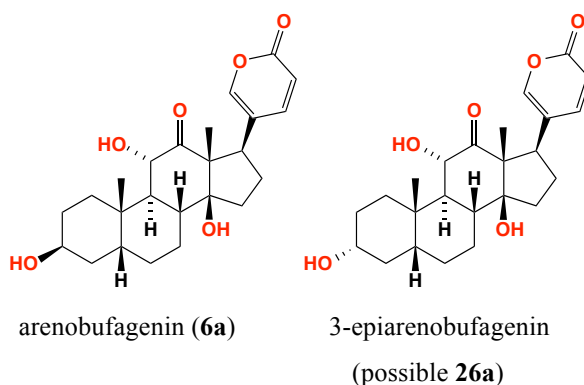
Two bacterial strains, isolated from the exterior of the parotoid gland (*ex situ*) (CMB-TD22) (A109) and the inner part of the parotoid gland (*in situ*) (CMB-TD37) exhibited moderate and low levels of biotransformation of marinobufagenin, respectively. The strains also exhibited the same biotransformation products as indicated by the retention of the compounds, *m/z* values and the UV profiles (Figure 5.18). Three compounds were detected but surprisingly all the compounds exhibited the same molecular mass, *m/z* 419 (Figure 5.18). CMB-TD22 (A109) showed moderate levels of biotransformation to yield uncharacterized metabolites **28a** (11%), **29a** (7%) and **30a** (12%), while CMB-TD37 (A124) exhibited lower levels of transformation to yield **28a** (2%), **29a** (4%) and **30a** (4%).
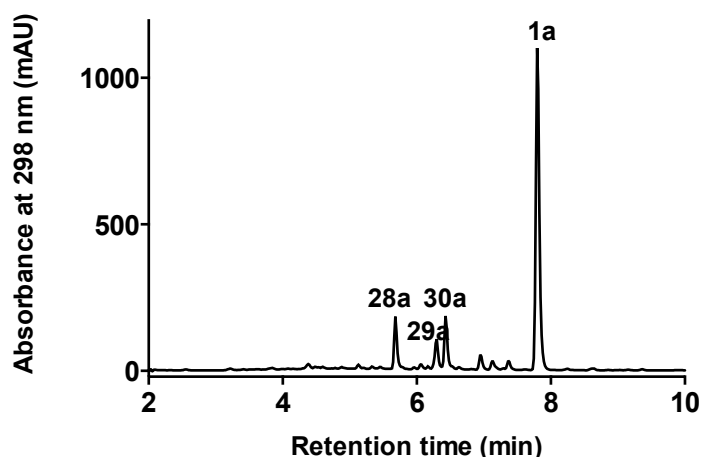
Figure 5.18 HPLC trace (298 nm) of A109 derived from CMB-TD22 analysed using Method 1. *m/z* 419 (**28a**), *m/z* 419 (**29a**), *m/z* 419 (**30a**)

A fungal strain (CMB-TD-42), isolated form the skin of the parotoid gland was cultivated in the presence of **1a** resulting in lower levels of biotransformation (Figure 5.19). Two biotransformation products, **6a** and **31a**, were identified based on the retention time, *m/z* values and the UV profile. Also, the UV profile of the biotransformation products exhibited a characteristic bufadienolide spectrum. The retention time and the *m/z* value of the peak at t_R = 5.7 min also matched with the retention time of **6a. 31a** was also *m/z* 417, which tentatively identified as an epimer of **6a** as described with bufagenins.
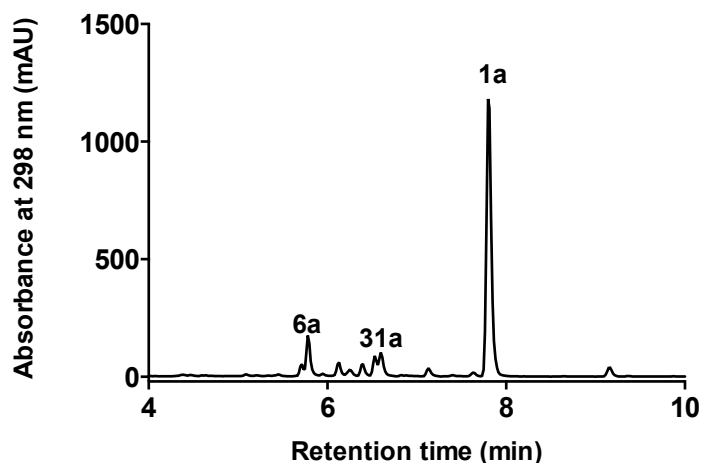
Figure 5.19 HPLC trace (298 nm) of A129 derived from CMB-TD42 analysed using Method 1. Arenobufagenin (**6a**), *m/z* 417 (**31a**)

Comparison of these most recent biotransformation trial with those reported by Hayes et al. clearly indicated the presence of bufagenin degrading microbes in the parotoid glands (from within and surface), however, the biotransformation products and the mechanism of degradation of the newly isolated microbes were different from that previously described.

secretion

marinobufagenin (**1a**)

ex situ

BtH

in situ

2c, **3c**, ← marinobufotoxin (**1c**) → **consume**
4c and **5c**

diversify

storage

Type II: Microbes   Type I: Microbes
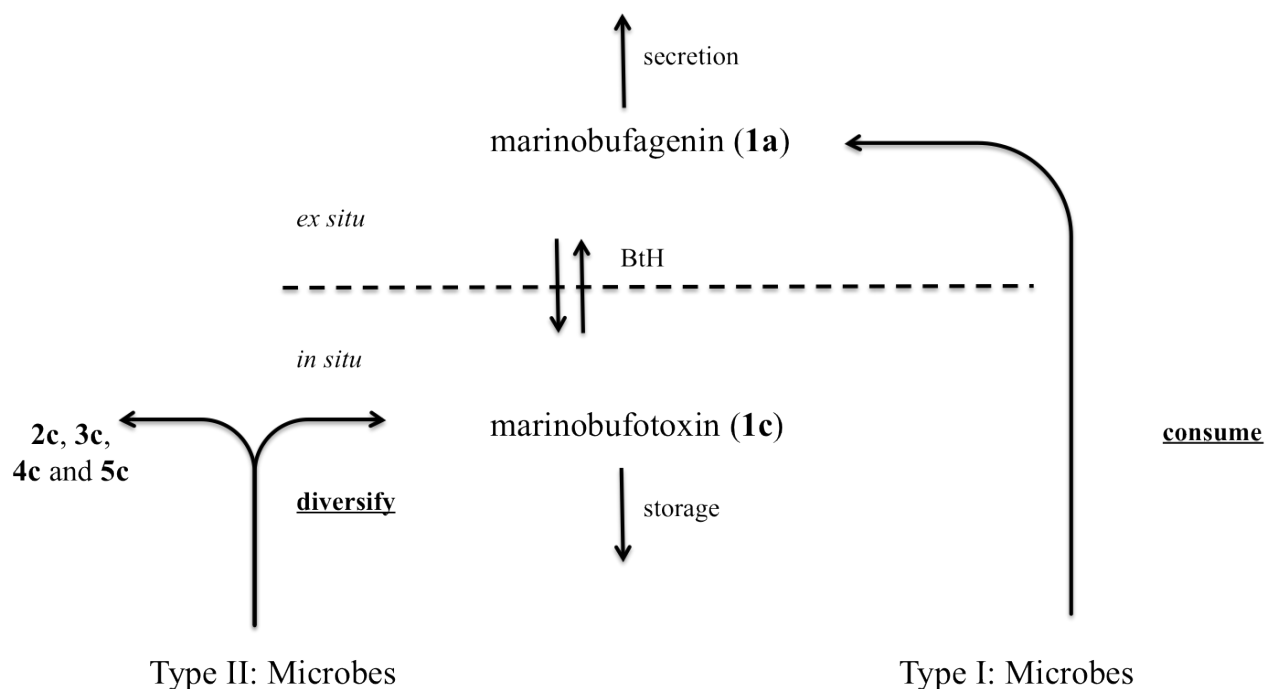
- transform bufotoxins/bufagenins
- enhance chemical diversity, and possibly improve toxin efficacy against diverse species

- consume bufagenins
- opportunistic
- may protect toad from more toxic bufagenins

Figure 5.20 Proposed role of biotransforming microbes in parotoid glands

Based on our observations two types of biotransforming microbes are proposed to be present within the parotoid gland, types 1 and 2 (Figure 5.20). Type 1 microbes are proposed to play a role in the degradation of bufagenins as reported by Hayes et al.[21] That said type 1 microbes are possibly opportunistic as they consume bufagenins as carbon source for growth and may also protect toads from accumulation of toxic bufagenins. Type 2 microbes are organisms that can potentially biotransform bufotoxins such as marinobufotoxin (**1c**) to yield other bufotoxin analogues such as telocinobufotoxin (**2c**), bufalitoxin (**3c**) and arenobufotoxin (**6c**). These microbes could possibly play a role in diversification of chemical diversity thereby improving the efficacy to cane toad parotoid toxins against diverse predatory species.

246

5.3 Conclusion

- Microbial degradation of bufadienolides by bacteria/fungi from parotoid gland and ovaries suggested that bufagenins are prone to biotransformation
- Bufotoxins are resistant to microbial degradation
- Identification of bacteria from *in situ* parotoid gland capable of diversifying bufagenin analogues suggesting possible role in the formation of various bufadienolide scaffolds in the parotoid toxin
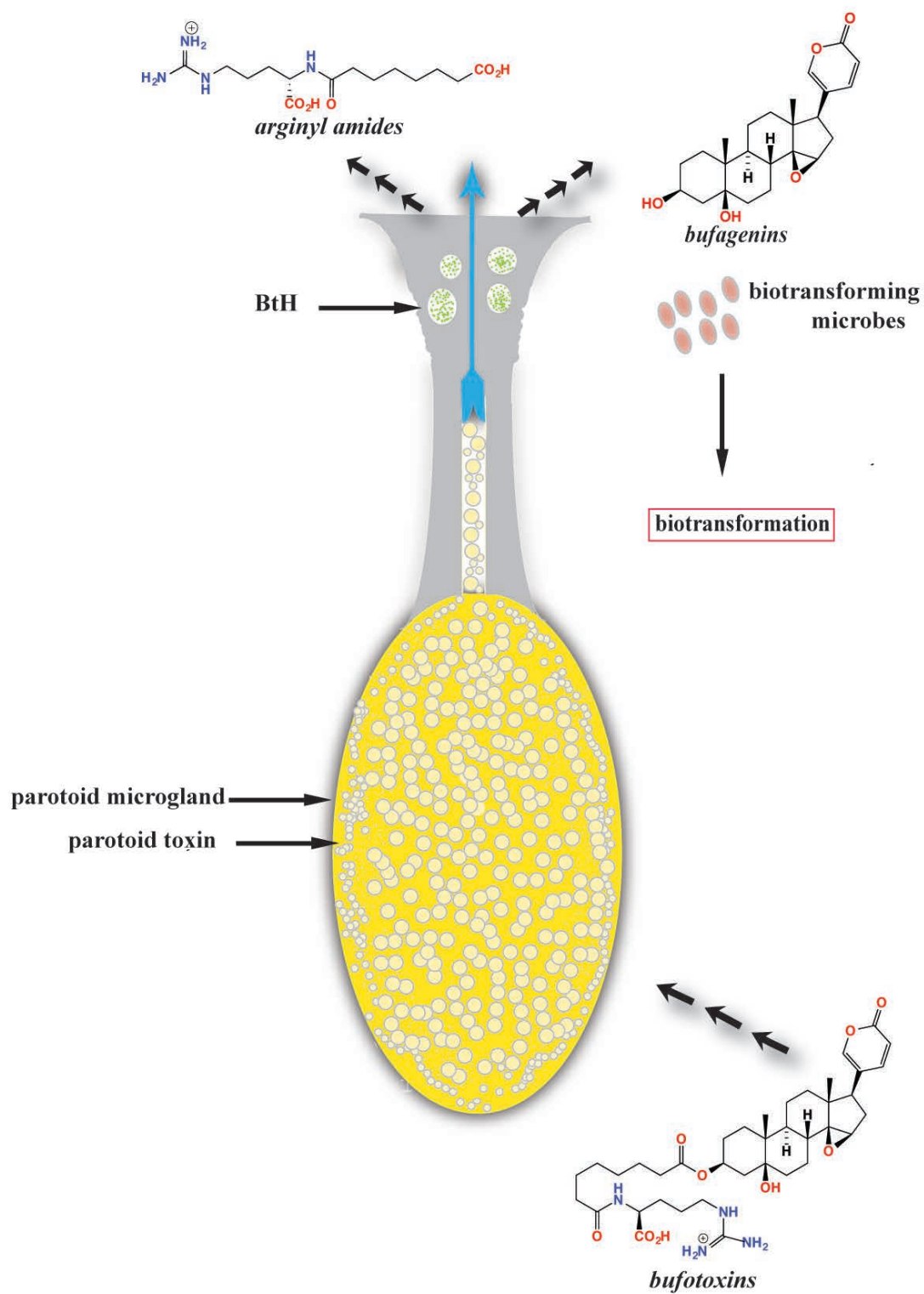
Figure 5.21 A diagrammatic representation of storage and release of parotoid toxin from a parotoid microgland based on recent findings. *In situ* bufotoxins are converted to *ex situ* bufagenins and amides by co-secretion of BtH. The converted bufagenins on the surface of the parotoid glands are biotransformed by the steroid-degrading microbes.

5.4 Experimental

5.4.1 Biotransformation of bufadienolides

5.4.1.1 Materials

Composition of nutrient agar medium: Peptone (Bacto) 4 g/L, NaCl (Univar) 1.5 g/L and Agar (Sigma) 18 g/L in H_2O.

Composition of nutrient broth: D-glucose (Sigma) 10 g/L, peptone (Bacto) 2 g/L, yeast extract (Bacto) 4 g/L and NaCl (Univar) 1.5 g/L in H_2O.

5.4.1.2 Growth of previously isolated biotransforming strains

Biotransforming strains, *C. testosteroni.* (from parotoid gland) and *A. johnsonii* (from ovary) were previously were stored at −80 °C in 10% aqueous glycerol. The glycerol stocks were thawed at room temperature and were streaked onto freshly prepared nutrient agar plates, which were incubated at 26.5 °C for 48 h.

5.4.1.3 Growth of bacterial strains in liquid medium

A single colony from the previously grown nutrient agar plate was selected and cultured in nutrient broth (10 mL) and incubated at 26.5 °C with shaking at 150 rpm until visible turbidity was achieved (24 h).

5.4.2 Biotransformation of marinobufagenin (1a)

Marinobufagenin in acetone (10 mg/mL; 50 μL) was added to each overnight culture (5 mL) of *C. testosteroni* and *Acinetobacter johnsonii* which were then incubated at 26.5 °C for further 72 h. 500 μL of cultures were extracted for every 0 h, 24 h, 48 h and 72 h time period respectively, with equal volumes of ethyl acetate (2 × 500 μL) and the organic layers were reduced to dryness under a stream of N_2 at 40 °C. The residues were redissolved in methanol (100 μL), filtered using 0.45 μm PTFE filter and analysed by HPLC-DAD-ESI-MS.

5.4.3 Biotransformation of marinobufotoxin (1c)

Marinobufotoxin in acetone (10 mg/mL; 50 μL) was added to each overnight culture (5 mL) of *C. testosteroni* and *A. johnstoni* which were then incubated at 26.5 °C for further 72 h. 500 μL of cultures were extracted for every 0 h, 24 h, 48 h and 72 h time period respectively, with equal

volumes of ethyl acetate (2 × 500 μL) and the organic layers were reduced to dryness under a stream of N_2 at 40 °C. The residues were redissolved in methanol (100 μL), filtered using 0.45 μm PTFE filter and analysed by HPLC-DAD-ESI-MS.

5.4.4 Biotransformation of marinobufagenin hemisuberate (1b)

Marinobufagenin hemisuberate in acetone (10 mg/mL; 50 μL) was added to each overnight culture (5 mL) of *C. testosteroni* and *A. johnsonii* which were then incubated at 26.5 °C for further 72 h. 500 μL of cultures were extracted for every 0 h, 24 h, 48 h and 72 h time period respectively, with equal volumes of ethyl acetate (2 × 500 μL) and the organic layers were reduced to dryness under a stream of N_2 at 40 °C. The residues were redissolved in methanol (100 μL), filtered using 0.45 μm PTFE filter and analysed by HPLC-DAD-ESI-MS.

5.4.5. Biotransformation of telocinobufagenin (2a)

Telocinobufagenin in acetone (10 mg/mL; 50 μL) was added to each overnight culture (5 mL) of *C. testosteroni*, *Acinetobacter johnsonii*, *Acinetobacter* sp. and *Flavobacterium* sp. which were then incubated at 26.5 °C for further 72 h. 500 μL of cultures were extracted for every 0 h, 24 h, 48 h and 72 h time period respectively, with equal volumes of ethyl acetate (2 × 500 μL) and the organic layers were reduced to dryness under a stream of N_2 at 40 °C. The residues were redissolved in methanol (100 μL), filtered using 0.45 μm PTFE filter and analysed by HPLC-DAD-ESI-MS.

5.4.6 Biotransformation of bufalin (3a)

Bufalin in acetone (10 mg/mL; 50 μL) was added to each overnight culture (5 mL) of *C. testosteroni*, *Acinetobacter johnsonii*, *Acinetobacter* sp. and *Flavobacterium* sp. which were then incubated at 26.5 °C for further 72 h. 500 μL of cultures were extracted for every 0 h, 24 h, 48 h and 72 h time period respectively, with equal volumes of ethyl acetate (2 × 500 μL) and the organic layers were reduced to dryness under a stream of N_2 at 40 °C. The residues were redissolved in methanol (100 μL), filtered using 0.45 μm PTFE filter and analysed by HPLC-DAD-ESI-MS

5.4.7 Isolation of microbes from the surface and the interior of the parotoid gland

Parotoid secretions from two (left) parotoid glands of two matured cane toads were directly squeezed onto sterile water, gently mixed and immediately an aliquot (50 μL) was added onto a nutrient agar plate and incubated for 5 days at 26.5 °C. Cane toads were then euthanized and

dissected to obtain two parotoid glands (right). An incision was made on the ventral portion of the parotoid gland and was directly swabbed onto a nutrient agar plate using a sterile tweezer followed by incubation for 5 days at 26.5 °C.

5.4.8 Biotransformation of marinobufagenin (1a) using micro bioreactors

The micro bioreactors and its accessories (including the sieved lid and the seal) were initially sterilized using autoclave. Sterile nutrient broth (2 mL) was added to each well of the 24-well plate micro bioreactor. A single colony of each microbe isolated from the parotoid secretions and parotoid gland was inoculated onto the broth and incubated for 12 h at 26.5 °C for unicellular bacterial colonies and 24 h for fungal and sporulating bacterial colonies. Marinobufagenin (15 mg/mL; 3 μL) was added to the cultures and was further incubated for 2 days for at 26.5 °C for unicellular bacterial colonies while 4 days for fungal and sporulating bacterial colonies. Cultures were extracted with equal volumes of ethyl acetate (2×2 mL) and the organic layers were filtered using 0.45 μm PTFE filter and reduced to dryness under a stream of N_2 at 40 °C. The residues were redissolved in methanol (50 μL) and analysed by HPLC-DAD-ESI-MS (Table 5.3).

Table 5.3 Biotransformation of marinobufagenin by newly isolated strains from parotoid glands

Strain code	Biotransformation products	Retention time (min)	Molecular mass (*m/z*)
CMB-TD29	arenobufagenin (**6a**)	5.81	417
	25a	6.28	363
	3-epi-arenobufagenin (**26a**)	5.74	417
CMB-TD49	arenobufagenin (**6a**)	5.81	417
	3-epi-arenobufagenin (**26a**)	5.74	417
	27a	6.25	345
CMB-TD22	**28a**	5.70	419
	29a	6.32	419
	30a	6.46	419
CMB-TD42	arenobufagenin (**6a**)	5.81	417
	31a	6.61	417

5.5 References

1. Wang, S. W.; Lin, H.; Tsai, S. C.; Hwu, C. M.; Chiao, Y. C.; Lu, C. C.; Chen, J. J.; Wang, G. J.; Chou, C. J.; Lin, L. C.; Chen, C. F.; Wang, P. S., Effects of methanol extract of Chansu on hypothalamic-pituitary-testis function in rats. *Metabolism* **1998,** *47*, 1211-1216.
2. Yeh, J. Y.; Huang, W. J.; Kan, S. F.; Wang, P. S., Effects of bufalin and cinobufagin on the proliferation of androgen dependent and independent prostate cancer cells. *Prostate* **2003,** *54*, 112-124.
3. Akimova, O. A.; Bagrov, A. Y.; Lopina, O. D.; Kamernitsky, A. V.; Tremblay, J.; Hamet, P.; Orlov, S. N., Cardiotonic steroids differentially affect intracellular Na^+ and $Na^+_{(i)}$/ $K^+_{(i)}$-independent signaling in C7-MDCK cells. *J. Biol. Chem.* **2005,** *280*, 832-839.
4. Zhan, J. X.; Guo, H. Z.; Ning, L. L.; Zhang, Y. X.; Guo, D., Efficient preparation of derivatives of resibufogenin using microbial catalytic technique. *Planta Med.* **2006,** *72*, 346-350.
5. Zhan, J. X.; Liu, W. H.; Guo, H. Z.; Zhang, Y. X.; Guo, D., Selective dehydrogenation of resibufogenin and cinobufagin at 3-OH by *Pseudomonas aeruginosa. Enzyme Microb. Technol.* **2003,** *33*, 29-32.
6. Zhan, J. X.; Zhang, Y. X.; Liu, W. H.; Guo, H. Z.; Guo, D., Directional modifications of resibufogenin by *Mucor subtilissimus* and *Pseudomonas aeruginosa. Biocatal. Biotransform.* **2003,** *21*, 141-143.
7. Ye, M.; Ning, L. L.; Zhan, J. X.; Guo, H. Z.; Guo, D., Biotransformation of cinobufagin by cell suspension cultures of *Catharanthus roseus* and *Platycodon grandiflorum. J. Mol. Catal. B-Enzym.* **2003,** *22*, 89-95.
8. Ye, M.; Qu, G. Q.; Guo, H. Z.; Guo, D., Specific 12 beta-hydroxylation of cinobufagin by filamentous fungi. *Appl. Environ. Microbiol.* **2004,** *70*, 3521-3527.
9. Ma, X. C.; Xin, X. L.; Liu, K. X.; Han, J.; Guo, D. A., Microbial transformation of cinobufagin by *Syncephalastrum racemosum. J. Nat. Prod.* **2008,** *71*, 1268-1270.
10. He, X. J.; Tang, J. S.; Qiao, A. M.; Wang, G. H.; Jiang, M. M.; Liu, R. H.; Yao, X. S., Cytotoxic biotransformed products from cinobufagin by *Mucor spinosus* and *Aspergillus niger. Steroids* **2006,** *71*, 392-402.
11. Ye, M.; Han, J.; An, D. G.; Tu, G. Z.; Guo, D., New cytotoxic bufadienolides from the biotransformation of resibufogenin by *Mucor polymorphosporus. Tetrahedron* **2005,** *61*, 8947-8955.
12. Ye, M.; Qu, G. Q.; Guo, H. Z.; Guo, D., Novel cytotoxic bufadienolides derived from bufalin by microbial hydroxylation and their structure-activity relationships. *J. Steroid Biochem. Mol. Biol.* **2004,** *91*, 87-98.
13. Ye, M.; Guo, D., Substrate specificity for the 12 beta-hydroxylation of bufadienolides by *Alternaria alternata. J. Biotechnol.* **2005,** *117*, 253-262.
14. Xiao-Chi, M.; Cui, H.; Zheng, H.; Guo, D. A., Microbial transformation of three bufadienolides by *Penicillium aurantigriseum* and its application for metabolite identification in rat. *J. Mol. Catal. B-Enzym.* **2007,** *48*, 42-50.
15. Ma, X. C.; Zheng, J.; Guo, D. A., Highly selective isomerization and dehydrogenation of three major bufadienolides at 3-OH by *Fusarium solani. Enzyme Microb. Technol.* **2007,** *40*, 1585-1591.
16. Borges, K. B.; Borges, W. D.; Duran-Patron, R.; Pupo, M. T.; Bonato, P. S.; Collado, I. G., Stereoselective biotransformations using fungi as biocatalysts. *Tetrahedron-Asymmetry* **2009,** *20*, 385-397.
17. Duetz, W. A., Microtiter plates as mini-bioreactors: miniaturization of fermentation methods. *Trends Microbiol.* **2007,** *15*, 469-475.
18. Xin, X. L.; Zhan, L. B.; Li, F. Y.; Ma, X. C.; Liu, K. X.; Han, J.; Guo, D. A., Microbial transformation of bufotalin by *Alternaria alternata* AS 3.4578. *J. Asian Nat. Prod. Res.* **2009,** *11*, 7-11.

19. Ye, M.; Guo, D., A new bufadienolide obtained from the biotransformation of cinobufagin by *Alternaria alternata*. *Nat. Prod. Res.* **2008,** *22*, 26-30.

20. Zhang, J.; Sun, Y.; Liu, J. H.; Yu, B. Y.; Xu, Q., Microbial transformation of three bufadienolides by Nocardia sp and some insight for the cytotoxic structure-activity relationship (SAR). *Bioorg. Med. Chem. Lett.* **2007,** *17*, 6062-6065.

21. Hayes, R. A.; Piggott, A. M.; Dalle, K.; Capon, R. J., Microbial biotransformation as a source of chemical diversity in cane toad steroid toxins. *Bioorg. Med. Chem. Lett.* **2009,** *19*, 1790-1792.

22. Skowasch, D.; Mobus, E.; Maser, E., Identification of a novel *Comamonas testosteroni* gene encoding a steroid-inducible extradiol dioxygenase. *Biochem. Biophys. Res. Commun.* **2002,** *294*, 560-566.

23. Marcus, P. I.; Talalay, P., Induction and purification of alpha-hydroxysteroid and beta-hydroxysteroid dehydrogenases. *J. Biol. Chem.* **1956,** *218*, 661-674.

24. Talalay, P.; Dobson, M. M.; Tapley, D. F., Oxidative degradation of testosterone by adaptive enzymes. *Nature* **1952,** *170*, 620-621.

25. Shimada, K.; Miyashiro, Y.; Nishio, T., Characterization of in vitro metabolites of toad venom using high-performance liquid chromatography and liquid chromatography-mass spectrometryt. *Biomed. Chromatogr.* **2006,** *20*, 1321-1327.

Chapter 6: Characterization of the cane toad egg extracts, with the emphasis on bufadienolides (bufolipins)

6.1 Introduction

The aim of this chapter is to characterize the bufadienolide composition of the eggs of *B. marinus*. *B. marinus* eggs have been reported to contain cardiotonic activity similar to that of adult parotoid secretions,[1] with eggs (pre-laying) removed from oviducts in 1994 reported to contain poly-hydroxylated bufagenins such as 11α-hydroxymarinobufagenin (**10a**), 11α,19-dihydroxymarinobufagenin (**11a**), 11α-hydroxytelocinobufagenin (**12a**), 19-hydroxytelocinobufagenin (**13a**), 11α,19-dihydroxytelocinobufagenin (**14a**) (Figure 6.1).[1] A subsequent 1998 report described telocinobufagenin (**2a**), hellebrigenin (**5a**), arenobufagenin (**6a**) and 5β-hydroxyarenobufagenin (**15a**) and three bufolipins, 11α, 19-dihydroxytelocinobufagenin-3-(14-hydroxy-7-tetradecanoic acid) ester (bufolipin A* (**1h**)), 11α, 19-dihydroxytelocinobufagenin-3-(14-hydroxytetradecanoic acid) ester (bufolipin B* (**2h**)) and 11α, 19-dihydroxytelocinobufagenin-3-(12-hydroxydodecanoic acid) ester (bufolipin C* (**3h**)) from oviducts of *B. marinus*.[2] Interestingly, in a recent finding by Crossland et al, bufolipin A (**1h**) was isolated from laid eggs while several other bufolipins and bufagenins were also identified.[3]

telocinobufagenin (**2a**)   hellebrigenin (**5a**)   arenobufagenin (**6a**)

11α-hydroxy marinobufagenin (**10a**)   11α-hydroxy telocinobufagenin (**11a**)   11α,19-dihydroxy marinobufagenin (**12a**)

11α19-dihydroxy
telocinobufagenin (**13a**)

19-hydroxy
telocinobufagenin (**14a**)

5β-hydroxyarenobufagenin (**15a**)

bufolipin A (**1h**)

bufolipin B (**2h**)
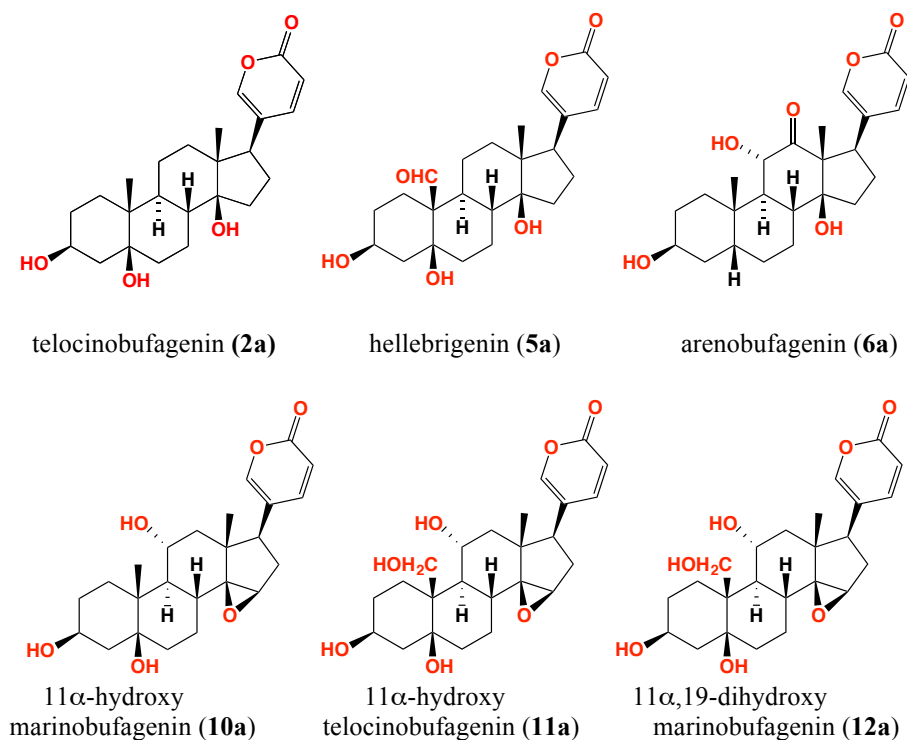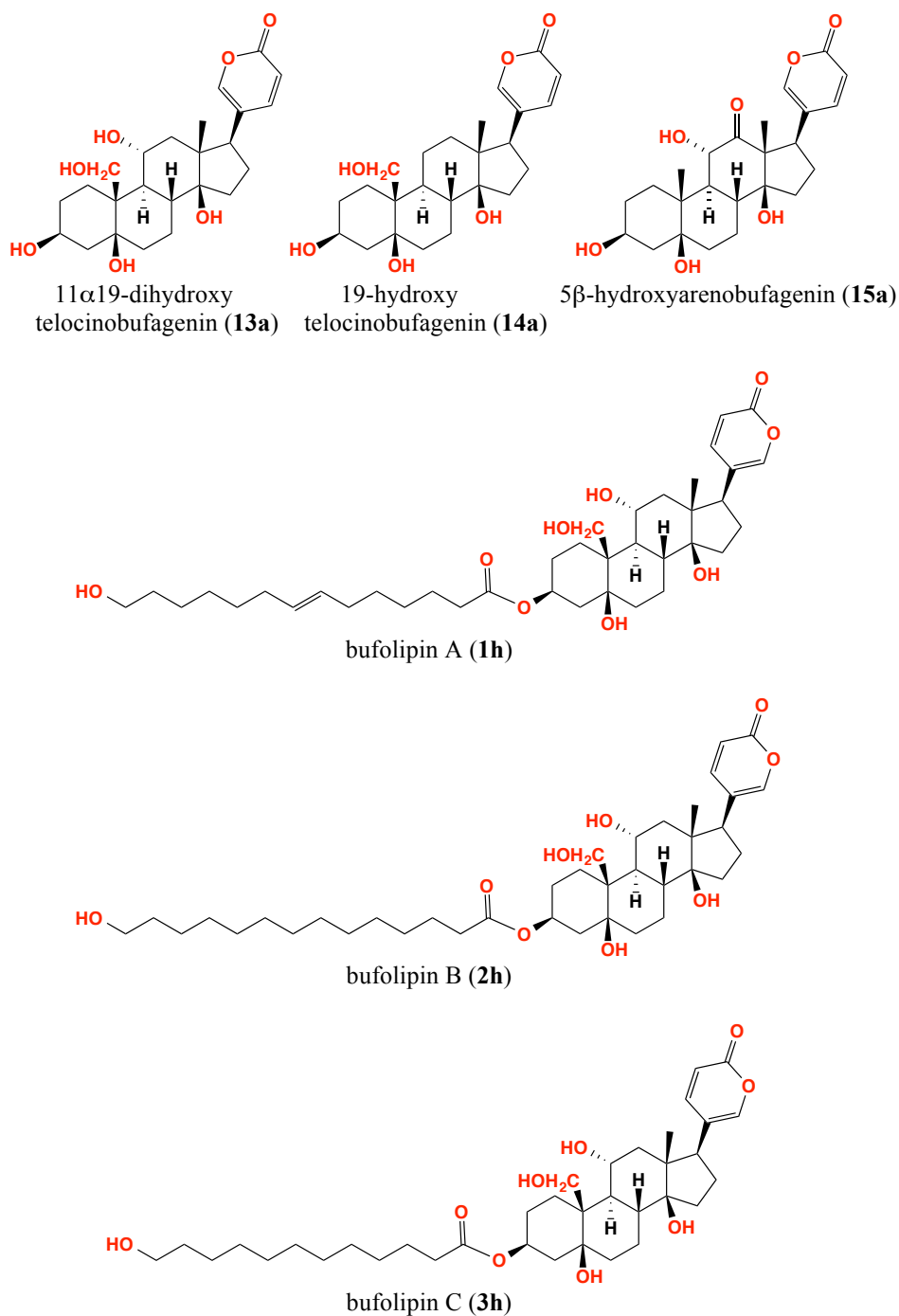
bufolipin C (**3h**)

Figure 6.1 Bufagenins and bufolipins found in eggs/ovaries of the cane toad

[*] Bufolipins terminology is coined by our group to describe the unique class of bufadienolides identified in *B. marinus* eggs

In this study all bufadienolides from *B. marinus* eggs including bufagenins and bufolipins will be isolated and characterized using analytical, preparative and semi-preparative HPLC-DAD, HPLC-DAD-MS, NMR and HRMS.

HPLC-DAD analytical methods used for the isolation and identification of bufolipins were developed with the use of bufagenin esters standards (comprising varying lengths of diacid esters)

previously synthesized (see Chapter 2). *B. marinus* eggs were subjected to trituration with hexane and *n*-BuOH, with bufadienolides (bufagenins and bufolipins) solubilized by *n*-BuOH. *n*-BuOH solubles were then subjected to fractionation using HPLC-DAD methods specific for bufagenins and bufolipins. Following isolation the bufadienolides were subjected to structure elucidation using NMR and HRMS.

6.2 Results and discussion

6.2.1 Analytical methodology for bufagenin esters

An HPLC-DAD based analytical methodology was developed specific for bufagenin esters (i.e. bufolipins) by identifying suitable reverse phase HPLC conditions. Synthetic bufagenin ester standards were prepared and subjected to analytical method development using several reverse phase columns (e.g. C_3, C_8, C_{18}, CN and phenyl) with C_8 providing the best resolution as previously observed by Crossland et al.[3] Solvent conditions including MeOH/H_2O, MeCN/H_2O at varying gradients (linear/isocratic) with (Method 4) and without (Method 5) TFA as modifier (0.01%) were considered, however, a linear gradient of MeCN/H_2O with TFA (0.01%) showed the best resolution (Figure 6.2). HPLC-DAD analysis without TFA showed broad peaks, however, since TFA could possibly react with bufagenin esters (as previously observed with bufotoxins), reverse-phase HPLC condition without TFA was considered as a suitable analytical methodology. For direct identification of compounds in crude egg extracts reverse phase HPLC condition with TFA was applied.
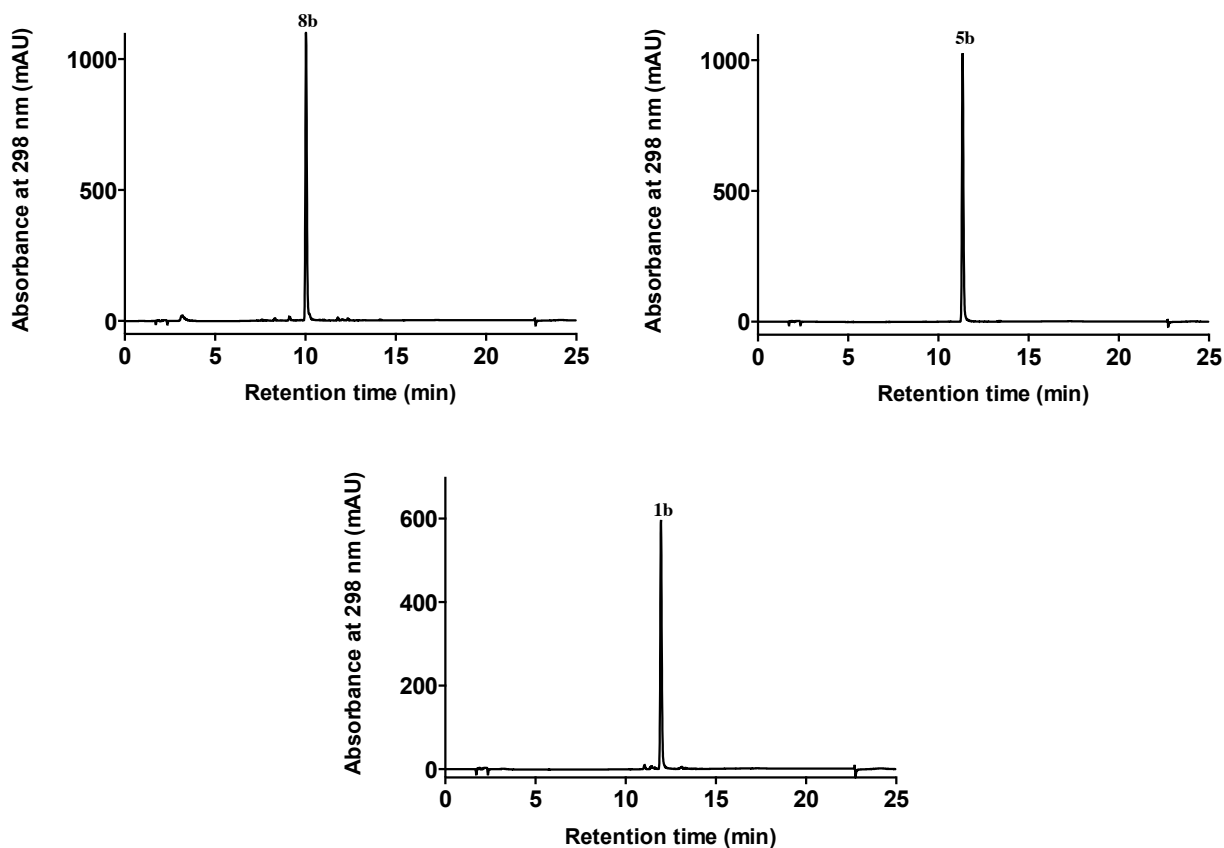
Figure 6.2 HPLC chromatograms and UV-Vis spectrum of synthetic bufolipins, marinobufagenin-3-succinate (**8b**), marinobufagenin-3-pimelate (**5b**) and marinobufagenin-3-suberate (**1b**) using Method 4.

Synthetic bufagenin esters exhibited analytical characteristics comparable to hydrophobic compounds due to the C-3 fatty acid ester linkage. As expected, the longer the fatty acid chain the more the hydrophobicity as evidenced from retention times.

An alternative analytical methodology (Method 5) for egg extracts was also developed using synthetic bufolipins. Since, the egg extracts consists of a mixture of bufagenins, bufotoxins and bufolipins along with significant amounts of fatty acids (Crossland et al),[3] a specific methodology to retain bufolipins (ie. bufagenin esters) for a longer time period on the C_8 reverse phase column was optimized using $MeCN/H_2O$ gradient without the use of TFA. Solvent conditions of Method 5 were optimized to begin with 90% $H_2O/MeCN$ and increasing the organic phase to 50% $H_2O/MeCN$ in only 5 min to separate all the polar compounds from the hydrophobic bufolipins. Followed by gradual increase of organic phase from 50% $H_2O/MeCN$ to 30% $H_2O/MeCN$ over 15 min over which is the expected range of retention time for the bufolipins. As expected, synthetic bufagenin esters showed retention times from 6.7 to 8.5 min using Method 5 (Figure 6.3).
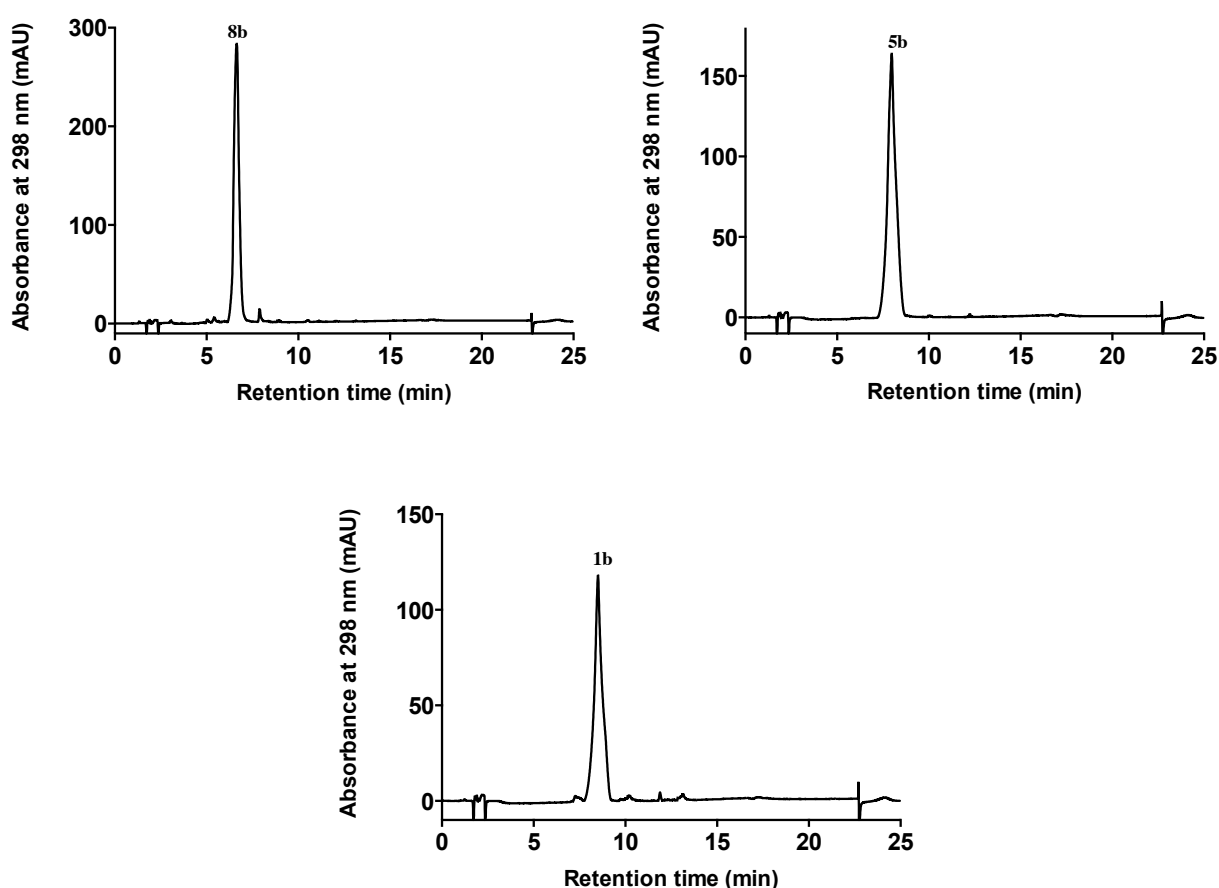
Figure 6.3 HPLC chromatograms and UV-Vis spectrum of synthetic bufolipins, marinobufagenin-3-succinate (**8b**), marinobufagenin-3-pimelate (**5b**) and marinobufagenin-3-suberate (**1b**) using Method 5.

6.2.2 Partitioning of egg extracts
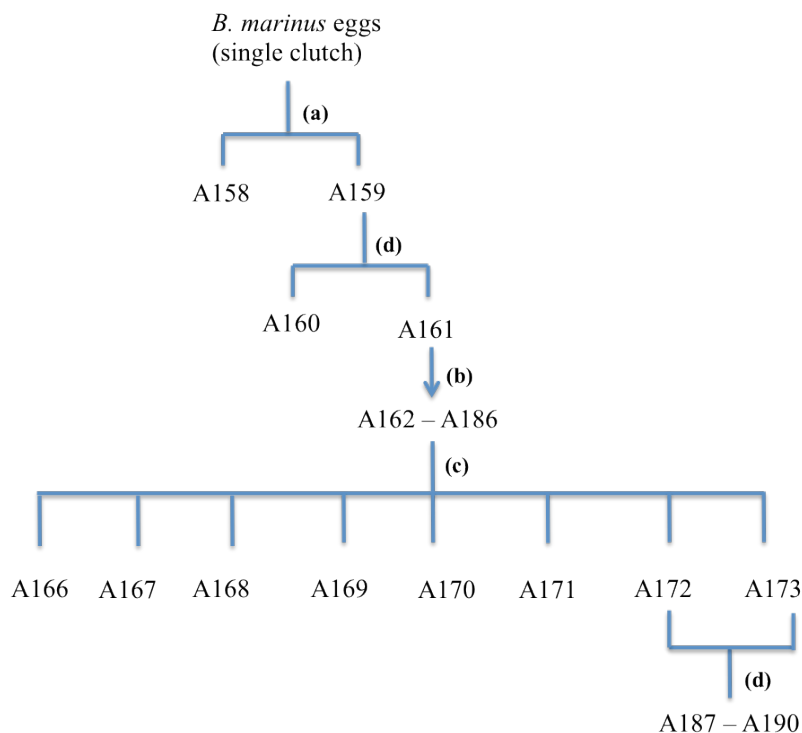
(a) – lyophilized, trituration with *n*-BuOH/H$_2$O
(b) – *n*-BuOH solubles concentrated under vacuum and triturated with *n*-BuOH/*n*-hexane (1:1)
(c) – *n*-BuOH solubles concentrated under vacuum and subjected to preparative HPLC using method 4 (Phenomenox, Luna-C$_8$ column, 250 x 21.2 mm, 10 μm, 20 mL/min, eluting with 10 – 100% MeCN/H$_2$O over 20 min)
(d) – semi-preparative HPLC using method 4a (Zorbax, C$_8$ column, 250 x 9.4 mm, 5 μm, 3.5 mL/min, eluting with 10 – 100% MeCN/H$_2$O over 20 min)

Scheme 6.1 Preparation of analytes A158 – A190.

A single wild harvested *B. marinus* egg mass was freeze-dried and extracted with MeOH to solubilize all bufadienolides, along with other structure classes including fatty acids, nucleic acids and lipids. The MeOH extract was concentrated *in vacuo* and then subjected to trituration with water and *n*-BuOH to generate fractions A158 and A159, respectively. The *n*-BuOH fraction (A159) solubilized all bufadienolides including bufolipins and fatty acids. To further concentrate bufolipins, A159 was concentrated *in vacuo* and then triturated with hexane followed by *n*-BuOH to generate fractions A160 and A161 respectively. The *n*-hexane solubilized fatty acids along with some bufolipins (A160), however, *n*-BuOH solubilized mostly bufolipins (A161). Fraction A161 was then subjected to preparative HPLC to yield fractions A162 – A186, of which, only two fractions, A172 and A173 were identified to contain bufolipins based on the UV response and HPLC-DAD-MS (Scheme 6.1). These two fractions were subsequently purified by semi-preparative HPLC to isolate two known and a mixture of five new bufolipins.

6.2.3 Identification of bufadienolides based on HPLC-DAD-MS analysis

A sample of A159 was dried *in vacuo*, re-dissolved in MeOH to a standard concentration (3 mg/mL) and subjected to HPLC-DAD-MS analysis using the above mentioned analytical methodology, Method 4 (Figure 6.4).
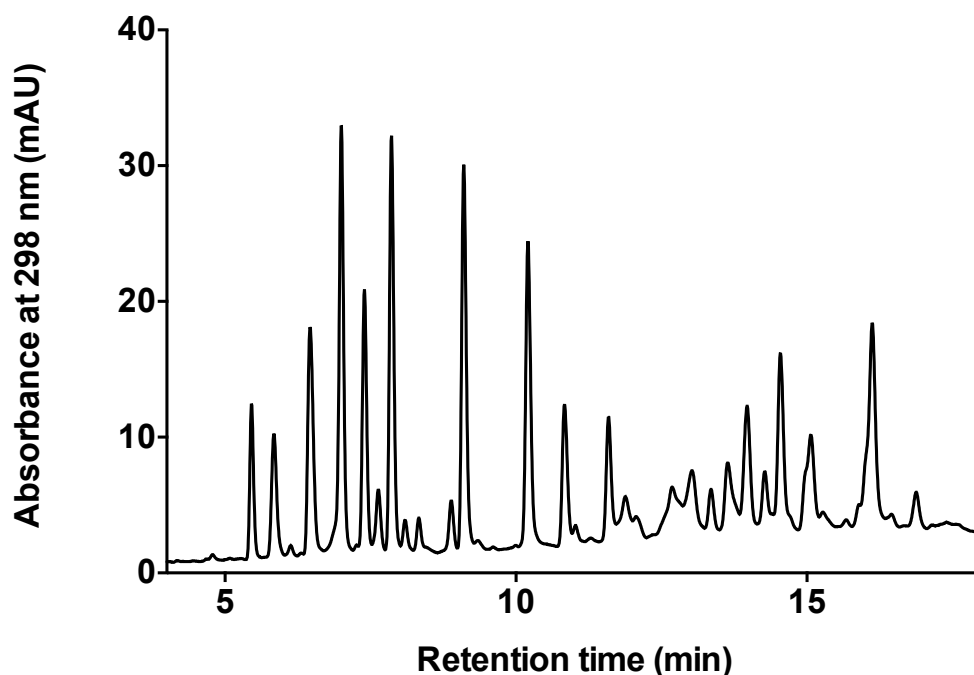
Figure 6.4 HPLC chromatogram of A159 analysed using Method 4.

Sharp peaks corresponding to bufadienolides were detected between the retention times 5 - 12 min based on the UV absorbance. Identification of bufadienolides was performed by isolation of individual peaks using preparative and semi-preparative HPLC, supported by MS and NMR analyses. An HPLC-DAD-MS analysis and comparison with bufadienolide standards previously described in Chapter 2 was also performed to identify bufadienolides in *B. marinus* eggs. Interestingly, no bufotoxins were identified in the *B. marinus* egg extracts, however, high amounts of bufagenins (5.2 – 10.1 min) and moderate to low amounts of bufolipins (10.5 – 11.8 min) were detected. Significant amounts of hydrophobic molecules (possibly bufolipins) (12.5 – 16.5 min) were also detected (Figure 6.5). Ionization of bufagenins was better than bufolipins while the hydrophobic molecules exhibited poor ionization.
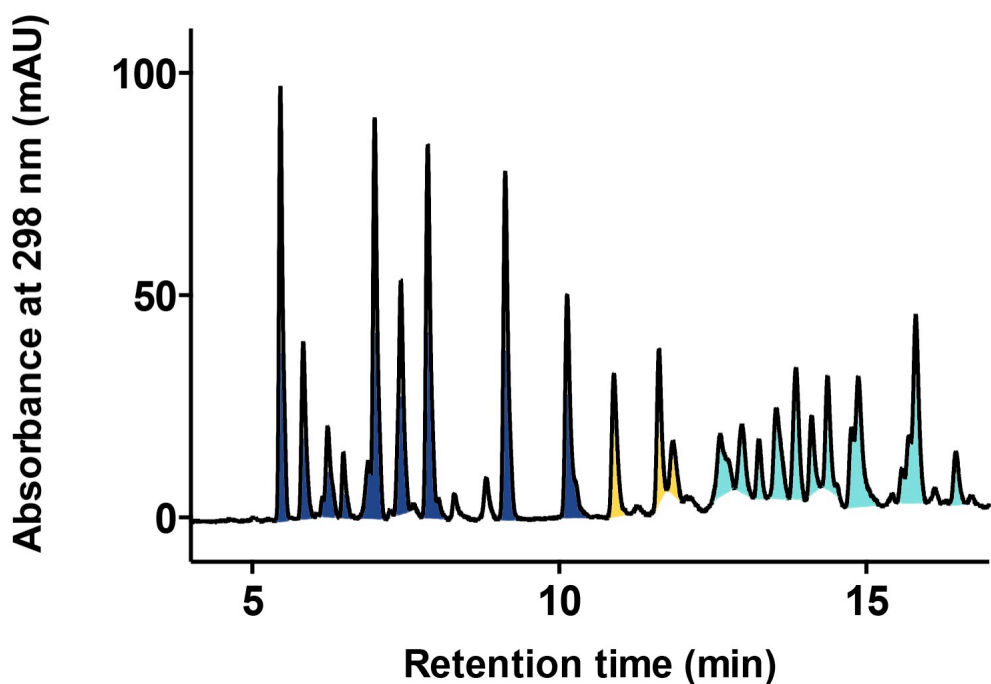
Figure 6.5 HPLC-DAD-MS chromatogram of A161 analysed using Method 4 exhibiting the presence of bufagenins (blue), bufolipins (yellow) and hydrophobic molecules (aqua)

Single mass ion extraction for each HPLC peak was performed to identify bugafenins and bufolipins based upon their range of molecular masses. Bufagenins showed ionization in the positive ESI mode and exhibited a m/z in the range between 400-440 while bufolipins showed better ionization in the negative ion ESI mode with a *m/z* >600 (Figure 6.6a, bufagenins (highlighted in blue), Figure 6.6b, bufolipins (highlighted in yellow)).
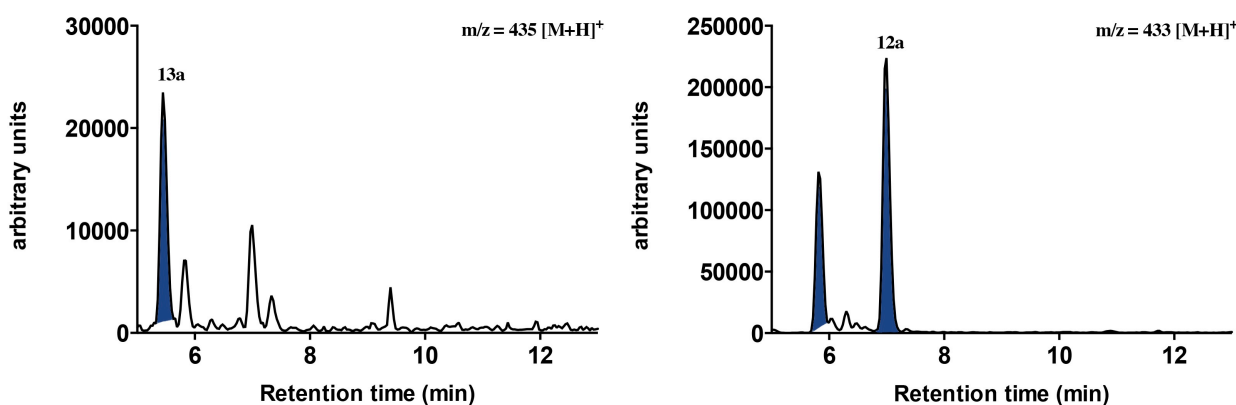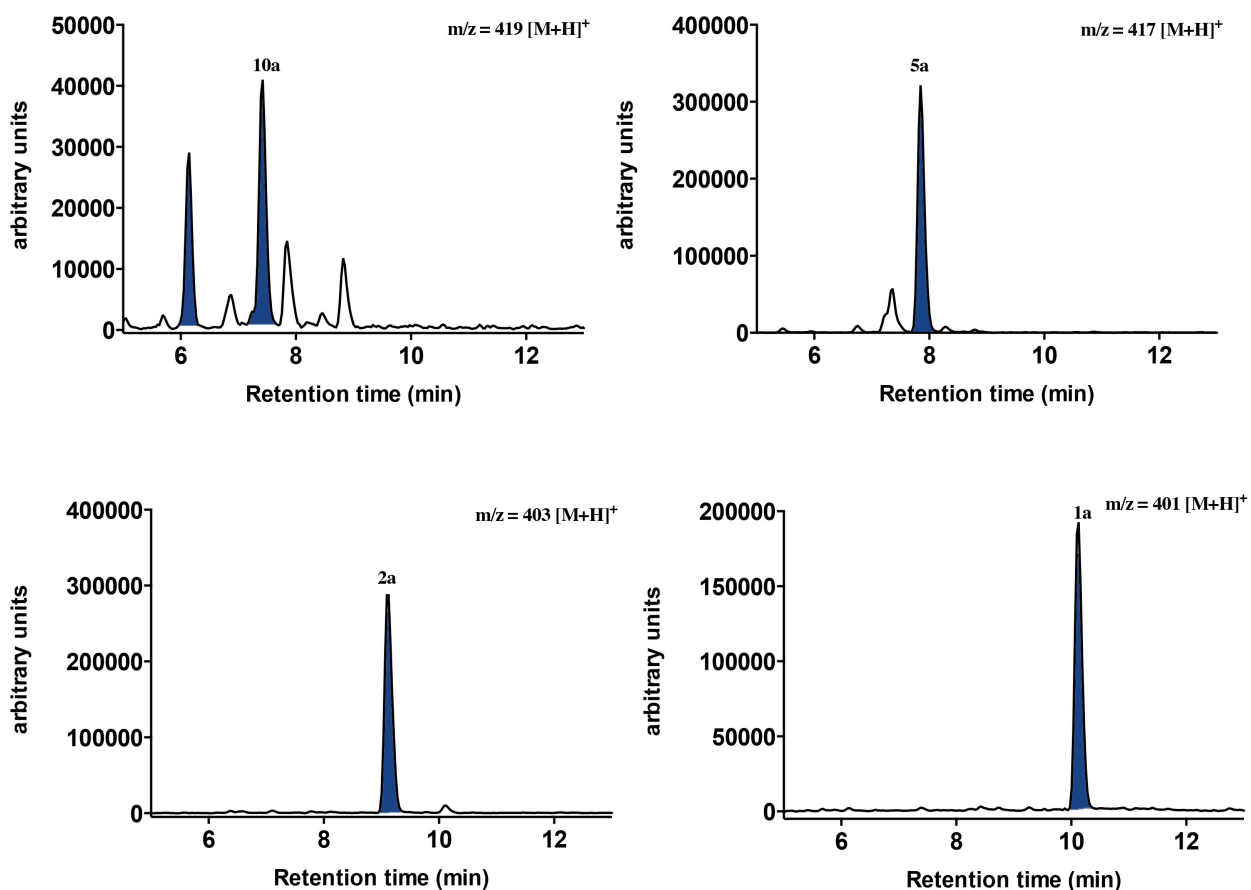
Figure 6.6a HPLC-DAD-ESI(+)-MS of A161 exhibiting single ion extraction of bufagenins
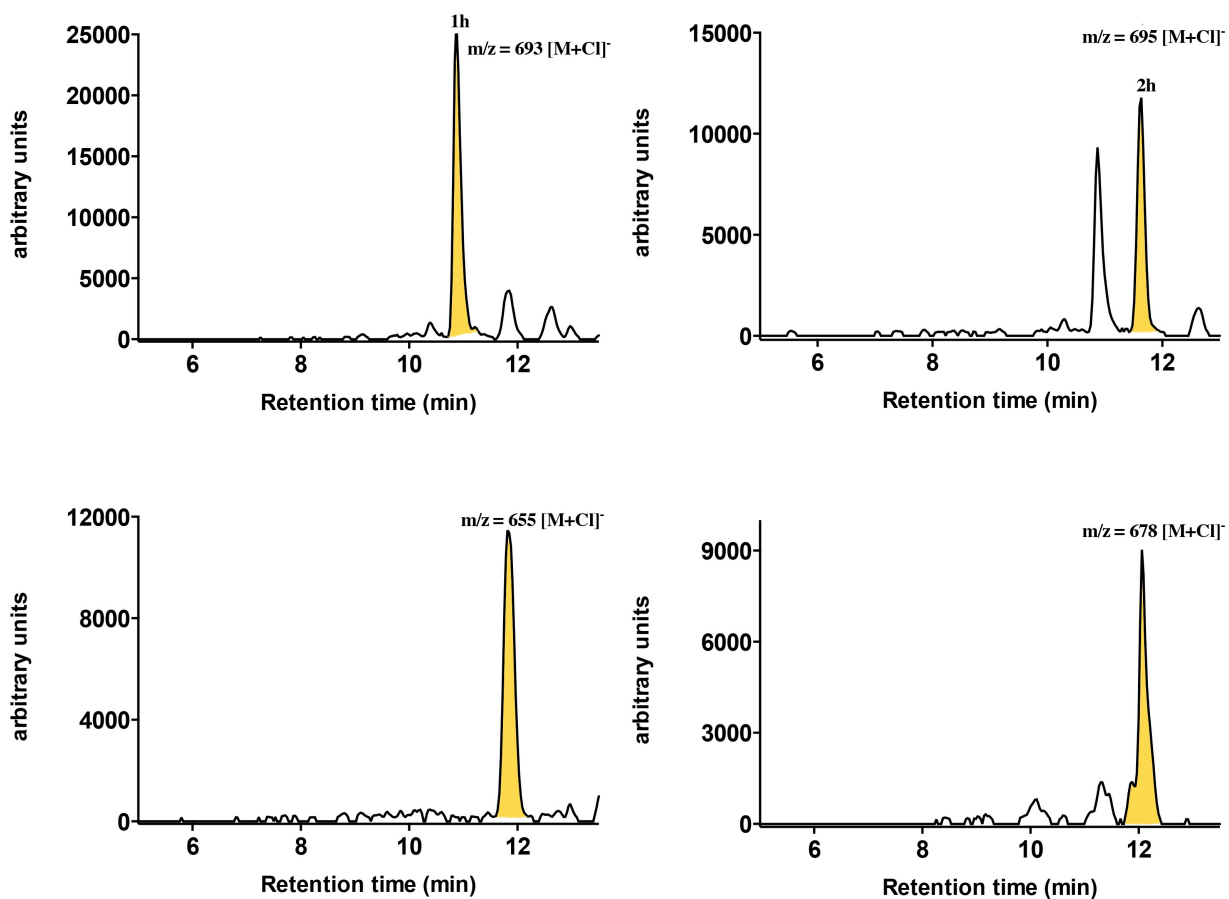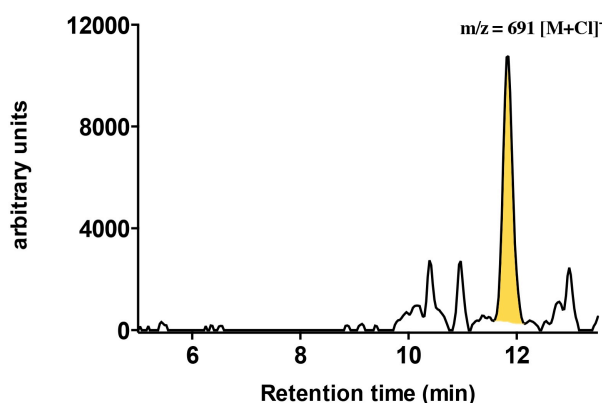
Figure 6.6b HPLC-DAD-ESI(-)-MS of A161 exhibiting single ion extraction of bufolipins

6.2.4 Isolation of bufagenins

The *n*-BuOH solubles of *B. marinus* eggs (A161) were subjected to purification using preparative HPLC-DAD (Figure 6.7) and individual peaks corresponding to bufadienolides were collected and subjected to characterization studies using HPLC-DAD-MS, HRMS and NMR.
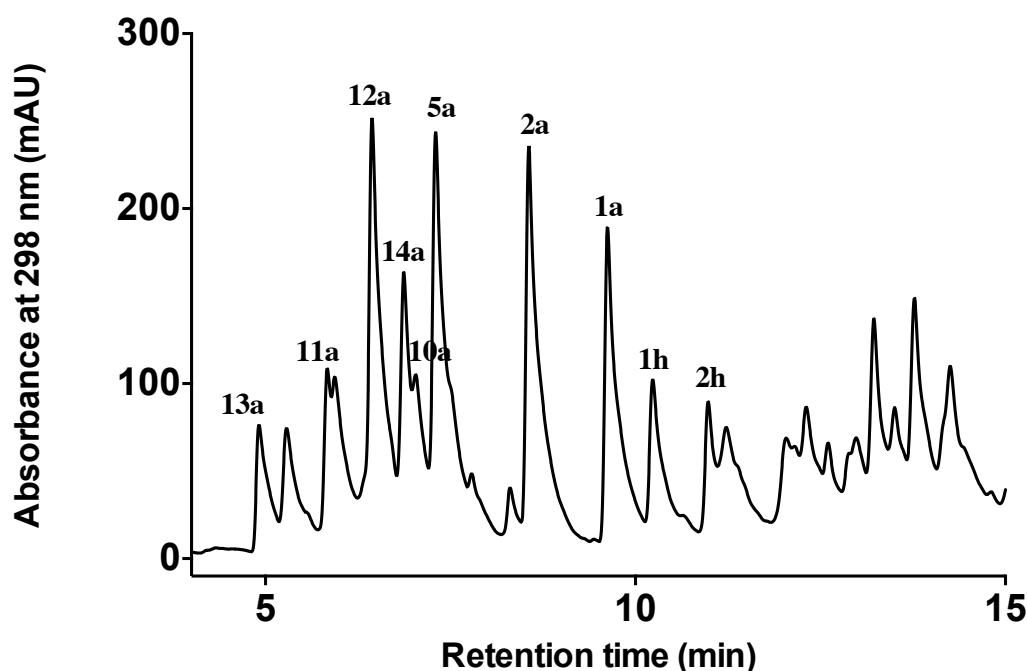
Figure 6.7 Purification of A161 using preparative HPLC-DAD

Previous published reports of bufagenins and bufolipins relied on a sampling of 182 toads yielding 2 – 20 mg of each bufadienolide (total >2g), whereas our studies was performed on a wild harvested egg mass from one cane toad.[1] Hence, characterization was performed on sub milligram scale on an individual and/or mixture of bufadienolides, employing sensitive tools like HRMS, NMR and LC-

MS. Using this approach, some of the fractions collected from preparative HPLC contained two or three bufagenins, making characterization difficult, however, previous reports of bufadienolides from eggs and ovaries of *B. marinus* provided helpful information. As fatty acids adsorbed on to the reverse phase C_8 column (during multiple injections) all the isolated bufagenins and bufolipins were contaminated with trace amounts of fatty acid. Subsequent purification of bufagenins using semi-preparative HPLC was difficult as the amount of bufadienolides (individual or mixture) recovered from preparative-HPLC were in the range of only 200 – 600 μg. That said co-injection of bufagenin standards (see Chapter 2) was also performed to identify some bufagenins present in *B. marinus* eggs.

Characterization of 11α,19-dihydroxy telocinobufagenin (**13a**) from Japanese *B. marinus* eggs has been previously reported.[1] In our study, **13a** was obtained as a pale white solid with HR(+)ESIMS analysis revealing a quasi-molecular ion (*m/z* 457.2193 [M+Na]$^+$) consistent with the molecular formula $C_{24}H_{34}O_7$ (Δmmu 0.85).[1] The UV-vis spectrum of **13a** exhibited the characteristic α-pyrone ring absorbance. All of the above indicated that 11α,19-dihydroxytelocinobufagenin (**13a**) was present in our egg extract.

Characterization of 11α,19-dihydroxymarinobufagenin (**12a**) from Japanese *B. marinus* eggs has been previously reported.[1] In our study **12a** was obtained as a pale white solid with HR(+)ESIMS analysis revealing a quasi-molecular ion (*m/z* 455.2040 [M+Na]$^+$) consistent with the molecular formula $C_{24}H_{32}O_7$ (Δmmu 0.85).[1] The UV-vis spectrum of **12a** exhibited the characteristic α-pyrone ring absorbance. All of the above indicated that 11α,19-dihydroxymarinobufagenin (**12a**) was present in our egg extract.

Characterization of 11α-hydroxymarinobufagenin (**10a**) from Japanese *B. marinus* eggs has been previously reported.[1] In our study **10a** was obtained as a pale white solid with HR(+)ESIMS analysis revealing a quasi-molecular ion (*m/z* 439.2100 [M+Na]$^+$) consistent with the molecular formula $C_{24}H_{32}O_6$ (Δmmu -2.07).[1] The UV-vis spectrum of **10a** exhibited the characteristic α-pyrone ring absorbance. All of the above indicated that 11α-hydroxymarinobufagenin (**10a**) was present in our egg extract.

Characterization of hellebrigenin (**5a**) from Japanese *B. marinus* ovaries has been previously reported.[2] In our study **5a** was obtained as a pale white solid with HR(+)ESIMS analysis revealing a quasi-molecular ion (*m/z* 439.2193 [M+H]$^+$) consistent with the molecular formula $C_{24}H_{32}O_6$

(Δmmu 1.45).[2] The ^{1}H NMR (CD$_3$OD) data for **5a** was identical to the literature data (see Chapter 2). The UV-vis spectrum of **5a** exhibited the characteristic α-pyrone ring absorbance, and on HPLC-DAD co-injection proved identical to an authentic standard of **5a** (see Chapter 2). All of the above confirmed hellebrigenin (**5a**) was present in our egg extract.

Characterization of telocinobufagenin (**2a**) from Japanese *B. marinus* ovaries has been previously reported.[2] In our study **2a** was obtained as a pale white solid with HR(+)ESIMS analysis revealing a quasi-molecular ion (*m/z* 403.2479 [M+H]$^+$) consistent with the molecular formula C$_{24}$H$_{34}$O$_5$ (Δmmu -2.98).[2] The ^{1}H NMR and ^{13}C NMR (CD$_3$OD) data for **2a** was identical to the literature data (see Chapter 2). The UV-vis spectrum of **2a** exhibited the characteristic α-pyrone ring absorbance and on HPLC-DAD co-injection proved identical to an authentic standard of **2a** (see Chapter 2). All of the above confirmed telocinobufagenin (**2a**) was present in our egg extract.

Characterization of marinobufagenin (**1a**) from Australian cane toad parotoid secretions has been previously reported.[4] In our study **1a** was obtained as a pale white solid with HR(+)ESIMS analysis revealing a quasi-molecular ion (*m/z* 401.2323 [M+H]$^+$) consistent with the molecular formula C$_{24}$H$_{32}$O$_5$ (Δmmu 2.32).[4] The ^{1}H NMR and ^{13}C NMR (CD$_3$OD) data for **1a** was identical to the literature data (see Chapter 2). The UV-vis spectrum of **1a** exhibited the characteristic α-pyrone ring absorbance and on HPLC-DAD co-injection proved identical to an authentic standard of **1a** (see Chapter 2). All of the above confirmed marinobufagenin (**1a**) was present in our egg extract.

11α-hydroxy
marinobufagenin (**10a**)

11α-hydroxy
telocinobufagenin (**11a**)

11α,19-dihydroxy
marinobufagenin (**12a**)

11α,19-dihydroxy
telocinobufagenin (**13a**)

19-hydroxy
telocinobufagenin (**14a**)

marinobufagenin (**1a**) telocinobufagenin (**2a**) hellebrigenin (**5a**)
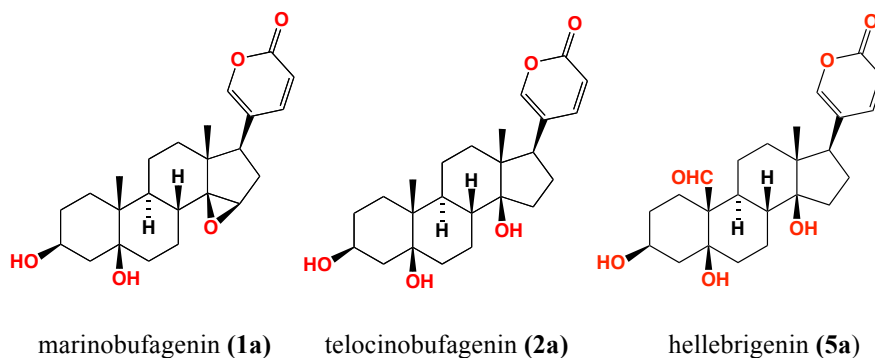
Figure 6.8 Bufagenins identified in A161

Due to the very low yields, two additional bufagenins detected in our egg extract (A161) could not be well characterized. Nevertheless, a single ion extraction for m/z 419 [M+H]$^+$ exhibited two peaks that we speculate may be due to **11a** and **14a**, both of which have previously been reported from Japanese *B. marinus* eggs.[1] In our study these two bufagenins exhibited HR(+)ESIMS quasi-molecular ions (m/z 441.2204 [M+Na]$^+$ and m/z 441.2224 [M+Na]$^+$), consistent with the molecular formula $C_{24}H_{34}O_6$,[1] and UV-vis spectra with characteristic α-pyrone ring absorbances. All of the above indicated that 11α-hydroxytelocinobufagenin (**11a**) and 19-hydroxytelocinobufagenin (**14a**) were present in our egg extract. Further analysis of HPLC-DAD-MS data for A161 indicated the presence of three additional isomeric bufagenins (t_R = 5.8, 6.2 and 6.8 min; Method 4), with UV-vis spectra characteristic of α-pyrone ring absorbance. At this time the structure of these bufagenins remains unknown.

6.2.5 Identification of bufolipins

Characterization of bufolipin A (**1h**) from Japanese *B. marinus* oviducts has been previously reported.[2] In our study **1h** was obtained as a pale white solid with HR(+)ESIMS analysis revealing a quasi-molecular ion (m/z 660.4216 [M+H]$^+$) consistent with the molecular formula $C_{38}H_{60}O_9$ (Δmmu 0.65).[2] The UV-vis spectrum of **1h** exhibited the characteristic α-pyrone ring absorbance and on HPLC-DAD co-injection proved identical to an in-house authentic standard of **1h** (previously isolated by Dr Angela Salim).[3] All of the above confirmed that bufolipin A (**1h**) was present in our egg extract.

Characterization of bufolipin B (**2h**) from Japanese *B. marinus* oviducts has been previously reported.[2] In our study, **2h** was obtained as a pale white solid with HR(+)ESIMS analysis revealing a quasi-molecular ion (m/z 658.4220 [M+H]$^+$) consistent with the molecular formula $C_{38}H_{58}O_9$ (Δmmu 0.50).[2] The UV-vis spectrum of **2h** exhibited the characteristic α-pyrone ring absorbance. All of the above indicated that bufolipin B (**2h**) was present in our egg extract.

bufolipin A (**1h**)

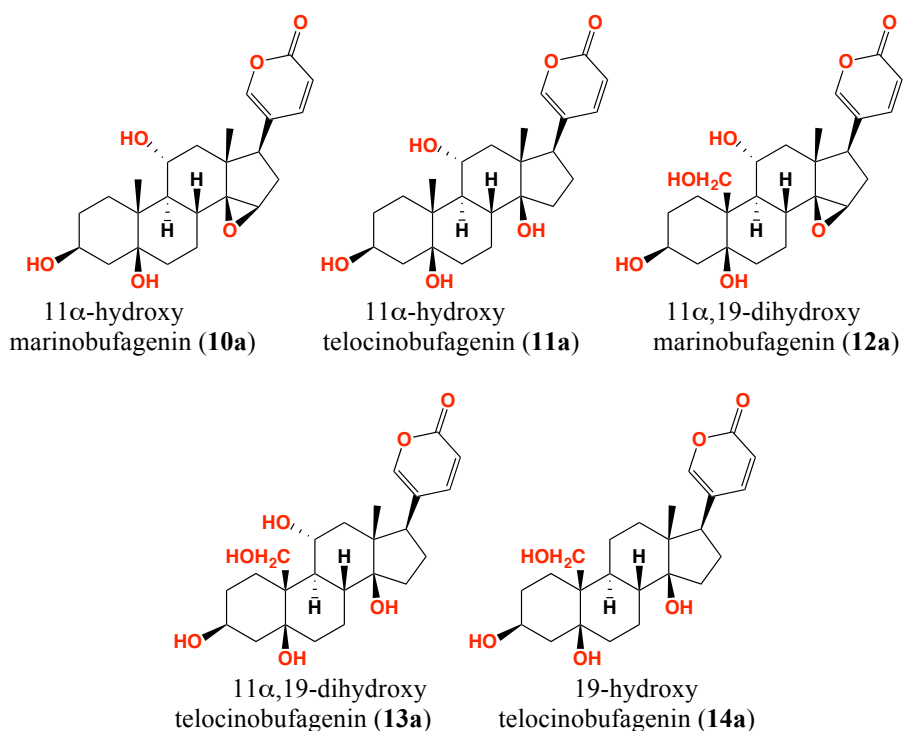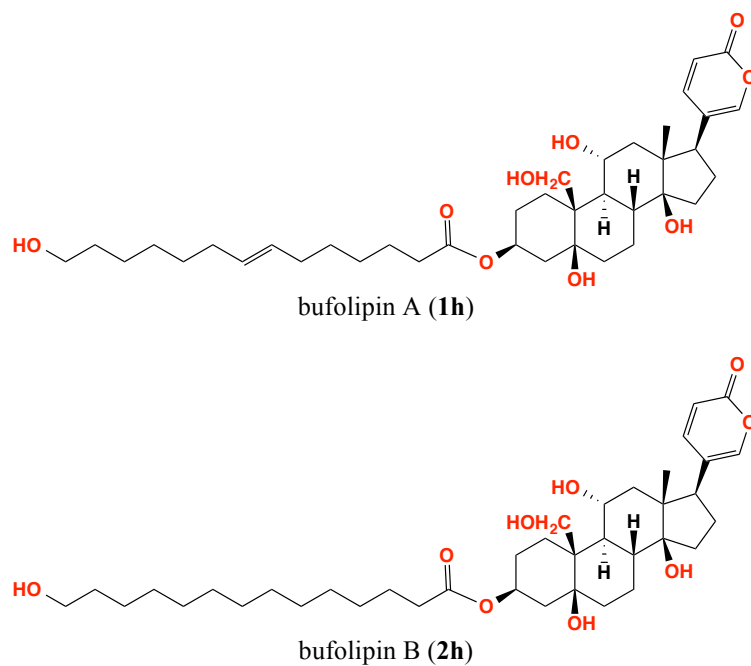
bufolipin B (**2h**)

Figure 6.9 Bufolipins identified in A161
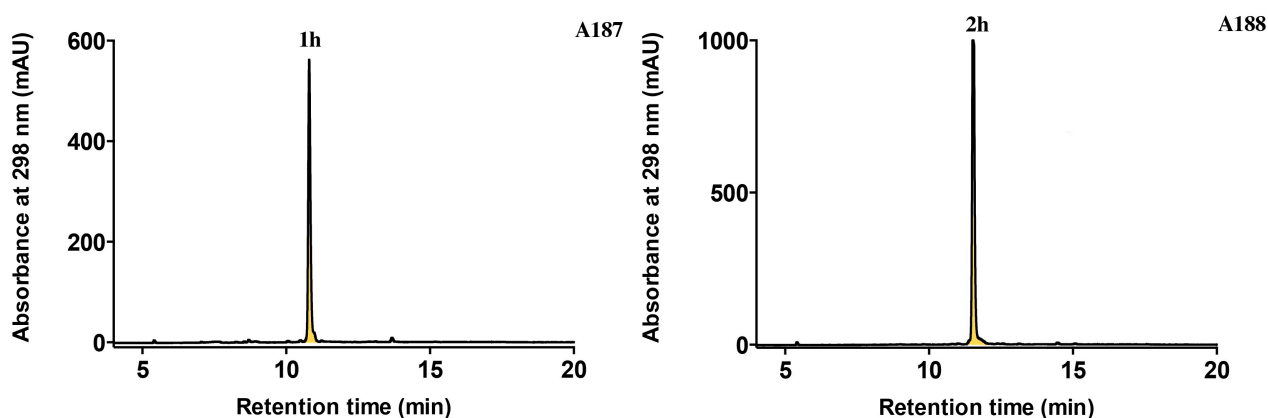
Figure 6.10 HPLC-DAD-MS profile of analytes A187 and A188

Further analysis of HPLC-DAD-MS data for A189 and A190 indicated the presence of four additional bufolipins (t_R = 12.0, 12.1, 12.4 and 13.2 min) (Method 4) with *m/z* [M+Cl]⁻ at 691, 655, 667 and 721, respectively, and with UV-vis spectra characteristic of α-pyrone ring absorbance. Figure 6.11 illustrates the mixture of unknown bufolipins present in A189 and A190 respectively.
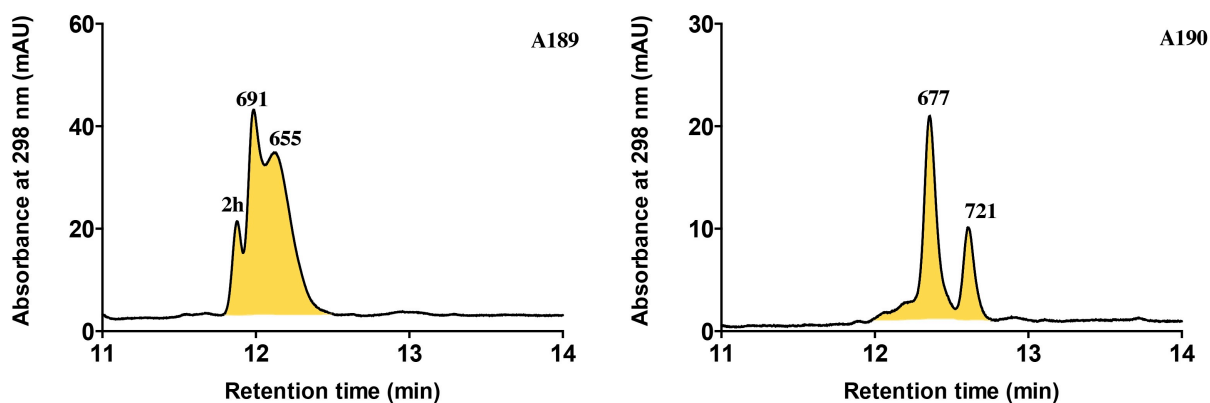
Figure 6.11 HPLC-DAD-MS profile of unknown bufolipins in fractions **4h** and **5h**

6.2.6 Discussion on bufadienolides from *B. marinus* eggs

Literature reports described of six bufagenins from pre-laid eggs obtained from 182 cane toads,[1] and two bufagenins and 3 bufolipins from the oviducts of 180 cane toads.[2] In our studies 8 known bufagenins and 2 bufolipins were identified from a single mass of eggs laid by one cane toad. Additional bufadienolides were detected but insufficient material was available to characterize and assign molecular structures. This study, demonstrated that the chemical diversity present in eggs is higher than previously reported.

6.2.7 Hydrolysis of bufolipins

Adult cane toad parotoid toxins are stored as bufotoxins and during the manual compression of the parotoid glands, bufotoxins are co-secreted with BtH and hydrolyzed into bufagenins. To identify the potential for BtH mediated hydrolysis of bufolipins in eggs. Pure bufolipin A (50 μg) was subjected to hydrolysis by BtH (2 μg) for 1 and 48 h time intervals, after which it was quenched with MeOH (500 μL), dried and re-dissolved in MeOH (50 μL) to generate analytes A191 and A192, respectively (Scheme 6.2). These analytes were then analysed using HPLC-DAD Method 1 (see Chapter 2).

bufolipin A

(a)

(b)　　　　　　(c)
A191　　　　　A192
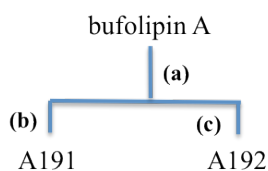
(a) – reaction with BtH (2 μg) at 37 °C
(b) – incubation for 1 h, quenched with MeOH (500 μL), dried and re-dissolved in MeOH (50 μL)
(c) – incubation for 48 h, quenched with MeOH (500 μL), dried and re-dissolved in MeOH (50 μL)

Scheme 6.2 Preparation of analytes A191 and A192.

Bufolipin A (**1h**) exposed to BtH for 1 h exhibited no hydrolysis. However, HPLC-DAD (Method 1) (see Chapter 2) analysis after 48 h (Figure 6.12) revealed moderate levels (28%) of hydrolysis to yield the bufagenin, 11α,19-dihydroxy telocinobufagenin (**13a**) and the fatty acid 14-hydroxytetradecanoic acid (**5.1**). Marinobufotoxin (**1c**) was used as a control (refer Figure 4.31B).
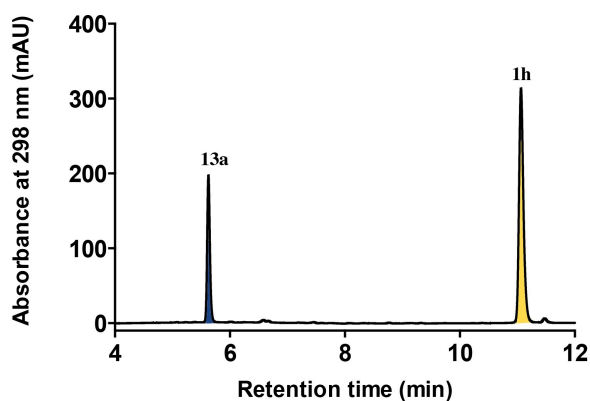
Figure 6.12 HPLC chromatogram (298 nm) of A192 analysed using Method 1

HPLC-DAD-MS confirmed the presence of 11α,19-dihydroxytelocinobufagenin (**13a**) (m/z 435, [M+H]), bufolipin A (**1h**) (m/z 659, [M+H]) and 14-hydroxytetradecanoic acid (**5.1**) (m/z 225, [M+H]) (Figure 6.13).
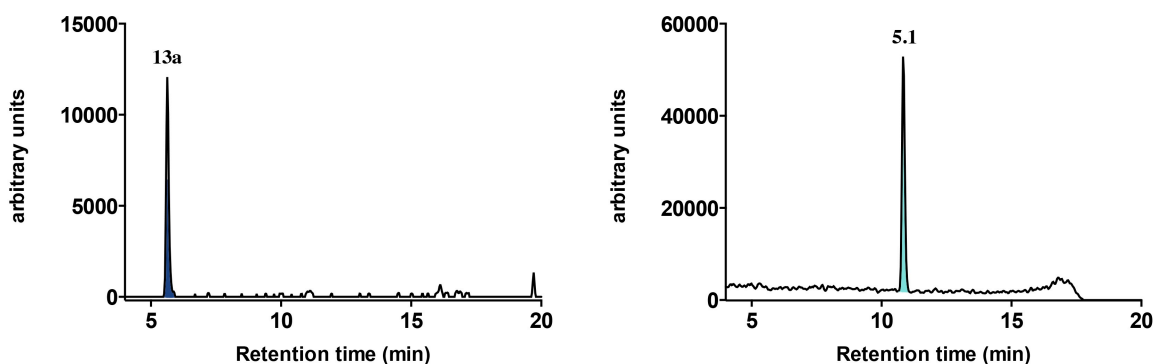
Figure 6.13 HPLC-DAD-MS analysis of A192 describing the single ion extraction for 11α,19-dihydroxytelocinobufagenin (**13a**) and 14-hydroxytetradecanoic acid (**5.1**)

6.2.8 Bufolipins as *B. marinus* tadpole attractants

Previous studies by Crossland et al showed that bufagenins and bufolipins attracted cane toad tadpoles, and can be used as toad specific baits.[3] These studies also determined that bufagenin baits lacked longevity as the bufagenins rapidly diffused into surrounding water with $t_{1/2}$ 48 h (data not shown). Bufolipins on the other hand are more hydrophobic than bufagenins and offer the prospect of longer lived baits. For practical reasons baits that continue to operate effectively for prolonged periods are deemed superior. Not withstanding their value, commercial supply of bufolipins from cane toad eggs is not practical. Hence, 'semi-synthetic bufolipin mimics' were synthesized from bufagenins recovered in high amounts from parotoid secretions. These bufolipin mimics were synthesized by esterification of bufagenins (e.g. **1a**) with long chain saturated fatty acids (e.g. octanoic acid) in a two-step reaction (Scheme 6.3). Synthetic bufolipins marinobufagenin-3-octanoate (**6h**) prepared as shown above showed better results (longevity) in cane toad tadpole attractant experiments (data not shown). Substantial amounts of synthetic bufolipins are required for field trials and required sourcing of large amounts of bufagenins.
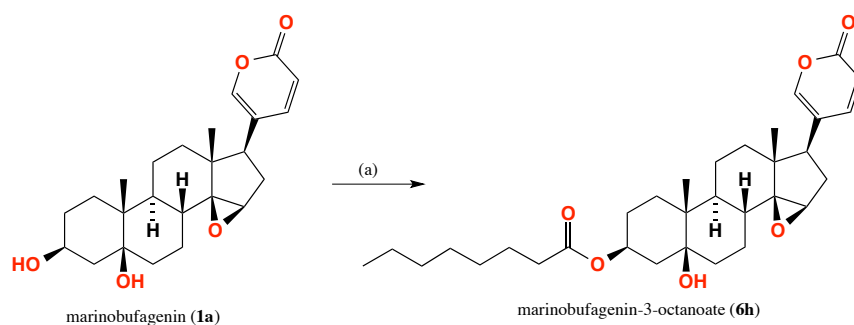
Scheme 6.3 Synthesis of bufolipins with octanoic acid (**5.1**) as example. (a) – reflux for 1 h with octanoic acid chloride and DMAP in pyridine
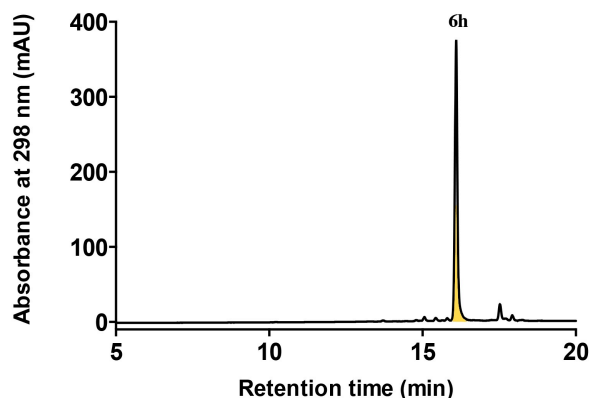
Figure 6.14 HPLC chromatogram of marinobufagenin-3-octanoate (**6h**) analysed using Method 4

271

6.2.8.1 Isolation of large amounts of bufagenins

Parotoid glands from 220 frozen cane toads were dissected, washed with H_2O and blended with MeOH using a tabletop blender. MeOH solubles along with tissue debris was subjected to filtration using Celite resin (Celite 545) to yield a mixture of bufadienolides and biogenic amines that was dried *in vacuo* to yield an oily residue, 11.2 g. This residue was subjected to sequential solvent trituration to yield *n*-hexane (1.6 g), EtOAc (5.8 g), *n*-BuOH (686 mg), MeOH (458 mg) and H_2O (3 g) solubles (Scheme 6.4). All samples were subjected to HPLC-DAD analysis using Method 1 (see Chapter 2) (Figure 6.14).

B. marinus
(parotoid glands)

⬇ (a)

A193 (11.2 g)

(b)	(c)	(d)	(e)	(f)
A194	A195	A196	A197	A198
(1.6 g)	(5.8 g)	(686 mg)	(458 mg)	(3 g)
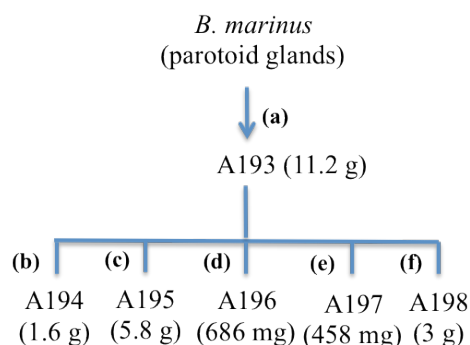
(a) – parotoid glands blended in MeOH and subjected to filtrations using Celite resin and flow through concentrated under vacuum
(b) – Trituration with *n*-hexane
(c) – Trituration with EtOAC
(d) – Trituration with *n*-BuOH
(e) – Trituration with MeOH
(f) – Trituration with H_2O

Scheme 6.4 Preparation of analytes A193 – A198.

EtOAc solubles (A195) contained only bufagenins and constituted more than 60% of parotoid secretions (based on mass recovery). *n*-BuOH solubles (A196) exhibited a mixture of bufotoxins (37%) and bufagenins (63%) with higher quantities of bufagenins (Figure 6.15). MeOH solubles (A197) consisted significant amount of bufotoxins (58%) followed by bufagenins (42%). Analysis of *n*-hexane solubles (A194) revealed the absence of bufadienolides. Armed with significant supply of bufagenins (>5.8 g) synthetic bufolipins can be synthesized as mentioned previously (Scheme 6.3) to support large scale field trials. These studies are ongoing.
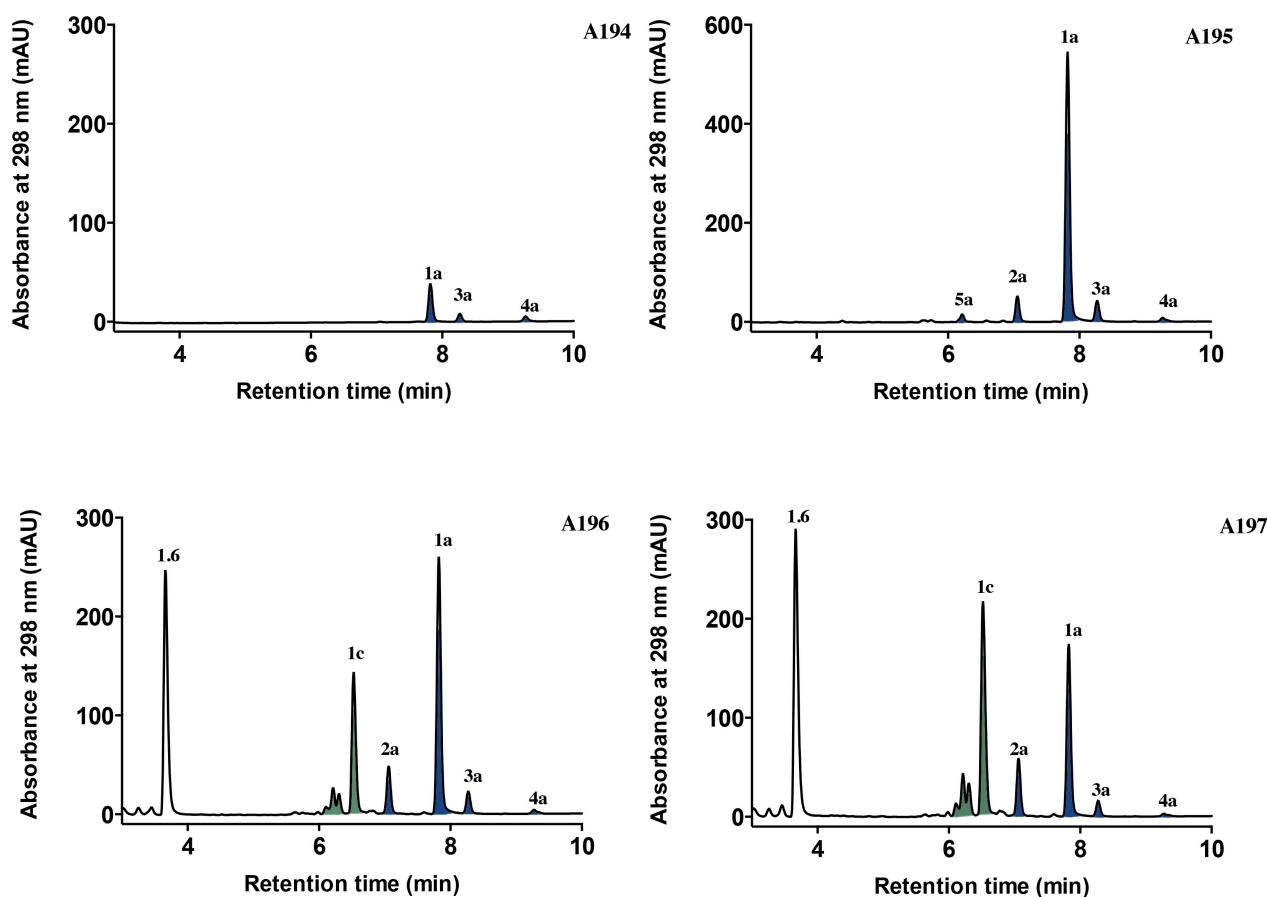
Figure 6.15 HPLC traces (298nm) of analytes A192 – A195 analysed using Method 1. Marinobufagenin (**1a**), telocinobufagenin (**2a**), bufalin (**3a**), resibufagenin (**4a**), arenobufagenin (**5a**), marinobufotoxin (**1c**) and dehydrobufotenin (**1.6**)

6.3 Conclusion

- Bufolipins were detected and isolated from *B. marinus* eggs using analytical methodologies developed using bufagenin ester standards

- *B. marinus* eggs contain bufagenins, bufolipins and hydrophobic molecules (such as fatty acids)

- Eight known bufagenins and two unknown bufagenins were identified in *B. marinus* eggs

- Two known and five uncharacterized bufolipins were detected in *B. marinus* eggs

- Synthetic bufolipins have previously been shown to attract *B. marinus* tadpoles at a similar potency to natural bufolipins. These synthetic bufolipins can be prepared by esterification of bufagenins obtained from extraction of adult can toad parotoid secretions. This current study has generated gram quantities of bufagenins for future elaboration in to synthetic bufolipins

6.4 Experimental

6.4.1 analytical methodologies for detection and isolation of bufolipins

Table 6.1 Analytical methods for the detection of bufolipins

	Method	Structure class	Conditions
HPLC-DAD	Method 4	bufolipins	Zorbax C_8 column, 150×4.6 mm, 5 μm, 1 mL/min, gradient from 90% H_2O/ MeCN to 100% MeCN over 15 min, hold at 100% MeCN over 5 min, with constant 0.01% modifier (TFA).
HPLC-DAD	Method 5	bufolipins	Zorbax C_8 column, 150×4.6 mm, 5 μm, 1 mL/min, gradient from 90-50% H_2O/ MeCN over 5 min, 50-30% H_2O/ MeCN over 15 min, 30% H_2O/ MeCN to 100% MeCN over 5 min, holding 100% MeCN for 5 min, with constant 0.01% modifier (TFA).

6.4.2 Isolation and identification of bufagenins and bufolipins from *B. marinus* eggs

A single clutch of *B. marinus* eggs from one cane toad was collected (USyd), lyophilized, solubilized in MeOH, filtered and the filtrate reduced to dryness under vacuum. The MeOH solubles were sequentially triturated with *n*-BuOH and H_2O and the *n*-BuOH solubles concentrated *in vacuo* and subjected to sequential trituration with *n*-hexane and *n*-BuOH. *n*-BuOH solubles was reduced to dryness under vacuum and subjected to preparative HPLC (Phenomenox, Luna C8 column, 250×21.2 mm, 10 μm, gradient from 90% H_2O/ MeCN to 100% MeCN over 15 min, holding 100% MeCN over 5 min and wash with 90% H_2O/ MeCN for 5 min, no TFA) to collect 25 fractions. Two fractions containing bufolipins were combined and purified using semi-preparative HPLC (Zorbax C_8 column, 250×9.4 mm, 5 μm, 1 mL/min, gradient from 90-50% H_2O/ MeCN over 5 min, 50-30% H_2O/ MeCN over 15 min, 30% H_2O/ MeCN to 100% MeCN over 5 min, hold at 100% MeCN for 5 min, no TFA).

6.4.3 Synthesis of octanoic acid chloride

A solution of octanoic acid (200 mg, 1.30 mmol) in thionyl chloride (3 mL) was refluxed for 6 h following which octanoic acid chloride was carefully obtained by distilling off the reaction mixture using Kugelrohr.

6.4.4 Synthesis of marinobufagenin-3-octanoate (6h)

A solution of marinobufagenin (**1a**) (5 mg, 12.5 μmol) is refluxed with octanoic acid chloride (25 μL) in the presence of DMAP (0.6 mg, 4.9 μmol) in pyridine (3 mL) for 1 h with constant stirring following which the reaction mixture was dried under N_2 at 40 °C and subjected to purification using semi-preparative HPLC (Zorbax C_{18} column, 250 × 9.4 mm, 5 μm, 1 mL/min, gradient from 90% H_2O/ MeCN to 100% MeCN over 15 min, holding 100% MeCN over 5 min, with constant 0.01% modifier (TFA)) to yield marinobufagenin-3-octanoate (1.2 mg) (Appendix Fig S30).

^{1}H NMR (CD$_3$OD, 600 MHz) δ$_H$ 0.76 (s, H-18), 0.92 (s, H-19), 1.38 (m, H-3′- H-7′), 2.72 (m, H-17), 2.78 (s, H-8′), 3.60 (s, H-15), 6.46 (dd, H-23), 7.42 (d, H-22), 7.94 (d, H-21) ppm. (Appendix Figure S30). colourless oil; $[\alpha]^{21}_D$ +37.8 (*c* 0.1, CHCl$_3$); HRESI(+)MS m/z 549.3187 (M+Na)$^+$ (calcd for $C_{32}H_{46}O_6$, 549.3180).

6.4.5 Isolation of bufagenins from parotoid secretions

Parotoid glands from 220 frozen toads were dissected and disrupted in a blender containing MeOH to release all the secretions. The MeOH solubles along with tissue debris was collected and was subjected to filtration using Celite resin (Celite 545) and the flow through was collected, reduced to dryness under vacuum and was triturated with *n*-hexane, EtOAc, *n*-BuOH, MeOH and H_2O.

6.5 References

1. Akizawa, T.; Mukai, T.; Matsukawa, M.; Yoshioka, M.; Morris, J. F.; Butler, V. P., Structures of novel bufadienolides in the eggs of a toad, *Bufo marinus*. *Chem. Pharm. Bull.* **1994,** *42*, 754-756.
2. Matsukawa, M.; Mukai, T.; Akizawa, T.; Miyatake, S.; Yoshioka, M.; Morris, J. F.; Butler, V. P., Isolation and characterization of novel endogenous digitalis-like factors in the ovary of the giant toad, *Bufo marinus*. *J. Nat. Prod.* **1998,** *61*, 1476-1481.
3. Crossland, M. R.; Haramura, T.; Salim, A. A.; Capon, R. J.; Shine, R., Exploiting intraspecific competitive mechanisms to control invasive cane toads (*Rhinella marina*). *Proc. R. Soc. B-Biol. Sci.* **2012,** *279*, 3436-3442.
4. Hayes, R. A.; Piggott, A. M.; Dalle, K.; Capon, R. J., Microbial biotransformation as a source of chemical diversity in cane toad steroid toxins. *Bioorg. Med. Chem. Lett.* **2009,** *19*, 1790-1792.

Figure S30 ^{1}H NMR (600 MHz, CD$_3$OD) spectrum for marinobufagenin-3-octanoate (**6h**)
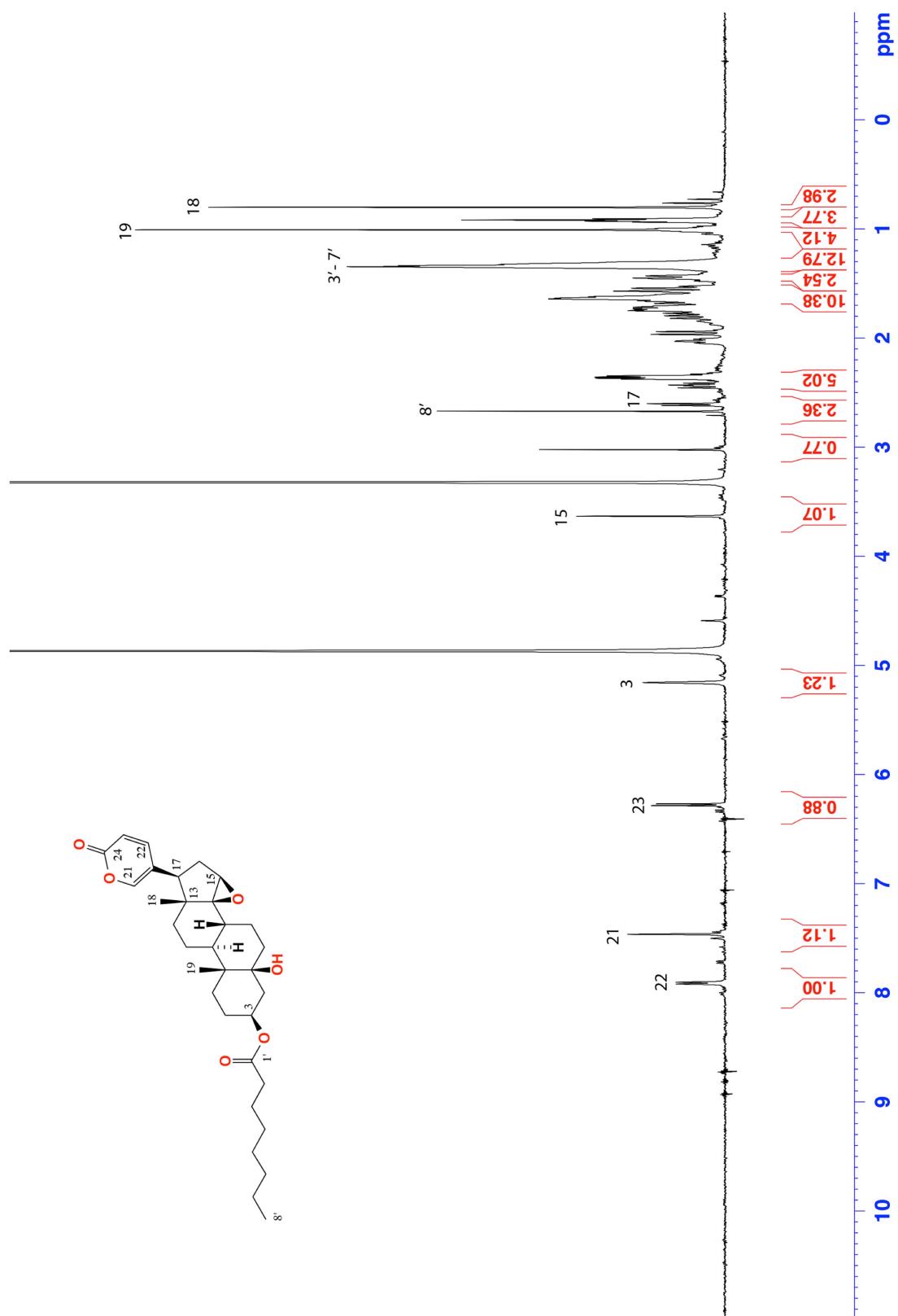
Chapter 7: Comparative analysis of the pharmacological properties of individual cane toad toxins

7.1 Introduction

7.1.1 Cane toad toxins and toxicity

The aim of the chapter is to investigate the toxicological/pharmacological properties of cane toad bufadienolides and arginyl amides. The language pertaining to cane toad toxins in the literature is often vague and inaccurate. For example, parotoid secretions are often described as venoms which conjures a particular view of there use as effective weapons. As venoms are typically injected by a specialized fang or spine, this description is quite inappropriate when applied to cane toads, which lack any such apparatus. Quite the opposite, cane toad toxin is only released involuntarily following physical pressure during a predatory attack – in which the toad is the victim not the aggressor.

This confusion also extends to attempts to use *in vitro* experiments to characterize the toxicity of cane toad toxins. Assays carried out on crude toxins[1,2] are of questionable value for a range of reasons; For example, as the diversity and ratio of chemicals present within a toxin sample can vary depending on the individual toad, the method of extraction, the method of handling and the method of storage, any assays carried out on uncharacterized toxin cannot be reproduced. Furthermore, the prospect that different chemical components could exert additive, complementary and/or synergistic effect needs to be considered.[2]

Finally, the choice of assay is critical as it underlines the relevance, reproducibility and reliability of any interpretation. Regrettably, many literature accounts of cane toad toxicity use poorly documented or questionable methodology, and extrapolate to conclusions that are not well defended. Consider the following SWOT analysis of some of the most common assays – Na^+/K^+ ATPase and cytotoxicity assays.

7.1.2 Conventional assays: a critique

Na^+/K^+ ATPase, an ion channel responsible for the transport of Na^+ and K^+, is expressed in various tissues as different isoforms, and bufadienolide toxicity is often correlated with inhibition of cardiac Na^+/K^+ ATPase. Although, Na^+/K^+ ATPase inhibition by bufadienolides had been described since 1960's, the typical assay system employs Na^+/K^+ ATPase isolated from pigs (liver or brain).[3, 4] For practical reasons the more ecologically relevant cardiac Na^+/K^+ ATPase sourced from crocodiles, snakes, quolls, is not available, which means published account of bufadienolide Na^+/K^+ ATPase

toxicity lack ecological relevance and yet they are often used to infer ecological significance! Several researchers have performed Na^+/K^+ ATPase inhibition assays using various assay platforms.[2, 4, 5] The most common assay platform is displacement of radio labeled ouabain by analytes such as bufadienolides where ouabain is viewed as a positive control. Again the ecological relevance is questionable as ouabain is a cardenolide glycoside not a bufadienolide, and the assay measures a ligand displacement not a loss of function. Perhaps an even larger risk is the willingness by some researchers to make quantitative comparisons between assay results obtained in different enzyme preparations, in different labs, using different protocols, such unqualified comparisons are of very little value.
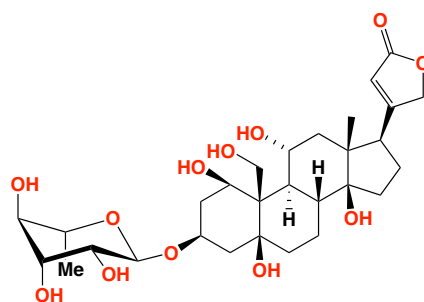
ouabain (**1.10**)

Table 7.1 List of pharmacological properties reported on various bufadienolide structure classes isolated from *B. marinus* reported from various countries (reused from Table 1.2)

Pharmacological properties (cell/tissue types)	bufagenins	bufotoxins	bufolipins	bufagenin sulfates	bufagenin glycosides
Na^+/K^+ ATPase inhibition					
human kidney[3]	**1a, 2a**				
C7-MDCK cells[2]	**1a, 3a**	**1c, 2c**			
dog Kidney/pig brain[4]	**3a**				
guinea pig heart[6]	**1a, 2a**	**1c, 2c, 8c**			
guinea pig heart[5]	**1a**	**1c**		**1f**	**1g**
dog kidney[7]			**1h, 2h, 3h**		
Cytotoxicity					
PLC/PRF/5 cells[8]	**1a, 2a, 3a, 4a, 5a**				
HL-60, HCT-8, SF295, MDA-MB435, PBLS[9]	**1a, 2a, 3a, 5a**				
A549, U373, HS683, MCF-7[10]				**2f**	
Antibiotic – *E. coli* and *S. aureus*[11]	**1a, 2a**				

A list of bufadienolides submitted for various Na^+/K^+ ATPase inhibition assays from various sources and cell types and different read outs are listed in Table 7.1. Since the assays had several different parameters it is difficult to compare their outcomes. For example, a study performed by

Shimada et al in 1985 reported marinobufotoxin (**1c**) is more potent than marinobufagenin (**1a**) while Akimova et al in 2005 reported the opposite.[2, 5] The former assay was performed on guinea pig Na^+/K^+ ATPase and the read out was monitored using HPLC analysis while the latter was performed on MDCK cell lines using a ouabain radio labeled displacement assay system. [2, 5] Although the radio ligand displacement assay is generally accessible and provides a measure of binding affinity, the fact that it does not address functionality, and that it lacks a consistent cell/tissue derived Na^+/K^+ ATPase (e.g. varying across pigs and dogs), and meaningful positive control, make the assay highly questionable.

Cytotoxicity exhibited by bufadienolides performed *in vitro* is often compared to the toxicity of cane toad toxins.[10] Cytotoxicity is mostly performed on mammalian cancer cell lines, which are ecologically irrelevant assay systems. Moreover, cytotoxicity exhibited by bufadienolide is not entirely due to Na^+/K^+ ATPase inhibition as several pathways could be potential targets. Also cytotoxicity could possibly vary for each cell types contradicting the results, as some bufadienolides could be cytotoxic to one cell type while non-cytotoxic to others. A list of bufadienolides subjected to various cytotoxicity assays including various cell types are listed in Table 7.1. As mentioned previously comparative SAR studies including all bufadienolide structure classes is difficult as different bufadienolides were subjected to cytotoxicity studies with different cell types. Strengths of cytotoxicity assays include accessibility, feasibility and direct measurement of toxicity exhibited against selected cell types. Lack of relevant cell/tissues from relevant source organism and difference in readouts based on cell types are the weaknesses. Opportunities include inclusion of various bufadienolide structure classes in a single assay platform for comparative studies. Threat includes the correlation of *in vitro* assay to an ecological context.

7.1.3 Cane toad toxicity – pharmacological or ecological

Both *in vitro* Na^+/K^+ ATPase inhibition and cytotoxicity are attributed to the pharmacological properties of bufadienolides and are difficult to link to an ecological role due to lack of relevant assay systems. In addition, the oral bioavailability of cane toad parotoid secretions plays a critical role in the ecological significance of bufadienolides. Predators that present with lower bufadienolide oral bioavailability could possibly survive being poisoned by cane toads.

Only one study on antibiotic activity of bufadienolides is reported.[11] The assay system included pathogenic bacteria like *Escherichia coli* and *Staphylococcus aureus*. It is highly unlikely to correlate the assay results to relevant ecological context since the assay did not include toad-

specific pathogenic strains. Hence the antibiotic activity is correlated to the pharmacological properties of bufadienolides and cannot be translated into ecological relevance.

In summary, "toxicity" of cane toad parotoid secretions could be differentiated into pharmacological and ecological toxicity. Pharmacological toxicity includes Na^+/K^+ ATPase inhibition, cytotoxicity and antimicrobial properties of bufadienolides under *in vitro* conditions while ecological toxicity indicates a relevant assay (*in vivo*) performed on cane toad predators. However, given the constraints in obtaining Na^+/K^+ ATPase from tissue samples from predators such as crocodiles, quolls, lizards or snakes and the ethics approval for performing such assays made it difficult to pursue such studies.

Owing to the strengths of pharmacological toxicity listed above, cytotoxicity and antimicrobial properties of bufadienolides have been detailed in this chapter. Although this approach includes some weaknesses one of the additional strengths of the current investigation is inclusion of various bufadienolide structure classes for a comparative study. Cytotoxicity of bufadienolides in this context refers to the cell toxicity exhibited on mammalian cells while the antimicrobial property indicates the toxicity against certain gram positive and gram-negative bacteria. In either case it is the toxicity exhibited by cane toad toxins on mammalian and prokaryotic cells and does not solely refer to analysis of drug like characteristics. Due to the lack of time toxicity exhibited against fungal cells could not be performed. Investigations on cardiotoxicity of bufadienolides are significant however an assay to selectively inhibit cardiomyocytes (cardiac muscle cells involved in conduction of action potential) and a read out to quantify the inhibition is currently unavailable. Steps were taken to establish such an assay involving human cardiomyocytes and selective ion channel stains to quantitatively represent the inhibition of Na^+/K^+ ATPase, however, due to lack of time the assay could not be completed. That said a future work (in collaboration with Dr Ivan Birros, GE Health Sciences) has been planned to establish cardiomyocytes assay. Hence, the toxicity studies described in the current chapter represents pharmacological toxicity and this cannot be extended to ecological context.

During our investigations on bufadienolide pharmacological properties arginyl amides were also included in various pharmacological studies (such as cytotoxicity and antimicrobial properties) (Scheme 7.1).
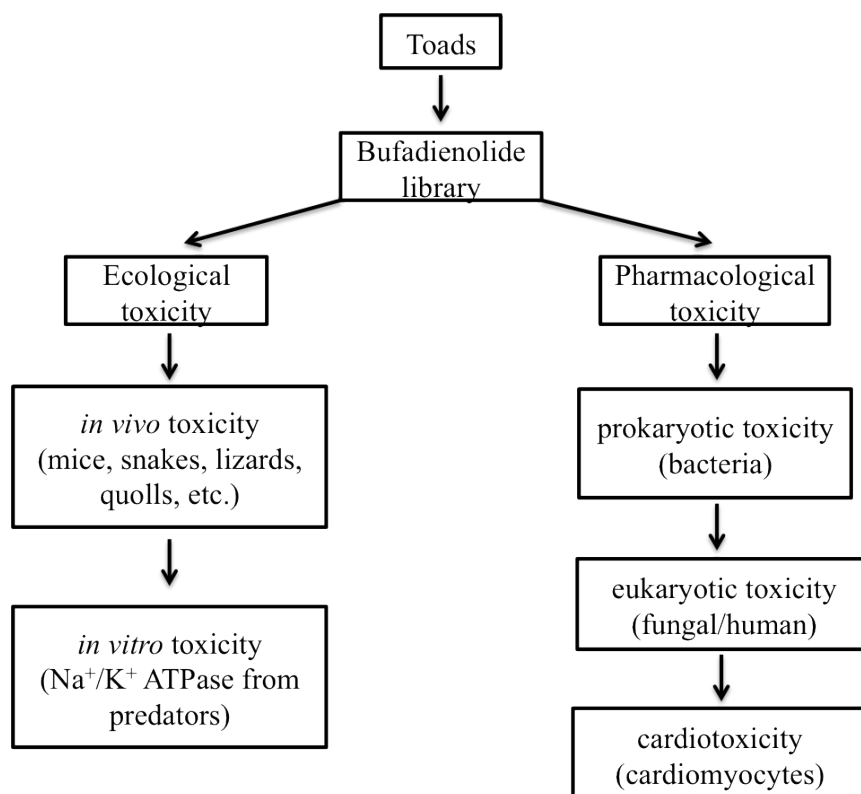
Scheme 7.1 Investigations of pharmacological activities of bufadienolides and arginyl amides

7.2 Results and discussion

7.2.1 Pharmacological toxicity studies on bufadienolides

Pharmacological toxicity studies on bufadienolides was performed by investigating the toxicity exhibited on prokaryotes (bacteria) and mammalian cells (cancer cell lines) by various structure classes of bufadienolides. Table 7.2 illustrates the bufadienolides and their pharmacological toxicity.

Table 7.2 Prokaryotic and mammalian cell toxicities of bufadienolides

Bufadienolide	Prokaryotic cytotoxicity*	Mammalian cytotoxicity**
marinobufagenin (**1a**)	✗	✓
telocinobufagenin (**2a**)	✗	✓
bufalin (**3a**)	✗***	✓
hellebrigenin (**5a**)	✗	✓
bufalin-3-acetate (**7a**)	✗	✓
marinobufagenin-3-suberate (**1b**)	✗	✗
telocinobufagenin-3-suberate (**2b**)	✗	✗
bufalin-3-suberate (**3b**)	✗	✓
marinobufagenin-3-pimelate (**5b**)	✗	✗
marinobufagenin-3-succinate (**9b**)	✗	✓
marinobufotoxin (**1c**)	✗	✓
telocinobufotoxin (**2c**)	✗	✓
bufalitoxin (**3c**)	✗	✓
bufolipin A (**1h**)	✗	✓
bufolipin B (**2h**)	✗	✓

*performed with *Bacillus subtilis*, *Escherichia coli*, *Pseudomonas aeruginosa*, and *Staphylococcus aureus* (strains ATCC 550 & ATCC 1900)
** performed with human SW 620 (colon cancer) and SF-295 (glioblastoma) cell lines
***moderate activity against *P. aeruginosa*
✓ MIC less than 64 μg/mL; IC_{50} less than 30 μM
✗ No antimicrobial; No cytotoxicity

Interestingly none of the bufadienolide structure classes were antibiotic to the pathogenic bacteria investigated *in vitro*. However, bufadienolides showed significant cytotoxicity against the mammalian cancer cell lines. Toxicity against mammalian cells is consistent with previous literature.[8] Bufadienolide structure classes exhibited a range of cytotoxicity levels based on substitutions at C-3, which are discussed in sections below.

7.2.2 Cytotoxicity of bufadienolides – An SAR study

7.2.2.1 Cytotoxicity of bufagenins

Bufagenins subjected to cytotoxicity assays against SW 620 (colon cancer) and SF-295 (glioblastoma) cell lines included marinobufagenin (**1a**), telocinobufagenin (**2a**), bufalin (**3a**) and hellebrigenin (**5a**) (Figure 7.1). The IC_{50} values exhibited by each bufagenin represented the half maximal inhibition of the growth of cells, which is indicated by the stain, MTT. The IC_{50} curves are illustrated in Figure 7.2 and the values in Table 7.3.
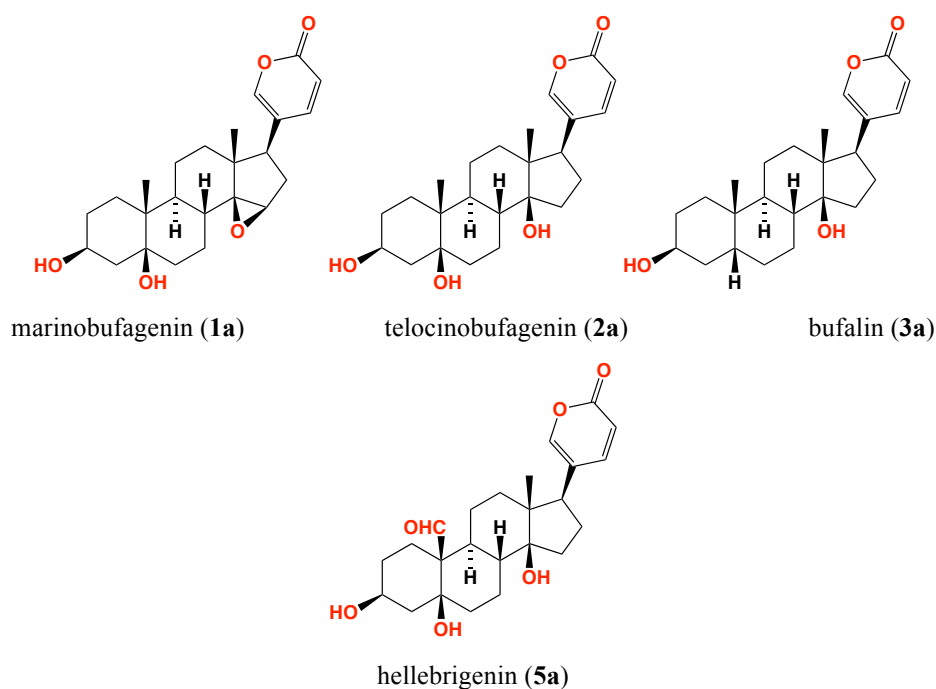
Figure 7.1 Bufagenins subjected to cytotoxicity assays
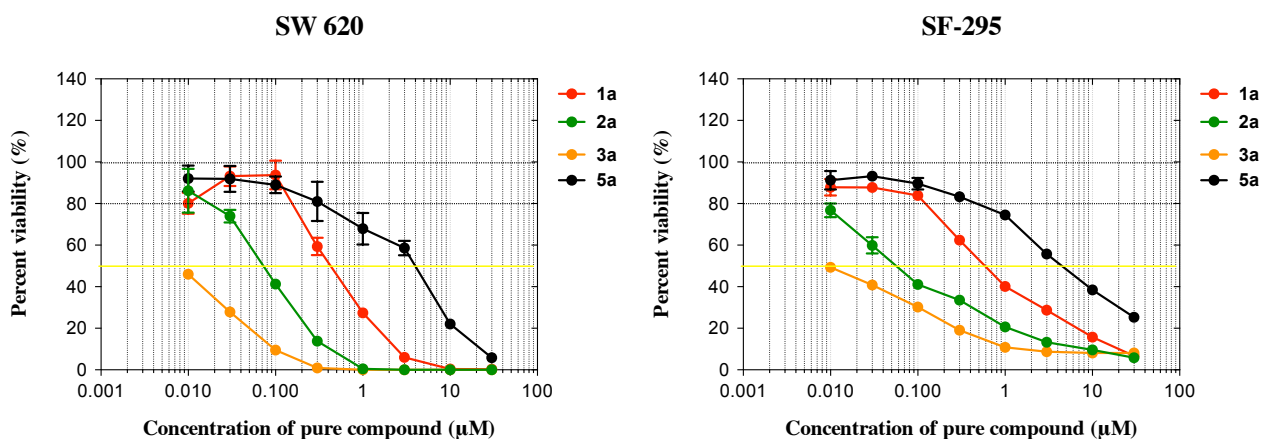
Figure 7.2 Cytotoxicity (IC_{50}) of bufagenins from parotoid secretions for SW 620 and SF-295 cell lines

The IC_{50} for bufagenins in the current investigation is in agreement with Kamano et al where bufalin (**3a**) was determined to be the most cytotoxic bufagenin followed by telocinobufagenin with

sub-nano molar potency.[8] A striking similarity of bufalin and telocinobufagenin is the hydroxyl at C-14, which could play a major role in the potent cytotoxicity. Cytotoxicity of hellebrigenin reduced to micromolar concentrations possibly due to an aldehyde substitution at C-10.

7.2.2.2 Cytotoxicity of bufagenin esters

Bufagenin esters subjected to cytotoxicity assays against SW 620 (colon cancer) and SF-295 (glioblastoma) cell lines included bufalin-3-acetate (**7a**), marinobufagenin-3-suberate (**1b**), telocinobufagenin-3-suberate (**2b**), bufalin-3-suberate (**3b**), marinobufagenin-3-pimelate (**5b**) and marinobufagenin-3-succinate (**9b**) (Figure 7.3). The IC$_{50}$ curves are illustrated in Figure 7.4 and the values in Table 7.3.

bufalin-3-acetate (**7a**) marinobufagenin-3-succinate (**9b**) marinobufagenin-3-pimelate (**5b**)

marinobufagenin-3-suberate (**1b**) telocinobufagenin-3-suberate (**2b**)

bufalin-3-suberate (**3b**)
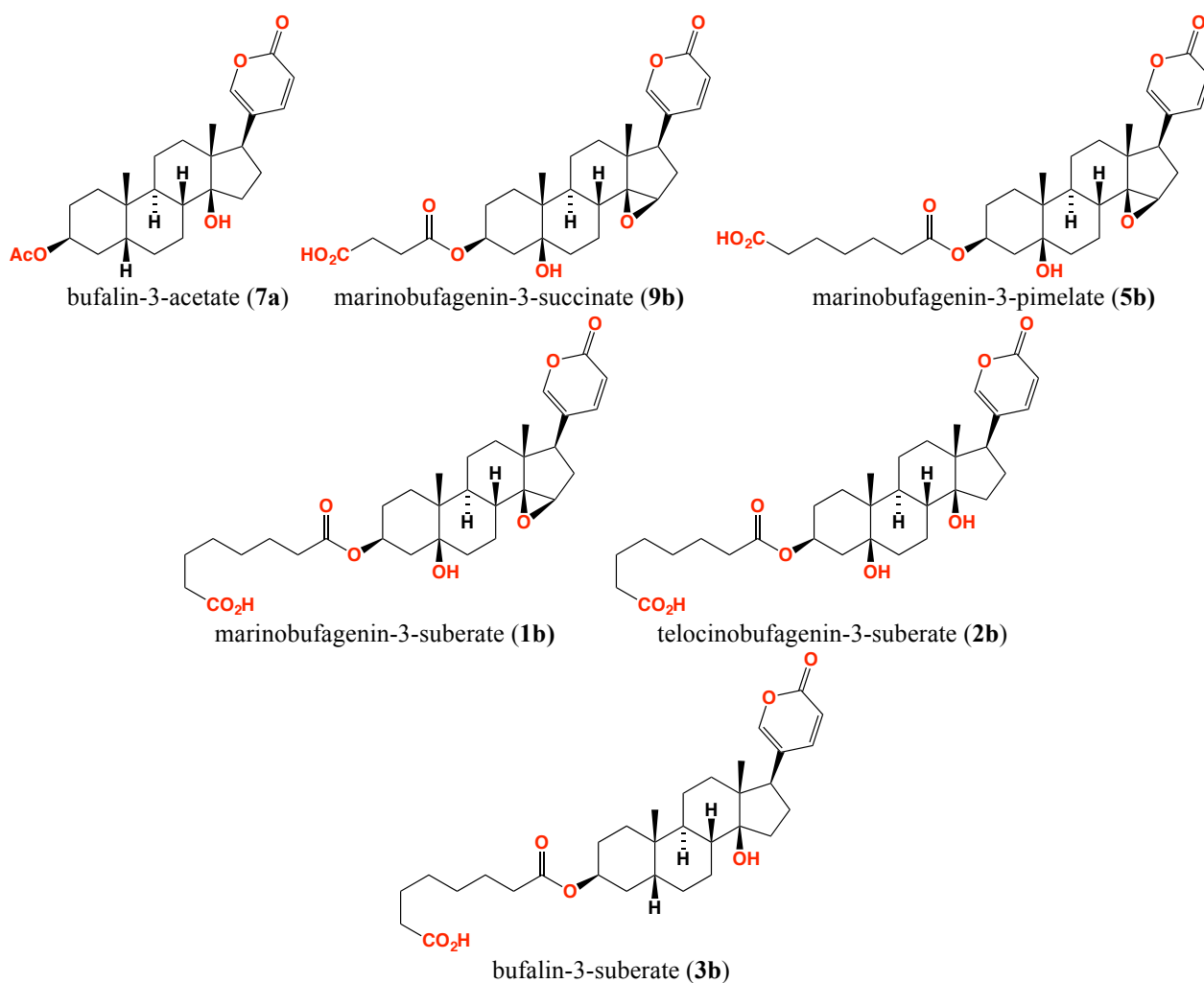
Figure 7.3 Bufagenin esters subjected to cytotoxicity assays
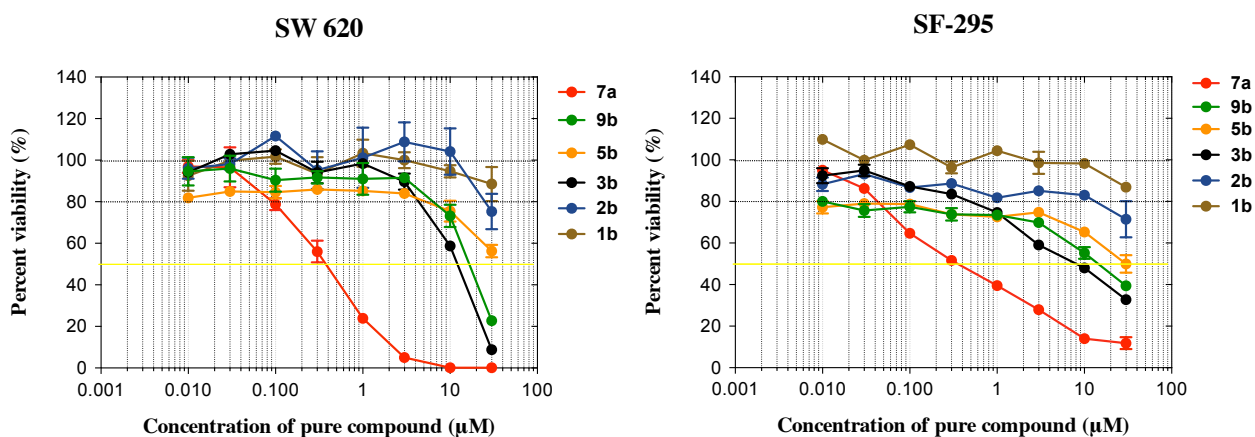
Figure 7.4 Cytotoxicity (IC$_{50}$) of bufagenin esters from parotoid secretions and synthetic analogues for SW 620 and SF-295 cell lines

Comparison of IC$_{50}$ values of bufagenin esters in the current investigations indicated that shorter the chain length of the ester at C-3 the higher is the cytotoxicity. Similarly, among marinobufagenin analogues, marinobufagenin-3-succinate (**8b**) with the shortest chain length (n=2) at C-3 showed IC$_{50}$ of 16.16 μM while other analogues are non-cytotoxic. Among the bufagenin esters subjected to cytotoxicity, bufalin analogues are more cytotoxic than marinobufagenin and telocinobufagenin analogues, which is consistent with previous investigations with bufagenins.[8]

7.2.2.3 Cytotoxicity of bufotoxins

Bufotoxins subjected to cytotoxicity assays against SW 620 (colon cancer) and SF-295 (glioblastoma) cell lines included marinobufotoxin (**1c**), telocinobufotoxin (**2c**) and bufalitoxin (**3c**) (Figure 7.5). The IC$_{50}$ curves are illustrated in Figure 7.6 and the values in Table 7.3.

marinobufotoxin (**1c**)　　　　　　　telocinobufotoxin (**2c**)

bufalitoxin (**3c**)
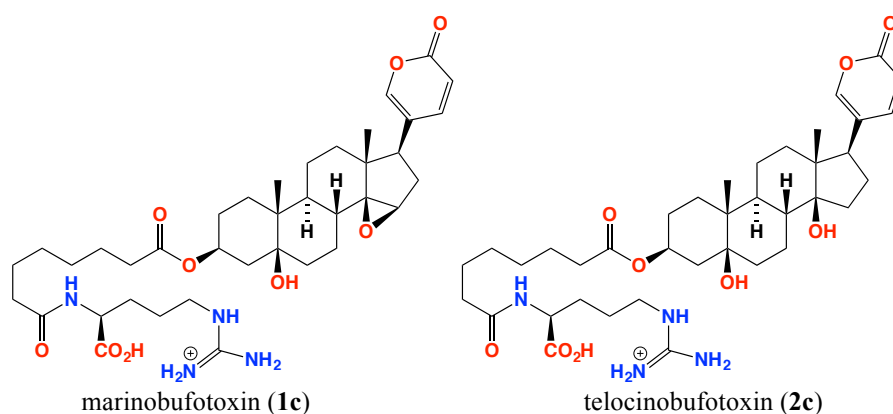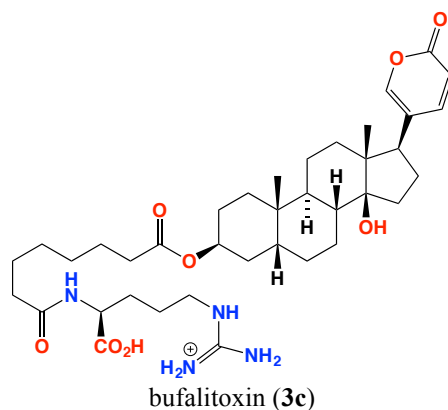
Figure 7.5 Bufotoxins subjected to cytotoxicity assays
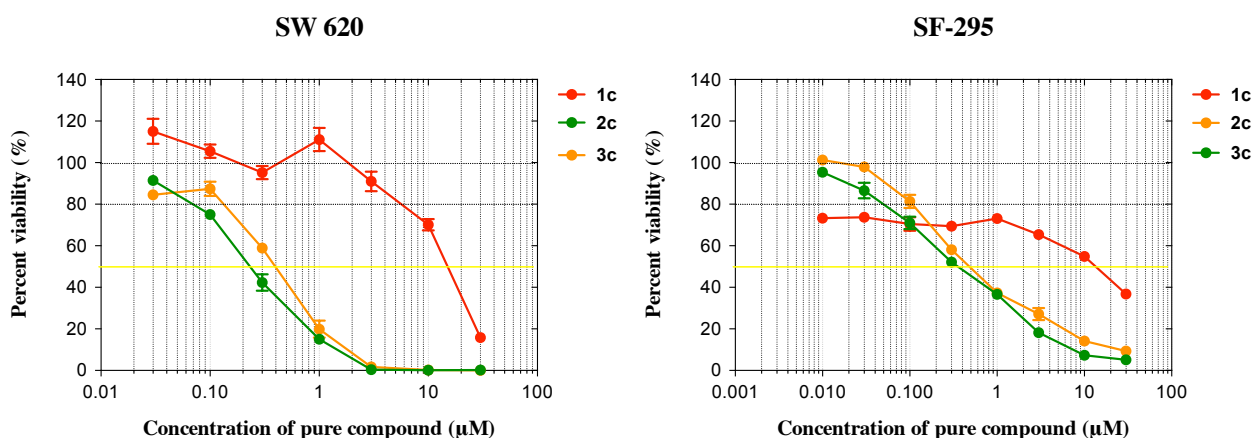
Figure 7.6 Cytotoxicity (IC$_{50}$) of bufotoxins for SW 620 and SF-295 cell lines

Cytotoxicity levels of bufotoxin in the current investigations revealed interesting findings, the dominant bufotoxin (>75%) in parotoid toxins *in situ*, marinobufotoxin (**1c**) showed the least cytotoxicity against SW 620 and SF-295, with a significant difference compared to other bufotoxins. The cytotoxicity levels comparison within the bufotoxin scaffold was similar to bufagenin and bufagenin esters scaffolds.

7.2.2.4 Cytotoxicity of bufolipins

Bufolipins subjected to cytotoxicity assays against SW 620 (colon cancer) and SF-295 (glioblastoma) cell lines included bufolipin A (**1h**) and bufolipin B (**2h**) (Figure 7.7). The IC$_{50}$ curves are illustrated in Figure 7.8 and the values in Table 7.3.

bufolipin A (**1h**)
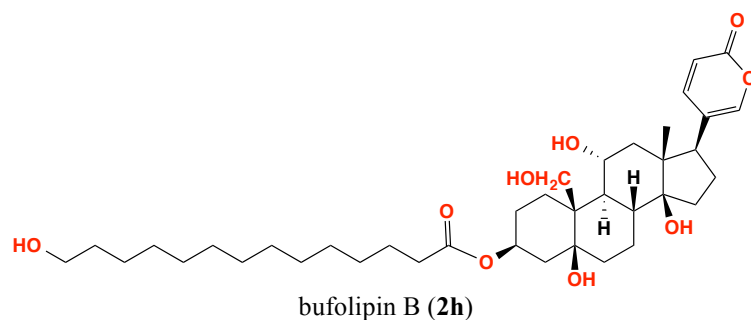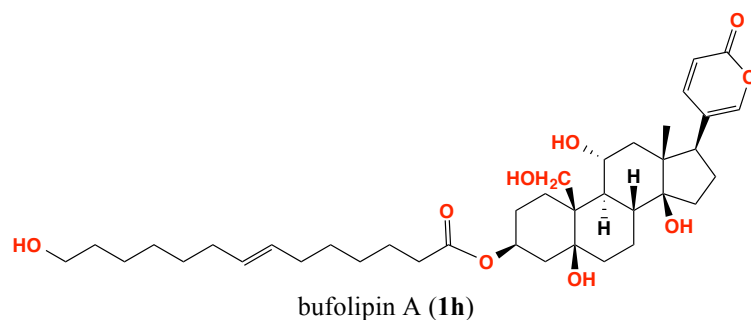
bufolipin B (**2h**)

Figure 7.7 Bufolipins subjected to cytotoxicity assays
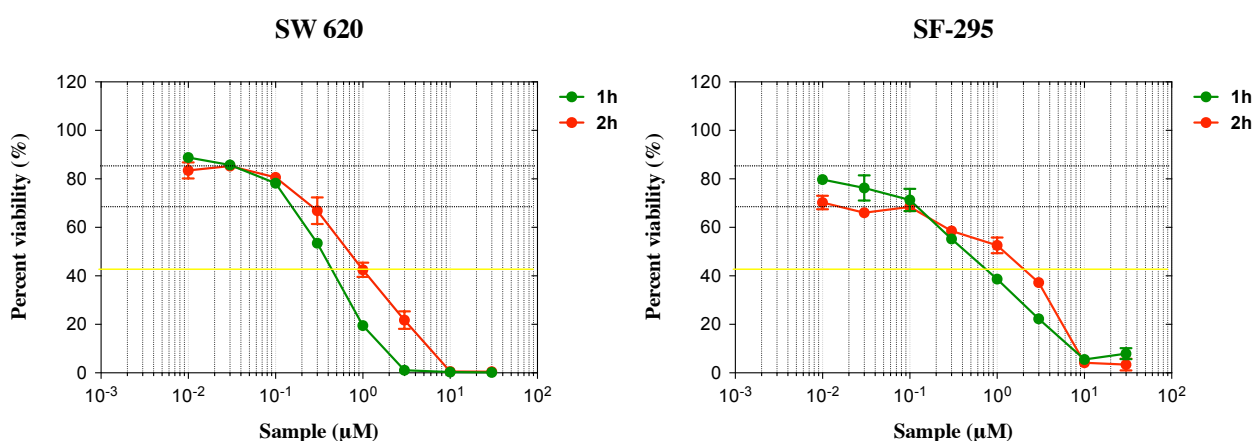
Figure 7.8 Cytotoxicity (IC_{50}) of bufolipins for SW 620 and SF-295 cell lines

Interestingly, cytotoxicity levels of bufolipins in the current investigations are also comparable to bufotoxins, such as bufalitoxin and telocinobufotoxin. In the case of bufagenin esters it was determined that long chain esters at C-3 could deter cytotoxicity levels, however, cytotoxicity levels of bufolipins clearly suggests the importance of terminal hydroxyl at C14′ of the fatty acid ester. Another important observation is that both bufolipin A and bufolipin C has C14 hydroxyl as in the case of bufalin and telocinobufagenin scaffolds, thus exhibiting higher cytotoxicity.

7.2.2.5 Discussion – SAR studies on cytotoxicity of bufadienolides

Table 7.3 IC_{50} values of bufadienolides against mammalian cancer cells

Structure class	Bufadienolide	IC_{50} (μM)	
		SW620	SF-295
bufagenin	marinobufagenin (**1a**)	0.44	0.68
bufagenin	telocinobufagenin (**2a**)	0.07	0.07
bufagenin	bufalin (**3a**)	0.01	0.01
bufagenin	hellebrigenin (**5a**)	2.67	4.74
bufagenin ester	bufalin-3-acetate (**7a**)	0.35	0.44
bufagenin ester	marinobufagenin-3-suberate (**1b**)	>30	>30
bufagenin ester	telocinobufagenin-3-suberate (**2b**)	>30	>30
bufagenin ester	bufalin-3-suberate (**3b**)	11.3	7.53
bufagenin ester	marinobufagenin-3-pimelate (**5b**)	>30	>30
bufagenin ester	marinobufagenin-3-succinate (**9b**)	16.16	24.04
bufotoxin	marinobufotoxin (**1c**)	14.92	20.26
bufotoxin	telocinobufotoxin (**2c**)	0.37	0.63
bufotoxin	bufalitoxin (**3c**)	0.23	0.38
bufolipin	bufolipin A (**1h**)	0.29	0.35
bufolipin	bufolipin B (**2h**)	0.58	0.38

The current investigation of SAR studies of cytotoxicity exhibited by bufadienolide structure classes including bufagenins, bufagenin esters, bufotoxins and bufolipins suggests that bufagenins are the most cytotoxic class of bufadienolides followed by bufolipins and bufotoxins (Table 7.3). A cross comparison of marinobufagenin scaffolds of bufadienolides indicates that marinobufagenin (**1a**) is the most toxic scaffold followed by bufolipins (**1h** and **2h**) and marinobufotoxin (**1c**) (Figure 7.9). We hypothesize that bufotoxins, besides providing physical, chemical and microbiological stabilities, also provides biological stability from self-intoxication. On the other hand, bufagenins exhibiting high to very high cytotoxicity are potent molecules generated from the pool of bufotoxins, similar to that of a "pro-drug" to "drug" metabolism. Bufolipins could also provide better solubility characteristics (hydrophobicity) and with a better cytotoxicity profiles they could be ideal bufadienolide delivery vehicles adopted by *B. marinus* eggs.
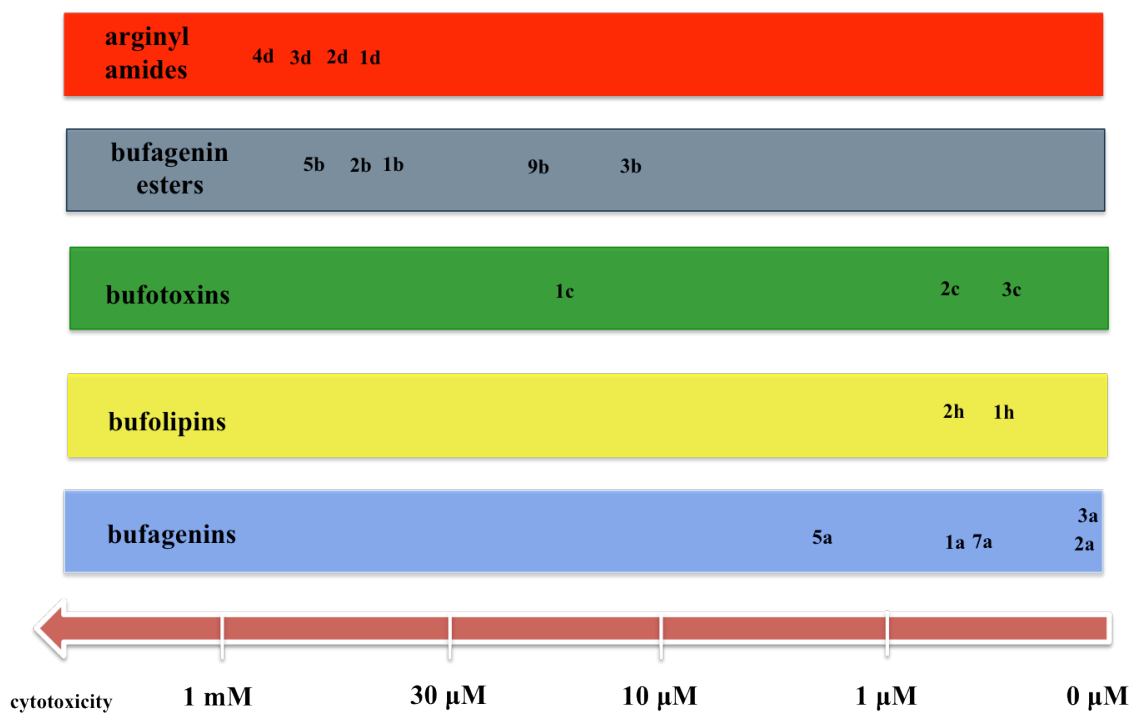
Figure 7.9 Structure activity relationship of bufadienolide structure classes based on cytotoxicity

7.2.2.6 Cytotoxicity of arginyl amides

Arginyl amides subjected to cytotoxicity assays against SW 620 (colon cancer) and SF-295 (glioblastoma) cell lines included suberoyl-L-arginine (**1d**), adipoyl-L-arginine (**2d**), pimeloyl-L-arginine (**3d**) and azeloyl-L-arginine (**1d**) (Figure 7.10). None of the arginyl amides exhibited cytotoxicity activity (Figure 7.11).

adipoyl-L-arginine (**2d**)

pimeloyl-L-arginine (**3d**)

suberoyl-L-arginine (**1d**)

azeloyl-L-arginine (**4d**)
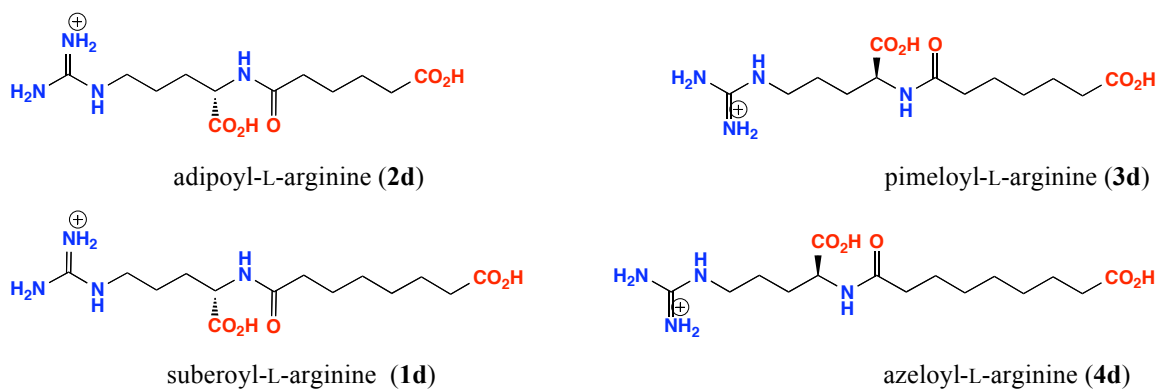
Figure 7.10 Arginyl amides subjected to cytotoxicity assays
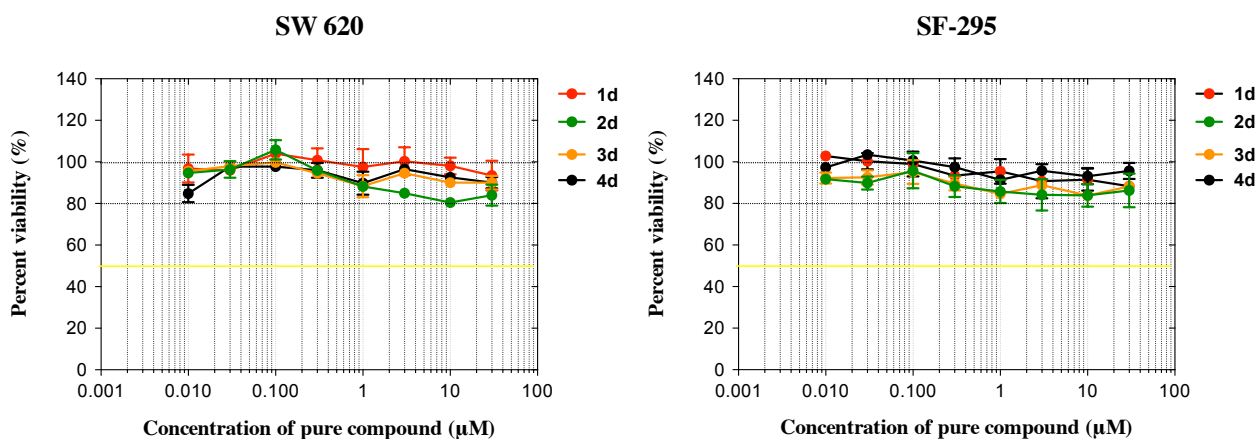
Figure 7.11 Cytotoxicity (IC$_{50}$) of arginyl amides for SW 620 and SF-295 cell lines

Arginyl amides such as suberoyl-L-arginine (**1d**) and pimeloyl-L-arginine (**3d**) are identified in parotoid secretions and are present in significant amounts (see Chapter 3). However, the absence of cytotoxicity observed with arginyl amides does not necessarily indicate an absence of ecological significance. Arginyl amides may act independently (possibly different targets) compared to bufadienolides. Figure 7.12 illustrates the relationship between the cytotoxicity values of marinobufotoxin (**1c**) and its hydrolysis products in our current investigation.
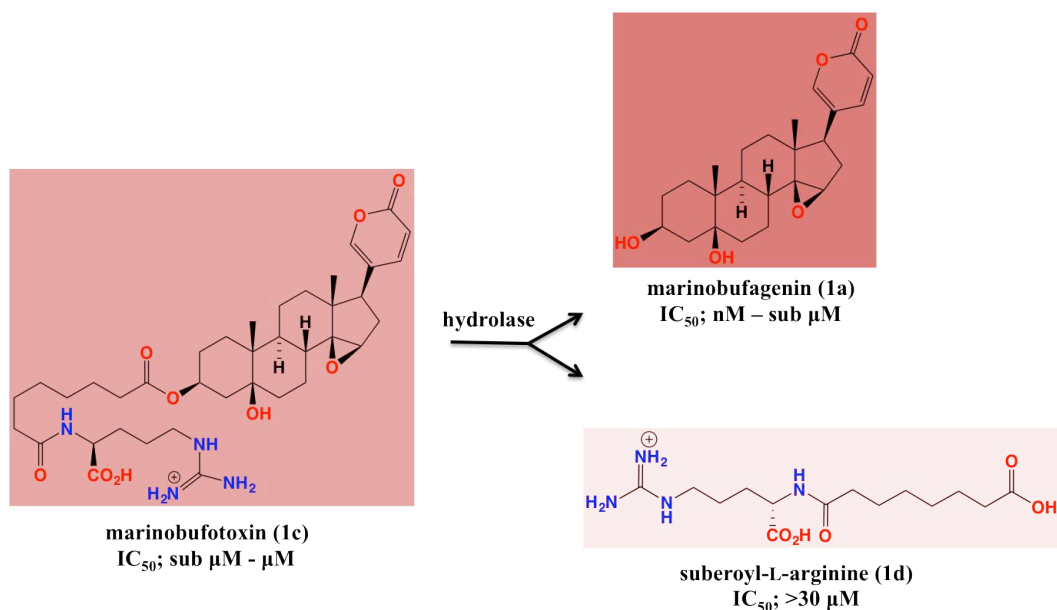
Figure 7.12 Cytotoxicity profiles of marinobufotoxin (**1c**) and its hydrolysis products

7.2.2.7 Synergism of bufagenins and suberoyl-L-arginine (1d)

Bufagenins and arginyl amides constituting parotoid secretions possibly exhibit synergistic activity on same or multiple targets. Hence both the structure classes were subjected to cytotoxicity assays at equimolar concentrations and no changes were observed. Following cytotoxicity studies investigation of another target, stimulation of nitric oxide (NO) production by arginyl amides.

7.2.3 Possible role of nitric oxide synthase in cane toad toxicity

For assessing the biological activity of arginyl amides we also investigated the possibility of activation of mammalian nitric oxide synthase (NOS). Nitric oxide synthase is an enzyme complex required to synthesize nitric oxide (NO) from L-arginine. There are three types of mammalian NOS (mNOS) expressed in nervous system (nNOS), immune system (iNOS in lungs) and endothelial cells (eNOS).[12] Endothelial NOS (eNOS) play a major role in generating NO, which mediates vasodilation of blood vessels resulting in increased blood flow.[13] eNOS utilizes L-arginine substrate to synthesize NO in the presence of co-factors such as Ca-calmodulin (Ca^{2+} bound calmodulin), FMN (flavin mononucleotide), FAD (flavin adenine dinucleotide), Heme and BH_4 (tetrahydrobiopterin) (Figure 7.13).[14] The NO biosynthesis is also inhibited by the synthetic agents N-nitro-L-arginine, N-methyl-L-arginine and N-nitro-arginine-methyl-ester.[14]

Since arginyl amides contain L-arginine we speculated that their presence may mediate NO production. For example, arginyl amides could possibly act as a substrate for eNOS leading to the production of NO with associated increases in blood flow. Such an event may accelerate the transport of cardiotoxic bufagenins leading to a more rapid (and effective) poisoning.

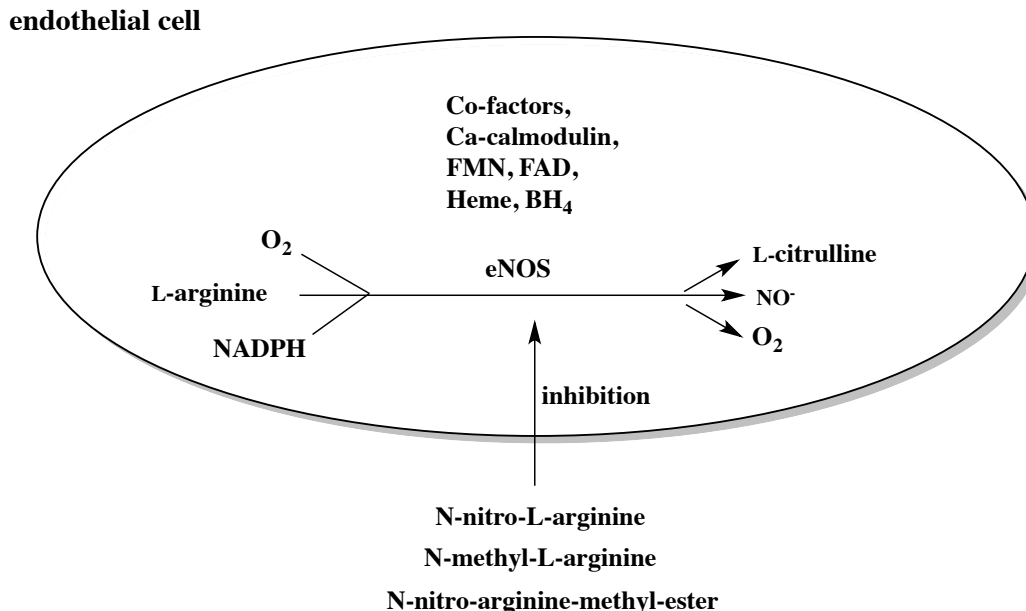**Figure 7.13** Description of NOS pathway in an endothelial cell indicating the substrates, co-factors for NO production as well as the inhibitors. Reproduced from Feletou et al 2006.

7.2.4 mNOS activation of arginyl amides

The arginyl amides suberoyl-L-arginine (**1d**), pimeloyl-L-arginine (**3d**), adipoyl-L-arginine (**2d**) and azeloyl-L-arginine (**4d**) were tested at four concentrations (5 mM, 1 mM, 100 μM and 10 μM) were

subjected to mNOS activation assay. Of the four arginyl amides subjected to mNOS activation, only suberoyl- L-arginine (**1d**) and pimeloyl- L-arginine (**3d**) that are naturally occurring analogues with **1d**, are present in substantial levels in the parotoid secretions. The assay was carried out using two cancer cell lines, SW620 (RPMI) and KB31 (DMEM) as a model for qualitatively assessing NOS activation of arginyl amides. The cell lines were cultivated from the frozen stock and maintained at a constant temperature of 15 °C. SW620 and KB31 exhibited about 70% confluence after 48 h of incubation. Arginyl amides were added to the cells aliquoted on to a 96-well plate and were incubated for 20 min followed by the addition of NO detection reagent and incubated for further 10 min as described by the manufacturer's protocol. NO detection reagent is a non-fluorescent substrate and reacts with the induced NO to generate a red fluorescent product, which is then detected using confocal microscopy. In a negative control an NO scavenger was added to the cells prior to the addition of NO detection reagent, to quench NO and associated fluorescence. Cells treated with L-arginine and NO detection reagent exhibited fluorescence and this represented the positive control. No fluorescence was detected with cells treated only with NO detection reagent.

7.2.4.1 Effect of suberoyl-L-arginine and pimeloyl-L-arginine compared to L-arginine

Cell lines, SW620 and KB31 treated with L-arginine exhibited high fluorescence at 1 mM and 5 mM concentrations which is in consistent with the values previously determined in-house assays by Dr Zeinab Khalil (Capon group). Surprisingly, suberoyl-L-arginine exhibited high fluorescence indicating the activation of mNOS at 100 μM compared to L-arginine in SW620 as well as KB31 cells (Figure 7.14 and Figure 7.15).

Pimeloyl-L-arginine (**3d**) on the other hand exhibited less mNOS activation compared to L-arginine at about 1 mM. Suberoyl-L-arginine exhibited mNOs activation at lower levels even at 10 μM in KB31 and SW 620 cell lines. Although the current investigation is a qualitative measure of mNOS activation, **1d** exhibited more activation than L-arginine based on the fluorescence observed at various concentrations (Figure 7.15).

Figure 7.14 mNOS activation identified in KB31 cells post treatment with A – KB31 cells with NO detection reagent, B – 1mM suberoyl-L-arginine (**1d**) with NO detection reagent and C – 1mM suberoyl-L-arginine (**1d**) with NO scavenger, D – 1mM L-arginine with NO detection reagent, E – 1mM L-arginine with NO scavenger . Bars – 0.6 μm.
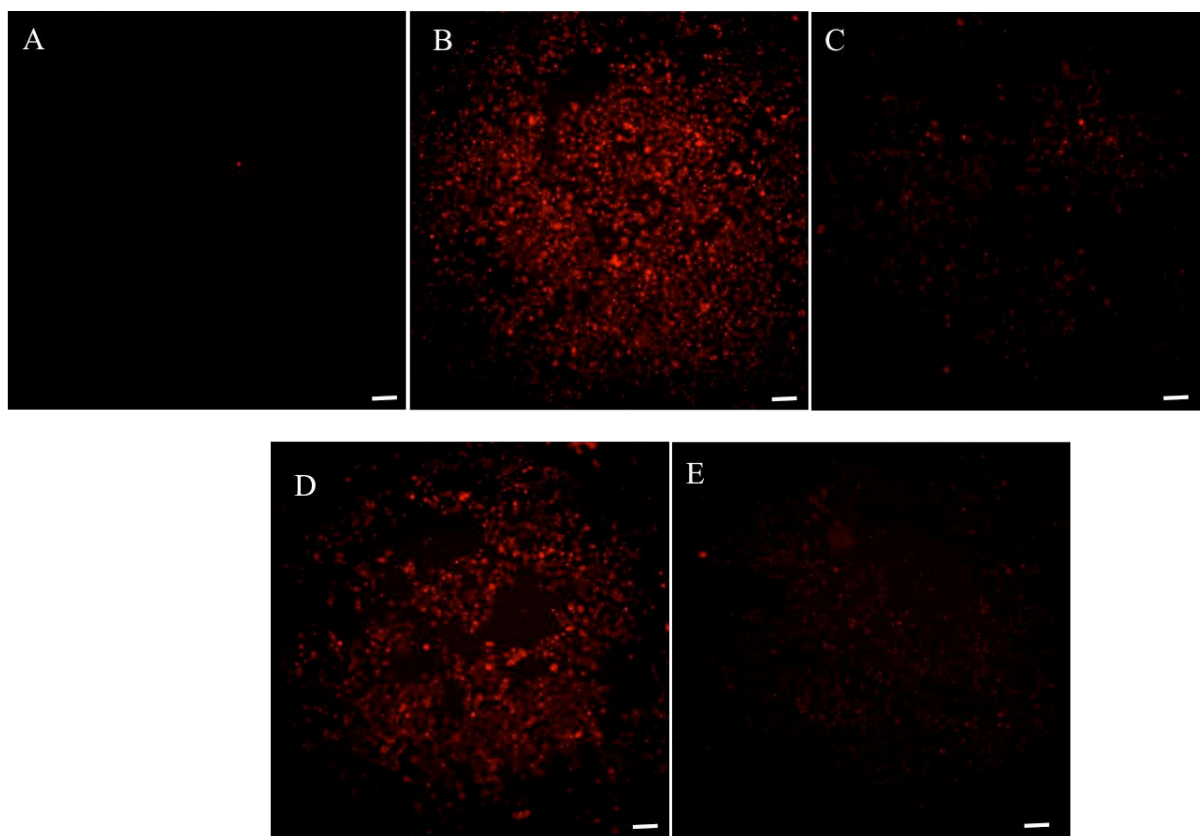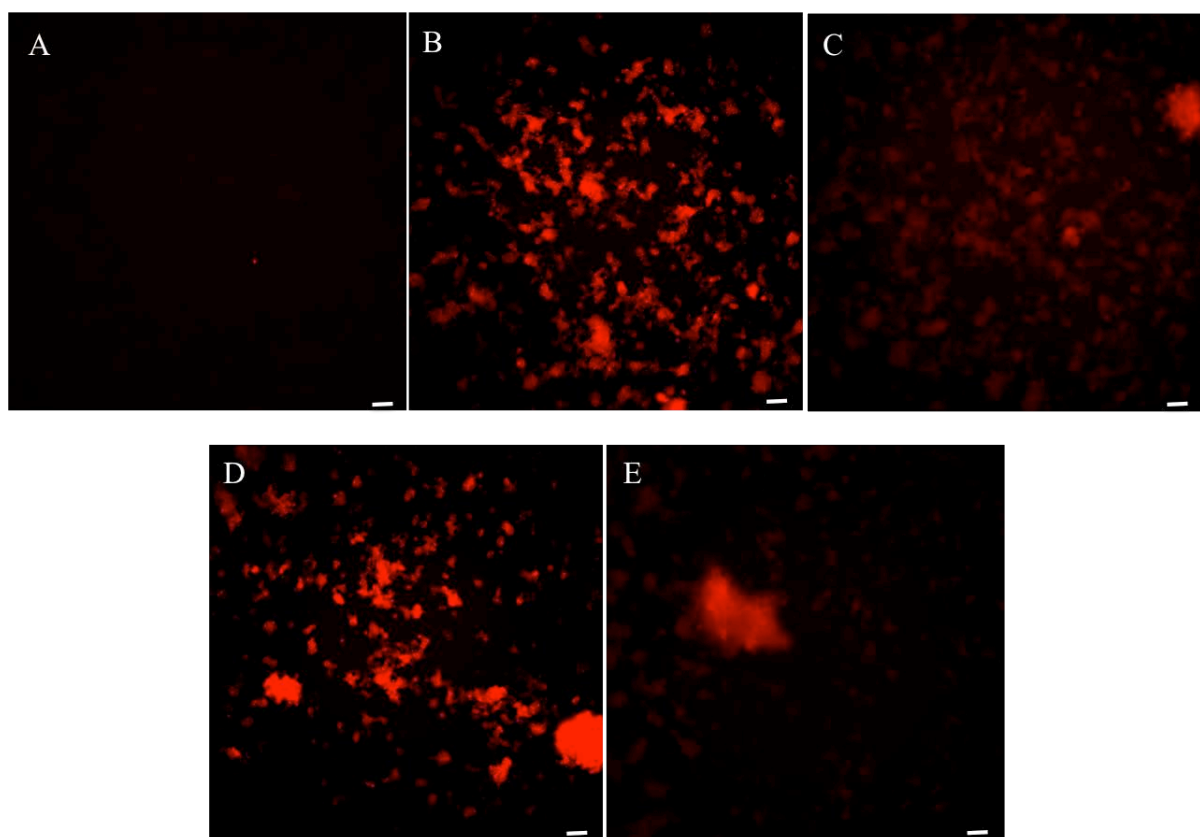

Figure 7.15 mNOS activation identified in SW620 cells post treatment with A – SW620 cells with NO detection reagent, B – 1mM suberoyl-L-arginine (**1d**) with NO detection reagent and C – 1mM suberoyl-L-arginine (**1d**) with NO scavenger, D – 1mM L-arginine with NO detection reagent, E – 1mM L-arginine with NO scavenger . Bars – 0.6 μm.

7.2.4.2 SAR studies on mNOS activation of arginyl amides

Arginyl amides with varying chain lengths including suberoyl-L-arginine (**1d**), adipoyl-L-arginine (**2d**), pimeloyl-L-arginine (**3d**) and azeloyl-L-arginine (**4d**) were subjected to mNOS activation in SW 620 and KB-31 cancer cell lines as explained above (Figure 7.16). Adipoyl-L-arginine and pimeloyl-L-arginine exhibited moderate mNOS activation and are comparable to L-arginine at 100 µM concentration. However, suberoyl-L-arginine and azeloyl-L-arginine showed higher fluorescence even at 10 µM levels. This observation suggests that longer the fatty acid ester, the higher the mNOS activation.
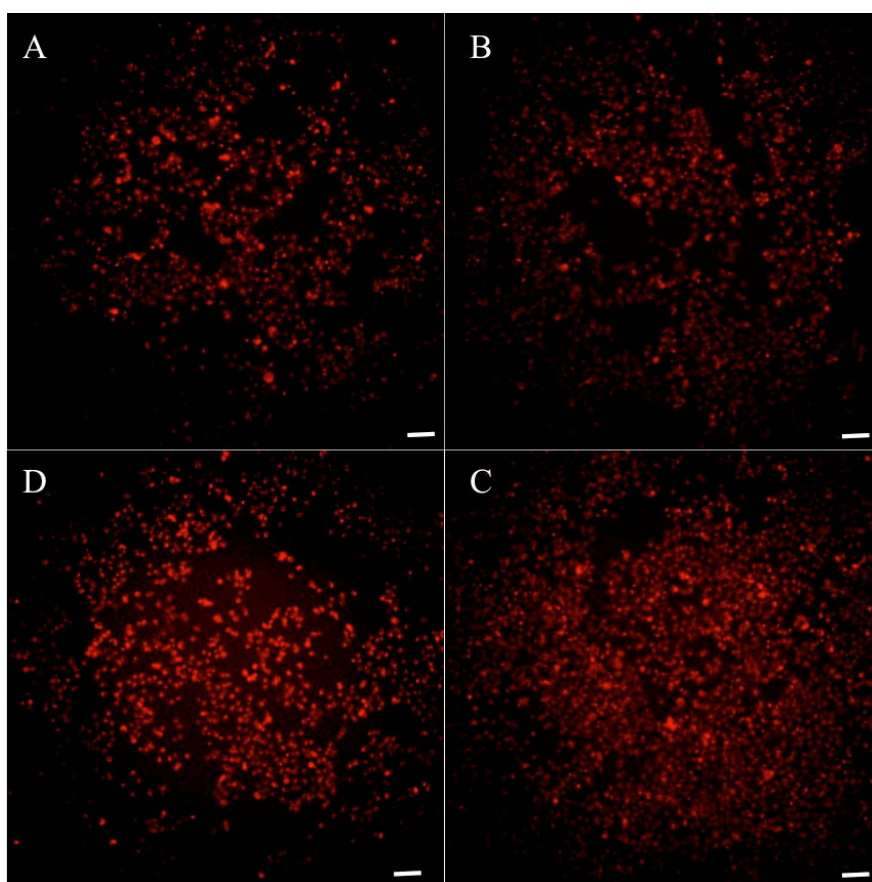
Figure 7.16 mNOS activation identified in KB-31 cells post treatment with 1mm A – adipoyl-L-arginine (**2d**), B – pimeloyl-L-arginine (**3d**), C- suberoyl-L-arginine (**1d**) and D - azeloyl-L-arginine (**4d**). Bars – 0.6 µm.

Fatty acid chain of arginyl amides plays a role in the activation of mNOS. The hydrophobicity of arginyl amides contributed by fatty acid could facilitate the transport through the cell membrane resulting in increased intake compared to L-arginine.

7.2.4.3 Discussion – mNOS activation by arginyl amides

Our analyses on mNOS activation suggests that arginyl amides, especially suberoyl-L-arginine (**1d**), the major arginyl amide in the parotoid secretions exhibits significant activation compared to the positive control, L-arginine. During a predatory attack, **1d** present in the parotoid secretions would lead to increased NO production resulting in a plausible vasodilation. It is speculated that this would result in increased transport/accessibility of the hydrophobic bufagenins into the cardiac region resulting in inhibition of cardiac Na^+/K^+ ATPase further leading to cardiac arrest (Figure 7.17).

Toxin delivery in cane toads follow a typical protoxin to toxin conversion mediated by BtH with bufagenins resulting in intoxication of predators while arginyl amides could possibly playing a role in intoxication by improving the bufagenin cardiotoxicity.
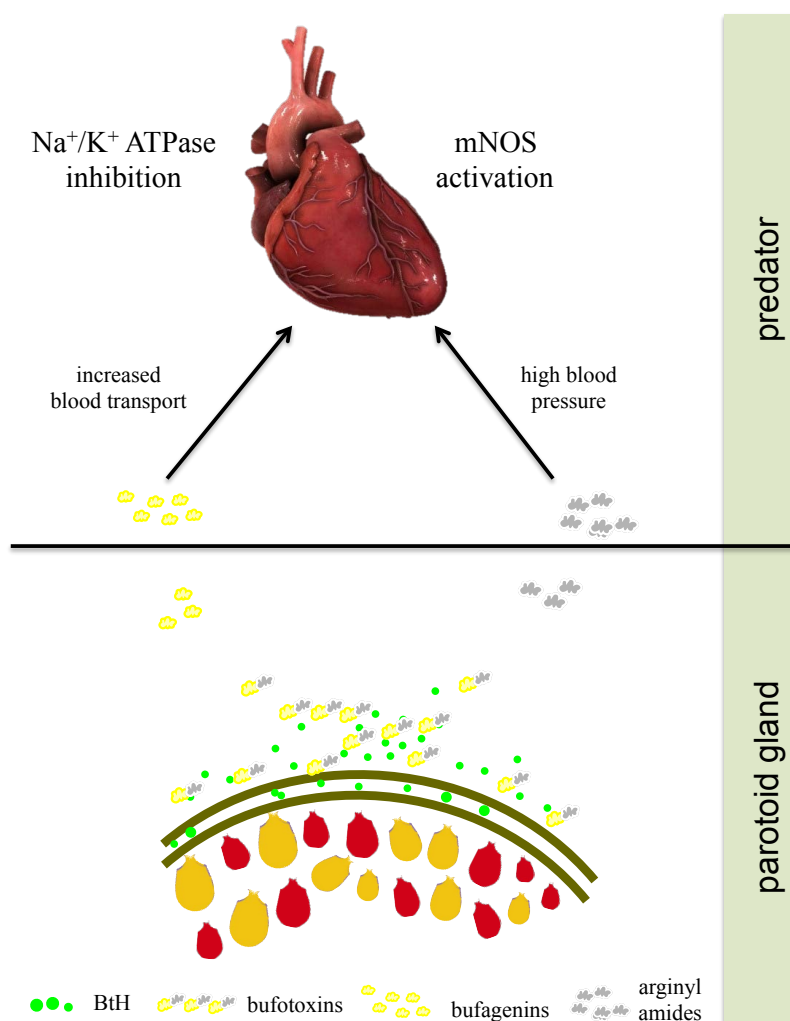
Figure 7.17 Proposed scheme of events following a predatory attack on cane toads

7.2.5 Antibacterial activity of bufadienolides and arginyl amides

Cane toad toxins including bufagenins, bufotoxins and arginyl amides were subjected to antimicrobial assays with various gram-positive and gram-negative strains including, *Bacillus subtilis* (ATCC 6633), *Escherichia coli* (ATCC11775), *Pseudomonas aeruginosa* (ATCC 10145), and *Staphylococcus aureus* (strains ATCC 9144 & ATCC 25923). The list of bufagenins (Figure 7.1), bufagenin esters (Figure 7.3), bufotoxins (Figure 7.5) and arginyl amides (Figure 7.18) subjected to bacterial cytotoxicity assays are mentioned above.

None of the bufadienolides and arginyl amides exhibited prokaryotic cytotoxicity against any of the bacteria subjected to the analysis. However, bufalin (**3a**) exhibited moderate antimicrobial activity against the Gram-negative bacteria *Pseudomonas aeruginosa* with a MIC of 1 μg/mL (Figure 7.14).
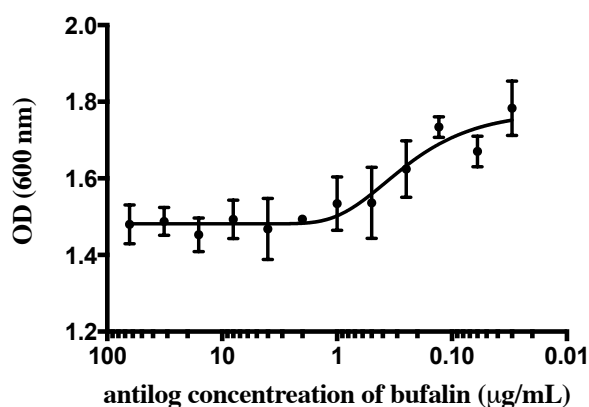
Figure 7.18 MIC (antilog) curve exhibited by bufalin (**3a**) on *Pseudomonas aeruginosa*

Cane toad toxins lack antimicrobial properties against pathogenic bacteria under current investigation. These results could not be directly compared to the antimicrobial properties of bufadienolides in parotoid gland *in situ* as the microbes experienced *in vivo* could be different from the current investigation. However, the *in situ* bufotoxins also provides resistance to microbial biotransformation as mentioned earlier in Chapter 5. These observations are consistent with out previous findings that *in situ* storage of bufotoxins provides multiple benefits to the cane toad parotoid glands including microbiological stability.

7.3 Conclusion

Toxicity of cane toads is a relative terminology as there are no relevant functional assays that explore targets (such as Na^+/K^+ ATPase) in a predatory species (such as crocodile, snakes, quolls etc) comparing bufadienolides (bufagenins, bufolipins and bufotoxins) and arginyl amides. However, some reports describe binding assays with bufadienolides and Na^+/K^+ ATPase from non-predatory species such as pigs. Our current investigations explored the cytotoxicity of cane toad chemical diversity and mNOS activation of arginyl amides as a measure of toxicity and identified that:

- Bufagenins are more cytotoxic (>30 fold) than bufotoxins and arginyl amides in our investigations

- Cytotoxicity of bufolipins are comparable to bufagenins

- Cane toad chemical diversity did not show antibacterial activity

- Arginyl amides are modest activators of mNOS

7.4 Experimental

7.4.1 Cytotoxicity

7.4.1.1 Cell lines and Cell Culture

The human colon cancer cell line SW620 and the human glioblastoma cell line SF-295 were provided by Susan E. Bates and Robert W. Robey of the National Cancer Institute (NCI), Bethesda, MD. These two cell lines were cultured in RPMI medium 1640 (Invitrogen, Carlsbad, CA).

7.4.1.2 Cytotoxicity Assay (MTT)

The MTT assay was used to evaluate the cytotoxicity of compounds against cancer cell lines (SW620 and SF295) as previously described[15]. Briefly, cells (2,000/well in 180 μL of RPMI 1640 supplemented with 10% FBS) were seeded evenly in a 96-well micro-plate which was then incubated for 18 h (37 °C; 5% CO_2) for attachment of cells. Compounds to be tested were dissolved in 5% DMSO (v/v) and diluted from a range of concentrations (0.001 μM to 3 μM for **3a** and 0.01 μM to 30 μM for all other compounds). Aliquots (20 μL) of each dilution (or of 5% DMSO for control wells) were added to the plate in duplicate. After 68 h incubation (37 °C; 5% CO_2), a solution of 3-(4,5-dimethylthiazol-2-yl)-2,5-diphenyltetrazolium bromide (MTT; Sigma, USA) in PBS was added to each well to a final concentration of 0.4 mg/mL and the plate was incubated for a further 4 h (37 °C; 5% CO_2). The medium was then carefully aspirated and precipitated formazan crystals were dissolved in DMSO (100 μL/well). Finally, the absorbance of each well at 580 nm was measured with a PowerWave XS Microplate Reader from Bio-Tek Instruments Inc. (Vinooski, VT). IC_{50} values (the concentration of the compound required for 50% inhibition of the cancer cells) were calculated using Prism 5.0 from GraphPad Software Inc. (La Jolla, CA).

7.4.2 mNOS activation assay

7.4.2.1 Reagents preparation according to manufacturer's instructions

The nitric oxide detection kit (ENZ-51013) including the NO scavenger 2-(4-carboxyphenyl)-4,4,5,5-tetramethylimidazoline-1-oxyl-3-oxide (c-PTIO) and matching 10×wash buffer was purchased from Enzo Life Sciences.

1. Dilution of NO detection reagent: An aliquot of the NO detection reagent (2.5 μL) was diluted 1:400 with pre-warmed culture medium (1 mL) immediately prior to use.

2. Positive control: The NO inducer (L-arginine) was supplied as a stock (100 mM) in deionized water. A final concentration per well is 1 mM. Therefore 2 μL of the stock is transferred to 198 μL of the cell culture medium.

3. Negative control: The NO Scavenger (c-PTIO) was supplied as lyophilized powder, which was dissolved in dry DMF (100 μL) to produce a stock solution of 4 mM.

4. 1X Wash buffer: The wash buffer was supplied as a 10X solution, which was diluted 1/10 with deionized water to give a 1X working concentration.

7.4.2.2 Cell Preparations

Two cell lines were chosen for the assay, KB-31 (adherent epithelial like, human cervix carcinoma) and SW620 (adherent epithelial like, human colorectal carcinoma). Both cells, KB-31 and SW620 were cultivated in 96 well plates 3 d prior to the experimental day to ensure 50-70% confluency in the day of the experiment. The cells were seeded in the plates in 2 different concentrations. KB-31 was seeded in plates to give final concentration 4000 cells/well, while SW620 was seeded in the plates to give final concentration 2000 cells/well. The plates were incubated at 37 °C for 3 d. On the day of the experiment, KB-31, 8000 cells/well gave confluency around 60% and for SW620, 8000 cells/well gave approx. confluency of 70% and the media used were DMEM for KB-31 and RPMI1640 for SW620 supplemented with L-glutamine and no phenol red. Cells were harvested and treated with compounds in 4 different concentrations (5 mM, 1 mM, 100 μM and 10 μM; 20 μL/well). Confocal microscopy was performed on a Zeiss LSM510 confocal laser-scanning microscope equipped with a Zeiss 63x/1.4NA oil-immersion objective. Confocal microscopy samples, in 12 mm coverglass bottom culture dishes (ProSciTech), were excited with a 543 nm He Ne laser and measured emissions filtered through a 560 nm long-pass filter. Images were accessed using Image J software (NIH).

7.4.3 Antimicrobial assay

MICs against all bacteria were measured by broth microdilution according to the Clinical and Laboratory Standards Institutes (CLSI) M7-A7 methodology. Briefly, serial two-fold dilutions of each compound was added into Costar non-treated polystyrene 96-well plates, and each well inoculated with 50 μL of bacterial strain including *Bacillus subtilis*, *Pseudomonas aeruginosa*, *Staphylococcus aureus* strain 9144, *Staphylococcus aureus* strain 25923 and *Escherichia coli* in MHB with a final concentration of approximate 5×10^5 CFU/ml. The MIC was the lowest antibiotic concentration that showed no visible growth after 24 h of incubation at 37 °C. Plates were subjected to spectrophotometric analysis (OD_{600nm}) using POLARstar Omega (BMG Labtech).

7.5 References

1. Halliday, D. C. T.; Venables, D.; Moore, D.; Shanmuganathan, T.; Pallister, J.; Robinson, A. J.; Hyatt, A., Cane toad toxicity: An assessment of extracts from early developmental stages and adult tissues using MDCK cell culture. *Toxicon* **2009,** *53*, 385-391.

2. Akimova, O. A.; Bagrov, A. Y.; Lopina, O. D.; Kamernitsky, A. V.; Tremblay, J.; Hamet, P.; Orlov, S. N., Cardiotonic steroids differentially affect intracellular Na^+ and $Na^+_{(i)}$/ $K^+_{(i)}$-independent signaling in C7-MDCK cells. *J. Biol. Chem.* **2005,** *280*, 832-839.

3. Touza, N. A.; Pocas, E. S. C.; Quintas, L. E. M.; Cunha, G.; Santos, M. L.; Noel, F., Inhibitory effect of combinations of digoxin and endogenous cardiotonic steroids on Na^+/K^+-ATPase activity in human kidney membrane preparation. *Life Sci.* **2011,** *88*, 39-42.

4. Hilton, P. J.; McKinnon, W.; Gravett, E. C.; Peron, J. M. R.; Frampton, C. M.; Nicholls, M. G.; Lord, G., Selective inhibition of the cellular sodium pump by emicymarin and 14 beta anhydroxy bufadienolides. *Steroids* **2010,** *75*, 1137-1145.

5. Shimada, K.; Ohishi, K.; Fukunaga, H.; Ro, J. S.; Nambara, T., Studies on steroids .213. structure activity relationship of bufotoxins and related-compounds for the inhibition of Na^+, K^+-adenosine triphosphatase. *J. Pharmacobio-Dyn.* **1985,** *8*, 1054-1059.

6. Shimada, K.; Sato, Y.; Nambara, T., Studies on steroids .230. Occurrence of marinobufotoxin and telocinobufotoxin homologs in the skin of *Bufo bankorensis borbour*. *Chem. Pharm. Bull.* **1987,** *35*, 2300-2304.

7. Matsukawa, M.; Mukai, T.; Akizawa, T.; Miyatake, S.; Yoshioka, M.; Morris, J. F.; Butler, V. P., Isolation and characterization of novel endogenous digitalis-like factors in the ovary of the giant toad, *Bufo marinus*. *J. Nat. Prod.* **1998,** *61*, 1476-1481.

8. Kamano, Y.; Kotake, A.; Hashima, H.; Inoue, M.; Morita, H.; Takeya, K.; Itokawa, H.; Nandachi, N.; Segawa, T.; Yukita, A.; Saitou, K.; Katsuyama, M.; Pettit, G. R., Structure-cytotoxic activity relationship for the toad poison bufadienolides. *Bioorg. Med. Chem.* **1998,** *6*, 1103-1115.

9. Cunha, G. A.; Resck, I. S.; Cavalcanti, B. C.; Pessoa, C. O.; Moraes, M. O.; Ferreira, J. R. O.; Rodrigues, F. A. R.; dos Santos, M. L., Cytotoxic profile of natural and some modified bufadienolides from toad *Rhinella schneideri* parotoid gland secretion. *Toxicon* **2010,** *56*, 339-348.

10. Gao, H.; Zehl, M.; Kaehlig, H.; Schneider, P.; Stuppner, H.; Moreno Y. Banuls, L.; Kiss, R.; Kopp, B., Rapid Structural Identification of Cytotoxic Bufadienolide Sulfates in Toad Venom from *Bufo melanosticus* by LC-DAD-MSn and LC-SPE-NMR. *J. Nat. Prod.* **2010,** *73*, 603-608.

11. Filho, G. A. C.; Schwartz, C. A.; Resck, I. S.; Murta, M. M.; Lemos, S. S.; Castro, M. S.; Kyaw, C.; Pires, O. R.; Leite, J. R. S.; Bloch, C.; Schwartz, E. F., Antimicrobial activity of the bufadienolides marinobufagin and telocinobufagin isolated as major components from skin secretion of the toad *Bufo rubescens*. *Toxicon* **2005,** *45*, 777-782.

12. Stuehr, D. J., Mammalian nitric oxide synthases. *Biochim. Biophys. Acta-Bioenerg.* **1999,** *1411*, 217-230.

13. Smith, C. J.; Santhanam, L.; Bruning, R. S.; Stanhewicz, A.; Berkowitz, D. E.; Holowatz, L. A., Upregulation of Inducible Nitric Oxide Synthase Contributes to Attenuated Cutaneous Vasodilation in Essential Hypertensive Humans. *Hypertension* **2011,** *58*, 935-942.

14. Feletou, M.; Vanhoutte, P. M., Endothelial dysfunction: a multifaceted disorder. *Am. J. Physiol.-Heart. Circul. Physiol.* **2006,** *291*, H985-H1002.

15. Huang, X. C.; Sun, Y. L.; Salim, A. A.; Chen, Z. S.; Capon, R. J., Parguerenes: Marine red alga bromoditerpenes as inhibitors of P-glycoprotein (ABCB1) in multidrug resistant human cancer cells. *Biochem. Pharmacol.* **2013,** *85*, 1257-68.

8. Conclusion

The current thesis describes cane toad parotoid glands and parotoid toxins, their storage and delivery, regulation of toxin levels, enzyme mediating toxin regulation, toxin distribution across adults and eggs and relationship with bacteria. Addressing all these domains required inputs from various disciplines including organic chemistry, analytical chemistry, biochemistry, proteomics and transcriptomics, imaging and microbiology. Profiling of cane toad toxins started in 1930's and it was always thought that cane toad parotoid glands contained bufagenins and secereted upon manual compression. In 1970's parotoid glands were studied and parotoid microglands containing parotoid toxins were identified, however, individual microglands were not dissected and studied until 2012. In 2008 bufagenin degrading bacterial strains were identified and the relationship between parotoid secretions and biotransforming bacteria was questioned.

Studies carried on in the current thesis further extended our existing knowledge on cane toad parotoid glands, parotoid toxin, parotoid secretions and the relationship with bacteria. A clear distinction between parotoid toxins and parotoid secretions was addressed with the help of chemical profiling, dissection analysis and microscopy. Identification of a protoxin to toxin conversion with the aid of *in situ* BtH exhibited significant understanding of a rare type of toxin storage and release mechanisms in Bufo species. Accordingly, the cytotoxicity studies correlated with the *in situ* bufotoxins being less cytotoxic compared to highly cytotoxic *ex situ* bufagenins. Another interesting finding is the identification of significant amounts of arginyl amides in parotoid secretions and their mNOS activation in mammalian cells. Distinction of bufagenin degrading strains and biotransforming strains is significant in understanding the relationship between bacteria and the parotoid glands. Also, existence of several new bufolipins was identified from *B. marinus* eggs, which also extends our undersanding of *B. marinus* chemical diversity. Figure 8.1 illustrates the trends in the understanding of cane toad parotoid secretions before and after the commencement of the current thesis.

The current findings may help us identify strategies to develop cane toad control solutions in Australia by exploiting our studies on BtH, bufagenin degrading bacteria and bufolipins (used as attractant pheromones).
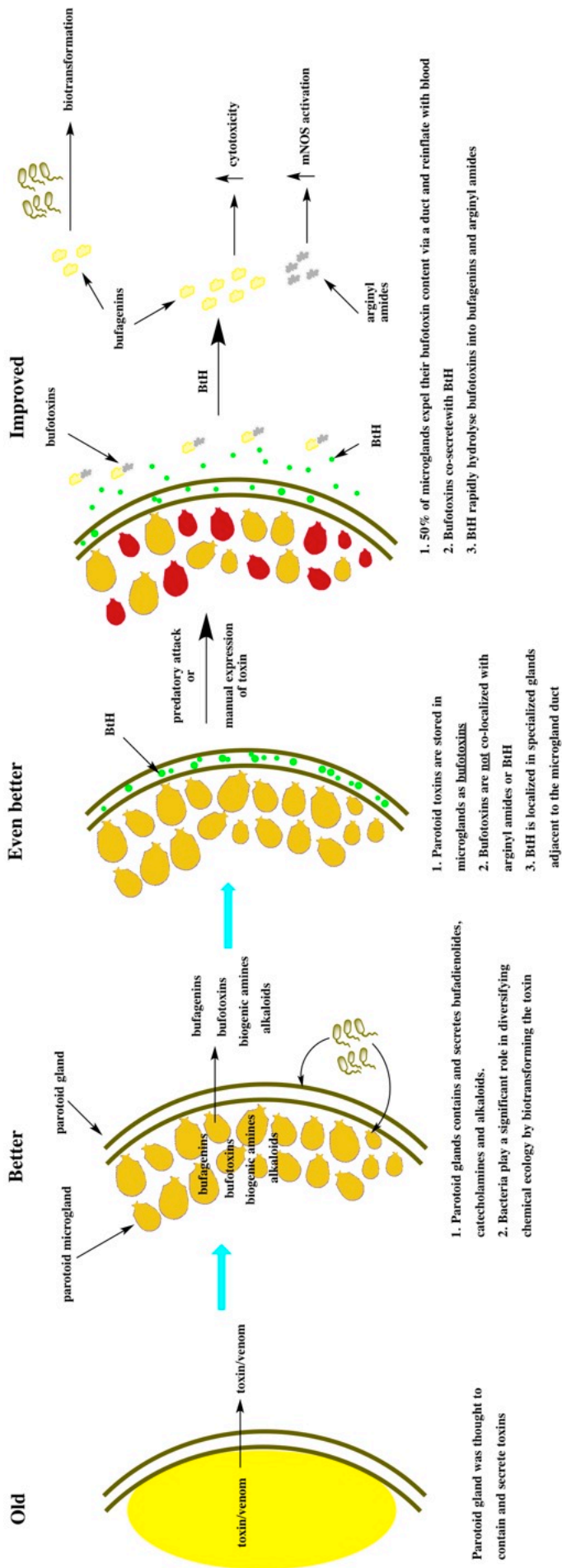
Figure 8.1 Trends in understanding of cane toad parotoid secretions and related events from 1900's to present

304

9. Future work

Investigation in the current thesis has led to new insights into the understanding of cane toad toxins resulting in interesting outcomes. Following are the list of future work:

- Protein crystallization – As discussed in chapter 4, isolation and identification of BtH protein sequence were performed. Since BtH belong to novel class of enzymes, structural information is significant. Parotoid secretions from 20 cane toads (40 parotoid glands) were collected and a large-scale purification of BtH (30 mg) was performed as mentioned before. Following this BtH will be subjected to crystal studies and the resulting crystals will be submitted to X-ray crystallography to identify the BtH crystal structure. This work is being performed in collaboration with A/Prof. Brett Collins (Institute for Molecular Biosciences) and is currently in progress.

- Bufolipins – Large scale synthesis of bufolipins (g scale) from previously isolated parotoid secretions (se Chapter 5) will be performed and submitted to toad tadpole attractant field trials which is being performed in collaboration with Prof. Rick Shine in Northern Territory.

- Identification of biotransforming bacteria – Biotransforming strains that were found to transform marinobufagenin (**1a**) into arenobufagenin (**6a**) will be subjected to identification using PCR based investigation. Also the ability of the strains to transform marinobufotoxin (**1c**) to arenobufotoxin (**6c**) (oxidations at steroidal C ring) will be performed as the strains were isolated from parotoid glands and identification of *in situ* biotransformation of bufotoxins would be significant. Also ability of such strains to biotransform other steroids including cholesterol and progesterone will be performed as modifications at C-10 and C-11 of steroidal C-ring would be a significant investigation.

- Pharmacology studies – antifungal assays for bufadienolides and arginyl amides using in-house fungi species such as *Candida albicans* and *Aspergillus niger*. A cardiomyocyte (Na^+/K^+ ATPase) inhibition of various structure classes of bufadienolides and arginyl amides.

- Attractant pheromones – bufagenins obtained from parotoid secretions would be subjected to microbial biotransformation to produce bufagenin-like structures found in eggs. These egg bufagenins would then be converted to bufolipins using established partial synthesis. These bufolipins would then be subjected to field trials for the identification of better attractant pheromone properties.